CARDIOVASCULAR TOXICITY ASSOCIATED WITH CANCER TREATMENT: STRATEGIES FOR DIAGNOSIS, MANAGEMENT AND CARDIOPROTECTION

EDITED BY: Zhi-Ren Zhang, Yue Li, Jun Pu, Yong Xia and Ming-Ming Wu
PUBLISHED IN: Frontiers in Pharmacology

frontiers Research Topics

ISSN 1664-8714
ISBN 978-2-83250-800-8
DOI 10.3389/978-2-83250-800-8

About Frontiers

Frontiers is more than just an open-access publisher of scholarly articles: it is a pioneering approach to the world of academia, radically improving the way scholarly research is managed. The grand vision of Frontiers is a world where all people have an equal opportunity to seek, share and generate knowledge. Frontiers provides immediate and permanent online open access to all its publications, but this alone is not enough to realize our grand goals.

Frontiers Journal Series

The Frontiers Journal Series is a multi-tier and interdisciplinary set of open-access, online journals, promising a paradigm shift from the current review, selection and dissemination processes in academic publishing. All Frontiers journals are driven by researchers for researchers; therefore, they constitute a service to the scholarly community. At the same time, the Frontiers Journal Series operates on a revolutionary invention, the tiered publishing system, initially addressing specific communities of scholars, and gradually climbing up to broader public understanding, thus serving the interests of the lay society, too.

Dedication to Quality

Each Frontiers article is a landmark of the highest quality, thanks to genuinely collaborative interactions between authors and review editors, who include some of the world's best academicians. Research must be certified by peers before entering a stream of knowledge that may eventually reach the public - and shape society; therefore, Frontiers only applies the most rigorous and unbiased reviews.
Frontiers revolutionizes research publishing by freely delivering the most outstanding research, evaluated with no bias from both the academic and social point of view. By applying the most advanced information technologies, Frontiers is catapulting scholarly publishing into a new generation.

What are Frontiers Research Topics?

Frontiers Research Topics are very popular trademarks of the Frontiers Journals Series: they are collections of at least ten articles, all centered on a particular subject. With their unique mix of varied contributions from Original Research to Review Articles, Frontiers Research Topics unify the most influential researchers, the latest key findings and historical advances in a hot research area! Find out more on how to host your own Frontiers Research Topic or contribute to one as an author by contacting the Frontiers Editorial Office: frontiersin.org/about/contact

CARDIOVASCULAR TOXICITY ASSOCIATED WITH CANCER TREATMENT: STRATEGIES FOR DIAGNOSIS, MANAGEMENT AND CARDIOPROTECTION

Topic Editors:
Zhi-Ren Zhang, Harbin Medical University, China
Yue Li, First Affiliated Hospital of Harbin Medical University, China
Jun Pu, Shanghai Jiao Tong University, China
Yong Xia, The Ohio State University, United States
Ming-Ming Wu, Harbin Medical University, China

Citation: Zhang, Z.-R., Li, Y., Pu, J., Xia, Y., Wu, M.-M., eds. (2022). Cardiovascular Toxicity Associated With Cancer Treatment: Strategies for Diagnosis, Management and Cardioprotection. Lausanne: Frontiers Media SA.
doi: 10.3389/978-2-83250-800-8

Table of Contents

frontiers in Pharmacology

ORIGINAL RESEARCH
published: 01 October 2021
doi: 10.3389/fphar.2021.748677

Dynamic Changes of Serum Heart Type-Fatty Acid Binding Protein in Cancer Patients Treated With Immune Checkpoint Inhibitors

Ming Yuan[1,2†], Li Zang[3†], Aiqing Xu[1], Mengqi Gong[1], Qing Liu[3], Bin Huo[3,4], Jinhuan Wang[3], Huaying Fu[1], Gary Tse[1], Leonardo Roever[5], Guangping Li[1], Haitao Wang[3,4] and Tong Liu[1]**

[1]Tianjin Key Laboratory of Ionic-Molecular Function of Cardiovascular Disease, Department of Cardiology, Tianjin Institute of Cardiology, Second Hospital of Tianjin Medical University, Tianjin, China, [2]Department of Cardiology, Biomedical Research (Therapy) Center, Sir Run Run Shaw Hospital, School of Medicine, Zhejiang University, Hangzhou, China, [3]Department of Oncology, Second Hospital of Tianjin Medical University, Tianjin, China, [4]Central Laboratory/Tianjin Research Institute of Urology, Second Hospital of Tianjin Medical University, Tianjin, China, [5]Department of Clinical Research, Federal University of Uberlândia, Uberlândia, Brazil

Objective: Immune checkpoint inhibitors (ICIs) are effective anti-cancer drugs that can improve survival in cancer patients, but their use may be associated with adverse cardiovascular side effects. Therefore, there is a clinical unmet need to identify non-invasive biomarker to detect subclinical cardiac toxicity after ICI treatment. The aim of this study is to examine the plasma levels of biomarkers in cancer survivors who were treated with ICIs.

Patients and Methods: In a cohort of 19 cancer patients, biomarkers were evaluated at baseline, 1 month, 3 and 6 months after ICI administration. These biomarkers, hypothesized to be mechanistically relevant to cardiotoxicity, included cardiac troponin I (cTnI), high-sensitivity C-reactive protein (Hs-CRP), N-terminal pro–B-type natriuretic peptide (NT-pro BNP), CK (creatine kinase), CK-MB (creatine kinase-MB), Pentraxin-related protein 3 (PTX3), growth differentiation factor 15 (GDF-15), heart type-fatty acid binding protein (H-FABP) and galectin 3 (Gal-3).

Results: H-FABP, but not other biomarkers, were increased at 3 months, which persisted at 6 months (529.28 ± 312.83 vs. 752.33 ± 283.65 vs. 808.00 ± 289.69 pg/ml, $p = 0.031$ and $p = 0.013$). Left ventricular ejection fraction (63.00 ± 4.15% vs. 63.74 ± 4.07%, $p > 0.05$) was not significantly reduced at this time point.

Conclusions: H-FABP, but not other biomarkers, were increased in patients who were treated using ICIs. H-FABP might be a more sensitive biomarker to detect ICI-related subclinical myocardial damage than traditional cardiac biomarkers.

Keywords: cardio-oncology, cardiotoxicity, immune checkpoint inhibitors, H-FABP, immune-related adverse events

OPEN ACCESS

Edited by:
Zhi-Ren Zhang,
Harbin Medical University, China

Reviewed by:
Leilei Cheng,
Fudan University, China
Tiangang Zhu,
Peking University people's hospital, China
Lilei Yu,
Wuhan University, China

***Correspondence:**
Haitao Wang
marveljwh@163.com
Tong Liu
liutongdoc@126.com

†These authors have contributed equally to this work

Specialty section:
This article was submitted to Cardiovascular and Smooth Muscle Pharmacology, a section of the journal Frontiers in Pharmacology

Received: *28 July 2021*
Accepted: *15 September 2021*
Published: *01 October 2021*

Citation:
Yuan M, Zang L, Xu A, Gong M, Liu Q, Huo B, Wang J, Fu H, Tse G, Roever L, Li G, Wang H and Liu T (2021) Dynamic Changes of Serum Heart Type-Fatty Acid Binding Protein in Cancer Patients Treated With Immune Checkpoint Inhibitors. Front. Pharmacol. 12:748677. doi: 10.3389/fphar.2021.748677

INTRODUCTION

Utilizing the immune system to recognize and target malignant cells has been a strategy used in oncology for many years (Thomas and Hassan, 2012). In the past decades, a major advancement has been the use of immune checkpoint inhibitors (ICIs) to block antibodies expressed on T lymphocytes, including cytotoxic T-lymphocyte-associated protein-4 (CTLA-4) and programmed cell death protein-1 (PD-1) (Ansell et al., 2015; Wolchok et al., 2017), or their corresponding ligands expressed on tumor cells, such as programmed cell death 1 ligand-1 (PD-L1) (Herbst et al., 2016; Gulley et al., 2017; Choueiri et al., 2018). ICIs including CTLA-4 (ipilimumab), PD-1 (nivolumab or pembrolizumab), and PD-L1 (atezolizumab, avelumab, or durvalumab), either as a monotherapy or combination therapy can induce tumor responses in melanoma, non-small cell lung cancer (NSCLC), renal cell cancer (RCC), head and neck squamous cell carcinoma, urothelial cancer, breast cancer and Hodgkin disease (Ribas and Wolchok, 2018). Whilst the use of ICIs has led to improvements in cancer survival, however, the suppression of immune responses producing a range of autoimmune adverse events. The most common immune-mediated adverse events in patients receiving ICIs are fatigue, rashes, diarrhea, colitis, pulmonary and renal systems were reported (Postow et al., 2018). These agents also carry a significant risk of cardiovascular morbidity, including LVEF decline, cardiomyopathy, and HF (Voskens et al., 2013; Wang et al., 2018). Myocarditis is an infrequent but potential fatal complication of ICIs. Myocarditis with clinical presentations ranging from asymptomatic cardiac biomarker elevation to heart failure, arrhythmia, cardiac fibrosis and pericarditis (Gibson et al., 2016; Mahmood et al., 2018; Neilan et al., 2018; Altan et al., 2019). Another study found that the incidence of myocarditis is 1.14% in a cohort of cancer patients treated with ICIs (Mahmood et al., 2018). Echocardiography and electrocardiography are routinely used but they show low sensitivity for the early prediction of myocardial damage. Whilst endomyocardial biopsy has the degree of specificity and sensitivity needed for diagnosing ICI-associated myocarditis, it is considered to be too invasive and expensive for serial monitoring. Therefore, there is an unmet clinical need to find useful diagnostic tools for the early identification or accurate prediction of those who may be suffering from ICI-related myocarditis. Early identification and preemptive cardioprotective treatment can reduce interruptions or discontinuations in cancer therapy, and reduce cardiovascular burden and potentially maximize the tolerable doses of ICIs to improve cancer-related mortality. The aim of this study is to investigate the changes of the plasma levels of biomarkers in cancer survivors who were treated with ICIs with a follow-up period of 6 months. The biomarkers reflected cardiomyocyte injury [cardiac troponin I (cTnI), CK (creatine kinase), CK-MB (creatine kinase-MB)]; inflammation [high-sensitivity C-reactive protein (Hs-CRP), Pentraxin-related protein (PTX3) and growth differentiation factor 15 (GDF-15)]; neurohormonal activation [N-terminal pro–B-type natriuretic peptide (NT-pro BNP)]; heart type-fatty acid binding protein (H-FABP); and fibrosis [galectin 3 (Gal-3)]Their associations with myocardial damage, occurring either concurrently or at a subsequent visit were determined.

METHODS

Study Population

The study protocol was approved by the institutional review boards of the participating institutions. The study is registered with the Chinese Clinical Trial Registry (registration number: ChiCTR18000162216). All participants provided informed consent. A total of 19 consecutive patients who never used the ICIs and hospitalized in the Oncology Department of Tianjin Medical University Second Hospital from June 2018 to June 2019 were enrolled to the study. Eligible patients were 18–85 years of age, diagnosed with cancer and planned for adjuvant therapy with ICIs. Patients with one of the following conditions were excluded: intolerance to ICIs treatment; severe left main coronary artery disease confirmed by angiography; presence of grade III or IV heart failure; acute myocardial infarction (acute or recovery period); hepatic insufficiency (AST/ALT >80U/L); severe renal insufficiency (eGER ≤ 30 m/min/1.73 m^2); thyroid disease; acute infectious diseases; mental illness; life expectancy is less than 6 months.

At baseline (before immune-therapy) and 1month, 3 months, 6 months after ICIs administration, demographics and clinical history were recorded. Transthoracic echocardiograms were obtained at each visit, and blood samples were obtained immediately before cancer therapy infusion at 1, 3, 6-month intervals.

Echocardiography

A transthoracic echocardiographic examination was performed in all patients using the Vivid-7 system equipped with a 2.4 MHz transducer (GE Medical Systems, Milwaukee, WI, USA). Left ventricular end systolic diameter (LVEDS), left ventricular end-diastolic diameter (LVEDD) and left ventricular ejection fraction (LVEF) were obtained using Simpson's method of discs in the apical 4- and 2-chamber views as recommended by the American Society of Echocardiography. All tracings were made by a single observer and the data measurement is done by two ultrasound doctors at a centralized reading center who was blinded to all other clinical or biomarker data.

Biomarkers

At the time of the echocardiography, venous blood samples were drawn from all participants and collected in standard tubes for plasma with EDTA. Place the collected blood samples properly, it is strictly forbidden to freeze whole blood to avoid hemolysis. After the blood culture sampling is completed, it should be sent to the biological laboratory for verification by a dedicated person immediately, generally not more than 2 h hemolysis specimens centrifuged at 3,000 rpm for 15 min, plasma was removed, allocated, and frozen at −80°C until assay. Measurement of cTnI, NT-proBNP, CK, CK-MB, Hs-CRP were performed on the clinical Laboratory System. Serum levels of GDF-15, Gal-3, PTX3 and H-FABP were assayed using commercially available ELISA kit (Cusabio Biotech Corporation, China). All

TABLE1 | Baseline Characteristics of study participants.

	All participants *N* = 19
Age at start of ICI,yrs	48.2 ± 11.6
Male	8 (42.1)
Body mass index, kg/m2	21.3 ± 2.7
Fasting glucose	5.47 ± 0.77
Medical History and Risk Factors	
History of hypertension	5 (26.3)
History of diabetes	4 (21.1)
Tobacco use	
Current	2 (10.5)
Former	2 (10.5)
Alcohol intake	6 (31.6)
Hypercholesterolemia	2 (10.5)
Prior myocardial infraction	1 (5.3)
Prior coronary stenting	1 (5.3)
Prior atrial fibrillation	0 (0)
Prior COPD	0 (0)
Prior chronic kidney disease	2 (10.5)
Primary Cancer Type	
Lung cancer	3 (15.8)
Rectal cancer	1 (5.3)
Female reproductive system tumor	4 (21.1)
Bladder Cancer	1 (5.3)
Breast cancer	2 (10.5)
Renal cell carcinoma	4 (10.5)
Melanmoa	1 (5.3)
Other	3 (15.8)
Pre-ICI home CV Medications	
Beta-blockers	2 (10.5)
Aspirin	1 (5.3)
Statin	1 (5.3)
Calcium-channel blocker	3 (15.8)
ACE inhibitors or ARBs	2 (10.5)
Current monotherapy ICI	
Nivolumab (anti-PD1)	10 (52.6)
Sintilimab (anti-PD1)	2 (10.5)
Durvalumab (anti-PDL1)	7 (36.8)
ICI combined chemotherapy or radiation	
Radiation	2 (10.5)
Bevacizumab	1 (5.3)
VEGF inhibitors	3 (15.8)
Other chemotherapy	3 (15.8)
Other immune side effects during treatment	
No other immune side effects	15 (78.9)
Thyroiditis	2 (10.5)
Iritis	1 (5.3)
Colitis	1 (5.3)

Values are mean ± SD or n (%). Abbreviations: ICI = immune checkpoint inhibitors; CV = cardiovascular; ACE = Angiotensin-converting enzyme; ARBs = Angiotensin receptor blocker; COPD: chronic obstructive pulmonary diseases; anti-PD1: anti-programmed cell death protein 1; VEGF inhibitors: vascular endothelial growth factor inhibitors.

measurements were performed on previously unthawed samples. Concentrations of unknown samples are determined using a standard curve that was constructed by plotting absorbance values against concentrations of the standards.

Statistical Methods

Each biomarker was evaluated at baseline, 1 month, 3 and 6 months. The normality of the distribution of each continuous variable was tested by the Kolmogorov–Smirnov test. Continuous variables were reported as means ± SD or median (interquartile range) as appropriate. Statistical analysis was performed using the ANOVA test for continuous variables. A p value of <0.05 was regarded as statistically significant. All tests were two tailed and analyses were performed using SPSS 22.0 Statistical Package Program (SPSS Inc., Chicago, IL, United States).

RESULTS

Patients Population

The baseline characteristics of the study cohort are shown in **Table 1**. The mean age of patients (N = 19) who using ICIs was 48.2 ± 11.6 years with 42.1% being male. Prior to ICIs administration, only one patient had previous myocardial infarction and coronary stenting, but the left ventricular ejection fraction (LVEF) was >50% in all those with a baseline measurement.

Indications and Side Effects of ICIs

The most common indications for ICIs were Renal cell carcinoma, lung cancer and female reproductive system tumor. Of the monotherapy at the time of presentation, anti-PD1 was the most frequent (63.1%) in cases. For better therapeutic effect and clinical prognosis, single ICI therapy administrated with radiation or other chemotherapy is presented in **Table 1**. More than one-half (78.9%) of the cases had not experienced other ICI-related side effect.

Cardiac function and biomarkers at 1, 3, 6 months after ICI therapy compared to baseline.

There were no myocarditis cases and other clinical adverse cardiovascular events within 6 months of starting therapy. Compared to baseline, there was no change in LVEF (p = 0.608), LVEDD (p = 0.105) or LVEDS (p = 0.178) 6 months after ICI therapy. (**Figure 1**; **Table 2**).

A number of biomarkers were evaluated before and after initiation of ICI therapy at different timepoints (**Table 2**). H-FABP levels were significantly elevated at 3 months which persisted at 6 months (p = 0.031 and p = 0.013), whereas GDF-15 was significantly lower only at 6 months (p = 0.017). Gal-3 was not significantly altered whilst PTX3 was significantly reduced at 1 month (p = 0.025, **Figure 2**). By contrast, no significant changes in cTnI (p = 0.24), D-dimer (p = 0.219), CK (p = 0.059) and CK-MB (p = 0.92) were observed at 1 month, 3 and 6 months (**Figure 3**).

DISCUSSION

The main findings of this prospective cohort study are that H-FABP levels, but not other biomarkers, were increased at three months in an absence of detectable reductions in LVEF.

ICIs have shown important benefits for improved treatment of several cancers, having demonstrated high response rates and prolonged overall survival in cancer patients. In 2015, the

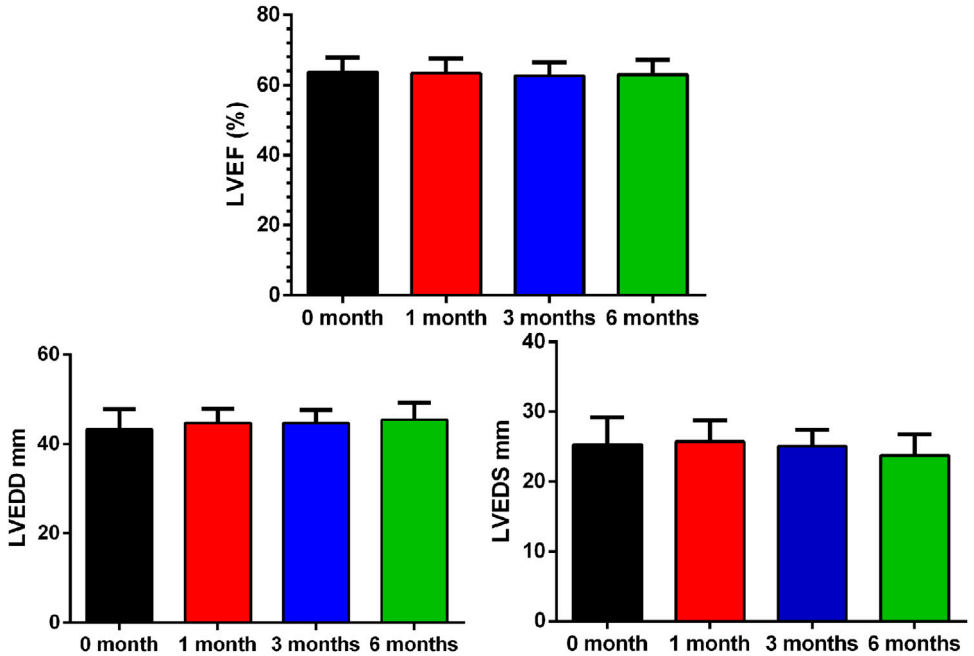

FIGURE 1 | Baseline and Interval Changes in Echocardiography. LVEF: left ventricular ejection fraction; LVEDD: left ventricular end diastolic diameter.

TABLE 2 | Baseline and Interval Changes in Echocardiography and Biomarker Levels Between Baseline and 1, 3 and 6 months.

	0 month	1 month	3 months	6 months
LVEF%	63.74 ± 4.07	63.41 ± 4.23	62.69 ± 3.79	63.00 ± 4.15
LVEDS mm	25.28 ± 3.93	25.73 ± 3.04	25.05 ± 2.37	23.76 ± 2.99
LVEDD mm	43.29 ± 4.46	44.74 ± 3.14	44.71 ± 2.98	45.43 ± 3.86
cTnI ng/ml	0.001 (0.001–0.002)	0.001 (0.001–0.0025)	0.0015 (0.001–0.002)	0.001 (0.001–0.001)
NT-proBNPng/L	82.30 (61.20–87.50)	64.00 (41.25–99.35)	79.45 (36.17–128.25)	147.00 (40.50–208.50)
D-dimer ng/ml	791.64 (478.43–2,187.79)	506.04 (430.01–1,042.59)	538.35 (303.43–925.55)	416.38 (297.23–938.05)
CK U/L	43.40 (34.70–88.90)	46.80 (37.00–87.00)	59.20 (34.52–85.12)	104.60 (50.55–177.37)
CK-MB U/L	17.16 ± 6.92	16.68 ± 5.79	18.01 ± 5.97	16.89 ± 11.42
Hs-CRP mg/L	10.08 (5.26–51.22)	7.98 (2.57–23.28)	9.28 (2.10–16.62)	3.71 (2.36–23.37)
GDF-15 pg/ml	1,075.85 ± 841.00	934.19 ± 623.22	870.14 ± 694.02	389.57 ± 199.74*
Gal-3 ng/ml	613.25 (462.99–957.24)	556.07 (428.21–759.64)	472.35 (443.52–540.28)	470.77 (439.40–536.31)
PTX3 pg/ml	398.82 ± 297.96	224.54 ± 143.58*	253.69 ± 166.15	310.02 ± 116.86
H-FABP pg/ml	529.28 ± 312.83	666.76 ± 187.87	752.33 ± 283.65*	808.00 ± 289.69*
Scr umol/l	62.42 ± 24.75	68.53 ± 21.90	65.54 ± 21.42	61.88 ± 14.63

*Abbreviations: LVEF: left ventricular ejection fraction; LVEDS: left ventricular end systolic diameter; LVEDD: left ventricular end diastolic diameter; cTnI: cardiac troponin I; NT-proBNP: N-terminal pro–B-type natriuretic peptide; CK: creatine kinase; Hs-CRP: high-sensitivity C-reactive protein; GDF-15: growth differentiation factor 15; Gal-3: galectin 3; PTX3: pentraxin-related protein 3; H-FABP: heart type-fatty acid binding protein. Values are mean ± SD or median (interquartile range); * was compared with the 0 month group, P < 0.05*

United States are almost 590,000 patients who are indicated for ICIs therapy (Andrews, 2015), and the ICIs market will experience considerable growth over the coming period (Webster, 2014). Nevertheless, the incidence of early and late adverse events associated with ICIs is unknown. ICIs are known to upregulate T-cell-mediated immune responses against cancer cells, although adverse events are a common occurrence, cardiotoxic effects are infrequent but are often associated with high mortality (Lyon et al., 2018). The immunotherapy trial data from Bristol-Myers Squibb found 18 cases (0.09%) of myocarditis among 20,594 subjects in the pharmacovigilance database. The incidence of myocarditis was higher in patients receiving a combination of nivolumab and ipilimumab (0.27%) than in those receiving nivolumab alone (0.06%) (Johnson et al., 2016). A multi-center registration study of 8 medical centers showed that the incidence of myocarditis was 1.14% (Mahmood et al., 2018). The median time from the application of ICIs to the onset of

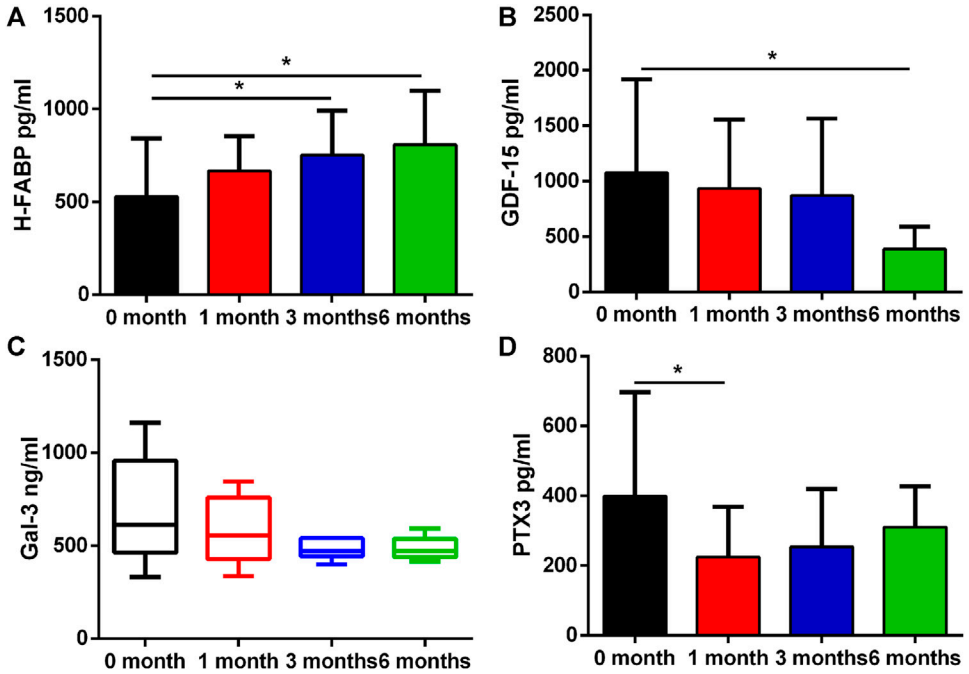

FIGURE 2 | Proteins that had differential plasma levels between baseline and 1, 3 and 6 months. Edges of boxes denote 25th and 75th percentiles, lines are median concentrations, and error bars are minimum and maximum concentrations. **(A)** NT-pro BNP: N-terminal pro–B-type natriuretic peptide; **(B)** D-dimer; **(C)** CK: creatine kinase; **(D)** CK-MB: creatine kinase-MB.

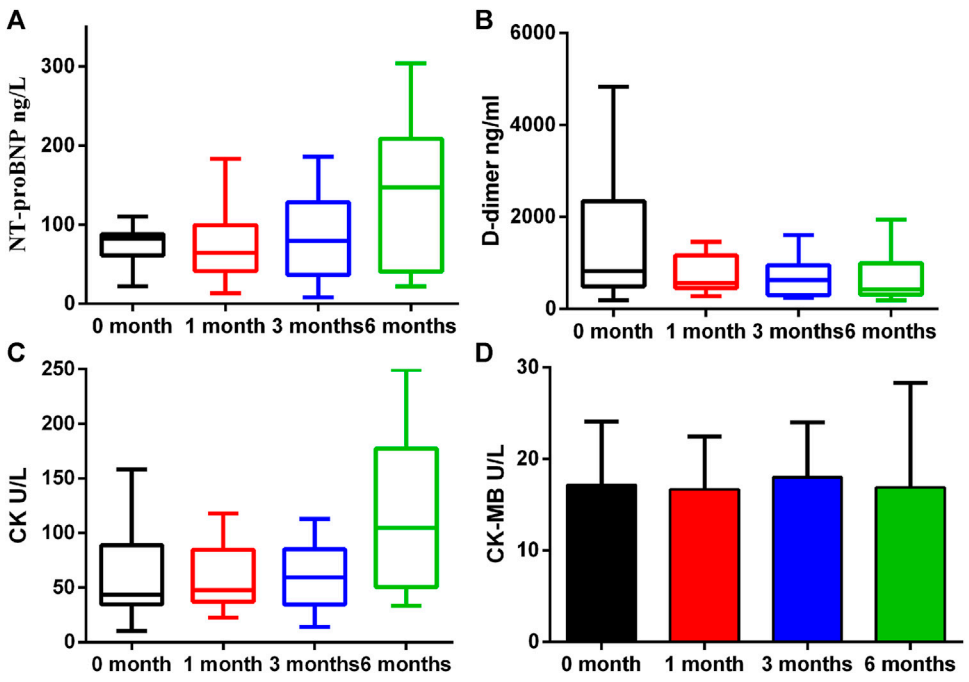

FIGURE 3 | Plasma concentration changes of H-FABP, GDF-15, Gal-3, and PTX3 over ICIs treatment time. Edges of boxes denote 25th and 75th percentiles, lines are median concentrations, and error bars are minimum and maximum concentrations. **(A)** H-FABP: heart type-fatty acid binding protein; **(B)** GDF-15: growth differentiation factor 15; **(C)** Gal-3: galectin 3; **(D)** PTX3: pentraxin-related protein 3.

myocarditis was 34 days, and the age of patients with myocarditis was 65 ± 13 years, of which 29% were women. Compared with the control group, patients with combined ICIs (34 vs. 2%) and diabetes (34 vs. 13%) had a higher incidence of myocarditis. Our results suggest that individual biomarkers may show early changes that can reflect subclinical cardiac dysfunction following use of ICIs.

Fatty acid-binding proteins (FABPs) are relatively small cytoplasmic proteins that are abundant in tissues with active fatty acid metabolism, including the heart and the skeletal muscles. In fact, heart-type FABP (H-FABP) is particularly important for cardiomyocyte energy homoeostasis, since 50–80% of the heart's energy is provided by the oxidation of fatty acids and H-FABP ensures intracellular transport of insoluble fatty acids. Following myocardial cell damage, H-FABP diffuse much more rapidly than troponins secretion into the interstitial space and appears in the circulation as early as 90 min after the onset of symptoms. Recently, H-FABP has become a newer perspective marker for the early detection of myocardial ischemia and necrosis, evaluated in the diagnostics and risk stratification of acute coronary syndromes (O'Donoghue et al., 2006; Viswanathan et al., 2010; Hai-Long et al., 2018). Experimentally, concentrations of H-FABP, as measured by the MSD immunoassay, have been found to increase in rats treated with various myotoxic compounds (Tonomura et al., 2012). ElGhandour at al. studied 40 non-Hodgkin's lymphoma patients treated with 6 cycles of cardiotoxic chemotherapy containing Doxorubicin (DOX). The authors concluded that H-FABP may serve as a reliable early predictor of cardiomyopathy induced by DOX. Our findings suggest that there is an association between H-FABP increase and subsequent myocardial dysfunction and provide evidence to support the importance of assessing changes in biomarkers over time. The utility of H-FABP appears to lie in evaluating levels after initial ICIs therapy exposure as opposed to baseline. To our knowledge, we describe for the first time an association between early changes in H-FABP levels and subsequent subclinical myocardial damage induced by treatment with ICIs. The heart-type-Fatty-Acid-Binding-Protein (H-FABP) is a protein, which is involved in intracellular myocardial transport. After myocardial necrosis H-FABP is rapidly released into the blood stream and was therefore investigated as a biomarker for acute myocardial infarction (AMI). In the study, H-FABP was detected to determine the potential utility for the early identification of cancer patients at risk for ICI-associated subclinical myocardial damage. Whilst H-FABP is a biomarker of cardiac dysfunction or damage, ICIs may cause systemic side effects that can lead to abnormal levels of this protein.

Gal-3 is a 26-kDa protein that is expressed by macrophages, plays a prominent role in tumor growth, metastasis, angiogenesis, and immune evasion and is believed to be a mediator of profibrotic pathways, stimulating cardiac fibroblasts to proliferate and deposit collagen. Gal-3 concentrations are elevated in patients with acute HF and are predictive of an increased risk of adverse outcomes (Shah et al., 2010). On the other hand, Gal-3 is highly expressed within the tumor microenvironment of aggressive cancers and whose expression correlates with poor survival particularly in patients with cancer (Vuong et al., 2019).

PTX3 is a member of the pentraxin family, the prototype of the pentraxin family is C reactive protein (CRP), a widely used clinical biomarker in human pathologies with an inflammatory or infectious origin (Lee et al., 2018). Nowadays, inflammation is considered an important determinant of cardiovascular disease and related risk factors including diabetes, hypertension (Libby, 2012). Among different inflammatory molecules, cytokines such as tumor necrosis factor (TNF)-α, interleukin (IL)-1β, and IL-6 were suggested pathophysiological players. Plasma PTX3 levels are elevated in patients with unstable angina pectoris (Inoue et al., 2007) and in patients undergoing coronary stenting (Kotooka et al., 2008). In heart failure, the plasma PTX3 level provides important prognostic information for the risk stratification of patients (Suzuki et al., 2008). GDF-15 is a member of the TGF-β cytokine superfamily that is produced in response to oxidative stress, inflammation, and injury (Wollert et al., 2007) and is an emerging marker in acute coronary syndromes and HF. The mechanisms of ICIs associated cardiotoxicity is unknown, and we found no significant association between either GDF-15 or PTX3 and ICI-associated subclinical myocardial damage. Irena et al. (Kaplanov et al., 2019) indicated that the particular importance to tumor-mediated inflammation is IL-1β, IL-1β is increased in most cancers, including breast cancer in advanced stages, where it is mainly expressed by cells in the microenvironment and enhances progression and metastasis. The reduction of inflammatory markers, such as GDF-15 and PTX3, in this study may be linked to increased survival and response to immune therapy. Further studies should explore the relationship between different biomarkers and outcomes after immune therapy.

Study Limitation

There are several limitations of this study. Firstly, a relatively small number of patients was enrolled. Further studies in a larger number of patients will be needed to define the potential role of new circulating biomarkers in the assessment of ICIs-induced subclinical myocardial injury. Secondly, follow-up was relative short at 6 months. Thirdly, myocarditis is more prevalent in patients with combined use of CTLA-4 and PD-1/PD-L1, but CTLA-4 has not yet been marketed in the Mainland and was therefore not included in this study. Lastly, the application of imaging such as cardiac magnetic resonance imaging (CMR) or speckle-tracking echocardiography would be able to quantify the degree and location of cardiac dysfunction more precisely. had been resonated, the accuracy of the diagnosis could be improved. For example, speckle tracking imaging is recommended by ESC for detecting subclinical cardiac damage. It can be used in combination with measurements of H-FABP levels for further patient monitoring and risk stratification.

CONCLUSION

H-FABP, but not other biomarkers, were increased in patients underwent ICIs therapy. H-FABP might be a more sensitive biomarker to detect ICI-related subclinical myocardial damage than traditional cardiac biomarkers.

DATA AVAILABILITY STATEMENT

The raw data supporting the conclusion of this article will be made available by the authors, without undue reservation, to any qualified researcher.

ETHICS STATEMENT

The studies involving human participants were reviewed and approved by The Ethic Committee of Second Hospital of Tianjin Medical University. The patients/participants provided their written informed consent to participate in this study.

AUTHOR CONTRIBUTIONS

Concept—TL, HW; Design—TL, HW, MY; Supervision—TL, GL; Fundings—TL; Materials—TL, MY; Data collection and/or processing—MY, LZ, AX, QL, BH, JW, HF; Analysis and/or interpretation—MY, MG; Literature search—MY, LZ, HW, TL; Writing—MY; Critical review—GT, LR, GL, TL.

FUNDING

This study was supported by grants from the National Natural Science Foundation of China (81970270, 81570298 to TL).

REFERENCES

Altan, M., Toki, M. I., Gettinger, S. N., Carvajal-Hausdorf, D. E., Zugazagoitia, J., Sinard, J. H., et al. (2019). Immune Checkpoint Inhibitor-Associated Pericarditis. *J. Thorac. Oncol.* 14 (6), 1102–1108. doi:10.1016/j.jtho.2019.02.026

Andrews, A. (2015). Treating with Checkpoint Inhibitors-Figure $1 Million Per Patient. *Am. Health Drug Benefits* 8 (Spec Issue), 9.

Ansell, S. M., Lesokhin, A. M., Borrello, I., Halwani, A., Scott, E. C., Gutierrez, M., et al. (2015). PD-1 Blockade with Nivolumab in Relapsed or Refractory Hodgkin's Lymphoma. *N. Engl. J. Med.* 372 (4), 311–319. doi:10.1056/NEJMoa1411087

Choueiri, T. K., Larkin, J., Oya, M., Thistlethwaite, F., Martignoni, M., Nathan, P., et al. (2018). Preliminary Results for Avelumab Plus Axitinib as First-Line Therapy in Patients with Advanced clear-cell Renal-Cell Carcinoma (JAVELIN Renal 100): an Open-Label, Dose-Finding and Dose-Expansion, Phase 1b Trial. *Lancet Oncol.* 19 (4), 451–460. doi:10.1016/s1470-2045(18)30107-4

Gibson, R., Delaune, J., Szady, A., and Markham, M. (2016). Suspected Autoimmune Myocarditis and Cardiac Conduction Abnormalities with Nivolumab Therapy for Non-small Cell Lung Cancer. *BMJ Case Rep.* 2016, bcr2016216228. doi:10.1136/bcr-2016-216228

Gulley, J. L., Rajan, A., Spigel, D. R., Iannotti, N., Chandler, J., Wong, D. J. L., et al. (2017). Avelumab for Patients with Previously Treated Metastatic or Recurrent Non-small-cell Lung Cancer (JAVELIN Solid Tumor): Dose-Expansion Cohort of a Multicentre, Open-Label, Phase 1b Trial. *Lancet Oncol.* 18 (5), 599–610. doi:10.1016/s1470-2045(17)30240-1

Hai-Long, W., Xiao-Hua, P., and Jian-Jun, Y. (2018). The Prognostic Value of Heart-type Fatty Acid Binding Protein in Patients with Acute Coronary Syndrome. *J. Coll. Physicians Surg. Pak* 28 (1), 56–60. doi:10.29271/jcpsp.2018.01.56

Herbst, R. S., Baas, P., Kim, D. W., Felip, E., Pérez-Gracia, J. L., Han, J. Y., et al. (2016). Pembrolizumab versus Docetaxel for Previously Treated, PD-L1-Positive, Advanced Non-small-cell Lung Cancer (KEYNOTE-010): a Randomised Controlled Trial. *Lancet* 387 (10027), 1540–1550. doi:10.1016/s0140-6736(15)01281-7

Inoue, K., Sugiyama, A., Reid, P. C., Ito, Y., Miyauchi, K., Mukai, S., et al. (2007). Establishment of a High Sensitivity Plasma Assay for Human Pentraxin3 as a Marker for Unstable Angina Pectoris. *Arterioscler Thromb. Vasc. Biol.* 27 (1), 161–167. doi:10.1161/01.ATV.0000252126.48375.d5

Johnson, D. B., Balko, J. M., Compton, M. L., Chalkias, S., Gorham, J., Xu, Y., et al. (2016). Fulminant Myocarditis with Combination Immune Checkpoint Blockade. *N. Engl. J. Med.* 375 (18), 1749–1755. doi:10.1056/NEJMoa1609214

Kaplanov, I., Carmi, Y., Kornetsky, R., Shemesh, A., Shurin, G. V., Shurin, M. R., et al. (2019). Blocking IL-1β Reverses the Immunosuppression in Mouse Breast Cancer and Synergizes with Anti-PD-1 for Tumor Abrogation. *Proc. Natl. Acad. Sci. U S A.* 116 (4), 1361–1369. doi:10.1073/pnas.1812266115

Kotooka, N., Inoue, T., Fujimatsu, D., Morooka, T., Hashimoto, S., Hikichi, Y., et al. (2008). Pentraxin3 Is a Novel Marker for Stent-Induced Inflammation and Neointimal Thickening. *Atherosclerosis* 197 (1), 368–374. doi:10.1016/j.atherosclerosis.2007.05.031

Lee, Y. T., Gong, M., Chau, A., Wong, W. T., Bazoukis, G., Wong, S. H., et al. (2018). Pentraxin-3 as a Marker of Sepsis Severity and Predictor of Mortality Outcomes: A Systematic Review and Meta-Analysis. *J. Infect.* 76 (1), 1–10. doi:10.1016/j.jinf.2017.10.016

Libby, P. (2012). Inflammation in Atherosclerosis. *Arterioscler Thromb. Vasc. Biol.* 32 (9), 2045–2051. doi:10.1161/atvbaha.108.179705

Lyon, A. R., Yousaf, N., Battisti, N. M. L., Moslehi, J., and Larkin, J. (2018). Immune Checkpoint Inhibitors and Cardiovascular Toxicity. *Lancet Oncol.* 19 (9), e447–e458. doi:10.1016/s1470-2045(18)30457-1

Mahmood, S. S., Fradley, M. G., Cohen, J. V., Nohria, A., Reynolds, K. L., Heinzerling, L. M., et al. (2018). Myocarditis in Patients Treated with Immune Checkpoint Inhibitors. *J. Am. Coll. Cardiol.* 71 (16), 1755–1764. doi:10.1016/j.jacc.2018.02.037

Neilan, T. G., Rothenberg, M. L., Amiri-Kordestani, L., Sullivan, R. J., Steingart, R. M., Gregory, W., et al. (2018). Myocarditis Associated with Immune Checkpoint Inhibitors: An Expert Consensus on Data Gaps and a Call to Action. *Oncologist* 23 (8), 874–878. doi:10.1634/theoncologist.2018-0157

O'Donoghue, M., de Lemos, J. A., Morrow, D. A., Murphy, S. A., Buros, J. L., Cannon, C. P., et al. (2006). Prognostic Utility of Heart-type Fatty Acid Binding Protein in Patients with Acute Coronary Syndromes. *Circulation* 114 (6), 550–557. doi:10.1161/circulationaha.106.641936

Postow, M. A., Sidlow, R., and Hellmann, M. D. (2018). Immune-Related Adverse Events Associated with Immune Checkpoint Blockade. *N. Engl. J. Med.* 378 (2), 158–168. doi:10.1056/NEJMra1703481

Ribas, A., and Wolchok, J. D. (2018). Cancer Immunotherapy Using Checkpoint Blockade. *Science* 359 (6382), 1350–1355. doi:10.1126/science.aar4060

Shah, R. V., Chen-Tournoux, A. A., Picard, M. H., van Kimmenade, R. R., and Januzzi, J. L. (2010). Galectin-3, Cardiac Structure and Function, and Long-Term Mortality in Patients with Acutely Decompensated Heart Failure. *Eur. J. Heart Fail.* 12 (8), 826–832. doi:10.1093/eurjhf/hfq091

Suzuki, S., Takeishi, Y., Niizeki, T., Koyama, Y., Kitahara, T., Sasaki, T., et al. (2008). Pentraxin 3, a New Marker for Vascular Inflammation, Predicts Adverse Clinical Outcomes in Patients with Heart Failure. *Am. Heart J.* 155 (1), 75–81. doi:10.1016/j.ahj.2007.08.013

Thomas, A., and Hassan, R. (2012). Immunotherapies for Non-small-cell Lung Cancer and Mesothelioma. *Lancet Oncol.* 13 (7), e301–10. doi:10.1016/s1470-2045(12)70126-2

Tonomura, Y., Matsushima, S., Kashiwagi, E., Fujisawa, K., Takagi, S., Nishimura, Y., et al. (2012). Biomarker Panel of Cardiac and Skeletal Muscle Troponins, Fatty Acid Binding Protein 3 and Myosin Light Chain 3 for the Accurate Diagnosis of Cardiotoxicity and Musculoskeletal Toxicity in Rats. *Toxicology* 302 (2-3), 179–189. doi:10.1016/j.tox.2012.07.012

Viswanathan, K., Kilcullen, N., Morrell, C., Thistlethwaite, S. J., Sivananthan, M. U., Hassan, T. B., et al. (2010). Heart-type Fatty Acid-Binding Protein Predicts Long-Term Mortality and Re-infarction in Consecutive Patients with Suspected Acute Coronary Syndrome Who Are Troponin-Negative. *J. Am. Coll. Cardiol.* 55 (23), 2590–2598. doi:10.1016/j.jacc.2009.12.062

Voskens, C. J., Goldinger, S. M., Loquai, C., Robert, C., Kaehler, K. C., Berking, C., et al. (2013). The price of Tumor Control: an Analysis of Rare Side Effects of Anti-CTLA-4 Therapy in Metastatic Melanoma from the Ipilimumab Network. *PLoS One* 8 (1), e53745. doi:10.1371/journal.pone.0053745

Vuong, L., Kouverianou, E., Rooney, C. M., McHugh, B. J., Howie, S. E. M., Gregory, C. D., et al. (2019). An Orally Active Galectin-3 Antagonist Inhibits Lung Adenocarcinoma Growth and Augments Response to PD-L1 Blockade. *Cancer Res.* 79 (7), 1480–1492. doi:10.1158/0008-5472.CAN-18-2244

Wang, D. Y., Salem, J. E., Cohen, J. V., Chandra, S., Menzer, C., Ye, F., et al. (2018). Fatal Toxic Effects Associated with Immune Checkpoint Inhibitors: A Systematic Review and Meta-Analysis. *JAMA Oncol.* 4 (12), 1721–1728. doi:10.1001/jamaoncol.2018.3923

Webster, R. M. (2014). The Immune Checkpoint Inhibitors: where Are We Now. *Nat. Rev. Drug Discov.* 13 (12), 883–884. doi:10.1038/nrd4476

Wolchok, J. D., Chiarion-Sileni, V., Gonzalez, R., Rutkowski, P., Grob, J. J., Cowey, C. L., et al. (2017). Overall Survival with Combined Nivolumab and Ipilimumab in Advanced Melanoma. *N. Engl. J. Med.* 377 (14), 1345–1356. doi:10.1056/NEJMoa1709684

Wollert, K. C., Kempf, T., Lagerqvist, B., Lindahl, B., Olofsson, S., Allhoff, T., et al. (2007). Growth Differentiation Factor 15 for Risk Stratification and Selection of an Invasive Treatment Strategy in Non ST-Elevation Acute Coronary Syndrome. *Circulation* 116 (14), 1540–1548. doi:10.1161/circulationaha.107.697714

Conflict of Interest: The authors declare that the research was conducted in the absence of any commercial or financial relationships that could be construed as a potential conflict of interest.

Publisher's Note: All claims expressed in this article are solely those of the authors and do not necessarily represent those of their affiliated organizations, or those of the publisher, the editors and the reviewers. Any product that may be evaluated in this article, or claim that may be made by its manufacturer, is not guaranteed or endorsed by the publisher.

frontiers in Pharmacology

ORIGINAL RESEARCH
published: 15 October 2021
doi: 10.3389/fphar.2021.733805

Schisandrin B Antagonizes Cardiotoxicity Induced by Pirarubicin by Inhibiting Mitochondrial Permeability Transition Pore (mPTP) Opening and Decreasing Cardiomyocyte Apoptosis

Hongwei Shi[1,2†], Heng Tang[3†], Wen Ai[4], Qingfu Zeng[5], Hong Yang[6], Fengqing Zhu[3], Yunjie Wei[7], Rui Feng[3], Li Wen[3], Peng Pu[3] and Quan He[3]**

[1]Department of Radiation Oncology, Hubei Cancer Hospital, Tongji Medical College, Huazhong University of Science and Technology, Wuhan, China, [2]Department of Oncology, Renmin Hospital of Wuhan University, Wuhan, China, [3]Department of Cardiology, The First Affiliated Hospital of Chongqing Medical University, Chongqing, China, [4]Shenzhen Nanshan District People's Hospital, Shenzhen, China, [5]Department of Vascular Surgery, The Second Affiliated Hospital of Nanchang University, Nanchang, China, [6]Department of Endocrine, The First Affiliated Hospital of Chongqing Medical University, Chongqing, China, [7]Department of Cardiology, Hubei Shiyan Taihe Hospital, Shiyan, China

Objective: Pirarubicin (THP), one of the anthracycline anticancer drugs, is widely used in the treatment of various cancers, but its cardiotoxicity cannot be ignored. Schisandrin B (SchB) has the ability to upregulate cellular antioxidant defense mechanism and promote mitochondrial function and antioxidant status. However, it has not been reported whether it can resist THP-induced cardiotoxicity. The aim of this study was to investigate the effect of SchB on THP cardiotoxicity and its mechanism.

Methods: The rat model of cardiotoxicity induced by THP was established, and SchB treatment was performed at the same time. The changes of ECG, cardiac coefficient, and echocardiogram were observed. The changes of myocardial tissue morphology were observed by H&E staining. Apoptosis was detected by TUNEL. The levels of LDH, BNP, CK-MB, cTnT, SOD, and MDA in serum were measured to observe the heart damage and oxidative stress state of rats. The expression of cleaved-caspase 9, pro/cleaved-caspase 3, Bcl-2/Bax, and cytosol and mitochondrial Cyt C and Bax was evaluated by western blot. H9c2 cardiomyocytes were cocultured with THP, SchB, and mPTP inhibitor CsA to detect the production of ROS and verify the above signaling pathways. The opening of mPTP and mitochondrial swelling were detected by mPTP kit and purified mitochondrial swelling kit.

Results: After 8 weeks, a series of cardiotoxicity manifestations were observed in THP rats. These adverse effects can be effectively alleviated by SchB treatment. Further studies showed that SchB had strong antioxidant and antiapoptotic abilities in THP cardiotoxicity.

OPEN ACCESS

Edited by:
Zhi-Ren Zhang,
Harbin Medical University, China

Reviewed by:
Jian Yang,
The First People's Hospital of Yichang, China
Ming He,
Nanchang University, China

***Correspondence:**
Peng Pu
pp841103@sina.com
Quan He
1355956791@sina.com

[†]These authors have contributed equally to this work

Specialty section:
This article was submitted to Cardiovascular and Smooth Muscle Pharmacology, a section of the journal Frontiers in Pharmacology

Received: 30 June 2021
Accepted: 30 August 2021
Published: 15 October 2021

Citation:
Shi H, Tang H, Ai W, Zeng Q, Yang H, Zhu F, Wei Y, Feng R, Wen L, Pu P and He Q (2021) Schisandrin B Antagonizes Cardiotoxicity Induced by Pirarubicin by Inhibiting Mitochondrial Permeability Transition Pore (mPTP) Opening and Decreasing Cardiomyocyte Apoptosis. Front. Pharmacol. 12:733805. doi: 10.3389/fphar.2021.733805

Conclusion: SchB has an obvious protective effect on THP-induced cardiotoxicity. The mechanism may be closely related to the protection of mitochondrial function, inhibition of mPTP opening, and alleviation of oxidative stress and apoptosis of cardiomyocytes.

Keywords: antiapoptotic, cardiotoxicity, schisandrin B, pirarubicin (THP), MPTP

INTRODUCTION

Pirarubicin (THP) is an anthracycline anticancer drug that has been widely used clinically. It has a broad antitumor spectrum and high clinical efficacy (Greish et al., 2005). However, it is also dose-dependent and exhibits cumulative cardiotoxicity (Von Hoff et al., 1979; Octavia et al., 2012). The clinical symptoms, such as arrhythmia and cardiac dysfunction, appear during the early treatment stages (Carvalho et al., 2014). Long-term anthracycline use has caused dose-dependent congestive heart failure and irreversible heart damage, which limits its clinical application (Casparini, 2006). Studies have shown that reactive oxygen species (ROS) and lipid peroxidation-induced oxidative stress and cardiomyocyte apoptosis play a leading role in THP-induced cardiotoxicity (Koh et al., 2002; Wang et al., 2017). Therefore, improving or alleviating oxidative stress injury and cardiomyocyte apoptosis might help to prevent and treat THP cardiotoxicity.

Schisandrin B has the ability to upregulate the cellular antioxidant defense mechanism and to promote mitochondrial function and antioxidant status, thus exhibiting a wide range of protective effects in many tissues in the body (Kim et al., 2004; Lam and Ko, 2012). Recent studies have found that long-term low-dose SchB treatment increases the function and antioxidant capacity of mitochondria in brain, heart, liver, and skeletal muscle of young and old rats (Chen and Ko, 2010; Lam and Ko, 2012). Based on the above results, we speculated that SchB might contribute to improving THP-induced cardiotoxicity. However, this hypothesis has not been confirmed *in vivo* or *in vitro*.

The present study investigated the antioxidant and antiapoptotic effects of SchB and explored their key pathways in THP-induced cardiotoxicity.

MATERIALS AND METHODS

Materials

Pirarubicin and schisandrin B, purity ≥98%, were obtained from Shanghai Aladdin Reagent Co., Ltd. (Shanghai, China). Mitochondrial permeability transition pore (mPTP) inhibitor cyclosporin A (CsA) was purchased from MCE company. Brain natriuretic peptide (BNP), creatine kinase MB (CK-MB), and cardiac troponin T (cTnT) test kits were all purchased from Jiangsu enzyme label Biotechnology Co., Ltd. (Jiangsu, China). Malondialdehyde (MDA), superoxide dismutase (SOD), and lactate dehydrogenase (LDH) test kits were obtained from Nanjing Jian Cheng Biological Engineering Research Institute (Nanjing, China). The antibody of cleaved-caspase 9, pro/cleaved-caspase 3, Bcl-2/Bax, Cyt C, and COX IV were obtained from Cell Signaling Technology. All chemicals and reagents were of analytical grade.

Animal Experiments

Animal Model

This study was performed according to the Guide for the Care and Use of Laboratory Animals and approved by the Animal Ethics Committee of the First Affiliated Hospital of Chongqing Medical University (CMU). 40 male SD rats (180–200 g) were obtained from the CMU experimental animal center. Rats were randomly distributed equally into four groups (n = 10 in each group): CON group (normal-diet-fed rats, equal volume of normal saline was injected into caudal vein), SchB group (SchB-diet-fed rats, 50 $mg.kg^{-1}$, equal volume of normal saline was injected into caudal vein), THP group [normal-diet-fed rats; THP (3 $mg.kg^{-1}$) was injected *via* caudal vein once a week], and THP + SchB group [SchB-diet-fed rats, 50 $mg.kg^{-1}$; THP (3 $mg.kg^{-1}$) was injected *via* caudal vein once a week]. Similar dietary feeding methods have also been published in our previous studies (Tang et al., 2021a; Tang et al., 2021b). The CON and THP group were fed with AIN-76A diet. AIN-76A diet contains approximately 5.2% fat (% by weight, approx. all from corn oil). SchB diet in the SchB group and SchB + THP group contains approximately 0.5‰ SchB in AIN-76A feed. After conversion, 0.5‰ SchB in diet = 50 mg/kg in rats. AIN-76A feed and the processing of SchB feed were performed by Jiangsu synergy pharmaceutical Bioengineering Co., Ltd.

The food consumption and body weight were measured twice a week.

Electrocardiogram and Doppler Echocardiography

The experiment ended at week 8. Rats were anesthetized with inhaled isoflurane (2%, maintenance dose was also 2%). Needle electrodes were inserted subcutaneously into the right upper limb, right lower limb, and left lower limb, respectively. The lead IV ECG was recorded by BL-420F biological function measurement system (Chengdu Taimeng Science and Technique Company). The R wave, S wave, T wave, and QT interval of rat ECG were measured on the system. The hair of the precordial region was removed, and the Doppler echocardiography was measured by Vivid E95 ultrasonic diagnostic apparatus with L8-18i-D probe (General Electric Company). When testing, the probe frequency was 18 MHz and the depth was 1.5 cm. EF, FS, LVIDd, and LVIDs in rat echocardiography were measured in the system. All operations were performed by professional ECG or echocardiography technicians, and the test results were checked by two or more cardiologists.

Sample Collection, Preparation, and Biochemical Indices

After fasting overnight, the rats were weighed and sacrificed under anesthesia. Blood samples were collected from abdominal aorta and centrifuged at 3,000 rpm for 30 min within 8 h. The supernatant was stored in a refrigerator at

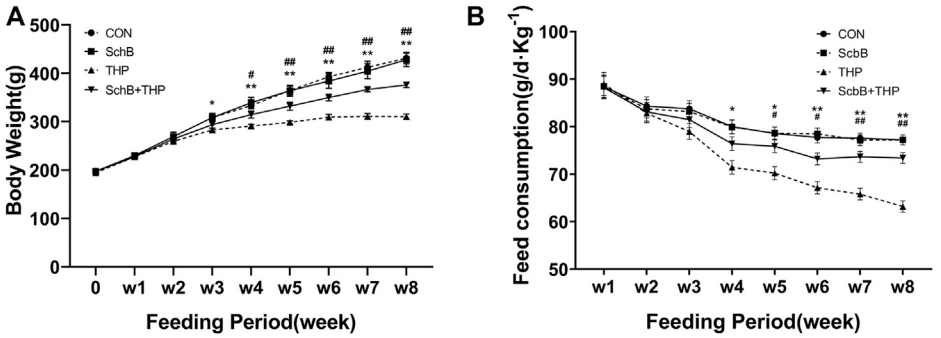

FIGURE 1 | SchB effectively improved the abnormal body weight and food intake of SD rats induced by THP. **(A)** From the third week, the body weight of rats injected with THP alone was significantly lower than that of normal rats (THP vs. CON, $p < 0.05$). The weight loss of THP rats was further reduced after 4 weeks ($p < 0.01$, THP vs. CON). In THP rats treated with SchB (50 mg*kg^{-1}), weight loss was significantly improved ($p < 0.05$, SchB + THP vs. THP). The improvement was more significant after the fifth week ($p < 0.01$, SchB + THP vs. THP). **(B)** From the fourth week, the food intake of rats injected with THP alone was significantly lower than that of normal rats (THP group vs. CON group, $p < 0.05$). The food intake of THP rats decreased further after 6 weeks ($p < 0.01$, THP and CON). In THP rats treated with SchB (50 mg*kg^{-1}), the food intake increased significantly ($p < 0.05$, SchB + THP vs. THP). The improvement was more significant after the seventh week ($p < 0.01$, SchB + THP vs. THP). All values are mean ± SD. $^{*}p < 0.05$ vs. CON, $^{**}p < 0.01$ vs. CON; $^{\#}p < 0.05$ vs. THP, and $^{\#\#}p < 0.01$ vs. THP.

−80°C. The serum LDH, BNP, CK-MB, cTnT, SOD, and MDA were measured as soon as possible according to the operation procedure of the kit. Heart samples were excised and weighed. The remaining heart tissue was stored in the −80°C refrigerator.

Histopathological Examination

The left ventricular free wall myocardial tissue was fixed with 4% paraformaldehyde solution, embedded in paraffin, and cut into 5 μm thick sections. Then, HE staining and TUNEL staining were performed according to the kit instructions to observe the tissue changes. TUNEL apoptosis detection kit (green fluorescence) was purchased from Beyotime Biological Reagent Co., Ltd (Jiangsu, China). The paraffin section was dewaxed in xylene, dehydrated with absolute alcohol, washed with distilled water, and then added 20 μg/ml proteinase K without DNase (37°C for 30 min) and then washed with PBS for 3 times. 50 μL TUNEL solution was added to the target area and incubated at 37°C for 60 min. After washing with PBS for 3 times, the antifluorescence quenching sealing solution was used to seal the plates, which were observed with Nikon eclipse 80i microscope (Nikon, Chiyoda, Japan). Apoptosis level = apoptotic cells/total cells × 100%.

Cell Experiments

CCK-8 Was Used to Determine the Optimal Concentration of SchB and the Coculture Effect of SchB and CsA

We used the CCK-8 cell activity test kit to explore the optimal concentration of SchB on cells and whether the coculture of SchB and CsA had additional effects. H9C2 cardiomyocytes were treated with 5 μM THP to establish the cell injury model. The concentration of SchB treatment was divided into 25 μM, 50 μM, 100 μM, and 200 μM to coculture with 5 μM THP to detect cell viability. 200 μM SchB was cultured alone to detect whether SchB had independent effects. In addition, the optimal concentration of SchB obtained was cocultured with 10 μm CsA to determine whether there was additional effect.

Cell Culture and Treatment

H9C2 cardiomyoblasts were purchased from the cell bank of Chinese Academy of Sciences and cultured in Dulbecco's modified eagle's high glucose medium (Gibco, China) and supplemented with 10% fetal bovine serum (Pan, Germany). The cell cultures were cultured in 5% CO_2 incubator at 37°C. H9C2 cardiomyocytes were divided into six groups: normal group (CON), SchB group (SchB, 50 μm, 24 h), THP group (THP, 5 μm, 22 h), THP and SchB coculture group (SchB, 50 μm, 24 h + THP, 5 μm, 22 h), CsA group (CsA, 10 μm, 22 h), and THP and CsA coculture group (CsA, 10 μm, 24 h + THP, 5 μm, 22 h). In the SchB + THP and CsA + THP group, the cells were preincubated with SchB (50 μm) or CsA (10 μm) for 2 h and then cocultured with THP (5 μm) for 22 h.

ROS and Mitochondrial Permeability Transition Pore Staining in H9C2 Cells

H9C2 cardiomyocytes were seeded into 24-well plates and treated according to the cell treatment scheme mentioned above. When the cell growth reached 70–80%, the staining was carried out according to the instructions of ROS staining and mPTP staining kit. The fluorescent dye of ROS was DCFH-DA, and the fluorescent dye of mPTP was Calcein AM, which was observed with Nikon eclipse 80i microscope (Nikon, Chiyoda, Japan). The two fluorescent dyes were purchased from Beyotime Biological Reagent Co., Ltd. (Jiangsu, China). The positive area was counted by ImageJ software (ImageJ 1.51J8).

Swelling Experiment of Purified Mitochondria *In Vitro*

The cells were cultured according to the above cell grouping. When the cells grow to 70–80%, the mitochondria of each group of cells are extracted according to the instructions of cell mitochondrial extraction kit (Beyotime Institute of Biotechnology). Then, the swelling degree of mitochondria in each group was detected according to the instructions of the purified mitochondrial swelling photometric determination kit (Shanghai haling Biotechnology Co., Ltd.).

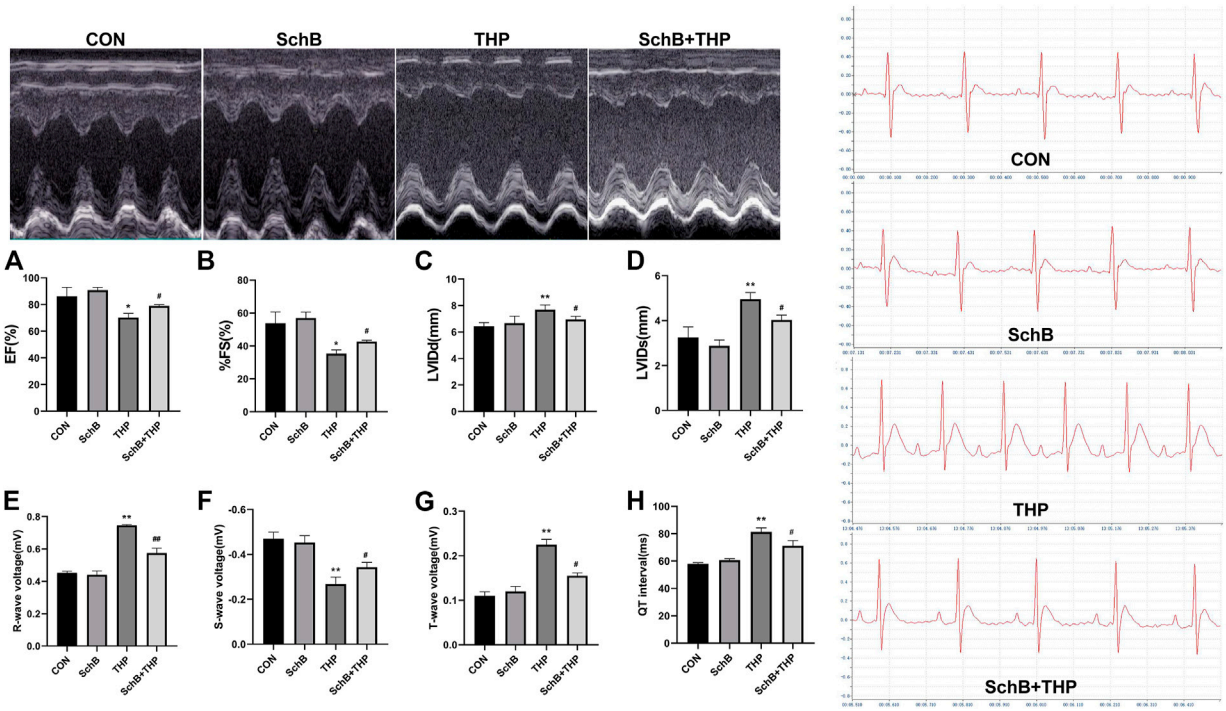

FIGURE 2 | SchB effectively improved the echocardiographic and ECG changes of SD rats induced by THP. Compared with normal rats, EF **(A)** and % FS **(B)** decreased and LVIDd **(C)** and LVIDs **(D)** thickened (THP vs. CON). Compared with normal SD rats, the ECG of THP rats was also abnormal (THP vs CON). The R wave **(E)** and T wave **(G)** voltage increased; S wave voltage decreased **(F)**; and QT interval **(H)** prolonged (THP vs. CON). After treatment with SchB (50 mg*kg^{-1}), the above changes were significantly improved (SchB + THP vs. THP). All values are mean ± SD. $^{*}p < 0.05$ vs. CON, $^{**}p < 0.01$ vs. CON, $^{\#}p < 0.05$ vs. THP, and $^{\#\#}p < 0.01$ vs. THP.

Western Blotting

Mitochondrial and cytoplasmic proteins were extracted from cells and heart tissues according to the cell and tissue mitochondrial separation kit. The protein concentration in supernatant was determined by BCA kit. About 20–40 μg heart tissue or cell lysate was used for twelve alkyl sulfate polyacrylamide gel electrophoresis and then transferred to the FL membrane (microporous). The expression level of specific protein was standardized as GAPDH or COX IV.

Statistical Analysis

Data were presented as mean ± SD. The significance of differences between groups was analyzed statistically using a one or two-way analysis of variance (ANOVA), followed by a Tukey's multiple-comparison post hoc test. Differences were considered significant at $p < 0.05$.

RESULTS

SchB Effectively Improved the THP-Induced Decrease of Body Weight and Food Intake in SD Rats

From the third and fourth week, the body weight (**Figure 1A**, $p < 0.05$) and food intake (**Figure 1B**, $p < 0.05$) of rats in the THP injection group decreased, and the difference was more significant at the fifth and sixth week ($p < 0.01$). After treatment with SchB, the above changes were significantly improved.

SchB Effectively Improved the Changes of ECG and Echocardiography Induced by THP in Rats

After 8 weeks, a series of ECG and echocardiogram (**Figure 2**) changes were observed in SD rats injected with THP alone, such as EF (**Figure 2A**) and FS (**Figure 2B**) decreased, LVIDd (**Figure 2C**) and LVIDs (**Figure 2D**) increased, R wave (**Figure 2E**) and T wave (**Figure 2F**) increased, S wave (**Figure 2G**) decreased, and QT interval (**Figure 2H**) prolonged. After SchB treatment, the above changes were significantly improved (**Figures 2A–H**, $p > 0.05$).

SchB Improves Myocardial Tissue and Cardiac Index Changes Induced by THP in Rats

As shown by H&E staining in **Figure 3**, compared with the CON group, the arrangement of cardiomyocytes in the THP injection group was disordered, the intercellular space was enlarged, and the cardiomyocytes were focal vacuolization or steatosis. However, after treatment with SchB, the histological changes of heart were mild.

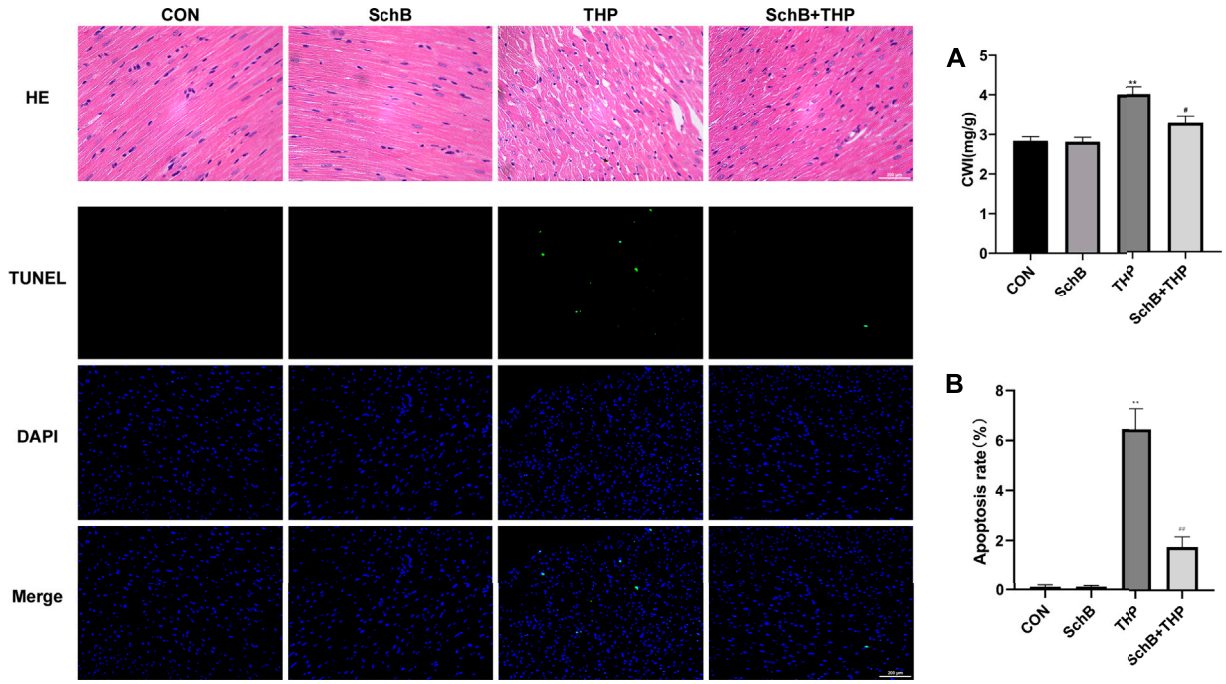

FIGURE 3 | SchB attenuated THP-induced cardiac histopathological changes, apoptosis, and increased CWI. The myocardial tissue structure of the CON and SchB group was normal. In the THP group, the arrangement of cardiomyocytes was disordered, the intercellular space was significantly increased, and the cardiomyocytes were focal vacuolization or steatosis. The vacuolation and steatosis of myocardial cells in rats treated with SchB were significantly improved. TUNEL staining showed that there was no apoptosis in the control group and SchB group. In the THP group, there was partial apoptosis. In the group of SchB + THP, a few or a single cell apoptosis was occasionally observed. The CWI of rats in the THP group was significantly higher than that in the normal group, and the CWI of rats in the SchB + THP group was significantly lower than that in the THP group. All values are the mean ± SD. $^{*}p < 0.05$ vs. CON, $^{**}p < 0.01$ vs. CON, $^{\#}p < 0.05$ vs. THP, and $^{\#\#}p < 0.01$ vs. THP.

The cardiac weight index (CWI) of THP (**Figure 3A**) group was also higher than that of the CON group, and the above changes were relieved after SchB treatment.

TUNEL staining (**Figure 3**) showed that there was no cardiomyocyte apoptosis in the CON and SchB groups, but partial cardiomyocyte apoptosis in the THP injection group. Apoptosis of cardiomyocytes was occasionally observed after treatment with SchB. Quantitative analysis can be found in **Figure 3B**.

SchB Alleviated the Changes of Blood Biochemical Indexes Induced by THP in Rats

In the blood, THP caused a decrease in SOD (**Figure 4A**) and an increase in MDA (**Figure 4B**), LDH (**Figure 4C**), CK-MB (**Figure 4D**), cTnT (**Figure 4E**), and BNP (**Figure 4F**). However, SchB treatment effectively improved these changes (**Figures 4A–F**, $p > 0.05$).

The Effect of SchB and THP on the Expression of Apoptosis-Related Proteins *In Vivo*

After 8 weeks of THP injection, the content of Cyt C (**Figure 5A**) decreased and Bax (**Figure 5B**) increased in mitochondria. In addition, the expression of procaspase 3 decreased, the expression of cleaved-caspase 3/9 and Cyt C increased, and the ratio of Bcl-2/Bax decreased (**Figure 5C**) in cytoplasm.

SchB treatment effectively alleviated the above changes. More evidence can be found in the semiquantitative analysis (**Figures 5A–C**).

The Optimum Concentration of SchB and the Coculture Effect of SchB and CsA

As shown in **Figure 6A**, under the condition of THP-induced cell injury, we detected the effects of four concentrations of SchB on cell activity. The results showed that THP significantly decreased cell activity. Although the cell activity of 25 μM SchB-treated cells increased slightly, there was no difference compared with the THP group. Three concentrations (50, 75, and 100 μM) of SchB treatment of cardiomyocytes significantly improved the decreased cell activity, but there is no difference among the three groups. The cells treated with the maximum concentration of 100 μM SchB also did not see significant cytotoxicity. Therefore, SchB concentration of 50 μM was selected for subsequent cell experiments.

The results of cotreatment of SchB and CsA showed that there was no significant difference in THP-induced cytotoxicity between SchB and CsA alone (**Figure 6B**).

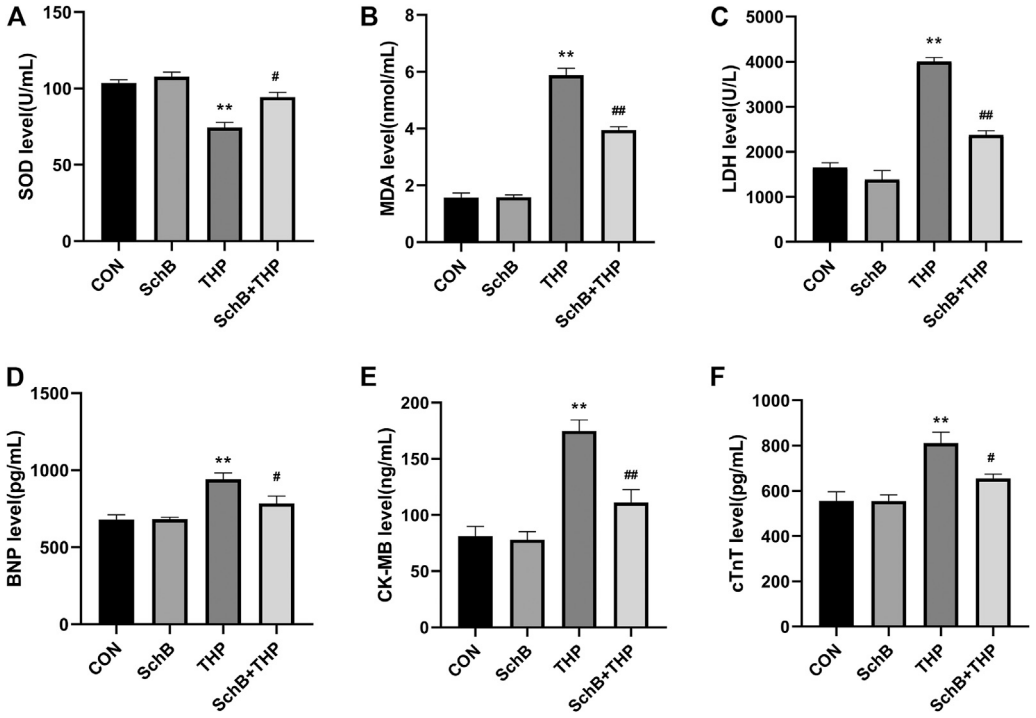

FIGURE 4 | SchB effectively improved the level of serum markers in heart injury induced by THP: **(A)** superoxide dismutase (SOD) levels, **(B)** malondialdehyde (MDA) levels, **(C)** lactate dehydrogenase (LDH) levels, **(D)** brain natriuretic peptide (BNP) levels, **(E)** creatine kinase MB (CK-MB) levels, and **(F)** cardiac troponin T (cTnT) levels. All values are mean ± SD. $^{*}p < 0.05$ vs. CON, $^{**}p < 0.01$ vs. CON, $^{\#}p < 0.05$ vs. THP, and $^{\#\#}p < 0.01$ vs. THP.

ROS Level of H9C2 Cardiomyocytes in Each Group

As shown in **Figure 6C**, THP induced H9C2 cells to produce a large amount of ROS, which decreased after both SchB and CsA treatment. ROS was almost absent in CON, SchB, and CsA groups.

Effects of SchB, THP, and CsA on Mitochondrial Permeability Transition Pore in H9C2 Cardiomyocytes

As shown in **Figure 6**, H9C2 cells in CON, SchB, and CsA groups showed bright green fluorescence, while only weak green fluorescence was observed in the THP group. The green fluorescence was more obvious in SchB + THP and CsA + THP groups, which was greatly improved compared with THP. Ionomycin was a strong positive control.

Effects of SchB, THP, and CsA on the Expression of Related Proteins in H9C2 Cardiomyocytes

As shown in **Figure 7**, THP caused the decrease of Cyt C content (**Figure 7A**) and the increase of Bax content (**Figure 7B**) in mitochondria. The above changes were alleviated by the treatment of mPTP inhibitor CsA (**Figure 7**). SchB treatment showed similar effect (**Figure 7**) in cytoplasm.

In addition, THP also increased the expression of cleaved-caspase 3/9 and Cyt C decreased the expression of procaspase 3 and decreased the ratio of Bcl-2/Bax (**Figure 7C**). After treatment with SchB or CsA, the above changes were alleviated effectively (**Figure 7C**). More evidence can be found in the semiquantitative analysis (**Figures 5A–C**).

DISCUSSION

Consistent with the expected results, THP caused cardiotoxicity in rats. After an intravenous injection of 10 $mgkg^{-1}$ THP for 8 weeks, a series of systemic and cardiac toxicity changes occurred in SD rats, including abnormal body weight and food intake, adverse changes in echocardiography and electrocardiogram readings, cardiac tissue structure damage, abnormal increase in myocardial injury markers, oxidative stress injury, and increase in cardiomyocyte apoptosis. SchB effectively improved toxicity at a dose of 50 $mgkg^{-1}$/D. Further studies have shown that the beneficial effects of SchB might be related to the inhibition of mPTP opening and decrease in cardiomyocyte apoptosis.

At present, it is generally believed that the mechanism of cardiotoxicity in anthracycline anticancer drugs involves oxidative stress, which increases cardiomyocyte apoptosis caused by ROS and calcium overload (Yao et al., 2015; Donato et al., 2017). High ROS level activates cytotoxic signals, leading to DNA damage, mitochondrial dysfunction, and decreasing protein synthesis. Consequently, this process induces cardiomyocyte apoptosis,

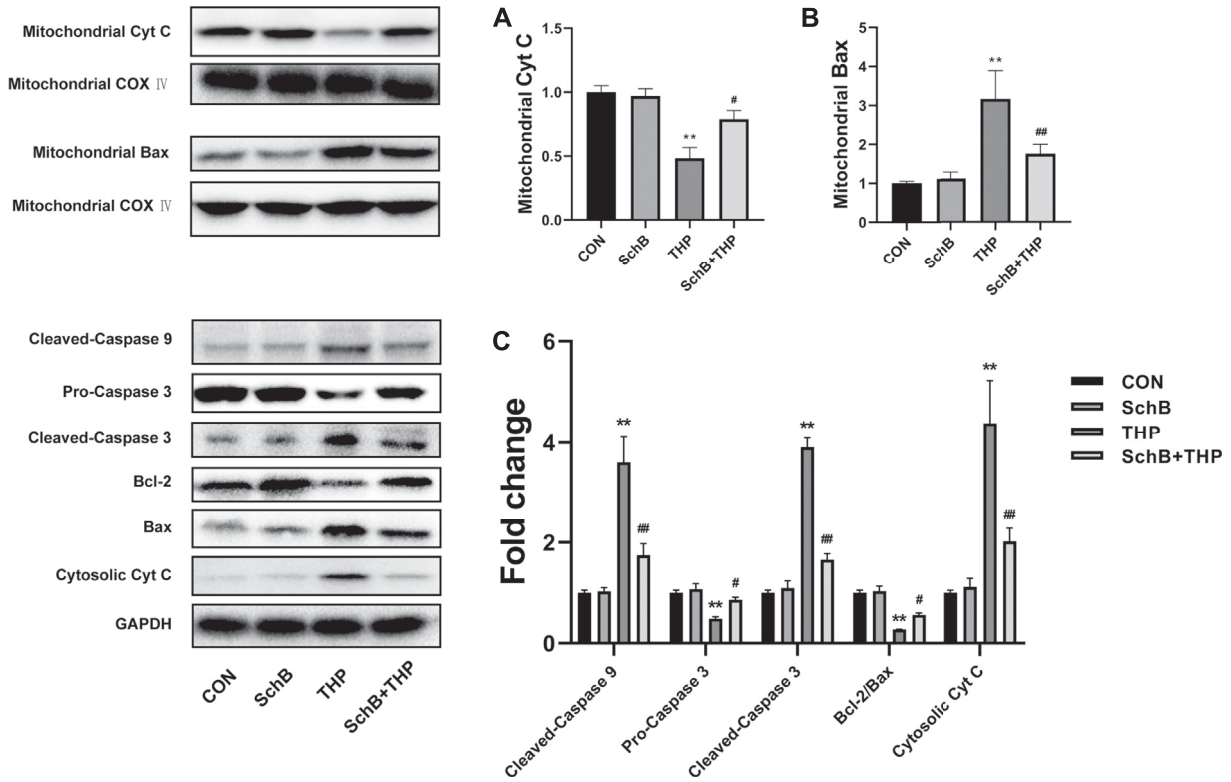

FIGURE 5 | SchB ameliorates THP-induced abnormal expression of apoptosis-related proteins in rat heart. The content of mitochondrial Cyt C **(A)** decreased and Bax **(B)** increased in the THP group, but reversed in the SchB + THP group **(C).** In the THP group, the expression of cytosolic Cyt C and cleaved-caspase 9/3 increased, while procaspase 3 and Bcl-2/Bax ratio decreased. The above changes were reversed in the SchB + THP group. More evidence can be found in the semiquantitative analysis **(A–C)**. All values are mean ± SD. $^{*}p < 0.05$ vs. CON, $^{**}p < 0.01$ vs. CON, $^{\#}p < 0.05$ vs. THP, and $^{\#\#}p < 0.01$ vs. *THP*.

leading to irreversible damage (Farías et al., 2017). Mitochondria are not only the main target of ROS damage but also an important site of ROS production (Donato et al., 2017). ROS oxidizes the thiol group of adenine nucleotide translocase (ANT) and causes the opening of mPTP (Li et al., 2018; Boyman et al., 2019). Presence of a large number of ROS results in apoptosis by destroying the mitochondrial membrane structure and releasing apoptosis-inducing factors (Zhang et al., 2019). At the same time, ROS also directly promotes the opening of mPTP, which leads to a decrease in mitochondrial membrane potential and the ROS bursting, forming a vicious circle and further aggravating mitochondria damage (Griffiths and Halestrap, 1995; Li et al., 2018). The mPTP is composed of nonspecific voltage-dependent anion channel (VDAC) located in the outer membrane, ANT located in the inner membrane, and Cyp D receptor located in the mitochondrial matrix (Fayaz et al., 2015). Under physiological conditions, only water and small molecular substances with a relative molecular weight of $<1.5\times10^3$ are allowed to pass through to maintain the electrochemical balance in mitochondria and form stable mitochondrial membrane potential (Mnatsakanyan et al., 2016; Green and Kroemer, 2004). Under various exogenous pathological stimuli, such as THP-induced heart injury, mPTP is opened abruptly, leading to mitochondrial membrane potential collapse, oxidative phosphorylation uncoupling, and ATP production disorder (Hausenloy and Yellon, 2003; Halestrap and Richardson, 2015). At the same time, the outer mitochondrial membrane ruptures, which promotes the release of Cyt C and other proapoptotic factors into the cytoplasm, initiate the caspase cascade apoptotic reaction and finally cause endogenous apoptosis. CsA is a classical mPTP inhibitor that specifically binds to Cyp D and inhibits the Cyp D and ANT binding, which also inhibits mPTP opening, reduces cell apoptosis, and plays a role in myocardial protection (Huang et al., 2014; Hurst et al., 2017). Studies have found that CsA pretreatment delays mPTP opening and improves cardiac systolic function and myocardial cell survival rate in cardiac surgery (Chiari et al., 2014).

Another interesting finding in this study was that SchB protected against THP-induced cardiotoxicity. Modern pharmacological studies have shown that SchB increases the activity or content of SOD and glutathione in tissue cells and resists the damage from free radicals to organisms (Ip and Ko, 1996; Xin et al., 2010; Hu et al., 2011; Jiang et al., 2015). Some scholars have found that MDA content in serum of MI/RI model rats treated with SchB was significantly lower than that of rats from the control group (Wang et al., 2003). In the present animal model, SchB increased SOD activity and decreased MDA content, which also fully reflected its strong antioxidant capacity. The latest research has shown that SchB significantly reduces the expression of p53 protein in a spinal cord injury

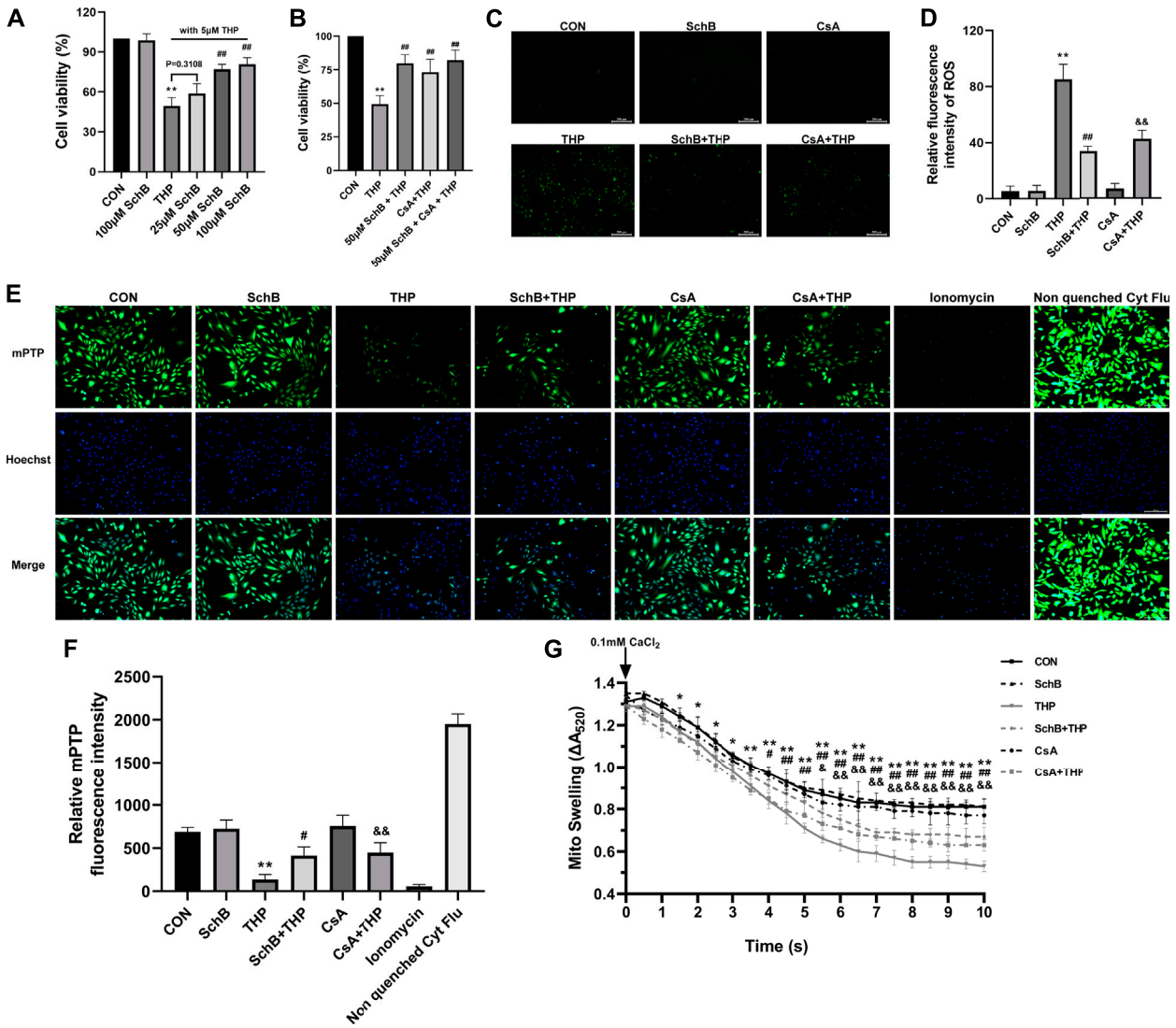

FIGURE 6 | SchB ameliorates THP-induced abnormal expression of apoptosis-related proteins in rat heart. **(A)** Screening of optimum treatment concentration of SchB. **(B)** Observation on the effect of coculture of SchB and CsA. **(C)** ROS staining in each group. **(D)** Quantification of relative fluorescence intensity of ROS in each group. **(E)** H9C2 cells in CON, SchB, and CsA groups showed bright green fluorescence, while only weak green fluorescence was observed in the THP group. The green fluorescence was more obvious in SchB + THP and CsA + THP groups, which was greatly improved compared with THP. Ionomycin was a strong positive control. Nonquenched Cyt Flu was that the cytoplasmic fluorescence is not quenched. **(F)** Fluorescence quantitative analysis. **(G)** Mitochondrial swelling was analyzed for 10 min. All values are mean ± SD. $^{*}p < 0.05$ vs. CON, $^{**}p < 0.01$ vs. CON, $^{\#}p < 0.05$ vs. THP, and $^{\#\#}p < 0.01$ vs *THP*.

mouse model and alleviates apoptosis in model mice (Xin et al., 2017). In addition, a study of ischemia-reperfusion injury in rats has found that the mitochondrial integrity of brain cells in the SchB treatment group was higher than that in the control group (Chiu et al., 2005). As mentioned above, mitochondria are the production sites of ATP and also the key organelle for oxidative stress and apoptosis. Mitochondrial dysfunction produces excessive active oxygen, which causes oxidative stress damage, opens up mPTP, and destroys ion homeostasis (Kim et al., 2003). Cyt C leaks into the cytoplasm, which leads to a series of events, such as caspase 9 activation and eventually mitochondrial-driven apoptosis (Jemmerson et al., 2005).

In general, SchB effectively inhibited the abnormal increase of oxidative stress induced by THP in rats. In addition, SchB seems to have the potential to inhibit mPTP opening similar to CsA and reduces the release of Cyt C from mitochondria to the cytoplasm. Finally, it alleviates cardiomyocyte apoptosis, which may be one of the molecular mechanisms of protecting myocardial mitochondria and preventing THP cardiotoxicity. However, the molecular mechanism of how SchB improves the increase of oxidative stress caused by THP *in vivo* is not clear. In addition, it is also not clear whether SchB directly affects mPTP opening like CsA. This is the limitation of our research and also the direction of our next work.

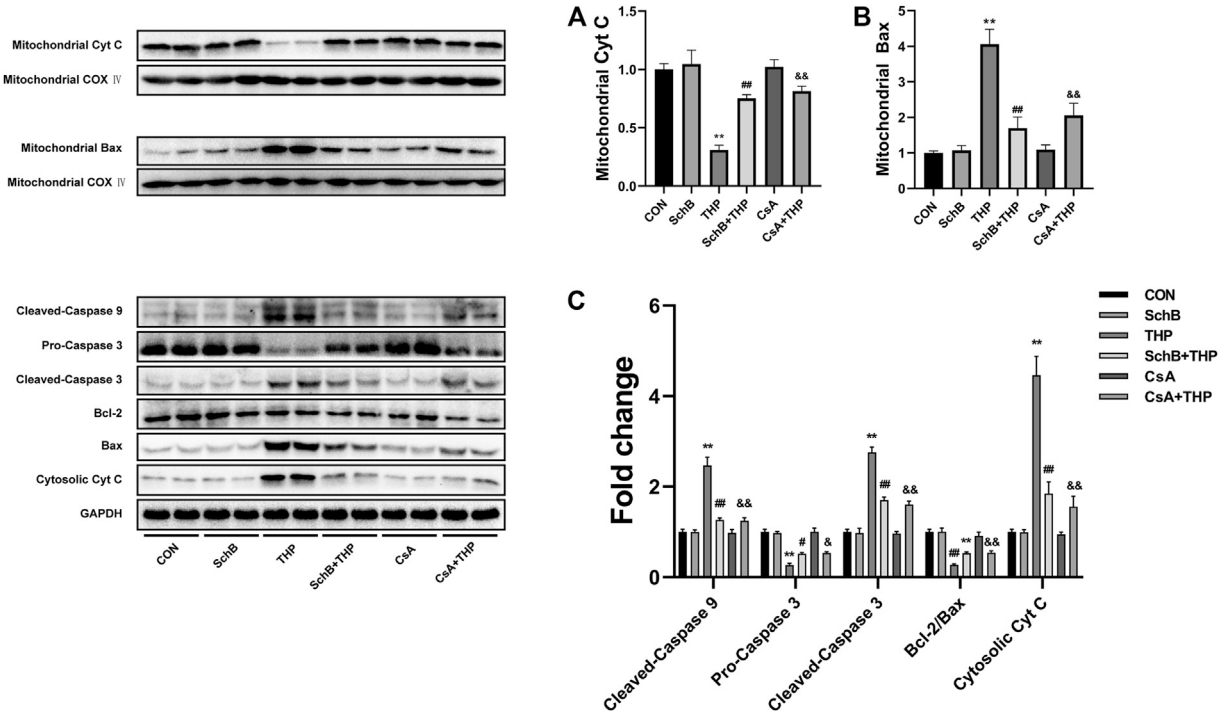

FIGURE 7 | SchB ameliorates THP-induced abnormal expression of apoptosis-related proteins in rat heart. THP caused the decrease of Cyt C **(A)** and increase of Bax **(B)** content in mitochondria. The above changes were alleviated by the treatment of mPTP inhibitor CsA. SchB treatment showed similar effects. In addition, THP also increased the expression of Cyt C and cleaved-caspase 3/9, decreased the expression of procaspase 3, and decreased the ratio of Bcl-2/Bax in cytoplasm **(C)**. After treatment with SchB or CsA, the above changes were alleviated effectively **(C)**. More evidence can be found in the semiquantitative analysis **(A–C)**. All values are mean ± SD. $^{*}p < 0.05$ vs. CON, $^{**}p < 0.01$ vs. CON, $^{\#}p < 0.05$ vs. THP, and $^{\#\#}p < 0.01$ vs. THP.

CONCLUSION

Although THP is an anthracycline anticancer drug modified by adriamycin, its cardiotoxicity cannot be ignored. SchB has an outstanding potential in the prevention and treatment of THP cardiotoxicity in rats and myocardial cell injury models. Its mechanism may be related to the reduction in oxidative stress, inhibition of mPTP opening, and ultimate reversal of myocardial cell apoptosis. The present study suggested the possible mechanism of SchB in THP cardiotoxicity and provided a theoretical basis for the clinical application of SchB in the future.

DATA AVAILABILITY STATEMENT

The original contributions presented in the study are included in the article/Supplementary Material. Further inquiries can be directed to the corresponding authors.

ETHICS STATEMENT

The animal study was reviewed and approved by the First Affiliated Hospital of Chongqing Medical University (CMU).

AUTHOR CONTRIBUTIONS

All the authors have made a significant contribution to this article, have seen and approved the final article, and have agreed to its submission to the "Obesity Facts." HS, WA, and HT made substantial contributions to the conception or design of the work and analysis and interpretation of data for the work, acquisition analysis and interpretation of data for the work, and revising article critically for important intellectual content. QZ, HY, FZ, YW, RF, and LW contributed to design of the work and analysis of data for the work. PP and QH drafted the work for important intellectual content and provided final approval of the version to be published. The authors agreed to be accountable for all aspects of the work in ensuring that questions related to the accuracy or integrity of any part of the work are appropriately investigated and resolved.

FUNDING

The study was supported by the National Natural Science Foundation of China (Grant number: 31501097), Chongqing Science and Health Joint Project (Grant number: 2020FYYX101), China Postdoctoral Science Foundation (Grant number: 2019M652612), and Natural Science Foundation of Hubei Province, China (Grant number: 2019CFB407). National Key R&D Program of China (Grant numbers: 2018YFC1311400, 2018YFC1311404).

REFERENCES

Boyman, L., Coleman, A. K., Zhao, G., Wescott, A. P., Joca, H. C., Greiser, B. M., et al. (2019). Dynamics of the Mitochondrial Permeability Transition Pore: Transient and Permanent Opening Events. *Arch. Biochem. Biophys.* 666, 31–39. doi:10.1016/j.abb.2019.03.016

Carvalho, F. S., Burgeiro, A., Garcia, R., Moreno, A. J., Carvalho, R. A., and Oliveira, P. J. (2014). Doxorubicin-Induced Cardiotoxicity: From Bioenergetic Failure and Cell Death to Cardiomyopathy. *Med. Res. Rev.* 34 (1), 106–135. doi:10.1002/med.21280

Casparini, M. (2006). Anthracycline Cardiotoxicity. *Eur. Paediatric Haematol. Oncol.* 11 (3), 237–240. doi:10.3109/08880019409141665

Chen, N., and Ko, M. (2010). Schisandrin B-Induced Glutathione Antioxidant Response and Cardioprotection Are Mediated by Reactive Oxidant Species Production in Rat Hearts. *Biol. Pharm. Bull.* 33 (5), 825–829. doi:10.1248/bpb.33.825

Chiari, P., Angoulvant, D., Mewton, N., Desebbe, O., Obadia, J. F., Robin, J., et al. (2014). Cyclosporine Protects the Heart during Aortic Valve Surgery. *Anesthesiology* 121 (2), 232–238. doi:10.1097/ALN.0000000000000331

Chiu, P. Y., Mak, D. H., Poon, M. K., and Ko, K. M. (2005). Role of Cytochrome P-450 in Schisandrin B-Induced Antioxidant and Heat Shock Responses in Mouse Liver. *Life Sci.* 77 (23), 2887–2895. doi:10.1016/j.lfs.2005.03.026

Donato, C., Antonella, D. A., Luigi, S., Lucia, P., Michela, I., Federico, Q., et al. (2017). Oxidative Stress and Cellular Response to Doxorubicin: A Common Factor in the Complex Milieu of Anthracycline Cardiotoxicity. *Oxidative Med. Cell Longevity.* 2017, 1521020. doi:10.1155/2017/1521020

Fayaz, S. M., Raj, Y. V., and Krishnamurthy, R. G. (2015). CypD: The Key to the Death Door. *CNS Neurol. Disord. Drug Targets.* 14 (5), 654–663. doi:10.2174/1871527314666150429113239

Farías, J. G., Molina, V. M., Carrasco, R. A., Zepeda, A. B., Figueroa, E., Letelier, P., et al. (2017). Antioxidant Therapeutic Strategies for Cardiovascular Conditions Associated with Oxidative Stress. *Nutrients* 9 (9), 966. doi:10.3390/nu9090966

Greish, K., Nagamitsu, A., Fang, J., and Maeda, H. (2005). Copoly(styrene-maleic Acid)-Pirarubicin Micelles: High Tumor-Targeting Efficiency with Little Toxicity. *Bioconjug. Chem.* 16 (1), 230–236. doi:10.1021/bc040297g

Griffiths, E. J., and Halestrap, A. P. (1995). Mitochondrial Non-specific Pores Remain Closed during Cardiac Ischaemia, but Open upon Reperfusion. *Biochem. J.* 307 (Pt 11), 93–98. doi:10.1042/bj3070093

Halestrap, A. P., and Richardson, A. P. (2015). The Mitochondrial Permeability Transition: a Current Perspective on its Identity and Role in Ischaemia/reperfusion Injury. *J. Mol. Cel Cardiol.* 78, 129–141. doi:10.1016/j.yjmcc.2014.08.018

Hausenloy, D. J., and Yellon, D. M. (2003). The Mitochondrial Permeability Transition Pore: its Fundamental Role in Mediating Cell Death during Ischaemia and Reperfusion. *J. Mol. Cel Cardiol.* 35 (4), 339–341. doi:10.1016/s0022-2828(03)00043-9

Hu, J. Y., Lu, T. L., Mao, C. Q., and Huang, Z. J. (2011). HPLC Simultaneous Determination of Six Lignans in Fructus Schisandrae. *Chin. J. Pharm. Anal.* 31 (12), 2225–2228. doi:10.16155/j.0254-1793.2011.12.013

Huang, K., Lu, S. J., Zhong, J. H., Xiang, Q., Wang, L., and Wu, M. (2014). Comparative Analysis of Different Cyclosporine A Doses on protection after Myocardial Ischemia/reperfusion Injury in Rat. *Asian Pac. J. Trop. Med.* 7 (2), 144–148. doi:10.1016/S1995-7645(14)60011-0

Hurst, S., Hoek, J., and Sheu, S. S. (2017). Mitochondrial Ca2+ and Regulation of the Permeability Transition Pore. *J. Bioenerg. Biomembr.* 49 (1), 27–47. doi:10.1007/s10863-016-9672-x

Ip, S. P., and Ko, K. M. (1996). The Crucial Antioxidant Action of Schisandrin B in Protecting against Carbon Tetrachloride Hepatotoxicity in Mice: a Comparative Study with Butylated Hydroxytoluene. *Biochem. Pharmacol.* 52 (11), 1687–1693. doi:10.1016/s0006-2952(96)00517-5

Jemmerson, R., Dubinsky, J. M., and Brustovetsky, N. (2005). Cytochrome C Release from CNS Mitochondria and Potential for Clinical Intervention in Apoptosis-Mediated CNS Diseases. *Antioxid. Redox Signal.* 7 (9-10), 1158–1172. doi:10.1089/ars.2005.7.1158

Jiang, E. P., Li, H., Yu, C. R., Yu, C. Y., Jing, S., Sun, H. X., et al. (2015). Schisandrin B Protects PC12 Cells against Oxidative Stress of Neurodegenerative Diseases. *Neuroreport* 26 (6), 360–366. doi:10.1097/WNR.0000000000000354

Kim, J. S., He, L., and Lemasters, J. J. (2003). Mitochondrial Permeability Transition: a Common Pathway to Necrosis and Apoptosis. *Biochem. Biophys. Res. Commun.* 304 (3), 463–470. doi:10.1016/s0006-291x(03)00618-1

Kim, S. R., Lee, M. K., Koo, K. A., Kim, S. H., Sung, S. H., Lee, N. G., et al. (2004). Dibenzocyclooctadiene Lignans from Schisandra Chinensis Protect Primary Cultures of Rat Cortical Cells from Glutamate-Induced Toxicity. *J. Neurosci. Res.* 76 (3), 397–405. doi:10.1002/jnr.20089

Koh, E., Ueda, Y., Nakamura, T., Kobayashi, A., Katsuta, S., and Takahashi, H. (2002). Apoptosis in Young Rats with Adriamycin-Induced Cardiomyopathy-Ccomparison with Pirarubicin, a New Anthracycline Derivative. *Pediatr. Res.* 51 (2), 256–259. doi:10.1203/00006450-200202000-00021

Lam, P. Y., and Ko, K. M. (2012). Schisandrin B as a Hormetic Agent for Preventing Age-Related Neurodegenerative Diseases. *Oxid Med. Cel Longev.* 2012 (3), 250825. doi:10.1155/2012/250825

Li, X., Chen, M., Yang, Z., Wang, W., Lin, H., and Xu, S. (2018). Selenoprotein S Silencing Triggers Mouse Hepatoma Cells Apoptosis and Necrosis Involving in Intracellular Calcium Imbalance and ROS-mPTP-ATP. *Biochim. Biophys. Acta Gen. Subj.* 1862, 2113–2123. doi:10.1016/j.bbagen.2018.07.005

Mnatsakanyan, N., Beutner, G., Porter, G. A., Alavian, K. N., and Jonas, E. A. (2016). Physiological Roles of the Mitochondrial Permeability Transition Pore. *J. Bioenerg. Biomembr.* 49 (1), 13–25. doi:10.1007/s10863-016-9652-1

Green, D. R., and Kroemer, G. (2004). The Pathophysiology of Mitochondrial Cell Death. *Science* 305 (5684), 626 –629. doi:10.1126/science.1099320

Octavia, Y., Tocchetti, C. G., Gabrielson, K. L., Janssens, S., Crijns, H. J., and Moens, A. L. (2012). Doxorubicin-induced Cardiomyopathy: From Molecular Mechanisms to Therapeutic Strategies. *J. Mol. Cel Cardiol.* 52 (6), 1213–1225. doi:10.1016/j.yjmcc.2012.03.006

Tang, H., Zeng, Q., Ren, N., Wei, Y., He, Q., Chen, M., et al. (2021). Kaempferide Improves Oxidative Stress and Inflammation by Inhibiting the TLR4/IκBα/NF-Kb Pathway in Obese Mice. *Iran J. Basic Med. Sci.* 24 (4), 493–498. doi:10.22038/ijbms.2021.52690.11892

Tang, H., Zeng, Q., Tang, T., Wei, Y., and Pu, P. (2021). Kaempferide Improves Glycolipid Metabolism Disorder by Activating PPARγ in High-Fat-Diet-Fed Mice. *Life Sci.* 270 (7), 119133. doi:10.1016/j.lfs.2021.119133

Von Hoff, D. D., Layard, M. W., Basa, P., Davis, H. L., Von Hoff, A. L., Rozencweig, M., et al. (1979). Risk Factors for Doxorubicin-Induced Congestive Heart Failure. *Ann. Intern. Med.* 91 (5), 710–717. doi:10.7326/0003-4819-91-5-710

Wang, L., Nishida, H., Ogawa, Y., and Konishi, T. (2003). Prevention of Oxidative Injury in PC12 Cells by a Traditional Chinese Medicine, Shengmai San, as a Model of an Antioxidant-Based Composite Formula. *Biol. Pharm. Bull.* 26 (7), 1000–1004. doi:10.1248/bpb.26.1000

Wang, Y., Zhang, Y., Sun, B., Tong, Q., and Ren, L. (2017). Rutin Protects against Pirarubicin-Induced Cardiotoxicity through TGF-β1-P38 MAPK Signaling Pathway. *Evid. Based Complement. Alternat Med.* 2017 (3-6), 1759385. doi:10.1155/2017/1759385

Xin, D. Q., Hu, Z. M., Huo, H. J., Yang, X. J., Han, D., Xing, W. H., et al. (2017). Schisandrin B Attenuates the Inflammatory Response, Oxidative Stress and Apoptosis Induced by Traumatic Spinal Cord Injury *via* Inhibition of P53 Signaling in Adult Rats. *Mol. Med. Rep.* 16 (1), 533–538. doi:10.3892/mmr.2017.6622

Xin, S., Yu, X., Jianguang, C., Qi, W., Dan, T., and Tan, L. (2010). e0126Study on anti-oxidative function of four kinds of schizandrae lignans. *Heart* 96 (Suppl. 3), A41. doi:10.1136/hrt.2010.208967.126

Yao, H., Shang, Z., Wang, P., Li, S., Zhang, Q., Tian, H., et al. (2015). Protection of Luteolin-7-O-Glucoside Against Doxorubicin-Induced Injury through PTEN/Akt and ERK Pathway in H9c2 Cells. *Cardiovasc. Toxicol.* 16 (2), 101–110. doi:10.1007/s12012-015-9317-z

Zhang, Q., Liu, J., Zhang, M., Wei, S., Li, R., Gao, Y., et al. (2019). Apoptosis Induction of Fibroblast-like Synoviocytes Is an Important Molecular-Mechanism for Herbal Medicine along with its Active Components in Treating Rheumatoid Arthritis. *Biomolecules* 9 (12), 795. doi:10.3390/biom9120795

Conflict of Interest: The authors declare that the research was conducted in the absence of any commercial or financial relationships that could be construed as a potential conflict of interest.

Publisher's Note: All claims expressed in this article are solely those of the authors and do not necessarily represent those of their affiliated organizations, or those of the publisher, the editors, and the reviewers. Any product that may be evaluated in this article, or claim that may be made by its manufacturer, is not guaranteed or endorsed by the publisher.

frontiers in Pharmacology

ORIGINAL RESEARCH
published: 11 November 2021
doi: 10.3389/fphar.2021.770580

Assessment of Myocardial Work in Cancer Therapy-Related Cardiac Dysfunction and Analysis of CTRCD Prediction by Echocardiography

Jingyuan Guan, Wuyun Bao, Yao Xu, Wei Yang, Mengmeng Li, Mingjun Xu, Yu Zhang and Mei Zhang**

The Key Laboratory of Cardiovascular Remodeling and Function Research, Chinese Ministry of Education, Chinese National Health Commission and Chinese Academy of Medical Sciences, The State and Shandong Province Joint Key Laboratory of Translational Cardiovascular Medicine, Qilu Hospital of Shandong University, Jinan, China

No study has examined myocardial work in subjects with cancer therapy-related cardiac dysfunction (CTRCD). Myocardial work, as a new ultrasonic indicator, reflects the metabolism and oxygen consumption of the left ventricle. The aim of this study was to test the relative value of new indices of myocardial work and global longitudinal strain (GLS) in detecting changes in myocardial function during the treatment of breast cancer by two-dimensional and three-dimensional echocardiography. We enrolled 79 breast cancer patients undergoing different tumor treatment regimens. Follow-up observation was conducted before and after chemotherapy. The effects of breast cancer chemotherapy and targeted therapy on the development of CTRCD [defined as an absolute reduction in left ventricular ejection fraction (LVEF) of >5% to <53%] were detected by two-dimensional and three-dimensional speckle tracking echocardiography. Our findings further indicate that LVEF, myocardial work index (GWI) and myocardial work efficiency (GWE) showed significant changes after the T6 cycle, and GLS showed significant changes after the T4 cycle ($p < 0.05$). The three-dimensional strain changes after T6 and T8 had no advantages compared with GLS. Body mass index (BMI), the GLS change rate after the second cycle of chemotherapy (G2v) and the 3D-GCS change rate after the second cycle of chemotherapy (C2v) were independent factors that could predict the occurrence of CTRCD during follow-up, among which BMI was the best predictor (area under the curve, 0.922). In conclusion, the current study determined that GLS was superior to GWI in predicting cardiac function in patients with tumors with little variation in blood pressure. BMI, G2v and C2v can be used to predict the occurrence of CTRCD.

Keywords: anthracycline, trastuzumab, cardiotoxicity, speckle tracking technology, myocardial work

OPEN ACCESS

Edited by:
Jun Pu,
Shanghai Jiao Tong University, China

Reviewed by:
Simona Sperlongano,
University of Campania Luigi Vanvitelli, Italy
Marcellino Monda,
Università della Campania Luigi Vanvitelli, Italy

****Correspondence:***
Yu Zhang
zhangyusdu@sina.cn
Mei Zhang
daixh@vip.sina.com

Specialty section:
This article was submitted to Cardiovascular and Smooth Muscle Pharmacology, a section of the journal Frontiers in Pharmacology

Received: *04 September 2021*
Accepted: *04 October 2021*
Published: *11 November 2021*

Citation:
Guan J, Bao W, Xu Y, Yang W, Li M, Xu M, Zhang Y and Zhang M (2021) Assessment of Myocardial Work in Cancer Therapy-Related Cardiac Dysfunction and Analysis of CTRCD Prediction by Echocardiography. Front. Pharmacol. 12:770580. doi: 10.3389/fphar.2021.770580

Abbreviations: CTRCD, heart dysfunction associated with cancer treatment; GLS, global longitudinal strain; LVEF, left ventricular ejection fraction; GWI, myocardial work index; GWE, myocardial work efficiency; BMI, body mass index; LV-PSL, left ventricular pressure-strain ring; T0, baseline before chemotherapy; T2, after the second cycle of chemotherapy; T4, after the fourth cycle of chemotherapy; T6, after the sixth cycle of chemotherapy; T8, after the eighth cycle of chemotherapy; SBP, systolic blood pressure; DBP, diastolic blood pressure; HR, heart rate; BSA, body surface area; Glu, blood glucose; TG, triglycerides; TC, total cholesterol; L2v, rate of change of LVEF at T2; G2v, rate of change of GLS at T2; I2v, rate of change of GWI at T2; E2v, rate of change of GWE at T2; S2v, rate of change of 3D-GLS at T2; C2v, rate of change of 3D-GCS at T2; A2v, rate of change of 3D-GAS at T2.

INTRODUCTION

Cardiovascular disease complicated by chemotherapy has become one of the important causes of posttreatment death in tumor patients (Giordano et al., 2016), among which the most devastating is the heart dysfunction associated with cancer treatment (CTRCD). In the course of treatment, regular follow-up examination is one of the most important methods to prevent cardio-related adverse reactions. Among them, echocardiography has become the most widely used examination method beyond multigated acquisition scanning (MUGA) and magnetic resonance imaging of the myocardium (CMR) due to its advantages including noninvasiveness and repeatability. At present, the most commonly used ultrasonic parameters are left ventricular ejection fraction (LVEF) and global longitudinal strain (GLS). Compared with 2D Speckle Tracking Echocardiogram (2D-STE), the three-dimensional strain measurement has no space limitation and has a more accurate and objective reference value (Zeng et al., 2021).

The left ventricular myocardial work index (GWI) is the area of the left ventricular pressure-strain ring (LV-PSL), which represents the work done by the myocardium from mitral valve closure to mitral valve opening and reflects the metabolism and oxygen consumption of the left ventricle. Its advantage lies in the correction of afterload, which overcomes the dependence of the left ventricular ejection fraction and left ventricular strain on the load (Russell et al., 2012; Hubert et al., 2018). At present, GWI and myocardial work efficiency (GWE) have been confirmed to change earlier than strain in left ventricular remodeling diseases caused by coronary heart disease and structural heart disease (Chan et al., 2019), and the role of myocardial work in the field of oncologic cardiology has not been reported. We followed up breast cancer patients treated with different regimens to explore the value of two-dimensional and three-dimensional speckle tracking in the early monitoring of cardiac function changes and to explore the risk factors for cardiotoxicity caused by breast cancer drug therapy.

METHODS

Study Population

A total of 79 female patients admitted to Qilu Hospital of Shandong University were enrolled in this study and were divided into three groups according to their treatment plans. Patients in G1 group who received anthracycline-free and non-targeted regimens [Docetaxel (T) 75 mg/m2 on day 1 and Carboplatin (Cb) AUC 6 on day 1, 21 days for a cycle, a total of six cycles]; G2 included patients treated with anthracycline-containing regimens without targeted therapy [Doxorubicin (A) 60 mg/m2 on day 1 or Epirubicin (E) 60–100 mg/m2 on day 1, Cyclophosphamide (C) 600 mg/m2 on day 1, 21 days for a cycle, a total of four cycles; Docetaxel (T) 100 mg/m2 iv on day 1, 21 days as a cycle, a total of four cycles]; G3 included patients treated with anthracyclines combined with targeted drugs [Doxorubicin (A) 50–60 mg/m2 on day 1 or Epirubicin (E) 80–100 mg/m2 on day 1, Cyclophosphamide (C) 600 mg/m2 on day 1, 21 days for a cycle, a total of four cycles; followed by Docetaxel (T) 100 mg/m2 on the first day, 21 days as a cycle, a total of four cycles. At the same time, Trastuzumab (H) was given at the first dose of 8 mg/kg, followed by 6 mg/kg for a period of 21 days, for a total of four cycles. Combined with or without Pertuzumab, first dose of 840 mg and then 420 mg for each period of 21 days, for a period of four cycles]. All patients underwent echocardiography before chemotherapy (T0) and after the end of chemotherapy cycle 2 (T2), cycle 4 (T4), cycle 6 (T6), and cycle 8 (T8).

The patients who met the following inclusion criteria were enrolled: 1) those aged less than 70 years old; 2) patients diagnosed with breast cancer by histology or cytopathology; 3) patients set to receive adjuvant chemotherapy combined with trastuzumab combined with or without pertuzumab; 4) those with no previous history of chemotherapy or radiotherapy. The major exclusion criteria included poor echocardiography image quality that did not allow complete analysis of the ultrasonic data; patients with heart failure, history of coronary heart disease, acute coronary syndrome or myocarditis, myocardial infarction, severe valvular disease, cardiomyopathy and other serious heart disease; and patients with persistent atrial fibrillation and severe arrhythmia. The study protocol was approved by the Ethics Committee of Shandong University Qilu Hospital (Ethics approval number: 2018163), and written informed consent was obtained from all participants.

Demographic Characteristics

Data on age, body mass index, current or previous smoking, diabetes mellitus, coronary artery disease, systolic blood pressure (SBP), diastolic blood pressure (DBP), and administration of antihypertensive drugs and statins were collected at enrollment. Serum levels of fasting blood glucose (GLU), serum triglycerides, total cholesterol, low-density lipoprotein cholesterol (LDL-C) and high-density lipoprotein cholesterol (HDL-C) were measured in the clinical laboratory departments of Qilu hospitals.

Echocardiography

All subjects were examined by a GE Vivid E95 or GE Vivid E9 color Doppler ultrasound with an M5S-D probe (probe frequency 1.4–4.6 Hz) and a 4V-D probe (probe frequency 1.5–4.0 Hz). Ultrasound images were collected, and bilateral brachial artery blood pressure was measured. In addition to standard echocardiography, the study included 3–5 cardiac cycles at frame rates of 50–70 frames per second on apical sections of four-, three- and two-chamber views that were stored digitally in original format for analysis. All strain analyses were performed using semiautomatic speckle tracking technology (EchoPAC203, GE Medical System, Milwaukee, Wisconsin) using the entire left ventricular model (the three apical views). Parts that were inadequately tracked were excluded. Three-dimensional full volume left ventricular acquisition using a maximum volume ratio matrix array sensor was attempted in all patients. The biplanar Simpson method was used to measure LVEF, while the measurement of GLS and myocardial work was based on automated function imaging (AFI). When the myocardial

TABLE 1 | Demographic and biochemical data in the different treatment groups [M (Q1~Q3)].

	G1 (*n* = 20)	G2 (*n* = 38)	G3 (n = 21)	*p*
Age (years)	48(44–53.5)	49(43–56)	48(44–49)	0.711
Weight (kg)	61(54.25–67.38)	61.5(56.75–65)	62(56–75.5)	0.713
Height (cm)	160(158–163.75)	160(158–162)	160(157.5–165)	0.77
SBP (mmHg)	124.5(110.5–129.75)	122.5(116–138.25)	128(118–139.5)	0.603
DBP (mmHg)	75.5(65.75–79.75)	76(69–86)	74(67–82)	0.665
HR (bpm)	81.5(78–85)	81.5(72.5–90.5)	77(72.5–84.5)	0.678
BMI (kg/m^2)	22.98(21.42–25.84)	23.98(21.93–26.51)	24.6(21.34–27.85)	0.665
BSA (m^2)	1.67(1.56–1.74)	1.66(1.61–1.73)	1.69(1.59–1.84)	0.674
Glu (mmol/L)	4.94(4.65–5.38)	4.99(4.72–5.39)	5.11(4.64–5.56)	0.936
LDL-C (mmol/L)	2.46(2.06–2.77)	2.55(2.19–3.05)	2.22(2.02–3.13)	0.457
HDL-C (mmol/L)	1.33(1.19–1.54)	1.31(1.08–1.61)	1.3(1.05–1.63)	0.917
TG (mmol/L)	1.13(0.78–1.46)	1.05(0.84–1.65)	1.05(0.72–1.54)	0.773
TC (mmol/L)	4.27(3.92–4.56)	4.57(3.93–4.99)	4.29(3.95–4.83)	0.484

SBP, systolic blood pressure; DBP, diastolic blood pressure; HR, heart rate; BMI, body mass index; BSA, body surface area; Glu, blood glucose; TG, triglycerides; TC, total cholesterol. Data are expressed as [M (Q1~Q3)].

tracking was not accurate, the myocardium could be manually adjusted.

Definitions of CTRCD

CTRCD (Zamorano et al., 2016) is defined as a reduction in LVEF of at least 5% from baseline to <53% (Negishi and Negishi, 2018) in absolute value, accompanied by symptoms or signs of heart failure, or a reduction in LVEF of at least 10% to an absolute value <53% without symptoms or signs of heart failure.

Statistical Analysis

Statistical analysis involved the use of SPSS version 26.0 (SPSS, Chicago, IL) and GraphPad Prism 9.0 (GraphPad, United States). All measurement data were tested for normality and homogeneity of variance. Measurement data meeting the normal distribution were measured as the mean ± SD ($\bar{X} \pm s$). Measurement data that did not meet the normal distribution were expressed as the median (interquartile range) [M (Q1~Q3)], and the data between groups were compared using the Mann-Whitney U test. Paired t tests were used to compare the data from the same patient before and after chemotherapy. Survival analysis was performed by the Kaplan-Meier method, and the log-rank test was used for univariate analysis between groups. Multivariate survival analysis was performed by a Cox proportional risk regression model. $p < 0.05$ indicated that the difference was statistically significant.

RESULTS

Patient Characteristics

A total of 206 breast cancer patients were screened from November 2018–January 2021. Among them, 79 were newly treated breast cancer patients who met the inclusion criteria and completed multicycle follow-up. All were female patients aged 22–66 years old, with a median age of 48 years old. There were 20 cases in the G1 group, 38 cases in the G2 group, and 21 cases in the G3 group. Among them, seven patients had hypertension, three patients had coronary heart disease, and three patients had diabetes. Eight patients were treated with dextroimide, and 26 patients were treated with other drugs (salvia miltiorrhiza polyphenol, cyclic adenosine glucamine, and safflower yellow). There were no significant differences in age, weight, height, BMI, body surface area (BSA), blood pressure, blood glucose or blood lipids among the different treatment groups ($p > 0.05$) (**Table 1**).

LVEF, GLS and GWI

Compared with the G1 group, GLS in T4 and LVEF, GWI and GWE in T6 were significantly decreased in the G2 and G3 groups ($p < 0.05$). With the progression of chemotherapy, the values of LVEF, GLS, GWI and GWE gradually decreased; GLS significantly decreased at T2; and LVEF, GWI and GWE significantly decreased at T4 (**Figure 1**).

The 3D-STE parameters of the research object are shown in **Table 2**. Compared with the basic condition before chemotherapy, 3D-GLS, 3D-GCS, 3D-GAS and 3D-GRS were significantly decreased ($p < 0.05$). The decrease in 3D-GLS and 3D-GCS in G2 and G3 was more obvious than that in G1, the changes were statistically significant in T6, and 3D-GAS and 3D-GRS were significantly changed in T8 (**Figure 2**).

LVEF decreased in the course of chemotherapy, and the degree of decrease was G3 > G2 > G1. GLS decreased in the course of chemotherapy, and the degree of decrease was G3 > G2 > G1. GWI showed a downward trend in the course of chemotherapy, the change in GWI in the G1 group was not obvious, and the change range was G3 > G2. GWI showed a downward trend during chemotherapy, with no significant change in the G1 group, a similar decrease in the G2 group and G3 group at T4, and G3 > G2 after G6. Note: LVEF, left ventricular ejection fraction; GLS, left ventricular overall longitudinal strain; GWI, global myocardial work index; GWE, myocardial work efficiency; T0, baseline before chemotherapy; T2, after the second cycle of chemotherapy; T4, after the fourth cycle of chemotherapy; T6, after the sixth cycle of chemotherapy; T8, after the eighth cycle of chemotherapy. $^*p < 0.01$ compared with G1.

3D-GLS, 3D-GCS, 3D-GAS and 3D-GRS all showed a downward trend during chemotherapy. The changes in

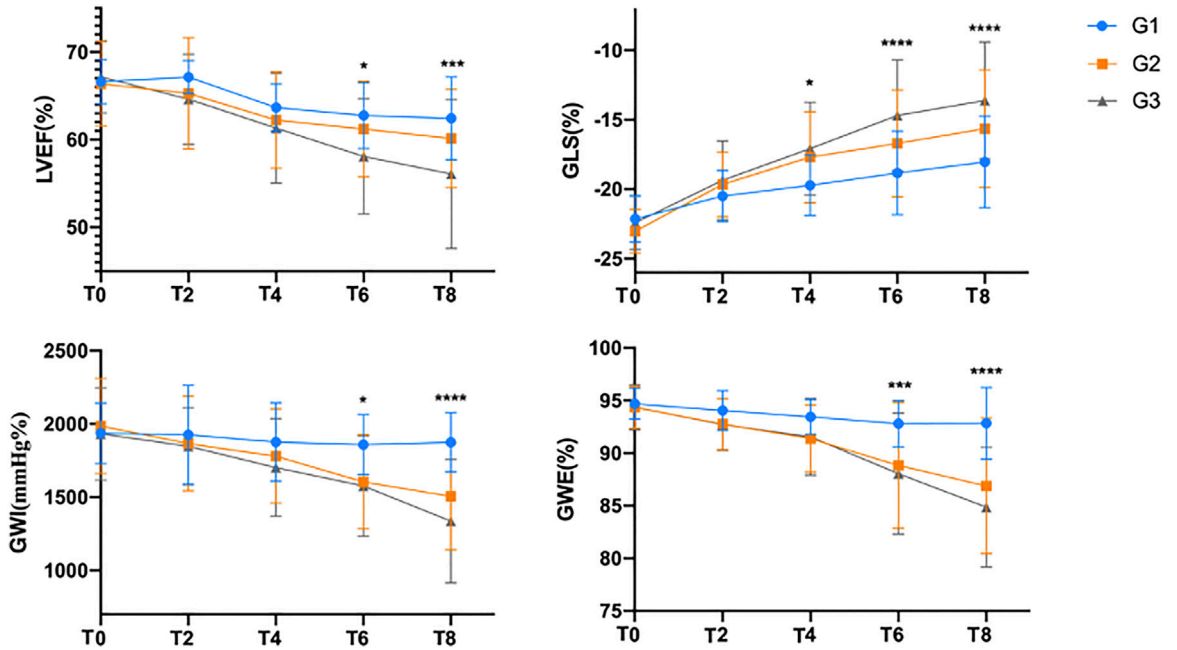

FIGURE 1 | Comparison of the assessment of left ventricular function before and after chemotherapy.

TABLE 2 | Left ventricular ultrasonography before and after chemotherapy ($\bar{X} \pm s$).

	T0	T2	T4	T6	T8
LVEF (%)	66.65 ± 4.13	65.57 ± 5.25	62.34 ± 5.21#	60.73 ± 5.65#	59.43 ± 6.99#
GLS (%)	−22.6 ± 1.77	−19.79 ± 2.38#	−18.17 ± 3.04#	−16.96 ± 3.65#	−15.94 ± 4.03#
GWI (mmHg%)	1959.14 ± 294.34	1876.75 ± 309.1*	1783.51 ± 314.37#	1661.89 ± 321.25#	1552.58 ± 400.26#
GWE (%)	94.44 ± 1.91	93.08 ± 2.36#	91.95 ± 3.12#	89.62 ± 5.49#	87.84 ± 6.33#
3D-GLS (%)	−19.81 ± 1.69	−18.09 ± 2.41#	−16.72 ± 2.76#	−15.82 ± 3.71#	−14.86 ± 4.03#
3D-GCS (%)	−24.61 ± 3.42	−21.73 ± 3.62#	−19.87 ± 3.84#	−18.16 ± 4.51#	−17.7 ± 4.37#
3D-GAS (%)	−31.46 ± 4.73	−29.65 ± 5.23#	−28.39 ± 4.75#	−27 ± 4.58#	−25.65 ± 4.48#
3D-GRS (%)	34.8 ± 9.06	33.54 ± 9.12	31.8 ± 7.04*	30.14 ± 7.05#	28.85 ± 7.14#

*LVEF, left ventricular ejection fraction; GLS, global longitudinal strain; GWI, global myocardial work index; GWE, myocardial work efficiency; 3D-GLS, left ventricular three-dimensional longitudinal peak strain; 3D-GCS, left ventricular three-dimensional peripheral peak strain; 3D-GAS, left ventricular three-dimensional area peak strain; 3D-GRS, left ventricular three-dimensional radial peak strain. #p < 0.05 compared with T0; *p < 0.01 compared with T0.*

3D-GLS, 3D-GAS and 3D-GRS in the G3 group were significantly higher than those in the G1 and G2 groups ($p < 0.05$). The degree of decrease in 3D-GCS was G3 > G2 > G1. Note: 3D-GLS, left ventricular three-dimensional longitudinal peak strain; 3D-GCS, left ventricular three-dimensional peripheral peak strain; 3D-GAS, left ventricular three-dimensional area peak strain; 3D-GRS, left ventricular three-dimensional radial peak strain. *$p <$ 0.01 compared with G1.

CTRCD

During the follow-up, a total of nine patients developed CTRCD (see **Supplementary Figure S1** for an example of image analysis). In the G1 group, one patient developed CTRCD at T8, and in the G2 group, one patient developed CTRCD at T2, one patient at T6, and one patient at T8. In the G3 group, one patient developed CTRCD at T2, two patients at T6, and two patients at T8.

The difference in clinical data between the event group ($n = 9$) and the nonevent group ($n = 70$) is shown in **Table 3**. There were no significant differences in age, systolic blood pressure, diastolic blood pressure, heart rate, blood glucose, HDL-C or TC between the two groups ($p > 0.05$), while BMI, BSA, LDL-C and TG in the event group were significantly increased ($p < 0.05$) (**Table 3**). L2v is defined as the rate of change of LVEF at T2, and G2v (GLS) compared with baseline, I2v (GWI), E2v (GWE), S2v (3D-GLS), C2v (3D-GCS), and A2v (3D-GAS) are similarly defined.

Age, diastolic blood pressure, heart rate, E2v and A2v were not correlated with the occurrence of CTRCD. Systolic blood pressure, BMI, BSA, serum glucose levels, serum LDL-C levels, serum HDL-C levels, serum TC levels, serum TG levels, L2v, G2v, I2v, S2v and C2v were significantly correlated with the occurrence of end events ($p < 0.05$) (**Supplementary Table S1**).

The BMI level and G2v and C2v as parameters for predicting the occurrence of CTRCD in breast cancer

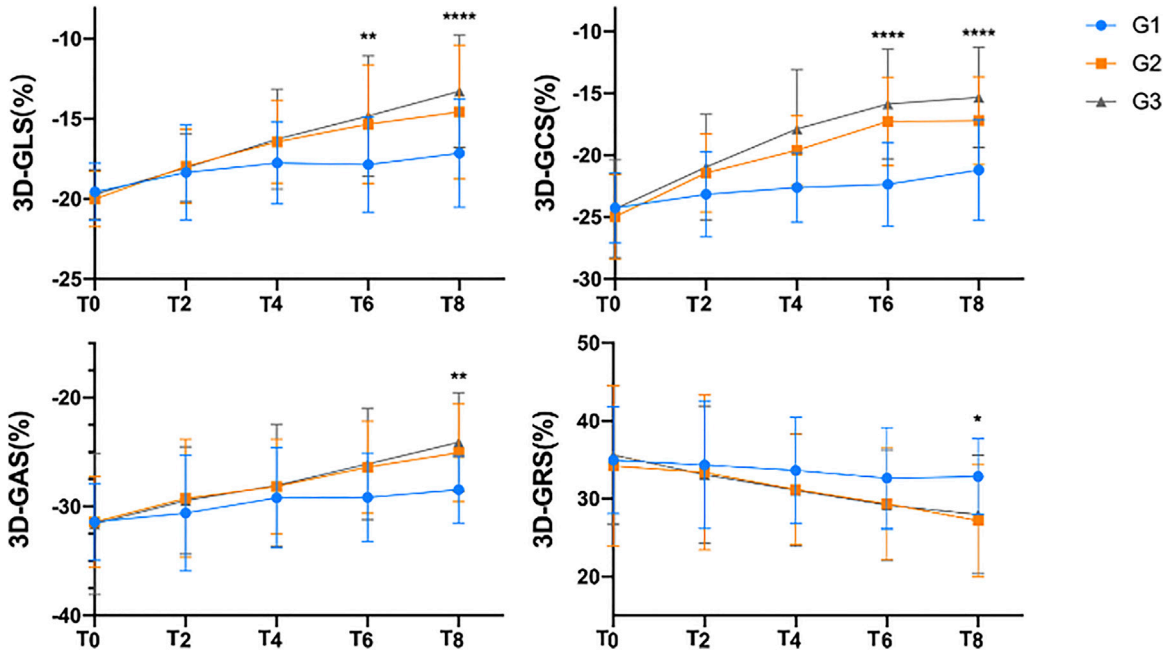

FIGURE 2 | Comparison of the three-dimensional strain indices before and after chemotherapy.

TABLE 3 | Differences in clinical influencing factors at baseline between the CTRCD and non-CTRCD groups ($\bar{X} \pm s$).

	CTRCD group (n = 9)	Non-CTRCD group (n = 70)	p
Age (years)	53.44 ± 9.4	48.09 ± 8.16	0.135
BMI (kg/m^2)	29.46 ± 2.7	23.79 ± 3.19	< 0.001
BSA (m^2)	1.83 ± 0.14	1.66 ± 0.12	0.006
SBP (mmHg)	121.78 ± 10.5	127.7 ± 17.38	0.167
DBP (mmHg)	77.22 ± 8.26	76.01 ± 10.97	0.669
HR (bpm)	79.78 ± 7	80.99 ± 11.56	0.663
Glu (mmol/L)	5.08 ± 0.95	5.19 ± 0.86	0.742
LDL-C (mmol/L)	3.05 ± 0.49	2.47 ± 0.6	0.008
HDL-C (mmol/L)	1.37 ± 0.32	1.3 ± 0.94	0.353
TG (mmol/L)	1.3 ± 0.94	1.31 ± 0.76	0.971
TC (mmol/L)	5.08 ± 0.73	4.45 ± 0.8	0.034

SBP, systolic blood pressure; DBP, diastolic blood pressure; HR, heart rate; BMI, body mass index; BSA, body surface area; Glu, blood glucose; TG, triglycerides; TC, total cholesterol. Data are expressed as the mean ± SD.

patients after tumor treatment showed good predictive value, with AUCs of 0.922 (95% CI: 0.858–0.987), 0.776 (95% CI: 0.600–0.952) and 0.703 (95% CI: 0.488–0.918), respectively. At the 95th percentile risk threshold, the sensitivities were 88.9, 55.6, and 66.7%, and the specificities were 88.6, 94.3, and 81.4%, respectively. Among them, BMI is the optimal parameter. When BMI is higher than 27.03, the probability of CTRCD is 1.301 times that with a BMI less than 27.03. (**Table 4**, **Figure 3**).

The ROC curves of BMI, G2v and C2v for predicting the occurrence of cardiotoxicity are shown. The area under the curve of BMI (0.922) was better than that of G2v (0.776) and C2v (0.703), and its predictive value for the occurrence of cardiotoxicity was the highest.

DISCUSSION

There were several important findings in the present study. First, the GWI and GWE decreased with chemotherapy, but their sensitivity was lower than that of GLS. Second, 3D strain parameters such as 3D-GLS, 3D-GCS, 3D-GAS and 3D-GRS changed significantly in the course of chemotherapy but did not show obvious advantages over GLS. Third, BMI can be used as an independent factor to predict the occurrence of CTRCD.

In this cohort study, we analyzed the changes in GLS parameters and myocardial work parameters from echocardiography over the duration of tumor therapy and the role of these changes in predicting the occurrence of CTRCD. The results showed that GLS had statistically significant changes earlier than GWI. Theoretically, myocardial work is calculated based on the left ventricle pressure applied to the strain, under normal circumstances, the changes in myocardial work and ventricular strain will show better consistency. However, in this study, some patients developed hypertension after receiving chemotherapy treatment, which can balance the reduction of strain, so that the change in myocardial work index occurred after the reduction of strain. We plan to further explore these hypotheses in a follow-up study of hypertensive patients with tumors.

Chan et al. (2019) used LV-PSL to assess myocardial function in a group of coronary angiography patients. The study included control patients, patients with hypertension, and patients with

TABLE 4 | Analysis of the Cox regression results in the CTRCD and non-CTRCD groups.

	B	SE	Wals	*p*	HR (95.0% CI)
L2v (%)	0.123	0.116	1.116	0.291	1.131 (0.9–1.42)
G2v (%)	0.082	0.032	6.616	0.01*	1.086 (1.02–1.156)
I2v (%)	0.013	0.028	0.21	0.646	1.013 (0.958–1.071)
S2v (%)	3.847	2.085	3.403	0.065	46.854 (0.786–2791.451)
C2v (%)	5.512	2.299	5.75	0.016*	247.692 (2.737–22419.074)
A2v (%)	–0.053	2.969	0	0.986	0.949 (0.003–319.475)
BMI (kg/m^2)	0.263	0.133	3.914	0.048*	1.301 (1.002–1.688)
BSA (m2)	0.849	2.775	0.094	0.76	2.336 (0.01–537.464)
LDL-C (mmol/L)	0.567	1.287	0.194	0.66	1.763 (0.142–21.945)
TC (mmol/L)	–0.054	0.905	0.004	0.953	0.948 (0.161–5.589)

SBP, systolic blood pressure; DBP, diastolic blood pressure; HR, heart rate; BMI, body mass index; BSA, body surface area; Glu, blood glucose; TG, triglycerides; TC, total cholesterol; L2v, rate of change of LVEF at T2; G2v, rate of change of GLS at T2; I2v, rate of change of GWI at T2; E2v, rate of change of GWE at T2; S2v, rate of change of 3D-GLS at T2; C2v, rate of change of 3D-GCS at T2; A2v, in the rate of change of 3D-GAS at T2. *p < *0.05.*

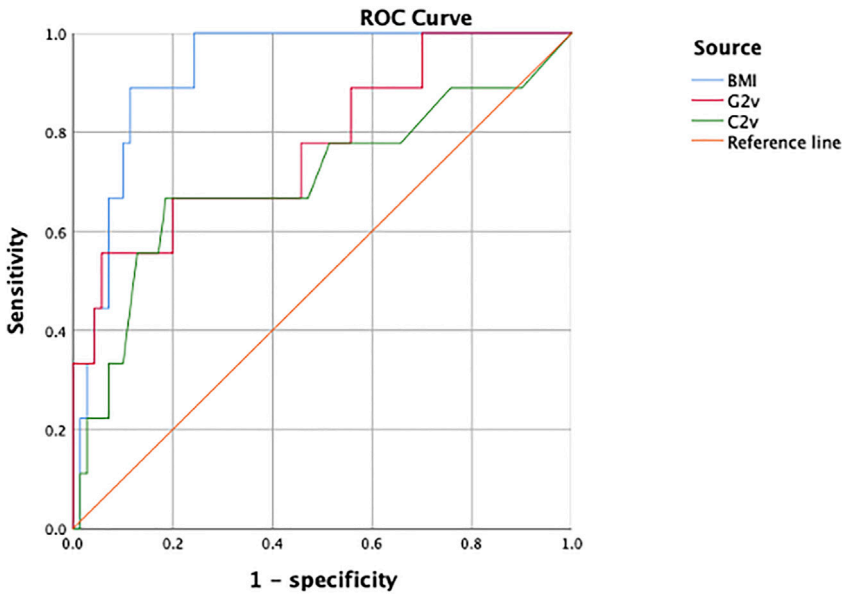

FIGURE 3 | ROC curves were used to analyze the predictive value of BMI, G2v and C2v for cardiotoxicity.

Index	Sensitivity (%)	Specificity (%)	AUC (95%CI)	Cutoff point	*P*
BMI (kg/m^2)	88.9	88.6	0.922(0.858–0.987)	27.03	< 0.001
G2v (%)	55.6	94.3	0.776(0.600–0.952)	22.7	< 0.001
C2v (%)	66.7	81.4	0.703(0.488–0.918)	16.5	< 0.001

cardiomyopathy. The results showed that the proportions of GCW and GWW increased in patients with hypertension and that GWE remained unchanged. In hypertensive patients with systolic blood pressure >160 mmHg, GLS and LVEF were normal and relatively unchanged, but the GWI was significantly higher than that of the control group, and the GWE of patients with cardiomyopathy decreased with the decrease in GLS and LVEF. The reduced efficiency reflects impairment in ventricular function. This study demonstrated that the GWI is more sensitive than GLS and LVEF in diseases associated with abnormal cardiomyocyte metabolism. However, the normal range of GWI and GWE in the Chinese population is still unknown due to the lack of large real-world studies evaluating cardiac function in normal controls. In this study, both GWI and GWE showed a downward trend with time after chemotherapy, and a significant change occurred after the second cycle of

treatment, indicating that the use of chemotherapy drugs reduced the cardiac ejection work and the cardiac ejection work efficiency and that GWI and GWE, as corresponding measurement indicators, were sensitive to the response to chemotherapy drugs.

Evidence that 3D-STE can predict subsequent changes in 2D LVEF was first presented by Mornoş et al. (2014). In this study, 3D-GLS, 3D-GCS and 3D-GAS all decreased significantly after the second cycle of treatment, while 3D-GRS decreased after the fourth cycle, showing good consistency with the change in two-dimensional strain, and it could not be concluded that three-dimensional strain was superior to two-dimensional strain. Previous studies have found that three-dimensional ultrasound parameters (including 3D LVEF, GCS, longitudinal strain and principal strain) change more significantly than two-dimensional ultrasound parameters in breast cancer patients treated with anthracyclines, and these abnormalities persist after 2 years of follow-up (Kang and Scherrer-Crosbie, 2019). Some studies (Zhang et al., 2018) showed that the decline in the measured values of three-dimensional ultrasonic parameters was significantly correlated with the subsequent decline in LVEF, in which GLS and GCS were correlated with the changes in systolic function at the same time and thereafter. The follow-up time of this study was short, and the value of two-dimensional strain and three-dimensional strain in the evaluation of long-term prognosis needs further study.

A recent meta-study on the cardiotoxicity of anthracyclines (Nesser et al., 2009) showed that overweight and obesity were significantly associated with the risk of cardiotoxicity with anthracyclines and anti-Her-2 targeted therapy, consistent with the increased risk of higher body mass index in patients receiving anthracyclines and anthracyclines followed by trastuzumab in this study. Patients of normal weight had the lowest risk of cardiotoxicity, overweight patients had a moderate risk, and obese patients had the highest risk. Obesity was an independent risk factor for heart failure in a large epidemiological study conducted by Kenchaiah et al. (2002). Obesity can lead to excessive epicardial adipose tissue deposition and fibrosis, increase cardiac output and myocardial oxygen consumption, and increase the prevalence of heart failure (HF), especially HF with reduced ejection fraction (HFpEF) (Powell-Wiley et al., 2021), which may include left ventricular centripetal remodeling, right ventricular dilatation, and right ventricular three-compartment dysfunction. This process, combined with the toxic effect of chemotherapy drugs on the heart, makes obese patients more prone to cardiac dysfunction after chemotherapy.

Of the three groups, the results showed that the G3 group, which received anthracyclines in combination with targeted drugs, had the most significant changes in cardiac function. At present, anthracyclines are still essential in the treatment of breast cancer, but a small number of patients have been treated with targeted drugs alone. This study was limited by the patients' economic burden and medical insurance status, and only a few patients were treated with double-targeted therapy alone (trastuzumab combined with pertuzumab). Therefore, patients who were treated with single-targeted therapy alone and double-targeted therapy alone were not compared and analyzed. We will conduct a comparative study of these two treatment regimens in the following study, aiming to explore whether pertuzumab can improve the treatment effect of patients while worsening their heart function.

CONCLUSION

In tumor patients with little change in blood pressure, the predictive value of GLS on cardiac function is better than that of myocardial work parameters and 3D echocardiographic parameters. BMI, G2v and C2v were independent predictors of cardiac function impairment in breast cancer patients receiving chemotherapy, among which BMI was the best predictor. Further prospective studies in hypertensive patients are needed to evaluate the value of myocardial work parameters in predicting CTRCD.

DATA AVAILABILITY STATEMENT

The original contributions presented in the study are included in the article/**Supplementary Material**, further inquiries can be directed to the corresponding authors.

ETHICS STATEMENT

The studies involving human participants were reviewed and approved by Ethics Committee of Qilu Hospital. The patients/participants provided their written informed consent to participate in this study. Written informed consent was obtained from the individual(s) for the publication of any potentially identifiable images or data included in this article.

AUTHOR CONTRIBUTIONS

All authors listed have made a substantial, direct, and intellectual contribution to the work and approved it for publication.

SUPPLEMENTARY MATERIAL

The Supplementary Material for this article can be found online at: https://www.frontiersin.org/articles/10.3389/fphar.2021.770580/full#supplementary-material

REFERENCES

Chan, J., Edwards, N. F. A., Khandheria, B. K., Shiino, K., Sabapathy, S., Anderson, B., et al. (2019). A New Approach to Assess Myocardial Work by Non-Invasive Left Ventricular Pressure-Strain Relations in Hypertension and Dilated Cardiomyopathy. *Eur. Heart J. Cardiovasc. Imaging* 20, 31–39. doi:10.1093/ehjci/jey131

Giordano, G., Spagnuolo, A., Olivieri, N., Corbo, C., Campagna, A., Spagnoletti, I., et al. (2016). Cancer Drug Related Cardiotoxicity during Breast Cancer Treatment. *Expert Opin. Drug Saf.* 15, 1063–1074. doi:10.1080/14740338.2016.1182493

Hubert, A., Le Rolle, V., Leclercq, C., Galli, E., Samset, E., Casset, C., et al. (2018). Estimation of Myocardial Work from Pressure-Strain Loops Analysis: an Experimental Evaluation. *Eur. Heart J. Cardiovasc. Imaging* 19, 1372–1379. doi:10.1093/ehjci/jey024

Kang, Y., and Scherrer-Crosbie, M. (2019). Echocardiography Imaging of Cardiotoxicity. *Cardiol. Clin.* 37, 419–427. doi:10.1016/j.ccl.2019.07.006

Kenchaiah, S., Evans, J. C., Levy, D., Wilson, P. W., Benjamin, E. J., Larson, M. G., et al. (2002). Obesity and the Risk of Heart Failure. *N. Engl. J. Med.* 347, 305–313. doi:10.1056/NEJMoa020245

Mornoș, C., Manolis, A. J., Cozma, D., Kouremenos, N., Zacharopoulou, I., and Ionac, A. (2014). The Value of Left Ventricular Global Longitudinal Strain Assessed by Three-Dimensional Strain Imaging in the Early Detection of Anthracyclinemediated Cardiotoxicity. *Hellenic J. Cardiol.* 55, 235–244.

Negishi, T., and Negishi, K. (2018). Echocardiographic Evaluation of Cardiac Function after Cancer Chemotherapy. *J. Echocardiogr* 16, 20–27. doi:10.1007/s12574-017-0344-6

Nesser, H. J., Mor-Avi, V., Gorissen, W., Weinert, L., Steringer-Mascherbauer, R., Niel, J., et al. (2009). Quantification of Left Ventricular Volumes Using Three-Dimensional Echocardiographic Speckle Tracking: Comparison with MRI. *Eur. Heart J.* 30, 1565–1573. doi:10.1093/eurheartj/ehp187

Powell-Wiley, T. M., Poirier, P., Burke, L. E., Després, J. P., Gordon-Larsen, P., Lavie, C. J., et al. (2021). Obesity and Cardiovascular Disease: A Scientific Statement from the American Heart Association. *Circulation* 143, e984–e1010. doi:10.1161/CIR.0000000000000973

Russell, K., Eriksen, M., Aaberge, L., Wilhelmsen, N., Skulstad, H., Remme, E. W., et al. (2012). A Novel Clinical Method for Quantification of Regional Left Ventricular Pressure-Strain Loop Area: A Non-Invasive index of Myocardial Work. *Eur. Heart J.* 33, 724–733. doi:10.1093/eurheartj/ehs016

Zamorano, J. L., Lancellotti, P., Rodriguez Muñoz, D., Aboyans, V., Asteggiano, R., Galderisi, M., et al. (2016). 2016 ESC Position Paper on Cancer Treatments and Cardiovascular Toxicity Developed under the Auspices of the ESC Committee for Practice Guidelines: The Task Force for Cancer Treatments and Cardiovascular Toxicity of the European Society of Cardiology (ESC). *Eur. Heart J.* 37, 2768–2801. doi:10.1093/eurheartj/ehw211

Zeng, Q., Wang, S., Zhang, L., Li, Y., Cheng, L., Wang, J., et al. (2021). Left Ventricular Remodeling and its Progression in Asymptomatic Patients with Chronic Aortic Regurgitation: Evaluation by Speckle-Tracking Echocardiography. *J. Am. Soc. Echocardiogr* 34, 360–369. doi:10.1016/j.echo.2020.11.018

Zhang, K. W., Finkelman, B. S., Gulati, G., Narayan, H. K., Upshaw, J., Narayan, V., et al. (2018). Abnormalities in 3-Dimensional Left Ventricular Mechanics with Anthracycline Chemotherapy Are Associated with Systolic and Diastolic Dysfunction. *JACC Cardiovasc. Imaging* 11, 1059–1068. doi:10.1016/j.jcmg.2018.01.015

Conflict of Interest: The authors declare that the research was conducted in the absence of any commercial or financial relationships that could be construed as a potential conflict of interest.

frontiers in Pharmacology

ORIGINAL RESEARCH
published: 06 December 2021
doi: 10.3389/fphar.2021.770631

Case Series of Steroid-Resistant Immune Checkpoint Inhibitor Associated Myocarditis: A Comparative Analysis of Corticosteroid and Tofacitinib Treatment

Cong Wang[1†], Jinyi Lin[1†], Yan Wang[2†], David H. Hsi[3], Jiahui Chen[1], Tianshu Liu[2], Yuhong Zhou[2], Zhenggang Ren[4], Zhaochong Zeng[5], Leilei Cheng[6] and Junbo Ge[1]**

[1]Department of Cardiology, Zhongshan Hospital, Shanghai Institute of Cardiovascular Diseases, Fudan University, Shanghai, China, [2]Department of Oncology, Zhongshan Hospital, Fudan University, Shanghai, China, [3]Department of Cardiology, Stamford Hospital, Stamford, CT, United States, [4]Department of Liver Medicine, Zhongshan Hospital, Fudan University, Shanghai, China, [5]Department of Radiotherapy, Zhongshan Hospital, Fudan University, Shanghai, China, [6]Department of Echocardiography, Zhongshan Hospital, Shanghai Institute of Cardiovascular Diseases, Shanghai Institute of Medical Imaging, Fudan University, Shanghai, China

Background: Immune checkpoint inhibitor (ICI)–associated myocarditis is an uncommon and potentially fatal immune-related adverse event (irAE). Although corticosteroids are recommended as the first-line treatment by current guidelines, patients still have variable responses to it, and the guidelines vary significantly in terms of treatment strategies.

Objectives: In this study, we performed a retrospective analysis of ICI-associated myocarditis in our hospital to propose a new comparative analysis to aid individualized treatment.

Methods: We reviewed detailed records of 24 patients with confirmed ICI-associated myocarditis in our hospital from July 1, 2019, to April 1, 2021. Although all the cases in our study received recommended initial corticosteroid treatment according to the guidelines, different responses to corticosteroid were observed during the process of subsequent corticosteroid tapering. Basing on troponin cardiac troponin T rebound during corticosteroid tapering, we propose a new classification analysis of ICI-associated myocarditis that included two subgroups: corticosteroid-sensitive (n = 8) and corticosteroid-resistant group (n = 16).

Results: Compared with corticosteroid-sensitive patients, larger doses of corticosteroid, longer period of treatment, and higher mortality rate were found in corticosteroid-resistant

Abbreviations: ICIs, immune checkpoint inhibitors; CTLA-4, cytotoxic T-lymphocyte–associated antigen 4; PD-1, programmed cell death protein 1; PD-L1, programmed cell death ligand 1; irAEs, immune-related adverse events; CMR, cardiac magnetic resonance imaging; JAKs, Janus kinases; LGE, late gadolinium enhancement; CPK, creatine phosphokinase; BNP, brain natriuretic peptide; AST, aspartate aminotransferase; ALT, alanine aminotransferase; TNF-α, tumor necrosis factor α; TKI, tyrosine kinase inhibitors; STAT, signal transducer and activator of transcription

OPEN ACCESS

Edited by:
Jun Pu,
Shanghai Jiao Tong University, China

Reviewed by:
Jingzheng Zheng,
Our Lady of Lourdes Medical Center, United States
Naoka Murakami,
Brigham and Women's Hospital and Harvard Medical School, United States
Feng Qian,
University at Albany, United States

***Correspondence:**
Junbo Ge
ge.junbo2@zs-hospital.sh.cn
Leilei Cheng
cheng.leilei@zs-hospital.sh.cn

†These authors have contributed equally to this work

Specialty section:
This article was submitted to Cardiovascular and Smooth Muscle Pharmacology, a section of the journal Frontiers in Pharmacology

Received: 04 September 2021
Accepted: 10 November 2021
Published: 06 December 2021

Citation:
Wang C, Lin J, Wang Y, Hsi DH, Chen J, Liu T, Zhou Y, Ren Z, Zeng Z, Cheng L and Ge J (2021) Case Series of Steroid-Resistant Immune Checkpoint Inhibitor Associated Myocarditis: A Comparative Analysis of Corticosteroid and Tofacitinib Treatment. Front. Pharmacol. 12:770631. doi: 10.3389/fphar.2021.770631

patients. Corticosteroid-resistant patients were characterized by more prominent ptosis, muscle weakness, elevated cardiac biomarkers, creatine kinase, and hepatic enzymes levels than that in the corticosteroid-sensitive patients. Tofacitinib (5 mg twice a day) was used in 11 corticosteroid-resistant patients, with seven patients recovered from ICI-associated myocarditis, showing a promising therapeutic effect.

Conclusion: Our group analysis of corticosteroid responsiveness in patients with ICI-associated myocarditis may help clinicians to apply individualized treatment in this high-risk cohort. In addition, tofacitinib could provide clinical benefits when used early in the corticosteroid-resistant patients and may provide a new option for the treatment of ICI-associated myocarditis.

Keywords: immune checkpoint inhibitor, myocarditis, corticosteroid, tofacitinib, cardiotoxicity

INTRODUCTION

Immune checkpoint inhibitors (ICIs) including monoclonal antibodies (mAbs) against cytotoxic T-lymphocyte–associated antigen 4 (CTLA-4), programmed cell death protein 1 (PD-1), and programmed cell death ligand 1 (PD-L1) have significantly improved cancer treatment and achieved unprecedented efficacy in some types of cancer (Sasidharan Nair and Elkord, 2018; Togashi et al., 2019). Since the advent of ipilimumab (CTLA-4 mAbs), the first ICI approved by the US Food and Drug Administration (FDA) in 2011, ICIs are routinely used in clinical treatments. There are more than 1,200 ICI-associated registered trials worldwide (Topalian, 2017; Ribas and Wolchok, 2018). With the growing indications of ICIs and their fundamental role in cancer therapies, more ICI-associated side effects have drawn attention of clinicians.

The mechanisms of ICIs are based on promoting T-cell–mediated antitumor activity by targeting the intrinsic immune "brakes" (immune checkpoints). Blockade of these inhibitory pathways by targeting PD-1, PD-L1, and CTLA-4 releases the brakes of tumor-reactive T cells antitumor activity and leads to the remarkable clinical benefit (Kallies et al., 2020; Waliany et al., 2021). Unfortunately, autoreactive T cells may also be inappropriately activated by ICIs, leading to a broad spectrum of adverse events termed immune-related adverse events (irAEs). Because of their widespread effects on the immune system, irAEs can influence almost every organ, including the colon, lungs, liver, skin, thyroid, and heart (Michot et al., 2016; Postow et al., 2018). ICI-related cardiotoxicity is uncommon but characterized by a high mortality rate (Wang et al., 2018). Previous studies have reported some types of cardiovascular irAEs, including myocarditis, pericardial disease, arrhythmia, acute coronary syndrome, and vasculitis (Khunger et al., 2020; Baik et al., 2021). Since the FDA approval of ipilimumab in 2011, six more ICIs have been approved for cancer therapy including nivolumab, pembrolizumab, cemiplimab atezolizumab, avelumab, and durvalumab (Vaddepally et al., 2020). Although the incidence of ICI-associated myocarditis is merely approximately 1%, the mortality rate of myocarditis is up to 50% despite intensive treatment (Al-Kindi and Oliveira, 2018; Anquetil et al., 2018; Palaskas et al., 2020). Both cardiologists and oncologists need to be familiar with ICI-associated myocarditis and treatment options.

Because of the large variability of clinical symptoms, there is no consensus on standard regimens of ICI-associated myocarditis currently. The treatment of ICI-associated myocarditis has largely been based on the therapy of viral myocarditis (Palaskas et al., 2020). Corticosteroids are usually the first-line treatment. While the early identification of corticosteroid effect is crucial for further therapy, there have been case reports of successfully treated ICI-associated myocarditis with intravenous immunoglobulin, mycophenolate, infliximab, plasmapheresis, and alemtuzumab (Arangalage et al., 2017; Norwood et al., 2017; Frigeri et al., 2018; Esfahani et al., 2019). However, the effectiveness of these agents is still unclear because of inadequate response to corticosteroids in many patients.

Currently, the severity of ICI-associated cardiotoxicity can be divided into four grades: grade 1 is the mildest (asymptomatic with laboratory abnormalities), and grade 4 is the most severe (moderate to severe cardiac impairment and life-threatening conditions) (Brahmer et al., 2018). However, this classification system may not clearly specify response to corticosteroid therapy. Mortality rate remained high in the commonly used corticosteroid therapy (Zhang et al., 2020). In this study, we proposed a new classification for ICI-associated myocarditis including two subgroups: corticosteroid-sensitive and corticosteroid-resistant group, according to the clinical presentations and outcomes, to guide the individualized treatment options. In this study, tofacitinib treatment was used in 11 cases of ICI-associated myocarditis who responded poorly to corticosteroid and immunosuppressive regiments. Tofacitinib demonstrated promising treatment effects for ICI-associated myocarditis.

METHODS

Patient Selection

This retrospective study was conducted in Zhongshan Hospital of Fudan University. We identified patients who received ICI treatment between July 2019 and April 2021. The inclusion criteria are as follows: (1) definitive diagnosis of myocarditis

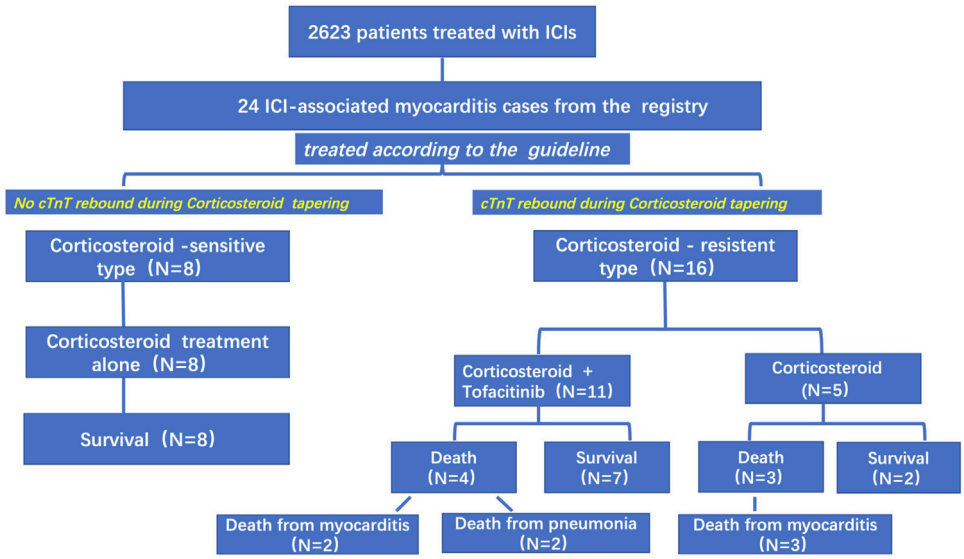

FIGURE 1 | Treatment for ICI-associated myocarditis. Based on the response to corticosteroids (troponin cTnT levels rebounding or not during corticosteroid tapering), we divided patients with ICI-associated myocarditis into corticosteroid-sensitive and corticosteroid-resistant groups.

such as abnormal cardiac magnetic resonance imaging (CMR), clinical syndrome of myocarditis, and positive biomarkers; (2) complete medical history and follow-up; and (3) endpoint events—cardiac recovery or death. Data extracted from the medical records included demographics, clinical presentation, medical treatment for myocarditis, laboratory data, discontinuation or withholding of ICIs, and patients' clinical outcomes. The study was approved by the Zhongshan Hospital Institutional Review Board.

Treatment and Evaluation

Once the diagnosis of myocarditis was identified, all patients in our study received recommended corticosteroid treatment according to the current guidelines (Brahmer et al., 2018; Haanen et al., 2018). To be specific, in mild cases (grade 1–2), 1 to 2 mg/kg methylprednisolone was given intravenously. The tapering period lasted for 4 to 6 weeks. For moderate to severe decompensation cases (grade 3–4), pulse therapy was administered by giving methylprednisolone 500 to 1,000 mg/d plus either antithymocyte globulin or other immune suppressants such as infliximab. For subsequent corticosteroid tapering, methylprednisolone was used 1 to 2 mg/kg/day for 3 days and then reduced by 10 to 20 mg every 3 to 5 days to 40 mg before changing into oral prednisolone finally. For pulse therapy, methylprednisolone was used in order of decreasing doses as follows: 500 mg for 3 days, 240 mg for 3 days, 120 mg for 3 days, 80 mg for 3 days, 60 mg for 3 days, and 40 mg for 3 days and then changed into oral prednisolone.

Janus kinase (JAK) pathway inhibitor tofacitinib was used in patients whose cardiac troponin T (cTnT) levels started to increase during corticosteroid tapering. We monitored patients closely by measuring troponin, creatine kinase, and renal and liver function every day or every other day. After reaching the plateau, these indicators were checked every 2 weeks together with electrocardiogram and echocardiography. Standard myocardial protection and antimyocardial remodeling medications such as coenzyme Q10, β-blockers, angiotensin-converting enzyme inhibitors, or angiotensin II receptor blockers were used in all patients with ICI-associated myocarditis. We tried to titrate all medications to the target dosages.

Statistical Analysis

Kaplan–Meier method was utilized to estimate the overall survival and differences in survival curves between the corticosteroid-sensitive and corticosteroid-resistant groups. Differences between groups were tested by Student *t* test. All statistical tests were two-sided with an α level of 0.05. Statistical analysis was performed by using SPSS version 19.

RESULTS

Baseline Characteristics

From July 1, 2019, to April 1, 2021, 2,623 patients in our center were treated with PD-1 or PD-L1 mAbs (**Figure 1**). Based on the inclusion criteria, 24 ICI-associated myocarditis patients (16 males and 8 females) were included in this study. ICI agents applied included pembrolizumab, toripalimab, sintilimab, cadonilimab, durvalumab and camrelizumab. Among them, four patients were treated with ICIs only while 20 patients were treated with ICIs plus chemotherapy or radiation therapy. Demographic and baseline clinical characteristics of these patients are presented in **Table 1**. The most common cancer diagnosis was gastric, hepatic, and colorectal cancer. All patients were in the stage 3 to 4 of cancer. The most common initial clinical presentation in our cohort was malaise, followed by

TABLE 1 | Baseline characteristics in patients with ICI-associated myocarditis.

Case	Age	Gender	Malignancy	Onset symptoms	Cardiovascular complications	Associated irAEs	ECG	TTE	CMR
1	66	Male	Gastric carcinoma	Asymptomatic	Atrial fibrillation	Creatine kinase elevation	Atrial fibrillation	Atrial enlargement, mild mitral regurgitation	Local edema and LGE
2	72	Male	Gastric carcinoma	Asymptomatic		Creatine kinase elevation	RBBB	No significant abnormality	Local edema and LGE
3	70	Female	Hepatic carcinoma	Asymptomatic		Creatine kinase elevation	Sinus rhythm	No significant abnormality	Local edema
4	67	Male	Hepatic carcinoma	Asymptomatic		Creatine kinase elevation	Sinus rhythm	Ventricular septal hypertrophy	Ventricular septal hypertrophy
5	66	Female	Colorectal carcinoma	Asymptomatic	Coronary artery fistula		Sinus rhythm	No significant abnormality	
6	72	Male	Lung carcinoma	Asymptomatic			Atrial premature beats	Aortic regurgitation	Local edema and LGE
7	63	Male	Gastric carcinoma	Asymptomatic			Sinus bradycardia	BAV	Local edema and LGE
8	38	Female	Leiomyosarcoma	Asymptomatic			Sinus tachycardia	No significant abnormality	Local edema and LGE
9	71	Male	Gastric carcinoma	Ptosis, muscle soreness, malaise		Creatine kinase elevation	Atrial premature beats	Dilated aorta	Local edema and LGE
10	68	Female	Hodgkin lymphoma, breast carcinoma	Chest congestion	Hypertension	Creatine kinase elevation	Atrial premature beats	No significant abnormality	Local LGE
11	57	Female	Cervical carcinoma	Chest congestion		Thyroiditis	ST changes	LVEF <50%	Wide LGE
12	65	Male	Head-neck carcinoma	Malaise		Creatine kinase elevation	T changes	Atrial enlargement, dilated aorta	Local edema and LGE
13	54	Male	Colorectal carcinoma	Malaise		Hepatitis	ST changes	Atrial enlargement	Local edema and LGE
14	63	Female	Gastric carcinoma	Ptosis, malaise		Creatine kinase elevation	T changes	Mild mitral regurgitation	No significant inflammation
15	71	Female	Esophageal carcinoma	Ptosis, muscle soreness		Creatine kinase elevation	First-degree AV block	No significant abnormality	
16	63	Female	Malignant melanoma	Ptosis, malaise		Creatine kinase elevation	Sinus rhythm	No significant abnormality	No significant inflammation
17	58	Male	Gastric carcinoma	Ptosis, malaise		Creatine kinase elevation	RBBB	LVEF <50%	
18	60	Male	Esophageal carcinoma	Malaise		Creatine kinase elevation	Sinus rhythm	Minimal pericardial effusion	Local edema
19	59	Male	Colorectal carcinoma	Ptosis, malaise	Hypertension	Creatine kinase elevation	Sinus rhythm	Atrial enlargement	Local edema and LGE
20	66	Male	Hepatic carcinoma	malaise		Creatine kinase elevation	ST changes	Dilated aorta; mild aortic regurgitation	Local edema and LGE
21	65	Male	Lung carcinoma	Ptosis, malaise			RBBB; ST changes; ventricular premature beat	Minimal pericardial effusion	Local edema and LGE
22	77	Male	Hepatic carcinoma	Ptosis, malaise	Hypertension	Creatine kinase elevation	Sinus tachycardia; first-degree AV block	Atrial enlargement	
23	53	Male	Hepatic carcinoma	Chest congestion, malaise		Creatine kinase elevation	Sinus tachycardia	Atrial enlargement	Local edema and LGE

(Continued on following page)

TABLE 1 | (*Continued*) Baseline characteristics in patients with ICI-associated myocarditis.

Case	Age	Gender	Malignancy	Onset symptoms	Cardiovascular complications	Associated irAEs	ECG	TTE	CMR
24	41	Male	Hepatic carcinoma	malaise		Creatine kinase elevation	Sinus tachycardia; ST changes	LVEF <50%; moderate mitral regurgitation	Wide LGE

BAV, bicuspid aortic valve; ECG, electrocardiogram; LVEF, left ventricular ejection fraction; RBBB, right bundle-branch block; TTE, transthoracic echocardiogram.

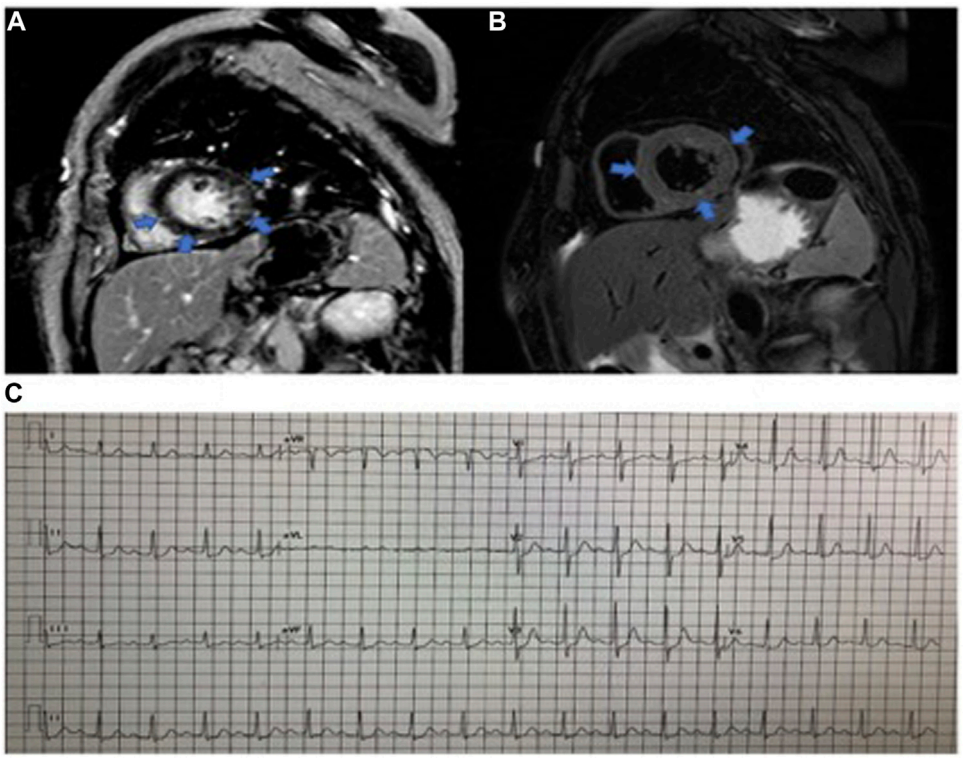

FIGURE 2 | Cardiac magnetic resonance imaging of myocarditis. **(A)** LGE image of fibrosis. **(B)**. Precontrast T2-weighted image of the same slice location as the image in the same patient. **(C)**. Eelectrocardiogram abnormalities: the prolongation of the PR interval, sinus tachycardia, and ST changes.

chest congestion, muscular soreness, and ptosis. Electrocardiographic abnormalities were detected in 18 patients (75%) including atrial or ventricular premature beats, sinus tachycardia, sinus bradycardia, ST-T changes, and atrial fibrillation. No patients had high-grade atrioventricular block or malignant arrhythmia. Echocardiographic abnormalities, such as left ventricular hypertrophy, left atrial enlargement, and valvular regurgitation, were detected in 11 patients. The most common CMR finding was late gadolinium enhancement (LGE), whereas functional abnormalities were detected in three patients (**Figure 2**).

The Comparative Analysis Based on Corticosteroid Responsiveness

Although all the cases in this study received recommended initial corticosteroid treatment according to the guidelines (Brahmer et al., 2018; Haanen et al., 2018), different responses to corticosteroid were observed in subsequent tapering. Troponin cTnT levels of eight patients gradually decreased accompanied by decrement of corticosteroid. However, the levels of troponin cTnT rebounded in 16 patients during corticosteroid tapering despite symptomatic remission after the initial treatment.

Based on troponin cTnT rebound during corticosteroid tapering, we classified patients with ICI-associated myocarditis into two subgroups: (1) corticosteroid-resistant ICI-associated myocarditis: troponin cTnT rebound during corticosteroid tapering; and (2) corticosteroid-sensitive ICI-associated myocarditis: no troponin cTnT rebound during corticosteroid tapering.

Eight corticosteroid-sensitive patients responded favorably to the treatment evidenced by gradually troponin cTnT decreasing, smooth corticosteroid tapering, and shorter treatment time. In 16 corticosteroid-resistant patients, troponin cTnT increased

TABLE 2 | Treatment of 24 patients with ICI-associated myocarditis.

Case	ICIs	Time to onset (days)	Combined anticancer drug	Combined therapy	Initial cTnT (ng/mL) (<0.003 ng/mL)	Time to corticosteroid treatment (days)	Initial corticosteroid dose	Total intravenous corticosteroid dose (mg)	Time to cTNT recovery (days)	Time to corticosteroid finished (days)	Outcome
1	Camrelizumab (anti–PD-1)	14	Oxaliplatin + 5-fluorouracil		0.094	5	Methylprednisolone 160 mg	1,280	51	72	Improved
2	Camrelizumab (anti–PD-1)	14			0.1	19	Methylprednisolone 120 mg	660	100	86	Improved
3	Sintilimab (anti–PD-1)	21			0.229	9	Methylprednisolone 80 mg	600	97	68	Improved
4	Pembrolizumab (anti–PD-1)	21			0.182	1	Methylprednisolone 50 mg	950	34	60	Improved
5	Pembrolizumab (anti–PD-1)	42	Regorafenib		0.033	5	Methylprednisolone 120 mg	930	27	61	Improved
6	Sintilimab (anti–PD-1	21	Paclitaxel + cisplatin		0.086	2	Methylprednisolone 40 mg	200	5	51	Improved
7	Cadonilimab (anti–PD-1/CTLA-4)	56	Oxaliplatin + capecitabine		0.05	2	Methylprednisolone 120 mg	540	3	65	Improved
8	Sintilimab (anti–PD-1)	63	Eribulin		0.136	7	Methylprednisolone 120 mg	540	5	67	Improved
9	Camrelizumab (anti–PD-1)	28	Oxaliplatin + capecitabine	Immunoglobulin + tofacitinib	0.507	1	Methylprednisolone 500 mg	3,090	104	107	Improved
10	Sintilimab (anti–PD-1)	21		Immunoglobulin + tofacitinib + plasmapheresis	0.508	8	Methylprednisolone 500 mg	2,880			Death from pneumonia
11	Pembrolizumab (anti–PD-1)	147	Bevacizumab + paclitaxel + cisplatin		0.328	6	Methylprednisolone 240 mg	1,660			Death from myositis progression
12	Toripalimab (anti–PD-1)	14	Gemcitabine	Infliximab 500 mg	0.072	1	Methylprednisolone 500 mg	4,000			Death from myositis progression
13	Camrelizumab (anti–PD-1)	28	Fruquintinib	Immunoglobulin + tofacitinib	0.048	2	Methylprednisolone 500 mg	3,120			Death from myositis progression
14	Camrelizumab (anti–PD-1)	42		Immunoglobulin + tofacitinib	0.348	6	Methylprednisolone 500 mg	3,330	118	121	Improved
15	Camrelizumab (anti–PD-1)	14	Paclitaxel		0.332	6	Methylprednisolone 80 mg	320			Death from myositis progression
16	Toripalimab (anti–PD-1	28		Immunoglobulin + tofacitinib	1.44	1	Methylprednisolone 40 mg	240	93	87	Improved
17	Camrelizumab (anti–PD-1)	14	Apatinib	Immunoglobulin + tofacitinib	2.09	10	Methylprednisolone 500 mg	3,500			Death from pneumonia
18	Cadonilimab (anti–PD-1/CTLA-4)	42		Immunoglobulin + tofacitinib	0.113	16	Methylprednisolone 500 mg	3,000	64	70	Improved
19	Pembrolizumab (anti–PD-1)	21	Fruquintinib	Immunoglobulin + tofacitinib	0.165	1	Methylprednisolone 240 mg	1,500	106	111	Improved
20	Pembrolizumab (anti–PD-1)	21	Lenvatinib	Tofacitinib	0.06	2	Methylprednisolone 80 mg	1,500	50	69	Improved
21	Sintilimab (anti–PD-1)	42	Cisplatin + docetaxel	Immunoglobulin	0.731	11	Methylprednisolone 200 mg	2,320	70	91	Improved
22	Toripalimab (anti–PD-1)	14	Bevacizumab	Immunoglobulin + tofacitinib	2.86	1	Methylprednisolone 500 mg	3,360			Death from myositis progression
23	Sintilimab (anti–PD-1)	63	Lenvatinib	Tofacitinib	0.403	21	Methylprednisolone 60 mg	540	55	70	Improved
24	Durvalumab (anti–PD-L1)	42	Bevacizumab	Immunoglobulin	0.122	2	Methylprednisolone 500 mg	3,900	62	98	Improved

again and required high-dose corticosteroid regimen with rapid tapering. Troponin cTnT rebound often occurred during second to third corticosteroid tapering. In this study, the initial methylprednisolone doses of corticosteroid-sensitive patients were approximately 1 to 2 mg/kg per day, and total intravenous dose was less than 1,500 mg. For corticosteroid-resistant patients, initial methylprednisolone dose was usually 500 mg, and total intravenous dose was much higher than that in the corticosteroid sensitive-group (**Table 2**).

In addition, infliximab (500 mg in one patient) and tofacitinib (5 mg twice a day in 11 patients) were used in corticosteroid-resistant patients. Interestingly, tofacitinib achieved a satisfactory therapeutic effect. Seven patients received tofacitinib treatment recovered from ICI-associated myocarditis, whereas two patients died of severe pneumonia, and the other two patients died of myocarditis progression.

Differences Between Two Groups

There is no significant difference of age and gender between corticosteroid-sensitive and corticosteroid-resistant group. According to the American Society of Clinical Oncology guidelines (Brahmer et al., 2018), myocarditis severity in corticosteroid-sensitive group was between grade 1 and grade 2. For corticosteroid-resistant group, grades of severity were between grade 2 and grade 3. Patients in the corticosteroid-resistant group had frequent symptoms of chest congestion, muscular soreness, and ptosis. Biomarkers troponin cTnT and creatine phosphokinase (CPK) were increased more significantly in the corticosteroid-resistant group than in the corticosteroid-sensitive group (**Table 3**). Our data revealed that corticosteroid-resistant patients have more complications such as myositis and autoimmune hepatitis. Therefore, the levels of aspartate aminotransferase (AST), alanine aminotransferase (ALT), and C-reactive protein were increased more in corticosteroid-resistant patients than in corticosteroid-sensitive group patients.

Survival

All eight corticosteroid-sensitive patients recovered from ICI-associated myocarditis. In the corticosteroid-resistant group, nine patients recovered from ICI-associated myocarditis (recovery rate = 56.3%), whereas the other seven patients died. The reason of death could be listed as follows: two patients died of septic shock due to severe pneumonia, and five patients died of cardiogenic shock due to the progression of myocarditis. Comparison of survival curves using log-rank test demonstrated a higher mortality in corticosteroid-resistant patients than that in the corticosteroid-sensitive patients ($p = 0.01$) (**Figure 3**).

DISCUSSION

In this study, we reported 24 ICI-associated myocarditis patients and analyzed some important clinical parameters. Based on the response to corticosteroids (troponin cTnT levels rebounding or not during corticosteroid tapering), we divided ICI-associated myocarditis patients into corticosteroid-sensitive and corticosteroid-resistant group. Corticosteroid-resistant patients could benefit from tofacitinib treatment. This illustrated the heterogeneity in etiology and pathophysiology in these patients. Response to corticosteroid treatment may predict the prognosis, guide the corticosteroid doses, and initiate additional immune suppression therapy (**Table 4**).

Previously, ICI-associated myocarditis had been reported with an incidence of 0.03% to 1.14% (Mahmood et al., 2018; Salem et al., 2018). Recent studies have indicated an increase in its incidence, which may be related to the expanding use of ICIs (Al-Kindi and Oliveira, 2018; Salem et al., 2018). Up until now, the precise mechanisms of ICI-associated myocarditis remain unclear. Suggested possibilities include shared antigens between the tumor and myocardium, T-cell receptor targeting homologous muscle antigen as the tumor antigen, or certain T-cell receptors targeting dissimilar antigens (Lv et al., 2011; Johnson et al., 2016; Khunger et al., 2020). Thus, T cells targeting the shared epitopes between tumor and myocardium may exist, and the ICIs can augment the T-cell effector function, resulting in the development of autoimmune myocarditis (Müller et al., 2018; Tocchetti et al., 2018). The degree and spectrum of inflammation may account for the variable clinical presentations and treatment effects.

The treatment of ICI-associated myocarditis has largely been based on the corticosteroids. According to the recommendations of the Society for Immunotherapy of Cancer, four grades of cardiovascular irAEs have been defined and used to guide initial corticosteroid doses (Puzanov et al., 2017). It is still difficult to predict the prognosis even if high-dose corticosteroid regimen was used. cTnT is a cardiac-specific biomarker of ongoing myocardial inflammation in myocarditis. Therefore, monitoring the changes of troponin T levels provides a reliable way to assess clinical situation in ICI-associated myocarditis cases. We would like to point out that our classification is based on the change of cTnT levels rather than the initial cTnT levels. As shown in **Figure 4**, two cases from the corticosteroid-resistant group had initial cTnT levels of less than 0.1 ng/mL, whereas the cTnT levels rebounded remarkably during corticosteroid tapering. Therefore, troponin cTnT rebound during corticosteroid tapering probably reflected ongoing myocardial inflammation and necrosis.

Once ICI-associated myocarditis was diagnosed, we used intravenous methylprednisolone 1 to 2 mg/kg daily before transition to oral prednisone 1 to 2 mg/kg per day followed by tapering doses over several weeks for corticosteroid-sensitive patients. For corticosteroid-resistant patients, we recommend intravenous methylprednisolone 500 mg daily before transition to oral prednisone 1 to 2 mg/kg daily. Other immunosuppressants were used in different centers including mycophenolate mofetil, antithymocyte globulin, and intravenous immunoglobulin (Arangalage et al., 2017; Norwood et al., 2017; Tay et al., 2017). One additional option for immunosuppression is the chimeric immunoglobulin G mAb to tumor necrosis factor α (TNF-α), named infliximab. By binding to TNF-α, a major proinflammatory cytokine, infliximab, leads to the downregulation of other cytokines and induces the apoptosis of TNF-producing cells, including T lymphocytes (Frigeri et al., 2018; Khunger et al., 2020). One of our corticosteroid-sensitive

TABLE 3 | Comparison of corticosteroid-sensitive and corticosteroid-resistant ICI-associated myocarditis patients.

Characteristics	Corticosteroid-sensitive (n = 8)	Corticosteroid-resistant (n = 16)	*p*
Age (years)	64.3 ± 3.9	61.9 ± 2.1	NS
Gender (M/F)	5/3	11/5	NS
ST2 (ng/mL)	69.1 ± 14.2	116.9 ± 31.1	NS
BNP (pg/mL)	244.0 ± 94.8	1,498.4 ± 531.3	NS
cTNT (ng/mL)	0.11 ± 0.02	0.63 ± 0.2	<0.05
CK (U/L)	384.6 ± 139.2	2,326.8 ± 654.4	<0.05
CKMB (U/L)	33.1 ± 7.5	125.9 ± 26.8	<0.05
CKMM (U/L)	351.4 ± 135.5	2,361.1 ± 665.0	<0.05
ALT (U/L)	33.3 ± 9.2	144.6 ± 28.3	<0.05
AST (U/L)	48.0 ± 11.9	182.8 ± 46.2	<0.05
CRP (mg/L)	4.4 ± 1.8	64.4 ± 25.2	<0.05

BNP, brain natriuretic peptide; CK, creatine kinase; NS, no significance; ST2, suppression of tumorigenicity 2.

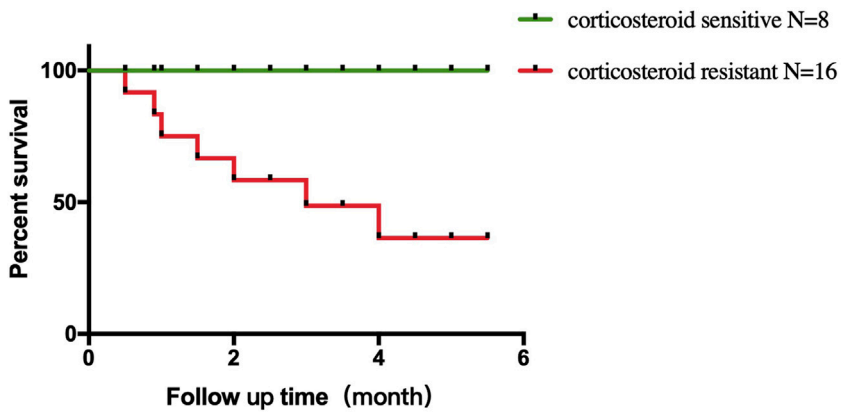

FIGURE 3 | Comparison of survival curves. Higher mortality in corticosteroid-resistant patients compared with corticosteroid-sensitive patients.

TABLE 4 | ICI-associated myocarditis: corticosteroid-sensitive and corticosteroid-resistant sub-type.

	Corticosteroid-sensitive	Corticosteroid-resistant
Characteristic	cTnT decrease during reduction of corticosteroid dose	cTnT rebound during reduction of corticosteroid dose
Symptoms	Asymptomatic or mild symptoms	Ptosis, muscle soreness, malaise
Laboratory tests	Mild to moderate increase of myocardial injury biomarker, hepatic enzymes, CPK, inflammation biomarker	Significant increase of myocardial injury biomarker, hepatic enzymes, CPK, inflammation biomarker
CMR	No significant abnormality	Edema and LGE
Treatment initial corticosteroid dose	Methylprednisolone 1–2 mg/kg per day	Methylprednisolone 500 mg × 3 days
Additional therapy		Tofacitinib 5 mg bid

patients and five corticosteroid-resistant patients received combined ICI agents and tyrosine kinase inhibitor (TKI) treatment. There is a strong impetus for combining TKI and ICI, given their complementary response profile and synergy in generating antitumor immunity. It has been demonstrated that ICI in conjunction with TKI enhanced efficacy in multiple tumor types (Ascierto et al., 2019; Rini et al., 2019). As both agents could cause cardiotoxicities, it is therefore possible that a higher rate of cardiotoxicity might be observed with combination regimens. Future clinical trials combining ICI and TKI should prospectively assess biomarkers of cardiotoxicity for better clinical understanding and comprehensive assessment.

Compared with traditional treatment modalities, we studied tofacitinib with interesting results. It is a JAK inhibitor, which blocks the production of proinflammatory cytokines through the suppression of JAK–signal transducer and activator of transcription (STAT) signal pathway (Angelini et al., 2020; Hosseini et al., 2020). It has been already used for rheumatoid arthritis, psoriatic arthritis, and ulcerative colitis (Moura and Fonseca, 2020; Chimenti et al., 2021). Increased expression of phosphorylated proteins of JAK-STAT

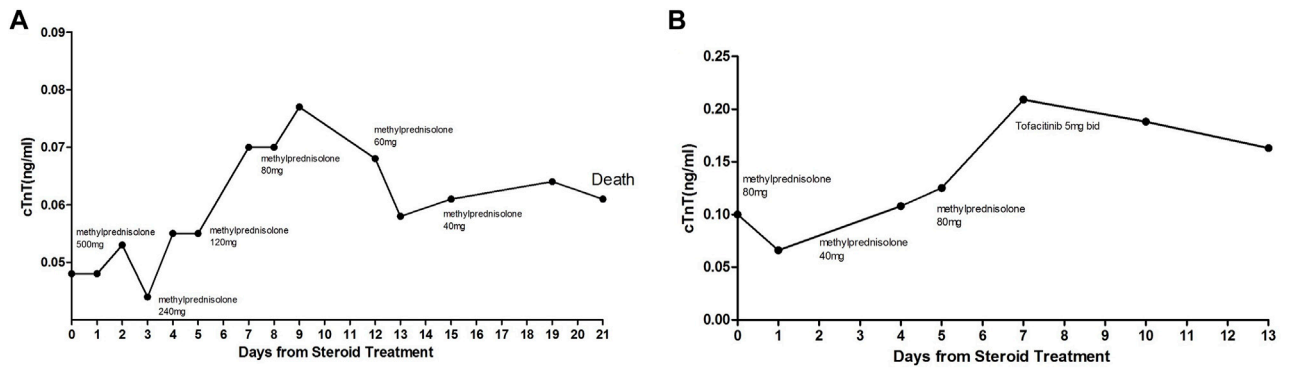

FIGURE 4 | Two cases from the corticosteroid-resistant group. Initial cTnT levels were less than 0.1 ng/mL; however, cTnT levels rebounded significantly during corticosteroid tapering.

pathway was observed in rat autoimmune myocarditis model; while being treated with JAK inhibitor, the cardiac function and myocardial inflammation were alleviated (Liu et al., 2016). A previous study proved that JAK/STAT signaling pathway played a vital role in the tumorigenesis and could promote tumor evasion by conferring high PD-L1 expression on tumor cells (Luo et al., 2018; Song et al., 2018). Therefore, targeting JAK/STAT pathway might also have a synergistic antitumor effect of ICI therapy. Tofacitinib was the first small molecule JAK inhibitor; it reversibly and competitively binds to the ATP binding site of the kinase domain of JAK (Flanagan et al., 2010). Compared with specific inflammatory pathway mAb, tofacitinib is a pan-JAK inhibitor, effecting JAK1, JAK2, JAK3, TYK2, IL-6, and type I interferons (Fernández-Clotet et al., 2018). Given the potential risks of inflammatory cytokine storm in corticosteroid-resistant patients, it is reasonable to observe the favorable results after tofacitinib treatment. Therefore, our findings may provide a new option for clinical treatment of refractory myocarditis confirmed by other investigators.

LIMITATION

Significant differences of clinical symptoms and laboratory and imaging tests could be observed between the two groups. Because of the limited cases, we were unable to construct a scoring system to predict the efficacy of corticosteroid therapy. Our initial experience was from a small and retrospective study without comparison to other possible treatment regimens. To confirm the validity of myocarditis treatment strategies in corticosteroid-sensitive and corticosteroid-resistant groups, a prospective and randomized clinical trial enrolling large patient samples will be of critical importance in the future.

CONCLUSION

Corticosteroid responsiveness in patients with ICI-associated myocarditis may guide clinicians to provide targeted treatment in this high-risk cohort. Based on our retrospective study, tofacitinib could offer additional clinical benefits when being used early in the corticosteroid-resistant patients and provide a new option for the treatment of ICI-associated myocarditis.

Clinical Perspectives: This new group analysis for ICI-associated myocarditis may guide individualized therapies in this high-risk population. Tofacitinib treatment may have impactful clinical benefits when being used early in corticosteroid-resistant patients.

DATA AVAILABILITY STATEMENT

The raw data supporting the conclusion of this article will be made available by the authors, without undue reservation.

ETHICS STATEMENT

The studies involving human participants were reviewed and approved by Zhongshan Hospital Fudan University. The patients/participants provided their written informed consent to participate in this study. Written informed consent was obtained from the individual(s) for the publication of any potentially identifiable images or data included in this article.

AUTHOR CONTRIBUTIONS

CW and JL: conception, design and interpretation of data; CW and YW: drafting of the manuscript; JC, YZ, and ZR: analysis and interpretation of data; DH, ZZ, and TL: revising the manuscript critically for important intellectual content; LC and JG: final approval of the manuscript submitted.

FUNDING

This study was supported by the National Natural Science Foundation of China (No. 81800349), Shanghai sailing program (18YF1404100), Clinical Research Project of Zhongshan Hospital (2020ZSLC21) and Smart medical treatment project of Zhongshan Hospital (2020ZHZS16).

REFERENCES

Al-Kindi, S. G., and Oliveira, G. H. (2018). Reporting of Immune Checkpoint Inhibitor-Associated Myocarditis. *Lancet* 392, 382–383. doi:10.1016/S0140-6736(18)31542-3

Angelini, J., Talotta, R., Roncato, R., Fornasier, G., Barbiero, G., Dal Cin, L., et al. (2020). JAK-inhibitors for the Treatment of Rheumatoid Arthritis: A Focus on the Present and an Outlook on the Future. *Biomolecules* 10, 1002. doi:10.3390/biom10071002

Anquetil, C., Salem, J. E., Lebrun-Vignes, B., Johnson, D. B., Mammen, A. L., Stenzel, W., et al. (2018). Immune Checkpoint Inhibitor-Associated Myositis: Expanding the Spectrum of Cardiac Complications of the Immunotherapy Revolution. *Circulation* 138, 743–745. doi:10.1161/CIRCULATIONAHA.118.035898

Arangalage, D., Delyon, J., Lermuzeaux, M., Ekpe, K., Ederhy, S., Pages, C., et al. (2017). Survival after Fulminant Myocarditis Induced by Immune-Checkpoint Inhibitors. *Ann. Intern. Med.* 167, 683–684. doi:10.7326/L17-0396

Ascierto, P. A., Ferrucci, P. F., Fisher, R., Del Vecchio, M., Atkinson, V., Schmidt, H., et al. (2019). Dabrafenib, Trametinib and Pembrolizumab or Placebo in BRAF-Mutant Melanoma. *Nat. Med.* 25, 941–946. doi:10.1038/s41591-019-0448-9

Baik, A., Tsai, K., Oh, D., and Aras, M. (2021). Mechanisms and Clinical Manifestations of Cardiovascular Toxicities Associated with Immune Checkpoint Inhibitors. *Clin. Sci. (Lon).* 135, 703–724. doi:10.1042/CS20200331

Brahmer, J. R., Lacchetti, C., Schneider, B. J., Atkins, M. B., Brassil, K. J., Caterino, J. M., et al. (2018). Management of Immune-Related Adverse Events in Patients Treated with Immune Checkpoint Inhibitor Therapy: American Society of Clinical Oncology Clinical Practice Guideline. *J. Clin. Oncol.* 36, 1714–1768. doi:10.1200/JCO.2017.77.6385

Chimenti, M. S., Conigliaro, P., Biancone, L., and Perricone, R. (2021). Update on the Therapeutic Management of Patients with Either Psoriatic Arthritis or Ulcerative Colitis: Focus on the JAK Inhibitor Tofacitinib. *Ther. Adv. Musculoskelet. Dis.* 13, 1759720X20977777. doi:10.1177/1759720X20977777

Esfahani, K., Buhlaiga, N., Thébault, P., Lapointe, R., Johnson, N. A., and Miller, W. H. (2019). Alemtuzumab for Immune-Related Myocarditis Due to PD-1 Therapy. *N. Engl. J. Med.* 380, 2375–2376. doi:10.1056/NEJMc1903064

Fernández-Clotet, A., Castro-Poceiro, J., and Panés, J. (2018). Tofacitinib for the Treatment of Ulcerative Colitis. *Expert Rev. Clin. Immunol.* 14, 881–892. doi:10.1080/1744666X.2018.1532291

Flanagan, M. E., Blumenkopf, T. A., Brissette, W. H., Brown, M. F., Casavant, J. M., Shang-Poa, C., et al. (2010). Discovery of CP-690,550: a Potent and Selective Janus Kinase (JAK) Inhibitor for the Treatment of Autoimmune Diseases and Organ Transplant Rejection. *J. Med. Chem.* 53, 8468–8484. doi:10.1021/jm1004286

Frigeri, M., Meyer, P., Banfi, C., Giraud, R., Hachulla, A. L., Spoerl, D., et al. (2018). Immune Checkpoint Inhibitor-Associated Myocarditis: A New Challenge for Cardiologists. *Can. J. Cardiol.* 34, 92–e3. doi:10.1016/j.cjca.2017.09.025

Haanen, J. B. A. G., Carbonnel, F., Robert, C., Kerr, K. M., Peters, S., Larkin, J., et al. (2018). Management of Toxicities from Immunotherapy: ESMO Clinical Practice Guidelines for Diagnosis, Treatment and Follow-Up. *Ann. Oncol.* 29, iv264–iv266. doi:10.1093/annonc/mdy162

Hosseini, A., Gharibi, T., Marofi, F., Javadian, M., Babaloo, Z., and Baradaran, B. (2020). Janus Kinase Inhibitors: A Therapeutic Strategy for Cancer and Autoimmune Diseases. *J. Cel Physiol* 235, 5903–5924. doi:10.1002/jcp.29593

Johnson, D. B., Balko, J. M., Compton, M. L., Chalkias, S., Gorham, J., Xu, Y., et al. (2016). Fulminant Myocarditis with Combination Immune Checkpoint Blockade. *N. Engl. J. Med.* 375, 1749–1755. doi:10.1056/NEJMoa1609214

Kallies, A., Zehn, D., and Utzschneider, D. T. (2020). Precursor Exhausted T Cells: Key to Successful Immunotherapy? *Nat. Rev. Immunol.* 20, 128–136. doi:10.1038/s41577-019-0223-7

Khunger, A., Battel, L., Wadhawan, A., More, A., Kapoor, A., and Agrawal, N. (2020). New Insights into Mechanisms of Immune Checkpoint Inhibitor-Induced Cardiovascular Toxicity. *Curr. Oncol. Rep.* 22, 65. doi:10.1007/s11912-020-00925-8

Liu, X., Zhang, X., Ye, L., and Yuan, H. (2016). Protective Mechanisms of Berberine against Experimental Autoimmune Myocarditis in a Rat Model. *Biomed. Pharmacother.* 79, 222–230. doi:10.1016/j.biopha.2016.02.015

Luo, N., Formisano, L., Gonzalez-Ericsson, P. I., Sanchez, V., Dean, P. T., Opalenik, S. R., et al. (2018). Melanoma Response to Anti-PD-L1 Immunotherapy Requires JAK1 Signaling, but Not JAK2. *Oncoimmunology* 7, e1438106. doi:10.1080/2162402X.2018.1438106

Lv, H., Havari, E., Pinto, S., Gottumukkala, R. V., Cornivelli, L., Raddassi, K., et al. (2011). Impaired Thymic Tolerance to α-myosin Directs Autoimmunity to the Heart in Mice and Humans. *J. Clin. Invest.* 121, 1561–1573. doi:10.1172/JCI44583

Mahmood, S. S., Fradley, M. G., Cohen, J. V., Nohria, A., Reynolds, K. L., Heinzerling, L. M., et al. (2018). Myocarditis in Patients Treated with Immune Checkpoint Inhibitors. *J. Am. Coll. Cardiol.* 71, 1755–1764. doi:10.1016/j.jacc.2018.02.037

Michot, J. M., Bigenwald, C., Champiat, S., Collins, M., Carbonnel, F., Postel-Vinay, S., et al. (2016). Immune-related Adverse Events with Immune Checkpoint Blockade: a Comprehensive Review. *Eur. J. Cancer*, 54, 139–148. doi:10.1016/j.ejca.2015.11.016

Moura, R. A., and Fonseca, J. E. (2020). JAK Inhibitors and Modulation of B Cell Immune Responses in Rheumatoid Arthritis. *Front. Med. (Lausanne).* 7, 607725. doi:10.3389/fmed.2020.607725

Müller, O., Spehlmann, M., and Frey, N. (2018). Cardio-toxicity of Checkpoint Inhibitors. *J. Thorac. Dis.* 10, S4400–S4404. doi:10.21037/jtd.2018.12.78

Norwood, T. G., Westbrook, B. C., Johnson, D. B., Litovsky, S. H., Terry, N. L., McKee, S. B., et al. (2017). Smoldering Myocarditis Following Immune Checkpoint Blockade. *J. Immunother. Cancer* 5, 91. doi:10.1186/s40425-017-0296-4

Palaskas, N., Lopez-Mattei, J., Durand, J. B., Iliescu, C., and Deswal, A. (2020). Immune Checkpoint Inhibitor Myocarditis: Pathophysiological Characteristics, Diagnosis, and Treatment. *J. Am. Heart Assoc.* 9, e013757. doi:10.1161/JAHA.119.013757

Postow, M. A., Sidlow, R., and Hellmann, M. D. (2018). Immune-Related Adverse Events Associated with Immune Checkpoint Blockade. *N. Engl. J. Med.* 378, 158–168. doi:10.1056/NEJMra1703481

Puzanov, I., Diab, A., Abdallah, K., Bingham, C. O., Brogdon, C., Dadu, R., et al. (2017). Managing Toxicities Associated with Immune Checkpoint Inhibitors: Consensus Recommendations from the Society for Immunotherapy of Cancer (SITC) Toxicity Management Working Group. *J. Immunother. Cancer* 5, 95. doi:10.1186/s40425-017-0300-z

Ribas, A., and Wolchok, J. D. (2018). Cancer Immunotherapy Using Checkpoint Blockade. *Science* 359, 1350–1355. doi:10.1126/science.aar4060

Rini, B. I., Plimack, E. R., Stus, V., Gafanov, R., Hawkins, R., Nosov, D., et al. (2019). Pembrolizumab Plus Axitinib versus Sunitinib for Advanced Renal-Cell Carcinoma. *N. Engl. J. Med.* 380, 1116–1127. doi:10.1056/NEJMoa1816714

Salem, J. E., Manouchehri, A., Moey, M., Lebrun-Vignes, B., Bastarache, L., Pariente, A., et al. (2018). Cardiovascular Toxicities Associated with Immune Checkpoint Inhibitors: an Observational, Retrospective, Pharmacovigilance Study. *Lancet Oncol.* 19, 1579–1589. doi:10.1016/S1470-2045(18)30608-9

Sasidharan Nair, V., and Elkord, E. (2018). Immune Checkpoint Inhibitors in Cancer Therapy: a Focus on T-Regulatory Cells, by Varun Sasidharan Nair and Eyad Elkord (Erratum). *Immunol. Cel Biol* 96, 236. doi:10.1111/imcb.12012

Song, T. L., Nairismägi, M. L., Laurensia, Y., Lim, J. Q., Tan, J., Li, Z. M., et al. (2018). Oncogenic Activation of the STAT3 Pathway Drives PD-L1 Expression in Natural killer/T-Cell Lymphoma. *Blood* 132, 1146–1158. doi:10.1182/blood-2018-01-829424

Tay, R. Y., Blackley, E., McLean, C., Moore, M., Bergin, P., Gill, S., et al. (2017). Successful Use of Equine Anti-thymocyte Globulin (ATGAM) for Fulminant Myocarditis Secondary to Nivolumab Therapy. *Br. J. Cancer* 117, 921–924. doi:10.1038/bjc.2017.253

Tocchetti, C. G., Galdiero, M. R., and Varricchi, G. (2018). Cardiac Toxicity in Patients Treated with Immune Checkpoint Inhibitors: It Is Now Time for Cardio-Immuno-Oncology. *J. Am. Coll. Cardiol.* 71, 1765–1767. doi:10.1016/j.jacc.2018.02.038

Togashi, Y., Shitara, K., and Nishikawa, H. (2019). Regulatory T Cells in Cancer Immunosuppression - Implications for Anticancer Therapy. *Nat. Rev. Clin. Oncol.* 16, 356–371. doi:10.1038/s41571-019-0175-7

Topalian, S. L. (2017). Targeting Immune Checkpoints in Cancer Therapy. *JAMA* 318, 1647–1648. doi:10.1001/jama.2017.14155

Vaddepally, R. K., Kharel, P., Pandey, R., Garje, R., and Chandra, A. B. (2020). Review of Indications of FDA-Approved Immune Checkpoint Inhibitors Per NCCN Guidelines with the Level of Evidence. *Cancers (Basel)* 12, 738. doi:10.3390/cancers12030738

Waliany, S., Lee, D., Witteles, R. M., Neal, J. W., Nguyen, P., Davis, M. M., et al. (2021). Immune Checkpoint Inhibitor Cardiotoxicity: Understanding Basic Mechanisms and Clinical Characteristics and Finding a Cure. *Annu. Rev. Pharmacol. Toxicol.* 61, 113–134. doi:10.1146/annurev-pharmtox-010919-023451

Wang, D. Y., Salem, J. E., Cohen, J. V., Chandra, S., Menzer, C., Ye, F., et al. (2018). Fatal Toxic Effects Associated with Immune Checkpoint Inhibitors: A Systematic Review and Meta-Analysis. *JAMA Oncol.* 4, 1721–1728. doi:10.1001/jamaoncol.2018.3923

Zhang, L., Zlotoff, D. A., Awadalla, M., Mahmood, S. S., Nohria, A., Hassan, M. Z. O., et al. (2020). Major Adverse Cardiovascular Events and the Timing and Dose of Corticosteroids in Immune Checkpoint Inhibitor-Associated Myocarditis. *Circulation* 141, 2031–2034. doi:10.1161/CIRCULATIONAHA.119.044703

Conflict of Interest: The authors declare that the research was conducted in the absence of any commercial or financial relationships that could be construed as a potential conflict of interest.

frontiers in Pharmacology

ORIGINAL RESEARCH
published: 05 January 2022
doi: 10.3389/fphar.2021.749899

Resolvin D1 Attenuates Doxorubicin-Induced Cardiotoxicity by Inhibiting Inflammation, Oxidative and Endoplasmic Reticulum Stress

Menglong Wang[1,2,3†], *Jishou Zhang*[1,2,3†], *Mengmeng Zhao*[1,2,3†], *Jianfang Liu*[1,2,3], *Jing Ye*[1,2,3], *Yao Xu*[1,2,3], *Zhen Wang*[1,2,3], *Di Ye*[1,2,3], *Dan Li*[4] *and Jun Wan*[1,2,3*]

[1]*Department of Cardiology, Renmin Hospital of Wuhan University, Wuhan, China,* [2]*Cardiovascular Research Institute, Wuhan University, Wuhan, China,* [3]*Hubei Key Laboratory of Cardiology, Wuhan, China,* [4]*Department of Pediatrics, Renmin Hospital of Wuhan University, Wuhan, China*

Resolvin D1 (RvD1) is a lipid mediator that promotes resolution of inflammation. However, the function of RvD1 in doxorubicin- (Dox-) induced cardiotoxicity remains to be clarified. This study aimed to investigate whether RvD1 could attenuate Dox-induced cardiac injury. The mice were divided into three groups: control, Dox (20 mg/kg, once, intraperitoneally), and Dox + RvD1. RvD1 (2.5 μg/kg, intraperitoneally) was injected daily for 5 days. Echocardiography was performed to evaluate the cardiac function, and the heart tissue and serum samples were collected for further analyses. The results showed that RvD1 attenuated the decreased ratio of heart weight/body weight and heart weight/tibia length, the increased level of creatine kinase and activity of lactate dehydrogenase after Dox treatment. RvD1 improved the ejection fraction and fractional shortening of left ventricular and attenuated the severity of apoptosis induced by Dox. As for the underlying pathways, the results showed that RvD1 reduced the expression of IL-1 and IL-6, and attenuated the phosphorylation of P65 in cardiac tissue. RvD1 attenuated the oxidative stress induced by Dox, as demonstrated by the attenuated levels of superoxide dismutase, glutathione, and malondialdehyde, decreased expression of Nox-2 and Nox-4 and increased expression of Nrf-2 and HO-1. In addition, RvD1 also inhibited the endoplasmic reticulum stress induced by Dox. These results indicate the potential therapeutic benefits of RvD1 in Dox-induced cardiotoxicity in mice, and the mechanism may be related to the attenuated inflammation, oxidative stress and endoplasmic reticulum stress.

Keywords: resolvin D1, doxorubicin, cardiotoxicity, oxidative stress, apopstosis

OPEN ACCESS

Edited by:
Ming-Ming Wu,
Harbin Medical University, China

Reviewed by:
Rabia Johnson,
South African Medical Research Council, South Africa
Lamiaa A. Ahmed,
Cairo University, Egypt

***Correspondence:**
Jun Wan
wanjun@whu.edu.cn

[†]*These authors have contributed equally to this work*

Specialty section:
This article was submitted to Cardiovascular and Smooth Muscle Pharmacology, a section of the journal Frontiers in Pharmacology

Received: *30 July 2021*
Accepted: *06 December 2021*
Published: *05 January 2022*

Citation:
Wang M, Zhang J, Zhao M, Liu J, Ye J, Xu Y, Wang Z, Ye D, Li D and Wan J (2022) Resolvin D1 Attenuates Doxorubicin-Induced Cardiotoxicity by Inhibiting Inflammation, Oxidative and Endoplasmic Reticulum Stress. Front. Pharmacol. 12:749899. doi: 10.3389/fphar.2021.749899

INTRODUCTION

Doxorubicin (Dox), an anthracycline-based chemotherapeutic drug, is routinely used in the treatment of a wide variety of cancers, including breast, ovarian, bladder, lung, thyroid, and stomach cancer (Buzdar et al., 1985). However, treatment with Dox has been reported to cause dose-dependent cardiac toxicity and heart failure (Lefrak et al., 1973). Dox-induced cardiotoxicity seriously impairs the quality of life and life expectancy of patients with cancer. Several studies have shown that oxidative stress and apoptosis of cardiomyocytes are associated with Dox-induced cardiotoxicity (Kalivendi et al., 2001). However, there are currently no effective drugs to prevent and treat the cardiotoxicity caused by Dox.

Resolvin D1 (RvD1) is a specialized pro-resolving lipid mediator, mainly derived from docosahexaenoic acid (DHA). RvD1 reduces excessive polymorphonuclear neutrophil infiltration and transmigration, promoting resolution of inflammation (Abdolmaleki et al., 2020). In addition, RvD1 reduces tissue damage by attenuating oxidative stress and apoptosis (Lee and Surh, 2013; Saito et al., 2018). RvD1 has a protective role in Dox-induced nephropathy (Zhang et al., 2013). The protective effect of RvD1 has also been reported in cardiovascular diseases, including myocardial injury, neointimal hyperplasia, and abdominal aortic aneurysm (Miyahara et al., 2013; Kain et al., 2015; Spinosa et al., 2018). Recently, RvD1 was reported to alleviate angiotensin II-induced hypertension and cardiac remodeling via blocking Ang II signaling and attenuating inflammation (Olivares-Silva et al., 2021; Salas-Hernández et al., 2021).

However, the function of RvD1 in Dox-induced cardiovascular injury remains unclear. The objective of our study was to determine the effect of RvD1 supplementation on Dox-induced myocardial damage and to identify the underlying mechanism, which may provide novel insights for the prevention and/or treatment of Dox-induced cardiotoxicity.

MATERIALS AND METHODS

Animals

Experimental mice were treated in accordance with the National Institute of Health Guidelines for the Care and Use of Laboratory Animals, and study was approved by the Ethics Committee for Animal Research of the Wuhan University (Institutional Animal Care and Use Committee Issue No.20181215). C57BL/6 male mice (6–8 weeks old, 21.5–22.5 g) were obtained from Vital River Experimental Animal Technology Co. Ltd. (Beijing, China). The mice were maintained in a standard laboratory at the Cardiovascular Research Institute of Wuhan University, and were housed in standard humidity/temperature-controlled environment (70% relative humidity, 22°C) in a light-controlled room (12/12 h light/dark cycle) with access to sterile rodent food and water. All the mice were individually caged. The mice were used for the experiment after acclimatization to the housing environment for 2 weeks. The mice were randomly divided into three groups: control (CTRL; n = 10), Dox (n = 15), and Dox + RvD1 (n = 10). The control group received only sterile saline. Mice in the Dox group were treated with Dox (20 mg/kg) once intraperitoneally (i.p.) (Wang et al., 2018; Zhang et al., 2020). Mice in the Dox + RvD1 group were treated with RvD1 (2.5 μg/kg, i.p.) 30 min before Dox administration and every day thereafter for the duration of the experiment. Both Dox and RvD1 were dissolved in 0.9% sterile saline. All mice were observed and weighed daily. The mice were sacrificed after 5 days of Dox treatment. The heart weight of mice was collected for the ratio of heart weight (HW)/body weight (BW) and HW/tibia length (TL). The left cardiac tissues were collected for detailed analyses.

Echocardiography

Echocardiography was performed on anesthetized (1.5–2% isoflurane) mice using a Mylab30CV ultrasound (Biosound Esaote, Inc.) equipped with a 10 MHz linear array ultrasound transducer. We defined end-systole and end-diastole as the phases in which the left ventricular (LV) end-diastolic diameter (LVEDd) and LV end-systolic diameter (LVEDs) were obtained. LV ejection fraction (LVEF) and LV fractional shortening (LVFS) were also analyzed via LV M-mode tracing with a sweep speed of 50 mm/s at the midpapillary muscle level.

Cardiomyocyte Injury Evaluation

The activity of lactate dehydrogenase (LDH), the concentrations of myocardial-bound creatine kinase (CK-MB) and cardiac troponinwere I (cTnI) assessed as indexes of cardiomyocyte injury. Both LDH activity, CK-MB levels and cTnI levels in serum were detected using kits (all purchased from Nanjing Jiancheng Bioengineering Institute, China) according to the manufacturer's instructions and as described in our previous study (Ye et al., 2018).

Oxidative Stress Evaluation

At the end of the experiment, the cardiac tissues were removed and washed in ice-cold phosphate-buffered saline. The cardiac tissues (30 mg) were added to 300 μL of phosphate-buffered saline, ground into homogenates, and centrifuged at 3,000 rpm at 4°C for 15 min to collect the supernatant. The activities of superoxide dismutase 1 (SOD1) and the level of malondialdehyde (MDA) and glutathione (GSH) were detected by commercially available kits purchased from Nanjing Jiancheng Bioengineering Institute (Nanjing, China) following the manufacturer's instructions.

Histological Analysis

Histological analysis was performed as described in our previous study (Ye et al., 2020a). Cardiac tissues were fixed with 4% paraformaldehyde for 5 days. Then, the tissues were embedded in paraffin and sliced into 4–5 μm sections and mounted onto slides. Cardiomyocyte vacuolization was analyzed by hematoxylin and eosin (H&E) staining using a commercially available kit (Millipore) and then visualized by light microscopy. Sections were also subjected to immunofluorescence staining. the sections were autoclaved for antigen retrieval and then blocked with 10% goat serumfor 10min. Next, the sections were incubatedwith primary antibodies against Phospho-NF-κB p65 (Abcam, Cambridge, United Kingdom) overnight at 4°C. The sections were rinsed with PBS for 20 min before incubating with two different IRDye® 800CW conjugated secondary antibodies for 60 min and subsequently counterstained with the SlowFade Gold antifade reagent containing DAPI. All the figures were captured with fluorescence microscope, and Image Pro Plus 6.0 (Media Cybernetics, Bethesda, MD, United States) was used for relative quantification.

TdT-Mediated dUTP Nick-End-Labeling Assay

TUNEL staining of the cardiac tissue was performed as described previously (Ye et al., 2020b). The sections of the cardiac tissue

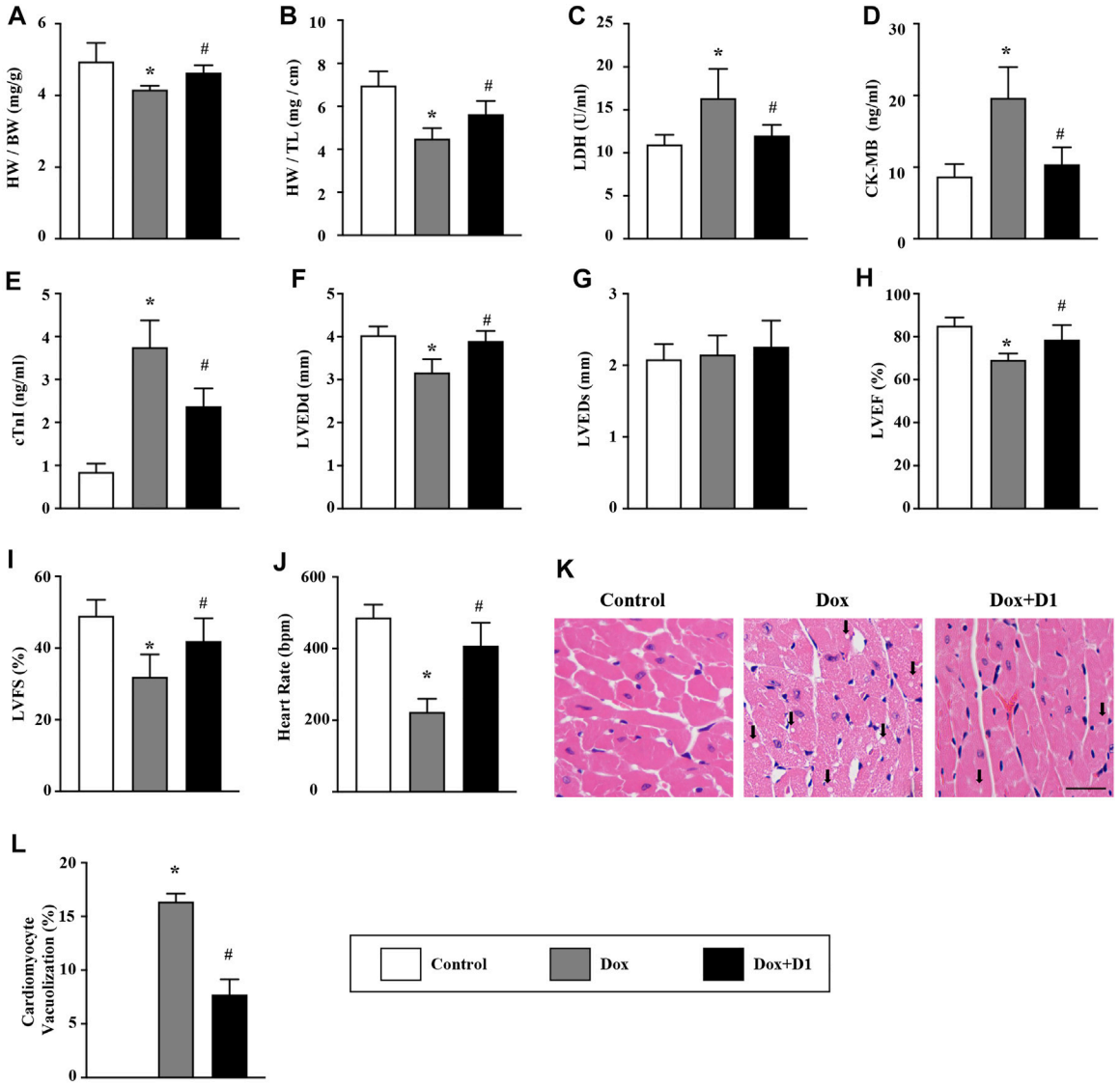

FIGURE 1 | RvD1 improved cardiac function in mice treated with Dox. **(A, B)** The ratio of HW/BW and HW/TL in different groups, n = 10. **(C–E)** Level of LDH, CK-MB and cTnI in the serum, n = 5. **(F–J)** Echocardiographic parameters in different groups, including LVEDd, LVEDs, LVEF, LVFS and heart rate, n = 6. **(K, L)** Vacuolated cardiomyocytes were detected in different groups by H&E staining and quantified, n = 4, bar = 25 μm. Data was presented as the mean ± standard deviation (SD) and compared with one-way ANOVA followed by Tukey's test. *$p < 0.05$ compared with the Control group. #$p < 0.05$ compared with the Dox group. HW, heart weight; BW, body weight; TL, tibia length; LDH, lactate dehydrogenase; CK-MB, myocardial-bound creatine kinase; cTnI, cardiac troponinwere I; LVEDd, left ventricular (LV) end-diastolic diameter; LVEDs, LV end-systolic diameter; LVEF, LV ejection fraction; LVFS, LV fractional shortening.

were analyzed using a TUNEL kit (Millipore, United States) following the manufacturer's instructions. Light microscopy was used to evaluate apoptotic cells, and Image Pro Plus software was used for relative quantification.

Western Blotting

We extracted and prepared total LV tissue protein with 1× RIPA buffer as reported previously (Ye et al., 2018). Proteins (50 μg) were separated by electrophoresis through a 10 or 12% sodium dodecyl sulfate polyacrylamide gel electrophoresis (SDS-PAGE) gel and transferred onto polyvinylidene fluoride membrane (IPFL00010, Millipore, Billerica, MA, United States). Then, the blots were blocked with 5% nonfat powdered milk and incubated overnight at 4°C with the primary antibodies. The primary antibodies used in this study were as follows: phospho-nuclear factor kappa-B p65 (p-P65, 1:500 dilution, Abcam, Cambridge, United Kingdom), nuclear factor kappa-B (NF-kB) p65 (T-P65, 1: 1000 dilution, Abcam), NADPH oxidase 2 (Nox-2, 1:200, Santa Cruz, CA, United States), NADPH oxidase 4 (Nox-4, 1:200, Santa Cruz), nuclear factor-erythroid 2-related factor 2 (Nrf-2, 1:500,

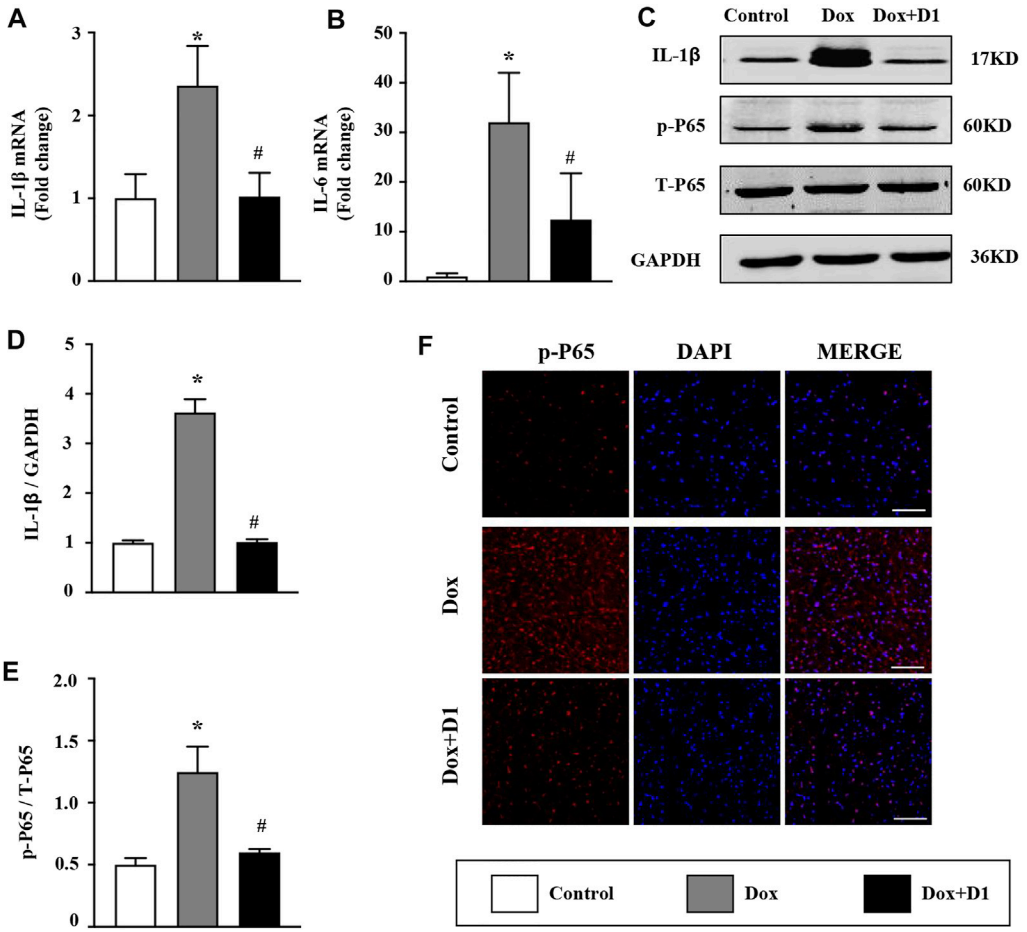

FIGURE 2 | RvD1 reduced Dox-induced inflammation in cardiac tissue. **(A, B)** mRNA expression levels of the inflammatory cytokines, IL-1β and IL-6 in different groups, n = 4. **(C–E)** Western blotting of p-p65 in different groups, n = 4. **(F)** Immunofluorescence analysis of p65 in different groups, n = 4, bar = 50 μm. Data was presented as the mean ± SD and compared using one-way ANOVA followed by Tukey's test. *$p < 0.05$ compared with the control group. #$p < 0.05$ compared with the Dox group.

Gene Technology, Shanghai, China), heme oxygenase-1 (HO-1, 1:500, Gene Technology), glucose-regulated protein 78 (GRP78, 1:500 dilution, Cell Signaling Technology), phospho-protein kinase R-like ER kinase (p-PERK, 1:200, Santa Cruz), caspase 12 (1: 1,000 dilution, Cell Signaling Technology), phospho-eukaryotic initiation factor 2α (*p*-eIF2α, 1:1,000 dilution, Cell Signaling Technology), activating transcription factor 6α (ATF-6α, 1:200 dilution, Santa Cruz Biotechnology), C/EBP homologous protein (CHOP, 1:1,000 dilution, Cell Signaling Technology), cleaved caspase 3 (c-caspase 3, 1:500, Cell Signaling Technology), B cell lymphoma-2 (Bcl-2, 1:500, Abcam), BCL2-associated X (Bax, 1:500, Abcam), and glyceraldehyde-3-phosphate dehydrogenase (GAPDH, 1:1,000, Cell Signaling Technology). After several washes, the blots were incubated with the secondary antibody (goat anti-rabbit antibody) at a dilution of 1:5,000 to 1:10,000 for 1 h at 25°C in the dark. The membranes were sequentially washed several times in the dark and scanned using the Odyssey Imaging System (LI-COR Biosciences, Lincoln, United States), and the band intensities were measured.

Real-Time Polymerase Chain Reaction Analysis

RNA was extracted from LV tissue using TRIzol (Invitrogen Life Technologies, Carlsbad, CA, United States). The concentration of RNA is measured by Nanodrop 2000 (Thermo Fisher Scientific, United States). The cDNA was synthesized from 2 μg of RNA from each group using oligo (DT) primers and the Transcriptor First Strand cDNA Synthesis Kit (Roche). RT+/RT-control was applied when cDNA was synthesized. Water without RNase and DNase was used to dilute DNA for three times before quantitative analysis. Quantitative analysis was conducted using a LightCycler 480 and SYBR Green Master Mix (Roche) follow the MIQE guidelines. The results were analyzed with the $2^{-\triangle\triangle Ct}$ method and normalized against GAPDH gene expression. Details of the primer sequences are presented in **Supplementary Table S1**.

Statistical Analysis

Data were analyzed using SPSS 24.0 software and are presented as the mean ± standard deviation (SD). Comparisons between groups were

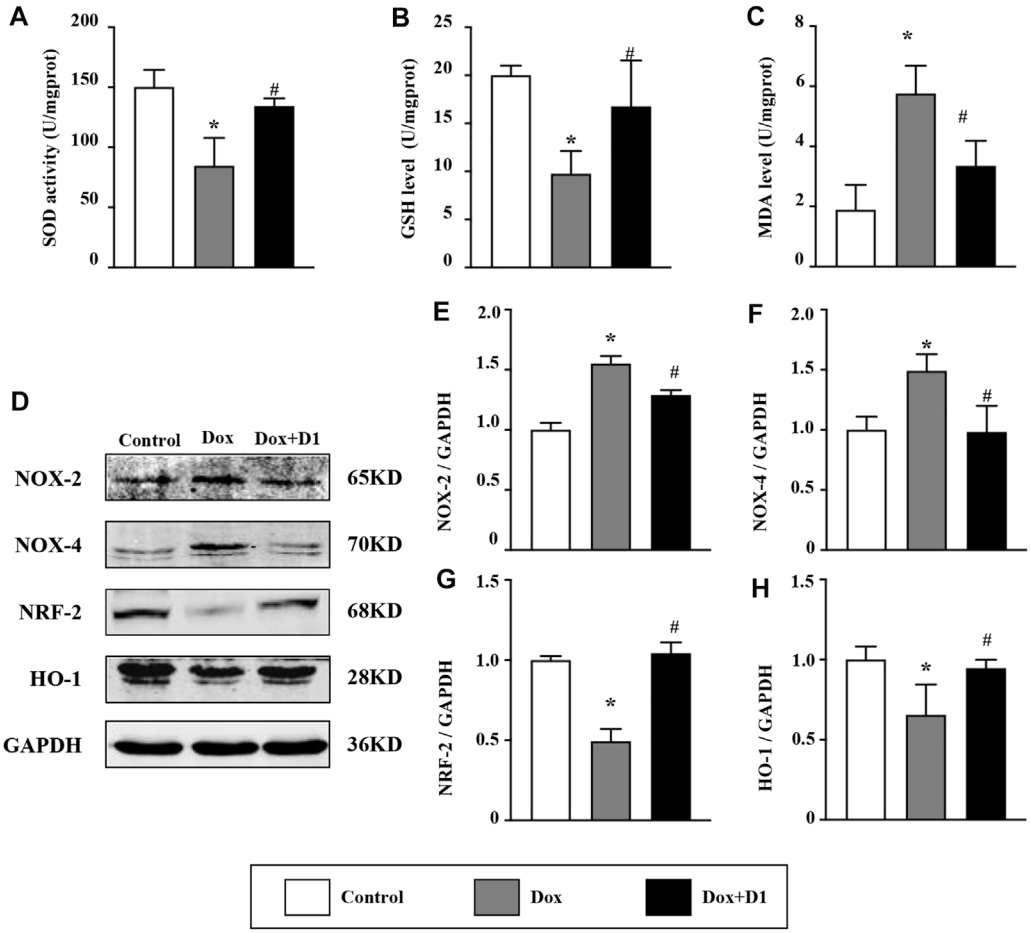

FIGURE 3 | RvD1 protected the cardiac tissue against Dox-induced oxidative stress. Levels of superoxide dismutase (SOD) **(A)**, glutathione (GSH) **(B)** and malondialdehyde (MDA) **(C)** in left heart tissue in the three groups, n = 5. Representative western blotting **(D)** and results of quantitation of Nox-2 **(E)**, Nox-4 **(F)**, Nrf-2 **(G)** and HO-1 **(H)** in different groups, n = 4. Data was presented as the mean ± SD and compared using one-way ANOVA followed by Tukey's test. *$p < 0.05$ compared with the control group. #$p < 0.05$ compared with the Dox group.

made using one-way analysis of variance (ANOVA) followed by Tukey's test. A p value <0.05 was considered statistically significant.

RESULTS

RvD1 Ameliorates Cardiac Dysfunction in Mice Treated With Dox

Compared to control mice, mice treated with Dox showed a decrease in the ratio of HW/BW and HW/TL. However, the administration of RvD1 improved the Dox-induced HW/BW and HW/TL ratios (**Figures 1A,B**). Compared to the control group, the levels of CK-MB, cTNI and activity of LDH in LV tissue were significantly increased in the Dox group. The administration of RvD1 reversed these trends (**Figures 1C–E**). In addition, the decreased LVEDd, LVEF, and LVFS in the Dox group were significantly improved by RvD1 treatment (**Figures 1F–I**). Histological examination revealed increased vacuolar accumulation in the Dox-treated mice, which was significantly improved in the Dox + RvD1 group (**Figures 1J,K**).

RvD1 Reduces Dox-Induced Inflammation in Cardiac Tissue

The expression of proinflammatory cytokines including IL-1β and IL-6 in the heart was significantly increased by Dox treatment (**Figures 2A,B**). Compared to the Dox group, a significant reduction in IL-1β and IL-6 level was observed in the Dox + RvD1 group (**Figures 2A,B**). In addition, the inhibitory effect of RvD1 on inflammation was further confirmed by western blotting and immunofluorescence examination, which showed that RvD1 reduced NF-kB signaling (**Figures 2C–E**). These results showed that RvD1 protects against heart injury by inhibiting inflammatory responses.

RvD1 Protects Cardiac Tissue Against Dox-Induced Oxidative Stress

Compared to the control group, the activity of SOD and the expression level of GSH were reduced in the Dox group.

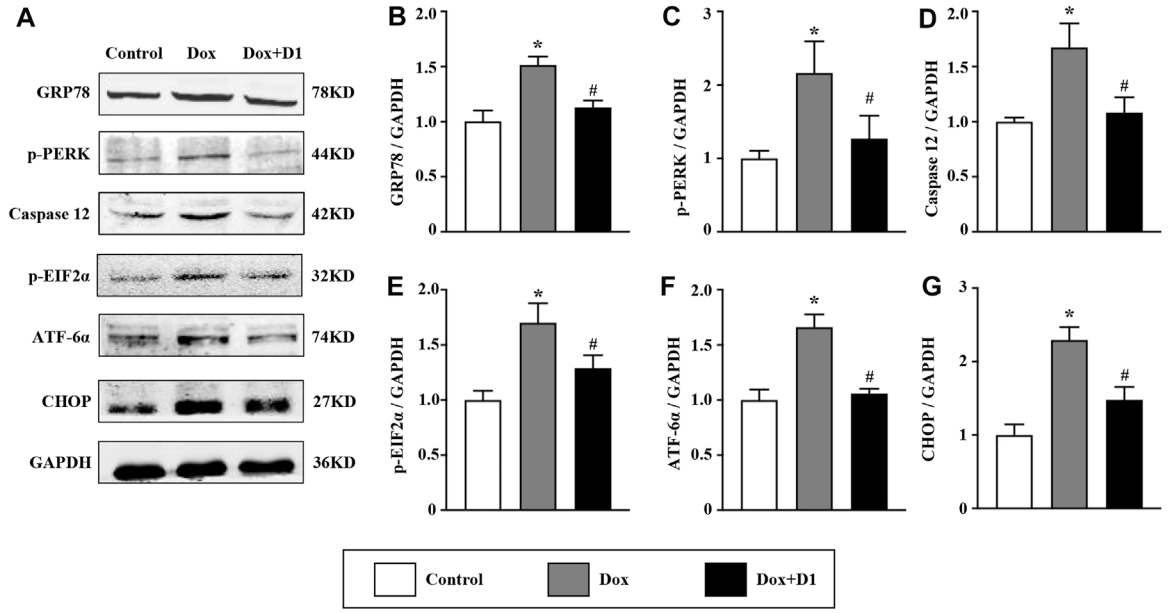

FIGURE 4 | RvD1 attenuated Dox-induced ER stress. Representative western blotting **(A)** and quantitative analysis showing the expression levels of glucose-regulated protein 78 (GRP78) **(B)**, protein kinase R-like ER kinase (PERK) **(C)**, caspase 12 **(D)**, phosphorylated eukaryotic translation initiation factor 2 (p-eif2α) **(E)**, activating transcription factor 6α (ATF6α) **(F)**, and C/EBP homologous protein (CHOP) **(G)** in different groups, n = 4. Data are presented as the mean ± SD and compared using one-way ANOVA followed by Tukey's test. *$p < 0.05$ compared with the control group. #$p < 0.05$ compared with the Dox group.

Whereas, MDA level was significantly increased in the Dox group (**Figures 3A–C**). However, treatment with RvD1 significantly restored SOD activity and GSH level, and reduced MDA level compared to the Dox-treated group (**Figures 3A–C**). In addition, western blotting results showed that the expression of Nox-2 and -4, which are important generators of reactive oxygen species (ROS), was reduced in the Dox + RvD1 group compared to the Dox-treated group (**Figures 3D–F**). The expression of Nrf-2 and HO-1, which play protective roles against oxidative stress, was increased in the Dox + RvD1 group compared to the Dox group (**Figures 3G,H**). These findings indicate that RvD1 treatment protects the cardiac tissue against Dox-induced oxidative stress.

RvD1 Attenuates Dox-Induced Endoplasmic Reticulum Stress

We investigated whether RvD1 attenuated ER stress, thereby reducing cardiotoxicity induced by Dox. The western blot results showed that RvD1 treatment reduced the expression of important markers that are indicative of the severity of ER stress (**Figure 4A**), including GRP78 and CHOP (**Figures 4B,G**). In addition, the administration of Dox increased the expression levels of caspase-12, p-PERK, p-eif2α, and ATF6α, which were attenuated by RvD1 treatment (**Figures 4C–F**). These results indicate that RvD1 treatment attenuated Dox-induced ER stress.

RvD1 Reduces Dox-Induced Apoptosis of Cardiomyocytes

Apoptosis is reported to be involved in Dox-induced cardiotoxicity (Wang et al., 2016a). We evaluated the severity of apoptosis and identified the potential signaling pathways associated with the RvD1 treatment on cardiomyocyte apoptosis. Compared to the control group, the mRNA level of Bax was increased while that of Bcl-2 was decreased in the Dox-treated group (**Figures 5A,B**). These changes were significantly reversed following treatment with RvD1. Similarly, western blotting results showed that Dox increased the expression levels of c-caspase 3 and Bax, and decreased Bcl-2 expression (**Figures 5C–G**). These changes were attenuated by RvD1. In addition, TUNEL assay showed that RvD1 treatment significantly reduced the number of Dox-induced apoptotic cells (**Figure 5H**). These results showed that RvD1 reduces Dox-induced cardiomyocyte apoptosis.

DISCUSSION

This study revealed that RvD1 attenuates Dox-induced cardiotoxicity. The possible mechanisms involved in RvD1-mediated attenuation of Dox-induced cardiotoxicity include regulation of inflammation, oxidative stress, autophagy dysfunction, ER stress, and apoptosis.

Dose-dependent cardiac toxicity and heart failure were reported in cancer patients treated with Dox, which

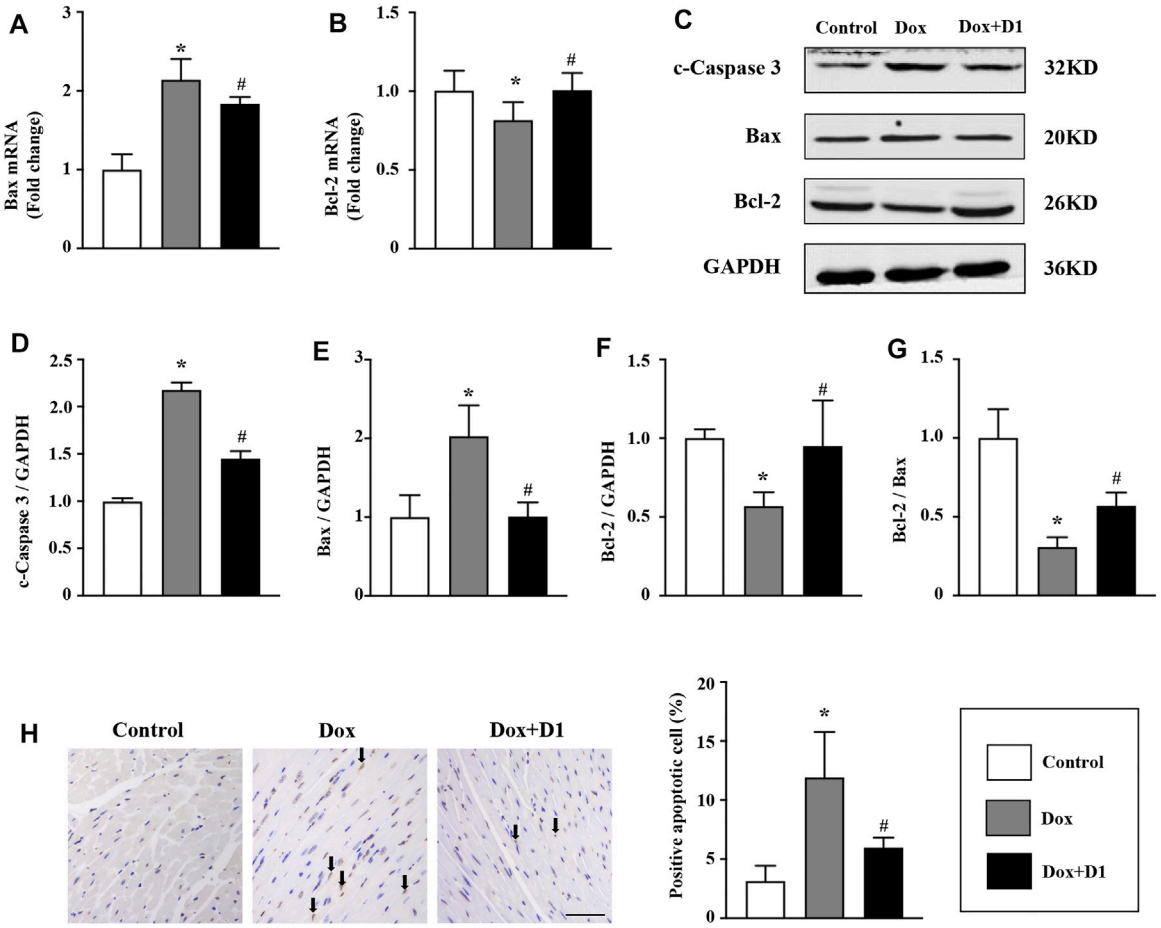

FIGURE 5 | RvD1 reduced Dox-induced apoptosis of cardiomyocytes. mRNA levels of Bax **(A)** and Bcl-2 **(B)** in different groups, n = 4. Representative western blotting **(C)** and quantitative analysis showing the expression levels of c-caspase-3 **(D)**, Bax **(E)**, and Bcl-2 **(F)** in different groups, n = 4. **(G)** Bcl-2/Bax in different groups. **(H)** TdT-mediated dUTP nick-end-labeling (TUNEL) assay results of the left cardiac tissue in different groups, n = 4, bar = 50 μm. Data are presented as the mean ± SD and compared using one-way ANOVA followed by Tukey's test. *$p < 0.05$ compared with the control group. #$p < 0.05$ compared with the Dox group.

seriously impaired the quality of life and life expectancy of patients with cancer (VON HOFF et al., 1979). Dox triggers splenic contraction and irreversible dysregulation of cyclooxygenase and lipoxygenase, which alter the inflammation resolution program in the myocardium, suggesting that resolvin supplementation may improve the cardiac injury induced by Dox (Jadapalli et al., 2018). RvD1, an important anti-inflammatory mediator, is mainly derived from DHA. DHA supplementation may attenuate Dox-induced cardiotoxicity by inhibiting the activation of NF-κB/iNOS/NO signaling pathway *in vitro* (Wang et al., 2016b). In addition, another study suggested that DHA pretreatment may protect H9C2 cells against Dox-induced injury by reducing ROS production (Hsu et al., 2014). However, the *in vivo* effects of RvD1 on Dox-induced cardiotoxicity remain unknown. In this study, RvD1 treatment increased the HW/BW ratio, reduced the level of cardiac injury biomarkers, and improved the EF and FS, all of which were compromised by Dox. Taken together, RvD1 ameliorated cardiac dysfunction in mice treated with Dox.

Inflammation is the body's defensive response to stimulation, such as infection or injury. Acute inflammatory responses such as surgery-induced tissue injury are self-limited processes that resolve on their own and are divided into initiation and resolution phases. Failed inflammation resolution can lead to immunopathology, such as systemic inflammation leading to organ dysfunction and death. Increasing evidence shows that polyunsaturated fatty acid-derived lipid mediators such as lipoxin A4, resolvins, and protectins are produced during the onset of inflammatory reactions. Their important biological roles have been demonstrated in a variety of cell types *in vitro* and in many animal models of diseases *in vivo* (Takano et al., 1997; Takano et al., 1998; Serhan and Petasis, 2011). Dox is reported to induce inflammatory responses through enhanced expression and release of proinflammatory cytokines by activating the NF-kB signaling pathway in the heart (Pecoraro et al., 2016). In the present study, we showed that Dox treatment provoked a series of inflammatory responses and increased the expression of inflammatory cytokines. The administration of RvD1 significantly reduced the expression of proinflammatory

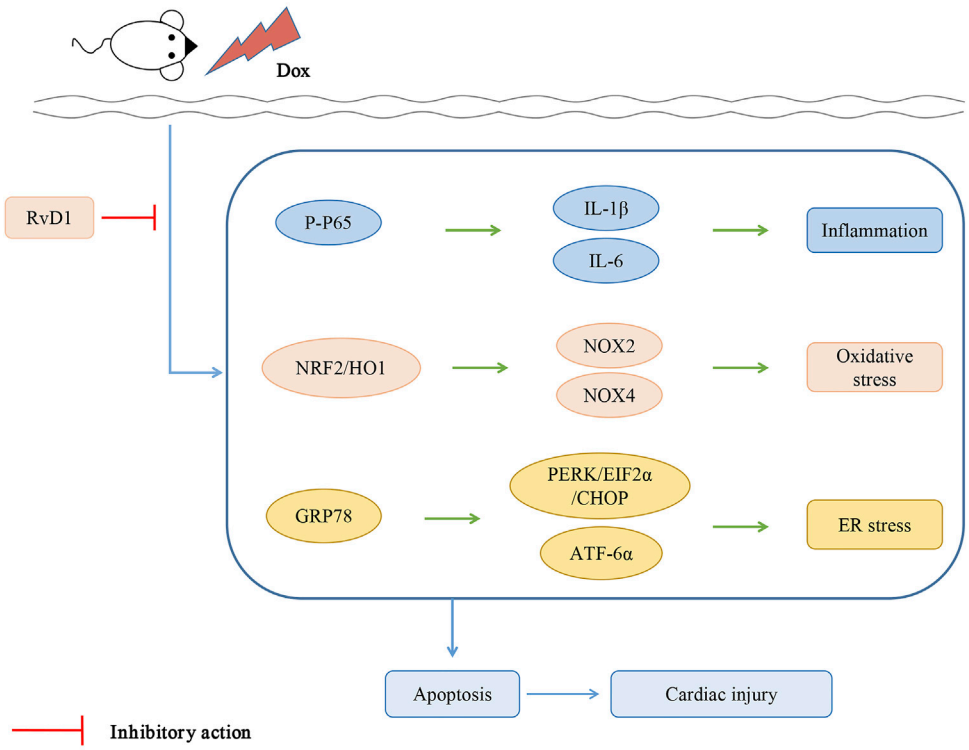

FIGURE 6 | Diagram depicting the regulation mechanism of RvD1 in Dox-induced cardiotoxicity.

cytokines, including IL-1β and IL-6, by suppressing the NF-kB signaling pathway. This study indicates that RvD1 confers a potential cardioprotective effect against Dox-induced cardiotoxicity through the inhibition of the inflammatory response.

ROS are generated during mitochondrial oxidative metabolism and in cellular response to xenobiotics, cytokines, and bacterial invasion (Ray et al., 2012). When ROS overwhelms the cellular antioxidant defense system, whether through increased levels of ROS or decreased cellular antioxidant capacity, oxidative stress occurs (Ray et al., 2012). RvD1 was reported to suppress oxidative stress by upregulating the expression of Nrf2 and HO-1 in other diseases (Saito et al., 2018). In the present study, lipid peroxidation products (MDA) and antioxidant enzymes (SOD and GSH) were used to estimate the oxidative stress in the cardiac tissues. Administration of RvD1 significantly attenuated the oxidative stress induced by Dox treatment. Dox induces the production of ROS through activation of the NADPH oxidase signaling pathway (Wojnowski et al., 2005). Nox-2 deficiency protects mice against cardiac injury after Dox treatment (Zhao et al., 2010). In this study, we found that RvD1 treatment inhibited oxidative stress by downregulating the expression of Nox-2 and Nox-4, the key NADPH oxidase subunit. In addition, ER stress plays an important role in the development of heart failure (Minamino et al., 2010). ER stress establishes a progressive pathological cycle with oxidative stress in endothelial dysfunction, diabetes, and heart, liver, kidney, or neurological diseases (Reyes-Fermín et al., 2020). ER stress plays an important role in oxidative stress, as it is also a source of ROS (Burgos-Morón et al., 2019). We evaluated the level of ER stress to further understand the underlying mechanisms behind RvD1-mediated protection against Dox-induced cardiotoxicity. ER stress-associated proteins were enhanced following Dox treatment but reduced after RvD1 administration. The RvD1-mediated protection against Dox-induced ER stress was achieved by downregulating the PERK and ATF-6 signaling pathways. These results indicate that RvD1 may suppress Dox-induced cardiotoxicity through the regulation of oxidative stress and ER stress.

Several studies have indicated that Dox promotes endoplasmic reticulum-induced apoptosis by activating the expression of pro-apoptotic factors and inhibiting the expression of anti-apoptotic factors (Chua et al., 2009). As a specific pro-apoptotic pathway, ER stress can activate the CHOP and caspase-12 pathways, thereby mediating apoptosis (Tabas and Ron, 2011). In the present study, RvD1 treatment reduced the expression of CHOP and caspase-12, leading to reduced myocardial apoptosis and improved cardiac dysfunction. In addition, CHOP is reported to regulate apoptosis factors, including Bax, Bcl-2,

and cleaved caspase-3, which are key determinants of cell death (Fu et al., 2010). Consistent with previous studies, our results showed that RvD1 treatment significantly enhanced the expression of Bcl-2 and reduced the expression of Bax and cleaved caspase-3. This study demonstrates that RvD1 protects cardiac tissues against Dox-induced apoptosis.

Our study has several limitations. First, the administeration of RvD1 before Dox may prevent the absorption of Dox into systemic circulation due to chemicophysical interaction. Second, our study suggests that RvD1 may improve Dox-induced cardiotoxicity via alleviating apoptosis. Further interventions may help to explore the mechanism. Third, we did not detect the systemic inflammation induced by Dox in this study.

CONCLUSION

RvD1 protects cardiac tissue against Dox-induced cardiotoxicity, possibly through the attenuation of inflammation, oxidative stress and ER stress (**Figure 6**).

DATA AVAILABILITY STATEMENT

The raw data supporting the conclusions of this article will be made available by the authors, without undue reservation.

ETHICS STATEMENT

The animal study was reviewed and approved by the Ethics Committee for Animal Research of the Wuhan University.

AUTHOR CONTRIBUTIONS

JZ, MW, and MZ contributed to the experimental design and wrote the manuscript. JY, ZW, and YX contributed to the acquisition and analysis of the data. DY, JL, DL, and JW reviewed the manuscript.

FUNDING

This study was supported by the Natural Science Foundation of Hubei Province (NO.2020CFB234) and the Fundamental Research Funds for Central Universities of the Central South University (NO.2042019kf0065).

SUPPLEMENTARY MATERIAL

The Supplementary Material for this article can be found online at: https://www.frontiersin.org/articles/10.3389/fphar.2021.749899/full#supplementary-material

REFERENCES

Abdolmaleki, F., Kovanen, P. T., Mardani, R., Gheibi-Hayat, S. M., Bo, S., and Sahebkar, A. (2020). Resolvins: Emerging Players in Autoimmune and Inflammatory Diseases. *Clin. Rev. Allergy Immunol.* 58, 82–91. doi:10.1007/s12016-019-08754-9

Burgos-Morón, E., Abad-Jiménez, Z., Marañón, A. M., Iannantuoni, F., Escribano-López, I., López-Domènech, S., et al. (2019). Relationship between Oxidative Stress, ER Stress, and Inflammation in Type 2 Diabetes: The Battle Continues. *J. Clin. Med.* 8, , 2019 1385.10.3390/jcm8091385

Buzdar, A. U., Marcus, C., Smith, T. L., and Blumenschein, G. R. (1985). Early and Delayed Clinical Cardiotoxicity of Doxorubicin. *Cancer* 55, 2761–2765. doi:10.1002/1097-0142(19850615)55:12<2761:aid-cncr2820551206>3.0.co;2-p

Chua, C. C., Gao, J., Ho, Y. S., Xu, X., Kuo, I. C., Chua, K. Y., et al. (2009). Over-expression of a Modified Bifunctional Apoptosis Regulator Protects against Cardiac Injury and Doxorubicin-Induced Cardiotoxicity in Transgenic Mice. *Cardiovasc. Res.* 81, 20–27. doi:10.1093/cvr/cvn257

Fu, H. Y., Okada, K., Liao, Y., Tsukamoto, O., Isomura, T., Asai, M., et al. (2010). Ablation of C/EBP Homologous Protein Attenuates Endoplasmic Reticulum-Mediated Apoptosis and Cardiac Dysfunction Induced by Pressure Overload. *Circulation* 122, 361–369. doi:10.1161/CIRCULATIONAHA.109.917914

Hsu, H. C., Chen, C. Y., and Chen, M. F. (2014). N-3 Polyunsaturated Fatty Acids Decrease Levels of Doxorubicin-Induced Reactive Oxygen Species in Cardiomyocytes -- Involvement of Uncoupling Protein UCP2. *J. Biomed. Sci.* 21, 101. doi:10.1186/s12929-014-0101-3

Jadapalli, J. K., Wright, G. W., Kain, V., Sherwani, M. A., Sonkar, R., Yusuf, N., et al. (2018). Doxorubicin Triggers Splenic Contraction and Irreversible Dysregulation of COX and LOX that Alters the Inflammation-Resolution Program in the Myocardium. *Am. J. Physiol. Heart Circ. Physiol.* 315, H1091–h1100. doi:10.1152/ajpheart.00290.2018

Kain, V., Ingle, K. A., Colas, R. A., Dalli, J., Prabhu, S. D., Serhan, C. N., et al. (2015). Resolvin D1 Activates the Inflammation Resolving Response at Splenic and Ventricular Site Following Myocardial Infarction Leading to Improved Ventricular Function. *J. Mol. Cel Cardiol* 84, 24–35. doi:10.1016/j.yjmcc.2015.04.003

Kalivendi, S. V., Kotamraju, S., Zhao, H., Joseph, J., and Kalyanaraman, B. (2001). Doxorubicin-induced Apoptosis Is Associated with Increased Transcription of Endothelial Nitric-Oxide Synthase. Effect of Antiapoptotic Antioxidants and Calcium. *J. Biol. Chem.* 276, 47266–47276. doi:10.1074/jbc.M106829200

Lee, H. N., and Surh, Y. J. (2013). Resolvin D1-Mediated NOX2 Inactivation Rescues Macrophages Undertaking Efferocytosis from Oxidative Stress-Induced Apoptosis. *Biochem. Pharmacol.* 86, 759–769. doi:10.1016/j.bcp.2013.07.002

Lefrak, E. A., Pitha, J., Rosenheim, S., and Gottlieb, J. A. (1973). A Clinicopathologic Analysis of Adriamycin Cardiotoxicity. *Cancer* 32, 302–314. doi:10.1002/1097-0142(197308)32:2<302:aid-cncr2820320205>3.0.co;2-2

Minamino, T., Komuro, I., and Kitakaze, M. (2010). Endoplasmic Reticulum Stress as a Therapeutic Target in Cardiovascular Disease. *Circ. Res.* 107, 1071–1082. doi:10.1161/CIRCRESAHA.110.227819

Miyahara, T., Runge, S., Chatterjee, A., Chen, M., Mottola, G., Fitzgerald, J. M., et al. (2013). D-series Resolvin Attenuates Vascular Smooth Muscle Cell Activation and Neointimal Hyperplasia Following Vascular Injury. *Faseb j* 27, 2220–2232. doi:10.1096/fj.12-225615

Olivares-Silva, F., De Gregorio, N., Espitia-Corredor, J., Espinoza, C., Vivar, R., Silva, D., et al. (2021). Resolvin-D1 Attenuation of Angiotensin II-Induced Cardiac Inflammation in Mice Is Associated with Prevention of Cardiac Remodeling and Hypertension. *Biochim. Biophys. Acta Mol. Basis Dis.* 1867, 166241. doi:10.1016/j.bbadis.2021.166241

Pecoraro, M., Del Pizzo, M., Marzocco, S., Sorrentino, R., Ciccarelli, M., Iaccarino, G., et al. (2016). Inflammatory Mediators in a Short-Time Mouse Model of Doxorubicin-Induced Cardiotoxicity. *Toxicol. Appl. Pharmacol.* 293, 44–52. doi:10.1016/j.taap.2016.01.006

Ray, P. D., Huang, B. W., and Tsuji, Y. (2012). Reactive Oxygen Species (ROS) Homeostasis and Redox Regulation in Cellular Signaling. *Cell Signal* 24, 981–990. doi:10.1016/j.cellsig.2012.01.008

Reyes-Fermín, L. M., Aparicio-Trejo, O. E., Avila-Rojas, S. H., Gómez-Sierra, T., Martínez-Klimova, E., and Pedraza-Chaverri, J. (2020). Natural Antioxidants' Effects on Endoplasmic Reticulum Stress-Related Diseases. *Food Chem. Toxicol.* 138, 111229.

Saito, P., Melo, C. P. B., Martinez, R. M., Fattori, V., Cezar, T. L. C., Pinto, I. C., et al. (2018). The Lipid Mediator Resolvin D1 Reduces the Skin Inflammation and Oxidative Stress Induced by UV Irradiation in Hairless Mice. *Front. Pharmacol.* 9, 1242. doi:10.3389/fphar.2018.01242

Salas-Hernández, A., Ruz-Cortés, F., Bruggendieck, F., Espinoza-Perez, C., Espitia-Corredor, J., Varela, N. M., et al. (2021). Resolvin D1 Reduces Expression and Secretion of Cytokines and Monocyte Adhesion Triggered by Angiotensin II, in Rat Cardiac Fibroblasts. *Biomed. Pharmacother.* 141, 111947.

Serhan, C. N., and Petasis, N. A. (2011). Resolvins and Protectins in Inflammation Resolution. *Chem. Rev.* 111, 5922–5943. doi:10.1021/cr100396c

Spinosa, M., Su, G., Salmon, M. D., Lu, G., Cullen, J. M., Fashandi, A. Z., et al. (2018). Resolvin D1 Decreases Abdominal Aortic Aneurysm Formation by Inhibiting NETosis in a Mouse Model. *J. Vasc. Surg.* 68, 93s–103s. doi:10.1016/j.jvs.2018.05.253

Tabas, I., and Ron, D. (2011). Integrating the Mechanisms of Apoptosis Induced by Endoplasmic Reticulum Stress. *Nat. Cel Biol* 13, 184–190. doi:10.1038/ncb0311-184

Takano, T., Clish, C. B., Gronert, K., Petasis, N., and Serhan, C. N. (1998). Neutrophil-mediated Changes in Vascular Permeability Are Inhibited by Topical Application of Aspirin-Triggered 15-Epi-Lipoxin A4 and Novel Lipoxin B4 Stable Analogues. *J. Clin. Invest.* 101, 819–826. doi:10.1172/JCI1578

Takano, T., Fiore, S., Maddox, J. F., Brady, H. R., Petasis, N. A., and Serhan, C. N. (1997). Aspirin-triggered 15-Epi-Lipoxin A4 (LXA4) and LXA4 Stable Analogues Are Potent Inhibitors of Acute Inflammation: Evidence for Anti-inflammatory Receptors. *J. Exp. Med.* 185, 1693–1704. doi:10.1084/jem.185.9.1693

VON Hoff, D. D., Layard, M. W., Basa, P., Davis, H. L., Jr., VON Hoff, A. L., Rozencweig, M., et al. (1979). Risk Factors for Doxorubicin-Induced Congestive Heart Failure. *Ann. Intern. Med.* 91, 710–717. doi:10.7326/0003-4819-91-5-710

Wang, L., Zhang, T. P., Zhang, Y., Bi, H. L., Guan, X. M., Wang, H. X., et al. (2016). Protection against Doxorubicin-Induced Myocardial Dysfunction in Mice by Cardiac-specific Expression of Carboxyl Terminus of Hsp70-Interacting Protein. *Sci. Rep.* 6, 28399. doi:10.1038/srep28399

Wang, Z., Wang, M., Liu, J., Ye, J., Jiang, H., Xu, Y., et al. (2018). Inhibition of TRPA1 Attenuates Doxorubicin-Induced Acute Cardiotoxicity by Suppressing Oxidative Stress, the Inflammatory Response, and Endoplasmic Reticulum Stress. *Oxid Med. Cel Longev* 2018, 5179468. doi:10.1155/2018/5179468

Wang, Z. Q., Chen, M. T., Zhang, R., Zhang, Y., Li, W., and Li, Y. G. (2016). Docosahexaenoic Acid Attenuates Doxorubicin-Induced Cytotoxicity and Inflammation by Suppressing NF-κB/iNOS/NO Signaling Pathway Activation in H9C2 Cardiac Cells. *J. Cardiovasc. Pharmacol.* 67, 283–289. doi:10.1097/FJC.0000000000000350

Wojnowski, L., Kulle, B., Schirmer, M., Schlüter, G., Schmidt, A., Rosenberger, A., et al. (2005). NAD(P)H Oxidase and Multidrug Resistance Protein Genetic Polymorphisms Are Associated with Doxorubicin-Induced Cardiotoxicity. *Circulation* 112, 3754–3762. doi:10.1161/CIRCULATIONAHA.105.576850

Ye, J., Huang, Y., Que, B., Chang, C., Liu, W., Hu, H., et al. (2018). Interleukin-12p35 Knock Out Aggravates Doxorubicin-Induced Cardiac Injury and Dysfunction by Aggravating the Inflammatory Response, Oxidative Stress, Apoptosis and Autophagy in Mice. *EBioMedicine* 35, 29–39. doi:10.1016/j.ebiom.2018.06.009

Ye, J., Wang, Y., Wang, Z., Liu, L., Yang, Z., Ye, D., et al. (2020). Interleukin-12p35 Deficiency Enhances Mitochondrial Dysfunction and Aggravates Cardiac Remodeling in Aging Mice. *Aging (Albany NY)* 12, 193–203. doi:10.18632/aging.102609

Ye, J., Wang, Y., Xu, Y., Wang, Z., Liu, L., Wang, M., et al. (2020). Interleukin-22 Deficiency Alleviates Doxorubicin-Induced Oxidative Stress and Cardiac Injury via the P38 MAPK/macrophage/Fizz3 axis in Mice. *Redox Biol.* 36, 101636. doi:10.1016/j.redox.2020.101636

Zhang, J., Wang, M., Ding, W., Zhao, M., Ye, J., Xu, Y., et al. (2020). Resolvin E1 Protects against Doxorubicin-Induced Cardiotoxicity by Inhibiting Oxidative Stress, Autophagy and Apoptosis by Targeting AKT/mTOR Signaling. *Biochem. Pharmacol.* 180, 114188. doi:10.1016/j.bcp.2020.114188

Zhang, X., Qu, X., Sun, Y. B., Caruana, G., Bertram, J. F., Nikolic-Paterson, D. J., et al. (2013). Resolvin D1 Protects Podocytes in Adriamycin-Induced Nephropathy through Modulation of 14-3-3β Acetylation. *PLoS One* 8, e67471. doi:10.1371/journal.pone.0067471

Zhao, Y., McLaughlin, D., Robinson, E., Harvey, A. P., Hookham, M. B., Shah, A. M., et al. (2010). Nox2 NADPH Oxidase Promotes Pathologic Cardiac Remodeling Associated with Doxorubicin Chemotherapy. *Cancer Res.* 70, 9287–9297. doi:10.1158/0008-5472.CAN-10-2664

Conflict of Interest: The authors declare that the research was conducted in the absence of any commercial or financial relationships that could be construed as a potential conflict of interest.

Publisher's Note: All claims expressed in this article are solely those of the authors and do not necessarily represent those of their affiliated organizations, or those of the publisher, the editors and the reviewers. Any product that may be evaluated in this article, or claim that may be made by its manufacturer, is not guaranteed or endorsed by the publisher.

frontiers in Pharmacology

REVIEW
published: 08 February 2022
doi: 10.3389/fphar.2022.811406

Understanding Anthracycline Cardiotoxicity From Mitochondrial Aspect

Junqi Huang[1†], Rundong Wu[2†], Linyi Chen[2], Ziqiang Yang[2], Daoguang Yan[2] and Mingchuan Li[2*]*

[1]Key Laboratory for Regenerative Medicine, Ministry of Education, College of Life Science and Technology, Jinan University, Guangzhou, China, [2]Department of Biology, College of Life Science and Technology, Jinan University, Guangzhou, China

Anthracyclines, such as doxorubicin, represent one group of chemotherapy drugs with the most cardiotoxicity. Despite that anthracyclines are capable of treating assorted solid tumors and hematological malignancies, the side effect of inducing cardiac dysfunction has hampered their clinical use. Currently, the mechanism underlying anthracycline cardiotoxicity remains obscure. Increasing evidence points to mitochondria, the energy factory of cardiomyocytes, as a major target of anthracyclines. In this review, we will summarize recent findings about mitochondrial mechanism during anthracycline cardiotoxicity. In particular, we will focus on the following aspects: 1) the traditional view about anthracycline-induced reactive oxygen species (ROS), which is produced by mitochondria, but in turn causes mitochondrial injury. 2) Mitochondrial iron-overload and ferroptosis during anthracycline cardiotoxicity. 3) Autophagy, mitophagy and mitochondrial dynamics during anthracycline cardiotoxicity. 4) Anthracycline-induced disruption of cardiac metabolism.

Keywords: anthracycline, cardiotoxicity, mitochondria, ROS, ferroptosis, mitophagy, metabolism

OPEN ACCESS

Edited by:
Yong Xia,
The Ohio State University, United States

Reviewed by:
Min Wu,
China Academy of Chinese Medical Sciences, China
Alessandra Ghigo,
University of Turin, Italy
Ming He,
Nanchang University, China

***Correspondence:**
Mingchuan Li
mingchuanli@jnu.edu.cn
Daoguang Yan
tydg@jnu.edu.cn

†These authors have contributed equally to this work

Specialty section:
This article was submitted to Cardiovascular and Smooth Muscle Pharmacology, a section of the journal Frontiers in Pharmacology

Received: *08 November 2021*
Accepted: *24 January 2022*
Published: *08 February 2022*

Citation:
Huang J, Wu R, Chen L, Yang Z, Yan D and Li M (2022) Understanding Anthracycline Cardiotoxicity From Mitochondrial Aspect. Front. Pharmacol. 13:811406. doi: 10.3389/fphar.2022.811406

INTRODUCTION

Anthracyclines, including doxorubicin, daunorubicin, epirubicin and idarubicin, are a family of antibiotics that are broadly used to treat solid tumors (ovary, breast, stomach, brain, and gastrointestinal tumors) and hematological malignancies (lymphoma and pediatric leukemia) (National Cancer Institute, 2020). Anthracyclines can be used alone or combined with other anti-cancer regimens, such as radiation therapy or monoclonal antibodies (Christodoulou et al., 2009). However, cardiovascular diseases arise as a leading cause of morbidity and mortality among cancer survivors receiving anthracycline therapy, largely limiting the clinical application of these drugs (Zamorano et al., 2016).

At present, there is no standard guideline to prevent anthracycline-associated cardiotoxicity. This is mainly because our understanding of the molecular mechanisms underlying anthracycline cardiotoxicity is still limited. It is currently known that anthracyclines primarily bind to topoisomerase 2 (TOP2) and induce DNA double-strand breaks in cancer cells (Tewey et al., 1984). Similarly in the heart, topoisomerase 2ß (TOP2ß) acts as the main target of anthracyclines in cardiomyocytes (Lyu et al., 2007; Zhang et al., 2012). Formation of ROS due to the redox cycling of anthracyclines is considered as another key mechanism that leads to oxidative stress damage in cardiomyocytes (Simůnek et al., 2009). Beside these, other mechanisms include anthracycline-induced disruption of iron metabolism, insulin resistance and inflammation (Ghigo et al., 2016).

More recently, disturbance of cardiac autophagy, especially mitochondrial autophagy (mitophagy), emerges as a newly recognized reason underlying anthracycline cardiotoxicity [reviewed in ref (Li M. et al., 2020)]. Anthracycline cardiotoxicity is likely to be multifactorial and complex [reviewed in refs (Vejpongsa and Yeh, 2014; Ghigo et al., 2016; Sala et al., 2020)]. Nevertheless, distinct mechanisms converge on anthracycline-induced mitochondrial dysfunction as a central event. In the heart, mitochondria are important organelles, which occupy around 30% of the total cardiomyocyte volume and supply 90% energy through oxidative phosphorylation (OXPHOS) for the cardiac biological processes (Piquereau et al., 2013). Thus, deciphering mitochondrial alterations at the molecular and functional levels is critical for anthracycline therapy. In this review, we will summarize the recent findings about anthracycline-induced cardiotoxicity, especially about mitochondria-related ROS production, iron-overload and ferroptosis, mitophagy and mitochondrial dynamics disruption, as well as cardiac metabolism alteration after mitochondrial dysfunction.

ANTHRACYCLINE CARDIOTOXICITY: PHENOMENON AND CURRENT TREATMENT

Anthracycline treatment results in acute, early and chronic cardiotoxicity. The acute side effects include supraventricular arrhythmia, transient left ventricle dysfunction and electrocardiographic changes, which occur immediately following treatment and are reversible after discontinuation of the therapeutic regimen. However, irreversible cardiac dysfunction may develop early after treatment completion, commonly within 1 year, or manifest several years after treatment (median = 7 years). Irreversible cardiac dysfunction may eventually lead to heart failure and lower the life quality of cancer survivors (Zamorano et al., 2016). For example, breast carcinoma and small cell lung carcinoma patients receiving doxorubicin treatment showed a 5% incidence of congestive heart failure at a cumulative dose of 400 mg/m^2. This incidence rate rapidly increased to 48% when 700 mg/m^2 was reached (Swain et al., 2003). Thus, early detection of cardiac dysfunction is important to prevent anthracycline cardiotoxicity. If anthracycline-induced cardiac dysfunction is identified early and interfered with heart failure medications, patients recover easily. In contrast, heart failure is difficult to treat if detected late after anthracycline therapy (Cardinale et al., 2010, 2015).

Phenomenon of chronic anthracycline cardiotoxicity includes enlargement of all chambers and thinning of the ventricular walls, which are classic appearances of a dilated heart, accompanied by continuous progressive decline of fractional shortening and ejection fraction (Vejpongsa and Yeh, 2014). Some studies also reported a decrease of left ventricle mass after anthracycline therapy (Jordan et al., 2018). Morphologically, clinical observations and animal studies both discovered myofibrillar loss, cardiomyocyte atrophy and cellular microvacuolization in anthracycline-treated hearts (Li et al., 2016, 2018). This may explain why chronic anthracycline cardiotoxicity is frequently irreversible. Cardiac fibrosis and inflammation were reported in some cases, although not representative enough (Zhao et al., 2010; Wang et al., 2016).

Strategies of preventing anthracycline-induced cardiac dysfunction include reduction of cumulative dose, liposome-based delivery, continuous infusions or use of less toxic analogues (such as epirubicin) (Vejpongsa and Yeh, 2014; Zamorano et al., 2016). At present, dexrazoxane, an iron chelator, is the only cardioprotective drug approved by Food and Drug Administration (FDA) and European Medicines Agent (EMA) to reduce anthracycline cardiotoxicity. Nevertheless, dexrazoxane was initially restricted to adult metastatic breast cancer patients receiving high cumulative dose of anthracyclines (European Medicines Agency, 2018a). Meanwhile, traditional cardiac medications, including angiotensin converting enzyme inhibitors (ACE inhibitors), angiotensin II receptor blockers (ARBs) and ß-adrenergic receptor antagonists (ß-blockers), are also tested in different studies to prevent anthracycline-associated cardiac side effects. Nevertheless, the results remain controversial, as some studies found a significant improvement of cardiac function by carvedilol (Kalay et al., 2006), nebivolol (Kaya et al., 2013) or carvedilol + enalapril (Bosch et al., 2013), whereas others reported no difference among placebo, metoprolol and enalapril groups (Georgakopoulos et al., 2010). More evidence is needed to clarify this point.

ANTHRACYCLINE-INDUCED MITOCHONDRIAL ROS PRODUCTION

The most widely accepted mechanism for anthracycline cardiotoxicity is the ability of these drugs to generate excessive reactive oxygen species (ROS) (**Figure 1A**). The special chemical structures of anthracyclines decide that they can be reduced to a semiquinone form. Inside the cells, this process is catalyzed by nicotinamide adenine dinucleotide phosphate (NADPH) oxidase and nitric oxide synthases (NOSs) in the cytoplasm [reviewed in refs (Rochette et al., 2015; Ghigo et al., 2016)], as well as by mitochondrial electron transport chain (ETC). All these components can transfer electrons to doxorubicin (DOX), for example, to form semiquinone doxorubicin (SQ-DOX). SQ-DOX is an unstable metabolite that could be oxidized by oxygen within mitochondria, accompanied by the release of ROS. This is further worsened by the fact that anthracyclines have high affinity to cardiolipin (Parker et al., 2001), a phospholipid exclusively localized at the inner mitochondrial membrane. Thus anthracyclines preferentially accumulate in mitochondria (Ichikawa et al., 2014). Excess ROS production can induce different types of cellular injury and ultimately lead to cell death. Considering the fact that mitochondria are extremely rich in cardiomyocytes and that the heart has lower levels of antioxidant enzymes, such as catalase and superoxide dismutase (SOD), compared to other organs (Li X. et al., 2020), it is reasonable that the heart is more susceptible to anthracycline-induced ROS generation.

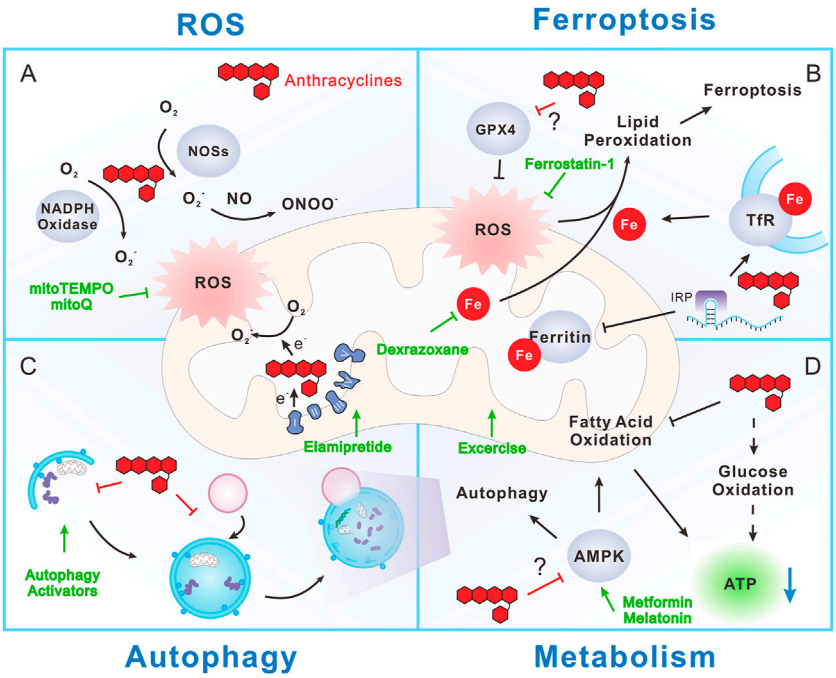

FIGURE 1 | Mitochondrial mechanism during anthracycline cardiotoxicity. **(A)** Anthracyclines promote reactive oxygen species (ROS) production through directly interfering with NADPH oxidase, nitric oxide synthases (NOSs) and mitochondrial electron transport chain (ETC). Mitochondria are the major producers of ROS, but in turn are injured by ROS. **(B)** Anthracyclines can disrupt iron metabolism by interacting with iron regulatory protein (IRP), resulting in promotion of transferrin receptor (TfR) expression and inhibition of ferritin expression. As a result, iron uptake is increased and iron storage is decreased, ultimately leading to free iron overload, especially in mitochondria. ROS can induce lipid peroxidation and consequent ferroptosis in an iron-dependent manner. Notably, anthracyclines inhibit Glutathione peroxidase 4 (GPX4), a phospholipid hydroperoxidase that inhibits lipid peroxidation, thus exacerbate ferroptosis. **(C)** Anthracyclines may disrupt autophagy and mitochondrial autophagy (mitophagy) through inhibition of autophagy initiation and blocking the fusion between autophagosome and lysosome. This prevents the efficient clearance of damaged cellular components including mitochondria and worsens anthracycline cardiotoxicity. However, whether autophagy is protective or detrimental during anthracycline cardiotoxicity is still controversial. **(D)** Anthracyclines largely reduce the utilization of fatty acid while transiently increase glucose oxidation (dashed arrow). The reprogram of fuel substrate utilization does not improve energy supply, but together with mitochondrial dysfunction, eventually lead to ATP reduction and energetic failure. AMPK is the main energy and nutrient sensor that promotes ATP production by activating anabolic processes, such as fatty acid oxidation and autophagy. Notably, AMPK is inhibited by anthracyclines with still unclear mechanism, which further exacerbates anthracycline-induced energetic failure. Strategies aiming at targeting mitochondrial features to reduce anthracycline cardiotoxicity include (green symbols): 1) Mitochondrial specific antioxidants, like mitoTEMPO and MitoQ. 2) Iron chelators, such as dexrazoxane. 3) Ferroptosis inhibitors, like ferrostatin-1. 4) Autophagy activators, such as PI3K/Akt/mTOR inhibitors and AMPK activators (metformin and melatonin). 5) Energetic stimulators, like elamipretide and aerobic exercise.

Mitochondrial respiration supplies ATP through electron transfer and the accompanied proton gradient. During this process, ROS are natural by-products under physiological conditions, but may be excessively produced under pathological situations, such as anthracycline stress. Mitochondrial ROS are primarily generated by the ETC complexes, including complex I, II, and III [reviewed in ref (Forrester et al., 2018)]. Complex I (also known as NADH dehydrogenase) is the major site wherein anthracyclines interrupt mitochondrial ROS production. Complex I catalyzes the production of NAD^+ from NADH and extracts 2 electrons to reduce FMN (flavin mononucleotide), the central unit of complex I. O_2^- is produced when O_2 reacts with reduced FMN (Forrester et al., 2018). Early studies demonstrated that anthracyclines can facilitate O_2^- generation by extracting electron from complex I to form semiquinone anthracycline. The oxidation of semiquinone anthracycline by O_2 promotes O_2^- generation (Davies and Doroshow, 1986; Marcillat et al., 1989). In addition, the extraction of electrons by anthracyclines hinders electron flow within ETC and, as a result, reduces ATP production. Later studies further revealed that the activities of complex II and III are also rapidly inhibited by anthracyclines, which do not contribute to ROS generation, suggesting that anthracyclines inactivate cardiac ETC through both oxidative and non-oxidative mechanisms (Marcillat et al., 1989; Pointon et al., 2010).

In summary, anthracycline-induced ROS production is pivotal factor that contribute to cardiomyocyte injury. It is worthy to note that ROS itself could boost secondary ROS generation, a process named ROS-induced ROS release (RIRR) (Zorov et al., 2014). RIRR hypothesis suggests that high level of ROS will cause irreversible opening of mitochondrial permeability transition pore (mPTP), leading to mitochondria damage and consequent ROS release from mitochondria to cytosol. The increased cytosolic ROS is rapidly absorbed by the adjacent normal mitochondria, thereby cascade amplification and release of ROS is achieved, ultimately triggering cell apoptosis (Zorov et al., 2014). In fact, a study in anthracycline-induced endotheliotoxicity models demonstrated that a stable level of

cytosolic ROS and rapid rise of mitochondrial ROS were observed in the early phase (4–8 h) after doxorubicin treatment, while a sudden 15-fold increase of cytosolic ROS occurs 16 h after doxorubicin exposure in human umbilical vein endothelial cells (HUVECs), suggesting that RIRR could contribute to the final ROS burst by anthracyclines (He et al., 2020). As anthracycline-induced cardiomyocyte mPTP opening and mitochondrial membrane potential loss are consistently observed in a large number of studies (He et al., 2018; Villa et al., 2021), it is supposed that RIRR also contributes to anthracycline cardiotoxicity, which awaits direct experimental confirmation.

MITOCHONDRIAL IRON-OVERLOAD AND FERROPTOSIS DURING ANTHRACYCLINE CARDIOTOXICITY

Disruption of iron homeostasis is another key reason for anthracycline cardiotoxicity. Since their discovery, anthracyclines are found capable of chelating free iron vigorously to form iron-anthracycline complexes, which further react with oxygen and promote ROS production (Gutteridge, 1984). Early studies demonstrated that animals fed with iron-rich food are more susceptible to doxorubicin-induced weight lost and cardiomyocyte apoptosis, suggesting a pivotal role of iron metabolism during anthracycline cardiotoxicity (Panjrath et al., 2007). Since anthracyclines boost ROS production, the iron-anthracycline complexes-related free radicals were initially considered as a contributor to anthracycline cardiotoxicity. Nevertheless, many antioxidant strategies failed to protect against anthracycline-induced myocardium injury in animal studies (Mukhopadhyay et al., 2009) and clinical settings (van Dalen et al., 2011). Thus, iron-anthracycline complexes and the related ROS production may have only limited effect in anthracycline cardiotoxicity. Instead, increasing evidence has supported the view that anthracyclines may directly interrupt iron metabolism, resulting in iron-overload and the consequent ferroptosis (**Figure 1B**).

Anthracyclines Interrupt Iron Metabolism

It is progressively clear that free iron accumulates in cardiomyocytes during anthracycline treatment, resulting in iron-overload that could be highly toxic (Ichikawa et al., 2014). Anthracycline-induced interruption of iron metabolism is a complex and multi-target process. Primarily, anthracyclines can interfere with the key iron-binding and -transporting proteins. For example, doxorubicinol, a doxorubicin metabolite, can sequester the Fe-S cluster of iron regulatory protein 1 (IRP-1), which serves as an important feedback regulator that strictly controls the expression of iron metabolism proteins (Minotti et al., 1998, 2001). Iron-doxorubicin complexes further reduce the available free iron pool, leading to a switch of IRP-1 to an iron-free state. Iron-free IRP-1 can bind to the iron-responsive elements (IREs) on the mRNA of iron metabolism-related proteins, such as transferrin receptor (TfR) and ferritin, and regulates their expression (Rouault, 2006). Upregulation of TfR and subsequently iron uptake are detected in doxorubicin-treated cells, whereby anti-TfR antibody effectively reduces doxorubicin-promoted iron uptake and cell death (Kotamraju et al., 2002). Beside disrupting IRP-1, doxorubicin can directly interact with the IREs of ferritin heavy and light chains (Canzoneri and Oyelere, 2008). The combinatorial altered expressions of TfR and ferritin lead to enhancement of iron uptake, inhibition of iron sequestration and ultimately iron-overload in cardiomyocytes. Moreover, deficiency of human hemochromatosis protein (also known as the HFE protein), which competes the interaction between TfR and transferrin, also leads to iron-overload and exacerbates doxorubicin-induced mitochondrial damage and mortality (Miranda et al., 2003). Notably, anthracycline-induced increment of iron contents preferentially accumulates in special subcellular compartments, especially the cardiac mitochondria. This may be due to the fact that mitochondria are the major cellular cites of iron utilization. Iron is required for the synthesis of heme and Fe-S clusters that are essential cofactors of enzymes involved in the tricarboxylic acid (TCA) cycle and the respiratory chain (Rizzollo et al., 2021). Accordingly, hearts from patients with anthracycline-related cardiomyopathy displayed higher iron levels in mitochondria, compared to those from patients with normal cardiac function or other types of heart failure (Ichikawa et al., 2014). Within the matrix, mitochondrial ferritin (FtMt) serves as an iron storage protein in mitochondria to avoid oxidative stress-related damage induced by high iron content. Correspondingly, FtMt deficient mice ($FtMt^{-/-}$) are more susceptible to anthracycine-induced mitochondrial damage, heart remodeling and mortality (Maccarinelli et al., 2014). In contrast, overexpression of mitochondrial iron exporters, such as ABC protein B8 (ABCB8), reduces mitochondrial free iron and protects the heart against anthracycline-induced cardiomyopathy (Ichikawa et al., 2014). Thus, anthracycline-induced disruption of iron metabolism eventually results in labile iron accumulation in mitochondria and finally cardiotoxicity.

Anthracyclines Induce Ferroptosis in Cardiomyocytes

A long-debated issue about anthracycline cardiotoxicity is which type of programmed cell death contributes mostly to the loss of terminally differentiated cardiomyocytes. It was initially reported that anthracyclines induce DNA damage and apoptosis (Arola et al., 2000). Nevertheless, later evidence suggested that anthracyclines trigger various types of programmed cell death, including necrosis (Zhang et al., 2016), pyroptosis (Wang et al., 2017), and autophagy (Lu et al., 2009). Thereinto, apoptosis, necrosis and pyroptosis are considered detrimental, while autophagy could be cardiac protective (Li et al., 2016, 2018). Intriguingly, disturbance of iron metabolism may eventually lead to another iron-dependent programmed cell death, ferroptosis. In fact, recent studies have highlighted the dominant role of ferroptosis in anthracycline cardiotoxicity (Fang et al., 2019; Tadokoro et al., 2020).

Ferroptosis is a recently identified form of programmed cell death that involves iron- and ROS-dependent damage to membrane lipids. It is characterized by the existence of small mitochondria with condensed mitochondrial membrane, pruning of mitochondria crista, as well as outer mitochondrial membrane rupture (Xie et al., 2016). Ferroptosis is genetically and biochemically distinct from other forms of programmed cell death, like apoptosis, necrosis, and autophagy. It can be triggered by activation of mitochondrial voltage-dependent anion channels, mitogen-activated protein kinases or over-activated endoplasmic reticulum stress. ROS production stimulated by these stresses directly induces peroxidation of phospholipids with polyunsaturated fatty acid (PUFA) chain in an iron-dependent manner, ultimately resulting in ferroptotic cell death. The cystine/glutamate antiporter system Xc^- maintains redox homeostasis by importing cystine to produce cysteine, which is used to synthesize the major antioxidant glutathione (GSH), thus inhibiting ferroptosis. In addition, glutathione peroxidase 4 (GPX4), nuclear factor erythroid 2-related factor 2 (NRF2) and heat shock protein beta-1 (HSPB1, also known as HSP27) negatively inhibit ferroptosis by limiting ROS production and reducing cellular iron uptake. In contrast, p53 inhibits SLC7A11, a key component of system Xc^-, while NADPH oxidase directly contributes to ROS production, both of which promote ferroptosis (Jiang et al., 2021). Doxorubicin treatment results in the suppression of GPX4, upregulation of PTGS2 (another key ferroptosis indicator) and lipid peroxidation of mitochondrial membrane, typical phenotypes of mitochondria-dependent ferroptosis, implying that anthracyclines induce ferroptosis in cardiomyocytes and hearts (Fang et al., 2019; Tadokoro et al., 2020; He et al., 2021). Consistently, inhibition of ferroptosis by pharmacological inhibitors (ferrostatin-1 or mitoTEMPO) or by genetic overexpression of GPX4 both significantly reduce doxorubicin-induced heart injury and mortality in mice (Fang et al., 2019; Tadokoro et al., 2020). Mechanistically, doxorubicin facilitates nuclear accumulation of the nuclear factor erythroid 2-related factor 2 (NRF2) and enables NRF2 to promote the expression of heme oxygenase 1 (HMOX1). HMOX1 can degrade heme to release free iron. As a result, iron accumulates in the heart after doxorubicin treatment, ultimately promoting mitochondrial-dependent ferroptosis (Fang et al., 2019). Moreover, anthracyclines downregulate GPX4, especially mitochondrial GPX4, thereby dampening the anti-ferroptosis effect of GPX4 and exacerbating cardiomyocyte injury (Tadokoro et al., 2020). Notably, inhibition of ferroptosis displays more efficient cardiac protection compared to repression of other types of programmed cell death, including apoptosis, necrosis and autophagy (Fang et al., 2019), further emphasizing the dominant role of iron-overload and ferroptosis in anthracycline-induced cardiotoxicity. Thus, ferroptosis inhibitors, such as ferrostatin-1 or mitoTEMPO, could be promising drugs to prevent anthracycline cardiotoxicity.

Overall, ferroptosis raises as a newly recognized programmed cell death. Past and recent evidence both highlight that anthracycline-induced iron-overload in mitochondria and the consequent mitochondria-dependent ferroptosis are dominant factors involved in anthracycline cardiotoxicity. It is worth further efforts to investigate whether ferroptosis inhibitors could act as cardioprotectant against anthracycline cardiotoxicity in the future.

AUTOPHAGY, MITOPHAGY AND MITOCHONDRIAL DYNAMICS IN ANTHRACYCLINE CARDIOTOXICITY

Autophagy and Mitophagy in Anthracycline Cardiotoxicity

Autophagy is another programmed cell death process that has received great attention. Since its discovery, autophagy is considered as a beneficial process that helps to maintain cellular homeostasis by facilitating the removal of aggregated proteins and damaged organelles, such as mitochondria (Chun and Kim, 2018). Nevertheless, uncontrolled amplification of autophagy can also be a final outcome, resulting in cell death (Nishida et al., 2008). Autophagy starts with the nucleation and elongation of double membrane vesicles, named autophagosomes, which can encapsulate ubiquitinated proteins destined to be degraded (Russell et al., 2013). The recognition of cargo proteins or organelles depends on matured microtubule-associated protein 1 light chain 3 (LC3-II) on the autophagosome membranes and proteins that carry a LC3-II interacting domain (LIR), such as sequestosome-1 (SQSTM1, also known as ubiquitin-binding protein p62) (Klionsky et al., 2021). Consequently, autophagosomes fuse with lysosomes to form autolysosomes, wherein the low pH environment and proteases control the degradation of targeted protein cargos. Autophagy is strictly regulated by the upstream signalling, including AMP activated protein kinase (AMPK)-regulated activation and PI3K/Akt/mTOR-mediated inhibition (Kim et al., 2011).

The detoxifying effect of this cellular recycling process in other types of cardiac diseases is well recognized (Sabbah et al., 2016), but whether autophagy is beneficial or detrimental in anthracycline-induced cardiotoxicity is still a subject of dispute. Previous studies reported that anthracyclines stimulate cardiac autophagy, which primarily contributes to cardiomyocyte death after drug treatment. An enhanced level of autophagy markers, including Beclin1, LC3-II, p62, autophagy-related protein (ATG) 5 (ATG5) and 7 (ATG7), are detected in anthracycline-treated cardiomyocytes and hearts (Zhang et al., 2011, 2019; Wang et al., 2014; Luo et al., 2018). In support of these findings, inhibition of Beclin1 attenuates anthracycline-induced cardiomyocyte death, whereas Beclin1 overexpression exacerbates anthracycline cardiotoxicity (Kobayashi et al., 2010). However, other studies demonstrated that anthracyclines in fact can block autophagy and that promotion of cardiac autophagy flux is protective against anthracycline cardiotoxicity (Kawaguchi et al., 2012; Sishi et al., 2013; Dutta et al., 2014; Li et al., 2016, 2018; Song et al., 2018; He et al., 2021). These controversial findings may be attributed to a lack of uniform models to study the role of autophagy in anthracycline cardiotoxicity [reviewed in ref. (Li M. et al.,

2020)]. Whether autophagy is protective or detrimental in anthracycline cardiotoxicity may be attribute to multiple reasons, including the lack of accurate analysis of autophagy flux, dose and duration of anthracycline treatment, as well as dynamic phases of the pathological development. Despite that no consensus has been made on the role of autophagy in anthracycline cardiotoxicity, most studies support the view that anthracyclines impair autophagy flux, resulting in the blockage of clearance and recycling of potentially toxic cellular components, such as damaged/dysfunctional mitochondria (**Figure 1C**).

Cardiomyocytes are abundant with mitochondria, which are the major source of ROS production. In turn, cardiomyocyte mitochondria are susceptible to ROS-induced damage. Mitochondrial autophagy, also called mitophagy, is essential for clearing damaged mitochondria and maintaining the functional ones (Saito and Junichi, 2015). In addition to the standard process of autophagy, mitophagy involves the participation of specific proteins, which work as labels for helping damaged-mitochondria recognition by LC3 and p62. These proteins include: 1) BCL2/adenovirus E1B 19 kDa interacting protein 3 (Bnip3), NIP3-like protein X (Nix, also known as Bnip3L), FUN14 domain containing 1 (FUNDC1) and cardiolipin, which are direct receptors of LC3 on the mitochondrial outer membrane, and 2) PTEN-inducible putative kinase 1 (PINK1) and Parkinson juvenile disease protein 2 (Parkin), which regulate mitochondrial protein ubiquitination and the recognition by p62 and LC3 (Saito and Junichi, 2015).

PINK1/Parkin-mediated recognition of damaged mitochondria by autophagosomes is the most studied mitophagy mechanism. PINK1 is a mitochondrial serine/threonine-protein kinase that locates in inner mitochondrial membrane. However, PINK1 fails to insert into the inner membrane when mitochondrial depolarization occurs, thereby accumulating at the outer mitochondrial membrane. Accumulated and activated PINK1 consequently recruits Parkin, an ubiquitin E3 ligase that ubiquitinates various proteins on the mitochondrial outer membrane, thus marking depolarized mitochondria to be recognized by p62, LC3 and autophagosomes (Narendra et al., 2008). Mitophagy is impaired in anthracycline-treated hearts, as a significant decrease of PINK1, Parkin and p62 in the mitochondria is detected after doxorubicin treatment (Hoshino et al., 2013). Precise analysis revealed that PINK1 and Parkin are suppressed by doxorubicin in early stages (2–8 days after treatment), but restore at later phases (14 days after treatment) (Hull et al., 2016). The mechanism about how anthracyclines inhibit PINK1, Parkin and the mitophagy process is still unclear, but may include the participation of apoptotic protein p53. Anthracyclines activate p53, subsequently promoting its direct binding and sequestering Parkin in the cytosol, thus hindering the recruitment of Parkin to mitochondria and preventing mitophagy initiation (Hoshino et al., 2013). Accordingly, both p53 deficiency and Parkin overexpression in cardiomyocytes restore mitophagy and attenuate anthracycline-induced cardiotoxicity (Hoshino et al., 2013).

Apart from the well-described PINK1/Parkin mechanism, Bnip3 and Nix (Bnip3L) are also essential players involved in mitophagy. Bnip3 and Nix are transcriptionally activated by hypoxia-HIF1α signalling axis and translocate to the outer mitochondrial membrane to trigger mitophagy. Notably, Bnip3 and Nix mediate mitophagy independent of the mitochondrial permeability transition pore opening and depolarization (Quinsay et al., 2010). Bnip3 contains a LIR domain that allows it to directly interact with LC3 and guide the recognition of mitochondria by autophagosome (Zhang and Ney, 2009; Saito and Junichi, 2015). Anthracyclines upregulate Bnip3 expression in a dose-dependent manner and promote its translocation to mitochondria (Dhingra et al., 2014). In line with a maladaptive role of Bnip3 in anthracycline cardiotoxicity, inhibition of Bnip3 with shRNA and expression of a mutant Bnip3 that lacks a mitochondria-binding domain, both rescued anthracycline-induced mitochondrial dysfunction in cardiomyocytes. Bnip3 deficiency ($Bnip3^{-/-}$) also protected the mice against anthracycline-induced mitochondrial injury and improved their survival (Dhingra et al., 2014). It is still unclear how anthracyclines activate Bnip3 in the heart. Anthracycline-induced ROS could be a trigger, as it is found that oxidative stress induces Bnip3 dimerization and activation in ischemia/reperfusion (I/R) hearts (Kubli et al., 2008). Notably, Bnip3 regulates both necrosis and the mitophagy process. It is worthy to further clarify whether both mechanisms are involved in Bnip3-mediated heart injury after anthracycline treatment.

Similar to the debate in autophagy, the role of mitophagy in anthracycline-induced cardiotoxicity is also unclear. Current evidence supports the view that anthracyclines inhibit PINK1/Parkin-regulated mitophagy and that restoration of mitophagy rescues anthracycline cardiotoxicity. In contrast, Bnip3, a dual marker of mitophagy and necrosis is upregulated by anthracyclines, prior to mitochondrial polarization. Anthracyclines appear to induce Bnip3 activation and promote necrosis (Dhingra et al., 2014), but it still needs to be clarified whether Bnip3-regulated mitophagy is involved in anthracycline cardiotoxicity. Moreover, chronic low-dose (Hoshino et al., 2013; Hull et al., 2016) and acute high-dose (Dhingra et al., 2014) anthracycline treatment regimens are used in different studies, resulting in the difficulty to reach a consensus whether mitophagy is injurious or protective during anthracycline cardiotoxicity.

Mitochondrial Dynamics in Anthracycline Cardiotoxicity

Mitochondria are highly dynamic organelles that change their morphology through fission and fusion. This process, namely mitochondrial dynamics, helps mitochondria to adapt to cellular stresses such as energy deficiency and ROS-induced injury, thereby ensuring mitochondrial function (Youle and van der Bliek, 2012). The fission process generates small spherical mitochondria, while the fusion process produces extended mitochondria and mitochondrial networks. Mitochondrial dynamics and autophagy/mitophagy constantly work together to eliminate injured and dysfunctional mitochondria. High resolution structured illumination microscopy (SIM) clearly showed that smaller mitochondria derived from mitochondria fission are always accompanied with a higher level of ROS and

loss of membrane potential, compared to the larger fission portion. These smaller mitochondria are destined for being degraded by mitophagy (Kleele et al., 2021). The mitochondrial fission process is mediated by fission factors, including mitochondrial fission factor (MFF), mitochondrial fission process 1 (MTFP1), dynamin-related protein 1 (DRP1), mitochondrial dynamics proteins of 49 kDa [MiD49 (also known as MIEF2)] and 51 kDa [MiD51 (also known as MIEF1)] (Kraus et al., 2021), whereas mitochondrial fusion is regulated by specific GTPases, including mitofusin 1 (MFN1), mitofusin 2 (MFN2) and optic atrophy 1 (OPA1) (Tilokani et al., 2018).

Dysregulation of mitochondrial dynamics were observed in various heart diseases, including cardiac hypertrophy, heart failure, dilated cardiomyopathy (DCM), ischemic heart disease [reviewed in ref (Ikeda et al., 2014)], as well as anthracycline-induced cardiomyopathy [reviewed in ref (Osataphan et al., 2020)]. Doxorubicin can decrease the expression of MFN1, MFN2 and OPA1, but increase DRP1 and promote mitochondria fragmentation (Li et al., 2014; Tang et al., 2017; Marques-Aleixo et al., 2018b; Catanzaro et al., 2019), suggesting that anthracyclines may inhibit mitochondrial fusion and promote mitochondrial fission. In rodent cardiomyocytes and hearts, doxorubicin exposure promotes phosphorylation of DRP1 at serine 616, which is essential for the activity of DRP1 to mediate mitochondrial fission (Dhingra et al., 2017; Xia et al., 2017). In line with this, DRP1 deficient animals are protected against anthracycline-induced cardiac dysfunction (Catanzaro et al., 2019). In addition, mitophagy inhibitor liensinine mitigates anthracycline-induced cardiotoxicity by inhibiting DRP1-mediated mitochondrial fission (Liang et al., 2020). These findings together suggest that anthracycline cardiotoxicity is mediated, at least in part, by the increased mitochondrial fragmentation, fission and the accelerated mitochondrial degradation by mitophagy. Inhibiting mitochondrial fission and mitophagy may provide beneficial effect against anthracycline cardiotoxicity. However, further studies are required to confirm whether the change of mitochondrial dynamics is a consequent of anthracycline-induced mitochondrial damage or a direct driver of cardiac injury.

ANTHRACYCLINE-INDUCED CARDIAC METABOLIC DISTURBANCE

As discussed above, mitochondria are the key energy factories of cardiomyocytes and major targets of anthracyclines. It is thus no doubt that anthracycline-induced long-term mitochondrial dysfunction can result in energy deficiency in cardiomyocytes. In fact, we and others all revealed that ATP production is impaired by anthracyclines (Li et al., 2018; Abdullah et al., 2019). Mitochondria isolated from acute and chronic anthracycline-treated hearts both showed significant suppression of mitochondrial respiration (Abdullah et al., 2019). Therefore, metabolic disturbance may also be a mechanism underlying anthracycline-induced cardiomyopathy (**Figure 1D**).

Anthracyclines Interrupt Myocardial Substrate Utilization

In physiological condition, hearts mainly use fatty acids (FAs) as substrates and rely on TCA cycle for ATP production. However, in the failing hearts, where mitochondria are impaired by ROS or other insults, cardiomyocytes switch to use glucose, lactate and a small amount of ketone bodies for energy production. Glycolysis then raises as a substituted metabolic mode to produce ATP when OXPHOS is suppressed (Doenst et al., 2013). In fact, anthracyclines increase translocation of glucose transporter 1 (GLUT1) to the plasma membrane (Hrelia et al., 2002), thereby enhancing transient glucose uptake in isolated cardiomyocytes (Hrelia et al., 2002), as well as in hearts of mice and Hodgkin disease patients (Baucknehet al., 2017; Sarocchi et al., 2018). In line with this, an increase of glycolytic flux (Carvalho et al., 2010) and key glycolytic enzymes, such as hexokinase (HK), phosphofructokinase (PFK) and pyruvate kinase (PK) (Li et al., 2018), were found in anthracycline-treated hearts. Nevertheless, glycolysis activation seems to be a transient and compensatory response that cannot meet the cellular energy demand in the long term, as glucose uptake returns to basal level later (3 h) after anthracycline treatment in cardiomyocytes (Hrelia et al., 2002). Moreover, persistent glucose usage may lead to several glucose-dependent non-ATP-generating pathways, such as pentose phosphate pathway (PPP), which serves as an important source of NADPH and ROS, and hexosamine biosynthetic pathway (HBP), which regulates protein O-GlcNAcylation (Doenst et al., 2013).

In contrast, long-chain fatty acid oxidation is inhibited in anthracycline-treated rat hearts (Carvalho et al., 2010). For instance, palmitate oxidation was reduced by 40–70% in cardiomyocytes isolated from acute or chronic anthracycline-treated animals (Abdel-aleem et al., 1997; Sayed-ahmed et al., 1999). Mechanistically, anthracyclines interrupt the activity of carnitine palmitoyl transferase I (CPT I), a mitochondrial membrane enzyme that converts long-chain acyl-CoA to long-chain acyl-carnitines and facilitates their transport into mitochondria. Therefore, anthracyclines inhibit the fatty-acid ß-oxidation process (Abdel-aleem et al., 1997). Accordingly, supplementation of L-carnitine was proved to attenuate anthracycline cardiotoxicity in animals (Andrieu-Abadie et al., 1999; Sayed-ahmed et al., 2000; Cabral et al., 2018) and in patients with non-Hodgkin lymphoma (Waldner et al., 2006).

Overall, when anthracyclines induce mitochondrial dysfunction, glucose oxidation is transiently activated while fatty acid oxidation is inhibited. The alteration of substrate utilization compensates early energy loss, but cannot meet the long-term cellular energy demand, thus resulting in maladaptive energetic failure. Strategies aiming for supplementing additional ATP production may work to mitigate anthracycline cardiotoxicity. For instance, an early study demonstrated that rats continuously administrated with fructose-1,6-diphosphate, a glycolytic intermediate, displayed significant improvement of cardiac function after acute and chronic anthracycline treatment (Danesi et al., 1990). Stimulating mitochondrial

respiration, by L-carnitine supplementation (Andrieu-Abadie et al., 1999; Sayed-ahmed et al., 2000; Cabral et al., 2018) or with OXPHOS medium filled with galactose/pyruvate/glutamine (Deus et al., 2015), also restored myocardial energy supply and mitigated anthracycline cardiotoxicity.

AMPK-Mediated Metabolic Homeostasis During Anthracycline Cardiotoxicity

AMPK is the main intracellular sensor and regulator of energy and nutrient signalling. It is canonically activated by the increase of AMP:ATP or ADP:ATP ratios that result from a variety of energy stresses, including starvation, exercise, ischemia or mitochondrial dysfunction. AMP and ADP can directly bind AMPK and promote its phosphorylation by liver-kinase-B1 (LBK1), thus increasing AMPK activity up to 100-fold. In contrast, ATP inhibits AMPK phosphorylation and activation. In addition, AMPK can also be phosphorylated by calcium/calmodulin-dependent kinase kinase 2 (CAMKKß) that is activated by different hormone stimulations. Once activated, AMPK can phosphorylate and regulate a variety of downstream proteins to promote catabolic processes such as fatty acid oxidation, glucose uptake, glycolysis, autophagy and mitochondrial fission, or inhibit anabolic processes such as synthesis of protein, fatty acid, glycogen and sterol (Garcia and Shaw, 2017).

Despite that anthracyclines induce mitochondrial dysfunction and energy deficiency, which are supposed to stimulate AMPK signalling, many studies revealed that AMPK as well as its downstream target acetyl-CoA carboxylase (ACC) are indeed inhibited by anthracyclines (Gratia et al., 2012; Kawaguchi et al., 2012; Wang et al., 2012). Accordingly, AMPKα1 deficient ($AMPK\alpha1^{-/-}$) mouse embryonic fibroblasts and cardiomyocytes are more susceptible to anthracycline treatment (Wang et al., 2012), but AMPK activation by a variety of strategies, such as prior starvation, 5-aminoimidazole-4-carboxamide ribonucleoside (AICAR) treatment and adenovirus-mediated AMPK constitutive activation (AMPK-CA), diminishes anthracycline-induced heart injury (Chen et al., 2011; Kawaguchi et al., 2012; Wang et al., 2012). In this view, instead of serving as a trigger to activate AMPK, energetic failure seems to be a result of anthracycline-regulated AMPK inhibition. As a result, catabolic processes aiming for increasing ATP production under anthracycline stress are inhibited following AMPK inhibition. This partially explains the inhibition of autophagy by anthracyclines, as AMPK inhibition results in direct reduction of ULK1 phosphorylation and blockage of autophagy initiation (Chen et al., 2011; Kawaguchi et al., 2012). Moreover, AMPK inhibition also reactivates mTORC1, which further promotes energy consumption, inhibits autophagy and worsens energetic stress (Gratia et al., 2012). Metformin, a well-recognized AMPK activator (Hawley et al., 2002), has also showed promising protective effects against anthracycline-induced heart injury (Asensio-López et al., 2011; Kobashigawa et al., 2014; Zilinyi et al., 2018). This further supports a fundamental role of AMPK in anthracycline-mediated metabolic disturbance. Nevertheless, the mechanism underlying how anthracyclines inhibit AMPK is still unclear and awaits further investigation.

Taken together, AMPK signalling is inhibited by anthracyclines, leading to the exacerbation of cardiac energetic stress, which further contributes to anthracycline cardiotoxicity. Reactivation of AMPK could be a potential strategy to attenuate anthracycline cardiotoxicity.

STRATEGIES TARGETING MITOCHONDRIAL MECHANISM TO REDUCE ANTHRACYCLINE CARDIOTOXICITY

Mitochondria are crucial for anthracycline-induced cardiotoxicity (**Figure 1**). Targeting mitochondrial mechanisms could provide potential strategies to attenuate anthracycline cardiotoxicity (Murabito et al., 2020). Anthracyclines promote excessive ROS production within the cytoplasm and mitochondria. Thus, antioxidants are initially tested in early studies to counterwork anthracycline cardiotoxicity. Nevertheless, antioxidants or ROS scavengers, such as the xanthine oxidase inhibitor allopurinol, the NADPH oxidase inhibitors apocynin and DPI, coenzyme Q10, L-carnitine, NAC and vitamins E and C, failed to mitigate anthracycline cardiotoxicity in animal (Berthiaume et al., 2005; Mukhopadhyay et al., 2009) and clinical studies (van Dalen et al., 2011), suggesting that general inhibition of ROS production is not sufficient to prevent anthracycline-induced cardiotoxicity. Moreover, some antioxidants are able to decrease anthracycline-induced oxidative stress but without preventing mitochondrial dysfunction (Berthiaume et al., 2005), implying that specifically targeting mitochondria-related ROS generation may be requisite. MitoTEMPO, a derivative of TEMPO, is a mitochondria-targeted superoxide mimetic. It can readily pass through lipid bilayers, accumulate in mitochondria, enhance superoxide dismutase (SOD) activity and scavenge mitochondrial O_2^-. Studies revealed that mitoTEMPO, but not TEMPO, can suppress anthracycline-induced lipid peroxidation specifically in mitochondria and reduce cardiomyopathy (Rocha et al., 2016; Fang et al., 2019). Other mitochondria-targeted antioxidants, like mitoquinone (mitoQ), also display protective effect against anthracycline-induced cardiotoxicity and endotheliotoxicity (Chandran et al., 2009; Clayton et al., 2020; Wu et al., 2020). Thus, mitoTEMPO and mitoQ are promising drugs to mitigate anthracycline-induced cardiomyopathy.

As discussed above, iron accumulates in mitochondria during anthracycline exposure. Therefore, iron chelators were primarily considered as pharmacological strategies to limit anthracycline cardiotoxicity. Nevertheless, dexrazoxane currently represents the only iron-chelating drug approved by FDA and EMA to prevent anthracycline-induced cardiomyopathy in breast cancer patients. The protective effect of dexrazoxane is primarily attributed to the scavenging of free iron (Xu et al., 2005). However, other iron chelators, such as desferrioxamine and deferasirox, failed to achieve the same protective effect (Voest

et al., 1994; Hasinoff et al., 2003), suggesting that dexrazoxane may protect the heart against anthracycline cardiotoxicity through mechanisms more than iron chelating. Later works revealed that dexrazoxane can also target and inhibit topoisomerase IIß (TOP2ß), avoiding the formation of anthracycline-TOP2ß-DNA cleavage complex and the consequent DNA double-strand breaks (Lyu et al., 2007; Hasinoff et al., 2020). The cardiac protective effect of dexrazoxane was proved in animal models (Alderton et al., 1990; Bjelogrlic et al., 2007) and was further validated in clinical trials on anthracycline-treated breast cancer patients (Venturini et al., 1996; Swain et al., 1997; Lopez et al., 1998). Nonetheless, its clinical use was initially restricted by FDA and EMA to adult breast cancer patients who receive therapeutic dose higher than 300 mg/m^2 doxorubicin or 540 mg/m^2 epirubicin, since it was debated that dexrazoxane may induce secondary hematological malignancies in pediatric patients (Tebbi et al., 2007; Lipshultz et al., 2010). However, new studies based on a large patient collection stated that dexrazoxane is cardioprotective and safe in pediatric leukemia patients receiving anthracycline therapy (Asselin et al., 2016). The EMA recently removed this contraindication for children and adolescents treated with high cumulative doses of anthracyclines (European Medicines Agency, 2018b).

Ferroptosis is a newly recognized programmed cell death that relies on both ROS generation and iron homeostasis disruption (Jiang et al., 2021). Studies in recent years highlighted that ferroptosis could be the dominant programmed cell death induced by anthracyclines, as inhibition of ferroptosis shows more efficient cardiac protection compared to blockage of apoptosis, necrosis or autophagy (Fang et al., 2019). Ferrostatin-1 is a widely-used ferroptosis inhibitor, potentially functioning through scavenging the alkoxyl radicals, interacting with ferrous iron and inhibiting lipid peroxidation (Miotto et al., 2020). Many studies have demonstrated that ferrostatin-1 efficiently attenuates anthracycline-induced ferroptosis, mitochondrial dysfunction and heart injury (Fang et al., 2019; Tadokoro et al., 2020; He et al., 2021). Notably, although ferrostatin-1 and dexrazoxane both inhibit ferroptosis and show similar protection against anthracycline-induced cardiac damage, they seem to function through different mechanisms. Ferrostatin-1 does not reduce the labile iron pool in the heart, whereas dexrazoxane attenuates cardiac free irons, after anthracycline treatment (Fang et al., 2019). Moreover, concomitant inhibition of ferroptosis and apoptosis with ferrostatin-1 and zVAD-FMK is more efficient than treating with ferrostatin-1 or Zvad-FMK alone and fully prevents anthracycline-induced cardiomyocyte death (Tadokoro et al., 2020). This suggests that anthracycline-induced cell death is not a single-factorial event.

The roles of autophagy and mitophagy in anthracycline-induced cardiotoxicity have been studied for decades, however, there is currently no autophagy-targeting compound being used in preclinical trials to reduce anthracycline cardiotoxicity. This is largely due to the controversy whether autophagy/mitophagy is beneficial or detrimental for anthracycline cardiotoxicity (Li M. et al., 2020). Nevertheless, some attempts targeting autophagy/mitophagy have been tried in animal models. Autophagy activators, such as mTOR inhibitor (rapamycin) (Ding et al., 2011), PI3Kγ inhibitors (AS605240, IPI145) (Li et al., 2018), show protective effect against anthracycline-induced heart injury in zebrafish and mouse. Other nonpharmacological interventions to promote autophagy, including prior starvation (Kawaguchi et al., 2012) and caloric restriction (Chen et al., 2011), also display cardioprotection during anthracycline treatment. Some studies suggested that inhibition of autophagy initiation could be beneficial, as anthracyclines inhibit the lysosome acidification, resulting in an accumulation of autophagosomes and autolysosomes (Li et al., 2016). In this regard, promotion of autophagy flux could be more precise than simple activation or inhibition of autophagy to prevent anthracycline cardiotoxicity. Unfortunately, selective drugs that target lysosome/autolysosome and facilitate autophagy flux are still not available. In contrast, inhibition of mitochondrial fission and mitophagy seems to be beneficial. The mitophagy inhibitor liensinine protects the heart against anthracycline-induced ROS generation and contractile dysfunction by decreasing DRP1 phosphorylation, inhibiting mitochondrial fragmentation and reducing mitophagy (Liang et al., 2020).

Mitochondria are the well-known energy factories of cardiomyocytes. Thus, anthracycline-induced mitochondrial dysfunction can ultimately lead to energy deficiency and metabolic disturbance. Strategies aiming at improving mitochondrial function could be capable to mitigate anthracycline cardiotoxicity. For example, elamipretide is a tetrapeptide designed to selectively target mitochondrial ETC and restore cellular bioenergetics. Animal studies (Gupta et al., 2016; Sabbah et al., 2016) and a small clinical trial (Daubert et al., 2017) all revealed that elamipretide can improve mitochondrial function and preserve cardiac contractility in canines and patients with heart failure. Although there is no direct evidence proving that elamipretide can prevent anthracycline-induced cardiomyopathy, the common feature of mitochondrial dysfunction during anthracycline cardiotoxicity suggests that elamipretide could be a promising drug. Interestingly, a recent work reported a mitochondria supplementation strategy in which mitochondria-rich extracellular vesicles (EVs), isolated from mesenchymal stem cells (MSCs), were transported to patient pluripotent stem cell-derived cardiomyocytes (iCMs). Mitochondria-rich EVs significantly promote ATP production and mitochondrial biogenesis and rescue iCMs from doxorubicin injury (O'Brien et al., 2021; Wang et al., 2021). Further, a recent work overviewed the tolerability and efficacy of exercise on cancer therapy-induced cardiovascular toxicity and concluded that aerobic exercise can improve peak oxygen uptake (VO2peak) and cardiorespiratory fitness (CRF) by an integrative assessment of global cardiovascular function (Scott et al., 2018). Physical activity was proved to mitigate anthracycline-induced mitochondriopathy in multiple animal studies [reviewed in ref (Marques-Aleixo et al., 2018a)]. The beneficial effect of exercise training primarily stems from the activation of mitochondrial biogenesis and adaption (MacInnis and Gibala, 2017), as well as the stimulation of energetic pathways such as AMPK signalling and the autophagy process (Marques-Aleixo et al., 2018b). Together, these animal and clinical evidence suggest that exercise training could be another potential strategy to prevent cardiotoxicity induced by anti-cancer therapy.

AMPK is a central mediator for cardiac metabolic homeostasis. A large set of studies proved that AMPK activators, like metformin (Asensio-López et al., 2011; Kobashigawa et al., 2014; Zilinyi et al., 2018) and melatonin (Liu et al., 2018; Li H. et al., 2020; Najafi et al., 2020; Arinno et al., 2021), can efficiently alleviate anthracycline-induced cardiac injury. The mechanism underlying the protective effect of AMPK activators is multi-factorial, for example, AMPK can facilitate fatty acid oxidation and promote cardiac autophagy. Based on these studies, a phase II clinical trial were carried out to validate whether metformin could reduce doxorubicin-induced cardiotoxicity in breast cancer patients (Avera McKennan Hospital & University Health Center, 2019). Unfortunately, this clinical trial was terminated due to slow accrual. Future clinical trials are needed to answer whether metformin or other AMPK activators could prevent anthracycline cardiotoxicity.

CONCLUSION

Cardiotoxicity induced by anthracyclines remains a hard stone that hampers their clinical applications in chemotherapy. Despite that the molecular mechanism underlying anthracycline cardiotoxicity is complex and multifactorial, emerging evidence supports the ideas that cardiac mitochondria are one of the pivotal targets of anthracyclines and mitochondrial dysfunction plays a determinant role in anthracycline cardiotoxicity (**Figure 1**). Anthracyclines have high affinity to the inner mitochondrial membrane protein cardiolipin and thus preferentially accumulate in mitochondria. Moreover, the special structures of anthracyclines decide that they are ideal substrates for redox reaction that produces excessive ROS which in turn injures mitochondria. In addition, anthracyclines interrupt iron metabolism and induce labile iron overload in mitochondria, which lead to cellular toxicity along with surplus ROS production. Thus, iron-dependent ferroptosis arises as a dominant programmed cell death that attributes to anthracycline-induced cardiomyocyte loss. Conversely, flux of another programmed cell death, autophagy, is impaired by anthracyclines. This restrains the efficient degradation and recycling of damaged cellular components including mitochondria, thereby exacerbating anthracycline-induced injury. Furthermore, anthracycline-associated mitochondrial dysfunction may reprogram the utilization of fuel substrates, including glucose and fatty acids, ultimately inducing metabolic disturbance and energetic failure.

Based on these aspects, pharmacological strategies aiming at reducing mitochondrial injury or restoring mitochondrial function could potentially lessen anthracycline cardiotoxicity. These strategies include the utilization of mitochondrial specific antioxidants, iron chelators, ferroptosis inhibitors, autophagy/mitophagy compounds and mitochondrial energetic stimulators. Some of these drugs showed protective effects in cardiomyocytes *in vitro* or animal models *in vivo*, yet failed to provide further benefits in preclinical studies. Despite almost 50 years of research, dexrazoxane remains the only FDA- and EMA-approved protectant to reduce cardiotoxicity in adult breast cancer patients who receive accumulative high dose anthracycline therapy. This could be due to the fact that anthracycline cardiotoxicity is a multi-factor event. For instance: 1) Dexrazoxane succeeds because it functions both as an iron chelator to reduce iron-overload and a TOP2ß inhibitor to mitigate DNA cleavage. 2) Antioxidant or iron chelator alone shows limited effects against anthracycline cardiotoxicity, while inhibition of ferroptosis by scavenging ROS and limiting iron-overload together displays more significant protection. 3) Concomitant inhibition of ferroptosis and apoptosis is more efficacious than supressing each process alone. The joint regimen fully prevents anthracycline-induced cardiomyocyte death. In the future, more bench work, preclinical and clinical studies are worth further testing, on one hand, whether the aforementioned mitochondria-targeted drugs could prevent anthracycline-induced cardiotoxicity and, on the other hand, whether targeting different mechanisms together could provide more efficient cardiac protection.

AUTHOR CONTRIBUTIONS

ML gave the first idea for the manuscript. JH, RW, LC, ZY, DY, and ML wrote the manuscript. JH, DY, and ML revised the manuscript. All authors listed have made substantial, direct, and intellectual contribution to the work and approved it for publication.

FUNDING

This work is supported by the grants from Guangzhou Basic and Applied Basic Research Foundation (202102020509 to JH), from the Program for Guangdong Introducing Innovative and Entrepreneurial Teams (2017ZT07S347 to JH), from National Natural Science Foundation of China (82000346 to ML), from Basic and Applied Basic Research Foundation of Guangdong Province (2019A1515110113 to ML) and from the Fundamental Research Funds for the Central Universities of Jinan University (21620338 to ML).

REFERENCES

Abdel-aleem, S., El-Merzabani, M. M., Sayed-Ahmed, M., Taylor, D. A., and Lowe, J. E. (1997). Acute and Chronic Effects of Adriamycin on Fatty Acid Oxidation in Isolated Cardiac Myocytes. *J. Mol. Cel Cardiol* 29, 789–797. doi:10.1006/jmcc.1996.0323

Abdullah, C. S., Alam, S., Aishwarya, R., Miriyala, S., Bhuiyan, M. A. N., and Panchatcharam, M., (2019). Doxorubicin-induced Cardiomyopathy Associated with Inhibition of Autophagic Degradation Process and Defects in Mitochondrial Respiration. *Sci. Rep.* 9, 1. 2002. doi:10.1038/s41598-018-37862-3

Alderton, P., Gross, J., and Green, M. D. (1990). Role of (±)-1,2-Bis(3,5-Dioxopiperazinyl-1-Yl)propane (ICRF-187) in Modulating Free Radical Scavenging Enzymes in Doxorubicin-Induced Cardiomyopathy. *Cancer Res.* 50, 5136–5142.

Andrieu-Abadie, N., Jaffrézou, J.-P., Hatem, S., Laurent, G., Levade, T., and Mercadier, J.-J. (1999). L-carnitine Prevents Doxorubicin-Induced Apoptosis of Cardiac Myocytes: Role of Inhibition of Ceramide Generation. *FASEB J.* 13, 1501–1510. doi:10.1096/fasebj.13.12.1501

Arinno, A., Maneechote, C., Khuanjing, T., Ongnok, B., Prathumsap, N., Chunchai, T., et al. (2021). Cardioprotective Effects of Melatonin and Metformin against Doxorubicin-Induced Cardiotoxicity in Rats Are through Preserving Mitochondrial Function and Dynamics. *Biochem. Pharmacol.* 192, 114743. doi:10.1016/j.bcp.2021.114743

Arola, O. J., Saraste, A., Pulkki, K., Kallajoki, M., Parvinen, M., and Voipio-Pulkki, L.-M. (2000). Acute Doxorubicin Cardiotoxicity Involves Cardiomyocyte Apoptosis. *Cancer Res.* 60, 1789–1792.

Asensio-López, M. C., Lax, A., Pascual-Figal, D. A., Valdés, M., and Sánchez-Más, J. (2011). Metformin Protects against Doxorubicin-Induced Cardiotoxicity: Involvement of the Adiponectin Cardiac System. *Free Radic. Biol. Med.* 51, 1861–1871. doi:10.1016/j.freeradbiomed.2011.08.015

Asselin, B. L., Devidas, M., Chen, L., Franco, V. I., Pullen, J., Borowitz, M. J., et al. (2016). Cardioprotection and Safety of Dexrazoxane in Patients Treated for Newly Diagnosed T-Cell Acute Lymphoblastic Leukemia or Advanced-Stage Lymphoblastic Non-hodgkin Lymphoma: A Report of the Children's Oncology Group Randomized Trial Pediatric Oncology Group 9404. *JCO* 34, 854–862. doi:10.1200/JCO.2015.60.8851

Avera McKennan Hospital & University Health Center (2019). *A Phase II Pilot Study Using Metformin to Reduce Cardiac Toxicity in Breast Cancer Patients*. Sioux Falls, South Dakota, United States: Avera McKennan Hospital & University Health Center, clinicaltrials.gov. Available at: https://clinicaltrials.gov/ct2/show/NCT02472353 (Accessed December 22, 2021).

Bauckneht, M., Ferrarazzo, G., Fiz, F., Morbelli, S., Sarocchi, M., Pastorino, F., et al. (2017). Doxorubicin Effect on Myocardial Metabolism as a Prerequisite for Subsequent Development of Cardiac Toxicity: A Translational 18F-FDG PET/CT Observation. *J. Nucl. Med.* 58, 1638–1645. doi:10.2967/jnumed.117.191122

Berthiaume, J. M., Oliveira, P. J., Fariss, M. W., and Wallace, K. B. (2005). Dietary Vitamin E Decreases Doxorubicin-Induced Oxidative Stress without Preventing Mitochondrial Dysfunction. *Cardiovasc. Toxicol.* 5, 257–267. doi:10.1385/CT:5:3:257

Bjelogrlic, S. K., Radic, J., Radulovic, S., Jokanovic, M., and Jovic, V. (2007). Effects of Dexrazoxane and Amifostine on Evolution of Doxorubicin Cardiomyopathy *In Vivo*. *Exp. Biol. Med. (Maywood)* 232, 1414–1424. doi:10.3181/0705-RM-138

Bosch, X., Rovira, M., Sitges, M., Domènech, A., Ortiz-Pérez, J. T., de Caralt, T. M., et al. (2013). Enalapril and Carvedilol for Preventing Chemotherapy-Induced Left Ventricular Systolic Dysfunction in Patients with Malignant Hemopathies: The OVERCOME Trial (preventiOn of Left Ventricular Dysfunction with Enalapril and caRvedilol in Patients Submitted to Intensive ChemOtherapy for the Treatment of Malignant hEmopathies). *J. Am. Coll. Cardiol.* 61, 2355–2362. doi:10.1016/j.jacc.2013.02.072

Cabral, R. E. L., Mendes, T. B., Vendramini, V., and Miraglia, S. M. (2018). Carnitine Partially Improves Oxidative Stress, Acrosome Integrity, and Reproductive Competence in Doxorubicin-Treated Rats. *Andrology* 6, 236–246. doi:10.1111/andr.12426

Canzoneri, J. C., and Oyelere, A. K. (2008). Interaction of Anthracyclines with Iron Responsive Element mRNAs. *Nucl. Acids Res.* 36, 6825–6834. doi:10.1093/nar/gkn774

Cardinale, D., Colombo, A., Bacchiani, G., Tedeschi, I., Meroni, C. A., Veglia, F., et al. (2015). Early Detection of Anthracycline Cardiotoxicity and Improvement with Heart Failure Therapy. *Circulation* 131, 1981–1988. doi:10.1161/CIRCULATIONAHA.114.013777

Cardinale, D., Colombo, A., Lamantia, G., Colombo, N., Civelli, M., De Giacomi, G., et al. (2010). Anthracycline-Induced Cardiomyopathy: Clinical Relevance and Response to Pharmacologic Therapy. *J. Am. Coll. Cardiol.* 55, 213–220. doi:10.1016/j.jacc.2009.03.095

Carvalho, R. A., Sousa, R. P. B., Cadete, V. J. J., Lopaschuk, G. D., Palmeira, C. M. M., Bjork, J. A., et al. (2010). Metabolic Remodeling Associated with Subchronic Doxorubicin Cardiomyopathy. *Toxicology* 270, 92–98. doi:10.1016/j.tox.2010.01.019

Catanzaro, M. P., Weiner, A., Kaminaris, A., Li, C., Cai, F., Zhao, F., et al. (2019). Doxorubicin-induced Cardiomyocyte Death Is Mediated by Unchecked Mitochondrial Fission and Mitophagy. *FASEB J.* 33, 11096–11108. doi:10.1096/fj.201802663R

Chandran, K., Aggarwal, D., Migrino, R. Q., Joseph, J., McAllister, D., Konorev, E. A., et al. (2009). Doxorubicin Inactivates Myocardial Cytochrome C Oxidase in Rats: Cardioprotection by Mito-Q. *Biophysical J.* 96, 1388–1398. doi:10.1016/j.bpj.2008.10.042

Chen, K., Xu, X., Kobayashi, S., Timm, D., Jepperson, T., and Liang, Q. (2011). Caloric Restriction Mimetic 2-Deoxyglucose Antagonizes Doxorubicin-Induced Cardiomyocyte Death by Multiple Mechanisms. *J. Biol. Chem.* 286, 21993–22006. doi:10.1074/jbc.M111.225805

Christodoulou, C., Kostopoulos, I., Kalofonos, H. P., Lianos, E., Bobos, M., Briasoulis, E., et al. (2009). Trastuzumab Combined with Pegylated Liposomal Doxorubicin in Patients with Metastatic Breast Cancer. *OCL* 76, 275–285. doi:10.1159/000207504

Chun, Y., and Kim, J. (2018). Autophagy: An Essential Degradation Program for Cellular Homeostasis and Life. *Cells* 7, 278. doi:10.3390/cells7120278

Clayton, Z. S., Brunt, V. E., Hutton, D. A., VanDongen, N. S., D'Alessandro, A., Reisz, J. A., et al. (2020). Doxorubicin-Induced Oxidative Stress and Endothelial Dysfunction in Conduit Arteries Is Prevented by Mitochondrial-specific Antioxidant Treatment. *JACC CardioOncol* 2, 475–488. doi:10.1016/j.jaccao.2020.06.010

Danesi, R., Bernardini, N., Marchetti, A., Bernardini, M., and Del Tacca, M. (1990). Protective Effects of Fructose-1,6-Diphosphate on Acute and Chronic Doxorubicin Cardiotoxicity in Rats. *Cancer Chemother. Pharmacol.* 25, 326–332. doi:10.1007/BF00686231

Daubert, M. A., Yow, E., Dunn, G., Marchev, S., Barnhart, H., Douglas, P. S., et al. (2017). Novel Mitochondria-Targeting Peptide in Heart Failure Treatment. *Circ. Heart Fail.* 10, e004389. doi:10.1161/CIRCHEARTFAILURE.117.004389

Davies, K. J., and Doroshow, J. H. (1986). Redox Cycling of Anthracyclines by Cardiac Mitochondria. I. Anthracycline Radical Formation by NADH Dehydrogenase. *J. Biol. Chem.* 261, 3060–3067. doi:10.1016/S0021-9258(17)35746-0

Deus, C. M., Zehowski, C., Nordgren, K., Wallace, K. B., Skildum, A., and Oliveira, P. J. (2015). Stimulating Basal Mitochondrial Respiration Decreases Doxorubicin Apoptotic Signaling in H9c2 Cardiomyoblasts. *Toxicology* 334, 1–11. doi:10.1016/j.tox.2015.05.001

Dhingra, A., Jayas, R., Afshar, P., Guberman, M., Maddaford, G., Gerstein, J., et al. (2017). Ellagic Acid Antagonizes Bnip3-Mediated Mitochondrial Injury and Necrotic Cell Death of Cardiac Myocytes. *Free Radic. Biol. Med.* 112, 411–422. doi:10.1016/j.freeradbiomed.2017.08.010

Dhingra, R., Margulets, V., Chowdhury, S. R., Thliveris, J., Jassal, D., Fernyhough, P., et al. (2014). Bnip3 Mediates Doxorubicin-Induced Cardiac Myocyte Necrosis and Mortality through Changes in Mitochondrial Signaling. *PNAS* 111, E5537–E5544. doi:10.1073/pnas.1414665111

Ding, Y., Sun, X., Huang, W., Hoage, T., Redfield, M., Kushwaha, S., et al. (2011). Haploinsufficiency of Target of Rapamycin Attenuates Cardiomyopathies in Adult Zebrafish. *Circ. Res.* 109, 658–669. doi:10.1161/CIRCRESAHA.111.248260

Doenst, T., Nguyen, T. D., and Abel, E. D. (2013). Cardiac Metabolism in Heart Failure: Implications beyond ATP Production. *Circ. Res.* 113, 709–724. doi:10.1161/CIRCRESAHA.113.300376

Dutta, D., Xu, J., Dirain, M. L. S., and Leeuwenburgh, C. (2014). Calorie Restriction Combined with Resveratrol Induces Autophagy and Protects 26-Month-Old Rat Hearts from Doxorubicin-Induced Toxicity. *Free Radic. Biol. Med.* 74, 252–262. doi:10.1016/j.freeradbiomed.2014.06.011

European Medicines Agency (2018a). *Dexrazoxane*. Amsterdam, Netherlands: European Medicines Agency. Available at: https://www.ema.europa.eu/en/medicines/human/referrals/dexrazoxane (Accessed July 18, 2021).

European Medicines Agency (2018b). *Cardioxane*. Amsterdam, Netherlands: European Medicines Agency. Available at: https://www.ema.europa.eu/en/medicines/human/referrals/cardioxane (Accessed July 18, 2021).

Fang, X., Wang, H., Han, D., Xie, E., Yang, X., Wei, J., et al. (2019). Ferroptosis as a Target for protection against Cardiomyopathy. *PNAS* 116, 2672–2680. doi:10.1073/pnas.1821022116

Forrester, S. J., Kikuchi, D. S., Hernandes, M. S., Xu, Q., and Griendling, K. K. (2018). Reactive Oxygen Species in Metabolic and Inflammatory Signaling. *Circ. Res.* 122, 877–902. doi:10.1161/CIRCRESAHA.117.311401

Garcia, D., and Shaw, R. J. (2017). AMPK: Mechanisms of Cellular Energy Sensing and Restoration of Metabolic Balance. *Mol. Cel* 66, 789–800. doi:10.1016/j.molcel.2017.05.032

Georgakopoulos, P., Roussou, P., Matsakas, E., Karavidas, A., Anagnostopoulos, N., Marinakis, T., et al. (2010). Cardioprotective Effect of Metoprolol and Enalapril in Doxorubicin-Treated Lymphoma Patients: A Prospective, Parallel-

Group, Randomized, Controlled Study with 36-month Follow-Up. *Am. J. Hematol.* 85, 894–896. doi:10.1002/ajh.21840

Ghigo, A., Li, M., and Hirsch, E. (2016). New Signal Transduction Paradigms in Anthracycline-Induced Cardiotoxicity. *Biochim. Biophys. Acta (Bba) - Mol. Cel Res.* 1863, 1916–1925. doi:10.1016/j.bbamcr.2016.01.021

Gratia, S., Kay, L., Potenza, L., Seffouh, A., Novel-Chaté, V., Schnebelen, C., et al. (2012). Inhibition of AMPK Signalling by Doxorubicin: at the Crossroads of the Cardiac Responses to Energetic, Oxidative, and Genotoxic Stress. *Cardiovasc. Res.* 95, 290–299. doi:10.1093/cvr/cvs134

Gupta, R. C., Vinita, S.-G., and Sabbah, H. N. (2016). Bendavia (Elamipretide) Restores Phosphorylation of Cardiac Myosin Binding Protein C on Serine 282 and Improves Left Ventricular Diastolic Function in Dogs with Heart Failure. *J. Am. Coll. Cardiol.* 67, 1443. doi:10.1016/S0735-1097(16)31444-9

Gutteridge, J. M. C. (1984). Lipid Peroxidation and Possible Hydroxyl Radical Formation Stimulated by the Self-Reduction of a Doxorubicin-Iron (III) Complex. *Biochem. Pharmacol.* 33, 1725–1728. doi:10.1016/0006-2952(84)90340-X

Hasinoff, B. B., Patel, D., and Wu, X. (2003). The Oral Iron Chelator ICL670A (Deferasirox) Does Not Protect Myocytes against Doxorubicin. *Free Radic. Biol. Med.* 35, 1469–1479. doi:10.1016/j.freeradbiomed.2003.08.005

Hasinoff, B. B., Patel, D., and Wu, X. (2020). The Role of Topoisomerase IIβ in the Mechanisms of Action of the Doxorubicin Cardioprotective Agent Dexrazoxane. *Cardiovasc. Toxicol.* 20, 312–320. doi:10.1007/s12012-019-09554-5

Hawley, S. A., Gadalla, A. E., Olsen, G. S., and Hardie, D. G. (2002). The Antidiabetic Drug Metformin Activates the AMP-Activated Protein Kinase Cascade via an Adenine Nucleotide-independent Mechanism. *Diabetes* 51, 2420–2425. doi:10.2337/diabetes.51.8.2420

He, H., Luo, Y., Qiao, Y., Zhang, Z., Yin, D., Yao, J., et al. (2018). Curcumin Attenuates Doxorubicin-Induced Cardiotoxicity via Suppressing Oxidative Stress and Preventing Mitochondrial Dysfunction Mediated by 14-3-3γ. *Food Funct.* 9, 4404–4418. doi:10.1039/C8FO00466H

He, H., Wang, L., Qiao, Y., Yang, B., Yin, D., and He, M. (2021). Epigallocatechin-3-gallate Pretreatment Alleviates Doxorubicin-Induced Ferroptosis and Cardiotoxicity by Upregulating AMPKα2 and Activating Adaptive Autophagy. *Redox Biol.* 48, 102185. doi:10.1016/j.redox.2021.102185

He, H., Wang, L., Qiao, Y., Zhou, Q., Li, H., Chen, S., et al. (2020). Doxorubicin Induces Endotheliotoxicity and Mitochondrial Dysfunction via ROS/eNOS/NO Pathway. *Front. Pharmacol.* 10, 1531. doi:10.3389/fphar.2019.01531

Hoshino, A., Mita, Y., Okawa, Y., Ariyoshi, M., Iwai-Kanai, E., Ueyama, T., et al. (2013). Cytosolic P53 Inhibits Parkin-Mediated Mitophagy and Promotes Mitochondrial Dysfunction in the Mouse Heart. *Nat. Commun.* 4, 2308. doi:10.1038/ncomms3308

Hrelia, S., Fiorentini, D., Maraldi, T., Angeloni, C., Bordoni, A., Biagi, P. L., et al. (2002). Doxorubicin Induces Early Lipid Peroxidation Associated with Changes in Glucose Transport in Cultured Cardiomyocytes. *Biochim. Biophys. Acta (Bba) - Biomembranes* 1567, 150–156. doi:10.1016/S0005-2736(02)00612-0

Hull, T. D., Boddu, R., Guo, L., Tisher, C. C., Traylor, A. M., Patel, B., et al. (2016). Heme Oxygenase-1 Regulates Mitochondrial Quality Control in the Heart. *JCI Insight* 1. doi:10.1172/jci.insight.85817

Ichikawa, Y., Ghanefar, M., Bayeva, M., Wu, R., Khechaduri, A., Prasad, S. V. N., et al. (2014). Cardiotoxicity of Doxorubicin Is Mediated through Mitochondrial Iron Accumulation. *J. Clin. Invest.* 124, 617–630. doi:10.1172/JCI72931

Ikeda, Y., Shirakabe, A., Brady, C., Zablocki, D., Ohishi, M., and Sadoshima, J. (2014). Molecular Mechanisms Mediating Mitochondrial Dynamics and Mitophagy and Their Functional Roles in the Cardiovascular System. *J. Mol. Cell Cardiol.* 78, 116–122. doi:10.1016/j.yjmcc.2014.09.019

Jiang, X., Stockwell, B. R., and Conrad, M. (2021). Ferroptosis: Mechanisms, Biology and Role in Disease. *Nat. Rev. Mol. Cel Biol* 22, 266–282. doi:10.1038/s41580-020-00324-8

Jordan, J. H., Castellino, S. M., Meléndez, G. C., Klepin, H. D., Ellis, L. R., Lamar, Z., et al. (2018). Left Ventricular Mass Change after Anthracycline Chemotherapy. *Circ. Heart Fail.* 11, e004560. doi:10.1161/CIRCHEARTFAILURE.117.004560

Kalay, N., Basar, E., Ozdogru, I., Er, O., Cetinkaya, Y., Dogan, A., et al. (2006). Protective Effects of Carvedilol against Anthracycline-Induced Cardiomyopathy. *J. Am. Coll. Cardiol.* 48, 2258–2262. doi:10.1016/j.jacc.2006.07.052

Kawaguchi, T., Takemura, G., Kanamori, H., Takeyama, T., Watanabe, T., Morishita, K., et al. (2012). Prior Starvation Mitigates Acute Doxorubicin Cardiotoxicity through Restoration of Autophagy in Affected Cardiomyocytes. *Cardiovasc. Res.* 96, 456–465. doi:10.1093/cvr/cvs282

Kaya, M. G., Ozkan, M., Gunebakmaz, O., Akkaya, H., Kaya, E. G., Akpek, M., et al. (2013). Protective Effects of Nebivolol against Anthracycline-Induced Cardiomyopathy: A Randomized Control Study. *Int. J. Cardiol.* 167, 2306–2310. doi:10.1016/j.ijcard.2012.06.023

Kim, J., Kundu, M., Viollet, B., and Guan, K.-L. (2011). AMPK and mTOR Regulate Autophagy through Direct Phosphorylation of Ulk1. *Nat. Cel Biol* 13, 132–141. doi:10.1038/ncb2152

Kleele, T., Rey, T., Winter, J., Zaganelli, S., Mahecic, D., Perreten Lambert, H., et al. (2021). Distinct Fission Signatures Predict Mitochondrial Degradation or Biogenesis. *Nature* 593 (7859), 435–439. doi:10.1038/s41586-021-03510-6

Klionsky, D. J., Abdel-Aziz, A. K., Abdelfatah, S., Abdellatif, M., Abdoli, A., Abel, S., et al. (2021). Guidelines for the Use and Interpretation of Assays for Monitoring Autophagy. *Autophagy* 17, 1–382. 4th edition. doi:10.1080/15548627.2015.1100356

Kobashigawa, L. C., Xu, Y. C., Padbury, J. F., Tseng, Y.-T., and Yano, N. (2014). Metformin Protects Cardiomyocyte from Doxorubicin Induced Cytotoxicity through an AMP-Activated Protein Kinase Dependent Signaling Pathway: An *In Vitro* Study. *PLOS ONE* 9, e104888. doi:10.1371/journal.pone.0104888

Kobayashi, S., Volden, P., Timm, D., Mao, K., Xu, X., and Liang, Q. (2010). Transcription Factor GATA4 Inhibits Doxorubicin-Induced Autophagy and Cardiomyocyte Death. *J. Biol. Chem.* 285, 793–804. doi:10.1074/jbc.M109.070037

Kotamraju, S., Chitambar, C. R., Kalivendi, S. V., Joseph, J., and Kalyanaraman, B. (2002). Transferrin Receptor-dependent Iron Uptake Is Responsible for Doxorubicin-Mediated Apoptosis in Endothelial Cells Role of Oxidant-Induced Iron Signaling in Apoptosis. *J. Biol. Chem.* 277, 17179–17187. doi:10.1074/jbc.M111604200

Kraus, F., Roy, K., Pucadyil, T. J., and Ryan, M. T. (2021). Function and Regulation of the Divisome for Mitochondrial Fission. *Nature* 590, 57–66. doi:10.1038/s41586-021-03214-x

Kubli, D. A., Quinsay, M. N., Huang, C., Lee, Y., and Gustafsson, Å. B. (2008). Bnip3 Functions as a Mitochondrial Sensor of Oxidative Stress during Myocardial Ischemia and Reperfusion. *Am. J. Physiology-Heart Circulatory Physiol.* 295, H2025–H2031. doi:10.1152/ajpheart.00552.2008

Li, D. L., Wang, Z. V., Ding, G., Tan, W., Luo, X., Criollo, A., et al. (2016). Doxorubicin Blocks Cardiomyocyte Autophagic Flux by Inhibiting Lysosome Acidification. *Circulation* 133, 1668–1687. doi:10.1161/CIRCULATIONAHA.115.017443

Li, H., Wang, C., Sun, P., Liu, D., Du, G., and Tian, J. (2020a). Melatonin Attenuates Doxorubicin-Induced Cardiotoxicity through Preservation of YAP Expression. *J. Cell Mol. Med.* 24, 3634–3646. doi:10.1111/jcmm.15057

Li, J., Li, Y., Jiao, J., Wang, J., Li, Y., Qin, D., et al. (2014). Mitofusin 1 Is Negatively Regulated by MicroRNA 140 in Cardiomyocyte Apoptosis. *Mol. Cell Biol.* 34 (10), 1788–1799. doi:10.1128/MCB.00774-13

Li, M., Russo, M., Pirozzi, F., Tocchetti, C. G., and Ghigo, A. (2020b). Autophagy and Cancer Therapy Cardiotoxicity: From Molecular Mechanisms to Therapeutic Opportunities. *Biochim. Biophys. Acta (Bba) - Mol. Cel Res.* 1867, 118493. doi:10.1016/j.bbamcr.2019.06.007

Li, M., Sala, V., De Santis, M. C., Cimino, J., Cappello, P., Pianca, N., et al. (2018). Phosphoinositide 3-Kinase Gamma Inhibition Protects from Anthracycline Cardiotoxicity and Reduces Tumor Growth. *Circulation* 138, 696–711. doi:10.1161/CIRCULATIONAHA.117.030352

Li, X., Lin, Y., Wang, S., Zhou, S., Ju, J., Wang, X., et al. (2020c). Extracellular Superoxide Dismutase Is Associated with Left Ventricular Geometry and Heart Failure in Patients with Cardiovascular Disease. *J. Am. Heart Assoc.* 9 (15), e016862. doi:10.1161/JAHA.120.016862

Liang, X., Wang, S., Wang, L., Ceylan, A. F., Ren, J., and Zhang, Y. (2020). Mitophagy Inhibitor Liensinine Suppresses Doxorubicin-Induced Cardiotoxicity through Inhibition of Drp1-Mediated Maladaptive Mitochondrial Fission. *Pharmacol. Res.* 157, 104846. doi:10.1016/j.phrs.2020.104846

Lipshultz, S. E., Scully, R. E., Lipsitz, S. R., Sallan, S. E., Silverman, L. B., Miller, T. L., et al. (2010). Assessment of Dexrazoxane as a Cardioprotectant in Doxorubicin-Treated Children with High-Risk Acute Lymphoblastic Leukaemia: Long-Term Follow-Up of a Prospective, Randomised, Multicentre Trial. *Lancet Oncol.* 11, 950–961. doi:10.1016/S1470-2045(10)70204-7

Liu, D., Ma, Z., Di, S., Yang, Y., Yang, J., Xu, L., et al. (2018). AMPK/PGC1α Activation by Melatonin Attenuates Acute Doxorubicin Cardiotoxicity via Alleviating Mitochondrial Oxidative Damage and Apoptosis. *Free Radic. Biol. Med.* 129, 59–72. doi:10.1016/j.freeradbiomed.2018.08.032

Lopez, M., Vici, P., Lauro, K. D., Conti, F., Paoletti, G., Ferraironi, A., et al. (1998). Randomized Prospective Clinical Trial of High-Dose Epirubicin and Dexrazoxane in Patients with Advanced Breast Cancer and Soft Tissue Sarcomas. *JCO* 16, 86–92. doi:10.1200/JCO.1998.16.1.86

Lu, L., Wu, W., Yan, J., Li, X., Yu, H., and Yu, X. (2009). Adriamycin-induced Autophagic Cardiomyocyte Death Plays a Pathogenic Role in a Rat Model of Heart Failure. *Int. J. Cardiol.* 134, 82–90. doi:10.1016/j.ijcard.2008.01.043

Luo, P., Zhu, Y., Chen, M., Yan, H., Yang, B., Yang, X., et al. (2018). HMGB1 Contributes to Adriamycin-Induced Cardiotoxicity via Up-Regulating Autophagy. *Toxicol. Lett.* 292, 115–122. doi:10.1016/j.toxlet.2018.04.034

Lyu, Y. L., Kerrigan, J. E., Lin, C.-P., Azarova, A. M., Tsai, Y.-C., Ban, Y., et al. (2007). Topoisomerase IIβ–Mediated DNA Double-Strand Breaks: Implications in Doxorubicin Cardiotoxicity and Prevention by Dexrazoxane. *Cancer Res.* 67, 8839–8846. doi:10.1158/0008-5472.CAN-07-1649

Maccarinelli, F., Gammella, E., Asperti, M., Regoni, M., Biasiotto, G., Turco, E., et al. (2014). Mice Lacking Mitochondrial Ferritin Are More Sensitive to Doxorubicin-Mediated Cardiotoxicity. *J. Mol. Med.* 92, 859–869. doi:10.1007/s00109-014-1147-0

MacInnis, M. J., and Gibala, M. J. (2017). Physiological Adaptations to Interval Training and the Role of Exercise Intensity. *J. Physiol.* 595, 2915–2930. doi:10.1113/JP273196

Marcillat, O., Zhang, Y., and Davies, K. J. A. (1989). Oxidative and Non-oxidative Mechanisms in the Inactivation of Cardiac Mitochondrial Electron Transport Chain Components by Doxorubicin. *Biochem. J.* 259, 181–189. doi:10.1042/bj2590181

Marques-Aleixo, I., Santos-Alves, E., Oliveira, P. J., Moreira, P. I., Magalhães, J., and Ascensão, A. (2018a). The Beneficial Role of Exercise in Mitigating Doxorubicin-Induced Mitochondrionopathy. *Biochim. Biophys. Acta (Bba) - Rev. Cancer* 1869, 189–199. doi:10.1016/j.bbcan.2018.01.002

Marques-Aleixo, I., Santos-Alves, E., Torrella, J. R., Oliveira, P. J., Magalhães, J., and Ascensão, A. (2018b). Exercise and Doxorubicin Treatment Modulate Cardiac Mitochondrial Quality Control Signaling. *Cardiovasc. Toxicol.* 18, 43–55. doi:10.1007/s12012-017-9412-4

Minotti, G., Recalcati, S., Mordente, A., Liberi, G., Calafiore, A. M., Mancuso, C., et al. (1998). The Secondary Alcohol Metabolite of Doxorubicin Irreversibly Inactivates Aconitase/iron Regulatory Protein-1 in Cytosolic Fractions from Human Myocardium. *FASEB J.* 12, 541–552. doi:10.1096/fasebj.12.7.541

Minotti, G., Ronchi, R., Salvatorelli, E., Menna, P., and Cairo, G. (2001). Doxorubicin Irreversibly Inactivates Iron Regulatory Proteins 1 and 2 in Cardiomyocytes Evidence for Distinct Metabolic Pathways and Implications for Iron-Mediated Cardiotoxicity of Antitumor Therapy. *Cancer Res.* 61, 8422–8428.

Miotto, G., Rossetto, M., Di Paolo, M. L., Orian, L., Venerando, R., Roveri, A., et al. (2020). Insight into the Mechanism of Ferroptosis Inhibition by Ferrostatin-1. *Redox Biol.* 28, 101328. doi:10.1016/j.redox.2019.101328

Miranda, C. J., Makui, H., Soares, R. J., Bilodeau, M., Mui, J., Vali, H., et al. (2003). Hfe Deficiency Increases Susceptibility to Cardiotoxicity and Exacerbates Changes in Iron Metabolism Induced by Doxorubicin. *Blood* 102, 2574–2580. doi:10.1182/blood-2003-03-0869

Mukhopadhyay, P., Rajesh, M., Bátkai, S., Kashiwaya, Y., Haskó, G., Liaudet, L., et al. (2009). Role of Superoxide, Nitric Oxide, and Peroxynitrite in Doxorubicin-Induced Cell Death *In Vivo* and *In Vitro*. *Am. J. Physiol. - Heart Circulatory Physiol.* 296, H1466–H1483. doi:10.1152/ajpheart.00795.2008

Murabito, A., Hirsch, E., and Ghigo, A. (2020). Mechanisms of Anthracycline-Induced Cardiotoxicity: Is Mitochondrial Dysfunction the Answer? *Front. Cardiovasc. Med.* 7, 35. doi:10.3389/fcvm.2020.00035

Najafi, M., Hooshangi Shayesteh, M. R., Mortezaee, K., Farhood, B., and Haghi-Aminjan, H. (2020). The Role of Melatonin on Doxorubicin-Induced Cardiotoxicity: A Systematic Review. *Life Sci.* 241, 117173. doi:10.1016/j.lfs.2019.117173

Narendra, D., Tanaka, A., Suen, D.-F., and Youle, R. J. (2008). Parkin Is Recruited Selectively to Impaired Mitochondria and Promotes Their Autophagy. *J. Cel Biol.* 183, 795–803. doi:10.1083/jcb.200809125

National Cancer Institute (2020). *Doxorubicin Hydrochloride*. Available at: https://www.cancer.gov/about-cancer/treatment/drugs/doxorubicinhydrochloride (Accessed July 18, 2021).

Nishida, K., Yamaguchi, O., and Otsu, K. (2008). Crosstalk between Autophagy and Apoptosis in Heart Disease. *Circ. Res.* 103, 343–351. doi:10.1161/CIRCRESAHA.108.175448

O'Brien, C. G., Ozen, M. O., Ikeda, G., Vaskova, E., Jung, J. H., Bayardo, N., et al. (2021). Mitochondria-Rich Extracellular Vesicles Rescue Patient-specific Cardiomyocytes from Doxorubicin Injury: Insights into the SENECA Trial. *JACC: CardioOncology* 3, 428–440. doi:10.1016/j.jaccao.2021.05.006

Osataphan, N., Phrommintikul, A., Chattipakorn, S. C., and Chattipakorn, N. (2020). Effects of Doxorubicin-Induced Cardiotoxicity on Cardiac Mitochondrial Dynamics and Mitochondrial Function: Insights for Future Interventions. *J. Cell Mol. Med.* 24, 6534–6557. doi:10.1111/jcmm.15305

Panjrath, G. S., Patel, V., Valdiviezo, C. I., Narula, N., Narula, J., and Jain, D. (2007). Potentiation of Doxorubicin Cardiotoxicity by Iron Loading in a Rodent Model. *J. Am. Coll. Cardiol.* 49, 2457–2464. doi:10.1016/j.jacc.2007.02.060

Parker, M. A., King, V., and Howard, K. P. (2001). Nuclear Magnetic Resonance Study of Doxorubicin Binding to Cardiolipin Containing Magnetically Oriented Phospholipid Bilayers. *Biochim. Biophys. Acta (Bba) - Biomembranes* 1514, 206–216. doi:10.1016/S0005-2736(01)00371-6

Piquereau, J., Caffin, F., Novotova, M., Lemaire, C., Veksler, V., Garnier, A., et al. (2013). Mitochondrial Dynamics in the Adult Cardiomyocytes: Which Roles for a Highly Specialized Cell? *Front. Physiol.* 4, 102. doi:10.3389/fphys.2013.00102

Pointon, A. V., Walker, T. M., Phillips, K. M., Luo, J., Riley, J., Zhang, S.-D., et al. (2010). Doxorubicin *In Vivo* Rapidly Alters Expression and Translation of Myocardial Electron Transport Chain Genes, Leads to ATP Loss and Caspase 3 Activation. *PLOS ONE* 5, e12733. doi:10.1371/journal.pone.0012733

Quinsay, M. N., Thomas, R. L., Lee, Y., and Gustafsson, A. B. (2010). Bnip3-mediated Mitochondrial Autophagy Is Independent of the Mitochondrial Permeability Transition Pore. *Autophagy* 6, 855–862. doi:10.4161/auto.6.7.13005

Rizzollo, F., More, S., Vangheluwe, P., and Agostinis, P. (2021). The Lysosome as a Master Regulator of Iron Metabolism. *Trends Biochem. Sci.* 46 (12), 960–975. doi:10.1016/j.tibs.2021.07.003

Rocha, V. C. J., França, L. S. D. A., de Araújo, C. F., Ng, A. M., de Andrade, C. M., Andrade, A. C., et al. (2016). Protective Effects of Mito-TEMPO against Doxorubicin Cardiotoxicity in Mice. *Cancer Chemother. Pharmacol.* 77, 659–662. doi:10.1007/s00280-015-2949-7

Rochette, L., Guenancia, C., Gudjoncik, A., Hachet, O., Zeller, M., Cottin, Y., et al. (2015). Anthracyclines/trastuzumab: New Aspects of Cardiotoxicity and Molecular Mechanisms. *Trends Pharmacol. Sci.* 36, 326–348. doi:10.1016/j.tips.2015.03.005

Rouault, T. A. (2006). The Role of Iron Regulatory Proteins in Mammalian Iron Homeostasis and Disease. *Nat. Chem. Biol.* 2, 406–414. doi:10.1038/nchembio807

Russell, R. C., Tian, Y., Yuan, H., Park, H. W., Chang, Y.-Y., Kim, J., et al. (2013). ULK1 Induces Autophagy by Phosphorylating Beclin-1 and Activating VPS34 Lipid Kinase. *Nat. Cel Biol* 15, 741–750. doi:10.1038/ncb2757

Sabbah, H. N., Gupta, R. C., Kohli, S., Wang, M., Hachem, S., and Zhang, K. (2016). Chronic Therapy with Elamipretide (MTP-131), a Novel Mitochondria-Targeting Peptide, Improves Left Ventricular and Mitochondrial Function in Dogs with Advanced Heart Failure. *Circ. Heart Fail.* 9, e002206. doi:10.1161/CIRCHEARTFAILURE.115.002206

Saito, T., and Junichi, S. (2015). Molecular Mechanisms of Mitochondrial Autophagy/Mitophagy in the Heart. *Circ. Res.* 116, 1477–1490. doi:10.1161/CIRCRESAHA.116.303790

Sala, V., Della Sala, A., Hirsch, E., and Ghigo, A. (2020). Signaling Pathways Underlying Anthracycline Cardiotoxicity. *Antioxid. Redox Signaling* 32, 1098–1114. doi:10.1089/ars.2020.8019

Sarocchi, M., Bauckneht, M., Arboscello, E., Capitanio, S., Marini, C., Morbelli, S., et al. (2018). An Increase in Myocardial 18-fluorodeoxyglucose Uptake Is Associated with Left Ventricular Ejection Fraction Decline in Hodgkin Lymphoma Patients Treated with Anthracycline. *J. Translational Med.* 16, 295. doi:10.1186/s12967-018-1670-9

Sayed-ahmed, M. M., Shaarawy, S., Shouman, S. A., and Osman, A.-M. M. (1999). Reversal of Doxorubicin-Induced Cardiac Metabolic Damage Byl-Carnitine. *Pharmacol. Res.* 39, 289–295. doi:10.1006/phrs.1998.0438

Sayed-ahmed, M. M., Shouman, S. A., Rezk, B. M., Khalifa, M. H., Osman, A.-M. M., and El-merzabani, M. M. (2000). Propionyl- L -Carnitine as Potential Protective Agent against Adriamycin-Induced Impairment of Fatty Acid Beta-Oxidation in Isolated Heart Mitochondria. *Pharmacol. Res.* 41, 143–150. doi:10.1006/phrs.1999.0583

Scott, J. M., Nilsen, T. S., Gupta, D., and Jones, L. W. (2018). Exercise Therapy and Cardiovascular Toxicity in Cancer. *Circulation* 137, 1176–1191. doi:10.1161/CIRCULATIONAHA.117.024671

Simůnek, T., Stérba, M., Popelová, O., Adamcová, M., Hrdina, R., and Gersl, V. (2009). Anthracycline-induced Cardiotoxicity: Overview of Studies Examining the Roles of Oxidative Stress and Free Cellular Iron. *Pharmacol. Rep.* 61, 154–171. doi:10.1016/s1734-1140(09)70018-0

Sishi, B. J. N., Loos, B., van Rooyen, J., and Engelbrecht, A.-M. (2013). Autophagy Upregulation Promotes Survival and Attenuates Doxorubicin-Induced Cardiotoxicity. *Biochem. Pharmacol.* 85, 124–134. doi:10.1016/j.bcp.2012.10.005

Song, R., Yang, Y., Lei, H., Wang, G., Huang, Y., Xue, W., et al. (2018). HDAC6 Inhibition Protects Cardiomyocytes against Doxorubicin-Induced Acute Damage by Improving α-tubulin Acetylation. *J. Mol. Cell Cardiol.* 124, 58–69. doi:10.1016/j.yjmcc.2018.10.007

Swain, S. M., Whaley, F. S., and Ewer, M. S. (2003). Congestive Heart Failure in Patients Treated with Doxorubicin. *Cancer* 97, 2869–2879. doi:10.1002/cncr.11407

Swain, S. M., Whaley, F. S., Gerber, M. C., Weisberg, S., York, M., Spicer, D., et al. (1997). Cardioprotection with Dexrazoxane for Doxorubicin-Containing Therapy in Advanced Breast Cancer. *JCO* 15, 1318–1332. doi:10.1200/JCO.1997.15.4.1318

Tadokoro, T., Ikeda, M., Ide, T., Deguchi, H., Ikeda, S., Okabe, K., et al. (2020). Mitochondria-dependent Ferroptosis Plays a Pivotal Role in Doxorubicin Cardiotoxicity. *JCI Insight* 5. doi:10.1172/jci.insight.132747

Tang, H., Tao, A., Song, J., Liu, Q., Wang, H., and Rui, T. (2017). Doxorubicin-induced Cardiomyocyte Apoptosis: Role of Mitofusin 2. *Int. J. Biochem. Cel Biol.* 88, 55–59. doi:10.1016/j.biocel.2017.05.006

Tebbi, C. K., London, W. B., Friedman, D., Villaluna, D., Alarcon, P. A. D., Constine, L. S., et al. (2007). Dexrazoxane-Associated Risk for Acute Myeloid Leukemia/Myelodysplastic Syndrome and Other Secondary Malignancies in Pediatric Hodgkin's Disease. *JCO* 25, 493–500. doi:10.1200/JCO.2005.02.3879

Tewey, K. M., Rowe, T. C., Yang, L., Halligan, B. D., and Liu, L. F. (1984). Adriamycin-induced DNA Damage Mediated by Mammalian DNA Topoisomerase II. *Science* 226, 466–468. doi:10.1126/science.6093249

Tilokani, L., Nagashima, S., Paupe, V., and Prudent, J. (2018). Mitochondrial Dynamics: Overview of Molecular Mechanisms. *Essays Biochem.* 62, 341–360. doi:10.1042/EBC20170104

van Dalen, E. C., Caron, H. N., Dickinson, H. O., and Kremer, L. C. (2011). Cardioprotective Interventions for Cancer Patients Receiving Anthracyclines. *Cochrane Database Syst. Rev.* 2011 (6), CD003917. doi:10.1002/14651858.CD003917.pub4

Vejpongsa, P., and Yeh, E. T. H. (2014). Prevention of Anthracycline-Induced Cardiotoxicity: Challenges and Opportunities. *J. Am. Coll. Cardiol.* 64, 938–945. doi:10.1016/j.jacc.2014.06.1167

Venturini, M., Michelotti, A., Mastro, L. D., Gallo, L., Carnino, F., Garrone, O., et al. (1996). Multicenter Randomized Controlled Clinical Trial to Evaluate Cardioprotection of Dexrazoxane versus No Cardioprotection in Women Receiving Epirubicin Chemotherapy for Advanced Breast Cancer. *JCO* 14, 3112–3120. doi:10.1200/JCO.1996.14.12.3112

Villa, F., Bruno, S., Costa, A., Li, M., Russo, M., Cimino, J., et al. (2021). The Human Fetal and Adult Stem Cell Secretome Can Exert Cardioprotective Paracrine Effects against Cardiotoxicity and Oxidative Stress from Cancer Treatment. *Cancers* 13, 3729. doi:10.3390/cancers13153729

Voest, E. E., van Acker, S. A. B. E., van der Vijgh, W. J. F., van Asbeck, B. S., and Bast, A. (1994). Comparison of Different Iron Chelators as Protective Agents against Acute Doxorubicin-Induced Cardiotoxicity. *J. Mol. Cell Cardiol.* 26, 1179–1185. doi:10.1006/jmcc.1994.1136

Waldner, R., Laschan, C., Lohninger, A., Gessner, M., Tüchler, H., Huemer, M., et al. (2006). Effects of Doxorubicin-Containing Chemotherapy and a Combination with L-Carnitine on Oxidative Metabolism in Patients with Non-hodgkin Lymphoma. *J. Cancer Res. Clin. Oncol.* 132, 121–128. doi:10.1007/s00432-005-0054-8

Wang, D. D., Cheng, R. K., and Tian, R. (2021). Combat Doxorubicin Cardiotoxicity with the Power of Mitochondria Transfer. *JACC: CardioOncology* 3, 441–443. doi:10.1016/j.jaccao.2021.08.001

Wang, L., Chen, Q., Qi, H., Wang, C., Wang, C., Zhang, J., et al. (2016). Doxorubicin-Induced Systemic Inflammation Is Driven by Upregulation of Toll-like Receptor TLR4 and Endotoxin Leakage. *Cancer Res.* 76, 6631–6642. doi:10.1158/0008-5472.CAN-15-3034

Wang, S., Song, P., and Zou, M.-H. (2012). Inhibition of AMP-Activated Protein Kinase α (AMPKα) by Doxorubicin Accentuates Genotoxic Stress and Cell Death in Mouse Embryonic Fibroblasts and Cardiomyocytes ROLE of P53 and SIRT1. *J. Biol. Chem.* 287, 8001–8012. doi:10.1074/jbc.M111.315812

Wang, X., Wang, X.-L., Chen, H.-L., Wu, D., Chen, J.-X., Wang, X.-X., et al. (2014). Ghrelin Inhibits Doxorubicin Cardiotoxicity by Inhibiting Excessive Autophagy through AMPK and P38-MAPK. *Biochem. Pharmacol.* 88, 334–350. doi:10.1016/j.bcp.2014.01.040

Wang, Y., Gao, W., Shi, X., Ding, J., Liu, W., He, H., et al. (2017). Chemotherapy Drugs Induce Pyroptosis through Caspase-3 Cleavage of a Gasdermin. *Nature* 547, 99–103. doi:10.1038/nature22393

Wu, W., Yang, B., Qiao, Y., Zhou, Q., He, H., and He, M. (2020). Kaempferol Protects Mitochondria and Alleviates Damages against Endotheliotoxicity Induced by Doxorubicin. *Biomed. Pharmacother.* 126, 110040. doi:10.1016/j.biopha.2020.110040

Xia, Y., Chen, Z., Chen, A., Fu, M., Dong, Z., Hu, K., et al. (2017). LCZ696 Improves Cardiac Function via Alleviating Drp1-Mediated Mitochondrial Dysfunction in Mice with Doxorubicin-Induced Dilated Cardiomyopathy. *J. Mol. Cell Cardiol.* 108, 138–148. doi:10.1016/j.yjmcc.2017.06.003

Xie, Y., Hou, W., Song, X., Yu, Y., Huang, J., Sun, X., et al. (2016). Ferroptosis: Process and Function. *Cell Death Differ* 23, 369–379. doi:10.1038/cdd.2015.158

Xu, X., Persson, H. L., and Richardson, D. R. (2005). Molecular Pharmacology of the Interaction of Anthracyclines with Iron. *Mol. Pharmacol.* 68, 261–271. doi:10.1124/mol.105.013383

Youle, R. J., and van der Bliek, A. M. (2012). Mitochondrial Fission, Fusion, and Stress. *Science* 337, 1062–1065. doi:10.1126/science.1219855

Zamorano, J. L., Lancellotti, P., Muñoz, D. R., Aboyans, V., Asteggiano, R., Galderisi, M., et al. (2016). 2016 ESC Position Paper on Cancer Treatments and Cardiovascular Toxicity Developed under the Auspices of the ESC Committee for Practice Guidelines. *Eur. Heart J.* 37, 2768–2801. doi:10.1093/eurheartj/ehw211

Zhang, J., and Ney, P. A. (2009). Role of BNIP3 and NIX in Cell Death, Autophagy, and Mitophagy. *Cel Death Differ* 16, 939–946. doi:10.1038/cdd.2009.16

Zhang, Q.-L., Yang, J.-J., and Zhang, H.-S. (2019). Carvedilol (CAR) Combined with Carnosic Acid (CAA) Attenuates Doxorubicin-Induced Cardiotoxicity by Suppressing Excessive Oxidative Stress, Inflammation, Apoptosis and Autophagy. *Biomed. Pharmacother.* 109, 71–83. doi:10.1016/j.biopha.2018.07.037

Zhang, S., Liu, X., Bawa-Khalfe, T., Lu, L.-S., Lyu, Y. L., Liu, L. F., et al. (2012). Identification of the Molecular Basis of Doxorubicin-Induced Cardiotoxicity. *Nat. Med.* 18, 1639–1642. doi:10.1038/nm.2919

Zhang, T., Zhang, Y., Cui, M., Jin, L., Wang, Y., Lv, F., et al. (2016). CaMKII Is a RIP3 Substrate Mediating Ischemia- and Oxidative Stress-Induced Myocardial Necroptosis. *Nat. Med.* 22, 175–182. doi:10.1038/nm.4017

Zhang, Y., Kang, Y.-M., Tian, C., Zeng, Y., Jia, L.-X., Ma, X., et al. (2011). Overexpression of Nrdp1 in the Heart Exacerbates Doxorubicin-Induced Cardiac Dysfunction in Mice. *PLOS ONE* 6, e21104. doi:10.1371/journal.pone.0021104

Zhao, Y., McLaughlin, D., Robinson, E., Harvey, A. P., Hookham, M. B., Shah, A. M., et al. (2010). Nox2 NADPH Oxidase Promotes Pathologic Cardiac Remodeling Associated

with Doxorubicin Chemotherapy. *Cancer Res.* 70, 9287–9297. doi:10.1158/0008-5472.CAN-10-2664

Zilinyi, R., Czompa, A., Czegledi, A., Gajtko, A., Pituk, D., Lekli, I., et al. (2018). The Cardioprotective Effect of Metformin in Doxorubicin-Induced Cardiotoxicity: The Role of Autophagy. *Molecules* 23, 1184. doi:10.3390/molecules23051184

Zorov, D. B., Juhaszova, M., and Sollott, S. J. (2014). Mitochondrial Reactive Oxygen Species (ROS) and ROS-Induced ROS Release. *Physiol. Rev.* 94, 909–950. doi:10.1152/physrev.00026.2013

Conflict of Interest: The authors declare that the research was conducted in the absence of any commercial or financial relationships that could be construed as a potential conflict of interest.

Publisher's Note: All claims expressed in this article are solely those of the authors and do not necessarily represent those of their affiliated organizations, or those of the publisher, the editors and the reviewers. Any product that may be evaluated in this article, or claim that may be made by its manufacturer, is not guaranteed or endorsed by the publisher.

frontiers in Pharmacology

ORIGINAL RESEARCH
published: 22 February 2022
doi: 10.3389/fphar.2022.850735

Long-Term Cardiac Damage Associated With Abdominal Irradiation in Mice

Zhaojia Wang[1†], Ziheng Jia[1†], Zandong Zhou[1], Xiaotong Zhao[2], Feng Wang[3], Xu Zhang[4], Gary Tse[1,5], Guangping Li[1], Yang Liu[2] and Tong Liu[1]**

[1]Tianjin Key Laboratory of Ionic-Molecular Function of Cardiovascular Disease, Department of Cardiology, Tianjin Institute of Cardiology, Second Hospital of Tianjin Medical University, Tianjin, China, [2]Institute of Radiation Medicine, Chinese Academy of Medical Sciences & Peking Union Medical College, Tianjin, China, [3]Department of Genetics, School of Basic Medical Sciences, Tianjin Medical University, Tianjin, China, [4]Tianjin Key Laboratory of Metabolic Diseases, Collaborative Innovation Center of Tianjin for Medical Epigenetics, Center for Cardiovascular Diseases, Research Center of Basic Medical Sciences, Department of Physiology and Pathophysiology, Tianjin Medical University, Tianjin, China, [5]Kent and Medway Medical School, Canterbury, United Kingdom

OPEN ACCESS

Edited by:
Zhi-Ren Zhang,
Harbin Medical University, China

Reviewed by:
Yunshan Cao,
Gansu Provincial Hospital, China
Ruijie Liu,
Grand Valley State University, United States
Chen Liu,
The First Affiliated Hospital of Sun Yat-sen University, China

***Correspondence:**
Tong Liu
liutongdoc@126.com
Yang Liu
liuyang@irm-cams.ac.cn

[†]These authors have contributed equally to this work

Specialty section:
This article was submitted to Cardiovascular and Smooth Muscle Pharmacology, a section of the journal Frontiers in Pharmacology

Received: *08 January 2022*
Accepted: *09 February 2022*
Published: *22 February 2022*

Citation:
Wang Z, Jia Z, Zhou Z, Zhao X, Wang F, Zhang X, Tse G, Li G, Liu Y and Liu T (2022) Long-Term Cardiac Damage Associated With Abdominal Irradiation in Mice. Front. Pharmacol. 13:850735. doi: 10.3389/fphar.2022.850735

Aims: Irradiation is an effective treatment for tumors but has been associated with cardiac dysfunction. However, the precise mechanisms remain incompletely elucidated. This study investigated the long-term cardiac damage associated with abdominal irradiation and explored possible mechanisms.

Methods and Results: Wild-type C57BL6/J mice were divided into two groups: untreated controls (Con) and treatment group receiving 15 Gy of abdominal gamma irradiation (AIR). Both groups received normal feeding for 12 months. The AIR group showed reductions in left ventricular ejection fraction (LVEF), fractional shortening (FS), left ventricular end-diastolic internal diameter (LVID; d), left ventricular end-diastolic volume (LV Vol. diastolic volume (LV Vol; d) and mitral transtricuspid flow late diastolic filling velocity (MV A). It also showed increased fibrosis, reduced conduction velocity and increased conduction heterogeneity. Non-targeted metabolomics showed the differential metabolites were mainly from amino acid metabolism. Further KEGG pathway annotation and enrichment analysis revealed that abnormalities in arginine and proline metabolism, lysine degradation, d-arginine and d-ornithine metabolism, alanine, aspartate and glutamate metabolism, and arginine biosynthesis.

Conclusion: Abdominal irradiation causes long-term damage to the non-irradiated heart, as reflected by electrical and structural remodeling and mechanical dysfunction associated with abnormal amino acid biosynthesis and metabolism.

Keywords: irradiation, cardiac function, cardiac remodeling, metabolomics, bystander effect

INTRODUCTION

Cancer is the leading cause of mortality worldwide (Soerjomataram and Bray, 2021; Sung et al., 2021). Approximately 19.3 million new cancer diagnoses are made whilst 10 million cancer-deaths are observed each year globally. Due to the early diagnosis and timely intervention of cancer treatment in recent years, deaths due to cancer itself have significantly receded, while cardiac disease and damage caused by tumor treatment have clearly become a major cause of non-neoplastic death

among cancer survivors (Curigliano et al., 2016; Armanious et al., 2018; Li H. et al., 2019; Alvarez-Cardona et al., 2020). Irradiation is an important treatment for cancer. However, it can exert adverse effects on normal and otherwise healthy tissues and organs, with significant negative impact on prognosis of cancer patients (Schaue and McBride, 2015; Nielsen et al., 2017; Chargari et al., 2019). For example, its related cardiac damage occurs in both short- and long-term (Groarke et al., 2014; Cao et al., 2021), while the early stages of cardiac dysfunction may be asymptomatic.

Long-term cardiac damage includes valvular heart disease, coronary heart disease, arrhythmia, pericardial stenosis, heart failure (Simone, 2017; Menezes et al., 2018; Nabialek-Trojanowska et al., 2020). Therefore, there is a need to better clarify the specific mechanisms underlying cardiac damage. The degree of cardiac damage is usually greater with a closer irradiation window and higher doses applied, as reflected by radiotherapy-related cardiac damage in the treatment of thoracic tumors such as breast cancer, lung cancer, and lymphoma (Bradley et al., 2015; Gkantaifi et al., 2019; Banfill et al., 2021).

By contrast, there are fewer reports of cardiac damage related to irradiation that do not directly target the heart. Previous studies have shown that oxidative stress in the heart after craniocerebral irradiation may be related to the bystander effect (Rashed et al., 2021). However, it is unclear whether other parts of the irradiation will also produce toxic effects on the heart directly. Clinical studies have reported that radiotherapy for peptic ulcer is a risk factor for coronary heart disease which can explain radiation-related cardiac dysfunction (Carr et al., 2005). Abdominal cancers are common (Sung et al., 2021) but there have been few mechanistic studies on the relationship between abdominal irradiation, possible cardiac dysfunction and the underlying mechanisms. Therefore, the aim of this study is to explore the long-term adverse effects on the heart caused by abdominal irradiation in a mouse model.

MATERIALS AND METHODS

Experimental Animal Models and Ethical Approval

All animal experiments were approved by the Institutional Committee for the Care and Use of Animals, Institute of Radiological Sciences, Chinese Academy of Medical Sciences (approval number: IRM-DWLL-2019149). Pathogen-free male C57BL6/J mice (6–8-week-old) were purchased from Beijing Vital River Laboratory Animal Technology Company. All the mice were equally divided into control group and abdominal irradiation group. Mice in irradiation group received a single dose of 15 Gy abdominal irradiation in a Gammacell-40^{137}Cesium gray irradiator (Atomic Energy of Canada Ltd., Chalk River, Ontario, Canada). All mice were subjected to echocardiographic, electrophysiological and metabolomic analyses at 12 months post-irradiation along with control mice. All the mice were fed in a standard environment (20 ± 1°C room temperature, 50 ± 10% relative humidity) for 12 h of light and dark cycling with ad libitum diet and water. For sampling, all mice were euthanised using anaesthetic exposure.

Echocardiography

Echocardiography was performed using the Vevo 2,100 high-resolution ultrasound imaging system. Isoflurane anaesthesia was used for supine fixation. Left ventricular end-diastolic internal diameter (LVEDD), left ventricular end-systolic internal diameter (LVESD), left ventricular end-diastolic volume (LV Vol; d) and left ventricular end-systolic volume (LV Vol; s) were measured and recorded in the short-axis view of the left heart. Left ventricular ejection fraction (LVEF) and shortening fraction (FS) were calculated as indicators of LV systolic function. In the apical four-chamber view, a sampling frame was placed at the mitral orifice and the left ventricular outflow tract to monitor mitral *trans*-tricuspid flow, early diastolic filling velocity (E) and late diastolic filling velocity (A), allowing quantification of the E/A ratio, reflecting diastolic function. Five different cardiac cycles were measured for each assessment.

Epicardial Electrogramming

Epicardial electrical activity was recorded by placing 6 x 6 electrode microelectrodes (electrode impedance: 1.5–1.7Q, PA03606060101, multi-electrode probe array) on the epicardial surface. Data were recorded by a multichannel system (EMS64-USB-1003, United Kingdom). The obtained activation waveforms were amplified by a filter amplifier and thus transmitted to a computer. All activation times were digitised and used to plot activation maps. The activation time is calculated as the point of maximum negative slope of the activation waveform. Conduction velocity (CV), inhomogeneity index and absolute inhomogeneity were calculated by EMapScope 4.0 software (MappingLab Ltd., United Kingdom).

Histological Analysis

For hematoxylin-eosin (HE) staining, paraffin-embedded tissues were dewaxed and hematoxylin stained for 3–8 min, followed by alcoholic fractionation with 1% hydrochloric acid for a few seconds and final immersion in eosin staining solution for 1–3 min. For Masson staining, dewaxed tissue sections were immersed in Weiger iron hematoxylin stain for 10 min. After grading with 0.5% hydrochloric acid ethanol for 15 s, the sections were stained with lychee red acid magenta solution for 8 min. This was followed by treatment with 1% phosphomolybdic acid in water for approximately 5 min and direct staining with aniline blue solution or bright green solution for a further 5 min. Finally, all sections were treated with 1% glacial acetic acid for 1 min. Relative quantitative analysis of the fibrosis in Masson stains is the mean of the six field positive area ratios (positive area divided by total area).

Non-Targeted Metabolomics Sample Preparation

15 mg of tissue was used for grinding (50 Hz, 5 min), followed by sonication in a water bath at 4°C for 10 min, and then left to

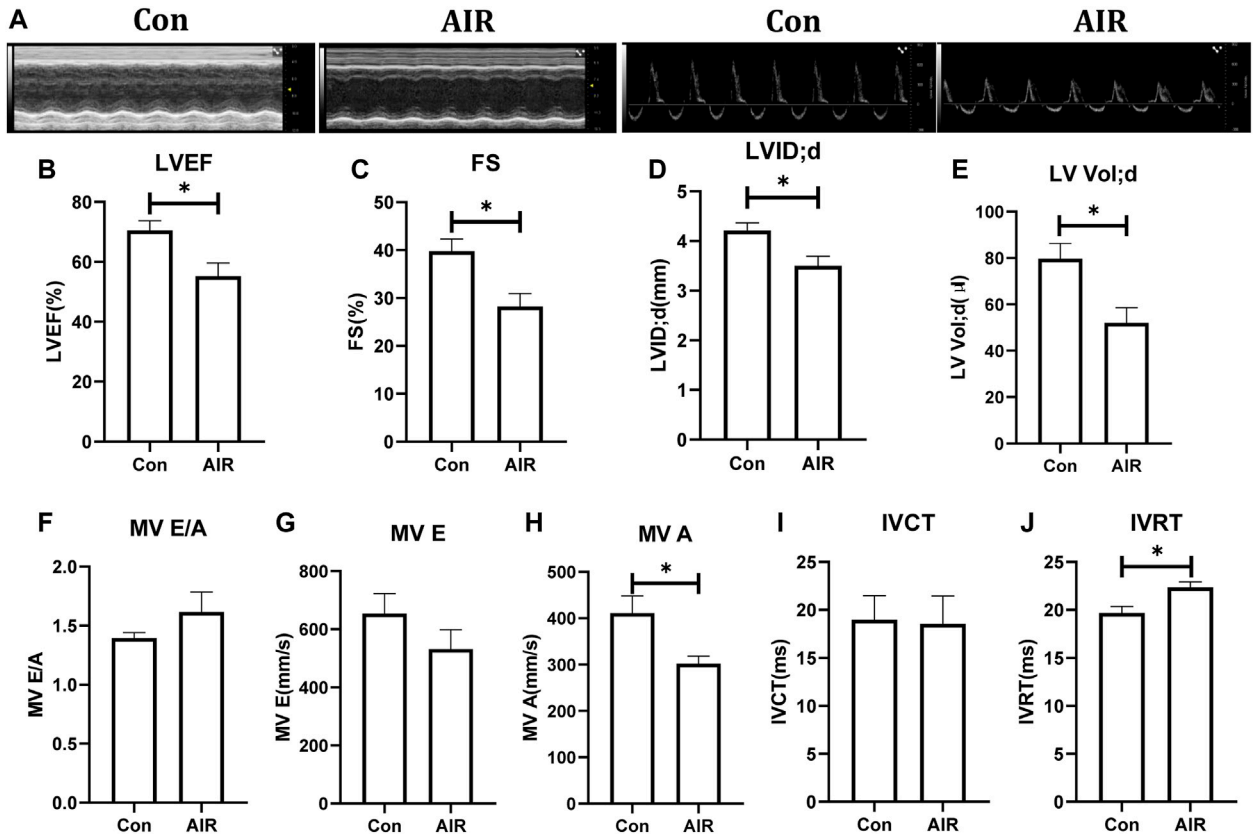

FIGURE 1 | Changes in cardiac function in mice with or without abdominal radiation. **(A)** Echocardiography shows in short-axis view (left) and apical four-chamber view (right). **(B)** Left ventricular ejection fraction (LVEF) (%). **(C)** Fractional shortening (FS) (%). **(D)** Left ventricular end-diastolic internal diameter (LVID; d). **(E)** Left ventricular end-diastolic volume (LV Vol; d). **(F)** Ratio of mitral transtricuspid flow early diastolic filling velocity and late diastolic filling velocity (MV E/A) **(G)** Mitral transtricuspid flow early diastolic filling velocity (MV E). **(H)** Mitral transtricuspid flow late diastolic filling velocity (MV A). **(I)** Isovolumic contraction time (IVCT). **(J)** Isovolumic relaxation time (IVRT). n = 5, $^{*}p < 0.05$.

stand for 1 h in a refrigerator at -20°C. The tissue was centrifuged at 25,000 rcf for 15 min at 4°C. After centrifugation, 600 μl of supernatant is placed in a cryogenic vacuum concentrator and 200 μl of reagent solution (acetonitrile: H2O = 7:3, v: v) is added to redissolve. The samples were vortex-shocked for 1 min, sonicated in a water bath at 4°C for 10 min, centrifuged at 25, 000 rcf for 15 min at 4°C and the supernatant was placed in a supernatant bottle. 20 μl of supernatant from each sample was mixed into QC quality control samples and used to assess the reproducibility and stability of the LC-MS analytical process.

Non-Targeted Metabolomics Analysis

LC-MS/MS technology was used for untargeted metabolomics analysis, using a high-resolution mass spectrometer Q Exactive (Thermo Fisher Scientific, United States) to collect data from positive and negative ions to improve metabolite coverage. LC-MS/MS data processing was performed using The Compound Discoverer 3.1 (Thermo Fisher Scientific, United States) software, which primarily included peak extraction, peak alignment and compound identification. Data pre-processing, statistical analysis, metabolite taxonomic annotation and functional annotation were performed using the metabolomics R package metaX and metabolome bioinformatics analysis pipeline developed by UW Genetics. The multivariate raw data were downscaled by PCA (Principal Component Analysis) to analyse the grouping, trends (within and between group similarities and differences) and outliers (presence of outlier samples) of the observed variables in the dataset. Using PLSDA (Partial Least Squares - Discriminant Analysis), VIP (Variable Importance in Projection) values for the first two main components of the model were combined with analysis of variability, ploidy change and student tests to screen for differential metabolites.

Statistical Analysis

Differences were considered statistically significant if $p < 0.05$ (*). Significance of differences between groups was analysed using t-tests. All data were analysed using SPSS 17.0.

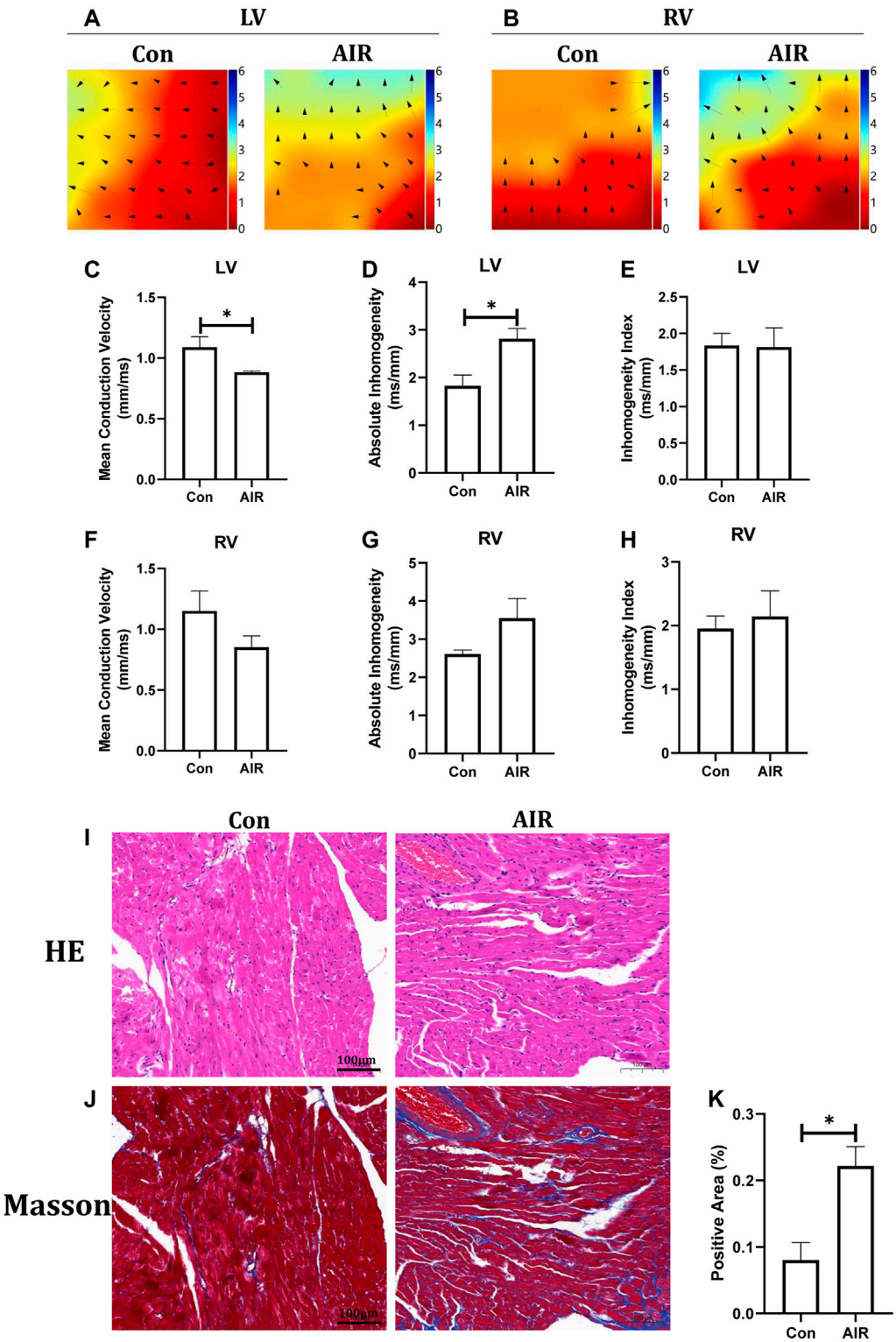

FIGURE 2 | Changes in ventricular electrical and structural remodeling in mice with or without abdominal radiation. Color-coded simulated epicardial activation map of with or without abdominal radiation in left ventricles **(A)** and right ventricles **(B)**. Mean epicardial electrical conduction velocity **(C)**, absolute inhomogeneity **(D)** and inhomogeneity index **(E)** of mice with or without abdominal radiation in left ventricles. Mean epicardial electrical conduction velocity **(F)**, absolute inhomogeneity **(G)** and inhomogeneity index **(H)** of mice with or without abdominal radiation in right ventricles. H&E stains **(I)** and Masson stains **(J)** of ventricle **(K)**. Relative quantitative analysis of the fibrosis in Masson stains of ventricle. The scale bar is 100 μm. n = 5, $^{*}p < 0.05$.

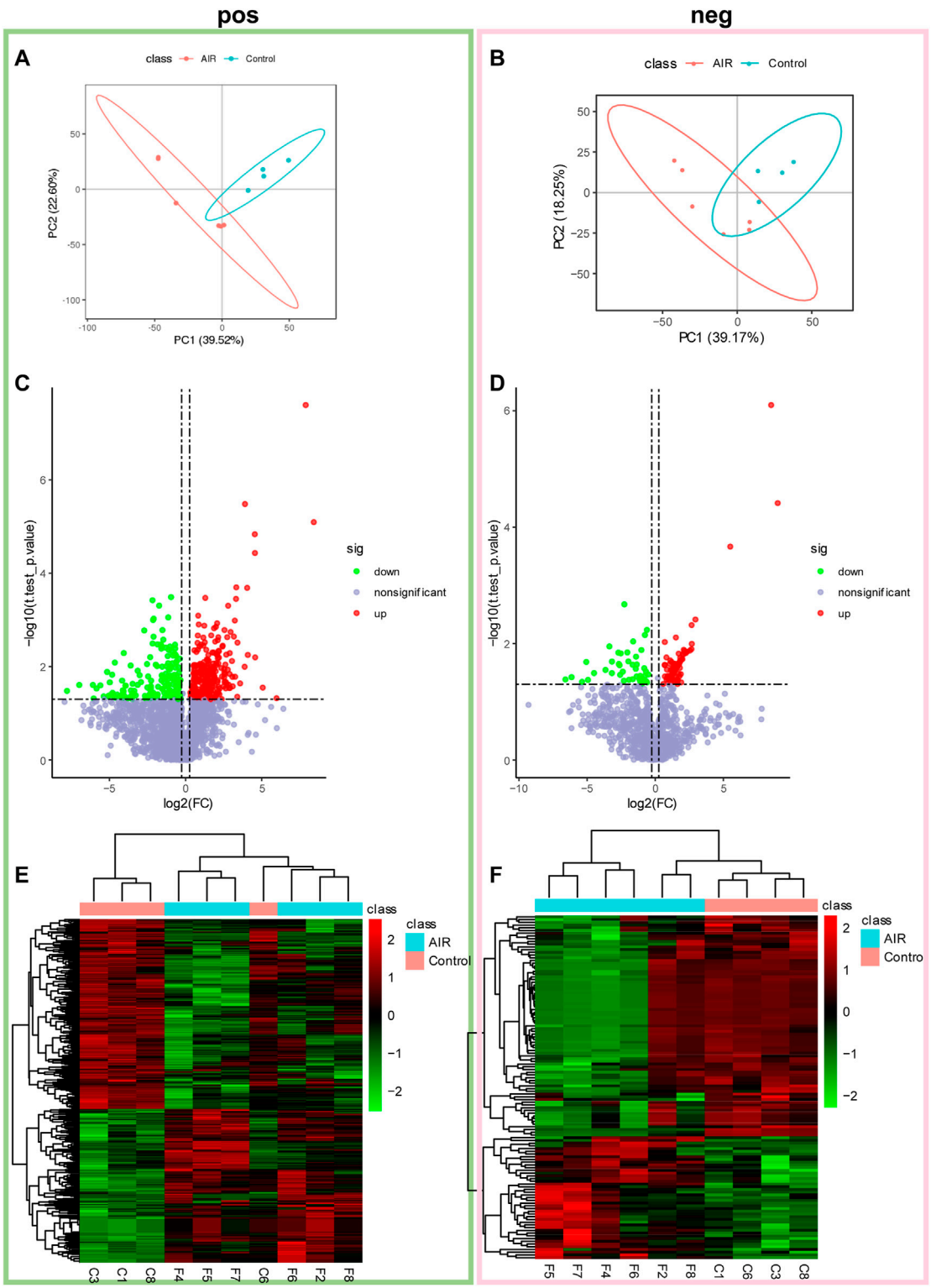

FIGURE 3 | Abdominal radiation significantly changes the tissue metabolic profile of ventricles. Extracted metabolites were analyzed in positive and negative modes as described. Partial least square-discriminant analysis (PLS-DA) and volcano plots of detected metabolites in positive mode and negative mode. In positive mode **(A)** and negative mode **(B)**, 2D scores plot shows PLS-DA discrimination between samples from ventricles of abdominal radiation group (AIR, red) and controls group (Control, blue). The shaded areas indicate the 95% confidence regions. Volcano plots show metabolites from ventricles in control group compared to abdominal radiation group in positive mode **(C)** and negative mode **(D)**. Significantly differential metabolites are highlighted in red (upregulated) and green (downregulated). Heatmap of the significantly altered metabolites between control and abdominal radiation group in positive mode **(E)** and negative mode **(F)**. Before cluster analysis, the data is processed by Log2 transformation and zero-mean normalization. The cluster analysis uses the PHEATMap function in the PHEATMap R package.

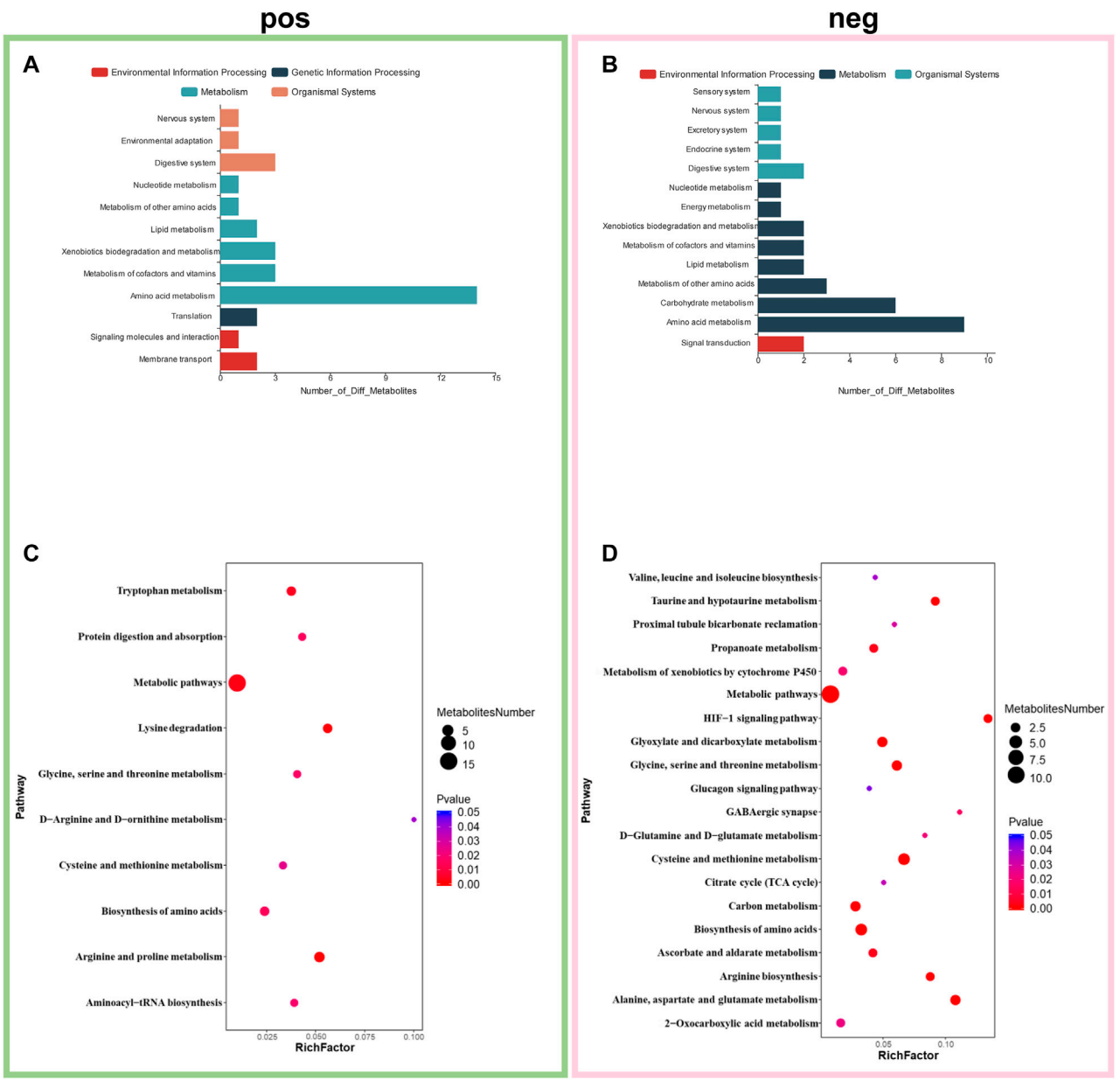

FIGURE 4 | Enrichment of differential metabolites and pathways. Classification and annotation of identified differential metabolites to in positive mode **(A)** and negative mode **(B)**. Metabolic pathway enrichment analysis in positive mode **(C)** and negative mode **(D)**. *$p < 0.05$, fold change≥1.2 or ≤0.83.

RESULTS

Abdominal Radiation-Related Damage on Ventricular Structure and Function

In the initial experiments, cardiac mechanical function and structure were examined using echocardiography. Left ventricular ejection fraction (LVEF), fractional shortening (FS), left ventricular end-diastolic internal diameter (LVID; d), left ventricular end-diastolic volume (LV Vol; d) and mitral transtricuspid flow late diastolic filling velocity (MV A) were reduced and isovolumic relaxation time (IVRT) was increased in the abdominal radiation group compared to the control group. Other parameters, such as mitral transtricuspid flow early diastolic filling velocity (MV E) and the ratio of mitral transtricuspid flow early diastolic filling velocity and late diastolic filling velocity (MV E/A) showed a tendency to deteriorate but the effects were not statistically significant (**Figures 1A–J**).

Electrical remodeling of the ventricles was evaluated using epicardial optical mapping. The mean electrical conduction velocity of the left ventricles was decreased and the absolute inhomogeneity, one of parameters of conduction heterogeneity, was increased in abdominal radiation group, suggesting an abnormal electrical conduction in the left ventricles. By

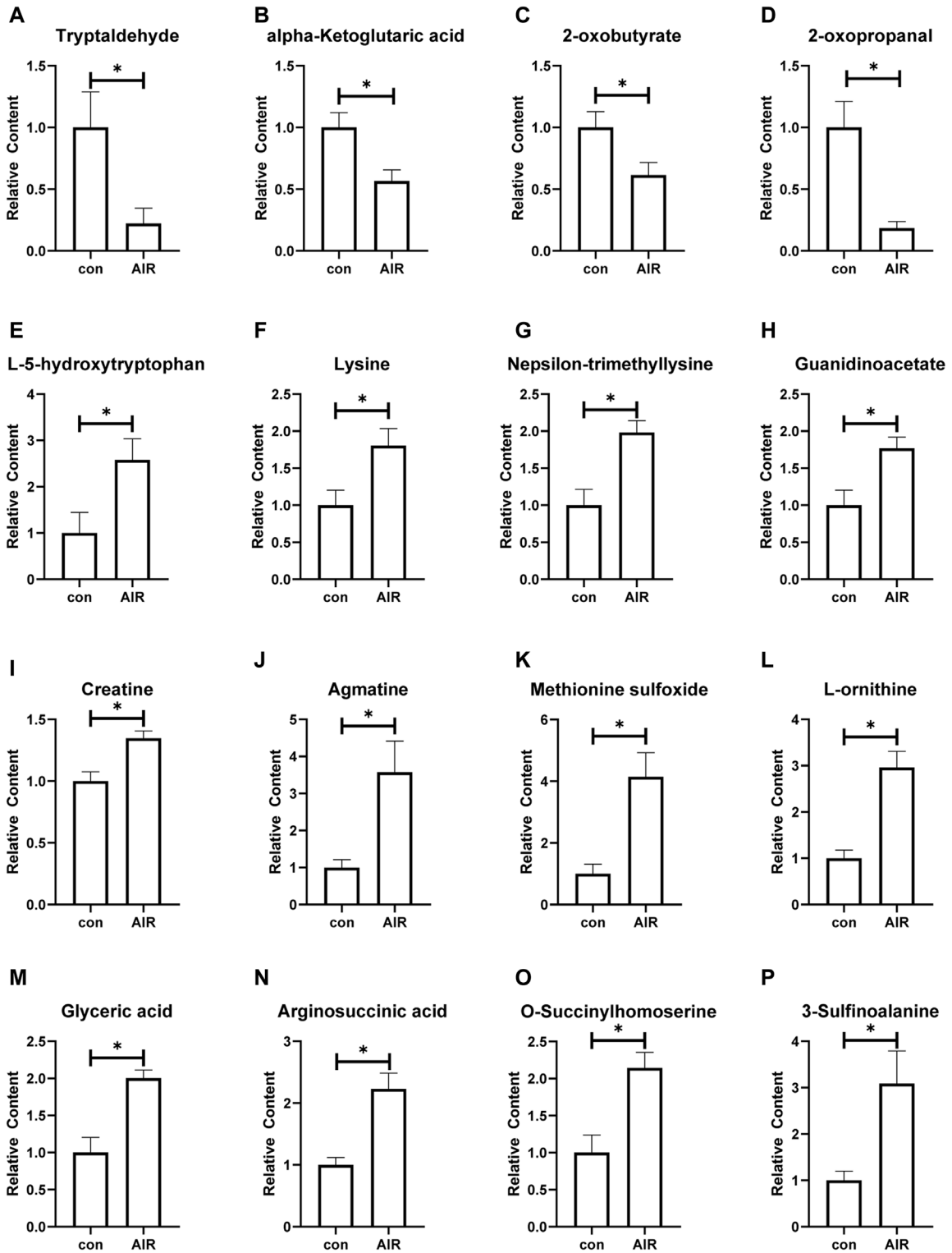

FIGURE 5 | Changes of amino acid metabolites of ventricles in mice with or without abdominal radiation. Relative content of tryptaldehyde **(A)**, alpha-ketoglutaric acid **(B)**, 2-oxobutyrate **(C)**, 2-oxopropanal **(D)**, l-5-hydroxytryptophan **(E)**, lysine **(F)**, nepsilon-trimethyllysine **(G)**, guanidinoacetate **(H)**, creatine **(I)**, agmatine **(G)**, methionine sulfoxide **(K)**, l-ornithine **(L)**, glyceric acid **(M)**, arginosuccinic acid **(N)**, *o*-succinylhomoserine **(O)**, 3-sulfinoalanine **(P)**. n = 4–6, $^*p < 0.05$.

contrast, the mean conduction velocity and heterogeneity of the right ventricles did not show significant changes (**Figures 2A–H**). Further tissue level studies using H&E stains showed no significant infiltration by inflammatory cells in abdominal radiation group (**Figure 2I**). Masson stain showed increased positive area of intramyocardial fibrosis, which could indicate ventricular structural remodeling in abdominal radiation group (**Figures 2J,K**).

Abdominal Radiation-Related Changes on Ventricular Small Molecule Metabolites

Subsequently, non-targeted metabolomics analysis was used to identify small molecular metabolites changes. Multiple variance statistical analysis (PCA and PLS-DA) and single variance analysis (folding variation (FC) and student tests) were used to identify changes in the levels of metabolites. PLS-DA of metabolites showed a distinct separation between abdominal radiation and control groups (**Figures 3A,B**). In the positive mode, a total of 474 metabolites were differentially expressed. Amongst these, 262 metabolites were up-regulated and 212 were down-regulated in control group compared to the abdominal radiated group. In the negative mode, 126 metabolites were significantly differentially expressed; among them, 81 metabolites were up-regulated and 45 were down-regulated in control group compared to the radiated samples (**Figures 3C–F**).

The KEGG and HMDB databases were used to classify and annotate the metabolites that were significantly different between the abdominal radiation and control groups. The identified differential metabolites were mainly concentrated in amino acid metabolism and carbohydrate metabolism (**Figures 4A,B**). Changes in amino acid metabolites are as follows: tryptaldehyde, alpha-ketoglutaric acid, 2-oxobutyrate, 2-oxopropanal decreased, while l-5-hydroxytryptophan, lysine, nepsilon-trimethyllysine, guanidinoacetate, creatine, agmatine, methionine sulfoxide, l-ornithine, glyceric acid, arginosuccinic acid, *o*-succinylhomoserine, 3-sulfinoalanine increasing (**Figure 5**).

Metabolic pathway enrichment analysis of the identified differential metabolites revealed that they were mainly enriched in arginine and proline metabolism, lysine degradation, tryptophan metabolism, biosynthesis of amino acids, protein digestion and absorption, glycine, serine and threonine metabolism, aminoacyl-tRNA biosynthesis, cysteine and methionine metabolism, d-arginine and d-ornithine metabolism, cysteine and methionine metabolism, alanine, aspartate and glutamate metabolism, biosynthesis of amino acids, glycine, serine and threonine metabolism, glyoxylate and dicarboxylate metabolism, HIF-1 signaling pathway, taurine and hypotaurine metabolism, arginine biosynthesis, carbon metabolism, propanoate metabolism, ascorbate and aldarate metabolism, gabaergic synapse, metabolism of xenobiotics by cytochrome P450, d-glutamine and d-glutamate metabolism and 2-Oxocarboxylic acid metabolism (**Figures 4C,D**).

Abdominal Radiation-Related Damage on Atrial Structure

The effects on structural and electrical remodelling in the atria were also examined. Epicardial optical mapping showed that the mean electrical conduction velocity of the left atrium was decreased, and the absolute inhomogeneity of the right atrium was increased in abdominal radiation group compared to control group (**Figures 6A–H**). By contrast, the absolute inhomogeneity of the left atrium and inhomogeneity index of the both left and right atrium trended to increase but the changes were not statistically significant. Similar to the findings in the ventricles, HE stains and Masson stains showed no significant infiltration by inflammatory cells and intramyocardial fibrosis in abdominal radiation group (**data not shown**).

DISCUSSION

In this study, long-term cardiac damage caused by abdominal irradiation in mice were examined. Cardiac mechanical dysfunction, associated with electrical and structural remodeling, was observed. These changes were associated with abnormalities in amino acid biosynthesis and metabolism.

The resultant cardiac damage by abdominal irradiation can be due to a number of reasons. It could be the bystander effect of radiotherapy, that is, the same effect of radiotherapy on cells, tissues or organs in non-irradiated areas (Wang et al., 2015; Fu et al., 2020). After irradiation, cells in the irradiated area can secrete cytokines, small molecular metabolites, exosomes or microvesicles containing various substances, and other media (Lin et al., 2017; Ariyoshi et al., 2019; Ni et al., 2020; Mukherjee et al., 2021), resulting in metabolic disorders, apoptosis, endoplasmic reticulum and golgi dysfunction of cells in non-irradiated areas (Yakovlev, 2015; Jella et al., 2018; Mladenov et al., 2018; Dong et al., 2020; Heeran et al., 2021; Yang et al., 2021). Earlier studies reported elevated levels of CRP in circulating blood, and splenic cells exhibited enhanced levels of oxidative stress and increased apoptosis after cranial irradiation in rats (El-Din et al., 2017). Isolated extracellular vesicles in the circulation of systemically irradiated mice were injected into unirradiated mice, resulting in increased levels of lipid peroxidation and reactive oxygen species in the spleen of bystander mice with spleen damage (Hargitai et al., 2021). However, the bystander effect of abdominal irradiation on the heart is still unclear. This study clarified that irradiation of the abdomen in mice can cause long-term damage to the structure and function of the heart in the non-irradiated position, which may be mediated by small molecular metabolites.

Several pathophysiological processes, such as myocardial fibrosis, atherosclerosis, microvascular and macrovascular ischemia, underlie the cardiac damage from irradiation. The possible mechanisms are also diverse, such as vascular damage, inflammatory response, platelet activation, calcium overload, endoplasmic reticulum and mitochondrial oxidative stress and autonomic dysfunction (Yusuf et al., 2017; Us et al., 2020; Zhang et al., 2020). Recent studies have shown that mRNA

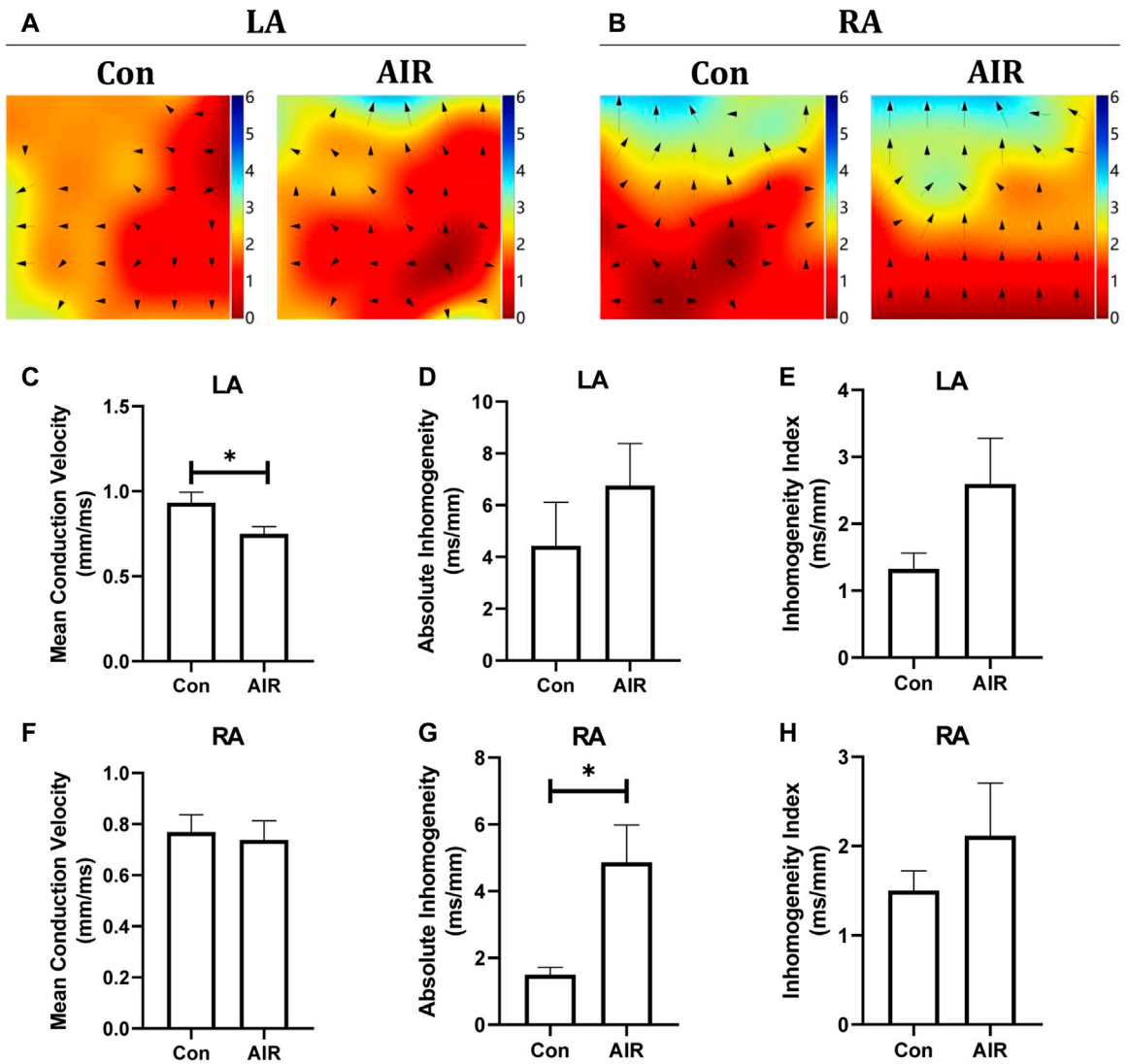

FIGURE 6 | Changes in cardiac electrical conduction of mice with or without abdominal radiation. Color-coded simulated epicardial activation map of mice in left atrium **(A)** and right atrium **(B)** with or without abdominal radiation. Mean epicardial electrical conduction velocity **(C)**, absolute inhomogeneity **(D)** and inhomogeneity index **(E)** of mice with or without abdominal radiation in left atrium. Mean epicardial electrical conduction velocity **(F)**, absolute inhomogeneity **(G)** and inhomogeneity index **(H)** of mice with or without abdominal radiation in right atrium. H&E stains (I) and Masson stains (J) of atrium. The scale bar is 100 μm.n = 5, $^{*}p < 0.05$.

levels of inflammasome-associated chemokines CCL2 and CCL5 and the adhesion molecule VCAM1 were significantly higher after direct radiation treatment of arteries compared to controls, suggesting that radiation-induced inflammatory factors play an important role in adverse cardiovascular effects (Christersdottir et al., 2019). We speculate that inflammatory factors from the radiotherapy site may enter the heart through the blood circulation and cause heart damage. In the rat model, it was found that the levels of inflammatory factors such as IL-4, IL-6, IL1-β and TNF-α and oxidative stress-related factors such as Malondialdehyde were significantly increased (Us et al., 2020). IL-6 acts on the gp130/STAT3 pathway to cause cardiomyocyte hypertrophy to provide a prerequisite for heart failure (Meléndez et al., 2010). TNF-α-mediated intracellular calcium overload leads to myocardial electrical activity and contractile dysfunction (Hanna and Frangogiannis, 2020). In addition, immune checkpoint inhibitors may increase the risk of radiation myocardial toxicity due to the fact that radiation myocardial toxicity may be mediated by the PD-1 axis and CD8-positive T cells (Du et al., 2018). This may be the reason for the changes in the function and structure of the cardiac changes in our animal model. In addition, heart damage related to craniocerebral radiotherapy may be related to oxidative stress (Rashed et al., 2021). This is consistent with the abnormal results of small molecule metabolites in our model.

Our study found abnormal amino acid metabolism of myocardial tissue in the abdominal radiation group. The metabolome results showed the decreased tryptaldehyde, alpha-ketoglutaric acid, 2-

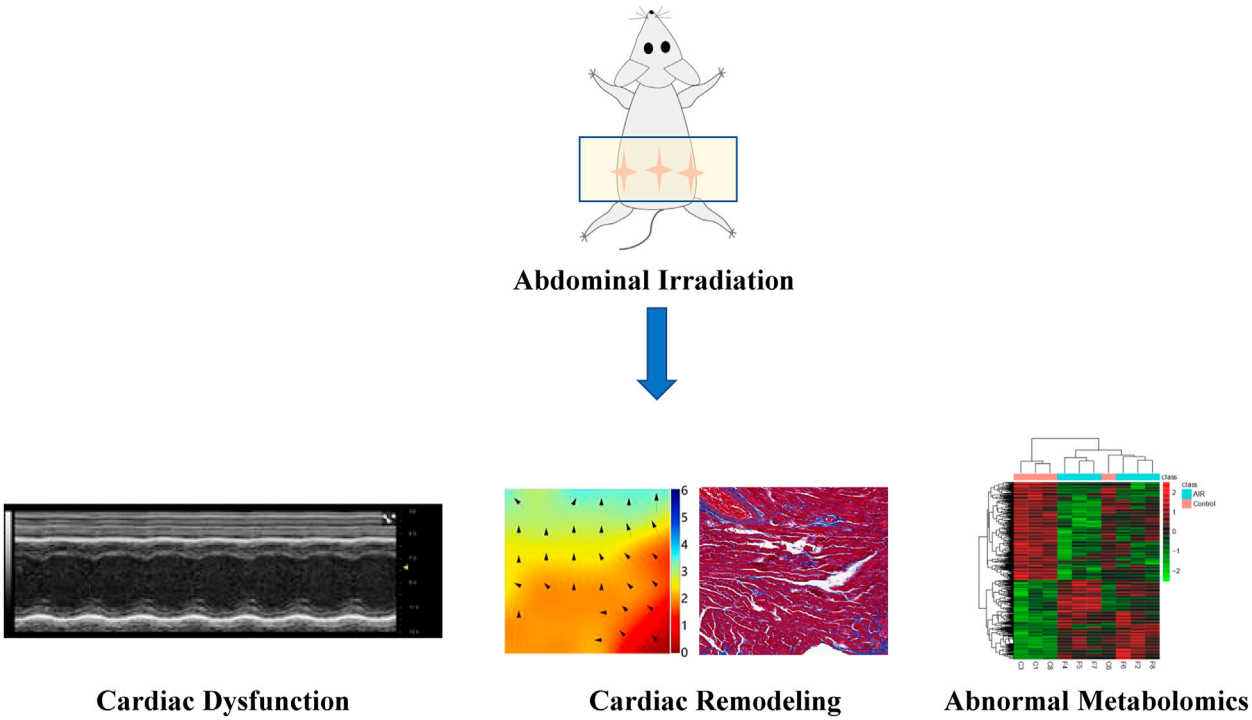

FIGURE 7 | Schematic image depicts long-term cardiac damage associated with abdominal irradiation in mice.

oxobutyrate, 2-oxopropanal and the increased l-5-hydroxytryptophan, lysine, nepsilon-trimethyllysine, guanidinoacetate, creatine, agmatine, methionine sulfoxide, l-ornithine, glyceric acid, arginosuccinic acid, *o*-succinylhomoserine, 3-sulfinoalanine increasing based on the findings. Kyoto Encyclopedia of Genes and Genomes database (https://www.genome.jp/kegg/) and Human Metabolome database (https://hmdb.ca/), we have analyzed the effect of different metabolite changes on the heart. Alpha-Ketoglutaric acid participates in the tricarboxylic acid cycle and eventually causes abnormal energy metabolism. It is also involved in metabolism of a variety of amino acids, such as alanine, aspartic acid and glutamic acid metabolism, lysine biosynthesis, histidine metabolism and so on. 2-oxobutyrate is a substance involved in the metabolism of a variety of amino acids (glycine, methionine, valine, leucine, serine, threonine, isoleucine), as well as the metabolism of propionic acid and C-5 branched-chain dibasic acid. It is also one of the degradation products of threonine. It can be converted into propionyl-CoA (and subsequently methylmalonyl-CoA, which can be converted into succinyl-CoA, a citric acid cycle intermediate), and thus enter the citric acid cycle. In addition, valine, leucine and isoleucine were also biosynthesized by propionic acid and C-5 branched-chain dibasic acid. 2-oxopropanal participates in the metabolism of glycine, serine and threonine, pyruvate metabolism, and propionic acid metabolism. Tryptaldehyde is involved in many enzymatic reactions. Therefore, when the content of the above substances is significantly reduced, it will not only reduce the energy supply of the heart, but also affect the synthesis and metabolism of the normal amino acids of the myocardium, and ultimately affect the changes in structure and function.

O-succinylhomoserine, 3-sulfinoalanine, and methionine sulfoxide are involved in the metabolism of cysteine and methionine metabolism. In this model, the content of O-succinylhomoserine, 3-sulfinoalanine, and methionine sulfoxide in the abdominal irradiation group all increased significantly, suggesting that the metabolism of cysteine or methionine was enhanced. N-acetylcysteine exerts a strong antioxidant effect on myocardial protection (Johnson et al., 2019; Mushtaq et al., 2021), the decrease of which may suggest that the model mouse myocardium may have reduced antioxidant capacity. Glyceric acid is a product of the pentose phosphate pathway, and its abnormally high levels in tissues can cause metabolic acidosis. And the pentose phosphate pathway can promote the production of reducing equivalents, such as NADPH, which will be used for reducing biosynthesis reactions in cells (Sun et al., 2017; Li Z. et al., 2019). Based on the previous results, our current results suggests that mice from the abdominal irradiation group may have a certain degree of hyperoxidation, which is consistent with the previously reported bystander effect of radiotherapy.

Arginosuccinic acid is synthesized from citrulline and aspartic acid and is used as the precursor of arginine in the urea cycle or citrulline-NO cycle. Arginosuccinate is the precursor of fumaric acid produced by argininosuccinate lyase in the citric acid cycle. The reduction of fumaric acid and malic acid was reported to be associated with right ventricular remodeling in severe pulmonary hypertension rats (Sakao et al., 2021), suggesting that arginine succinate utilization disorder may ultimately affect energy metabolism and ventricular remodeling. Guanidinoacetate (GAA) is involved in the metabolism of glycine,

serine and threonine, the metabolism of arginine and proline, and the production of creatine. The main metabolic function of creatine is producing creatine phosphate through the enzyme creatine kinase and phosphate group, which leads to ATP regeneration. Therefore, we speculate that the increase in myocardial guanidinoacetate will result in an increase in the production of creatine, and creatine utilization disorders could eventually affect the energy supply of the heart.

L-5-hydroxytryptophan is an aromatic amino acid produced from the essential amino acid L-tryptophan. When 5-hydroxytryptophan levels were high enough, it could be a neurotoxin and a metabolic toxin. It is reported that long-term use of L-5-HTP provides significant protection against the development of deoxycorticosterone acetate-salt-treated (DOCA)-induced hypertension and cardiac hypertrophy in rats (Fregly et al., 1987). Long-term-use of L-5-HTP can effectively reduce the increase in blood pressure in the DS model (Baron et al., 1991). In addition, L-5-hydroxytryptophan can also increase renin activity (Barney et al., 1981), thereby affecting the structure and function of the heart. Therefore, the increase in L-5-hydroxytryptophan in the AIR group observed in this study could be a compensatory protective effect or an unclear toxic effect. Tryptophan could generate indole-3-acetic acid (IAA) (Leveau and Gerards, 2008), and IAA degrading is involved in tricarboxylate cycling, gluconeogenesis, and carbon/nitrogen sensing (Leveau and Gerards, 2008), which may induced the cardiac dysfunction in AIR group. Lysine (Lys) is an essential amino acid that not only participates in protein synthesis, but also promotes the cross-linking of collagen peptides. Lysine is also often involved in histone modification and therefore affects the epigenome. According to reports, the acetylation of histone lysine is associated with myocardial remodeling (Peng et al., 2021; Han et al., 2022), and the lysine methylation of histone promotes the reprogramming of myocardial cells by fibroblasts (Singh et al., 2021). Meanwhile, histone lysine-specific demethylase one induced renal fibrosis (Dong et al., 2022; Zhang et al., 2022). However, a large increase in lysine was observed in the abdominal radiation group of this study, combined with the enrichment of other metabolites concentrated in the lysine metabolic pathway, further indicating that the large accumulation of lysine, but its role in the changes in cardiac structure and function is still need further verification.

Abnormalities in amino acid metabolism could be implicated in cardiac dysfunction and remodeling. However, the upstream and downstream regulatory mechanisms need to be further explored. Through KEGG pathway analysis, we speculate that some pathways may lead to changes in small molecular metabolites, and ultimately lead to abnormal cardiac function and remodeling. Our research found that differential metabolites are mainly enriched in HIF-1 signaling pathway, which participates in the regulation of many biological processes related to metabolic differences (Denko, 2008), especially oxygen homeostasis. HIF-1 is a switch that controls the recognition and response of cells to changes in oxygen status. HIF-1 controls oxygen utilization by regulating glucose metabolism and redox homeostasis (Semenza, 2014; Zhang et al., 2019). Radiation can activate the HIF-1 signaling pathway by damaging endothelial cells, and regulate vascular endothelial growth factor (VEGF) and CXCL12 (C-X-C motif chemokine 12) to increase the effect of killing target cells (Meijer et al., 2012; Sun et al., 2019; Huang and Zhou, 2020). For normal cell metabolism, radiation-dependent HIF1α converts oxidative phosphorylation to glycolysis and increase radiation resistance (Lall et al., 2014). However, this study found that irradiation of the abdomen of mice activated the cardiac HIF-1 pathway. Whether this change protects or damages the cardiac response related to the bystander phenomenon requires further research. Besides, the mechanism of HIF-1 activation also needs further study.

Limitations

Although this study revealed that long-term cardiac damage caused by remote abdominal irradiation is related to metabolic remodeling, especially amino acid metabolic remodeling, and downstream involving apoptosis, it did not clarify the specific pathway mechanism. Meanwhile, this study did not measure RV function, electrocardiogram and baseline echocardiographic parameters.

CONCLUSION

Abdominal irradiation causes long-term damage to the non-irradiated heart, as reflected by electrical and structural remodeling and mechanical dysfunction associated with abnormal amino acid biosynthesis and metabolism (**Figure 7**).

DATA AVAILABILITY STATEMENT

The original contributions presented in the study are included in the article/supplementary materials, further inquiries can be directed to the corresponding authors.

ETHICS STATEMENT

The animal study was reviewed and approved by Institutional Committee for the Care and Use of Animals, Institute of Radiological Sciences, Chinese Academy of Medical Sciences.

AUTHOR CONTRIBUTIONS

Concept—TL, YL, ZW; Fundings—TL; Materials—XZ, ZW; Data collection and/or processing—ZW, ZJ, ZZ; Analysis and/or interpretation—ZW, ZJ; Writing—ZW, ZJ; Critical review—GT, GL, TL, YL, XZ, FW.

ACKNOWLEDGMENTS

We thank all the staff and participants of this study for their important contributions. And we also thank National Natural Science Foundation of China (81970270, 82170327 to TL), Tianjin Natural Science Foundation (20JCZDJC00340, 20JCZXJC00130 to TL) and Tianjin Key Medical Discipline (Specialty) Construction Project.

REFERENCES

Alvarez-Cardona, J. A., Ray, J., Carver, J., Zaha, V., Cheng, R., Yang, E., et al. (2020). Cardio-Oncology Education and Training: JACC Council Perspectives. *J. Am. Coll. Cardiol.* 76 (19), 2267–2281. doi:10.1016/j.jacc.2020.08.079

Ariyoshi, K., Miura, T., Kasai, K., Fujishima, Y., Nakata, A., and Yoshida, M. (2019). Radiation-Induced Bystander Effect Is Mediated by Mitochondrial DNA in Exosome-like Vesicles. *Scientific Rep.* 9, 9103. doi:10.1038/s41598-019-45669-z

Armanious, M. A., Mohammadi, H., Khodor, S., Oliver, D. E., Johnstone, P. A., and Fradley, M. G. (2018). Cardiovascular Effects of Radiation Therapy. *Curr. Probl. Cancer* 42 (4), 433–442. doi:10.1016/j.currproblcancer.2018.05.008

Banfill, K., Giuliani, M., Aznar, M., Franks, K., McWilliam, A., Schmitt, M., et al. (2021). Cardiac Toxicity of Thoracic Radiotherapy: Existing Evidence and Future Directions. *J. Thorac. Oncol.* 16 (2), 216–227. doi:10.1016/j.jtho.2020.11.002

Barney, C. C., Threatte, R. M., Kikta, D. C., and Fregly, M. J. (1981). Effects of Serotonin and L-5-Hydroxytryptophan on Plasma Renin Activity in Rats. *Pharmacol. Biochem. Behav.* 14 (6), 895–900. doi:10.1016/0091-3057(81)90380-4

Baron, A., Riesselmann, A., and Fregly, M. J. (1991). Reduction in the Elevated Blood Pressure of Dahl Salt-Sensitive Rats Treated Chronically with L-5-Hydroxytryptophan. *Pharmacology* 42 (1), 15–22. doi:10.1159/000138763

Bradley, J. D., Paulus, R., Komaki, R., Masters, G., Blumenschein, G., Schild, S., et al. (2015). Standard-dose versus High-Dose Conformal Radiotherapy with Concurrent and Consolidation Carboplatin Plus Paclitaxel with or without Cetuximab for Patients with Stage IIIA or IIIB Non-small-cell Lung Cancer (RTOG 0617): a Randomised, Two-By-Two Factorial Phase 3 Study. *Lancet Oncol.* 16 (2), 187–199. doi:10.1016/s1470-2045(14)71207-0

Cao, L., Xu, C., Yi, P., Li, H., Lin, Y., Cai, G., et al. (2021). Asparaginyl Endopeptidase (AEP) Regulates Myocardial Apoptosis in Response to Radiation Exposure via Alterations in NRF2 Activation. *Am. J. Cancer Res.* 11 (4), 1206–1225.

Carr, Z. A., Land, C. E., Kleinerman, R. A., Weinstock, R. W., Stovall, M., Griem, M. L., et al. (2005). Coronary Heart Disease after Radiotherapy for Peptic Ulcer Disease. *Int. J. Radiat. Oncol. Biol. Phys.* 61 (3), 842–850. doi:10.1016/j.ijrobp.2004.07.708

Chargari, C., Deutsch, E., Blanchard, P., Gouy, S., Martelli, H., Guérin, F., et al. (2019). Brachytherapy: An Overview for Clinicians. *CA: a Cancer J. clinicians* 69 (5), 386–401. doi:10.3322/caac.21578

Christersdottir, T., Pirault, J., Gistera, A., Bergman, O., Gallina, A. L., Baumgartner, R., et al. (2019). Prevention of Radiotherapy-Induced Arterial Inflammation by Interleukin-1 Blockade. *Eur. Heart J.* 40 (30), 2495. doi:10.1093/eurheartj/ehz206

Curigliano, G., Cardinale, D., Dent, S., Criscitiello, C., Aseyev, O., Lenihan, D., et al. (2016). Cardiotoxicity of Anticancer Treatments: Epidemiology, Detection, and Management. *CA: a Cancer J. clinicians* 66 (4), 309–325. doi:10.3322/caac.21341

Denko, N. C. (2008). Hypoxia, HIF1 and Glucose Metabolism in the Solid Tumour. *Nat. Rev. Cancer* 8 (9), 705–713. doi:10.1038/nrc2468

Dong, C., Tu, W. Z., He, M. Y., Fu, J. M., Kobayashi, A., Konishi, T., et al. (2020). Role of Endoplasmic Reticulum and Mitochondrion in Proton Microbeam Radiation-Induced Bystander Effect. *Radiat. Res.* 193 (1), 63–72. doi:10.1667/rr15469.1

Dong, L., Yu, L., and Zhong, J. (2022). Histone Lysine-specific Demethylase 1 Induced Renal Fibrosis via Decreasing Sirtuin 3 Expression and Activating TGF-β1/Smad3 Pathway in Diabetic Nephropathy. *Diabetol. Metab. Syndr.* 14 (1), 2. doi:10.1186/s13098-021-00771-z

Du, S. S., Zhou, L., Alexander, G. S., Park, K., Yang, L. F., Wang, N. D., et al. (2018). PD-1 Modulates Radiation-Induced Cardiac Toxicity through Cytotoxic T Lymphocytes. *J. Thorac. Oncol.* 13 (4), 510–520. doi:10.1016/j.jtho.2017.12.002

El-Din, A. A. M., Abdelrazzak, A. B., Ahmed, M. T., and El-Missiry, M. A. (2017). Radiation Induced Bystander Effects in the Spleen of Cranially-Irradiated Rats. *Br. J. Radiol.* 90 (1080), 20170278. doi:10.1259/bjr.20170278

Fregly, M. J., Lockley, O. E., and Sumners, C. (1987). Chronic Treatment with L-5-Hydroxytryptophan Prevents the Development of DOCA-Salt-Induced Hypertension in Rats. *J. Hypertens.* 5 (5), 621–628. doi:10.1097/00004872-198710000-00018

Fu, J., Zhu, L., Tu, W., Wang, X., Pan, Y., Bai, Y., et al. (2020). Macrophage-Mediated Bystander Effects after Different Irradiations through a P53-dependent Pathway. *Radiat. Res.* 193 (2), 119–129. doi:10.1667/RR15354.1

Gkantaifi, A., Papadopoulos, C., Spyropoulou, D., Toumpourleka, M., Iliadis, G., Kardamakis, D., et al. (2019). Breast Radiotherapy and Early Adverse Cardiac Effects. The Role of Serum Biomarkers and Strain Echocardiography. *Anticancer Res.* 39 (4), 1667–1673. doi:10.21873/anticanres.13272

Groarke, J. D., Nguyen, P. L., Nohria, A., Ferrari, R., Cheng, S. S., and Moslehi, J. (2014). Cardiovascular Complications of Radiation Therapy for Thoracic Malignancies: the Role for Non-invasive Imaging for Detection of Cardiovascular Disease. *Eur. Heart J.* 35 (10), 612–623. doi:10.1093/eurheartj/eht114

Han, X., Peng, C., Huang, L., Luo, X., Mao, Q., Wu, S., et al. (2022). EGCG Prevents Pressure Overload-Induced Myocardial Remodeling by Downregulating Overexpression of HDAC5 in Mice. *Int. J. Mol. Med.* 49 (1), 11. doi:10.3892/ijmm.2021.5066

Hanna, A., and Frangogiannis, N. G. (2020). Inflammatory Cytokines and Chemokines as Therapeutic Targets in Heart Failure. *Cardiovasc. Drugs Ther.* 34 (6), 849–863. doi:10.1007/s10557-020-07071-0

Hargitai, R., Kis, D., Persa, E., Szatmari, T., Safrany, G., and Lumniczky, K. (2021). Oxidative Stress and Gene Expression Modifications Mediated by Extracellular Vesicles: An *In Vivo* Study of the Radiation-Induced Bystander Effect. *Antioxidants* 10 (2), 156. doi:10.3390/antiox10020156

Heeran, A. B., Berrigan, H. P., Buckley, C. E., Bottu, H. M., Prendiville, O., Buckley, A. M., et al. (2021). Radiation-induced Bystander Effect (RIBE) Alters Mitochondrial Metabolism Using a Human Rectal Cancer *Ex Vivo* Explant Model. *Translational Oncol.* 14 (1), 100882. doi:10.1016/j.tranon.2020.100882

Huang, R. X., and Zhou, P. K. (2020). DNA Damage Response Signaling Pathways and Targets for Radiotherapy Sensitization in Cancer. *Signal. Transduct. Target. Ther.* 5 (1), 60. doi:10.1038/s41392-020-0150-x

Jella, K. K., Moriarty, R., McClean, B., Byrne, H. J., and Lyng, F. M. (2018). Reactive Oxygen Species and Nitric Oxide Signaling in Bystander Cells. *PloS one* 13 (4), e0195371. doi:10.1371/journal.pone.0195371

Johnson, R., Sangweni, N. F., Mabhida, S. E., Dludla, P. V., Mabasa, L., Riedel, S., et al. (2019). An *In Vitro* Study on the Combination Effect of Metformin and N-Acetyl Cysteine against Hyperglycaemia-Induced Cardiac Damage. *Nutrients* 11 (12), 2850. doi:10.3390/nu11122850

Lall, R., Ganapathy, S., Yang, M., Xiao, S., Xu, T., Su, H., et al. (2014). Low-dose Radiation Exposure Induces a HIF-1-Mediated Adaptive and Protective Metabolic Response. *Cel Death Differ.* 21 (5), 836–844. doi:10.1038/cdd.2014.24

Leveau, J. H. J., and Gerards, S. (2008). Discovery of a Bacterial Gene Cluster for Catabolism of the Plant Hormone Indole 3-acetic Acid. *FEMS Microbiol. Ecol.* 65 (2), 238–250. doi:10.1111/j.1574-6941.2008.00436.x

Li, H., Cao, L., Yi, P.-Q., Xu, C., Su, J., Chen, P.-Z., et al. (2019). Pituitary Adenylate Cyclase-Activating Polypeptide Ameliorates Radiation-Induced Cardiac Injury. *Am. J. translational Res.* 11 (10), 6585–6599.

Li, Z., Li, J., Zhang, S., Chen, G., Chi, S., Li, X., et al. (2019). Metabolomics Analysis of Gut Barrier Dysfunction in a Trauma-Hemorrhagic Shock Rat Model. *Biosci. Rep.* 39 (1), BSR20181215. doi:10.1042/BSR20181215

Lin, X. Z., Wei, F. X., Major, P., Al-Nedawi, K., Al Saleh, H. A., and Tang, D. M. (2017). Microvesicles Contribute to the Bystander Effect of DNA Damage. *Int. J. Mol. Sci.* 18 (4), 788. doi:10.3390/ijms18040788

Meijer, T. W. H., Kaanders, J., Span, P. N., and Bussink, J. (2012). Targeting Hypoxia, HIF-1, and Tumor Glucose Metabolism to Improve Radiotherapy Efficacy. *Clin. Cancer Res.* 18 (20), 5585–5594. doi:10.1158/1078-0432.Ccr-12-0858

Meléndez, G. C., McLarty, J. L., Levick, S. P., Du, Y., Janicki, J. S., and Brower, G. L. (2010). Interleukin 6 Mediates Myocardial Fibrosis, Concentric Hypertrophy, and Diastolic Dysfunction in Rats. *Hypertension.* 56 (2), 225–231. doi:10.1161/HYPERTENSIONAHA.109.148635

Menezes, K. M., Wang, H. C., Hada, M., and Saganti, P. B. (2018). Radiation Matters of the Heart: A Mini Review. *Front. Cardiovasc. Med.* 5, 83. doi:10.3389/fcvm.2018.00083

Mladenov, E., Li, F. H., Zhang, L. H., Klammer, H., and Iliakis, G. (2018). Intercellular Communication of DNA Damage and Oxidative Status

Underpin Bystander Effects. *Int. J. Radiat. Biol.* 94 (8), 719–726. doi:10.1080/09553002.2018.1434323

Mukherjee, S., Dutta, A., and Chakraborty, A. (2021). External Modulators and Redox Homeostasis: Scenario in Radiation-Induced Bystander Cells. *Mutat. Research-Reviews Mutat. Res.* 787, 108368. doi:10.1016/j.mrrev.2021.108368

Mushtaq, I., Bashir, Z., Sarwar, M., Arshad, M., Ishtiaq, A., Khan, W., et al. (2021). N-acetyl Cysteine, Selenium, and Ascorbic Acid Rescue Diabetic Cardiac Hypertrophy via Mitochondrial-Associated Redox Regulators. *Molecules (Basel, Switzerland)* 26 (23), 7285. doi:10.3390/molecules26237285

Nabialek-Trojanowska, I., Lewicka, E., Wrona, A., Kaleta, A. M., Lewicka-Potocka, Z., Raczak, G., et al. (2020). Cardiovascular Complications after Radiotherapy. *Cardiol. J.* 27 (6), 836–847. doi:10.5603/CJ.a2018.0120

Ni, N., Ma, W. W., Tao, Y. L., Liu, J., Hua, H., Cheng, J. W., et al. (2020). Exosomal MiR-769-5p Exacerbates Ultraviolet-Induced Bystander Effect by Targeting TGFBR1. *Front. Physiol.* 11, 603081. doi:10.3389/fphys.2020.603081

Nielsen, K. M., Offersen, B. V., Nielsen, H. M., Vaage-Nilsen, M., and Yusuf, S. W. (2017). Short and Long Term Radiation Induced Cardiovascular Disease in Patients with Cancer. *Clin. Cardiol.* 40 (4), 255–261. doi:10.1002/clc.22634

Peng, B., Peng, C., Luo, X., Wu, S., Mao, Q., Zhang, H., et al. (2021). JNK Signaling-dependent Regulation of Histone Acetylation Are Involved in Anacardic Acid Alleviates Cardiomyocyte Hypertrophy Induced by Phenylephrine. *PloS one* 16 (12), e0261388. doi:10.1371/journal.pone.0261388

Rashed, E. R., Abdel-Rafei, M. K., and Thabet, N. M. (2021). Roles of Simvastatin and Sildenafil in Modulation of Cranial Irradiation-Induced Bystander Multiple Organs Injury in Rats. *Inflammation* 44 (6), 2554–2579. doi:10.1007/s10753-021-01524-w

Sakao, S., Kawakami, E., Shoji, H., Naito, A., Miwa, H., Suda, R., et al. (2021). Metabolic Remodeling in the Right Ventricle of Rats with Severe Pulmonary Arterial Hypertension. *Mol. Med. Rep.* 23 (4), 227. doi:10.3892/mmr.2021.11866

Schaue, D., and McBride, W. H. (2015). Opportunities and Challenges of Radiotherapy for Treating Cancer. *Nat. Rev. Clin. Oncol.* 12 (9), 527–540. doi:10.1038/nrclinonc.2015.120

Semenza, G. L. (2014). Hypoxia-Inducible Factor 1 and Cardiovascular Disease. *Annu. Rev. Physiol.* 76, 39–56. doi:10.1146/annurev-physiol-021113-170322

Simone, C. B. (2017). Thoracic Radiation Normal Tissue Injury. *Semin. Radiat. Oncol.* 27 (4), 370–377. doi:10.1016/j.semradonc.2017.04.009

Singh, V. P., Pinnamaneni, J. P., Pugazenthi, A., Sanagasetti, D., Mathison, M., Martin, J. F., et al. (2021). Hippo Pathway Effector Tead1 Induces Cardiac Fibroblast to Cardiomyocyte Reprogramming. *J. Am. Heart Assoc.* 10 (24), e022659. doi:10.1161/JAHA.121.022659

Soerjomataram, I., and Bray, F. (2021). Planning for Tomorrow: Global Cancer Incidence and the Role of Prevention 2020-2070. *Nat. Rev. Clin. Oncol.* 18 (10), 663–672. doi:10.1038/s41571-021-00514-z

Sun, S., Hu, F., Wu, J., and Zhang, S. (2017). Cannabidiol Attenuates OGD/R-induced Damage by Enhancing Mitochondrial Bioenergetics and Modulating Glucose Metabolism via Pentose-Phosphate Pathway in Hippocampal Neurons. *Redox Biol.* 11, 577–585. doi:10.1016/j.redox.2016.12.029

Sun, X. W., Gan, L., Na, A., Ge, L. L., Chen, B. Q., and Liu, J. M. (2019). Combination with Stereotactic Body Radiotherapy Offers a Promising Strategy to Overcome Resistance to Immunotherapy in Advanced Renal Cell Cancer. *J. Oncol.* 2019, 12. doi:10.1155/2019/1483406

Sung, H., Ferlay, J., Siegel, R. L., Laversanne, M., Soerjomataram, I., Jemal, A., et al. (2021). Global Cancer Statistics 2020: GLOBOCAN Estimates of Incidence and Mortality Worldwide for 36 Cancers in 185 Countries. *Ca-a Cancer J. Clinicians* 71 (3), 209–249. doi:10.3322/caac.21660

Us, S. B., Vezir, O., Yildirim, M., Bayrak, G., Yalin, S., Balli, E., et al. (2020). Protective Effect of N-Acetyl Cysteine against Radiotherapy-Induced Cardiac Damage. *Int. J. Radiat. Biol.* 96 (5), 661–670. doi:10.1080/09553002.2020.1721605

Wang, H. Z., Yu, K. N., Hou, J., Liu, Q., and Han, W. (2015). Radiation-induced Bystander Effect: Early Process and Rapid Assessment. *Cancer Lett.* 356 (1), 137–144. doi:10.1016/j.canlet.2013.09.031

Yakovlev, V. A. (2015). Role of Nitric Oxide in the Radiation-Induced Bystander Effect. *Redox Biol.* 6, 396–400. doi:10.1016/j.redox.2015.08.018

Yang, Z., Zhang, Q. N., Luo, H. T., Shao, L. H., Liu, R. F., Kong, Y. R., et al. (2021). Effect of Carbon Ion Radiation Induces Bystander Effect on Metastasis of A549 Cells and Metabonomic Correlation Analysis. *Front. Oncol.* 10, 601620. doi:10.3389/fonc.2020.601620

Yusuf, S. W., Venkatesulu, B. P., Mahadevan, L. S., and Krishnan, S. (2017). Radiation-Induced Cardiovascular Disease: A Clinical Perspective. *Front. Cardiovasc. Med.* 4, 66. doi:10.3389/fcvm.2017.00066

Zhang, P., Yang, P., Hong, L., Cai, X. Y., Zeng, Z. Y., Wu, X. C., et al. (2020). Oxidative Stress in Radiation-Induced Cardiotoxicity. *Oxid. Med. Cell Longev.* 2020, 3579143. doi:10.1155/2020/3579143

Zhang, Q., Yan, Q., Yang, H. F., and Wei, W. Y. (2019). Oxygen Sensing and Adaptability Won the 2019 Nobel Prize in Physiology or Medicine. *Genes Dis.* 6 (4), 328–332. doi:10.1016/j.gendis.2019.10.006

Zhang, X., Li, L. X., Yu, C., Nath, K. A., Zhuang, S., and Li, X. (2022). Targeting Lysine-specific Demethylase 1A Inhibits Renal Epithelial-Mesenchymal Transition and Attenuates Renal Fibrosis. *FASEB J.* 36 (1), e22122. doi:10.1096/fj.202101566R

Conflict of Interest: The authors declare that the research was conducted in the absence of any commercial or financial relationships that could be construed as a potential conflict of interest.

Publisher's Note: All claims expressed in this article are solely those of the authors and do not necessarily represent those of their affiliated organizations, or those of the publisher, the editors and the reviewers. Any product that may be evaluated in this article, or claim that may be made by its manufacturer, is not guaranteed or endorsed by the publisher.

frontiers in Pharmacology

REVIEW
published: 08 March 2022
doi: 10.3389/fphar.2022.854592

Immunomodulatory Treatment Strategies Targeting B Cells for Heart Failure

*Xinxin Zhang†, Yuxi Sun†, Ning Wang, Yanli Zhang, Yunlong Xia and Ying Liu**

Heart Failure and Structural Cardiology Division, First Affiliated Hospital of Dalian Medical University, Dalian, China

Cardio-oncology, a nascent specialty, has evolved as a concerted strategy to address the cardiovascular complications of cancer therapies. On the other hand, emerging evidence has shown that some anti-tumor drugs, such as CD20-targeted rotuximab, also have markedly cardioprotective effects in addition to treating cancers. Rituximab is a CD20-targeted monoclonal antibody and kill tumor B-cells through antibody-mediated and antibody-independent pathways, indicating that B cells participate and promote the progression of cardiovascular diseases. In this review, we mainly present the evidence that B cells contribute to the development of hypertrophy, inflammation, and maladaptive tissue remodeling, with the aim of proposing novel immunomodulatory therapeutic strategies targeting B cells and their products for the treatment of heart failure.

Keywords: cardio-oncology, CD20, b cells, rituximab, cardiovascular diseases, heart failure

OPEN ACCESS

Edited by:
Zhi-Ren Zhang,
Harbin Medical University, China

Reviewed by:
Chen Liu,
The First Affiliated Hospital of Sun Yat-sen University, China
Huaying Fu,
Second Hospital of Tianjin Medical University, China

****Correspondence:***
Ying Liu
yingliu.med@gmail.com

†These authors have contributed equally to this work and share first authorship

Specialty section:
This article was submitted to Cardiovascular and Smooth Muscle Pharmacology, a section of the journal Frontiers in Pharmacology

Received: *14 January 2022*
Accepted: *18 February 2022*
Published: *08 March 2022*

Citation:
Zhang X, Sun Y, Wang N, Zhang Y, Xia Y and Liu Y (2022) Immunomodulatory Treatment Strategies Targeting B Cells for Heart Failure. Front. Pharmacol. 13:854592. doi: 10.3389/fphar.2022.854592

INTRODUCTION

With the rapid development of early detective tools and therapeutic strategies for cancer patients, mortality rates attributed to cancer have remarkably declined. However, this improved survival status is achieved at the expense of anti-tumor treatment-induced cardiovascular diseases (CVDs), either caused by direct cardiotoxicity of anticancer treatment or preexisting CVDs or cardiovascular risk factors (Zamorano et al., 2016). Manifestations of adverse cardiovascular complications for cancer therapy include cancer therapeutics-related cardiac dysfunction (CTRCD) (reduction in left ventricular ejection fraction or heart failure), premature coronary artery disease, valvular disorders, pericardial injury, and arrhythmia. As the survival rates for patients with malignant tumors significantly increase, CVDs have become the second leading cause of long-term morbidity and mortality among cancer survivors (Howlader et al., 2010; Siegel et al., 2012; Bodai and Tuso 2015; Curigliano et al., 2016). Therefore, Cardio-oncology, a novel medical discipline focusing on the identification, prevention, and treatment of cardiovascular complications related to cancer therapy, has emerged. Currently, research on how to avoid adverse cardiovascular response and reverse the unfavorable CVD outcomes in patients with anti-tumor therapies has become a hot spot for both oncologists and cardiologists. Intriguingly, some recent studies have demonstrated that some anti-tumor drugs (such as CD20-targeted rituximab), in addition to treating cancers, also show markedly cardioprotective effects, but the specific mechanism has not been clarified (Uchida et al., 2004; Cang et al., 2012; Waldman et al., 2020). Therefore, exploring the potential value of anti-tumor drugs in the treatment of heart failure (HF) may provide new targets and ideas for remedying HF.

Increasing evidence shows that besides direct cardiotoxicity of anticancer treatment, malignant tumors are associated with CVDs through common risk factors, such as smoking, obesity, diabetes, hypertension and hyperlipidemia, diet, alcohol, exercise, age, sex, and race. The famous CANTOS study illuminated that in patients with previous myocardial infarction and a high-sensitivity

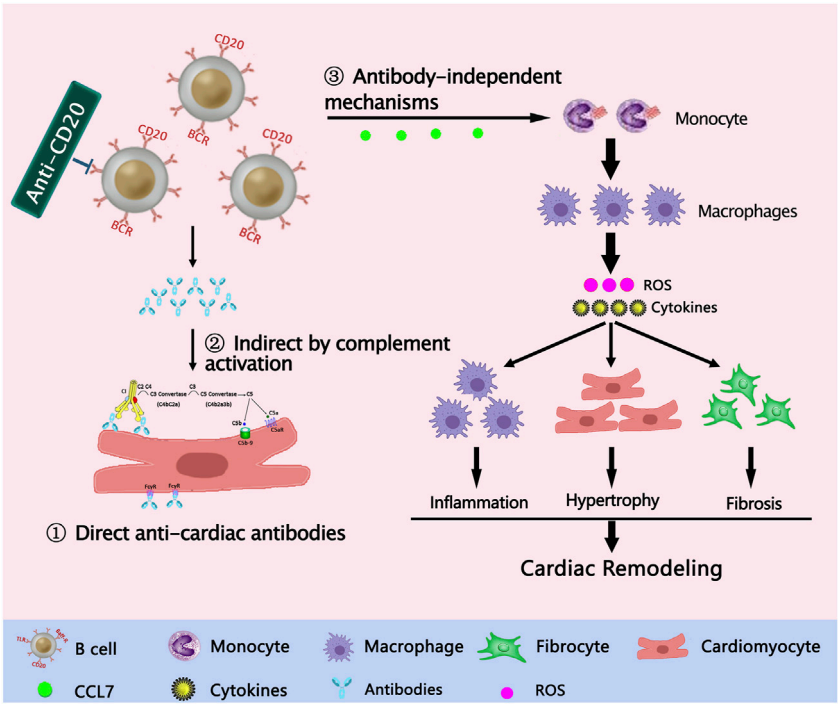

FIGURE 1 | Potential mechanisms of B cell participation in cardiac remodeling and heart failure. ①Direct effects of anti-cardiac antibodies; ②Indirect by complement activation; ③ Antibody-independent mechanisms.

C-reactive protein level of 2 mg or more per liter, anti-inflammatory therapy targeting the interleukin-1β innate immunity pathway with canakinumab not only led to a significantly lower rate of recurrent cardiovascular events, but also markedly reduced incident lung cancer and lung cancer mortality, suggesting that immune-inflammatory mechanism may be a common pathophysiological basis for cancers and CVDs (Ridker, et al., 2017a; Ridker, et al., 2017b).

IMMUNE INFLAMMATORY MECHANISM IN MYOCARDIAL REMODELING

Inflammation, as a defensive response to various pathogens, is regulated by innate and adaptive immune systems. The innate immune system is a highly conserved system that operates by nonspecific mechanisms and functions as a first line of defense, mainly relying on macrophages, dendritic cells, neutrophils, circulating monocytes, granulocytes, and even some non-immune cells that adopt immunological functions as needed. In contrast, the adaptive immune system is highly specific and able to remember and effectively mount responses against previously encountered immunological threats, which relies on the ability of T and B lymphocytes.

In addition to resisting the invasion of pathogens, immune responses also participate in various CVDs. Adequate evidence elucidates that multiple types of immune cells are involved in the process of myocardial remodeling and HF, such as neutrophils, monocytes/macrophages, and lymphocytes. Neutrophils are the most abundant white blood cells circulating in the human peripheral blood, and they respond quickly to acute injuries. In ischemic cardiomyopathy, neutrophils infiltrate the infarcted myocardium and mediate tissue damage. Removal of neutrophils significantly attenuate myocardial necrosis caused by ischemia-reperfusion (Frangogiannis, 2014). Recent studies have shown that neutralization of protein S100A9, secreted by neutrophils, ameliorated Ang II-induced hypertension, ventricular hypertrophy and fibrosis, indicating that neutrophils could act as an important regulator in pathophysiological ventricular remodeling (Wu et al., 2014). In addition, some previous studies have shown that bone marrow-derived monocytes were recruited into myocardial tissue after Ang II infusion and differentiated into M1 type macrophages, which secreted various inflammatory cytokines and chemokines, promoting myocardial cells apoptosis and fibroblasts transdifferentiation (Wang et al., 2014). Wenzel et al. observed selective ablation of lysozyme M-positive (LysM) myelomonocytic cells by low-dose diphtheria toxin attenuated Ang II-induced blood pressure increase, improved vascular endothelial and smooth muscle dysfunction, reduced vascular superoxide formation and the expression of NADPH oxidase subunits gp91phox and p67phox in mice. Moreover, our previous studies found that angiotensin II (Ang II) activated AT1RPKA-proteasome pathway, which promotes degradation of IκBα and MKP-1 and activation of STAT1 and NF-κB, thereby leading to Th1 differentiation. Th1 cells are generally considered to be associated with the occurrence of various adverse cardiovascular diseases (Qin et al., 2018). In another research, Gröschel et al. reported

mice lacking functional recombination activation gene 2 (Rag2), without clymphocytes, were protected during the transition from hypertrophy to heart failure following transverse aortic constriction (TAC) (Groschel et al., 2018). Currently, novel evidence has come to light that B lymphocytes may also play an essential role in the initiation and progression of HF through direct (by secreting antibodies) or indirect (by cytokines/chemokines secretion) pathways.

B CELLS BIOLOGY CHARACTERISTICS

B Cell Subgroups

B cells can be divided into two lineages, B1 cells and B2 cells. These 2 cell subsets differ considerably in ontogeny, function, location, and surface marker expression (Naradikian et al., 2016). In general, B1 cells (based on the expression of surface marker CD5, B1 cells can be further subdivided into B1a and B1b subsets) represent the vast majority of B cells in newborns, and mainly originate from fetal liver and omentum. In adults, B1 cells mainly exist in the pleural cavity and peritoneal cavity, and respond to T cell-independent antigens by secreting polyreactive natural immunoglobulin M (IgM) antibodies (Douna and Kuiper, 2016). B2 cells are produced postnatally, and represent the vast majority of B cells in adults, including a dominant population of follicular B cells and a smaller population of marginal zone (MGZ) B cells (Montecino-Rodriguez and Dorshkind, 2012). In a physiological state, B2 cells are produced in waves that parallel the waves of development of hematopoietic stem cells (HSCs), and circulate in lymphatic organs such as blood, thymus, spleen and lymph nodes. Functionally, B2 cells contribute to T-cell dependent humoral and adaptive immune responses through isotype class switching and affinity maturation (Montecino-Rodriguez and Dorshkind, 2012). In short, B1a cells don't regenerate after birth but are kept alive by self-replication, while B1b cells and B2 cells are produced throughout life (Melchers, 2015).

B Cell Surface Markers

B cells have a variety of surface molecules, which mediate different biological functions. The B cell receptor (BCR) is generally regarded as the characteristic surface marker and one of the most important receptors for B cells to sense external environment. Its most important function is as a receptor that recognizes various extracellular antigens in response to bacterial and viral infections for conferring host defense. The CD19/CD21/CD81 complex is the B-cell co-receptors, which can strengthen B cells activation signaling. CD20 is a transmembrane phospholipid protein that appears in the stages from pre-B cells to mature B cells, and is encoded by the MS4A1 gene. Notably, in addition to being expressed in normal B cells, CD20 is also expressed in B lymphocyte-derived lymphomas, leukemias, and neoplasms involved in immune and inflammatory diseases.

B Cell Biological Function

Although B cells are traditionally known for their ability to produce antibodies, they can also perform other critical functions in the context of immune responses. B1 cells can generate natural IgM antibodies in the absence of specific stimulation, while B2 cells differentiate into plasma cells that produce high concentration of antibodies and long-lived memory B cells when the BCR is engaged by an antigen (Savage and Baumgarth, 2015). In addition, B cells could identify antigens through the BCR, internalize them for processing and present them to $CD4^+$ T cells in the germinal centers. Moreover, B cells could secrete cytokines and chemokines, which exert a series of important biological effects. For example, B cells activate innate immune response through the secretion of IFN-γ, IL-6, and IL-17 (Shen and Fillatreau, 2015); promote $CD4^+$ T cell polarization through both MHC-II-dependent and MHC-II-independent mechanisms; modulate the maturation and growth of lymphoid structures through secreting LTα1β2 (Shen and Fillatreau, 2015); regulate the mobilization of monocytes through production of CCL7(Zouggari et al., 2013); recruit T cell to inflamed tissue through generating PEPITEM(Chimen et al., 2015). In contrast, some B cell subsets, mainly referred to as Bregs or B10 cells, also act as negative regulators of immune response through the secretion of IL-10, IL-35, and TFG-β. These immunosuppressive B cells could support immunologic tolerance, resolve acute inflammatory response, and maintain the homeostasis of certain types of natural killer cells (Shen and Fillatreau, 2015).

THE ROLE OF B CELLS IN CARDIAC REMODELING AND HEART FAILURE

B Cells in the Naive Myocardium and Human Heart

In the naive murine heart, B cells have been reported to be the most prevalent leukocytes (Adamo et al., 2018; Bonner et al., 2012). Myocardial B cells account for almost 10% of circulating B cells which adhere to the naive heart vascular endothelium and arrest their transit when they pass through the heart. Prior studies reported that the vast majority (>95%) of myocardial B cells remain intravascular, whereas few (<5%) cross the endothelium into myocardial tissue (Adamo et al., 2020a). Ramos et al. further observed that there were two subgroups of murine $B220^+$ (CD45R) lymphocytes in the naive cardiac muscle: a larger population of IgM^{high} IgD^{low} cells and a smaller population of IgM^{low} IgD^{high} cells (Ramos et al., 2017). Currently, there have been limited evidence to support the presence of B cells in normal human hearts. Data from histological analysis of autopsies indicate that B cells are present at a frequency similar to that of $CD4^+$and $CD8^+$ T cells in normal human hearts (Noutsias et al., 2002). Moreover, the presence of B cells in the human heart is also supported by some rare case reports of primary cardiac B cell lymphoma (Grantomo et al., 2018; Thiagaraj et al., 2018; Li et al., 2019). In human specimens, B cells have also been discovered within the pericardial fat, with a relative increase in the size of pericardial-fat-associated lymphoid clusters in patients with coronary artery disease (Horckmans et al., 2018).

B Cells and Cardiovascular Diseases

In recent years, different mouse models have been used to explore the association between myocardial B cell and CVDs, especially in these fields of ischemia reperfusion (I/R) and myocardial infarction (MI). In a I/R mouse model, Yan and his colleagues observed that

the frequency of myocardial $CD19^+$ B cells markedly increased after MI, peaking between day 5 and 7 after injury and returning to baseline soon. In addition, they found that the time course of B cell numbers in the myocardium after I/R injury differed from that observed after permanent coronary ligation, with B cells peaking in number 2 days earlier and returning to baseline faster (Yan et al., 2013). Zouggari et al. studied a mouse model of permanent coronary ligation and found that $B220^+$ B cells infiltrated into the myocardium and localized around the infarct zone after injury (Zouggari et al., 2013). They also explored the link between B lymphocytes and adverse left ventricular (LV) remodeling for the first time. In another fundamental study about cardiac hypertrophy and remodeling, TAC surgery was reported to induce an increase in the number of myocardial $CD19^+$ B cells at 4 weeks postoperatively (Wu et al., 2017). These findings suggest that specific subsets of cardiac B cells are model-dependent, showing different function in various models.

Currently, few studies have been performed on the role of B cells in the human heart. In a study about human acute ischemic cardiomyopathy, patients with ST-segment MI had a slight decrease in the number of circulating $B220^+$ cells at 1.5 h after myocardial reperfusion, which was followed by an remarkable increase above pre-reperfusion levels at 24 h after reperfusion (Boag et al., 2015). A cohort analysis of 56 patients with dilated cardiomyopathy (DCM) showed that HF patients had higher percentages of $CD19^+$ B cells and actively replicating $CD19^+$ B cell in peripheral blood than healthy volunteers. Additionally, they found that patients with DCM also had an increase in the percentage of TNF-producing B cells, which correlated directly with indices of cardiac dysfunction and myocardial fibrosis, whereas no change in the percentage of IL-10-producing B cells compared to healthy controls (Yu et al., 2013). In another study enrolled patients with non-ischemic cardiomyopathy, the investigators discovered that patients with HF showed an increased percentage of circulating Bregs ($CD19^+$ $CD5^+$ $CD1d^+$ $IL\text{-}10^+$ cells) in peripheral blood (Guo et al., 2015). In an *in vitro* study, mononuclear cells were isolated from patients with DCM and cultured for 48 h. The results showed that DCM patients had a lower prevalence of IL-10-producing B cells than healthy volunteers, and reduced IL-10 production efficiency was always associated with cardiac dysfunction (Jiao et al., 2018). Overall, the limited evidence provided by human studies about the involvement of B cells in cardiovascular disease suggests that the findings in animal models may be applicable to humans (Adamo et al., 2020b).

POTENTIAL MECHANISMS OF B CELL PARTICIPATION IN CVDS

Emerging evidence indicates that B cells play a critical role in the context of myocardial adaptation to injury through various mechanisms, including antibody-mediated mechanisms and antibody-independent mechanisms. (**Figure 1**).

Antibody-Mediated Mechanisms Contributing to Cardiac Dysfunction and Heart Failure

Antibody-dependent mechanisms contributing to cardiac injury mainly include direct effects of anti-cardiac antibodies and the activation of the complement system following the formation of antigen–antibody complexes.

Direct Anti-Cardiac Antibodies

A recent fundamental study has observed the important role of natural IgM antibody in myocardial I/R injury and identified a specific clone of B1 cells which could generate a type of natural antibodies that promote myocardial damage (Zhang et al., 2004; Zhang et al., 2006). Another study about myocardial I/R injury also showed that coronary artery ligation produced myocardial infarction (MI) and depressed ejection fraction, while these adverse effects were markedly reduced in Ig-deficient mice, indicating that antibodies play an important role in the development and progression of cardiac remodeling and heart failure (Keppner et al., 2018). In animal model, antibodies against specific cardiac proteins have also been shown to be sufficient to lead to cardiomyopathy (Matsui et al., 1997). For example, antibodies against troponin I were found to produce severe dilated cardiomyopathy in PD-1-deficient mice (Okazaki et al., 2003). Another cohort study identified anti-desmoglein-2 (Anti-DSG2) antibodies as a sensitive and specific biomarker for arrhythmogenic right ventricular cardiomyopathy (ARVC). In humans, the level of anti-DSG2 antibodies correlated with the burden of premature ventricular contractions; *In vitro*, the antibodies caused gap junction dysfunction, which was a common feature of ARVC. Anti-DSG2 antibodies likely explain the cardiac inflammation frequently identified in ARVC and may represent a new therapeutic target (Chatterjee et al., 2018).

A histological analysis of human myocardial tissue with end-stage HF showed immunoglobulin G (IgG) deposition was found in up to 70% of heart tissue samples (Youker et al., 2014). Almost 50% of biopsies were IgG3-positive, with a smaller proportion of C3c deposition stained positive. The presence of IgG3 and C3c in the myocardium has been proven to correlate with the duration and severity of HF(van den Hoogen et al., 2019). Moreover, both left ventricular diastolic dysfunction and end-stage HFrEF patients showed elevated levels of circulating IgG1 and IgG3, suggesting there was an antibody-mediated immune response in cardiac remodeling (van den Hoogen et al., 2019).

The Effects of Complement on Myocardial Injury

The complement system is an important component of innate immune responses, and can be activated through three pathways during HF. Classical pathway is initially activated by IgM or IgG antigen/antibody complexes, and induces the formation of the Membrane Attack Complex (MAC) through a series of cascade reactions (Nesargikar et al., 2012). Alternative pathway means that the complement system is activated by direct binding of bacteria and yeast independent of antibody interaction (Nesargikar et al., 2012). Lectin pathway is the most recently

discovered one that is capable of activating the complement system. The initiating molecules for this pathway are collectins (mannose-binding lectin and ficolin), which are multimeric lectin complexes (Nesargikar et al., 2012).

In recent years, there has been sufficient evidence to demonstrate that the complement system participates in the development of HF. In murine sepsis models, C5a, an important protein molecule of the complement system, has been verified to play an essential role in inotropic dysfunction *via* C5aR-mediated signaling pathway (Niederbichler et al., 2006). In a murine model of hypertension, blocking C5a receptors with inhibitors mitigated cardiac hypertrophy and perivascular fibrosis, and remarkably improved cardiac function, indicating that C5a was deeply involved in adverse cardiac remodeling (Zhang et al., 2014). Moreover, C5a is an effective chemokine that attracts a variety of bone marrow derived inflammatory cells to sites of injury and activates pro-fibrotic process through modulating TGF-β/Smad2/3 signaling pathway in the heart (Nesargikar et al., 2012; Zhang et al., 2014). In addition to C5a, C5b-9, the MAC complex, has also been shown to be closely associated with HF. C5b-9 has been proved to induce tumour necrosis factor-α (TNF-α) expression in cardiomyocytes, which contributes to cardiomyocyte hypertrophy, fibrosis, and apoptosis (Zwaka et al., 2002). All of these pathophysiological processes are critical components of injury in HF(Torre-Amione et al., 1996; Yu et al., 2013). Additionally, in a cohort study, compared with healthy volunteers, patients with HF exhibited increased circulating levels of complement activated cleavage end product C5b-9, which were tightly associated with disease severity (Wang and Cai, 2020).

Antibody-Independent Mechanisms Leading to Cardiac Injuries

In addition to acting through antibodies and complement, activated B cell could secrete cytokines and chemokines to directly modulate cardiac function and induce cardiac remodeling. B cells have been shown to be directly involved in cardiac remodeling through up-regulating cytokines of TGF-β and IL-6, and be responsible for maintaining a harmful inflammatory environment through production of TNF-α, IL-1β and IL-6 (Garcia-Rivas et al., 2020). TNF-α-secreting B cells in DCM patients were associated with increased cardiac fibrosis, as confirmed by late gadolinium enhancement on cardiac magnetic resonance imaging and elevated serum type iii pro-collagen levels (Yu et al., 2013).

B cells also exert biological effects by altering cardiac function through the secretion of chemokines. A recent study reported that mature B lymphocytes selectively produce chemokines CCL7, which can induce $Ly6C^{hi}$ monocyte mobilization and recruitment to the heart, leading to worsened tissue injury and deterioration of myocardial function in a mouse model of ischemia-reperfusion injury (Zouggari et al., 2013). In this study, genetic (Baff receptor deficiency) or antibody-mediated (CD20-or Baff-specific antibody) depletion of mature B cells impeded CCL7 production and monocyte mobilization, reduced cardiac injury and improved heart function. The authors further found that the circulating concentrations of CCL7 and BAFF in patients with acute myocardial infarction were markedly higher compared to healthy controls, and elevated levels of CCL7 and BAFF always predicted an increased risk of death or recurrence of myocardial infarction (Zouggari et al., 2013). In another study on acute kidney injury, the researchers also found that B cells produced chemokine CCL7, with the potential to facilitate neutrophil and monocyte recruitment to the injured kidney, aggravating renal impairment. CCL7 blockade in mice markedly reduced myeloid cell infiltration into the kidney and ameliorated acute kidney injury (Inaba et al., 2020).

ANTI-CD20 MEDIATED B CELL DEPLETION AS A THERAPEUTIC STRATEGY FOR HEART FAILURE

In cancer patients, the capacity of immune system to detect and eliminate malignant cells is dramatically impaired. Immunotherapy aims at retraining the affected immune system and restoring their anti-cancer functions (Lobenwein et al., 2021). In recent years, a large number of studies have shown that compared with traditional chemotherapy approaches, immunotherapy drugs have shown significant effects in improving overall survival, and have gradually become an important pillar of systemic treatment for various cancer types (Waldmann 2003; Pardoll 2012). As an important immunotherapy drug, monoclonal antibodies aim to disrupt the essential activities of tumor cells and cancer immune evasion in order to increase apoptosis and immune recognition of cancer cells. The new drug could inhibit tumor growth and metastasis by targeting specific receptors that are crucial for signaling pathways in dysregulated cancer cells and immune cells (Waldman et al., 2020). CD20 is an atypical tetraspanin expressed only on mature B cells and becomes a clinical target for the treatment of B-cell lymphoma. Rituximab is a CD20-targeted monoclonal antibody that binds to CD20 molecules and kills tumor B-cells through antibody-dependent cytotoxicity (ADCC) and complement-dependent cytotoxicity (CDC). Mechanistically, rituximab crosslinks the CD20 receptor present on most B cells, leading to FcγR-mediated B cell depletion (Uchida et al., 2004). FcγRs are present on cardiac fibroblasts and cardiomyocytes, and FcγR signal transduction promotes cardiomyocyte fibrosis by activating the apoptotic pathway, reduces calcium transients and cell shortening, and induces cardiomyocyte apoptosis (Staudt et al., 2007; Haudek et al., 2008; Keppner et al., 2018).

In clinical practice, CD20 depleting agents are not only approved for B cell-related cancers, but also increasingly used on- and off-label for autoimmune diseases, such as rheumatoid arthritis (RA), multiple sclerosis (MS) and systemic lupus erythematosus (SLE) (Cang et al., 2012). Clear evidence that B cell depletion may be effective for autoimmune therapy comes from an MS study which showed rituximab treatment can

increase remission rates and reduce the development of new lesions (Hauser et al., 2008). Orrelizumab, another CD20-specific cytolytic antibody, has also been shown to be suitable for the treatment of patients with relapsed or primary progressive forms of MS(Boz et al., 2019; Sabatino et al., 2019; Fox et al., 2021). In addition, studies in mouse models of Type 1 Diabetes Mellitus (T1DM), MS, and RA have also shown the protective effect of B cell depletion, which is consistent with an increasing number of highly suggestive studies (Serreze et al., 1998; Yanaba et al., 2007; Matsushita et al., 2008). In short, CD20 targeted monoclonal antibodies provide excellent efficacy in the treatment of both B cell derived tumors and autoimmune diseases.

In addition to anti-tumor and anti-autoimmune diseases, anti-CD20 treatments have been found to exert beneficial effects on cardiac remodeling and HF. Using a TAC pressure overload model of myocardial hypertrophy, Ma et al. found administration of rituximab markedly improved heart function, and suppressed heart chamber dilation, myocyte hypertrophy, fibrosis and oxidative stress through regulating calcineurin A, ERK1/2, STAT3, TGFβ/Smad2/3 and IKKα/β/NF-κB signaling pathways, suggesting that rituximab may be a promising drug for treating hypertrophic disease (Ma et al., 2019). In a mouse model of ischemia-reperfusion injury, researchers observed that the mice treated with anti-CD20 monoclonal antibodies had reduced cardiac adverse LV remodeling and improved cardiac function following permanent coronary artery ligation of the left anterior descending artery (Zouggari et al., 2013). Moreover, Tschope et al. presented a case series of six patients with subacute and chronic endomyocardial biopsy-confirmed $CD20^+$ B-lymphocyte-associated DCM treated with standard HF therapy in combination with rituximab. Of these, five DCM patients improved clinically several weeks after receiving a standard infusion protocol with rituximab, as indicated by decreased NYHA functional class, improved left ventricular ejection fraction, and reduced B-cell infiltration in endomyocardial biopsies (Sanchez-Trujillo et al., 2019). Based on these encouraging data, small-scale clinical trials investigating the effect of B cell depletion in the context of heart failure with reduced ejection fraction are being planned (ClinicalTrials.gov Identifier: NCT03332888) (44), and clinical trials in patients with ST-segment myocardial infarction are ongoing (ClinicalTrials. govmIdentifier: NCT03072199) (Sanchez-Trujillo et al., 2019).

There is also some literature supporting other B cell-targeting therapies. In a basic study, using a pressure overload mouse model induced by Ang II-infusion, the researchers found that administration of monoclonal antibodies targeting CD22, another important molecule present on the surface of B cells, led to decreased myocyte hypertrophy and myocardial fibrosis, as well as reduced concentrations of inflammatory cytokines, such as IL-1β and TNF-α(Cordero-Reyes et al., 2016). Belimumab, BAFF-specific antibody, specifically targets the BAFF receptor and acts as an effective B cell depleting agent. Currently, Belimumab is mainly used for the treatment of resistant SLE in adults, showing excellent efficacy in reducing flares and overall disease activity when combined with standard therapy (Blair and Duggan, 2018). Additionally, the most established agents targeting BCR signaling are Bruton tyrosine kinase (BTK) inhibitors and PI3K isoform-specific inhibitors, and their introduction into the clinic is rapidly changing the treatment of B-cell malignancies (Burger, 2019). In the future, BTK inhibitors and PI3K isoform-specific inhibitors could provide another therapeutic possibility for H, although there may be some controversy.

CONCLUSION

While most attention has been paid to the cardiovascular toxicity associated with anti-tumor therapy, some drugs have also shown great cardioprotective effects. Anti-CD20 agents have been preliminarily proved to improve left ventricle function in patients with refractory DCM, suggesting that B cells play a prominent role in cardiac remodeling and HF. Mechanically, B cells promote cardiac injuries through antibody-dependent and antibody-independent pathways. Notably, the specific B-cell subpopulation mediated myocardial damage needs to be further verified in the future research, as this would support trials of more specific therapeutics. Overall, it would be of great significance to identify the excellent cardioprotective effects of certain anti-tumor medications and apply them to the treatment of vascular diseases.

AUTHOR CONTRIBUTIONS

XZ and YS were responsible for writing the manuscript; NW assisted YZ to collect and sort relevant literatures; YX and YL were mainly in charge of revising the paper and polishing the language. Everyone in author list made an outstanding contribution.

FUNDING

This work was supported by the National Natural Science Foundation of China (Nos. U1908209 and 82170385).

REFERENCES

Adamo, L., Rocha-Resende, C., and Mann, D. L. (2020b). The Emerging Role of B Lymphocytes in Cardiovascular Disease. *Annu. Rev. Immunol.* 38, 99–121. doi:10.1146/annurev-immunol-042617-053104

Adamo, L., Rocha-Resende, C., Lin, C. Y., Evans, S., Williams, J., Dun, H., et al. (2020a). "Myocardial B Cells Are a Subset of Circulating Lymphocytes with Delayed Transit through the heart.". *JCI Insight* 5. doi:10.1172/jci.insight.134700

Adamo, L., Staloch, L. J., Rocha-Resende, C., Matkovich, S. J., Jiang, W., Bajpai, G., et al. (2018). "Modulation of Subsets of Cardiac B Lymphocytes Improves

Cardiac Function after Acute injury.". *JCI Insight* 3. doi:10.1172/jci.insight.120137

Blair, H. A., and Duggan, S. T. (2018). Belimumab: A Review in Systemic Lupus Erythematosus. *Drugs* 78 (3), 355–366. doi:10.1007/s40265-018-0872-z

Boag, S. E., Das, R., Shmeleva, E. V., Bagnall, A., Egred, M., Howard, N., et al. (2015). T Lymphocytes and Fractalkine Contribute to Myocardial Ischemia/reperfusion Injury in Patients. *J. Clin. Invest.* 125 (8), 3063–3076. doi:10.1172/JCI80055

Bodai, B. I., and Tuso, P. (2015). Breast Cancer Survivorship: a Comprehensive Review of Long-Term Medical Issues and Lifestyle Recommendations. *Perm J.* 19 (2), 48–79. doi:10.7812/TPP/14-241

Bönner, F., Borg, N., Burghoff, S., and Schrader, J. (2012). Resident Cardiac Immune Cells and Expression of the Ectonucleotidase Enzymes CD39 and CD73 after Ischemic Injury. *PLoS One* 7 (4), e34730. doi:10.1371/journal.pone.0034730

Boz, C., Terzi, M., Özer, B., Turkoglu, R., Karabudak, R., Efendi, H., et al. (2019). Comparative Analysis of Fingolimod versus Teriflunomide in Relapsing-Remitting Multiple Sclerosis. *Mult. Scler. Relat. Disord.* 36, 101376. doi:10.1016/j.msard.2019.101376

Burger, J. A. (2019). Bruton Tyrosine Kinase Inhibitors: Present and Future. *Cancer J.* 25 (6), 386–393. doi:10.1097/PPO.0000000000000412

Cang, S., Mukhi, N., Wang, K., and Liu, D. (2012). Novel CD20 Monoclonal Antibodies for Lymphoma Therapy. *J. Hematol. Oncol.* 5, 64. doi:10.1186/1756-8722-5-64

Chatterjee, D., Fatah, M., Akdis, D., Spears, D. A., Koopmann, T. T., Mittal, K., et al. (2018). "An Autoantibody Identifies Arrhythmogenic Right Ventricular Cardiomyopathy and Participates in its pathogenesis.". *Eur. Heart JX* 39 (44), 3932–3944. doi:10.1093/eurheartj/ehy567

Chimen, M., McGettrick, H. M., Apta, B., Kuravi, S. J., Yates, C. M., Kennedy, A., et al. (2015). Homeostatic Regulation of T Cell Trafficking by a B Cell-Derived Peptide Is Impaired in Autoimmune and Chronic Inflammatory Disease. *Nat. Med.* 21 (5), 467–475. doi:10.1038/nm.3842

Cordero-Reyes, A. M., Youker, K. A., Trevino, A. R., Celis, R., Hamilton, D. J., Flores-Arredondo, J. H., et al. (2016). Full Expression of Cardiomyopathy Is Partly Dependent on B-Cells: A Pathway that Involves Cytokine Activation, Immunoglobulin Deposition, and Activation of Apoptosis.". *J. Am. Heart Assoc.* 5. doi:10.1161/JAHA.115.002484

Curigliano, G., Cardinale, D., Dent, S., Criscitiello, C., Aseyev, O., Lenihan, D., et al. (2016). Cardiotoxicity of Anticancer Treatments: Epidemiology, Detection, and Management. *CA Cancer J. Clin.* 66 (4), 309–325. doi:10.3322/caac.21341

Douna, H., and Kuiper, J. (2016). Novel B-Cell Subsets in Atherosclerosis. *Curr. Opin. Lipidol.* 27 (5), 493–498. doi:10.1097/MOL.0000000000000335

Fox, E., Lovett-Racke, A. E., Gormley, M., Liu, Y., Petracca, M., Cocozza, S., et al. (2021). A Phase 2 Multicenter Study of Ublituximab, a Novel Glycoengineered Anti-CD20 Monoclonal Antibody, in Patients with Relapsing Forms of Multiple Sclerosis. *Mult. Scler.* 27 (3), 420–429. doi:10.1177/1352458520918375

Frangogiannis, N. G. (2014). "The Inflammatory Response in Myocardial Injury, Repair, and remodelling.". *Nat. Rev. Cardiol.* 11 (5), 255–265. doi:10.1038/nrcardio.2014.28

García-Rivas, G., Castillo, E. C., Gonzalez-Gil, A. M., Maravillas-Montero, J. L., Brunck, M., Torres-Quintanilla, A., et al. (2020). The Role of B Cells in Heart Failure and Implications for Future Immunomodulatory Treatment Strategies. *ESC Heart Fail.* 7 (4), 1387–1399. doi:10.1002/ehf2.12744

Grantomo, J., Pratita, J., Rachmat, J., and Saraswati, M. (2018). A Rare Case of Primary Cardiac Lymphoma and the Role of Early Surgical Debulking: a Case report.". *Eur. Heart J. Case Rep.* 2, yty116. doi:10.1093/ehjcr/yty116

Groschel, C., Sasse, A., Monecke, S., Rohrborn, C., Elsner, L., Didie, M., et al. (2018). "CD8(+)-T Cells with Specificity for a Model Antigen in Cardiomyocytes Can Become Activated after Transverse Aortic Constriction but Do Not Accelerate Progression to Heart Failure.". *Front. Immunol.* 9, 2665. doi:10.3389/fimmu.2018.02665

Guo, Y., Cen, Z., Wei, B., Wu, W., and Zhou, Q. (2015). Increased Circulating Interleukin 10-secreting B Cells in Patients with Dilated Cardiomyopathy. *Int. J. Clin. Exp. Pathol.* 8 (7), 8107–8114.

Haudek, S. B., Trial, J., Xia, Y., Gupta, D., Pilling, D., and Entman, M. L. (2008). Fc Receptor Engagement Mediates Differentiation of Cardiac Fibroblast Precursor Cells. *Proc. Natl. Acad. Sci. U S A.* 105 (29), 10179–10184. doi:10.1073/pnas.0804910105

Hauser, S. L., Waubant, E., Arnold, D. L., Vollmer, T., Antel, J., Fox, R. J., et al. (2008). B-cell Depletion with Rituximab in Relapsing-Remitting Multiple Sclerosis. *N. Engl. J. Med.* 358 (7), 676–688. doi:10.1056/NEJMoa0706383

Horckmans, M., Bianchini, M., Santovito, D., Megens, R. T. A., Springael, J. Y., Negri, I., et al. (2018). Pericardial Adipose Tissue Regulates Granulopoiesis, Fibrosis, and Cardiac Function after Myocardial Infarction. *Circulation* 137 (9), 948–960. doi:10.1161/CIRCULATIONAHA.117.028833

Howlader, N., Ries, L. A., Mariotto, A. B., Reichman, M. E., Ruhl, J., and Cronin, K. A. (2010). Improved Estimates of Cancer-specific Survival Rates from Population-Based Data. *J. Natl. Cancer Inst.* 102 (20), 1584–1598. doi:10.1093/jnci/djq366

Inaba, A., Tuong, Z. K., Riding, A. M., Mathews, R. J., Martin, J. L., Saeb-Parsy, K., et al. (2020). B Lymphocyte-Derived CCL7 Augments Neutrophil and Monocyte Recruitment, Exacerbating Acute Kidney Injury. *J. Immunol.* 205 (5), 1376–1384. doi:10.4049/jimmunol.2000454

Jiao, J., Lu, Y. Z., Xia, N., Wang, Y. Q., Tang, T. T., Nie, S. F., et al. (2018). Defective Circulating Regulatory B Cells in Patients with Dilated Cardiomyopathy. *Cell Physiol Biochem* 46 (1), 23–35. doi:10.1159/000488405

Keppner, L., Heinrichs, M., Rieckmann, M., Demengeot, J., Frantz, S., Hofmann, U., et al. (2018). Antibodies Aggravate the Development of Ischemic Heart Failure. *Am. J. Physiol. Heart Circ. Physiol.* 315 (5), H1358–H1367. doi:10.1152/ajpheart.00144.2018

Li, Y., Zhou, Z., Xin, F., Zhang, C., Zhang, R., Sun, D., et al. (2019). Primary Cardiac Lymphoma in Both Atria: A Case Report. *J. Clin. Ultrasound* 47 (9), 561–563. doi:10.1002/jcu.22738

Lobenwein, D., Kocher, F., Dobner, S., Gollmann-Tepekoylu, C., and Holfeld, J. (2021). "Cardiotoxic Mechanisms of Cancer Immunotherapy - A Systematic review.". *Int. J. Cardiol.* 323, 179–187. doi:10.1016/j.ijcard.2020.08.033

Ma, X. L., Lin, Q. Y., Wang, L., Xie, X., Zhang, Y. L., and Li, H. H. (2019). Rituximab Prevents and Reverses Cardiac Remodeling by Depressing B Cell Function in Mice. *Biomed. Pharmacother.* 114, 108804. doi:10.1016/j.biopha.2019.108804

Matsui, S., Fu, M. L., Katsuda, S., Hayase, M., Yamaguchi, N., Teraoka, K., et al. (1997). Peptides Derived from Cardiovascular G-Protein-Coupled Receptors Induce Morphological Cardiomyopathic Changes in Immunized Rabbits. *J. Mol. Cel Cardiol* 29 (2), 641–655. doi:10.1006/jmcc.1996.0307

Matsushita, T., Yanaba, K., Bouaziz, J. D., Fujimoto, M., and Tedder, T. F. (2008). Regulatory B Cells Inhibit EAE Initiation in Mice while Other B Cells Promote Disease Progression. *J. Clin. Invest.* 118 (10), 3420–3430. doi:10.1172/JCI36030

Melchers, F. (2015). Checkpoints that Control B Cell Development. *J. Clin. Invest.* 125 (6), 2203–2210. doi:10.1172/JCI78083

Montecino-Rodriguez, E., and Dorshkind, K. (2012). B-1 B Cell Development in the Fetus and Adult. *Immunity* 36 (1), 13–21. doi:10.1016/j.immuni.2011.11.017

Naradikian, M. S., Hao, Y., and Cancro, M. P. (2016). Age-associated B Cells: Key Mediators of Both Protective and Autoreactive Humoral Responses. *Immunol. Rev.* 269 (1), 118–129. doi:10.1111/imr.12380

Nesargikar, P. N., Spiller, B., and Chavez, R. (2012). The Complement System: History, Pathways, cascade and Inhibitors. *Eur. J. Microbiol. Immunol. (Bp)* 2 (2), 103–111. doi:10.1556/EuJMI.2.2012.2.2

Niederbichler, A. D., Hoesel, L. M., Westfall, M. V., Gao, H., Ipaktchi, K. R., Sun, L., et al. (2006). An Essential Role for Complement C5a in the Pathogenesis of Septic Cardiac Dysfunction. *J. Exp. Med.* 203 (1), 53–61. doi:10.1084/jem.20051207

Noutsias, M., Pauschinger, M., Schultheiss, H., and U, K. (2002). "Phenotypic Characterization of Infiltrates in Dilated Cardiomyopathy - Diagnostic Significance of T-Lymphocytes and Macrophages in Inflammatory cardiomyopathy.". *Med. Sci. Monit.* 8, CR478–87.

Okazaki, T., Tanaka, Y., Nishio, R., Mitsuiye, T., Mizoguchi, A., Wang, J., et al. (2003). Autoantibodies against Cardiac Troponin I Are Responsible for Dilated Cardiomyopathy in PD-1-Deficient Mice. *Nat. Med.* 9 (12), 1477–1483. doi:10.1038/nm955

Pardoll, D. M. (2012). The Blockade of Immune Checkpoints in Cancer Immunotherapy. *Nat. Rev. Cancer* 12 (4), 252–264. doi:10.1038/nrc3239

Qin, X. Y., Zhang, Y. L., Chi, Y. F., Yan, B., Zeng, X. J., Li, H. H., et al. (2018). Angiotensin II Regulates Th1 T Cell Differentiation through Angiotensin II Type 1 Receptor-PKA-Mediated Activation of Proteasome. *Cel Physiol Biochem* 45 (4), 1366–1376. doi:10.1159/000487562

Ramos, G. C., van den Berg, A., Nunes-Silva, V., Weirather, J., Peters, L., Burkard, M., et al. (2017). Myocardial Aging as a T-Cell-Mediated Phenomenon. *Proc. Natl. Acad. Sci. U S A.* 114 (12), E2420–E2429. doi:10.1073/pnas.1621047114

Ridker, P. M., Everett, B. M., Thuren, T., MacFadyen, J. G., Chang, W. H., Ballantyne, C., et al. (2017a). Antiinflammatory Therapy with Canakinumab for Atherosclerotic Disease. *N. Engl. J. Med.* 377 (12), 1119–1131. doi:10.1056/NEJMoa1707914

Ridker, P. M., MacFadyen, J. G., Thuren, T., Everett, B. M., Libby, P., and Glynn, R. J., (2017b). Effect of Interleukin-1β Inhibition with Canakinumab on Incident Lung Cancer in Patients with Atherosclerosis: Exploratory Results from a Randomised, Double-Blind, Placebo-Controlled Trial. *Lancet* 390 (10105), 1833–1842. doi:10.1016/S0140-6736(17)32247-X

Sabatino, J. J., Jr., Zamvil, S. S., and Hauser, S. L. (2019). "B-Cell Therapies in Multiple Sclerosis.". *Cold Spring Harb Perspect. Med.* 9. doi:10.1101/cshperspect.a032037

Sanchez-Trujillo, L., Jerjes-Sanchez, C., Rodriguez, D., Panneflek, J., Ortiz-Ledesma, C., Garcia-Rivas, G., et al. (2019). Phase II Clinical Trial Testing the Safety of a Humanised Monoclonal Antibody Anti-CD20 in Patients with Heart Failure with Reduced Ejection Fraction, ICFEr-RITU2: Study protocol.". *BMJ Open* 9, e022826. doi:10.1136/bmjopen-2018-022826

Savage, H. P., and Baumgarth, N. (2015). Characteristics of Natural Antibody-Secreting Cells. *Ann. N. Y Acad. Sci.* 1362, 132–142. doi:10.1111/nyas.12799

Serreze, D. V., Fleming, S. A., Chapman, H. D., Richard, S. D., Leiter, E. H., and Tisch, R. M. (1998). B Lymphocytes Are Critical Antigen-Presenting Cells for the Initiation of T Cell-Mediated Autoimmune Diabetes in Nonobese Diabetic Mice. *J. Immunol.* 161 (8), 3912–3918.

Shen, P., and Fillatreau, S. (2015). Antibody-independent Functions of B Cells: a Focus on Cytokines. *Nat. Rev. Immunol.* 15 (7), 441–451. doi:10.1038/nri3857

Siegel, R., DeSantis, C., Virgo, K., Stein, K., Mariotto, A., Smith, T., et al. (2012). Cancer Treatment and Survivorship Statistics, 2012. *CA Cancer J. Clin.* 62 (4), 220–241. doi:10.3322/caac.21149

Staudt, A., Eichler, P., Trimpert, C., Felix, S. B., and Greinacher, A. (2007). Fc(gamma) Receptors IIa on Cardiomyocytes and Their Potential Functional Relevance in Dilated Cardiomyopathy. *J. Am. Coll. Cardiol.* 49 (16), 1684–1692. doi:10.1016/j.jacc.2006.11.051

Thiagaraj, A., Kalamkar, P., Rahman, R., Farah, V., and Poornima, I. (2018). An Unprecedented Case Report of Primary Cardiac Lymphoma Exclusive to Left Ventricle: a Diagnostic and Therapeutic challenge.". *Eur. Heart J. Case Rep.* 2, yty029. doi:10.1093/ehjcr/yty029

Torre-Amione, G., Kapadia, S., Lee, J., Durand, J. B., Bies, R. D., Young, J. B., et al. (1996). Tumor Necrosis Factor-Alpha and Tumor Necrosis Factor Receptors in the Failing Human Heart. *Circulation* 93 (4), 704–711. doi:10.1161/01.cir.93.4.704

Uchida, J., Hamaguchi, Y., Oliver, J. A., Ravetch, J. V., Poe, J. C., Haas, K. M., et al. (2004). The Innate Mononuclear Phagocyte Network Depletes B Lymphocytes through Fc Receptor-dependent Mechanisms during Anti-CD20 Antibody Immunotherapy. *J. Exp. Med.* 199 (12), 1659–1669. doi:10.1084/jem.20040119

van den Hoogen, P., de Jager, S. C. A., Huibers, M. M. H., Schoneveld, A. H., Puspitasari, Y. M., Valstar, G. B., et al. (2019). Increased Circulating IgG Levels, Myocardial Immune Cells and IgG Deposits Support a Role for an Immune Response in Pre- and End-Stage Heart Failure. *J. Cel Mol Med* 23 (11), 7505–7516. doi:10.1111/jcmm.14619

Waldman, A. D., Fritz, J. M., and Lenardo, M. J. (2020). A Guide to Cancer Immunotherapy: from T Cell Basic Science to Clinical Practice. *Nat. Rev. Immunol.* 20 (11), 651–668. doi:10.1038/s41577-020-0306-5

Waldmann, T. A. (2003). Immunotherapy: Past, Present and Future. *Nat. Med.* 9 (3), 269–277. doi:10.1038/nm0303-269

Wang, L., Li, Y. L., Zhang, C. C., Cui, W., Wang, X., Xia, Y., et al. (2014). Inhibition of Toll-like Receptor 2 Reduces Cardiac Fibrosis by Attenuating Macrophage-Mediated Inflammation. *Cardiovasc. Res.* 101 (3), 383–392. doi:10.1093/cvr/cvt258

Wang, W., and Cai, D. (2020). Complement Components sC5b-9 and CH50 Predict Prognosis in Heart Failure Patients Combined with Hypertension. *Am. J. Hypertens.* 33 (1), 53–60. doi:10.1093/ajh/hpz140

Wu, L., Zhao, F., Dai, M., Li, H., Chen, C., Nie, J., et al. (2017). P2y12 Receptor Promotes Pressure Overload-Induced Cardiac Remodeling via Platelet-Driven Inflammation in Mice. *Hypertension* 70 (4), 759–769. doi:10.1161/HYPERTENSIONAHA.117.09262

Wu, Y., Li, Y., Zhang, C., Wang, X. A., Li, H., and Du, J. (2014). S100a8/a9 Released by CD11b+Gr1+ Neutrophils Activates Cardiac Fibroblasts to Initiate Angiotensin II-Induced Cardiac Inflammation and Injury. *Hypertension* 63 (6), 1241–1250. doi:10.1161/HYPERTENSIONAHA.113.02843

Yan, X., Anzai, A., Katsumata, Y., Matsuhashi, T., Ito, K., Endo, J., et al. (2013). Temporal Dynamics of Cardiac Immune Cell Accumulation Following Acute Myocardial Infarction. *J. Mol. Cel Cardiol* 62, 24–35. doi:10.1016/j.yjmcc.2013.04.023

Yanaba, K., Hamaguchi, Y., Venturi, G. M., Steeber, D. A., St Clair, E. W., and Tedder, T. F. (2007). B Cell Depletion Delays Collagen-Induced Arthritis in Mice: Arthritis Induction Requires Synergy between Humoral and Cell-Mediated Immunity. *J. Immunol.* 179 (2), 1369–1380. doi:10.4049/jimmunol.179.2.1369

Youker, K. A., Assad-Kottner, C., Cordero-Reyes, A. M., Trevino, A. R., Flores-Arredondo, J. H., Barrios, R., et al. (2014). High Proportion of Patients with End-Stage Heart Failure Regardless of Aetiology Demonstrates Anti-cardiac Antibody Deposition in Failing Myocardium: Humoral Activation, a Potential Contributor of Disease Progression. *Eur. Heart J.* 35 (16), 1061–1068. doi:10.1093/eurheartj/eht506

Yu, M., Wen, S., Wang, M., Liang, W., Li, H. H., Long, Q., et al. (2013). TNF-α-secreting B Cells Contribute to Myocardial Fibrosis in Dilated Cardiomyopathy. *J. Clin. Immunol.* 33 (5), 1002–1008. doi:10.1007/s10875-013-9889-y

Zamorano, J. L., Lancellotti, P., Rodriguez Muñoz, D., Aboyans, V., Asteggiano, R., Galderisi, M., et al. (2016). 2016 ESC Position Paper on Cancer Treatments and Cardiovascular Toxicity Developed under the Auspices of the ESC Committee for Practice Guidelines: The Task Force for Cancer Treatments and Cardiovascular Toxicity of the European Society of Cardiology (ESC). *Eur. Heart J.* 37 (36), 2768–2801. doi:10.1093/eurheartj/ehw211

Zhang, C., Li, Y., Wang, C., Wu, Y., and Du, J. (2014). Antagonist of C5aR Prevents Cardiac Remodeling in Angiotensin II-Induced Hypertension. *Am. J. Hypertens.* 27 (6), 857–864. doi:10.1093/ajh/hpt274

Zhang, M., Austen, W. G., Jr., Chiu, I., Alicot, E. M., Hung, R., Ma, M., et al. (2004). Identification of a Specific Self-Reactive IgM Antibody that Initiates Intestinal Ischemia/reperfusion Injury. *Proc. Natl. Acad. Sci. U S A.* 101 (11), 3886–3891. doi:10.1073/pnas.0400347101

Zhang, M., Michael, L. H., Grosjean, S. A., Kelly, R. A., Carroll, M. C., and Entman, M. L. (2006). The Role of Natural IgM in Myocardial Ischemia-Reperfusion Injury. *J. Mol. Cel Cardiol* 41 (1), 62–67. doi:10.1016/j.yjmcc.2006.02.006

Zouggari, Y., Ait-Oufella, H., Bonnin, P., Simon, T., Sage, A. P., Guérin, C., et al. (2013). B Lymphocytes Trigger Monocyte Mobilization and Impair Heart Function after Acute Myocardial Infarction. *Nat. Med.* 19 (10), 1273–1280. doi:10.1038/nm.3284

Zwaka, T. P., Manolov, D., Ozdemir, C., Marx, N., Kaya, Z., Kochs, M., et al. (2002). Complement and Dilated Cardiomyopathy: a Role of Sublytic Terminal Complement Complex-Induced Tumor Necrosis Factor-Alpha Synthesis in Cardiac Myocytes. *Am. J. Pathol.* 161 (2), 449–457. doi:10.1016/s0002-9440(10)64201-0

Conflict of Interest: The authors declare that the research was conducted in the absence of any commercial or financial relationships that could be construed as a potential conflict of interest.

frontiers in Pharmacology

ORIGINAL RESEARCH
published: 22 March 2022
doi: 10.3389/fphar.2022.832045

Pyrrolidine Dithiocarbamate Might Mitigate Radiation-Induced Heart Damage at an Early Stage in Rats

*Yajing Wu[1], Lina Liu[1], Shengliang Lv[1], Yi Wang[1], Shuai Wang[1], Sheng Wang[2], Jiandong Zhang[3] and Jun Wang[1]**

[1]Department of Radiation Oncology, Fourth Hospital of Hebei Medical University, Shijiazhuang, China, [2]Hebei Key Laboratory of Neurophysiology, Shijiazhuang, China, [3]Department of Radiation Oncology, The First Affiliated Hospital of Shandong First Medical University, Jinan, China

Objective: Radiation-induced heart damage (RIHD) is becoming an increasing concern due to offsetting clinical benefits of radiotherapy to a certain extent. Pyrrolidine dithiocarbamate (PDTC) as an antioxidant has been implicated in cardioprotective effects. We aimed to investigate whether pyrrolidine dithiocarbamate could attenuate heart damage at an early stage post-irradiation and unveil the potential mechanisms.

Methods: A total of 15 adult male Sprague–Dawley rats were randomized into the control, irradiation (IR), and PDTC plus irradiation (PDTC + IR) groups. Hearts were irradiated with a single fraction of 20.0 Gy. Rats received daily intraperitoneal injection of PDTC for 14 days. At the 14th day post-irradiation, echocardiography was performed, and rats were killed. Morphological damage was examined by hematoxylin–eosin (HE) stain and Masson's trichrome stain. The collagen volume fraction (CVF) was applied for semi-quantitative analysis. The protein levels were analyzed by Western blot and mRNA levels by quantitative real-time PCR.

Results: No significant damage to systolic function of left ventricular was induced at an early stage post-irradiation. HE staining of cardiac tissue showed that the disordered arrangement of myocardial cells and abnormal cell infiltration were alleviated in the PDTC + IR group. The increased CVF in the irradiation group was inhibited in the PDTC + IR group (22.05 ± 2.64% vs. 9.99 ± 1.65%, $p < 0.05$). The protein levels of nuclear factor-kappa B (NF-κB), hypoxia-inducible factor-1α (HIF-1α), and COL-1 were downregulated after treatment with PDTC ($p < 0.05$), and there was a declining trend in the protein of the connective tissue growth factor (CTGF). The mRNA expression of NF-κB and HIF-1α in the PDTC plus irradiation group was lower than that in the irradiation group ($p < 0.05$), and there was a declining trend in the mRNA expression of the connective tissue growth factor and COL-1.

Conclusion: PDTC alleviates myocardial cell disordered arrangement, abnormal cell infiltration, and pro-fibrotic change at an early stage in rats with radiation-induced heart damage. Such a protective effect is closely associated with the downregulation of NF-κB.

Keywords: acute radiation-induced heart pro-fibrotic damage, left ventricular function, nuclear factor-kappa B, pyrrolidine dithiocarbamate, hypoxia-inducible factor-1α, connective tissue growth factor

OPEN ACCESS

Edited by:
Jun Pu,
Shanghai Jiao Tong University, China

Reviewed by:
Jia-Yi Chen,
Shanghai Jiao Tong University, China
Matteo A Russo,
San Raffaele Pisana (IRCCS), Italy
Zhouguang Hui,
Chinese Academy of Medical Sciences and Peking Union Medical College, China

****Correspondence:***
Jun Wang
wangjunzr@163.com

Specialty section:
This article was submitted to Cardiovascular and Smooth Muscle Pharmacology, a section of the journal Frontiers in Pharmacology

Received: *09 December 2021*
Accepted: *28 February 2022*
Published: *22 March 2022*

Citation:
Wu Y, Liu L, Lv S, Wang Y, Wang S, Wang S, Zhang J and Wang J (2022) Pyrrolidine Dithiocarbamate Might Mitigate Radiation-Induced Heart Damage at an Early Stage in Rats. Front. Pharmacol. 13:832045. doi: 10.3389/fphar.2022.832045

1 INTRODUCTION

A total of 2 million new cancer patients are diagnosed per year, and improvements in cancer therapies have increased cancer survivors (Survivorship, 20192019). Among these survivors, cardiovascular disease is the leading cause of non-cancer-related mortality (Mehta et al., 2018). Detrimental effects on the cardiovascular system related to cancer treatments are a clinical challenge for cardiologists and oncologists. Radiotherapy may cause damage to both acute and chronic epicardial coronary artery and microcirculatory as well as fibrotic changes in the valve or pericardium (Chang et al., 2017). Pericarditis and pericardial effusions are the early-onset side effects that develop within weeks, while others have a late onset, often 10–20 years after treatment such as valvular heart disease and heart failure (Hufnagle et al., 2021). The mechanisms of radiation-induced cardiac damage are complicated, multi-factorial, and under-recognized, initial inflammation or oxidative stress and subsequent fibrosis seem to be the potential events (Ping et al., 2020). Accumulating evidence generally indicates that the main pathological manifestation of radiation-induced heart damage (RIHD) is myocardial fibrosis, and that radiation-induced heart fibrosis is usually considered as chronic manifestation. So far there are no approaches to reverse RIHD (Boerma 2012; Gürses et al., 2014). The administration of a palladium lipoic acid complex (POLY-MVA) mitigated the damage of radiation to mitochondria. Nonetheless, POLY-MVA did not mitigate adverse cardiac remodeling at 18 weeks after rats were exposed to the local heart with X-rays (Sridharan et al., 2017). Therefore, it is necessary to explore the pathogenesis of RIHD and find an effective intervention against RIHD at an early stage.

Recently, we demonstrated that radiation-induced myocardial fibrotic change could be observed as early as 14 days after exposure to irradiation, and the mechanisms might be attributed to the activation of oxidative stress and endoplasmic reticulum stress (Wang et al., 2016). NF-κB is considered as a redox-sensitive transcription factor and a regulator of the inflammatory process (Han et al., 2013; Sies et al., 2017). The p65/50 heterodimer is a common pattern of NF-κB, which exists in the cytoplasm as an inactive component bound to the inhibitor of κB alpha (IκB α). Once activated, the protein of IκB is phosphorylated and ubiquitinated, subunits of the NF-κB including p65 and P50 are released. NF-κB classical pathway activation is mainly marked by the formation of P50 and P65. Studies have also showed that ionizing radiation could induce NF-κB activation (Meng et al., 2003), and in the experimental studies of tumor cells, the activation of the NF-κB pathway was also confirmed (Cataldi et al., 2003; Lam et al., 2015). However, evidence of the role of NF-κB in acute RIHD is lacking. Irradiation could induce a reduction in the myocardial micro-vessel density (Sridharan et al., 2017) and subsequent myocardial ischemia and hypoxia. NF-κB increased the HIF-1 mRNA expression as an important factor, and this was followed by transcription of some pro-inflammatory genes (Korbecki et al., 2021). Hypoxia-inducible factor-1α (HIF-1α) is also one of the classic factors which can lead to fibrosis and upregulates the expression of many fibrosis-related genes, such as the connective tissue growth factor (CTGF) and transforming growth factor-β1 (TGF-β1). CTGF can increase the synthesis of fibrosis-related factors, such as collagen type I, and accelerate the proliferation of fibroblast (Zhou et al., 2013). Whether NF-κB, HIF-1α, and CTGF were activated at the acute stage of RIHD and participated in the process of radiation-induced myocardial fibrosis remains unexplored.

PDTC, an oxidant and an inhibitor of NF-κB, could inhibit cardiac inflammatory response, relieve ventricular remodeling, maintain normal tissue structure, and protect cardiac function in the rat's model with hypertension and myocardial ischemia (Theuer et al., 2002; Cau et al., 2015). There are very few reports about the effect of PDTC on RIHD, especially at an early stage post-irradiation. The most important finding in our previous data was that radiation-induced heart damage at a very early stage could be inhibited. We previously reported that chronic intermittent hypobaric hypoxia (CIHH) treatment prior to irradiation alleviated the early myocardial fibrosis by inhibiting oxidative stress and endoplasmic reticulum stress (Wang et al., 2016). Evidence of the protective effect of PDTC on RIHD is unavailable, and it is worth exploring whether PDTC could exert cardiac protection by the downregulation of NF-κB.

Here, we asked whether PDTC could alleviate RIHD in a rat model at an early stage and sought to investigate and delineate the putative cellular mechanism. Our data indicated that PDTC attenuated morphological damage and pro-fibrotic cardiac changes at an early stage in rat hearts subjected to irradiation, most likely *via* the inhibition of NF-κB, HIF-1α, and COL-1, providing a potentially clinical strategy to attenuate RIHD.

2 MATERIALS AND METHODS

2.1 Animals

A total of 15 adult male Sprague–Dawley rats aged 10 weeks, weighed 200–250 g were obtained from the Experimental Animal Center of Hebei Medical University (Shijiazhuang, China), with Guide for the Care and Use of Laboratory Animals, and it was approved by the Animal Care and Ethical Committee of Hebei Medical University. All rats were randomized into three groups: control, irradiation, and PDTC plus irradiation. The program was approved by the Animal Care and Ethical Committee of Hebei Medical University. Animals were synchronized for a 12:12-h light–dark cycle (lights on at 8 am and lights off at 8 pm), housed individually, and allowed to move freely in standard plastic cages in a climate-controlled room (22 ± 1°C). Food and water were provided *ad libitum*.

2.2 Pyrrolidine Dithiocarbamate Treatment

PDTC (p8765-5G, SIGMA, United States) was dissolved in physiological saline (0.9%) on the experiment day. In the PDTC plus irradiation group, rats received an intraperitoneal injection of PDTC at a dosage of 120 mg/kg 30 min prior to radiation and continued to receive the daily injection until the 14th day after radiation when cardiac tissue was harvested. Rats in

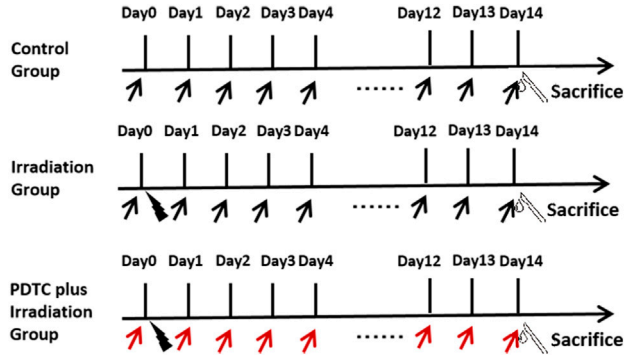

FIGURE 1 | Schedule of the experiment. Hearts of rats were irradiated with a single fraction of 20.0 Gy (black lightning bolt). PDTC (red arrow) or normal saline (black arrow) was intraperitoneally administrated at the dosage of 120 mg/kg 30 min prior to irradiation and continued to receive the daily injection until the 14th day post-irradiation.

control and irradiation groups were administrated with the corresponding volume of normal saline (**Figure 1**).

2.3 Irradiation treatment

Rats were anesthetized with 10% chloral hydrate (0.35 ml/100 g) and were irradiated with a single fraction of 20.0 Gy from a precise type medical high-energy linear accelerator (Elekta Corporation, Sweden) operated at 6 MV X-ray and with a dose rate of 1.87 Gy/min. Radiation was delivered locally to rat hearts using parallel opposed fields (anterior:posterior 1:1) with a diameter of 19 mm, while the rest of the rat body parts was shielded with lead plates (**Figure 1**).

2.4 Left Ventricular Function Measurement *In Vivo*

At the 14th day after irradiation, echocardiography was used for heart wall dimension measurements and to measure left ventricular ejection fraction (LVEF) by a well-trained investigator. The study measured the LV diastole and systole according to the main laws of the American Society of Echocardiography (Lang et al., 2015). Echocardiography was performed with a high-frequency transducer probe (VisualSonics MS400, FUJIFILM VisualSonics, Inc. Toronto, Canada, with a frequency range of 18–38 MHZ). Initially, the rats were anesthetized with 3% isofurane (80% oxygen) and placed supinely on an electrical heating pad (37°C). During examination, the isofurane concentration was reduced to a minimum (1–2%) to obtain constant and comparable heart rates shown by ECG. Additionally, prewarmed ultrasound gel was applied to reduce cold stimulation to small animals. Interventricular septum and para-sternal short-axis images were acquired. Conventional indicators were measured from the LV M-mode in short-axis view for three consecutive cardiac cycles and then averaged; these indicators included the LV wall thickness, diameter, fractional shortening (FS [LV end-diastolic diameter–LV end-systolic diameter]/LV end-diastolic diameter×100), and ejection fraction (EF [LV end-diastolic volume–LV end-systolic volume]/LV end-diastolic volume×100).

2.5 Histological Evaluations

2.5.1 Hematoxylin–Eosin (HE) Staining

At the 14th day after irradiation, cardiac tissues were harvested, and morphological changes in myocardial cells and interstitial were observed *via* HE staining. Hearts were dissected rapidly from the mediastinum and placed in 10% buffered formaldehyde for 24 h. An average of 3- to 4-mm-thickness longitudinal tissue slices showing the four chambers of the heart were taken after following the routine tissue processing. Sections (5 μm thick) were stained using hematoxylin and eosin for general tissue characterization. The nucleus of a normal myocardial cell was stained blue, and the cytoplasm was stained red. Fibroblast cells were distributed among the myocardial cells. The nucleus of a normal fibroblast cell was stained dark blue, and the cytoplasm was stained red.

2.5.2 Masson's Trichrome Stain

Total collagen accumulation was determined by preparing tissue sections with Masson's trichrome stain, and collagen volume fraction (CVF) was applied for semi-quantitative analysis of myocardial collagen (Wang et al., 2016). Briefly, the myocyte and collagen were stained red and green, respectively, with Masson's trichrome staining. CVF was applied for semi-quantitative analysis of myocardial collagen *via* an image processing system (Motic Med 6.0, Xiamen, China). Interstitial CVF was calculated as the area occupied by the green-dyed tissue, divided by the total myocardial area under direct vision. For each animal, five microscopic fields were examined, and the average of CVF was computed.

2.6 Determination of Nuclear Factor-Kappa B, Hypoxia-Inducible Factor-1α, Connective Tissue Growth Factor, and COL-1 Protein *via* Western Blot

At the 14th day after irradiation, rat heart tissue was harvested, snap frozen, crushed in liquid nitrogen, and then weighed. The tissue powder was homogenized with ice-cold Roche buffer with protease inhibitors (300 μl), and then was centrifuged at 20,000 g for 15 min at 4°C. The supernatant was collected to detect the protein level by BCA assay and diluted to the same concentration by thoroughly mixing with lysis buffer and loading buffer based on the concentration determined. SDS-PAGE was performed on 10% gradient gels. Samples, each containing 20 μg of protein, were added in the same amount of the sample-loading buffer. After electrophoresis, proteins were transferred to a polyvinylidene difluoride membrane and were blocked with 5% skim milk TBST buffer. Blots were incubated with primary antibodies overnight at 4°C and incubated with horseradish peroxidase-conjugated secondary antibody (EarthOx, Millbrae, CA). The signal was detected using the Clinx chemiluminescence's system (Shanghai, China). Primary antibodies P50 (ab32360, Abcam, United States), P65 (ab7970, Abcam, United States), HIF-1 alpha (sc-10790, SANTA CRUZ

Biotech Corp, United States), CTGF (ab6992, Abcam, United States), COL-1 (COL1A antibody) (sc-59772, SANTA CRUZ Biotech Corp, United States), and beta-actin (Bioworld Technology Corporation) were used for Western blot analysis. The best concentration of primary antibody (P50:1:1,000; P65: 1: 400; HIF-1 alpha: 1:100; CTGF: 1:1,000; COL-1: 1:400; and β -actin:1:5,000) were determined.

2.7 Detection of Nuclear Factor-Kappa B, Hypoxia-Inducible Factor-1α, Connective Tissue Growth Factor, and COL-1 mRNA *via* Quantitative Real-Time Polymerase Chain Reaction

On the 14th day after irradiation, to assess the mRNA levels of NF-κB and the downstream pathway, 50 mg of myocardial tissue were harvested, snap frozen, crushed in liquid nitrogen, and then weighed. Total RNA was extracted using an RNeasy Mini Kit (Qiagen, CA). RNA levels were quantified using 1 μl of each sample, and the process was repeated twice. The first strand cDNA was synthesized from 1 μg of each total RNA sample using reverse transcriptase. The temperature protocol for cDNA reverse transcription reactions was as follows: 25°C for 5 min, 50°C for 15 min, and 85°C for 5 min, and then the cDNA sample was frozen at −20°C. Primer Premier 5.0 (Premier Corporation, Canada) was used to design primers (sequences in Table 1). The primers were frozen at −20°C. PCR for each gene was performed with an Applied Biosystems QuantStudio 6 Flex fluorescent quantitative PCR instrument and SYBR Green I, and the amplification and melt curves were obtained. The thermal cycler protocol for all PCR reactions was as follows: 95°C for 2 min, 95°C for 15 s, and 60°C for 1 min for a total of 42 cycles. The $2^{-\triangle\triangle CT}$ method was used for relative quantitative analysis, and the difference among the samples was detected.

2.8 Statistical Analysis

Data were analyzed by Statistical Product and Service Solutions (SPSS) version 22.0 statistical software (IBM Co., Armonk, NY, United States). First, a normality test was conducted, and one way analysis of variance (ANOVA) was adopted for comparisons in three groups. The non-normality test was compared by using the rank sum test. When the homogeneity of variance was assumed, the LSD method was used for pairwise comparison, and if not, Dunnett's C test was used for pairwise comparison. Data were expressed as mean ± standard error. The criterion for statistical significance was $p < 0.05$.

3 RESULTS

3.1 No Significant Damage to Systolic Function of Left Ventricular Was Induced by Irradiation at a Very Early Stage

The evaluation of left ventricular function was performed at the 14th day after the irradiation injury. Electrocardiograph of the short axis view of the M-mode in rat hearts was shown with the interventricular septum image (**Figure 2A**) and para-sternal short axis view (**Figure 2B**). LVEF and LVFS are commonly used to evaluate the cardiac systolic function. Both the parameters of LVEF and LVFS were lower in the irradiation group than that in the control group, but there was no significance among the groups ($p > 0.05$ for both, **Figures 2C,D**). In parallel, there was no significant difference of LVEF and LVFS between the irradiation and PDTC + irradiation groups. The results indicated that no abnormal impairment of left ventricular systolic function was detected at a very early stage in an RIHD rat model.

3.2 No Significant Structural Changes Was Induced by Irradiation in Echocardiography and Pyrrolidine Dithiocarbamate-Alleviated Radiation-Induced Myocardial Morphological Change

Images of the interventricular septum (**Figure 2A**) and para-sternal short axis (**Figure 2B**) were displayed with the M-mode. The left ventricle posterior wall (LVPW) thickness at diastole and systole, interventricular septal (IVS) thickness at diastole and systole, and left ventricular internal diameters (LVID) at diastole and systole were similar between the control and irradiation groups (**Figure 3B–G**).

HE staining was performed to observe the general morphological characters of myocardial tissue. Myocardial cell edema, arrangement disorder, pyknosis of myocardial nuclei, and abnormal cells infiltration could be observed after irradiation. However, the aforementioned damage was attenuated in the PDTC plus irradiation group compared with the irradiation group (**Figure 3A**).

3.3 Pyrrolidine Dithiocarbamate-Alleviated Radiation Induced Myocardial Pro-Fibrotic Change

Masson's trichrome stain was performed to determine whether the pro-fibrotic change at a very early stage in rats subjected to irradiation. As shown in **Figure 4A**, collagen fibers in the irradiation group were more widely distributed in the myocardial interstitium than in the control group, but this increase in distribution was significantly attenuated in the PDTC plus irradiation group. The semi-quantitative analysis of Masson's trichrome stain (**Figure 4B**) indicated that the collagen volume fraction (CVF) of the irradiation group was significantly higher than that of the control group (22.05 ± 2.64% vs. 3.76 ± 0.79%, $p < 0.01$, $n = 5$), but the enhancement was inhibited by PDTC treatment (9.99 ± 1.65% vs. 22.05 ± 2.64%, $p < 0.05$, $n = 5$).

Similar pattern could be observed in the COL-1 protein level as detected by Western blot, which is a marker of fibrosis. The level of COL-1 protein was increased in the irradiation group compared with the control group (0.52 ± 0.05 vs. 0.32 ± 0.04, $p < 0.01$, $n = 5$, **Figure 4C**), but the increase in COL-1 in the PDTC plus irradiation group was much smaller than that in the irradiation group (0.36 ± 0.03 vs. 0.52 ± 0.05, $p < 0.05$, $n = 5$, **Figure 4C**).

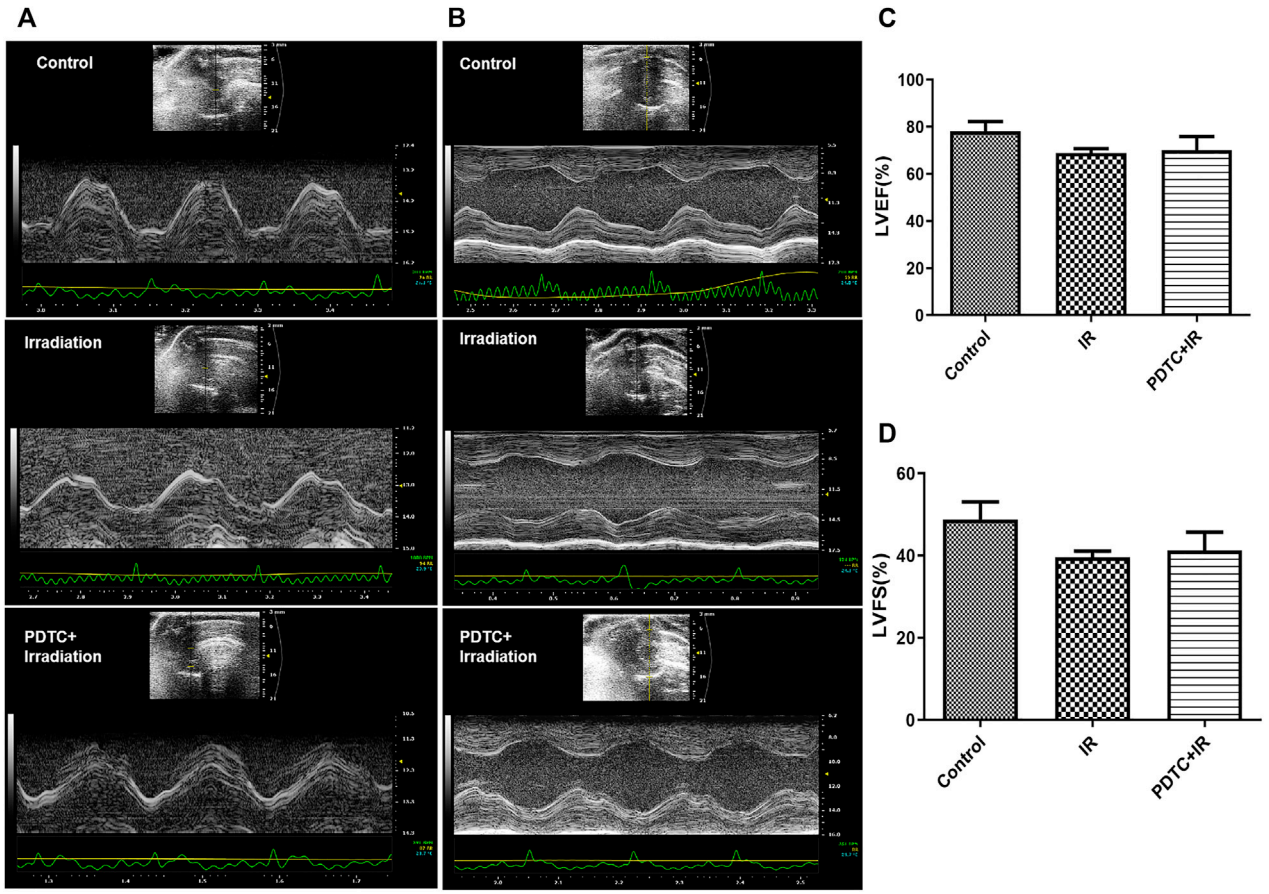

FIGURE 2 | Electrocardiographs of the short axis view in M-mode in rat hearts. **(A)** Interventricular septum image. **(B)** Para-sternal short axis view. **(C)** LVEF of rats from each group. **(D)** LVFS of rats from each group.

Furthermore, according to **Figure 4D**, it showed that the level of COL-1 mRNA in the irradiation group was higher than that in the control group (2.65 ± 0.25 vs. 1.26 ± 0.24, $p < 0.05$, $n = 5$), but the increase trend of COL-1 mRNA in the PDTC plus irradiation group was slightly smaller than that in the irradiation group (1.85 ± 0.55 vs. 2.65 ± 0.25, $0.05 < p < 0.10$, $n = 5$).

3.4 Pyrrolidine Dithiocarbamate-Attenuated Radiation Induced Myocardial Inflammation and Downstream Pathway

3.4.1 Effects of Pyrrolidine Dithiocarbamate on the Nuclear Factor-Kappa B Pathway

NF-κB classical pathway activation is mainly marked by the formation of P50 and P65. The expression of P50 and P65, the two main proteins of activation of NF-κB, was analyzed using Western blot to address whether NF-κB as one of the inflammation master switch was activated by radiation. As shown in **Figures 5A,B**, the expression of P50 and P65 proteins in the irradiation group was significantly higher than that in the controls (0.43 ± 0.04 vs. 0.2 ± 0.03, $p < 0.01$ for P50; 0.68 ± 0.07 vs. 0.45 ± 0.02, $p < 0.01$ for P65, $n = 5$), suggesting the involvement of NF-κB activation in irradiation-induced heart damage. PDTC treatment inhibited the increase in the expression of both P50 and P65 induced by irradiation (0.23 ± 0.02 vs. 0.43 ± 0.04, $p < 0.01$ for P50; 0.51 ± 0.05 vs. 0.68 ± 0.07, $p < 0.05$ for P65, $n = 5$, **Figures 5A,B**).

Results of qPCR (**Figures 5C,D**) showed that mRNA levels of both P50 and P65 were significantly higher in the irradiation group than in the controls (1,79 ± 0.17 vs. 1.08 ± 0.16, $p < 0.05$ for P50; 1.98 ± 0.20 vs. 1.28 ± 0.10, $p < 0.05$ for P65, $n = 5$), but the increase in RQ was significantly decreased in the PDTC plus irradiation group (1.18 ± 0.17 vs. 1.79 ± 0.17, $p < 0.05$ for P50; 1.40 ± 0.07 vs. 1.98 ± 0.20, $p < 0.05$ for P65, $n = 5$), which was consistent with the results of Western blot.

3.4.2 Effects of Pyrrolidine Dithiocarbamate on Hypoxia-Inducible Factor-1α and Connective Tissue Growth Factor

Activated NF-κB increased the HIF-1 mRNA expression. HIF-1α might increase the expression of many fibrosis-related genes, such as CTGF. Therefore, it was hypothesized that the expression of HIF-1α and CTGF genes was regulated by the activated NF-κB, and they might serve as the intermediate connection to radiation-induced cardiac fibrosis. As shown in **Figure 6A**, the HIF-1α protein level in the irradiation group was significantly higher than

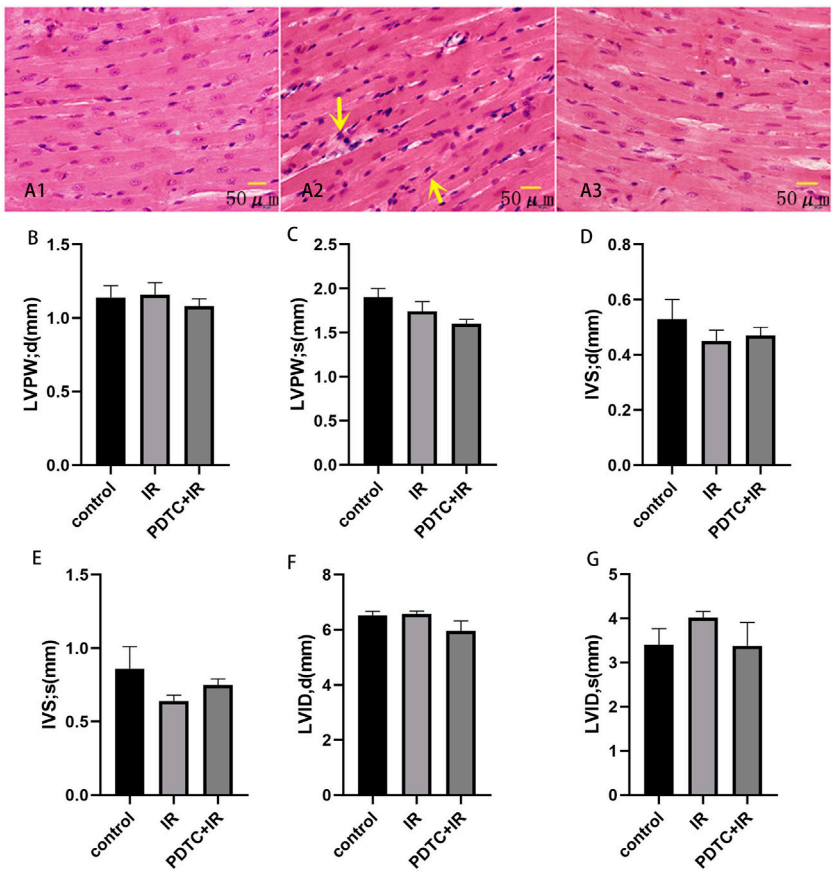

FIGURE 3 | Effects of PDTC on myocarditis reaction (n = 5). Transverse section in the cardiac muscles of rats *via* HE staining for the observation of cardiac injury (×200). **(A1)**: control group; **(A2)**: irradiation group; **(A3)**: PDTC + irradiation group. Arrows were abnormal cells infiltration. **(B,C)** show the thickness of LVPW at diastole and systole. **(D,E)** show the thickness of IVS at diastole and systole. **(F,G)** show LVID at diastole and systole.

that in the controls (0.31 ± 0.03 vs. 0.16 ± 0.01, $p < 0.01$, $n = 5$), but the enhancement was significantly inhibited by PDTC treatment (0.22 ± 0.04 vs. 0.31 ± 0.03, $p < 0.05$, $n = 5$). As shown in **Figure 6B**, the CTGF protein level in the irradiation group was significantly higher than that of the control group (0.52 + 0.05 vs. 0.32 ± 0.04, $p < 0.01$, $n = 5$), but the increase was slightly smaller in the PDTC plus irradiation group than that in the irradiation group (0.36 ± 0.03 vs. 0.52 + 0.05, $0.05 < p < 0.10$, $n = 5$).

Results of qPCR (**Figure 6C**) showed that HIF-1α mRNA was 2.65 ± 0.08 in the irradiation group, exhibiting an increase compared with 1.70 ± 0.23 in the control group ($p < 0.01$, $n = 5$), but the increase was dramatically inhibited by PDTC treatment (1.59 ± 0.30 vs. 2.65 ± 0.08, $p < 0.01$, $n = 5$). As shown in **Figure 6D**, the CTGF mRNA level in the irradiation group was 3.06 ± 0.47, a significant increase compared with 1.42 ± 0.17 of the control group ($p < 0.05$, n = 5); but the upward trend was slightly inhibited by PDTC treatment (1.88 + 0.55 vs. 3.06 ± 0.47, $0.05 < p < 0.10$, $n = 5$).

3.5 PPI Network Analysis

The PPI network was used to analyze the interactions among NF-κB, HIF-1α, CTGF, and COL-1 (mainly including COL-1A1 and COL-1A2) (**Figure 7**). There was a stepwise interaction among NF-κB, HIF-1α, CTGF, and COL-1A1 or COL-1A2.

4 DISCUSSION

This study was conducted to mainly evaluate the function of left ventricular systolic function *in vivo*, observe histological manifestations, and initially explore the putative mechanisms, and assessed the protective effects of PDTC treatment on RIHD at an early stage. First, we found that there was no significant difference in left ventricular systolic function at the 14th day after irradiation. Second, the histopathological results displayed myocardial cell edema, myocardial cell-disordered arrangement, abnormal cell infiltration, and pro-fibrotic cardiac change in irradiated hearts. Third, enhanced levels of P50, P65, HIF-1α, CTGF, and COL-1 occurred when challenged by irradiation. Finally, the most important finding was that PDTC treatment, to some extent, alleviated cardiac damage at a very early stage in locally irradiated hearts, which might be attributed to suppress NF-κB.

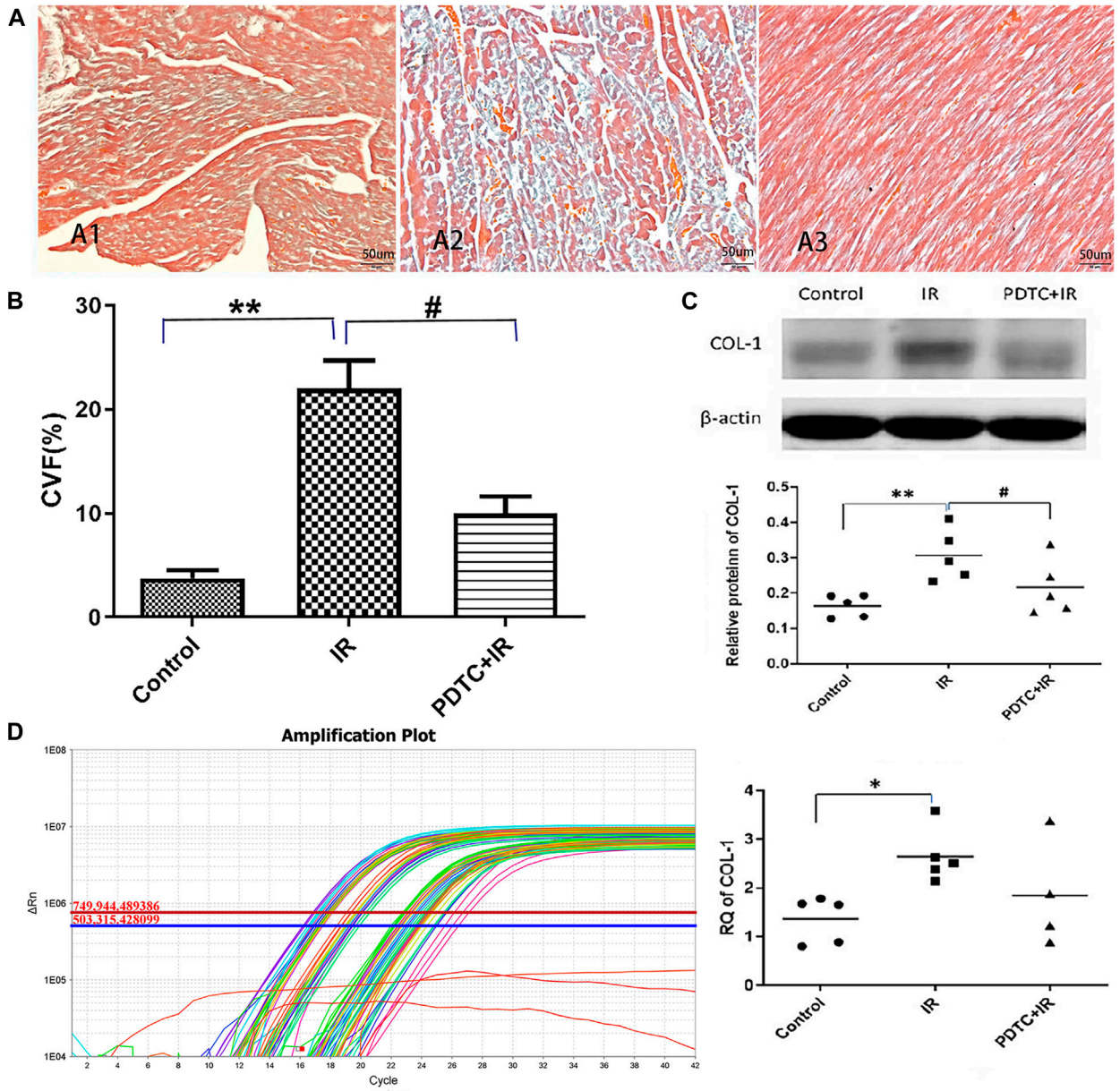

FIGURE 4 | Effects of PDTC treatment on radiation-induced myocardial fibrosis. **(A)** Transverse section in the myocardial of rats *via* Masson's trichrome staining for the observation of cardiac fibrosis (×200). All the collagen fibers were stained blue. **(A1)** Normal appearance in the control group. **(A2)** Damage characterized by myocardial interstitial fibrosis in the irradiation group. **(A3)** Little of collagen deposited at myocardial interstitial tissue in the PDTC + irradiation group. **(B)** Quantitative analysis showing collagen volume fraction (CVF) in each group. **(C)** Expression of COL-1 was revealed by Western blot in each group. **(D)** Expression of COL-1 was revealed by qPCR in each group. n = 5 for each group. *$p < 0.05$ for irradiation vs. control group; **$p < 0.01$ for irradiation vs. control group; #$p < 0.05$ for PDTC + irradiation vs. irradiation group.

Our data showed that there was no significant impairment of the left ventricular systolic function *in vivo* at the 14th day after irradiation in rats, consistent with previous studies also showed that no change in cardiac function occurred 4 months after radiation, and the deterioration of heart function occurred 4–6 months after radiation (Boerma et al., 2008; Mezzaroma et al., 2012). Our previous finding also indicated that the basic left ventricular function of isolated rat hearts was also not impaired at the 14th day post-radiation (Wang et al., 2016). The heart had its own reserve capacity, and it might keep a relative normal function at a compensatory stage in a short time after adverse stress. Echocardiography, an assessment of cardiac function *in vivo*, was a non-invasive and repeatable examination. Compared with the previous detection of isolated cardiac function, echocardiography data could be similar to the performance of patients who experienced thoracic radiotherapy.

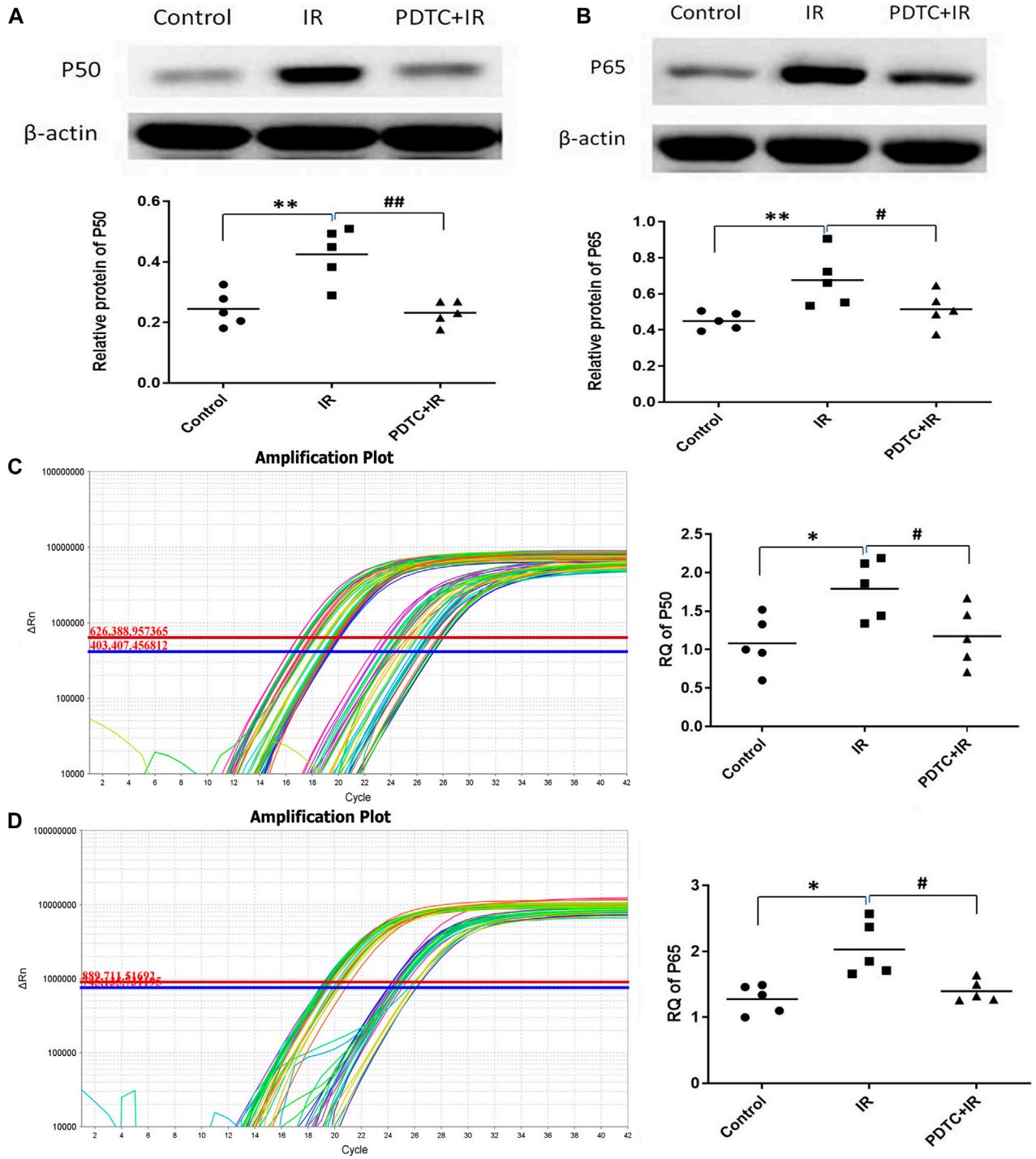

FIGURE 5 | Effects of PDTC treatment on the expression of NF-κB protein and mRNA in the myocardium. **(A)** and **(B)** show the expression of P50 and P65 proteins revealed by Western blot. **(C)** and **(D)** show the mRNA levels of P50 and P65 analyzed by qPCR ($n = 5$). $^{*}p < 0.05$ for irradiation vs. control group; $^{**}p < 0.01$ for irradiation vs. control group; $^{\#}p < 0.05$ for PDTC + irradiation vs. irradiation group; $^{\#\#}p < 0.05$ for PDTC + irradiation vs. irradiation group.

Left ventricular systolic function might not be a very sensitive index of cardiac injury at an early stage due to the cardiac reserve capacity and compensatory ability. In other words, cardiac damage might occur without the impairment of the cardiac systolic function. Therefore, we euthanized the rats and performed HE and Masson's trichrome staining to check the cardiac morphological changes. HE staining was mainly used to observe the morphology and arrangement of cardiomyocytes.

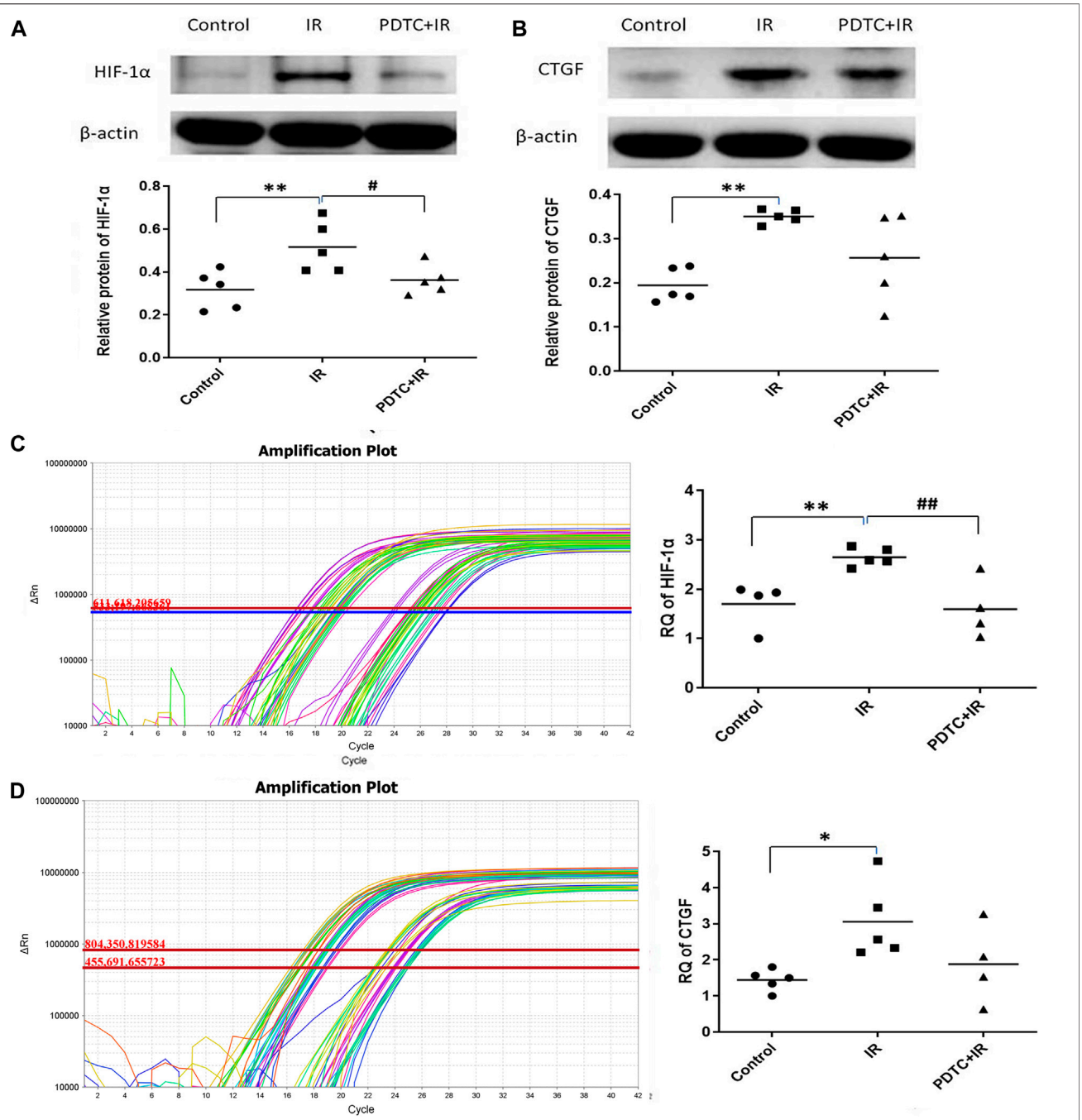

FIGURE 6 | Effects of PDTC on the expression of HIF-1α and CTGF proteins and mRNAs in myocardial tissue. **(A)** and **(B)** show the HIF-1α and CTGF protein levels revealed by Western blot **(C)** and **(D)** show the mRNA levels of HIF-1α and CTGF analyzed by qPCR. $n = 5$. $^{*}p < 0.05$ for irradiation vs. control group; $^{**}p < 0.01$ for irradiation vs. control group; $^{\#}p < 0.05$ for PDTC + irradiation vs. irradiation group; $^{\#\#}p < 0.05$ for PDTC + irradiation vs. irradiation group.

Masson's trichrome staining was a common method to assess fibrosis in the hearts with collagen being stained green. Previous studies indicated that rats were exposed to local heart irradiation with a single dose of 18, 20, or 24 Gy and were observed for 3–6 months; alterations myocardial inflammatory infiltration and interstitial fibrosis were progressed in time-dependent and dose-dependent manners (Sridharan et al., 2012; Gürses et al., 2014). Yi et al. (2020) indicated that cardiac tissue presented disordered arrangement of myocardial cells at the 21st day after irradiation in mice. In the present study, we found disordered arrangement of myocardial cells and abnormal cell infiltration at the 14th day after irradiation, suggesting that a much earlier change of myocardial cells might have occurred. As for which kind of cell infiltration, immunofluorescence or

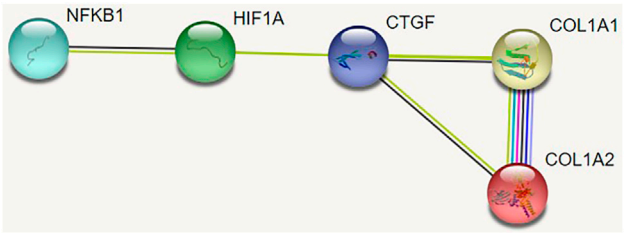

FIGURE 7 | PPI network was used to analyze interactions between NF-κB, HIF-1α, CTGF, and COL-1A.

immunohistochemistry with specific markers could be used. In parallel, we also found the onset of cardiac fibrosis based on the results of Masson's trichrome staining and the expression of COL-1 at the 14th day post-irradiation. Above all, PDTC might alleviate myocardial cell-disordered arrangement, abnormal cell infiltration, and fibrotic change induced by radiation. Up to now, it was the first study to find that PDTC had a protective effect on radiation-induced heart damage at an early stage.

The mechanism of RIHD at an early stage was not well understood, and there were several hypotheses according to preclinical evidence. Activation of inflammatory response or oxidative stress and fibrosis has been reported (Schultz-Hector and Trott 2007; Tapio 2016; Ping et al., 2020). NF-κB is an inducer of inflammation. Weintraub and Halle revealed that NF-κB increased in the irradiated vessel areas (Halle et al., 2010; Weintraub et al., 2010). In the present study, the local heart of the rat model was irradiated, and both mRNA and protein expression of cardiac tissue were detected. As a result, NF-κB was activated. Combined with the aforementioned disordered arrangement of myocardial cells or abnormal cell infiltration and fibrosis, we speculated that perhaps there was a relationship between the disordered arrangement of myocardial cells and fibrosis. After the PPI network analysis, we hypothesized that HIF-1α and CTGF were the bridge between NF-κB and COL-1. Van Uden indicated that NF-κB directly regulated the expression of HIF-1α under the normal oxygen condition (Van Uden et al., 2008). Additionally, HIF-1α could regulate the secretion of fibrogenic cytokine CTGF, promote the synthesis of collagen type I and fibronectin, and increase the proliferation of fibroblast (Angelini et al., 2015). Preliminarily, we observed an increase in the protein and mRNA levels of NF-κB, HIF-1α, and protein of COL-1 after irradiation to the local heart in a rat model. The levels of CTGF mRNA and protein only showed a trend of attenuation by PDTC but did not reach statistical significance. One possible explanation is that there are extremely complex interactions between HIF-1α and CTGF. Haydont observed that TGF-β1 directly activated the transcription of the CTGF gene after mesenchymal cells were exposed to irradiation (Haydont et al., 2008). Vozenin-Brotons indicated that the lower concentration of TGF-β1 sustained the expression of CTGF in intestinal radiation fibrosis (Vozenin-Brotons et al., 2003). Thus, we deduced that only suppressing NF-κB might be inadequate to interfere with the transcription and expression of CTGF. Meanwhile, the results of Western blot revealed that radiation-induced COL-1 increased by irradiation, but the mRNA level of COL-1 did not reach statistical significance. Theoretically, transcription of mRNA was prior to the translation of protein, but the processes of transcription and translation had their own half-lives and occurred at different times. At the end point of the present study (at the 14th day post-radiation), transcription of COL-1 mRNA was low, but the translation of COL-1 protein was high. This finding provided a new insight into RIHD at a very early stage. Confident study on the NF-κB/HIF-1α/CTGF/COL-1 signaling pathway was regulated by the activation of NF-κB in rat myocardial cells or primary cultures *in vitro* experiments or transgenic animals was needed.

PDTC is an antioxidant and an inhibitor of NF-κB. PDTC played an anti-inflammatory role, which could interfere with the production of pro-inflammatory cytokines and inhibit the activation of NF-κB (Cuzzocrea et al., 2002). Practically, PDTC has been examined for its preclinical safety evaluation in the liver, brain, nerves, and fat tissues and has reached the standard of safety application (Chabicovsky et al., 2010). In a rat model with hypertension and myocardial ischemia, PDTC has been identified to inhibit cardiac inflammatory response, relieve ventricular remodeling, maintain normal tissue structure, and protect cardiac function (Theuer et al., 2002; Cau et al., 2015). In the present study, PDTC treatment might alleviate structural damage in the locally irradiated heart. Such a protective effect might be associated with the suppression of NF-κB. Taken together, these results suggested that the suppression of NF-κB, HIF-1α, CTGF, and COL-1 might be a potential mechanism for the cardiac protection of PDTC. Furthermore, due to the advantage of safe, easy application, and low cost, PDTC might be a promising agent for the clinical therapy of RIHD.

There are several limitations to be mentioned herein. First, we observed the effects of PDTC on left ventricular systolic function and cardiac inflammation and pro-fibrotic cardiac change only at the 14th day after irradiation. Therefore, long-term studies, especially up to 3–6 months, are needed. Second, we observed primary cardiac injury in rats by HE staining did not evaluate the pro-inflammatory cell infiltrate and the kind of cells are involved with specific markers. Third, we showed that NF-κB, HIF-1α, CTGF, and COL-1 might be related to the early stage of radiation-induced cardiac injury. PPI network analysis indicated that there might be a stepwise interaction between NF-κB, HIF-1α, CTGF, and COL-1A1 or COL-1A2; however, confident study that signaling expression regulated by the activation of the NF-κB/HIF-1α/CTGF/COL-1 signaling pathway regulated by the activation of NF-κB in rat myocardial cells or primary cultures *in vitro* experiments or transgenic animals was needed to be conducted.

5 CONCLUSION

In conclusion, this study demonstrated that radiation-induced myocardial cell edema, partial myocardial cell-disordered arrangement, inflammation infiltration, and pro-fibrotic cardiac change could be observed as early as the 14 days after irradiation in rats, but there was no significant damage

to the function of left ventricular at the very early stage. PDTC treatment to some extent alleviated structural damage in the locally irradiated heart. Such a protective effect might be associated with the suppression of NF-κB. This study provides evidence that PDTC might be a potential clinical approach to address RIHD.

DATA AVAILABILITY STATEMENT

The raw data supporting the conclusions of this article will be made available by the authors, without undue reservation.

ETHICS STATEMENT

The animal study was reviewed and approved by the Animal Care and Ethical Committee of Hebei Medical University.

AUTHOR CONTRIBUTIONS

JW designed the experiments, analyzed the data, and revised the manuscript. YW designed and performed experiments, analyzed the data, and wrote the manuscript. SL performed the experiments of echocardiography, Western blotting, and RT-PCR at the Department of Physiology of Hebei Medical University. LL and SW managed the rats and established the RIHD animal model. YW and JZ reviewed and embellished the manuscript. SW analyzed the data and provided technical support. All authors read and approved the final manuscript.

FUNDING

The authors gratefully acknowledge the financial supports by the Hebei Clinical Research Center for Radiation Oncology under Grant number 2057702D. The work was supported by the Natural Science Foundation of Hebei Province (H2021206293 and H2020206348) and the Innovative Research Group Project of Hebei Province Natural Science Foundation (H2021206203). It was a great honor that part of the manuscript as an abstract entitled "PDTC Attenuates Radiation Induced Heart Damage Through Inhibition of Activation of NF-kB and Its Downstream Pathway in Rats" (ID: 3427) was selected for presentation during the ASTRO's 59th Annual Meeting in 2017.

REFERENCES

Angelini, A., Li, Z., Mericskay, M., and Decaux, J. F. (2015). Regulation of Connective Tissue Growth Factor and Cardiac Fibrosis by an SRF/MicroRNA-133a Axis. *PLoS One* 10, e0139858. doi:10.1371/journal.pone.0139858

Boerma, M. (2012). Experimental Radiation-Induced Heart Disease: Past, Present, and Future. *Radiat. Res.* 178, 1–6. doi:10.1667/rr2933.1

Boerma, M., Roberto, K. A., and Hauer-Jensen, M. (2008). Prevention and Treatment of Functional and Structural Radiation Injury in the Rat Heart by Pentoxifylline and Alpha-Tocopherol. *Int. J. Radiat. Oncol. Biol. Phys.* 72 (1), 170–177. doi:10.1016/j.ijrobp.2008.04.042

Cataldi, A., Rapino, M., Centurione, L., Sabatini, N., Grifone, G., Garaci, F., et al. (2003). NF-kappaB Activation Plays an Antiapoptotic Role in Human Leukemic K562 Cells Exposed to Ionizing Radiation. *J. Cel Biochem* 89, 956–963. doi:10.1002/jcb.10560

Cau, S. B., Guimaraes, D. A., Rizzi, E., Ceron, C. S., Gerlach, R. F., and Tanus-Santos, J. E. (2015). The Nuclear Factor kappaB Inhibitor Pyrrolidine Dithiocarbamate Prevents Cardiac Remodelling and Matrix Metalloproteinase-2 Up-Regulation in Renovascular Hypertension. *Basic Clin. Pharmacol. Toxicol.* 117, 234–241. doi:10.1111/bcpt.12400

Chabicovsky, M., Prieschl-Grassauer, E., Seipelt, J., Muster, T., Szolar, O. H., Hebar, A., et al. (2010). Pre-clinical Safety Evaluation of Pyrrolidine Dithiocarbamate. *Basic Clin. Pharmacol. Toxicol.* 107, 758–767. doi:10.1111/j.1742-7843.2010.00573.x

Chang, H. M., Okwuosa, T. M., Scarabelli, T., Moudgil, R., and Yeh, E. T. H. (2017). Cardiovascular Complications of Cancer Therapy: Best Practices in Diagnosis, Prevention, and Management: Part 2. *J. Am. Coll. Cardiol.* 70 (20), 2552–2565. doi:10.1016/j.jacc.2017.09.1095

Cuzzocrea, S., Chatterjee, P. K., Mazzon, E., Dugo, L., Serraino, I., Britti, D., et al. (2002). Pyrrolidine Dithiocarbamate Attenuates the Development of Acute and Chronic Inflammation. *Br. J. Pharmacol.* 135, 496–510. doi:10.1038/sj.bjp.0704463

Gürses, İ., Özeren, M., Serin, M., Yücel, N., and Erkal, H. Ş. (2014). Histopathological Evaluation of Melatonin as a Protective Agent in Heart Injury Induced by Radiation in a Rat Model. *Pathol. - Res. Pract.* 210 (12), 863–871. doi:10.1016/j.prp.2014.08.006

Halle, M., Gabrielsen, A., Paulsson-Berne, G., Gahm, C., Agardh, H. E., Farnebo, F., et al. (2010). Sustained Inflammation Due to Nuclear Factor-Kappa B Activation in Irradiated Human Arteries. *J. Am. Coll. Cardiol.* 55, 1227–1236. doi:10.1016/j.jacc.2009.10.047

Han, W., Li, H., Cai, J., Gleaves, L. A., Polosukhin, V. V., Segal, B. H., et al. (2013). NADPH Oxidase Limits Lipopolysaccharide-Induced Lung Inflammation and Injury in Mice through Reduction-Oxidation Regulation of NF-Kb Activity. *J. Immunol.* 190, 4786–4794. doi:10.4049/jimmunol.1201809

Haydont, V., Riser, B. L., Aigueperse, J., and Vozenin-Brotons, M. C. (2008). Specific Signals Involved in the Long-Term Maintenance of Radiation-Induced Fibrogenic Differentiation: a Role for CCN2 and Low Concentration of TGF-Beta1. *Am. J. Physiol. Cel Physiol* 294, C1332–C1341. doi:10.1152/ajpcell.90626.2007

Hufnagle, J. J., Andersen, S. N., and Maani, E. V. (2021). "Radiation Therapy Induced Cardiac Toxicity," in *StatPearls [Internet]* (Treasure Island (FL: StatPearls Publishing).

Korbecki, J., Simińska, D., Gąssowska-Dobrowolska, M., Listos, J., Gutowska, I., Chlubek, D., et al. (2021). Chronic and Cycling Hypoxia: Drivers of Cancer Chronic Inflammation through HIF-1 and NF-Kb Activation: A Review of the Molecular Mechanisms. *Int. J. Mol. Sci.* 22 (19), 10701. doi:10.3390/ijms221910701

Lam, R. K., Han, W., and Yu, K. N. (2015). Unirradiated Cells rescue Cells Exposed to Ionizing Radiation: Activation of NF-Kb Pathway in Irradiated Cells. *Mutat. Res.* 782, 23–33. doi:10.1016/j.mrfmmm.2015.10.004

Lang, R. M., Badano, L. P., Mor-Avi, V., Afilalo, J., Armstrong, A., Ernande, L., et al. (2015). Recommendations for Cardiac Chamber Quantification by Echocardiography in Adults: an Update from the American Society of Echocardiography and the European Association of Cardiovascular Imaging. *Eur. Heart J. Cardiovasc. Imaging* 16, 233–270. doi:10.1093/ehjci/jev014

Mehta, L. S., Watson, K. E., Barac, A., Beckie, T. M., Bittner, V., Cruz-Flores, S., et al. (2018). Cardiovascular Disease and Breast Cancer: where These Entities Intersect: a Scientific Statement from the American Heart Association. *Circulation* 137 (8), e30–66. doi:10.1161/CIR.0000000000000556

Meng, A., Yu, T., Chen, G., Brown, S. A., Wang, Y., Thompson, J. S., et al. (2003). Cellular Origin of Ionizing Radiation-Induced NF-kappaB Activation *In Vivo*

and Role of NF-kappaB in Ionizing Radiation-Induced Lymphocyte Apoptosis. *Int. J. Radiat. Biol.* 79, 849–861. doi:10.1080/09553000310001622814

Mezzaroma, E., Di, X., Graves, P., Toldo, S., Van Tassell, B. W., Kannan, H., et al. (2012). A Mouse Model of Radiation-Induced Cardiomyopathy. *Int. J. Cardiol.* 156 (2), 231–233. doi:10.1016/j.ijcard.2012.01.038

Ping, Z., Peng, Y., Lang, H., Xinyong, C., Zhiyi, Z., Xiaocheng, W., et al. (2020). Oxidative Stress in Radiation-Induced Cardiotoxicity. *Oxid Med. Cel Longev* 2020, 3579143. doi:10.1155/2020/3579143

Schultz-Hector, S., and Trott, K. R. (2007). Radiation-induced Cardiovascular Diseases: Is the Epidemiologic Evidence Compatible with the Radiobiologic Data? *Int. J. Radiat. Oncol. Biol. Phys.* 67, 10–18. doi:10.1016/j.ijrobp.2006.08.071

Sies, H., Berndt, C., and Jones, D. P. (2017). Oxidative Stress. *Annu. Rev. Biochem.* 86, 715–748. doi:10.1146/annurev-biochem-061516-045037

Sridharan, V., Seawright, J. W., Antonawich, F. J., Garnett, M., Cao, M., Singh, P., et al. (2017). Late Administration of a Palladium Lipoic Acid Complex (POLY-MVA) Modifies Cardiac Mitochondria but Not Functional or Structural Manifestations of Radiation-Induced Heart Disease in a Rat Model. *Radiat. Res.* 187 (3), 361–366. doi:10.1667/RR14643.1

Sridharan, V., Tripathi, P., Sharma, S. K., Moros, E. G., Corry, P. M., Lieblong, B. J., et al. (2012). Cardiac Inflammation after Local Irradiation Is Influenced by the Kallikrein-Kinin System. *Cancer Res.* 72, 4984–4992. doi:10.1158/0008-5472.CAN-12-1831

Survivorship, N. C. I. Oo. C. (2019). *Statistics: National Cancer Institute: Statistics*. United States: National Cancer Institute. Available from: https://cancercontrol.cancer.gov/ocs/statistics.

Tapio, S. (2016). Pathology and Biology of Radiation-Induced Cardiac Disease. *J. Radiat. Res.* 57 (5), 439–448. doi:10.1093/jrr/rrw064

Theuer, J., Dechend, R., Muller, D. N., Park, J. K., Fiebeler, A., Barta, P., et al. (2002). Angiotensin II Induced Inflammation in the Kidney and in the Heart of Double Transgenic Rats. *BMC Cardiovasc. Disord.* 2, 3. doi:10.1186/1471-2261-2-3

Van Uden, P., Kenneth, N. S., and Rocha, S. (2008). Regulation of Hypoxia-Inducible Factor-1alpha by NF-kappaB. *Biochem. J.* 412, 477–484. doi:10.1042/BJ20080476

Vozenin-Brotons, M. C., Milliat, F., Sabourin, J. C., de Gouville, A. C., François, A., Lasser, P., et al. (2003). Fibrogenic Signals in Patients with Radiation Enteritis Are Associated with Increased Connective Tissue Growth Factor Expression. *Int. J. Radiat. Oncol. Biol. Phys.* 56, 561–572. doi:10.1016/s0360-3016(02)04601-1

Wang, J., Wu, Y., Yuan, F., Liu, Y., Wang, X., Cao, F., et al. (2016). Chronic Intermittent Hypobaric Hypoxia Attenuates Radiation Induced Heart Damage in Rats. *Life Sci.* 160, 57–63. doi:10.1016/j.lfs.2016.07.002

Weintraub, N. L., Jones, W. K., and Manka, D. (2010). Understanding Radiation-Induced Vascular Disease. *J. Am. Coll. Cardiol.* 55, 1237–1239. doi:10.1016/j.jacc.2009.11.053

Yi, P., Li, H., Fang, Y., Su, J., Xu, C., Cao, L., et al. (2020). Administration of Trastuzumab with Heart Irradiation Induced Acute Cardiotoxicity in Mice. *Am. J. Cancer Res.* 10 (2), 536–544.

Zhou, J. J., Wei, Y., Zhang, L., Zhang, J., Guo, L. Y., Gao, C., et al. (2013). Chronic Intermittent Hypobaric Hypoxia Prevents Cardiac Dysfunction through Enhancing Antioxidation in Fructose-Fed Rats. *Can. J. Physiol. Pharmacol.* 91, 332–337. doi:10.1139/cjpp-2012-0059

Conflict of Interest: The authors declare that the research was conducted in the absence of any commercial or financial relationships that could be construed as a potential conflict of interest.

Publisher's Note: All claims expressed in this article are solely those of the authors and do not necessarily represent those of their affiliated organizations, or those of the publisher, the editors and the reviewers. Any product that may be evaluated in this article, or claim that may be made by its manufacturer, is not guaranteed or endorsed by the publisher.

frontiers | Frontiers in Pharmacology

ORIGINAL RESEARCH
published: 04 April 2022
doi: 10.3389/fphar.2022.823975

Setanaxib (GKT137831) Ameliorates Doxorubicin-Induced Cardiotoxicity by Inhibiting the NOX1/NOX4/Reactive Oxygen Species/MAPK Pathway

Hui Zheng[1], *Nannan Xu*[2], *Zihao Zhang*[3], *Fen Wang*[1], *Jie Xiao*[4]* and *Xiaoping Ji*[1]*

[1]The Key Laboratory of Cardiovascular Remodeling and Function Research, Chinese Ministry of Education, Chinese National Health Commission and Chinese Academy of Medical Sciences, The State and Shandong Province Joint Key Laboratory of Translational Cardiovascular Medicine, Department of Cardiology, Qilu Hospital, Cheeloo College of Medicine, Shandong University, Jinan, China, [2]Department of Infectious Diseases, Qilu Hospital, Cheeloo College of Medicine, Shandong University, Jinan, China, [3]Department of Cardiology, Weihai Central Hospital, Weihai, China, [4]Department of Critical Care Medicine, Qilu Hospital, Cheeloo College of Medicine, Shandong University, Jinan, China

OPEN ACCESS

Edited by:
Zhi-Ren Zhang,
Harbin Medical University, China

Reviewed by:
Jwu-Lai Yeh,
Kaohsiung Medical University, Taiwan
Çimen Karasu,
Gazi University, Turkey

***Correspondence:**
Xiaoping Ji
jixiaoping@sdu.edu.cn
Jie Xiao
chrisy-4619.202@163.com

Specialty section:
This article was submitted to Cardiovascular and Smooth Muscle Pharmacology, a section of the journal Frontiers in Pharmacology

Received: *28 November 2021*
Accepted: *16 March 2022*
Published: *04 April 2022*

Citation:
Zheng H, Xu N, Zhang Z, Wang F, Xiao J and Ji X (2022) Setanaxib (GKT137831) Ameliorates Doxorubicin-Induced Cardiotoxicity by Inhibiting the NOX1/NOX4/Reactive Oxygen Species/MAPK Pathway. Front. Pharmacol. 13:823975. doi: 10.3389/fphar.2022.823975

Background: Doxorubicin (DOX)-induced cardiotoxicity is a highly concerning issue, and the mechanism by which DOX induces cardiotoxicity is likely to be multifactorial. NADPH oxidase (NOX) is associated with DOX-induced cardiotoxicity. Setanaxib (GKT137831), a preferential direct inhibitor of NOX1 and NOX4, can delay or prevent the progression of many cardiovascular disorders by inhibiting reactive oxygen species (ROS) generation. In this study, we investigated the role of GKT137831 in ameliorating DOX-induced cardiotoxicity and the potential mechanisms of its action.

Methods and Results: The mice model of cardiotoxicity induced by DOX was established, and GKT137831 treatment was performed at the same time. Neonatal rat cardiomyocytes (NRCMs) were treated with DOX or GKT137831 for *in vitro* experiments. We found that DOX administration impaired cardiac function *in vivo*, reflected by decreased left ventricular ejection fraction (LVEF) and fractional shortening (FS%). DOX also impaired the viability of NRCMs *in vitro*. In addition, DOX increased the levels of NOX1 and NOX4 expression and ROS production and the cardiomyocyte apoptosis rate, both *in vivo* and *in vitro*. GKT137831 improved cardiac function, as indicated by the increased LVEF and FS%. *In vitro,* GKT137831 improved NRCM viability. It also decreased ROS production and the cardiomyocyte apoptosis rate. Apoptotic indices, such as cleaved PARP (c-PARP), cleaved caspase 3 (CC3) and BAX expression levels, were decreased, and the antiapoptotic index of Bcl-2 expression was increased. DOX markedly activated phosphorylated JNK, ERK and p38 proteins in NRCMs. Specific inhibitors of JNK (SP600125), ERK (PD98059) or p38 (SB203580) inhibited DOX-induced apoptosis of NRCMs. GKT137831 pretreatment inhibited excessive DOX-induced MAPK pathway activation.

Conclusion: This study revealed that GKT137831 can alleviate DOX-induced cardiomyocyte apoptosis by inhibiting NOX1/4-driven ROS production. The upregulation of MAPK pathway induced by NOX1/4-derived ROS production may be

the potential mechanism of GKT137831 action. GKT137831 may be a potential drug candidate to ameliorate DOX-induced cardiotoxicity.

Keywords: doxorubicin, cardiotoxicity, GKT137831, NADPH oxidase, apoptosis

INTRODUCTION

Doxorubicin (DOX), the most commonly used anthracycline, remains a prominent treatment in numerous types of cancers. However, dose-dependent cardiotoxicity induced by DOX became apparent soon after its widespread use in the 1970s (Von Hoff et al., 1979). The exact mechanism by which DOX induces cardiotoxicity is likely multifactorial, involving direct pathways affected by reactive oxygen species (ROS) generation (Singal and Iliskovic, 1998) and topoisomerase 2β (Zhang et al., 2012), as well as other indirect pathways.

NADPH oxidases (NOXs) constitute a group of plasma membrane-associated enzymes with the sole function of producing ROS (Altenhofer et al., 2012). The family has seven members, NOX1-5 and the dual oxidase DUOX1-2. These isoforms differ in their regulation, tissue and cellular distribution, subcellular localization and the ROS type that they produce (Elbatreek et al., 2021). NOX-derived ROS are essential modulators of signal transduction pathways that control key physiological activities (Manea et al., 2015). However, excessive and sustained release of NOX-derived ROS may play pathological roles in various diseases, including atherosclerosis (Sheehan et al., 2011; Douglas et al., 2012), hypertension (Touyz et al., 2019), diabetic kidney disease (Jha et al., 2016) and lung fibrosis (Louzada et al., 2021). Furthermore, NOX has been proposed to be involved in another potential enzymatic system leading to ROS production after DOX treatment, and NOX-derived ROS may be involved in the pathological development of DOX-induced cardiotoxicity (Zeng C. et al., 2020; Cheng et al., 2020).

Setanaxib (GKT137831) is a specific dual NOX1 and NOX4 inhibitor. Recent studies have shown that GKT137831 plays a protective role in many cardiovascular disorders. For instance, GKT137831 attenuated the development of diabetes-associated atherosclerosis (Gray et al., 2013) and prevented hypertensive cardiac remodeling and hypertrophy (Zhao et al., 2015; Zeng et al., 2019). However, studies investigating the role of GKT137831 in DOX-induced cardiotoxicity are rare.

Considering the important role of NOX in DOX-induced cardiotoxicity, we hypothesize that GKT137831 may reduce NOX1/NOX4-derived ROS production, thereby reducing ROS-induced apoptosis, and the potential mechanisms of GKT137831 action is discussed in this study.

MATERIALS AND METHODS

Reagents and Antibodies

DOX (MB1087) was obtained from Dalian Meilun Biotechnology Co., Ltd., China. Setanaxib (GKT137831), sodium carboxymethyl cellulose (CMC-Na; S6703), acetylcysteine (NAC; S1623), SP600125 (S1460), PD98059 (S1177), and SB203580 (S1076) were obtained from Selleck Chemicals (Houston, TX, United States). An *In Situ* Cell Death Detection kit, TMR red, for use at room temperature (RT) (cat. no. 12156792910) was obtained from Roche Diagnostics (Mannheim, Germany). A lactate dehydrogenase (LDH) assay kit (C0016), JC-1 kit (C2006), and ROS assay kit (S0033S) were obtained from Beyotime (Shanghai, China). A frozen section reactive oxygen detection kit (BB-470513) was obtained from Shanghai Beibo Biotechnology Co., Ltd., China.

Antibodies against NOX4 were purchased from Invitrogen (PA5-53304, CA, United States), and Abcam (ab133303, Cambridge, United Kingdom). An antibody against NOX1 (PA5-103220) was purchased from Invitrogen. An antibody against cardiac troponin I (66376-1-Ig) was purchased from Proteintech (Wuhan, China). Antibodies against PARP (#9542), cleaved caspase 3 (#9661), JNK (#9252), p-p44/42 MAPK (Erk1/2) (#4370), p44/42 MAPK (Erk1/2) (#4695), p-p38 MAPK (#4511), p38 MAPK (#8690), and β-actin (#4970) were purchased from Cell Signaling Technology (Shanghai, China). Antibodies against Bcl-2 (ab182858), Bax (ab32503), 4-Hydroxynonenal (4-HNE, ab46545), and p-JNK (ab76572) were purchased from Abcam.

Animal Experiments

Eight-week-old male C57BL/6J mice were obtained from ViewSolid Biotech (Beijing, China). After 1 week of adaptive feeding, the mice were randomly assigned to four groups: a control, control + GKT137831, DOX, and DOX + GKT137831 group, n = 10, 10, 20, 20 per group, respectively. To establish the DOX and DOX + GKT137831 groups, mice were injected with a cumulative dose of 20 mg/kg DOX [5 mg/kg Intraperitoneal (i.p.) injection at 0, 7, 14, and 21 days], while an equivalent volume of saline was administered by i.p. injection to the control and control + GKT137831 groups. After the first injection, the control + GKT137831 and DOX + GKT137831 group mice were treated with GKT137831 (60 mg/kg/d) by gavage, and an equivalent volume of 0.5% CMC-Na was administered to the control and DOX group mice by gavage. The mice were euthanized 6 weeks after the first injection. All animal experimental protocols complied with the Animal Management Rules of the Chinese Ministry of Health (document no. 55, 2001) and conformed to National Institutes of Health (NIH) guidelines (the Guide for the Care and Use of Laboratory Animals; NIH Publication No. 85-23, revised 1996).

Echocardiography

Transthoracic echocardiography was performed using a VisualSonics Vevo 2100 system equipped with an MS400 transducer (Visual Sonics). Anesthesia (5% isoflurane) was administered, and the mice remained under general anesthesia

with continuous administration of 2% isoflurane during echocardiogram acquisition. Indices of systolic function were obtained from long-axis M-mode scans. The parameters collected included left ventricular ejection fraction (LVEF), fractional shortening (FS%), end-systolic interventricular septal wall thickness (IVSS), end-diastolic interventricular septal wall thickness (IVSD), left ventricular end-systolic diameter (LVESD), left ventricular end-diastolic diameter (LVEDD), left ventricular end-systolic posterior wall (LVPWs), and left ventricular end-diastolic posterior wall (LVPWd).

Histological Analysis

Heart tissues were harvested, washed, fixed immediately in 4% paraformaldehyde and embedded in paraffin. Five-micrometer sections were collected and subjected to hematoxylin and eosin (HE) and Masson's trichrome staining. Immunofluorescence (IF) was performed to assess the expression of NOX1 and NOX4 after DOX treatment *in vivo*. To monitor oxidative stress status, frozen heart sections were stained with dihydroethidium (DHE). Transmission electron microscopy (TEM) was used to observe ultrastructural changes.

Immunofluorescence

After paraffin-embedded mouse heart section rehydration, heat antigen retrieval, 3% H_2O_2 treatment, 0.4% Triton X-100 (T8200; Solarbio, Beijing, China) treatment and washing with PBS, slides with the sections were blocked with 5% goat serum (SL038; Solarbio) for 30 min at 37°C, followed by overnight incubation with primary antibodies against NOX1 (1:200 dilution), NOX4 (1:200 dilution), and cTnI (1:200 dilution) at 4°C in a humid chamber. After washing, the slides were incubated with secondary antibodies (1:200 dilution, ZSGB-BIO) for 1 h at 37°C. The slides were covered with a drop of DAPI (Abcam) before being observed with a microscope (Nikon).

Neonatal Rat Rardiomyocytes Culture and Treatment

Culture of primary NRCMs was prepared as described previously (Li et al., 2014). NRCMs were incubated in high-glucose DMEM (HG-DMEM) supplemented with 8% horse serum, 5% newborn calf serum, penicillin (100 U/ml), streptomycin (100 mg/ml) and 100 μM bromodeoxyuridine. The cells were then diluted and plated in different culture dishes according to the specific experimental requirements. 24 h after plating, the culture medium was changed to HG-DMEM supplemented with 1.6% horse serum, 1% newborn calf serum, penicillin (100 U/ml), streptomycin (100 mg/ml) and 100 μM bromodeoxyuridine for another 48 h. On the fourth day after plating, experiments were initiated. In some experiments, NRCMs were treated with different concentrations of DOX for 24 h or pretreated with GKT137831 (5 μmol/L) for 1 h, NAC (10 mmol/L) for 1 h, SP600125 (10 μmol/L) for 1 h, PD98059 (10 μmol/L) for 1 h, SB203580 (10 μmol/L) for 1 h and then stimulated with DOX (2 μmol/L) for 24 h. Cells were then processed for further examination, such as IF microscopy or Western blotting.

Cell Injury Evaluation

Cell damage was assessed by determining the level of LDH from the cells with an LDH detection kit according to the manufacturer's instructions. The absorbance of the samples was measured with a microplate reader at a wavelength of 490 nm.

Measurement of Reactive Oxygen Species

Evaluation of the level of intracellular ROS was carried out with a reactive oxygen species assay kit. Measurements were based on the manufacturer's instructions. Cells treated with Rosup (50 μg/ml) for 20 min were used as positive controls.

Western Blot Analysis

Proteins were separated by 10% or 12% sodium dodecyl sulfate-polyacrylamide gel electrophoresis (SDS-PAGE) and then transferred to PVDF membranes (Millipore, United States). After the membranes were blocked with 5% skimmed milk for 1 h at room temperature, they were incubated with primary antibodies against NOX4 (1:1,000), NOX1 (1:1,000), PARP (1:1,000), Bcl-2 (1:2,000), BAX (1:1,000), cleaved caspase-3 (1:1,000), 4-HNE (1:2,000), p-JNK (1:5,000), JNK (1:1,000), p-ERK (1:1,000), ERK (1:1,000), p-p38 (1:1,000), p38 (1:1,000), and β-actin (1:1,000) overnight at 4°C. The membranes were then washed with TBST, followed by incubation with the appropriate horseradish peroxidase-conjugated secondary antibody (1:5,000 dilution; ZSGB-BIO, Beijing, China) for 1 h at room temperature. Protein bands were visualized using an Amersham Imager 680 electrochemiluminescence instrument (General Electric Company).

JC-1 Staining

Mitochondrial membrane potential (ΔΨm) was measured with a JC-1 kit based on the manufacturer's instructions. Briefly, after removing the culture medium, the cells were rinsed with PBS, and 500 μl of fresh medium was added, and then, 500 μl of JC-1 stain was added and incubated for 20 min in a 37°C incubator with 5% CO_2. Then, the supernatant was removed, and the cells were washed twice with JC-1 stain (1×). Next, we added 1 ml of fresh HG-DMEM. We then observed and photographed the cells with a laser scanning confocal microscope (LSM710; Zeiss).

TUNEL Staining

Apoptotic cells in the myocardium and the neonatal rat cardiomyocyte (NRCM) were detected by the use of a commercial DNA fragmentation detection kit (*In Situ* Cell Death Detection Kit, TMR red; Roche) followed by the manufacturer's instructions.

Statistics Analysis

The results are expressed as the means ± SD. All experiments were independently repeated at least three times. Statistical comparisons between 2 groups were performed *via* Student's t-test (data with normal distribution and homogeneity of variance) or Mann-Whitney test (data not normally distributed or without homogeneity of variance). Statistical comparisons between multiple groups were carried out by one-way ANOVA followed by LSD test (data with normal distribution and homogeneity of variance) or Kruskal-Wallis test followed by Dunn's test (data not normally distributed or

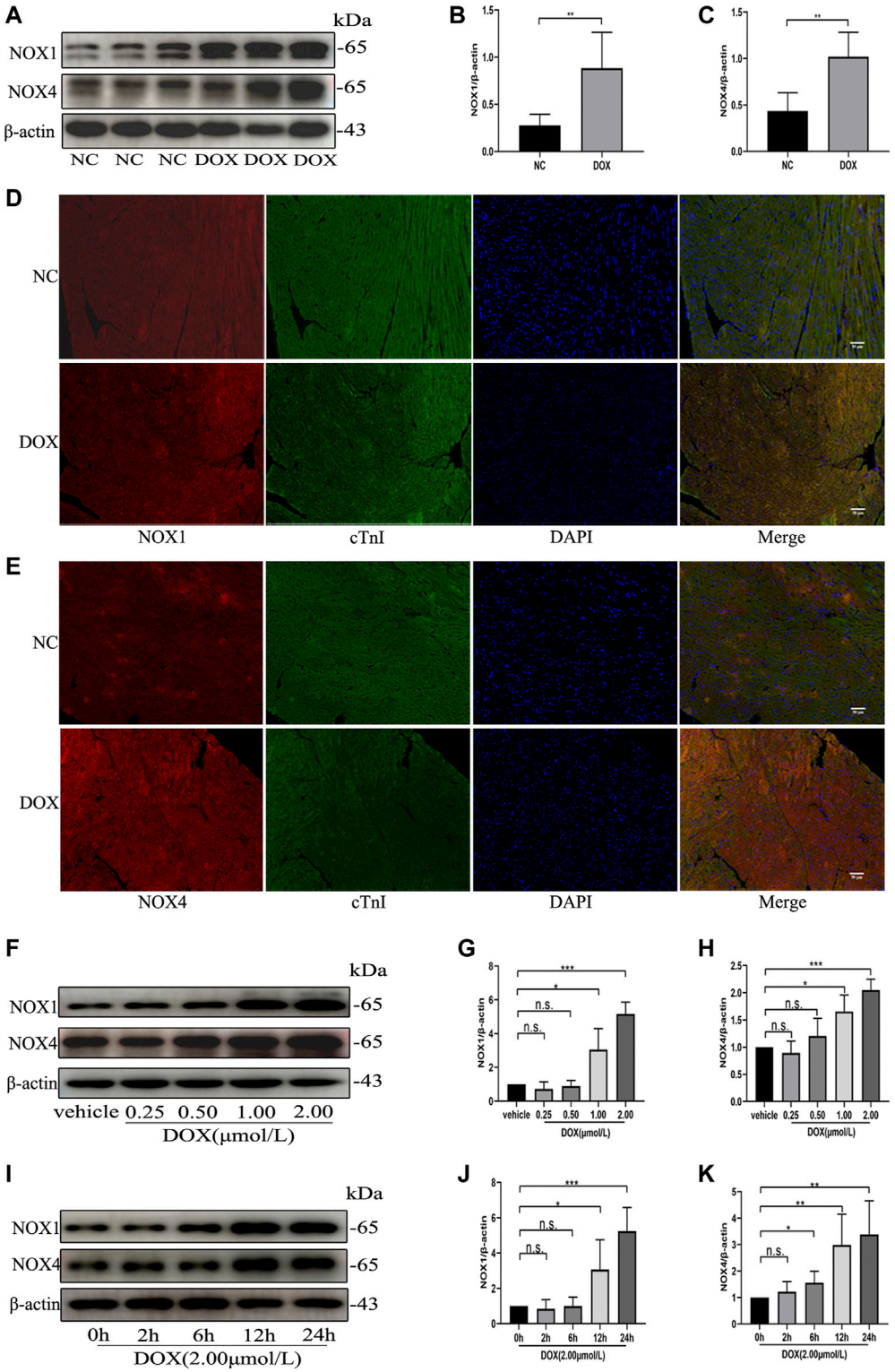

FIGURE 1 | The protein levels of NOX1 and NOX4 were increased by DOX both *in vivo* and *in vitro*. **(A)** Representative western blot analysis of NOX1 and NOX4 in myocardial tissue. **(B,C)** Quantification of NOX1 and NOX4 expression relative to the β-actin level (n = 6 per group). **(D,E)** Representative images of NOX1 and NOX4 expression in myocardial tissue detected by the immunofluorescence. The nuclei were stained with DAPI (Scale bar = 50 μm). **(F)** Representative western blot analysis of NOX1 and NOX4 of NRCMs treated with DOX of different concentrations for 24 h **(G,H)** Quantification of NOX1 and NOX4 expression relative to the β-actin level (n = 3). **(I)** Representative western blot analysis of NOX 1 and NOX 4 of NRCMs treated with DOX for different time. **(J,K)** Quantification of NOX1 and NOX4 expression relative to the β-actin level (n = 4–5). *p < 0.05, **p < 0.01, ***p < 0.001, n. s., not significant. NOX, NADPH oxidase; DOX, doxorubicin; cTnI, Cardiac troponin I.

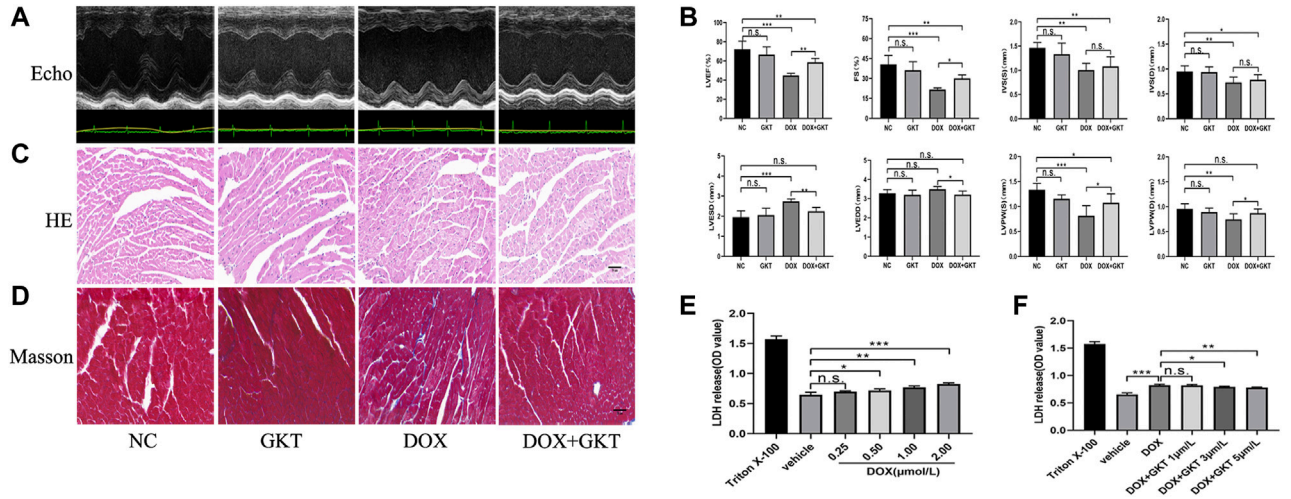

FIGURE 2 | GKT137831 alleviated DOX-induced cardiac dysfunction *in vivo* and attenuated diminished cell viability *in vitro*. **(A)** Representative M-mode echocardiograms. **(B)** Echocardiographic analysis of LVEF, FS, IVSS, IVSD, LVESD, LVEDD, LVPWS, and LVPWD ($n = 5–6$ per group). **(C,D)** Representative images with HE and Masson's trichrome staining in myocardial tissue (scar bar = 50 μm). **(E)** NRCMs were stimulated with DOX for 24 h and followed by LDH assay to evaluate the cell viability ($n = 4$). **(F)** NRCMs were pretreated with different concentrations of GKT for 1 h before DOX (2 μM) stimulation. The cell viability was evaluated by LDH assay ($n = 4$). $^{*}p < 0.05$, $^{**}p < 0.01$, $^{***}p < 0.001$, n. s., not significant. Echo, echocardiography; DOX, doxorubicin; GKT, GKT137831; LVEF, left ventricular ejection fraction; FS, fractional shortening; IVSS, end-systolic inter-ventricular septal wall thickness; IVSD, end-diastolic inter-ventricular septal wall thickness; LVESD, left ventricular end-systolic diameter; LVEDD, left ventricular end-diastolic diameter; LVPWS, left ventricular end-systolic posterior wall; LVPWD, left ventricular end-diastolic posterior wall; LDH, lactic dehydrogenase.

without homogeneity of variance). Kaplan-Meier survival analysis was completed using the Log-rank (Mantel-Cox) test. The data were analyzed using SPSS 26.0 and GraphPad Prism 8.0 software. $p < 0.05$ was considered to be statistically significant.

RESULTS

The Protein Levels of NOX1 and NOX4 Were Increased by Doxorubicin Both *in vivo* and *in vitro*

We first examined the effect of DOX on Nox1 and Nox4 protein expression in the mouse myocardium. As shown in **Figures 1A–E**, Western blot and immunofluorescence analyses demonstrated that the protein levels of NOX1 and NOX4 were significantly increased in the DOX-treated mouse myocardium, comparing with the control group. The Western blot analysis also demonstrated that the protein expression of NOX1 and NOX4 in the NRCMs was increased in a dose-dependent and time-dependent manner (**Figures 1F–K**) after DOX exposure. These results indicated that upregulation of NOX1 and NOX4 expression might be involved in DOX-induced cardiotoxicity.

GKT137831 Alleviated Doxorubicin-Induced Cardiac Dysfunction *in vivo* and Attenuated Diminished Cell Viability *in vitro*

After 6 weeks of treatment, all mice in the control group and the control + GKT137831 group survived. In contrast, 55% (11/20) mice survived in the DOX-treated group and 65% (13/20) mice survived in the DOX + GKT137831 group, and there was no significant difference between the two groups ($p > 0.05$, **Supplementary Figure S1**). As depicted in **Figures 2A,B**, the graph of echocardiogram data and the statistical results showed that DOX administration decreased the LVEF (EF %), FS (FS%), thickness of IVS, LVPW and increased the LVESD. Though LVEDD increased, which had no significant difference compared with the control group. GKT137831 treatment was highly effective in attenuating DOX-induced LV dilation and worsening of EF% and FS%, although GKT137831 itself exhibited little effect. *In vivo*, HE and Masson's staining showed that the cardiomyocytes in the DOX-treated group were disorganized, with increased cytoplasmic vacuolization and myocardial fibrosis. Following treatment with GKT137831, DOX-induced cardiomyocyte injury was alleviated, as indicated by attenuated morphological changes and decreased cytoplasmic vacuolization and fibrosis (**Figures 2C,D**). *In vitro*, we stimulated NRCMs with DOX to determine whether pretreatment with GKT137831 attenuated diminished cell viability by detecting the release of LDH from NRCMs. Increased LDH release is conversely correlated with cell activity. As shown in **Figure 2E**, DOX stimulation resulted in reduced cell viability in a dose-dependent manner; however, pretreatment with GKT137831 attenuated DOX-induced cardiotoxicity (**Figure 2F**). These results indicated that GKT137831, a dual NOX1 and NOX4 inhibitor, may play a protective role in DOX-induced cardiotoxicity.

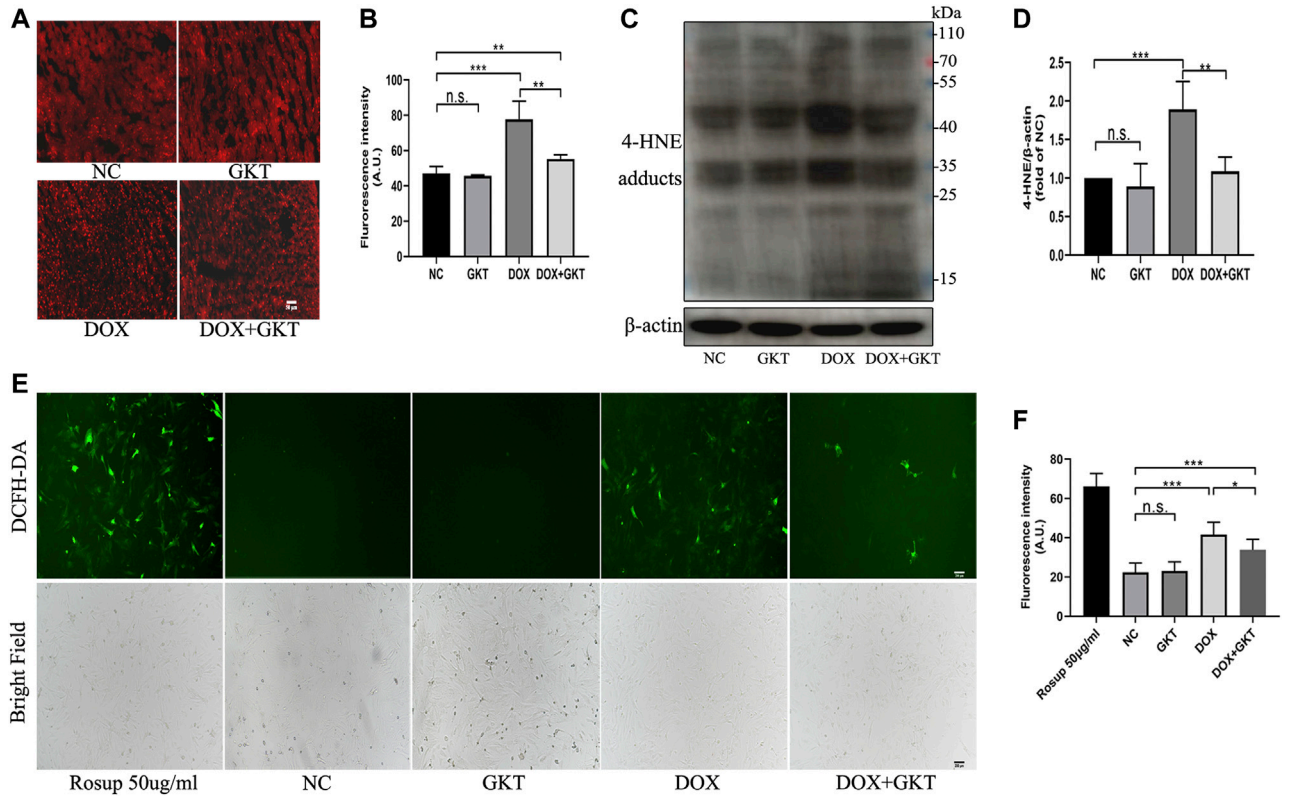

FIGURE 3 | GKT137831 ameliorated oxidative stress both *in vivo* and *in vitro*. **(A,B)** Representative images of myocardial tissue with DHE staining (scar bar = 50 μm) and fluorescence intensity analysis in different groups (n = 5 per group). **(C,D)** Representative images of western blotting for 4-HNE and quantifications by densitometric analysis, β-actin was used as a loading control (n = 5 per group). **(E,F)** Intracellular ROS generation in NRCMs was detected using DCFH-DA probe then evaluated by fluorescence microscopy (scar bar = 200 μm) and fluorescence intensity analysis. NRCMs were pretreated with GKT (5 μM) for 1 h, and then treated with DOX (2 μM) for 24 h. Rosup was used as a ROS positive control (n = 3). $^{*}p < 0.05$, $^{**}p < 0.01$, $^{***}p < 0.001$, n. s., not significant. Abbreviations: DOX, doxorubicin; GKT, GKT137831; DHE, dihydroethidium: 4-HNE, 4-hydroxynonenal: DCFH-DA, dichlorodihydrofluorescein diacetate; AU, arbitrary unit.

GKT137831 Ameliorated Oxidative Stress Both *in vivo* and *in vitro*

First, the Western blot analysis indicated that GKT137831 treatment could inhibit the protein expression of NOX1 and NOX4 compared with the DOX-treated group both *in vivo* and *in vitro* (**Supplementary Figure S2**). Oxidative stress is suggested to be the main cause of DOX-induced cardiotoxicity, thus we detected ROS levels both *in vivo* and *in vitro*. *In vivo*, compared with the control mice, the DHE fluorescence intensity of DOX treated mice was significantly enhanced (**Figures 3A,B**). Western blot-determined level of 4-HNE was also remarkably increased in the hearts of DOX-treated mice (**Figures 3C,D**). These effects were ameliorated by GKT137831 treatment. *In vitro*, a DCFH-DA fluorescence probe was used to measure intracellular ROS in the different groups. As shown in **Figures 3E,F**, GKT137831 pretreatment ameliorated DOX-induced ROS production, as measured by the green fluorescence intensity of DCFH-DA. All these results indicated that GKT137831 ameliorates NOX1/4-derived ROS both *in vivo* and *in vitro*.

GKT137831 Alleviated Doxorubicin-Induced Mitochondrial Damage Both *in vivo* and *in vitro*

Considering that mitochondria are the major subcellular targets of DOX, we performed TEM to examine mitochondrial morphology *in vivo*. We found that DOX induced abnormal changes in mitochondrial structure, including irregular arrangement, swelling, vacuolated and disrupted cristae in the mouse heart. The effects were alleviated by GKT137831 treatment (**Figure 4A**). *In vitro*, JC-1 staining indicated that Δψm disruption triggered by DOX was partially restored by pretreatment with GKT137831 (**Figure 4B**). These results indicated that GKT137831 may alleviate DOX-induced mitochondrial damage.

GKT137831 Reduced Doxorubicin-Induced Cardiomyocyte Apoptosis *in vivo*

Excess levels of ROS can lead to activation of cell death processes such as apoptosis (Redza-Dutordoir and Averill-Bates, 2016). The proportion of TUNEL-positive cells was significantly increased in

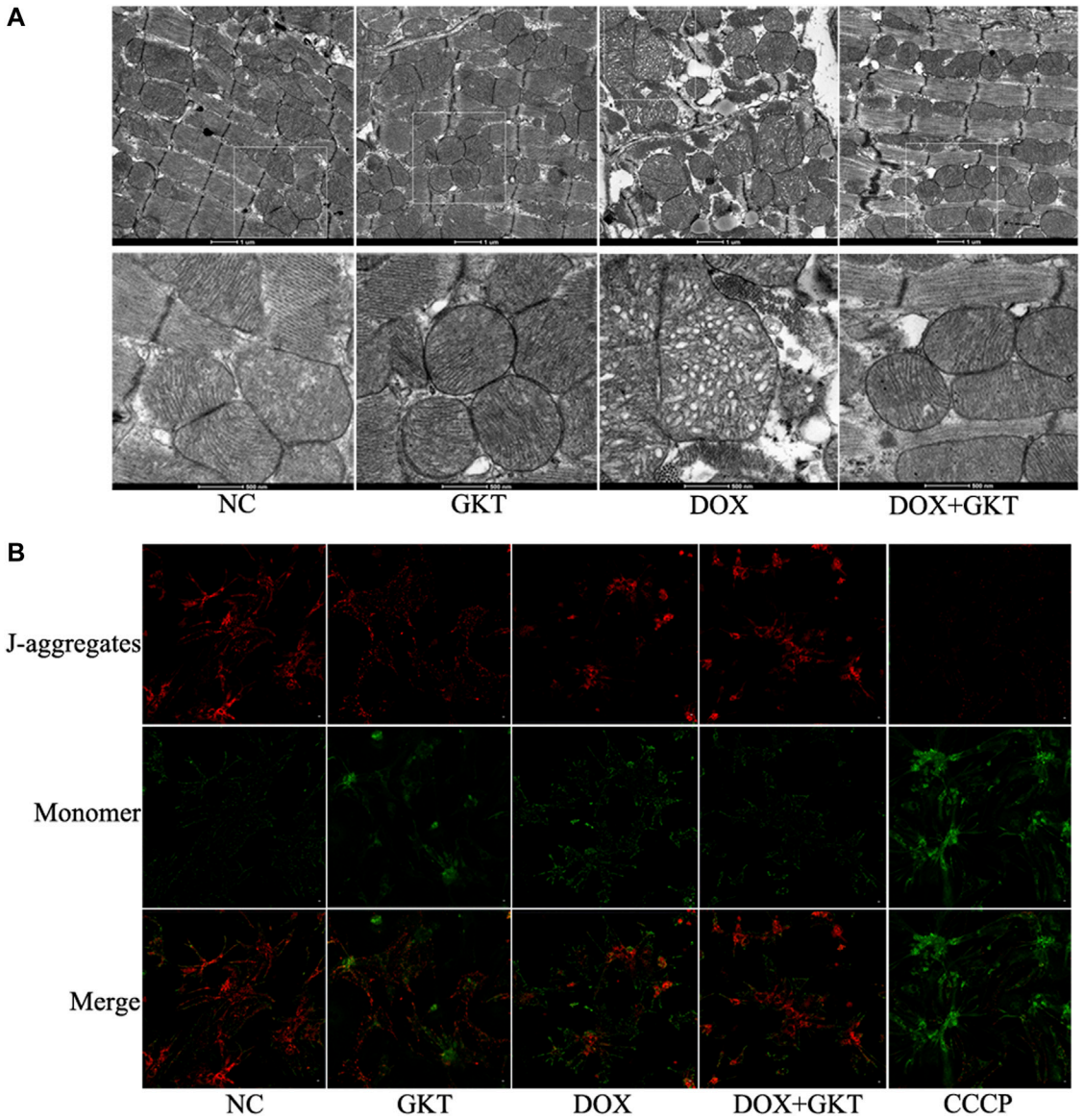

FIGURE 4 | GKT137831 alleviated DOX-induced mitochondrial damage both *in vivo* and *in vitro*. **(A)** Representative transmission electron microscopy image of cardiac mitochondrial ultrastructure. **(B)** Mitochondrial membrane potential measured with JC-1 staining (scale bar = 50 μm). CCCP was used as a positive control. DOX, doxorubicin; GKT, GKT137831; CCCP, carbonyl cyanide m-chlorophenylhydrazone.

DOX-treated mouse hearts. In contrast, fewer TUNEL-positive cells were observed in the GKT137831-treated mice subjected to DOX. GKT137831 treatment itself did not affect the TUNEL-positive cells in the absence of DOX treatment (**Figures 5A,C**). A Western blot analysis demonstrated that the expression of cleaved PARP, BAX and cleaved caspase three was significantly increased, but the expression level of Bcl-2 was downregulated in DOX-treated hearts compared with control hearts, suggesting activation of the apoptotic pathway, and these effects were suppressed by GKT137831 treatment (**Figures 5B,D–G**). These results indicated that GKT137831 may ameliorate DOX-induced cardiomyocyte apoptosis *in vivo* by suppressing NOX1/4-derived ROS production.

GKT137831 Reduced Doxorubicin-Induced Apoptosis of Neonatal Rat Cardiomyocytes

Next, we stimulated NRCMs with DOX to determine whether GKT137831 pretreatment reduced DOX-induced apoptosis *in vitro*. As shown in **Figures 6A,C–F**, pretreatment with GKT137831 attenuated DOX-induced apoptosis, which was confirmed by Western blot analysis of cleaved PARP, Bcl-2, BAX and cleaved caspase three expression. In addition, TUNEL staining revealed that pretreatment with GKT137831 significantly decreased the percentage of TUNEL-positive cells (**Figures 6B,G**). These results indicated that GKT137831 may ameliorate DOX-induced apoptosis in NRCMs by suppressing NOX1/4-derived ROS.

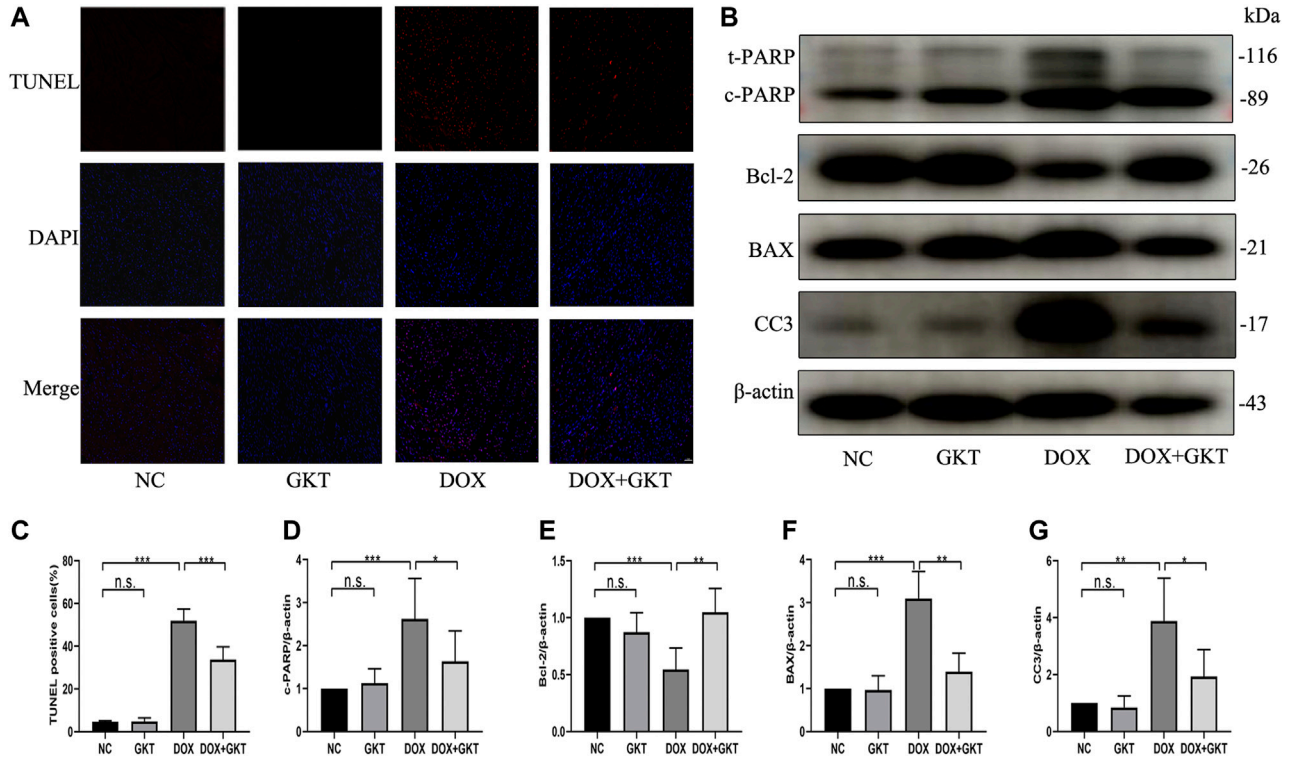

FIGURE 5 | GKT137831 reduced DOX-induced cardiomyocyte apoptosis *in vivo*. **(A,C)** Representative images of TUNEL staining in myocardial tissue (scale bar = 50 μm) and related quantification of TUNEL staining ($n = 5$ per group). **(B)** Representative western blot analysis of c-PARP, Bcl-2, BAX, and CC3 in myocardial tissue, and quantifications by densitometric analysis **(D,E,F,G)**, β-actin was used as a loading control ($n = 5–7$ per group). $^{*}p < 0.05$, $^{**}p < 0.01$, $^{***}p < 0.001$, n. s., not significant. DOX, doxorubicin; GKT, GKT137831; c-PARP, cleaved PARP; CC3, cleaved caspase 3.

GKT137831 Ameliorated Doxorubicin-Induced Apoptosis by Inhibiting the MAPK Pathway

To test the effect of DOX on the activation of MAPK pathway, NRCMs were treated with DOX for the indicated times. As shown in **Figures 7A,E–G**, DOX enhanced the phosphorylation and activation of JNK, ERK, and p38 in a time-dependent manner; however, DOX treatment did not induce significant changes in the total levels of JNK, ERK or p38. When we used specific inhibitors against JNK (SP600125), ERK (PD98059) or p38 (SB203580), the levels of the apoptosis indicators cleaved PARP and cleaved caspase three were decreased (**Figures 7B,H,I**). As shown in **Figures 7C,J**, the proportion of TUNEL-positive NRCMs was markedly decreased. After pretreatment with GKT137831, the phosphorylation and activation of JNK, ERK, and p38 were decreased in DOX-treated NRCMs. To confirm that ROS can trigger MAPK pathway, NAC was used as the positive control (**Figures 7D,K–M**). These results revealed that NOX1/4-derived ROS participate in the activation of MAPK pathway and that GKT137831 ameliorates DOX-induced apoptosis by inhibiting MAPK pathway activation to a certain extent.

DISCUSSION

DOX, the most commonly used anthracycline, plays a prominent role in many cancer treatments. Despite its potency, the clinical application of DOX is limited by its cumulative and dose-related cardiotoxicity. The exact mechanism of DOX-induced cardiotoxicity is multifactorial, and the most widely accepted hypothesis suggests that DOX is related to ROS production (Singal and Iliskovic, 1998). In the myocardium, mitochondria are the major subcellular target of DOX, and its inner membrane consists of cardiolipin, which shows a strong affinity for DOX (Goormaghtigh et al., 1986; Goormaghtigh et al., 1990). Redox cycling of DOX-derived quinone–semiquinone by the NADH dehydrogenase (complex I) of the mitochondrial electron transport chain and the Haber-Weiss reaction without enzymatic involvement are considered to be the major sources of ROS after DOX challenge (Davies and Doroshow, 1986; Berthiaume and Wallace, 2007). However, neither antioxidant nor iron chelation can completely prevent DOX-induced cardiotoxicity (McGowan et al., 2017), suggesting the complexity of the oxidative stress induced.

NADPH oxidase (NOX) is a multicomponent enzyme complex that consists of the membrane-bound subunits

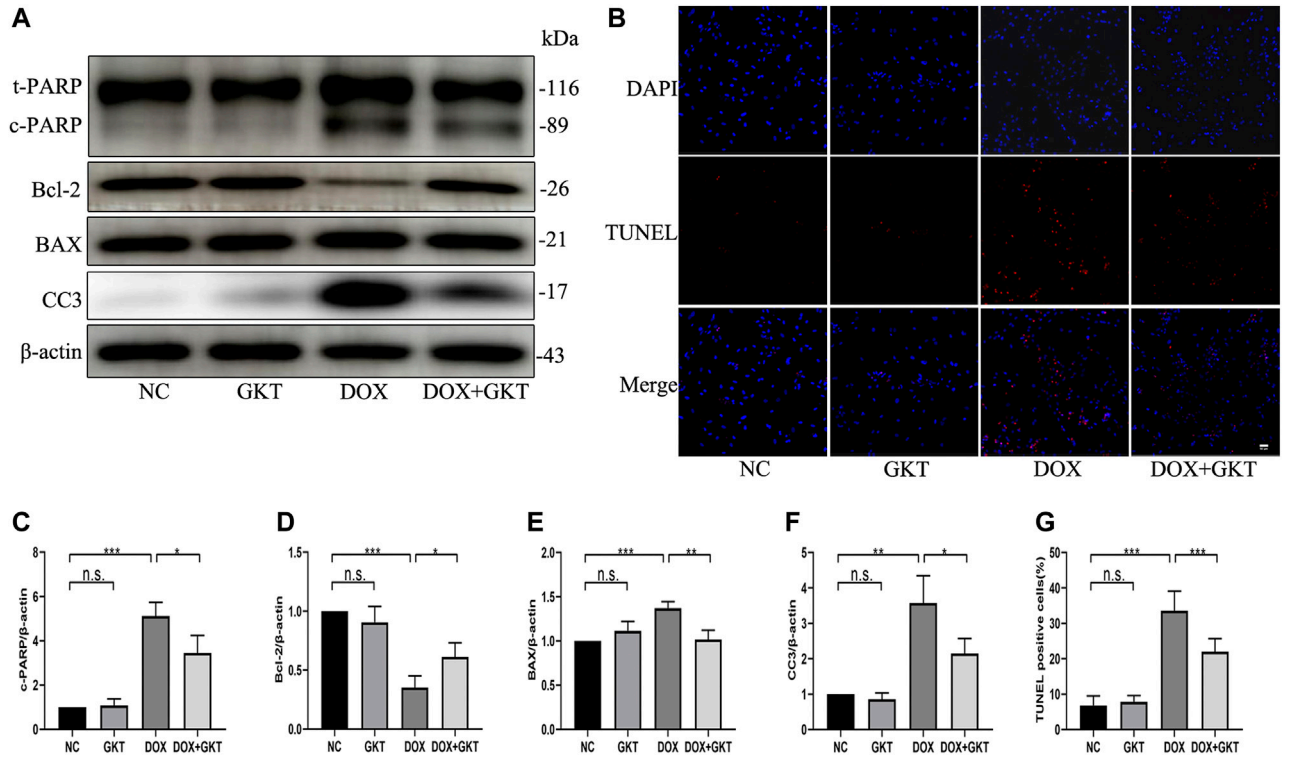

FIGURE 6 | GKT137831 reduced DOX-induced apoptosis of NRCMs. **(A)** Representative western blot analysis of c-PARP, Bcl-2, BAX, and CC3 and quantifications by densitometric analysis **(C,D,E,F)**, β-actin was used as a loading control ($n = 3$). **(B,G)** Representative images of TUNEL staining in NRCMs (scale bar = 50 μm) and related quantification of TUNEL staining ($n = 3$). NRCMs were pretreated with GKT (5 μM) for 1 h, and then treated with DOX (2 μM) for 24 h. $^{*}p < 0.05$, $^{**}p < 0.01$, $^{***}p < 0.001$, n. s., not significant. DOX, doxorubicin; GKT, GKT137831; c-PARP, cleaved PARP; CC3, cleaved caspase 3.

gp91^{phox} and p22^{phox}, the cytosolic regulatory subunits p47^{phox} and p67^{phox}, and the small GTP-binding protein Rac1 (Sumimoto, 2008). It has been proposed that another potential enzymatic system leads to ROS production after DOX treatment. The NOX complex plays an important role in enhancing superoxide production caused by the chemical interaction of DOX and NADPH (Deng et al., 2007). DOX can promote NOX activation, and a series of studies have demonstrated that NOX-derived ROS are implicated in DOX-induced cardiac apoptosis (Gilleron et al., 2009; Zhao et al., 2010). For example, gp91phox-knockout (Deng et al., 2007) or NOX2-deficient mice are resistant to DOX-induced cardiotoxicity (Wojnowski et al., 2005; Zhao et al., 2010; McLaughlin et al., 2017); Rac1 genetic deletion in cardiomyocytes and its inhibitor NSC23766 showed protection against DOX-induced cardiotoxicity (Ma et al., 2013). Therefore, targeting NOXs may be an effective way to reduce DOX-induced cardiotoxicity.

GKT137831 is a preferential direct inhibitor of NOX1 and NOX4 (Elbatreek et al., 2021). It has good pharmacokinetic properties and bioavailability with one or two daily doses administered to rodents or patients (Gorin et al., 2015; Gage and Thippeswamy, 2021). It is also well tolerated and delays or prevents the progression of a range of cardiovascular disorders. For example, GKT137831 attenuated plaque formation by inhibiting ROS generation and reducing the adhesion of inflammatory cells to the vascular wall (Gray et al., 2013); it also markedly attenuated cardiac remodeling by decreasing ROS levels (Zhao et al., 2015) and attenuated hypertensive cardiac hypertrophy by suppressing cardiac inflammation and activating Akt and ERK1/2 (Zeng SY. et al., 2020). It has also been recently tested in clinical trials focused on certain noncardiovascular disorders; for example, a phase II clinical trial with type 2 diabetes nephropathy patients (NCT02010242) and a phase II clinical trial with primary biliary cholangitis patients (NCT03226067) showed GKT137831 efficacy at several primary or secondary endpoints.

Our results showed that DOX increased the levels of NOX1 and NOX4 expression, which was accompanied by elevated ROS production both *in vivo* and *in vitro*. Moreover, DOX triggered apoptosis by increasing the levels of cleaved PARP, cleaved caspase 3, and BAX and reducing the Bcl-2 level. However, GKT137831 treatment decreased ROS generation and attenuated apoptosis. These results indicated that GKT137831 treatment can inhibit NOX1/4-derived ROS production to relieve DOX-induced cardiomyocyte apoptosis.

Then, we further explored the potential mechanism by which GKT137831 reduced DOX-induced myocardium apoptosis. ROS can trigger apoptosis *via* multiple mechanisms, and MAPK pathway is established redox-sensitive mediators involved in the modulation of apoptosis (Son et al., 2011; Kumar et al.,

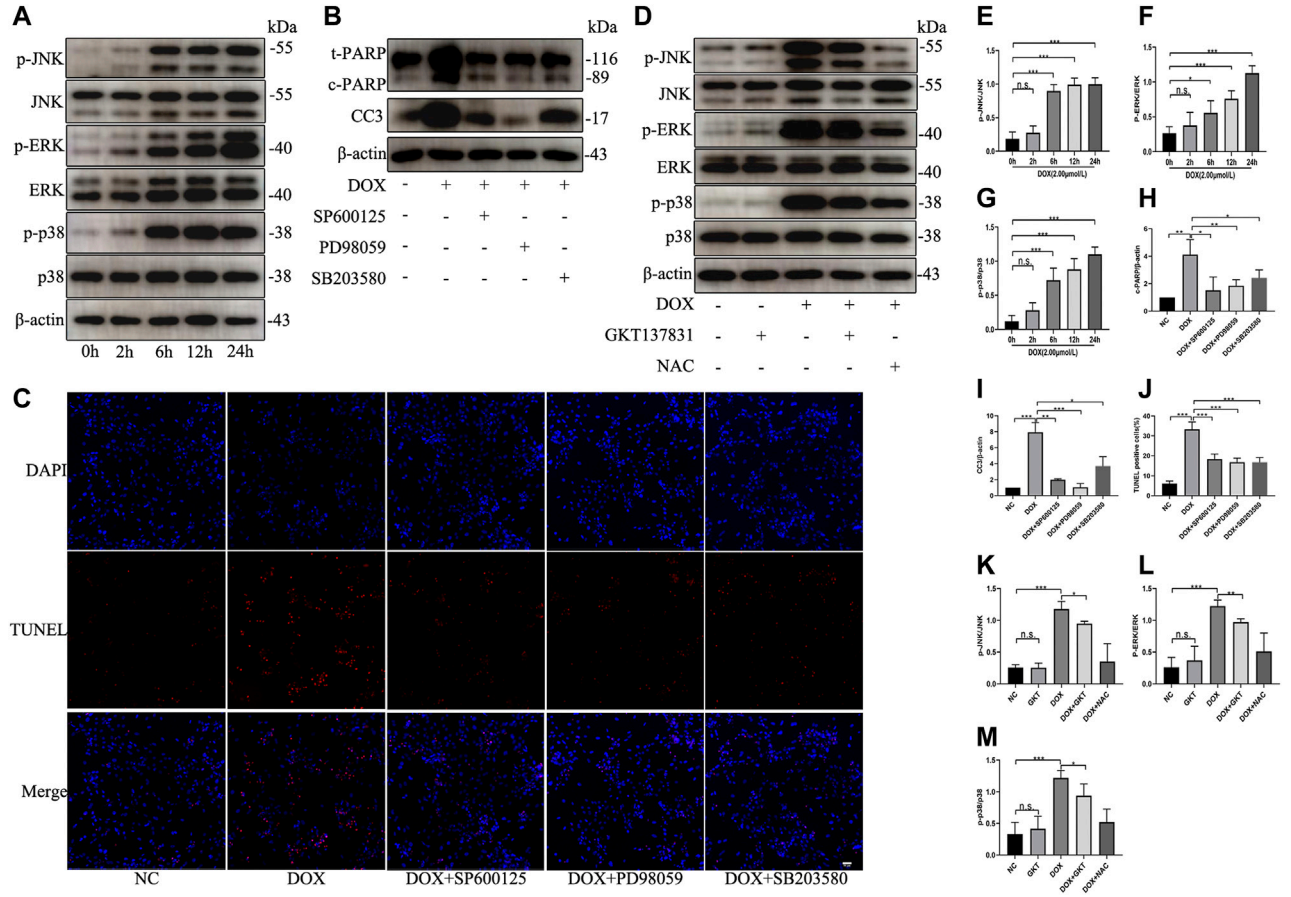

FIGURE 7 | GKT137831 ameliorated DOX-induced apoptosis by inhibiting the MAPK pathway. **(A)** Time-dependent effects of DOX on activation of JNK, ERK, and p38 MAPK were evaluated by Western blot. β-actin was used as a loading control. Relative protein expression levels of p-JNK/JNK **(E)**, p-ERK/ERK **(F)**, and p-p38/p38 **(G)** were quantified (n = 3–4). **(B)** NRCMs were pretreated with SP600125 (JNK inhibitor) or PD098059 (ERK1/2 inhibitor) or with SB203580 (p38 inhibitor) for 1 h and then treated with DOX for 24 h **(H,I)** The protein expressions of c-PARP and CC3 were determined by Western blot and quantifications by densitometric analysis (n = 3–4). **(C,J)** Representative images of TUNEL staining in NRCMs (scale bar = 50 μm) and related quantification of TUNEL staining (n = 3). **(D)** NRCMs pretreated with GKT or NAC for 1 h, and then treated with DOX for 24 h **(K,L,M)** The phosphorylation levels of JNK, ERK, and p38 were evaluated by Western blot, and quantifications by densitometric analysis (n = 3–4). $^{*}p < 0.05$, $^{**}p < 0.01$, $^{***}p < 0.001$, n. s., not significant. DOX, doxorubicin; GKT, GKT137831; NAC, acetylcysteine; c-PARP, cleaved PARP; CC3, cleaved caspase 3.

2020). In the present study, we found that DOX exposure activated MAPK pathway in NRCMs. Specific inhibitors against JNK (SP600125), ERK (PD98059) or p38 (SB203580) may abolish DOX-induced apoptosis of NRCMs, and the levels of the apoptosis indicators cleaved PARP and cleaved caspase three were decreased. GKT137831 pretreatment inhibited excessive DOX-induced MAPK pathway activation. These results indicated that GKT137831 attenuates cardiac apoptosis possibly through modulation of MAPK signaling pathway, although the precise mechanism remains to be determined.

In this study, GKT137831 was administered as a protective agent immediately after DOX exposure, and further investigations are required to address whether delayed GKT137831 intervention can attenuate established cardiomyopathy. Additional studies are also needed to determine whether GKT137831 protects against DOX-associated cardiotoxicity without compromising its antitumor effects.

CONCLUSION

Our studies demonstrated that GKT137831 can inhibit Nox1/4-derived ROS production to relieve DOX-induced cardiomyocyte apoptosis. Mechanistically, GKT137831inhibits the excessive activation of MAPK pathway induced by Nox1/4-derived ROS. Thus, GKT137831 may be a potential drug candidate to ameliorate DOX-induced cardiotoxicity.

DATA AVAILABILITY STATEMENT

The original contributions presented in the study are included in the article/**Supplementary Material**, further inquiries can be directed to the corresponding authors.

ETHICS STATEMENT

The animal study was reviewed and approved by the Animal Ethics Committee of Shandong University.

AUTHOR CONTRIBUTIONS

XJ conceived and designed the experiments. HZ, NX, and ZZ performed the experiments. HZ and NX analyzed the data, researched the data and contributed to the discussion. JX and FW contributed reagents, materials and analytic tools. HZ wrote the manuscript. XJ reviewed and edited the manuscript.

FUNDING

The present study was supported by the National Key Research and Development Program (grant number 2017YFC1308303), the National Natural Science Foundation of China (grant number 81873522), the Shandong Provincial Natural Science Foundation of China (grant number ZR2020QH007) and the Clinical Research Center of Shandong University (grant number 2020SDUCRCA009).

SUPPLEMENTARY MATERIAL

The Supplementary Material for this article can be found online at: https://www.frontiersin.org/articles/10.3389/fphar.2022.823975/full#supplementary-material

REFERENCES

Altenhofer, S., Kleikers, P. W., Radermacher, K. A., Scheurer, P., Rob Hermans, J. J., Schiffers, P., et al. (2012). The NOX Toolbox: Validating the Role of NADPH Oxidases in Physiology and Disease. *Cell Mol. Life Sci.* 69 (14), 2327–2343. doi:10.1007/s00018-012-1010-9

Berthiaume, J. M., and Wallace, K. B. (2007). Adriamycin-induced Oxidative Mitochondrial Cardiotoxicity. *Cell Biol Toxicol.* 23 (1), 15–25. doi:10.1007/s10565-006-0140-y

Cheng, D., Chen, L., Tu, W., Wang, H., Wang, Q., Meng, L., et al. (2020). Protective Effects of Valsartan Administration on Doxorubicin-induced Myocardial Injury in Rats and the Role of Oxidative Stress and NOX2/NOX4 Signaling. *Mol. Med. Rep.* 22 (5), 4151–4162. doi:10.3892/mmr.2020.11521

Davies, K. J., and Doroshow, J. H. (1986). Redox Cycling of Anthracyclines by Cardiac Mitochondria. I. Anthracycline Radical Formation by NADH Dehydrogenase. *J. Biol. Chem.* 261 (7), 3060–3067. doi:10.1016/s0021-9258(17)35746-0

Deng, S., Kruger, A., Kleschyov, A. L., Kalinowski, L., Daiber, A., and Wojnowski, L. (2007). Gp91phox-containing NAD(P)H Oxidase Increases Superoxide Formation by Doxorubicin and NADPH. *Free Radic. Biol. Med.* 42 (4), 466–473. doi:10.1016/j.freeradbiomed.2006.11.013

Douglas, G., Bendall, J. K., Crabtree, M. J., Tatham, A. L., Carter, E. E., Hale, A. B., et al. (2012). Endothelial-specific Nox2 Overexpression Increases Vascular Superoxide and Macrophage Recruitment in ApoE$^{-/-}$ Mice. *Cardiovasc. Res.* 94 (1), 20–29. doi:10.1093/cvr/cvs026

Elbatreek, M. H., Mucke, H., and Schmidt, H. H. H. W. (2021). NOX Inhibitors: from Bench to Naxibs to Bedside. *Handb Exp. Pharmacol.* 264, 145–168. doi:10.1007/164_2020_387

Gage, M. C., and Thippeswamy, T. (2021). Inhibitors of Src Family Kinases, Inducible Nitric Oxide Synthase, and NADPH Oxidase as Potential CNS Drug Targets for Neurological Diseases. *CNS Drugs* 35 (1), 1–20. doi:10.1007/s40263-020-00787-5

Gilleron, M., Marechal, X., Montaigne, D., Franczak, J., Neviere, R., and Lancel, S. (2009). NADPH Oxidases Participate to Doxorubicin-Induced Cardiac Myocyte Apoptosis. *Biochem. Biophys. Res. Commun.* 388 (4), 727–731. doi:10.1016/j.bbrc.2009.08.085

Goormaghtigh, E., Huart, P., Brasseur, R., and Ruysschaert, J. M. (1986). Mechanism of Inhibition of Mitochondrial Enzymatic Complex I-III by Adriamycin Derivatives. *Biochim. Biophys. Acta* 861 (1), 83–94. doi:10.1016/0005-2736(86)90374-3

Goormaghtigh, E., Huart, P., Praet, M., Brasseur, R., and Ruysschaert, J. M. (1990). Structure of the Adriamycin-Cardiolipin Complex. Role in Mitochondrial Toxicity. *Biophys. Chem.* 35 (2-3), 247–257. doi:10.1016/0301-4622(90)80012-v

Gorin, Y., Cavaglieri, R. C., Khazim, K., Lee, D. Y., Bruno, F., Thakur, S., et al. (2015). Targeting NADPH Oxidase with a Novel Dual Nox1/Nox4 Inhibitor Attenuates Renal Pathology in Type 1 Diabetes. *Am. J. Physiol. Ren. Physiol.* 308 (11), F1276–F1287. doi:10.1152/ajprenal.00396.2014

Gray, S. P., Di Marco, E., Okabe, J., Szyndralewiez, C., Heitz, F., Montezano, A. C., et al. (2013). NADPH Oxidase 1 Plays a Key Role in Diabetes Mellitus-Accelerated Atherosclerosis. *Circulation* 127 (18), 1888–1902. doi:10.1161/CIRCULATIONAHA.112.132159

Jha, J. C., Thallas-Bonke, V., Banal, C., Gray, S. P., Chow, B. S., Ramm, G., et al. (2016). Podocyte-specific Nox4 Deletion Affords Renoprotection in a Mouse Model of Diabetic Nephropathy. *Diabetologia* 59 (2), 379–389. doi:10.1007/s00125-015-3796-0

Kumar, R. R., Arora, K., Goswami, S., Sakhare, A., Singh, B., Chinnusamy, V., et al. (2020). MAPK Enzymes: a ROS Activated Signaling Sensors Involved in Modulating Heat Stress Response, Tolerance and Grain Stability of Wheat under Heat Stress. *3 Biotech.* 10 (9), 380. doi:10.1007/s13205-020-02377-0

Li, S., Wang, W., Niu, T., Wang, H., Li, B., Shao, L., et al. (2014). Nrf2 Deficiency Exaggerates Doxorubicin-Induced Cardiotoxicity and Cardiac Dysfunction. *Oxid. Med. Cel Longev.* 2014, 748524. doi:10.1155/2014/748524

Louzada, R. A., Corre, R., Ameziane El Hassani, R., Meziani, L., Jaillet, M., Cazes, A., et al. (2021). NADPH Oxidase DUOX1 Sustains TGF-β1 Signalling and Promotes Lung Fibrosis. *Eur. Respir. J.* 57 (1). doi:10.1183/13993003.01949-2019

Ma, J., Wang, Y., Zheng, D., Wei, M., Xu, H., and Peng, T. (2013). Rac1 Signalling Mediates Doxorubicin-Induced Cardiotoxicity through Both Reactive Oxygen Species-dependent and -independent Pathways. *Cardiovasc. Res.* 97 (1), 77–87. doi:10.1093/cvr/cvs309

Manea, S. A., Constantin, A., Manda, G., Sasson, S., and Manea, A. (2015). Regulation of Nox Enzymes Expression in Vascular Pathophysiology: Focusing on Transcription Factors and Epigenetic Mechanisms. *Redox Biol.* 5, 358–366. doi:10.1016/j.redox.2015.06.012

McGowan, J. V., Chung, R., Maulik, A., Piotrowska, I., Walker, J. M., and Yellon, D. M. (2017). Anthracycline Chemotherapy and Cardiotoxicity. *Cardiovasc. Drugs Ther.* 31 (1), 63–75. doi:10.1007/s10557-016-6711-0

McLaughlin, D., Zhao, Y., O'Neill, K. M., Edgar, K. S., Dunne, P. D., Kearney, A. M., et al. (2017). Signalling Mechanisms Underlying Doxorubicin and Nox2 NADPH Oxidase-Induced Cardiomyopathy: Involvement of Mitofusin-2. *Br. J. Pharmacol.* 174 (21), 3677–3695. doi:10.1111/bph.13773

Redza-Dutordoir, M., and Averill-Bates, D. A. (2016). Activation of Apoptosis Signalling Pathways by Reactive Oxygen Species. *Biochim. Biophys. Acta* 1863 (12), 2977–2992. doi:10.1016/j.bbamcr.2016.09.012

Sheehan, A. L., Carrell, S., Johnson, B., Stanic, B., Banfi, B., and Miller, F. J., Jr. (2011). Role for Nox1 NADPH Oxidase in Atherosclerosis. *Atherosclerosis* 216 (2), 321–326. doi:10.1016/j.atherosclerosis.2011.02.028

Singal, P. K., and Iliskovic, N. (1998). Doxorubicin-induced Cardiomyopathy. *N. Engl. J. Med.* 339 (13), 900–905. doi:10.1056/NEJM199809243391307

Son, Y., Cheong, Y. K., Kim, N. H., Chung, H. T., Kang, D. G., and Pae, H. O. (2011). Mitogen-activated Protein Kinases and Reactive Oxygen Species: How Can ROS Activate MAPK Pathways? *J. Signal. Transduct.* 2011, 792639. doi:10.1155/2011/792639

Sumimoto, H. (2008). Structure, Regulation and Evolution of Nox-Family NADPH Oxidases that Produce Reactive Oxygen Species. *FEBS J.* 275 (13), 3249–3277. doi:10.1111/j.1742-4658.2008.06488.x

Touyz, R. M., Anagnostopoulou, A., Camargo, L. L., Rios, F. J., and Montezano, A. C. (2019). Vascular Biology of Superoxide-Generating NADPH Oxidase 5-implications in Hypertension and Cardiovascular Disease. *Antioxid. Redox Signal.* 30 (7), 1027–1040. doi:10.1089/ars.2018.7583

Von Hoff, D. D., Layard, M. W., Basa, P., Davis, H. L., Jr., Von Hoff, A. L., Rozencweig, M., et al. (1979). Risk Factors for Doxorubicin-Induced Congestive Heart Failure. *Ann. Intern. Med.* 91 (5), 710–717. doi:10.7326/0003-4819-91-5-710

Wojnowski, L., Kulle, B., Schirmer, M., Schlüter, G., Schmidt, A., Rosenberger, A., et al. (2005). NAD(P)H Oxidase and Multidrug Resistance Protein Genetic Polymorphisms Are Associated with Doxorubicin-Induced Cardiotoxicity. *Circulation* 112 (24), 3754–3762. doi:10.1161/CIRCULATIONAHA.105.576850

Zeng, S. Y., Yang, L., Yan, Q. J., Gao, L., Lu, H. Q., and Yan, P. K. (2019). Nox1/4 Dual Inhibitor GKT137831 Attenuates Hypertensive Cardiac Remodelling Associating with the Inhibition of ADAM17-dependent Proinflammatory Cytokines-Induced Signalling Pathways in the Rats with Abdominal Artery Constriction. *Biomed. Pharmacother.* 109, 1907–1914. doi:10.1016/j.biopha.2018.11.077

Zeng, C., Duan, F., Hu, J., Luo, B., Huang, B., Lou, X., et al. (2020a). NLRP3 Inflammasome-Mediated Pyroptosis Contributes to the Pathogenesis of Non-ischemic Dilated Cardiomyopathy. *Redox Biol.* 34, 101523. doi:10.1016/j.redox.2020.101523

Zeng, S. Y., Yan, Q. J., Yang, L., Mei, Q. H., and Lu, H. Q. (2020b). Inhibition of the ROS-EGFR Pathway Mediates the Protective Action of Nox1/4 Inhibitor GKT137831 against Hypertensive Cardiac Hypertrophy via Suppressing Cardiac Inflammation and Activation of Akt and ERK1/2. *Mediators Inflamm.* 2020, 1078365. doi:10.1155/2020/1078365

Zhang, S., Liu, X., Bawa-Khalfe, T., Lu, L. S., Lyu, Y. L., Liu, L. F., et al. (2012). Identification of the Molecular Basis of Doxorubicin-Induced Cardiotoxicity. *Nat. Med.* 18 (11), 1639–1642. doi:10.1038/nm.2919

Zhao, Y., McLaughlin, D., Robinson, E., Harvey, A. P., Hookham, M. B., Shah, A. M., et al. (2010). Nox2 NADPH Oxidase Promotes Pathologic Cardiac Remodeling Associated with Doxorubicin Chemotherapy. *Cancer Res.* 70 (22), 9287–9297. doi:10.1158/0008-5472.CAN-10-2664

Zhao, Q. D., Viswanadhapalli, S., Williams, P., Shi, Q., Tan, C., Yi, X., et al. (2015). NADPH Oxidase 4 Induces Cardiac Fibrosis and Hypertrophy through Activating Akt/mTOR and NFκB Signaling Pathways. *Circulation* 131 (7), 643–655. doi:10.1161/CIRCULATIONAHA.114.011079

Conflict of Interest: The authors declare that the research was conducted in the absence of any commercial or financial relationships that could be construed as a potential conflict of interest.

Publisher's Note: All claims expressed in this article are solely those of the authors and do not necessarily represent those of their affiliated organizations, or those of the publisher, the editors and the reviewers. Any product that may be evaluated in this article, or claim that may be made by its manufacturer, is not guaranteed or endorsed by the publisher.

frontiers | Frontiers in Pharmacology

ORIGINAL RESEARCH
published: 12 April 2022
doi: 10.3389/fphar.2022.859755

Naringin Interferes Doxorubicin-Induced Myocardial Injury by Promoting the Expression of ECHS1

Zirui Zhao[1,2,3†], Shilei Yang[1,2†], Yawen Deng[3], Liang Wang[4], Yifen Zhang[3,5], Zhenyu Feng[3], Han Li[3], Zhongchao Chi[1,2], Yunpeng Xie[3] and Deshi Dong[1,2*]*

[1]Department of Pharmacy, The First Affiliated Hospital of Dalian Medical University, Dalian, China, [2]College of Pharmacy, Dalian Medical University, Dalian, China, [3]Institute of Cardiovascular Diseases, The First Affiliated Hospital of Dalian Medical University, Dalian, China, [4]Department of Clinical Pharmacy, Huludao Center Hospital, Huludao, China, [5]Department of Critical Care Medicine, The First Affiliated Hospital of Dalian Medical University, Dalian, China

Doxorubicin (DOX) leads to myocardial cell damage and irreversible heart failure, which limits the clinical application of DOX. Naringin has biological functions of inhibiting inflammation, oxidative stress and apoptosis. Our aim was to investigate whether Naringin could prevent DOX-related cardiotoxicity in mice. Naringin was administered by gavage and mice were intraperitoneally injected with doxorubicin (1 mg/kg/day) for 15 days. H&E, Masson, TUNEL and others experiments were examined. NRVMs and H9C2 cells were treated with Naringin and DOX *in vitro*. Using IF, ELISA and Western Blot to detect the effect of Naringin and ECHS1 on cells. The results showed that Naringin could prevent DOX related cardiac injury, inhibit cardiac oxidative stress, inflammation and apoptosis *in vivo* and *in vitro*. Inhibition of ECHS1 could interfere the effect of Naringin on DOX-induced myocardial injury. Naringin may provide a new cardiac protective tool for preventing the cardiotoxicity of anthracycline drugs.

Keywords: doxorubicin, apoptosis, oxidative stress, inflammation, Naringin, ECHS1

OPEN ACCESS

Edited by:
Zhi-Ren Zhang,
Harbin Medical University, China

Reviewed by:
Mohammad H. Abukhalil,
Al-Hussein Bin Talal University, Jordan
Eylem Taskin,
Adiyaman University, Turkey

***Correspondence:**
Deshi Dong
deshidong@163.com
Yunpeng Xie
xieyunpeng@dmu.edu.cn

†These authors have contributed equally to this work

Specialty section:
This article was submitted to Cardiovascular and Smooth Muscle Pharmacology, a section of the journal Frontiers in Pharmacology

Received: *21 January 2022*
Accepted: *16 March 2022*
Published: *12 April 2022*

Citation:
Zhao Z, Yang S, Deng Y, Wang L, Zhang Y, Feng Z, Li H, Chi Z, Xie Y and Dong D (2022) Naringin Interferes Doxorubicin-Induced Myocardial Injury by Promoting the Expression of ECHS1. Front. Pharmacol. 13:859755. doi: 10.3389/fphar.2022.859755

INTRODUCTION

In recent years, with the improvement of cancer diagnosis and treatment, cancer has gradually become a chronic disease, and the survival time of cancer patients has also been prolonged. But studies show that nearly half of cancer patients die from non-cancer events, with cardiovascular disease as the leading cause of death (Howlader et al., 2010; Jemal et al., 2010).

Currently, cancer treatment-related cardiotoxicity is mainly classified into two categories: type I and type II (Moudgil and Yeh, 2016). Type I chemotherapy-related cardiotoxicity refers to the presence of dose-dependent myocardial necrosis and large area of irreversible damage in cardiomyocytes after chemotherapy, which is mainly caused by anthracycline (Khouri et al., 2012). The mechanism is mainly positive correlation with cumulative dose, but the mechanism of myocardial injury has not been fully elucidated. At present, it is believed to be related to excessive production of reactive oxygen species (Antonucci et al., 2021), lipid peroxidation (Quagliariello et al., 2019), DNA damage (Qiao et al., 2020) and accumulation of tumor suppressor proteins (Li et al., 2019).

Polyphenolic compounds (flavonoids, anthocyanins, and phenolic acids) are known for their antioxidant properties, free radical scavenging, and iron chelation properties (Balea et al., 2018). Naringin is a flavonoid that is a phenolic compound found in grapefruit and other citrus

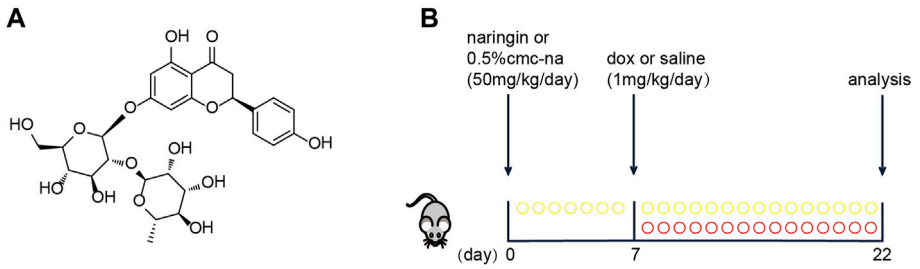

FIGURE 1 | (A) Basic structure of Naringin (NR). **(B)** Schematic protocol for mice treatments showing models of exposure doxorubicin (DOX), which were performed in mice to test the efficacy of Naringin (NR).

(**Figure 1A**). It has a variety of pharmacological and therapeutic properties, including anti-cancer, anti-inflammatory, and antioxidant effects (Raha et al., 2020). Naringin in myocardial infarction, Ischemia and reperfusion (Rajadurai and Prince, 2009), cardiac hypertrophy (Park et al., 2018) and other cardiovascular diseases play a role in cardiac protection. It has been reported that Naringin could protect doxorubicin-induced myocardial injury in rats (Jian et al., 2017), but it has not been involved in mice.

The mitochondrial short-chain enoyl-CoA hydratase encoded by the ECHS1 gene exists in the mitochondrial matrix as a 160 kU homohexamer. ECHS1 is involved in the second step of β-oxidation of short-chain fatty acids in mitochondria. Its role is to hydrate the trans-double bond between carbon 2 and carbon 3 in trans-2,3-enoyl CoA Forms L-3 hydroxyacyl CoA (Sharpe and Mckenzie, 2018).

In this study, the protective effect of Naringin and ECHS1 on doxorubicin-induced myocardial injury was found *in vivo* in mice.

MATERIALS AND METHODS

Animals and Treatment

Male C57BL/6J mice (8 weeks-old) were purchased from Aisaikesi (Shenyang). The mice were randomly divided into four groups. Sham group, Naringin group, DOX group and Naringin + DOX group. The mice were administered Naringin (50 mg/kg) solution dissolved in 0.5% CMC-Na or 0.5% CMC-Na via oral gavage for 22 days and at seventh day the mice were intraperitoneal injected with Doxorubicin hydrochloride (1 mg/kg) or saline for consecutive 15 days (**Figure 1B**). At the end of treatment, all mice were intraperitoneally anesthetized to collect the hearts and blood samples for determining heart injury and serum biomarker levels. All procedures were approved by the Animal Care and Use Committee of Dalian Medical University.

Hematoxylin & Eosin Staining

Hematoxylin & eosin (H&E) staining were carried out according to experiment protocol. Briefly, after the mice hearts were fixed with 4% formaldehyde overnight, they were embedded in paraffin and made into 5 μm sections. The cardiac tissues transversely sectioned from middle segment were stained with H&E for the assessment of myofilament morphology and injury.

Wheat Germ Agglutinin

For the assessment of the cardiomyocyte cross-sectional area, sections were stained with 50 μg/ml WGA for 60 min, and then it was calculated by measuring 15–20 cells per slid.

Primary Neonatal Rat Ventricular Myocytes Isolation and H9C2 Treatment

NRVMs were isolated from 1-2-day-old Sprague-Dawley (SD) rats. The heart tissue was cut into pieces and washed with precooled phosphate buffer saline (PBS), and then digested continuously with 0.25% trypsin. The cells were pre-incubated with Dulbecco's Minimum Essential Medium/F12 (DMEM/F12) containing 10% (vol/vol) fetal bovine serum (FBS) (Life-Lab, AC03L055) and 1% penicillin-streptomycin (PS). Then, the harvested cells were incubated on 100 mm^2 culture dishes at 37°C with 5% CO_2. H9C2 cells were obtained from American type culture collection (ATCC). H9C2 cells were cultured in the DMEM containing D-Glucose-(4.5 g/L) with 10% (vol/vol) FBS and 1% PS at 37°C with 5% CO_2.

NRVMs and H9C2 cells were treated with Naringin at a dose of 50 μM in culture medium after cell generation, Doxorubicin hydrochloride was administrated at a dose of 5 μM after Naringin treatment.

Terminal Deoxynucleotidyl Transferase dUTP NickEnd Labeling Assay

TUNEL Assay kit was used to evaluate cardiac apoptosis according to the manufacturer's protocol (US EVERBRIGHT, T6014). The apoptotic cells were visualized by fluorescence microscopy and apoptosis was indicated as the ratio of TUNEL-positive nuclei/total stained cell nuclei in five images per heart tissue.

Catalase, Malondialdehyde, Lactate dehydrogenase, Superoxide Dismutase and Glutathione-Peroxidase Kit Assay

Catalase (CAT), malondialdehyde (MDA), activities of lactate dehydrogenase (LDH), superoxide dismutase (SOD) and Total Glutathione peroxidase (GSH-Px) were measured respectively using assay kits (CAT, MDA, LDH, and SOD kits: Nanjing

Jiancheng Company, China; GSH-Px kit: Solarbio, China). The absorbance was detected using EnSpire microplatereader (Tecan, Switzerland).

Quantitative Real-Time PCR Analysis

Total RNA was isolated from NRVMs or heart tissues using TRIzol (Invitrogen) according to the manufacturer's protocol. cDNA was used for PCR amplification with gene-specific primers for *cybb* and *nox4*. First-strand cDNA was produced from 1 μg of total RNA from each sample using PrimeScript RT reagent kit according to the manufacturer's protocol (Yeasen, 11141ES60). The mRNA levels of genes were analyzed using SYBR Green Premix on an Applied Biosystems 7,500 Fast thermocycler. *actn2* was used as the endogenous control.

Table Primer sequences

Gene Forward primer (5′–3′) Reverse primer (5′–3′)

Cybb GCTACGCCTTCAACACCAAG AGTTCGTCCCCT TCTCCTGT

Nox4 CGGGATTTGCTACTGCCTCCAT TGACTCCTC AAATGGGCTTCC

Actn2 ATGCGGTTCCACAAGATTGC AGCCCTTCTTTG GCAGATGTT

Immunofluorescence Staining

Immunofluorescence staining was performed to detect the expression levels of Bcl-2 (Arigo) and γ-H2AX (abcam) of the cells. After washing with PBS three times, cells were fixed with 4% paraformaldehyde for 30 min, permeated with 0.1% Triton X-100 for 15 min, and then blocked with 3% fetal bovine serum albumin. Cells were incubated with the primary antibodies (anti-Bcl-2, anti-γ-H2AX) overnight at 4°C in a humidified chamber, and then incubated with a green fluorescent secondary antibody (diluted 1:200; Beyotime) for 2 h at room temperature. At last, the slide was staining with DAPI for 10 min and added anti-fluorescence quenching agent. The images were analyzed using a Nikon microscope (Tokyo, Japan).

MitoSOX Red

MitoSOX Red Assay kit was used to detect the mitochondrial superoxide. H9C2 cells were grown till about 70% confluence and the fresh media were added before experiments. MitoSOX was added to a concentration of 5 μM according to manufacturer's protocol. Before analysis with confocal microscope, cells were kept 30 min in CO_2 incubator at 37°C. The digital images were taken by an inverted confocal laser scanning microscope.

Cell Viability and Cytotoxicity Assay

H9C2 cells were seeded in a 96-well plate and incubated with DOX for 24 h. Cell viability and Cytotoxicity assay was evaluated by Cell Counting Kit-8 (CCK8).

Western Blot Analysis

H9C2 cells were lysed with radioimmunoprecipitation assay (RIPA) buffer supplemented with PMSF (PMSF: RIPA = 1: 100), and the supernatants were collected by centrifugation at 13,300 *g* for 15 min at 4°C. The proteins were separated by 12.5% SDS-PAGE and then transferred to polyvinylidene difluoride (PVDF) membranes by the Bio-Rad Western blotting system. After blocking with 5% non-fat milk for 2 h at room temperature, the membranes were incubated with the primary antibodies (anti-Bcl-2, anti-β-actin) overnight at 4°C and then followed by incubation with secondary antibodies (1:2,500) for 1 h at room temperature. Protein bands were visualized using an ECL kit and Image-Pro Plus 6.0 software was applied to quantify the band intensity values.

Transfection

In the experiments with si-ECHS1 inhibition, H9C2 cells were divided into five groups: Control, NR (50 μM), DOX (5 μM), NR + DOX (50 μM), NR + DOX (50 μM)+si-ECHS1. si-ECHS1 (5′-3': GGG ACC AUA UCA CCC GGA UTT; 5′-3': AUU CCG GGU GAU AUG GUC CCT T) was transfected with LipFiter 3.0 (Hanbio) for 24 h, followed by subsequent operations.

Enzyme Linked Immunosorbent Assay

The levels of inflammation factors in heart tissue or H9C2 cells was measured using IL-1β (Elabscience, China), IL-6 (Elabscience, China) and TNF-α (Elabscience, China) ELISA kits according to the manufacturer's recommendations, The OD is measured spectrophotometrically at a wavelength of 450 nm, the contents of IL-1β, IL-6 and TNF-α were calculated according to the standard curve.

Data Analysis

Results were expressed as mean ± standard deviation (SD). When the data were normally distributed, the difference between the two groups was analyzed by independent *t*-test, and the comparison between multiple groups was analyzed by one-way ANOVA. Differences were considered to be significant at $p < 0.05$.

RESULTS

Naringin Inhibits the Effect of Doxorubicin on Myocardial Atrophy *in vivo*

To demonstrate the role of Naringin in myocardial injury induced by doxorubicin. Mice were treated Naringin by gavage and then intraperitoneal injection of doxorubicin at a cumulative dose of 15 mg/kg for 2 weeks. The results showed that the heart weight and size of mice treated with doxorubicin significantly decreased, while Naringin increased the heart weight and size of mice treated with doxorubicin (**Figures 2A,B**). However, the heart weight/body weight ratio of mice did not different among the four groups (**Figure 2C**), possibly because the body weight of mice also decreased after treatment with doxorubicin (**Figure 2D**). The tibia length of the mice did not change, so the heart weight/tibia length (HW/TL) results were the same as the heart weight of the mice (**Figure 2E**). We also did WGA staining to observe the size of myocardial cells in each group. The results showed that

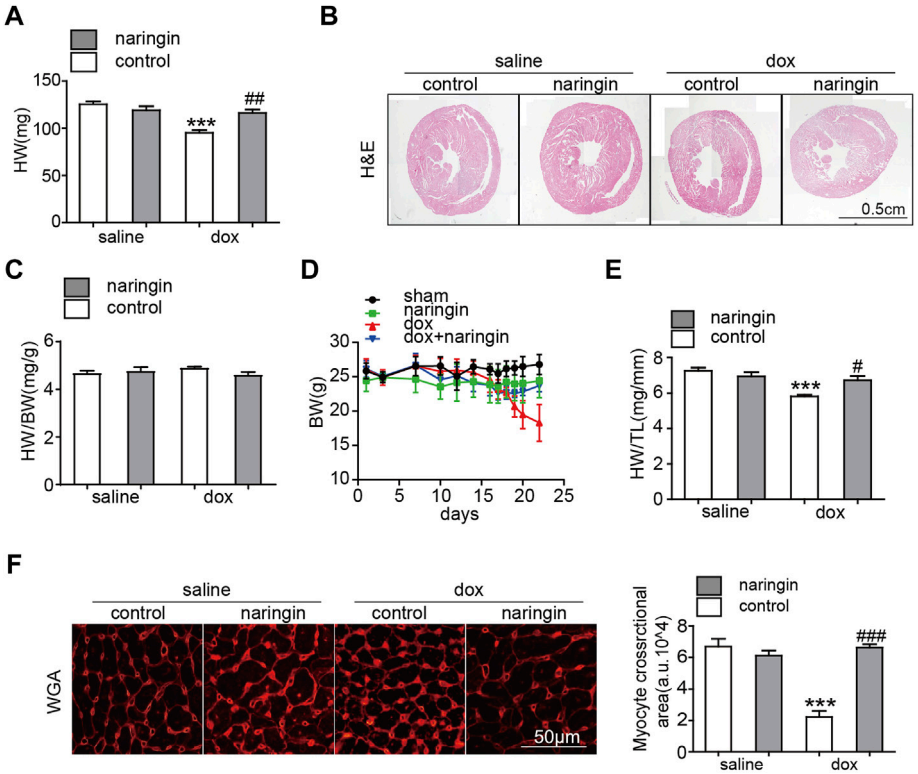

FIGURE 2 | Naringin inhibits the effect of DOX on myocardial atrophy *in vivo*. **(A)** Heart weight of four groups. **(B)** H&E staining of heart sections (Scale bar 1,500 μm). **(C)** Effect of NR on the ratios of heart weight to body weight (HW/BW). **(D)** Body weight of four groups. **(E)** Effect of NR on the ratios of heart weight to tibia length (HW/TL). **(F)** Heart cross-sections were stained with WGA, (left panel). Quantification of the relative myocyte cross-sectional area with quantification analysis (right panel). $^{***}p < 0.001$ DOX versus control group; $^{\#}p < 0.05$, $^{\#\#}p < 0.01$, and $^{\#\#\#}p < 0.001$ DOX versus NR + DOX.

myocardial cells in DOX group were significantly smaller, which was consistent with the results in the literature. However, after Naringin treatment, the size of mouse cardiomyocytes increased (**Figure 2F**). Thus, Naringin could protect the size of mouse cardiomyocytes induced by doxorubicin.

Naringin Inhibits the Effect of Doxorubicin on Apoptosis, Inflammation and Oxidative Stress *in vivo*

There are vacuoles of different sizes in the cytoplasm and nucleus of the denatured cells, and the cells are honeycomb or reticular. Severe denaturation, vesicle mutual fusion into a large vesicle, the nucleus hung in the center, or was squeezed in the side, cytoplasm blank, shape such as balloon. Vacuolation occurs in heart tissue from chemotherapy patients and doxorubicin-induced mice. Here, a large number of vacuolated cardiomyocytes were found in doxorubicin-induced mouse heart tissues by H&E staining, while the number of vacuolated cardiomyocytes was significantly reduced after treatment with Naringin (**Figure 3A**). Subsequently, we measured the degree of LDH, a marker of myocardial injury. The results showed that doxorubicin promoted the increase of LDH concentration, which was decreased after Naringin treatment (**Figure 3B**). Doxorubicin could induce apoptosis of cardiomyocytes. Oxidative stress is also a pathway by which cardiomyocytes are damaged by doxorubicin. We detected the concentration level of CAT, GSH-PX, MDA and SOD. They play a crucial role in the balance of oxidation and antioxidant in the organism and is closely related to the occurrence and development of many diseases. In this experiment, the concentration of CAT, GSH-PX and SOD was inhibited by doxorubicin, while the concentration of CAT, GSH-PX and SOD increased after Naringin treatment (**Figures 3C–E**). The concentration of MDA was increased by doxorubicin, while the concentration of MDA decreased after Naringin treatment (**Figure 3F**). The mRNA expression levels of oxidative stress related factors NOX2 (cybb) and *nox4* were also detected. The results showed that DOX could significantly promote the expression of cybb and *nox4*, while Naringin inhibited this phenomenon (**Figures 3G,H**). Next, TUNEL assay was performed to verify whether Naringin has protective effect on doxorubicin-induced apoptosis of cardiomyocytes. The results showed that doxorubicin could indeed induce apoptosis of mouse cardiomyocytes. Naringin, on the other hand, protects cardiomyocytes from apoptosis (**Figure 3I**). And we examined the marker of apoptosis bcl-2 and Bax by Western Blot. The results showed that Naringin could inhibited the expression of Bax and increase the expression of Bcl-2 induced by DOX (**Figure 3J**). Local tissue non-specific

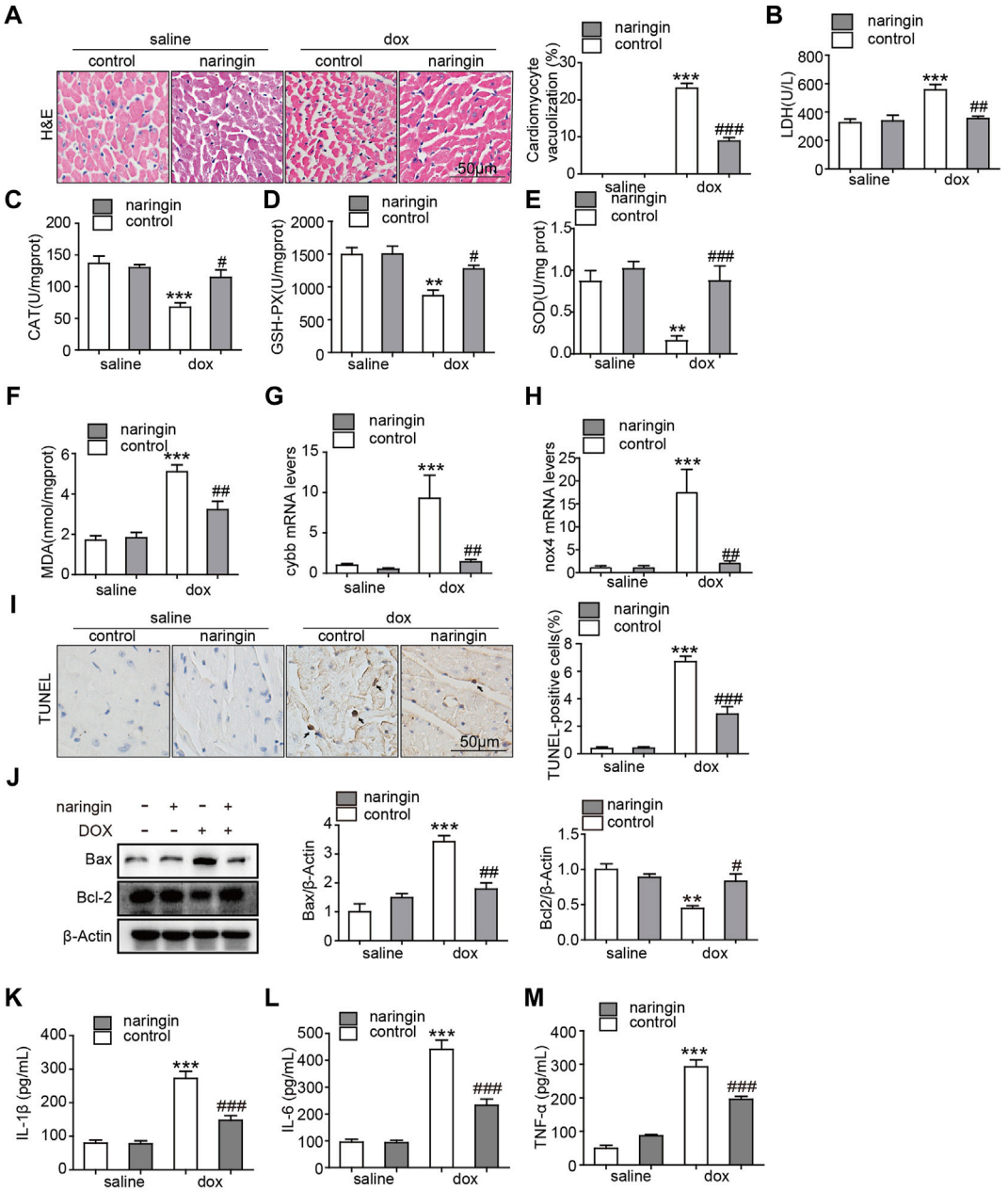

FIGURE 3 | Naringin inhibits the effect of DOX on apoptosis, inflammation and Oxidative stress *in vivo* **(A)** Naringin protects heart from vacuolization induced by DOX. H&E staining of heart sections (left panel), with quantification analysis (right panel). **(B)** The content of LDH (lactic acid dehydrogenase) activity in cardiac. **(C)** The content of CAT activity in cardiac. **(D)** The content of GSH-PX activity in cardiac. **(E)** The content of SOD activity in cardiac. **(F)** The content of MDA activity in cardiac. **(G)** Cardiac mRNA expression level of *cybb* was measured by qPCR analysis. **(H)** Cardiac mRNA expression level of *nox4* was measured by qPCR analysis. **(I)** Mice heart sections were conducted TUNEL staining for determination of apoptotic cells (black arrows indicate TUNEL positive cells, left panel) with quantification of apoptotic cells with quantification analysis (right panel). **(J)** The expression of Bax, Bcl-2 and β-actin detected by Western Blot. **(K–M)** The level of IL-1β, IL-6 and TNF-α detected by ELISA. $^{***}p < 0.001$ DOX versus control group; $^{\#\#}p < 0.01$, and $^{\#\#\#}p < 0.001$ DOX versus NR + DOX.

inflammation caused by DOX chemotherapy. We examined the level of IL-1β, IL-6 and THF-α. The results showed that Naringin could inhibited the level of IL-1β, IL-6 and THF-α induced by DOX (**Figures 3K–M**). These results suggested that Naringin could reduce cardiac injury by inhibiting apoptosis, inflammation and oxidative stress induced by doxorubicin *in vivo*.

Naringin Inhibits the Effect of Doxorubicin on Apoptosis, Inflammation and Oxidative Stress *in vitro*

We have shown that Naringin protects against doxorubicin-induced myocardial damage *in vivo*. Next, we verified this conclusion *in vitro* experiments. First, we used CCK8 assay to

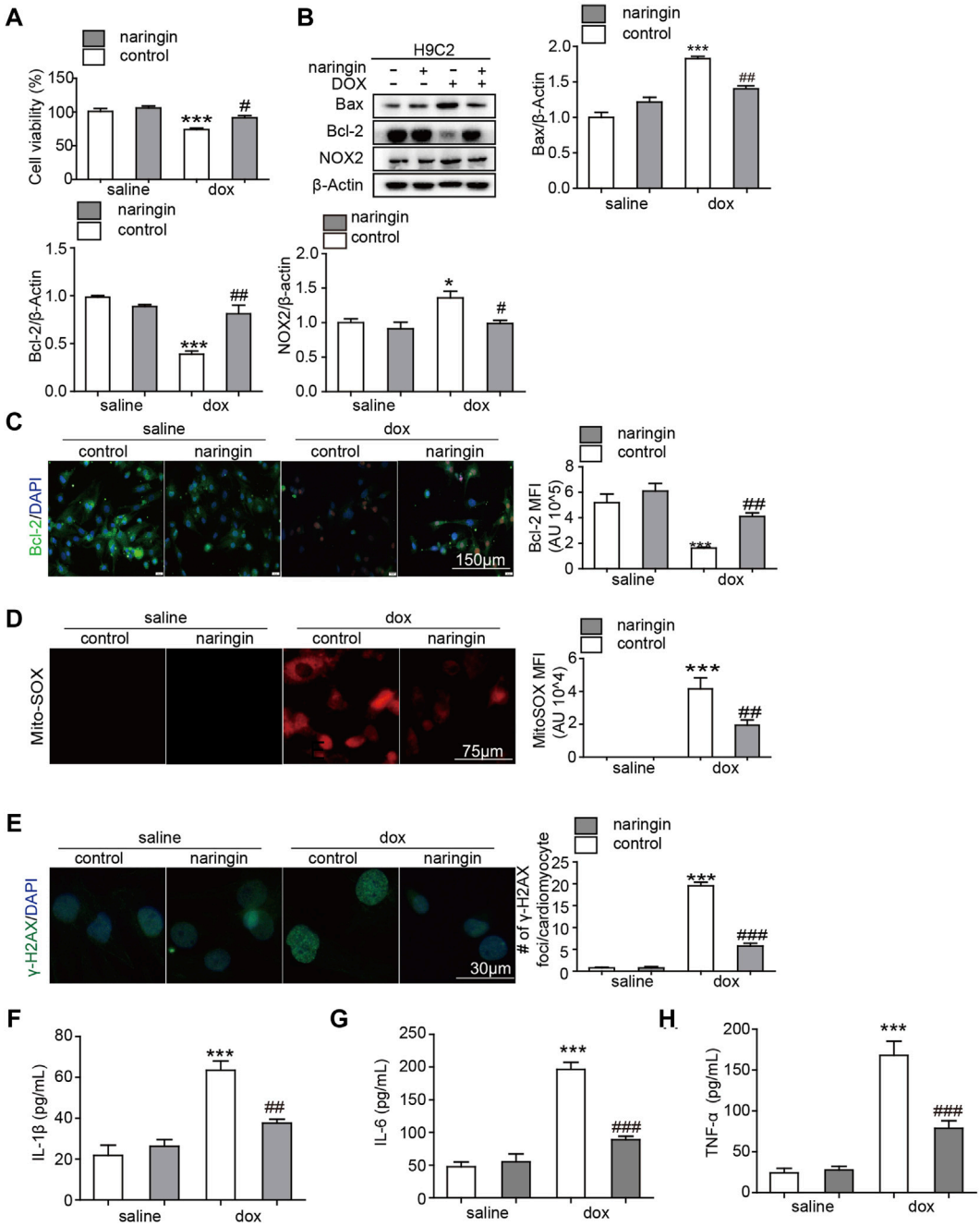

FIGURE 4 | Naringin inhibits the effect of DOX on apoptosis, inflammation and Oxidative stress *in vitro* **(A)** Effect of Naringin on H9C2 cells in the presence of DOX. Cell counting kit 8-based cell viability assays show Cell viability of H9C2 cells in the presence of DOX. **(B)** Effects of Naringin on the protein expression levels of Bcl-2, Bax and NOX2 in H9C2 cells (left panel) with quantification analysis (right panel). **(C)** Naringin treatment increases Dox-Induced Bcl-2 Secretion in NRVMS, which displays representative imaging of bcl-2 immunofluorescence staining. Bcl-2 cells are in green, DAPI in blue. **(D)** Representative Mito-SOX fluorescence images indicate the level of mitochondrial damage (left panel) with quantification of Mito-SOX florescence intensity. **(E)** Representation image of IF staining of the DNA damage markers γ-H2AX (left panel). The average number of γ-H2AX foci in γ-H2AX-positive NRVMS. **(F–H)** The level of IL-1β, IL-6 and TNF-α detected by ELISA. $^{***}p < 0.001$ DOX versus control group; $^{\#\#}p < 0.01$, and $^{\#\#\#}p < 0.001$ DOX versus NR + DOX.

test whether Naringin inhibited the cardiotoxicity of doxorubicin. The results showed that doxorubicin could inhibit the proliferation of H9C2 cells and promote their death. Naringin, on the other hand, could protect H9C2 to some extent (**Figure 4A**). Next, Western blot experiments were used to observe the apoptosis and ROS. The results showed DOX

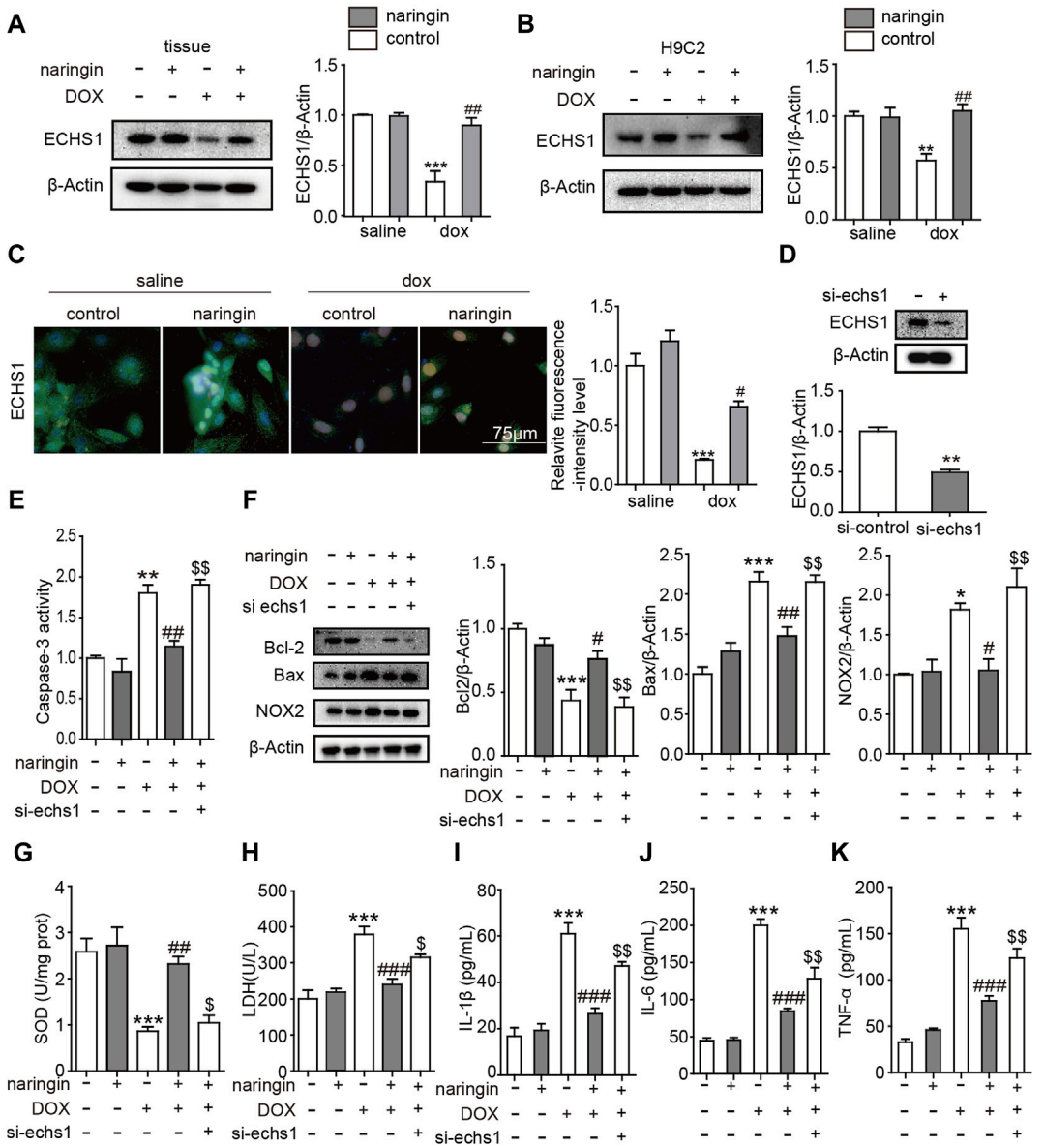

FIGURE 5 | Inhibition of ECHS1 interferes the effect of Naringin on DOX-induced on apoptosis, inflammation and Oxidative stress *in vitro*. **(A)** the protein expression levels of ECHS1 in heart tissue (left panel) with quantification analysis (right panel); **(B)** the protein expression levels of Bcl-2 in H9C2 cells (left panel) with quantification analysis (right panel); **(C)** representative imaging of ECHS1 immunofluorescence staining. ECHS1 cells are in green, DAPI in blue.; **(D)** the protein expression levels of ECHS1 after si-ECHS1 transfection; **(E)** the activity of caspase3 in different group; **(F)** the protein expression levels of Bcl-2, BAX, NOX2 and β-actin in heart tissue (left panel) with quantification analysis (right panel). **(G)** The content of SOD activity in H9C2. **(H)** The content of LDH activity in H9C2. **(I–K)** The level of IL-1β, IL-6 and TNF-α detected by ELISA. $^{**}p < 0.01$, $^{***}p < 0.001$ DOX versus control group or si- ECHS1 versus control group; $^{\#\#}p < 0.01$, and $^{\#\#\#}p < 0.001$ DOX versus NR + DOX; $^{\$\$}p < 0.01$ NR + DOX versus NR + DOX + si- ECHS1.

induced the expression of Bax and NOX2, while Naringin inhibited the expression of Bax and NOX2 induced by DOX in H9C2 cells (**Figure 4B**). And we used IF to detect the expression of bcl-2. The results showed DOX decreased the expression of Bcl-2, while Naringin increased the expression of Bcl-2 induced by DOX in H9C2 cells (**Figure 4C**). MitoSox™ Red reagent is a novel fluorescent dye that specifically targets mitochondria in living cells. MitoSox™ red reagents are oxidized by superoxide and produce red fluorescence. Next, we used MitoSox™ to observe the effects of DOX and Naringin on oxidative stress. The results showed that the mitochondria of cells induced by doxorubicin showed a large amount of red color, while the red color decreased after treatment with Naringin (**Figure 4D**). γ-H2AX could detect genomic damage as well as environmental and physical damage caused by cytotoxic chemicals. In this study, doxorubicin could promote

the expression of γ-H2AX in the nucleus, while Naringin could inhibit this phenomenon (**Figure 4E**). We examined the level of IL-1β, IL-6 and THF-α. The results showed that Naringin could inhibited the level of IL-1β, IL-6 and THF-α induced by DOX (**Figures 4F,G**).

Inhibition of ECHS1 Interferes the Effect of Naringin on Doxorubicin-Induced on Apoptosis, Inflammation and Oxidative Stress *in vitro*

We have proved Naringin inhibits the effect of DOX on apoptosis, inflammation and Oxidative stress *in vitro*. Next we looked at what proteins were involved. Oxygen free radicals produced by DOX cause cell damage and could peroxidize unsaturated fatty acids. ECHS1 mutations lead to decreased fatty acid mitochondrial β-oxidation activity, thereby reducing the formation of important energy substrates (such as acetyl CoA), reducing the production of ATP, leading to energy deficiency in the catabolic state (such as fever, after viral infection), and increasing organs. The susceptibility to dysfunction is especially obvious in tissues and organs that rely on fatty acids and ketone bodies as energy sources (such as heart tissue) (Haack et al., 2015). So we guess whether ECHS1 plays a role in the above results. First of all, we verified that DOX could inhibit the expression of ECHS1 in tissues and cells, and after treatment with Naringin, the expression of ECHS1 increased significantly (**Figures 5A–C**). Next, we constructed the siRNA of ECHS1, and verified by WB that ECHS1 did interfere with the sequence effectively (**Figure 5D**). Finally, we transfected si-ECHS1 in the presence of both DOX and Naringin, and found that after transfection of si-ECHS1, the activity of caspase3 increased (**Figure 5E**), the expression of apoptosis-related protein bcl-2 decreased, the expression of BAX increased, and the expression of oxidative stress-related protein NOX2 increased (**Figure 5F**). The concentration of SOD was inhibited by DOX, while the concentration of SOD increased after Naringin treatment. However, the level of SOD was decreased again after ECHS1 knockdown (**Figure 5G**). Then we measured the degree of LDH. The results showed that DOX promoted the increase of LDH concentration, which was decreased after Naringin treatment. However, the level of LDH was increased again after ECHS1 knockdown (**Figure 5H**). We examined the level of IL-1β, IL-6 and THF-α. The results showed that Naringin could inhibited the level of IL-1β, IL-6 and THF-α induced by DOX. However, the level of IL-1β, IL-6 and THF-α was increased again after echs1 knockdown (**Figures 5I–K**).

DISCUSSION

Anthracyclines are currently the most widely used anticancer drugs (Martins-Teixeira and Carvalho, 2020). As its classic representative, DOX has significant dose cumulative cardiotoxicity, which could eventually lead to heart failure with a poor prognosis and a 2-years mortality of up to 50%

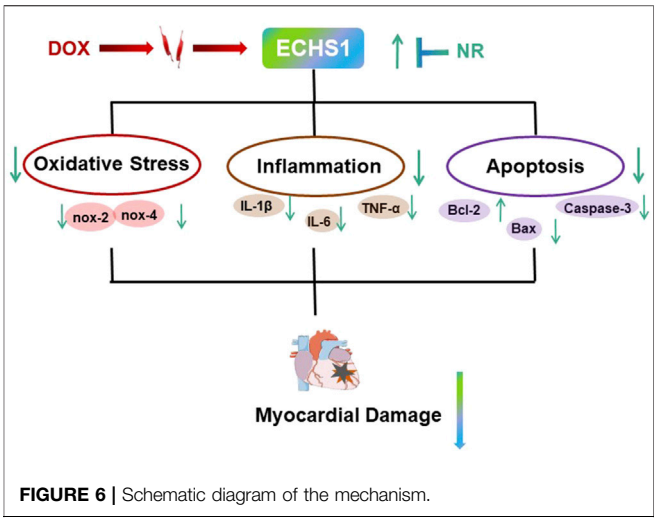

FIGURE 6 | Schematic diagram of the mechanism.

without treatment (Cardinale et al., 2020). Currently, there is no specific protocol to prevent DOX-induced cardiotoxicity. To standardize the treatment of heart failure caused by DOX, reduce the symptoms, improve the quality of life, and find a drug will have important clinical significance (Rochette et al., 2015).

In this study, we investigated the role of Naringin in myocardial injury induced by DOX in mice (**Figure 6**). Naringin has been extensively studied in cancer, rheumatic disease and a variety of cardiovascular diseases (Bai et al., 2019; Heidary et al., 2020; Yang et al., 2020), and its main mechanism is to protect cells from oxidative stress (Zhou et al., 2019) and apoptosis (Zhao et al., 2020). The pathogenic mechanism of doxorubicin is also the induction of oxidative stress and apoptosis (Hu et al., 2020; Zhang et al., 2020). The results show that Naringin did protect against DOX-induced myocardial injury, oxidative stress, and apoptosis. Naringin could increase HW/TL ratio and inhibit LDH level. Mitochondria are the centers of cell energy metabolism. Mitochondria are especially abundant in the sarcoplasm of myocardium (Cai et al., 2015), which adapts to the characteristics of continuous rhythmic contraction of myocardium. So the heart is also more vulnerable to oxidative stress. The results in this paper were the same as those reported, DOX increased oxidative stress level, decreased SOD level and increased mRNA level of oxidative stress related factors in mouse myocardium. However, Naringin could promote the increase of SOD level and reduce the mRNA level of oxidative stress related factors. So Naringin reduced the level of DOX-induced oxidative stress, which was one of the reasons for protecting the mouse heart from damage.

Apoptosis of cardiomyocytes is also one of the causes of heart damage (Imam et al., 2018; Zhou et al., 2021). In this study, we found that DOX could promote apoptosis of cardiomyocytes, inhibit cell activity, and induce vacuolation. This result was consistent with previous studies. After Naringin treatment, the number of apoptosis and vacuolation of myocardial cells decreased. The expression levels of apoptosis-related proteins were decreased.

IL-6 is a pleiotropic cytokine, which is related to pro-inflammatory and anti-inflammatory effects. TNF-α and IL-1β are key pro-inflammatory cytokines involved in the induction of inflammatory response. Inflammation is an important mechanism that triggers DOX-induced myocardial damage. In this article, we tested the expression levels of three cytokines to prove that NR could regulate DOX-induced inflammation through ECHS1.

ECHS1 encodes for short-chain enoyl-CoA hydratase, a key component in b-oxidation. This enzyme is also involved in the isoleucine and valine catabolic pathways. Its lack of clinical manifestations include severe psychomotor developmental delay, epilepsy, neurodegeneration, dystonia, respiratory insufficiency, metabolic acidosis, and feeding difficulties. In this study, we found that DOX could inhibit the expression of ECHS1. Naringin could promote the expression of ECHS1 induced by DOX. And after interfering with ECHS1, the levels of cell apoptosis, inflammation and oxidative stress showed a tendency to increase again.

Evidence suggests that Naringin couldimprove gentamicin-induced renal toxicity and related mitochondrial dysfunction, apoptosis and inflammation in rats, and inhibit fructose production of mitochondrial ROS and mitochondrial dysfunction in cardiomyocytes (Sahu et al., 2014). Naringin reduces cardiac hypertrophy by regulating ampK-MTOR signaling pathway (Park et al., 2018). Studies have shown that Naringin inhibits cardiomyocyte apoptosis induced by high glucose by reducing mitochondrial dysfunction and regulating the activation of P38 signaling pathway (Huang et al., 2013). These studies suggest that Naringin has a protective effect on diseases by inhibiting mitochondrial dysfunction.

ECHS1 is a multifunctional mitochondrial matrix enzyme involved in the oxidation of essential amino acids such as fatty acids and valine. Lack of ECHS1 leads to mitochondrial encephalopathy (Haack et al., 2015), and ECHS1 plays an important role in maintaining mitochondrial function.

Therefore, given the critical roles of Naringin and ECHS1 in maintaining mitochondrial function, we hypothesized that ECHS1 plays a role in Naringin against DOX-induced myocardial injury.

Because Naringin is a dihydroflavone compound, which exists in natural products, there was no difference between the Naringin group and the control group after the mice were given intragastric gavage. So Naringin has the potential of clinical application.

DATA AVAILABILITY STATEMENT

The raw data supporting the conclusions of this article will be made available by the authors, without undue reservation.

ETHICS STATEMENT

The animal study was reviewed and approved by The Animal Care and Use Committee of Dalian Medical University.

AUTHOR CONTRIBUTIONS

Methodology, Software, Writing–Original Draft Preparation: ZZ, SY, YD, LW, YZ, ZF, HL, ZC. Supervision, Writing–Review & Editing, Conceptualization: YX, DD.

FUNDING

This work was supported by Natural Science Foundation of Liaoning Province (Grant no. 2019-ZD-0652), Scientific research project of Liaoning Provincial Department of Education (LJKZ0857), Dalian Medical Science Research Project (Grant no. 1912006) and Natural Science Foundation of China (Grant no. 82070380) and Youth Science and Technology Star Project of Dalian (2020RQ073).

REFERENCES

Antonucci, S., Di Sante, M., Tonolo, F., Pontarollo, L., Scalcon, V., Alanova, P., et al. (2021). The Determining Role of Mitochondrial Reactive Oxygen Species Generation and Monoamine Oxidase Activity in Doxorubicin-Induced Cardiotoxicity. *Antioxid. Redox Signal.* 34 (7), 531–550. doi:10.1089/ars.2019.7929

Bai, J., Li, S., Wu, G., Ma, L., Li, C., Liu, H., et al. (2019). Naringin Inhibits Lipopolysaccharide-Induced Activation of Microglia Cells. *Cel Mol Biol (Noisy-le-grand)* 65 (5), 38–42. doi:10.14715/cmb/2019.65.5.6

Balea, Ş. S., Pârvu, A. E., Pop, N., Marín, F. Z., and Pârvu, M. (20182018). Polyphenolic Compounds, Antioxidant, and Cardioprotective Effects of Pomace Extracts from Feteasc㠠Neagr㠠Cultivar. *Oxid. Med. Cel. Longev.* 2018, 8194721. doi:10.1155/2018/8194721

Cai, R., Gu, J., Sun, H., Liu, X., Mei, W., Qi, Y., et al. (2015). Induction of SENP1 in Myocardium Contributes to Abnormities of Mitochondria and Cardiomyopathy. *J. Mol. Cel. Cardiol.* 79, 115–122. doi:10.1016/j.yjmcc.2014.11.014

Cardinale, D., Iacopo, F., and Cipolla, C. M. (2020). Cardiotoxicity of Anthracyclines. *Front. Cardiovasc. Med.* 7, 26. doi:10.3389/fcvm.2020.00026

Haack, T. B., Jackson, C. B., Murayama, K., Kremer, L. S., Schaller, A., Kotzaeridou, U., et al. (2015). Deficiency of ECHS1 Causes Mitochondrial Encephalopathy with Cardiac Involvement. *Ann. Clin. Transl Neurol.* 2 (5), 492–509. doi:10.1002/acn3.189

Heidary Moghaddam, R., Samimi, Z., Moradi, S. Z., Little, P. J., Xu, S., and Farzaei, M. H. (2020). Naringenin and Naringin in Cardiovascular Disease Prevention: A Preclinical Review. *Eur. J. Pharmacol.* 887, 173535. doi:10.1016/j.ejphar.2020.173535

Howlader, N., Ries, L. A., Mariotto, A. B., Reichman, M. E., Ruhl, J., and Cronin, K. A. (2010). Improved Estimates of Cancer-specific Survival Rates from Population-Based Data. *J. Natl. Cancer Inst.* 102 (20), 1584–1598. doi:10.1093/jnci/djq366

Hu, C., Zhang, X., Zhang, N., Wei, W. Y., Li, L. L., Ma, Z. G., et al. (2020). Osteocrin Attenuates Inflammation, Oxidative Stress, Apoptosis, and Cardiac Dysfunction in Doxorubicin-Induced Cardiotoxicity. *Clin. Transl Med.* 10 (3), e124. doi:10.1002/ctm2.124

Huang, H., Wu, K., You, Q., Huang, R., Li, S., and Wu, K. (2013). Naringin Inhibits High Glucose-Induced Cardiomyocyte Apoptosis by Attenuating Mitochondrial Dysfunction and Modulating the Activation of the p38 Signaling Pathway. *Int. J. Mol. Med.* 32 (2), 396–402.

Imam, F., Al-Harbi, N. O., Al-Harbi, M. M., Ansari, M. A., Al-Asmari, A. F., Ansari, M. N., et al. (2018). Apremilast Prevent Doxorubicin-Induced Apoptosis and Inflammation in Heart through Inhibition of Oxidative Stress Mediated Activation of NF-Kb Signaling Pathways. *Pharmacol. Rep.* 70 (5), 993–1000. doi:10.1016/j.pharep.2018.03.009

Jemal, A., Ward, E., and Thun, M. (2010). Declining Death Rates Reflect Progress against Cancer. *PLoS One* 5 (3), e9584. doi:10.1371/journal.pone.0009584

Jian, C. Y., Ouyang, H. B., Xiang, X. H., Chen, J. L., Li, Y. X., Zhou, X., et al. (2017). Naringin Protects Myocardial Cells from Doxorubicin-induced A-poptosis P-artially by I-nhibiting the p38MAPK P-athway. *Mol. Med. Rep.* 16 (6), 9457–9463. doi:10.3892/mmr.2017.7823

Khouri, M. G., Douglas, P. S., Mackey, J. R., Martin, M., Scott, J. M., Scherrer-Crosbie, M., et al. (2012). Cancer Therapy-Induced Cardiac Toxicity in Early Breast Cancer: Addressing the Unresolved Issues. *Circulation* 126 (23), 2749–2763. doi:10.1161/CIRCULATIONAHA.112.100560

Li, J., Wang, P. Y., Long, N. A., Zhuang, J., Springer, D. A., Zou, J., et al. (2019). p53 Prevents Doxorubicin Cardiotoxicity Independently of its Prototypical Tumor Suppressor Activities. *Proc. Natl. Acad. Sci. U S A.* 116 (39), 19626–19634. doi:10.1073/pnas.1904979116

Martins-Teixeira, M. B., and Carvalho, I. (2020). Antitumour Anthracyclines: Progress and Perspectives. *ChemMedChem* 15 (11), 933–948. doi:10.1002/cmdc.202000131

Moudgil, R., and Yeh, E. T. (2016). Mechanisms of Cardiotoxicity of Cancer Chemotherapeutic Agents: Cardiomyopathy and beyond. *Can. J. Cardiol.* 32 (7), 863–e5. doi:10.1016/j.cjca.2016.01.027

Park, J. H., Ku, H. J., Kim, J. K., Park, J. W., and Lee, J. H. (2018). Amelioration of High Fructose-Induced Cardiac Hypertrophy by Naringin. *Sci. Rep.* 8 (1), 9464. doi:10.1038/s41598-018-27788-1

Qiao, X., van der Zanden, S. Y., Wander, D. P. A., Borràs, D. M., Song, J. Y., Li, X., et al. (2020). Uncoupling DNA Damage from Chromatin Damage to Detoxify Doxorubicin. *Proc. Natl. Acad. Sci. U S A.* 117 (26), 15182–15192. doi:10.1073/pnas.1922072117

Quagliariello, V., Coppola, C., Mita, D. G., Piscopo, G., Iaffaioli, R. V., Botti, G., et al. (2019). Low Doses of Bisphenol A Have Pro-inflammatory and Pro-oxidant Effects, Stimulate Lipid Peroxidation and Increase the Cardiotoxicity of Doxorubicin in Cardiomyoblasts. *Environ. Toxicol. Pharmacol.* 69, 1–8. doi:10.1016/j.etap.2019.03.006

Raha, S., Kim, S. M., Lee, H. J., Yumnam, S., Saralamma, V. V., Ha, S. E., et al. (2020). Naringin Induces Lysosomal Permeabilization and Autophagy Cell Death in AGS Gastric Cancer Cells. *Am. J. Chin. Med.* 48 (3), 679–702. doi:10.1142/S0192415X20500342

Rajadurai, M., and Prince, P. S. (2009). Naringin Ameliorates Mitochondrial Lipid Peroxides, Antioxidants and Lipids in Isoproterenol-Induced Myocardial Infarction in Wistar Rats. *Phytother. Res.* 23 (3), 358–362. doi:10.1002/ptr.2632

Rochette, L., Guenancia, C., Gudjoncik, A., Hachet, O., Zeller, M., Cottin, Y., et al. (2015). Anthracyclines/trastuzumab: New Aspects of Cardiotoxicity and Molecular Mechanisms. *Trends Pharmacol. Sci.* 36 (6), 326–348. doi:10.1016/j.tips.2015.03.005

Sahu, B. D., Tatireddy, S., Koneru, M., Borkar, R. M., Kumar, J. M., Kuncha, M., et al. (2014). Naringin Ameliorates Gentamicin-Induced Nephrotoxicity and Associated Mitochondrial Dysfunction, Apoptosis and Inflammation in Rats: Possible Mechanism of Nephroprotection. *Toxicol. Appl. Pharmacol.* 277 (1), 8–20. doi:10.1016/j.taap.2014.02.022

Sharpe, A. J., and Mckenzie, M. (2018). Mitochondrial Fatty Acid Oxidation Disorders Associated with Short-Chain Enoyl-CoA Hydratase (ECHS1) Deficiency. *Cells* 7 (6), 46. doi:10.3390/cells7060046

Yang, J., Yuan, L., Wen, Y., Zhou, H., Jiang, W., Xu, D., et al. (2020). Protective Effects of Naringin in Cerebral Infarction and its Molecular Mechanism. *Med. Sci. Monit.* 26, e918772. doi:10.12659/MSM.918772

Zhang, X., Hu, C., Kong, C. Y., Song, P., Wu, H. M., Xu, S. C., et al. (2020). FNDC5 Alleviates Oxidative Stress and Cardiomyocyte Apoptosis in Doxorubicin-Induced Cardiotoxicity via Activating AKT. *Cell Death Differ* 27 (2), 540–555. doi:10.1038/s41418-019-0372-z

Zhao, H., Liu, M., Liu, H., Suo, R., and Lu, C. (2020). Naringin Protects Endothelial Cells from Apoptosis and Inflammation by Regulating the Hippo-YAP Pathway. *Biosci. Rep.* 40 (3), BSR20193431. doi:10.1042/BSR20193431

Zhou, C., Lai, Y., Huang, P., Xie, L., Lin, H., Zhou, Z., et al. (2019). Naringin Attenuates Alcoholic Liver Injury by Reducing Lipid Accumulation and Oxidative Stress. *Life Sci.* 216, 305–312. doi:10.1016/j.lfs.2018.07.031

Zhou, N. Q., Fang, Z. X., Huang, N., Zuo, Y., Qiu, Y., Guo, L. J., et al. (2021). aFGF Targeted Mediated by Novel Nanoparticles-Microbubble Complex Combined with Ultrasound-Targeted Microbubble Destruction Attenuates Doxorubicin-Induced Heart Failure via Anti-apoptosis and Promoting Cardiac Angiogenesis. *Front. Pharmacol.* 12, 607785. doi:10.3389/fphar.2021.607785

Conflict of Interest: The authors declare that the research was conducted in the absence of any commercial or financial relationships that could be construed as a potential conflict of interest.

Publisher's Note: All claims expressed in this article are solely those of the authors and do not necessarily represent those of their affiliated organizations, or those of the publisher, the editors and the reviewers. Any product that may be evaluated in this article, or claim that may be made by its manufacturer, is not guaranteed or endorsed by the publisher.

frontiers | Frontiers in Pharmacology

ORIGINAL RESEARCH
published: 20 April 2022
doi: 10.3389/fphar.2022.863322

Oleoylethanolamide as a New Therapeutic Strategy to Alleviate Doxorubicin-Induced Cardiotoxicity

Yeyu Qin[1†], Jing Xie[1†], Ruihe Zheng[1,2], Yuhang Li[3] and Haixia Wang[4]*

[1]Department of Pharmacy, Hainan General Hospital (Hainan Affiliated Hospital of Hainan Medical University), Haikou, China, [2]Medical College, Xiamen University, Xiamen, China, [3]Xiamen Institute of Rare-Earth Materials, Haixi Institutes, Chinese Academy of Sciences, Xiamen, China, [4]Department of Medical Oncology, Hainan General Hospital (Hainan Affiliated Hospital of Hainan Medical University), Haikou, China

Doxorubicin (DOX) is one of the most common chemotherapeutic anti-cancer drugs. However, its clinical use is restricted by serious cardiotoxicity. Oleoylethanolamide (OEA), a structural congener of endocannabinoid anandamide, is the endogenous agonist of peroxisome proliferator activated-receptor α (PPARα) and transient receptor potential cation channel vanilloid-1 (TRPV1), and involved in many physiological processes. The present study aimed to determine whether OEA treatment protects against DOX-induced cytotoxicity (DIC) and gain insights into the underlying mechanism that mediate these effects. Our data revealed that Oleoylethanolamide treatment improved the myocardial structure in DOX-challenged mice by attenuating cardiac oxidative stress and cell apoptosis. OEA also alleviated DOX-induced oxidative stress and apoptosis dysregulation in HL-1 cardiomyocyte. These effects were mediated by activation of TRPV1 and upregulation of PI3K/ Akt signaling pathway. Inhibition of TRPV1 and PI3K reversed the protective effects of OEA. Taken together, our data suggested that OEA protects against DIC through a TRPV1- mediated PI3K/ Akt pathway.

Keywords: oleoylethanolamide (OEA), doxorubicin (DOX)-induced cardiotoxicity (DIC), peroxisome proliferator activated-receptor α (PPARα), transient receptor potential cation channel vanilloid-1 (TRPV1), PI3K/ akt signaling oleoylethanolamide (OEA), PI3K/ akt signaling

OPEN ACCESS

Edited by:
Zhi-Ren Zhang,
Harbin Medical University, China

Reviewed by:
Eman Soliman,
Zagazig University, Egypt
Beshay Zordoky,
University of Minnesota Twin Cities, United States

****Correspondence:***
Haixia Wang
wanghaixia74@163.com

†These authors have contributed equally to this work

Specialty section:
This article was submitted to Cardiovascular and Smooth Muscle Pharmacology, a section of the journal Frontiers in Pharmacology

Received: *27 January 2022*
Accepted: *30 March 2022*
Published: *20 April 2022*

Citation:
Qin Y, Xie J, Zheng R, Li Y and Wang H (2022) Oleoylethanolamide as a New Therapeutic Strategy to Alleviate Doxorubicin-Induced Cardiotoxicity. Front. Pharmacol. 13:863322. doi: 10.3389/fphar.2022.863322

INTRODUCTION

Doxorubicin (DOX), a DNA topoisomerase II inhibitor, is commonly used for the treatment of a wide variety of cancers, including carcinomas, sarcomas and hematological cancers (Renu et al., 2018; Al-Malky et al., 2020). However, the clinical use of DOX is limited by cumulative cardiotoxicity, which can cause irreversible myocardial injury, manifested as a series of pathological changes including cardiomyopathy, arrhythmia, cardiac insufficiency and even heart failure in some cases (Renu et al., 2018). Although the specific regulatory mechanism of DOX-induced cardiotoxicity (DIC) remains unclear, it is thought to involve oxidative stress, fibrosis, autophagy and apoptosis dysregulation (Renu et al., 2018). To date, there are a limited number of drugs (e.g., dexrazoxane) that can be used for alleviating DIC (Seifert et al., 1994; Al-Malky et al., 2020). New therapeutic approaches that could prevent and treat DIC are still highly desired for patients.

Oleoylethanolamide (OEA) is a structural congener of endocannabinoid anandamide (Bowen et al., 2017). It is generated on-demand by small intestinal enterocytes and its production is

stimulated by food intake (Fu et al., 2003). OEA can interact with different receptors in animals, including peroxisome proliferator activated-receptor α (PPARα) and transient receptor potential cation channel vanilloid-1 (TRPV1) (Ahern, 2003; Fu et al., 2003). In fact, as a drug, OEA modulates many physiological processes, including food intake, inflammation, neuro-protection, lipid metabolism and atherosclerotic plaques development *via* the activation of the PPARα signaling (Fu et al., 2003; Zhou et al., 2012; Yang et al., 2016; Bowen et al., 2017; Wu et al., 2019). Besides PPARα, OEA was suggested to act also as a medium-potency agonist of TRPV1 (Ahern, 2003). However, the role of TRPV1 in OEA's actions remains less-well known.

OEA play beneficial roles in inflammation, apoptosis and oxidative stress related diseases (Pandey et al., 2009), opening up the possibility that OEA would have a therapeutic effect on DIC. In the current study, we examined whether treatment of OEA could attenuate DIC. We found that OEA significantly alleviated DOX-induced cardiac oxidative stress, cell apoptosis and tissues damage *in vivo* and *in vitro*. These therapeutic effects could be blocked by TRPV1 antagonist capsazepine and PI3K inhibitor LY294002. Our results identified OEA as a promising therapy for DIC.

METHODS

Drugs

Doxorubicin was purchased from Macklin Biochemical (Cat. #D807083). OEA (Cat. #Z130746), LY294002 (Cat. #L124970), fenofibrate (Cat. #F129682), capsazepine (Cat. #C126558) was purchased from Aladdin. GW6471 (Cat. # 11697) and nonivamide (Cat. # 25328) was purchased from Cayman chemical.

Animals and Treatments

The animal experiments were approved by the Institutes of Health and approved by the Animal Care and Use Committee of Hainan Medical University. C57BL/6 male mice (20–25 g) were purchased from the Vital River Laboratory Animal Technology Co., Ltd. Mice were group-housed in ventilated cages with controlled temperature (25 ± 1°C), relative humidity (55 ± 10%) and a 12-h day/night cycle at 20–25°C. Standard mouse chow and tap water were provided ad libitum.

The DIC model was reproduced as previously reported (Tadokoro et al., 2020). $N = 6$ mice for control and each DIC group. Briefly, DOX (6 mg/kg) or its vehicle was intravenously administered to mice at 9:00 a.m. at days 1, 2, and 4. Mice were intraperitoneally treated with OEA (15 or 30 mg/kg) at 2:00 p.m. (Fu et al., 2003). once daily, PI3K inhibitor LY294002 (10 mg/kg) once daily, or TRPV1 antagonist capsazepine (5 mg/kg) at 6:00 p.m. once daily for 14 consecutive days. All mice were then sacrificed at day 15 and the heart was excised and collected.

Histological Analysis

Hearts were excised, sectioned, fixed in 10% (w/v) formalin for 24 h, followed by embedding in paraffin. The specimen was embedded in paraffin, cut in 5 μm sections and stained with Masson's trichrome, and were photographed using a digital microscope at the magnification of ×400 (Sun et al., 2020). The severity of fibrosis was determined by the previous reported method (Sun et al., 2020). Total three sections per heart were analyzed. The score was calculated from three different and nonoverlapping fields in each section, and the average value was taken for each heart. The trained operator and data analysis were blinded to the experimental groups.

Immunofluorescence

Immunofluorescence staining was performed according to standard protocols (Sun et al., 2020; Li et al., 2021). The paraffin embedded heart sections and cell slides were incubated with the following primary antibodies at 4C overnight: goat anti-8-hydroxy-2′-deoxyguanosine (8-OHdG) (Sigma, Cat. # AB5830, 1:500 dilution) and rabbit anti-caspase-3 antibody (Abcam, Cat. # ab32351, 1:500 dilution). After washing, sections were incubated with donkey anti-goat IgG 647 (Abcam, Cat. # ab150135, 1:1,000 dilution) or goat anti-rabbit IgG 555 (Abcam, Cat. # ab150078, 1: 1,000 dilution) at room temperature for 2 h, and counterstained with 1 μg/ml DAPI. All fluorescence images were obtained using the Nikon Eclipse Ti-U fluorescence microscope and analyzed from five randomly selected fields by ImageJ.

TdT-Mediated dUTP Nick End-Labeling Staining

TUNEL staining was performed using the *in situ* Apoptosis Detection Kit (Takara Bio, Cat. # MK500) according to supplier's protocol (Liang et al., 2020). Briefly, the paraffin-embedded heart tissue sections were deparaffinized in xylene, rehydrated in aqueous solutions with decreasing alcohol content, and digested with proteinase K at room temperature for 15 min. The slides were then incubated with the TUNEL reaction mixture at 37°C for 1 h in a humidified chamber, followed by incubation with 4′,6-diamidino-2-phenylindole (DAPI) for 10 min.

Serum Biochemical and Immunochemical Analyses

Serum levels of cardiac troponin I (cTnI) (Nanjing Jiancheng Bioengineering Institute, Cat. #H149-2), heart-type fatty acid-binding protein (H-FABP) (Dldevelop, Cat. # DL-FABP3-Mu) and myoglobin (Dldevelop, Cat. # DL-MYO-Mu) were measured using corresponding enzyme-linked immunosorbent assay (ELISA) kits following the manufacturer's instructions (Kalantary-Charvadeh et al., 2019). Serum creatine kinase isoform MB (CK-MB) level was measured by using a colorimetric assay kit (Sigma, Cat. # MAK116) following the manufacturer's instructions (Kalantary-Charvadeh et al., 2019).

Thiobarbituric Acid Reactive Substances

TBARS were determined using a previous reported method (Sahu et al., 2019). Heart samples were homogenized in ice-cold potassium phosphate buffer (3 ml, 50 mM, pH 6, containing 0.32 M sucrose) for 3 min, and the mixture were allowed to react with 0.5 ml of 3% sodium dodecyl sulfate, 2 ml of 0.1 N HC1, 0.3 ml of 10%

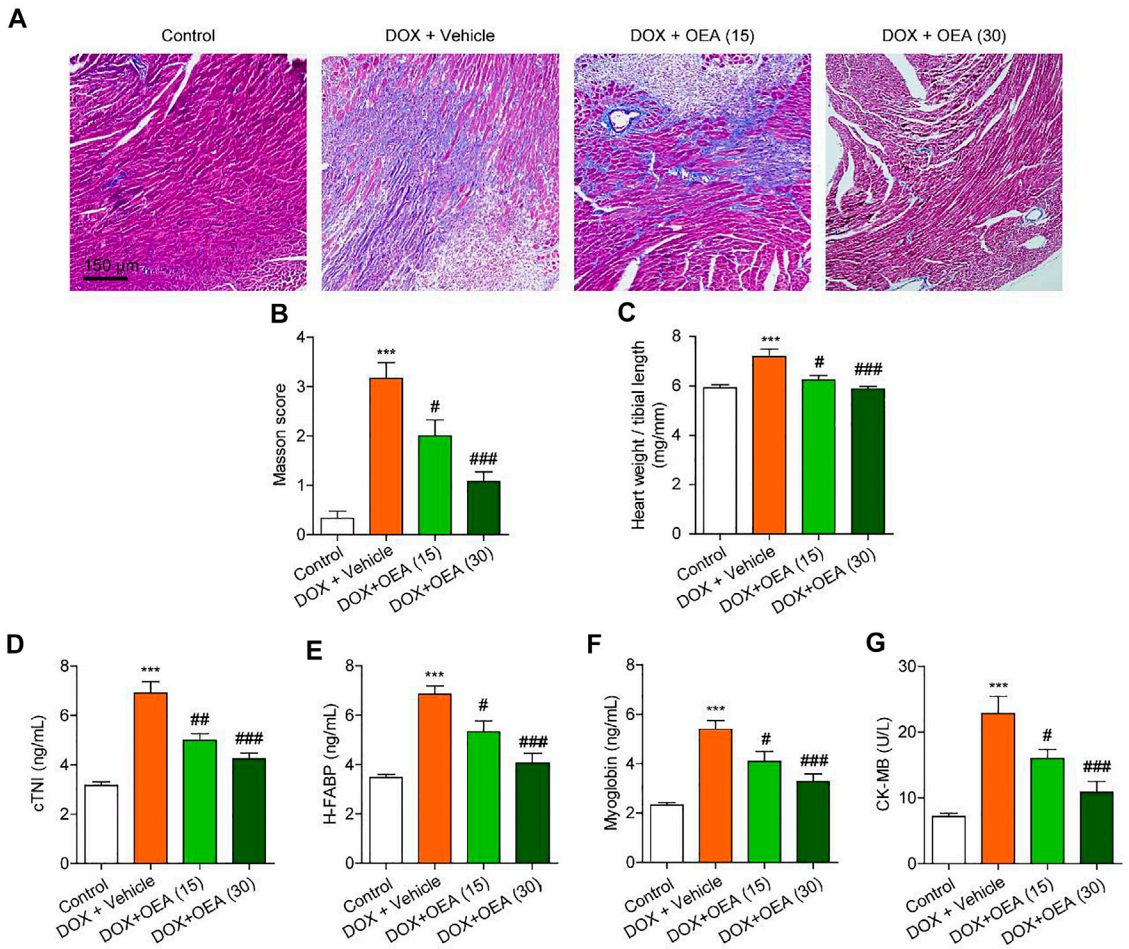

FIGURE 1 | OEA alleviates DIC in mice. Mice with or without DOX (6 mg/kg, i. v.) challenge were treated with OEA (15 or 30 mg/kg, i. v.) for 14 days concurrently with DOX challenge. Heart tissues were isolated at day 15 for analysis. Representative histopathological sections of heart tissues by **(A)** Masson's trichrome staining. **(B)** Myocardial fibrosis in the areas as described in **(A)** were graded. The effects of OEA or its vehicle on (C) heart weight/ tibial length ratio, serum levels of **(D)** cTNI **(E)** H-FABP **(F)** myoglobin and **(G)** CK-MB in mice. Data are expressed as mean ± SEM, $n = 6$. ***, $p < 0.001$ vs. control. #, $p < 0.05$; ##, $p < 0.01$; ###, $p < 0.001$ vs. DOX + vehicle.

phosphotungstic acid, and 1 ml of 0.7% 2-thiobarbituric acid at 90 °C for 30 min. The mixture was extracted with 5 ml L-butanol. After a brief centrifugation, the supernatants were collected and continuously scanned at a wavelength of 515 nm excitation and 555 nm emission. The values were defined as the amount of TBARS (malondialdehyde equivalents) per Gram of heart. Malondialdehyde standards were prepared from 1,1,3,3-tetramethoxypropane.

Glutathione-S-Transferase

GST activity was determined using a fluorescent assay kit (Thermo Fisher, Cat. # EIAGSTF) following the manufacturer's instructions (Sahu et al., 2019).

Cell Culture and Treatment

HL-1 cardiomyocytes (Sigma, Cat. # SCC065) were cultured in supplemented Claycomb Medium (Sigma, Cat. # 51800C) in an incubator at 37°C with 5% CO_2 atmosphere. Adult derived primary human cardiomyocytes (Celprogen, Cat # 36044-15) were cultured in complete growth media (Celprogen, Cat #M36044-15S) in an incubator at 37°C with 5% CO_2 atmosphere. Cells were plated into 12-well plate and cultured until 80% confluence. Cells were then incubated with vehicle (0.1% DMSO), OEA (30 μM), capsazepine (10 μM), GW6471 (5 μM), nonivamide (10 μM), fenofibrate (100 μM), LY294002 (10 μM) for 30 min, or TRPV1 siRNA (5′-GUUCGUGACAAGCAUGUACTT-3′, 3′-TTCAAGCACUGU UCGUACAUG-5′, 30 nM) and HiPerfect transfection reagent (Qiagen, 301704) for 18 h before challenged by 2 μM DOX. After 24 h, cells were harvested for analysis (Liu et al., 2020).

For immunofluorescence staining, HL-1 cells were cultured on coverslips under the same conditions as described above. HL-1 cardiomyocytes were fixed in 4% paraformaldehyde and 0.4% Triton X-100 (Aladdin, Cat. #T109026) for 30 min at room temperature, respectively. The cells were then washed 3 times with PBS and blocked with goat serum (Boster, Cat. # AR0009) at 37 °C for 1 h before immunofluorescence staining (Zhou et al., 2019; Sun et al., 2020).

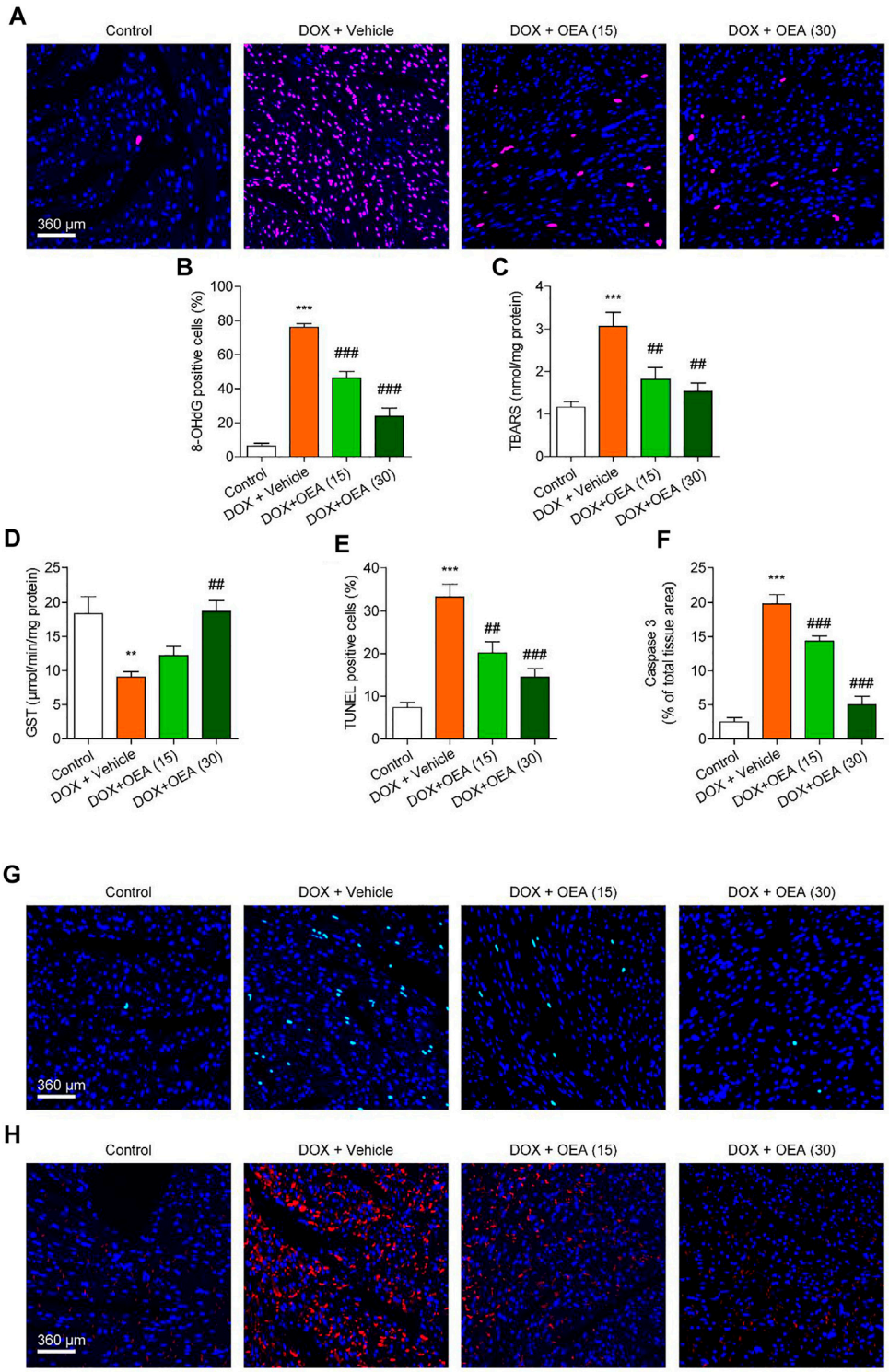

FIGURE 2 | OEA inhibited DOX-induced myocardial oxidative stress and apoptosis in mice. Mice with or without DOX (6 mg/kg, i. v.) challenge were treated with OEA (15 or 30 mg/kg, i. v.) for 14 days concurrently with DOX challenge. Heart tissues were isolated at day 15 for analysis. **(A)** Immunofluorescence staining of 8-OHdG in myocardial tissues. **(B)** 8-OHdG positive cells shown in **(A)** were counted. The effects of OEA or its vehicle on **(C)** TBARS and **(D)** GST in myocardial tissues. **(E)** TUNEL positive cells shown in **(G)** were counted. **(F)** Fluorescence quantification for caspase three in **(H)** were calculated. **(G)** Detection of apoptotic cells in mice cardiac tissues by TUNEL staining. **(H)** Immunofluorescence staining of caspase three in myocardial tissues. Data are expressed as mean ± SEM, $n = 6$. ***, $p < 0.001$ vs. control. #, $p < 0.05$; ##, $p < 0.01$; ###, $p < 0.001$ vs. DOX + vehicle.

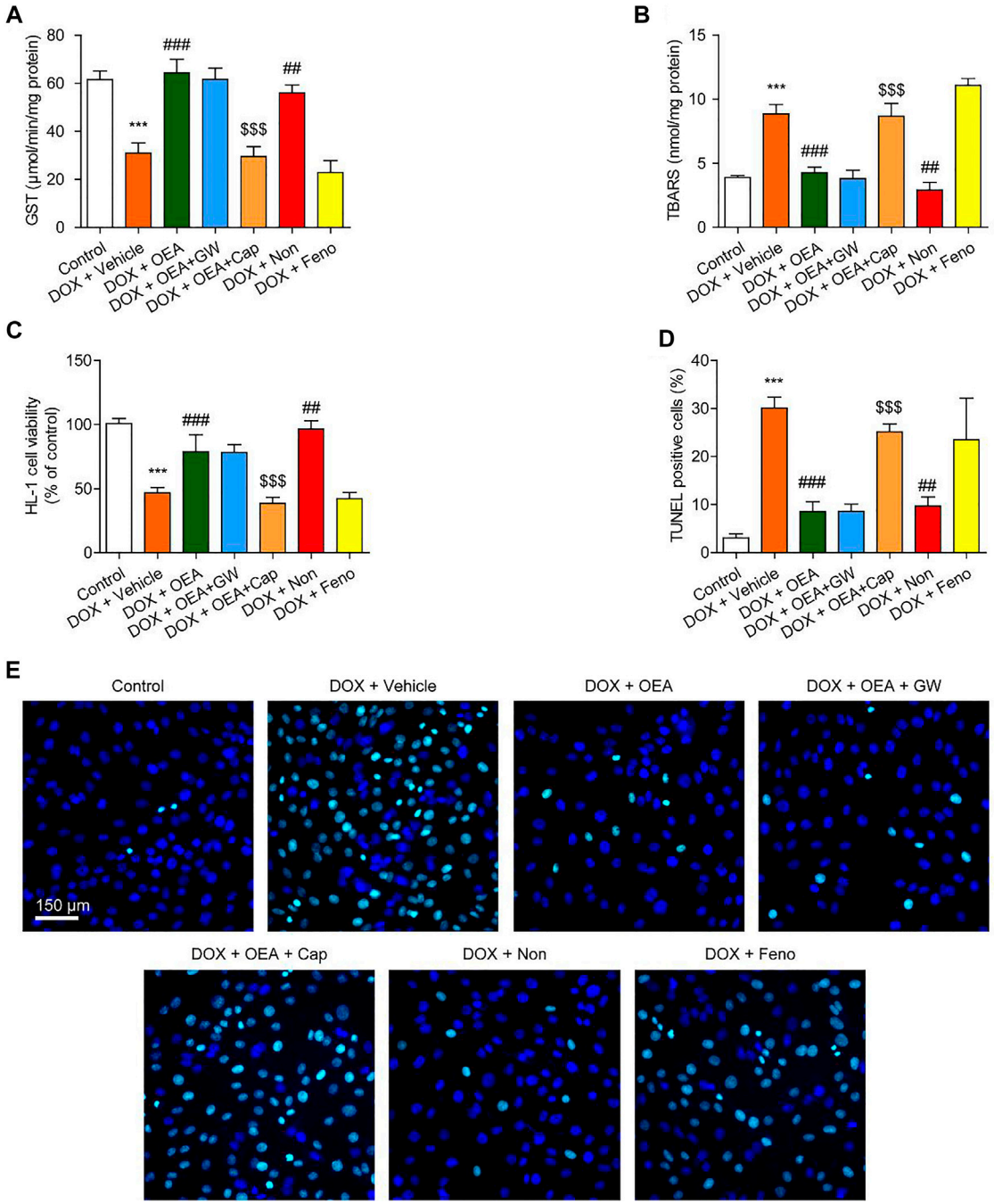

FIGURE 3 | OEA inhibited DOX-induced oxidative stress and apoptosis in cardiomyocytes through TRPV1 pathway. HL-1 cells were treated with 0.1% DMSO, OEA (30 μM), GW6471 (5 μM), capsazepine (10 μM), nonivamide (10 μM), fenofibrate (100 μM) for 30 min. Cells were then treated with DOX (2 μM) for 24 h. Levels of **(A)** GST **(B)** TBARS and **(C)** cell viability was assessed in HL-1 cardiomyocytes. **(D)** TUNEL positive cells shown in **(E)** were counted. **(E)** TUNEL staining of HL-1 cardiomyocytes. Data are expressed as mean ± SEM, $n = 4$. ***, $p < 0.001$ vs. control. ##, $p < 0.01$; ###, $p < 0.001$ vs. DOX + vehicle. $$$, $p < 0.001$ vs. DOX + OEA.

Cell Proliferation Assay

Cell viability were measured using the cell counting kit-8 (CCK8) (Dojindo, Cat. # CK04) according to the manufacturer's instructions (Liu et al., 2020). Cells were seeded into 96-well plates at a density of 1,000 per well and cultured under the same conditions as described above. Tetrazolium reagent (10 μl) provided from the kit was added into each well, and incubated at 37°C for 1 h. The

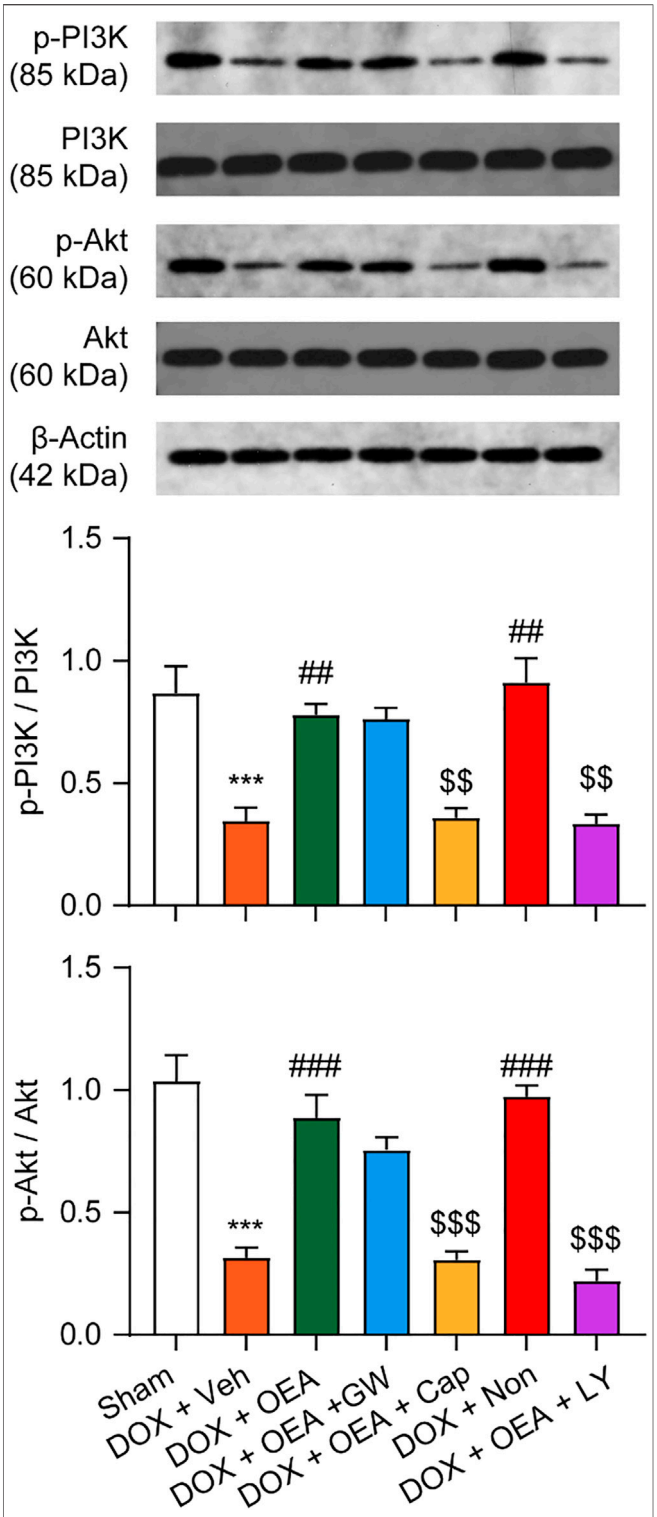

FIGURE 4 | OEA promotes TRPV1-mediated PI3K/ Akt signaling in cardiomyocytes. HL-1 cells were treated with 0.1% DMSO, OEA (30 μM), GW6471 (5 μM), capsazepine (10 μM) and nonivamide (10 μM) for 30 min. Cells were then treated with DOX (2 μM) for 24 h. PI3K, Akt, p-PI3K and p-Akt was determined using western blot analysis.

plate was measured at a wavelength of 450 nm using a microplate reader. Percent cell proliferation was defined as the relative percentage (%) of treated cells relative to untreated control group.

Western Blot

Western blotting was performed according to standard protocols (Tadokoro et al., 2020). The following antibodies were used: rabbit anti-PI3K antibody (Abcam, Cat. # ab86714, 1:1,000 dilution), rabbit anti-p-Akt antibody (Abcam, Cat. # ab222489, 1:1,000 dilution), rabbit anti-β-actin (Sigma, Cat. # A5441, 1: 50,000 dilution). As secondary agents, horseradish peroxidase-coupled goat anti-rabbit antibody was used. Bands were visualized with an enhanced chemiluminescence detection kit (Thermo, WP20005). All results were quantified using ImageJ software, with β-actin as the internal standard.

Statistical Analysis

The results are presented as the means ± SEM. One-way ANOVA was used to analyze the differences between experimental groups, followed by Tukey's Multiple Comparison Test using GraphPad Prism 9.0 software. In all cases, $p < 0.05$ was considered to indicate a statistically significant difference.

RESULTS

OEA Alleviates DOX-Induced Cardiotoxicity in Mice

We first assessed the potential protective effects of OEA on DIC. As shown in **Figure 1A**, Masson staining revealed that DOX challenge increased the degree of myocardial fibrosis, while OEA reduced the formation of fibrosis foci in the mice heart (**Figures 1A–C**). Furthermore, cTnI, H-FABP, myoglobin and CK-MB are sensitive markers of cardiomyocyte damage in the serum. DOX treatment elicited a drastic increase in the levels of cTnI, H-FABP, myoglobin and CK-MB in the serum of DIC mice, while OEA dose-dependently reduced the increment of these markers (**Figures 1D–G**). In addition, treatment of normal mice with OEA alone did not affect the histological features of heart and levels of cTnI, H-FABP, myoglobin and CK-MB (**Supplementary Figure S1**). Taken together, these data illustrate that OEA exhibits a protective role in DIC.

OEA Inhibits DOX-Induced Cardiac Oxidative Stress and Apoptosis in Mice

Dox chemotherapy has been reported to induce cardiotoxicity *via* lipids peroxidation and oxidative DNA damage in cardiomyocytes (Minotti et al., 1996). Cardiac TBARS and 8-OHdG are the markers of lipid peroxidation and oxidative DNA damage, respectively (Valavanidis et al., 2009; Aguilar Diaz De Leon and Borges, 2020). Dox caused significant up-regulation in expressions of 8-OHdG, a marker of oxidative DNA damage, and TBARS, a marker of lipid peroxidation, which were dose-

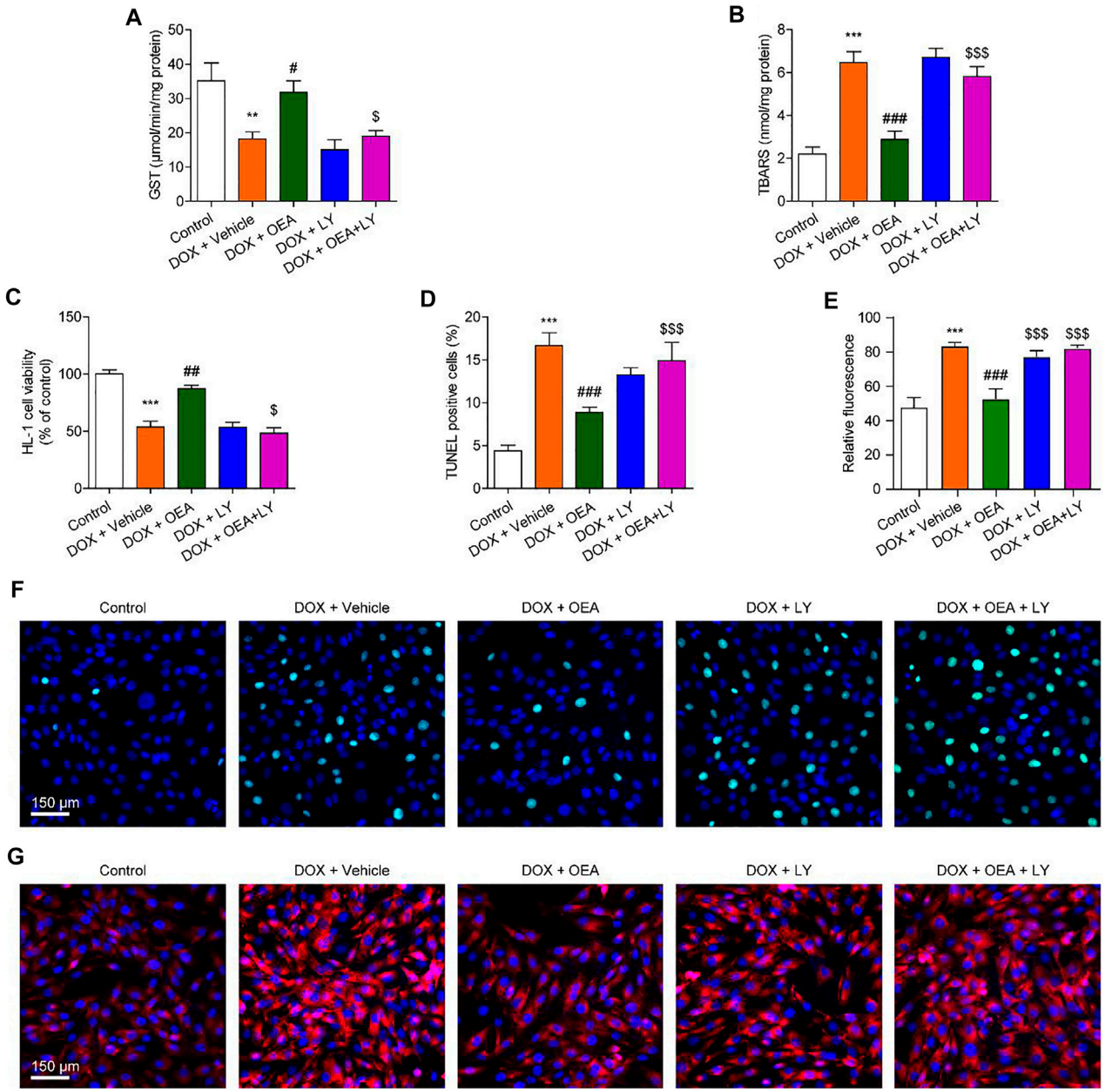

FIGURE 5 | Inhibition of the PI3K-Akt signaling blocks the protective effects of OEA in cardiomyocytes. HL-1 cells were treated with 0.1% DMSO, OEA (30 μM) and LY294002 (10 μM) for 30 min. Cells were then treated with DOX (2 μM) for 24 h. Levels of **(A)** GST **(B)** TBARS and **(C)** cell viability was assessed in HL-1 cardiomyocytes. **(D)** TUNEL positive cells shown in **(F)** were counted. **(E)** Fluorescence quantification for caspase three in **(G)** were calculated. **(F)** TUNEL staining of HL-1 cardiomyocytes. **(G)** Immunofluorescence staining of caspase three in HL-1 cardiomyocytes. Data are expressed as mean ± SEM, $n = 4$. ***, $p < 0.001$ vs. control. #, $p < 0.05$; ##, $p < 0.01$; ###, $p < 0.001$ vs. DOX + vehicle. $, $p < 0.05$; $$, $p < 0.01$; $$$, $p < 0.001$ vs. DOX + OEA.

dependently reduced by OEA treatment (**Figures 2A–C**). DOX challenge caused oxidative stress to the myocardial tissues *via* depletion of endogenous anti-oxidant enzyme GST, while OEA significantly restored activities of these anti-oxidant enzymes (**Figure 2D**). Cardiomyocyte apoptosis plays an important role in the pathophysiology of DIC. There were more TUNEL-positive cells in the heart of DOX-treated mice than in that of normal mice (**Figures 2E,G**). Simultaneous up-regulation of cleaved caspase three confirmed the cells apoptosis in the cardiac tissue of DOX-treated mice (**Figures 2F,H**). On the other hand, OEA treatment significantly attenuated DOX-induced cell apoptosis (**Figures 2F–H**). Overall, these observations suggested that OEA inhibited cardiac oxidative stress and apoptosis in DIC mice.

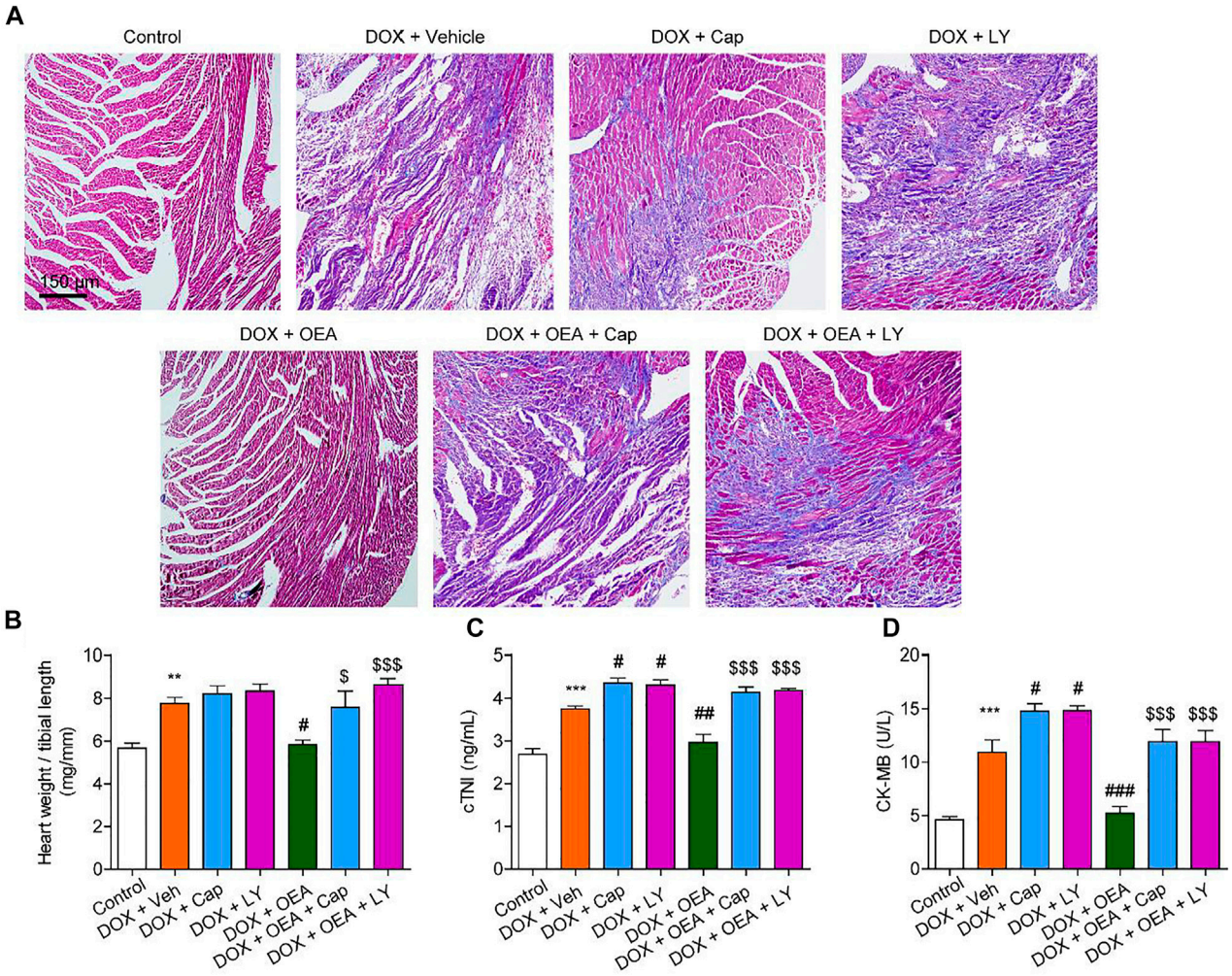

FIGURE 6 | OEA attenuates DIC in mice through a PI3K-dependent pathway. Mice with or without DOX (6 mg/kg, i. v.) challenge were treated with OEA (30 mg/kg, i. v.), capsazepine (5 mg/kg, i. v.) and LY294002 (10 mg/kg, i. v.) for 14 days concurrently with DOX challenge. Heart tissues were isolated at day 15 for analysis. **(A)** Representative histopathological sections of heart tissues by Masson staining. The effects of OEA and LY294002 on **(B)** heart weight/ tibial length ratio, serum levels of **(C)** cTNI and **(D)** CK-MB in mice. Data are expressed as mean ± SEM, $n = 6$. ***, $p < 0.001$ vs. control. #, $p < 0.05$ vs. DOX + vehicle. $$$, $p < 0.001$ vs. DOX + OEA.

OEA Inhibits DIC in HL-1 Cardiomyocytes Through a TRPV1-dependent Pathway

We further investigated the mechanism whereby OEA prevents DIC in HL-1 cardiomyocytes. OEA is known as an agonist of PPARα and TRPV1 (Ahern, 2003; Fu et al., 2003), thus we investigated whether OEA prevents oxidative stress and cell apoptosis through PPARα and/ or TRPV1 pathways. Consistent with *in vivo* results, OEA treatment reduced cardiac oxidative stress in DOX-challenged HL-1 cells (**Figures 3A,B**). The protective effects of OEA were completely prevented by TRPV1 antagonist capsazepine, but not by PPARα antagonist GW6471 (**Figures 3A,B**). In addition, TRPV1 agonist nonivamide but not PPARα agonist fenofibrate improved cellular oxidative defense in HL-1 cells treated with DOX (**Figures 3A,B**). We also measured cells viability and apoptosis at 24 h after DOX challenge. Treatment of OEA increased cells viability and reduced cells apoptosis (**Figures 3C–E**). The beneficial effects of OEA were impaired after pre-treatment with TRPV1 antagonist capsazepine but not PPARα antagonist GW6471 (**Figures 3C–E**). To confirm the role of TRPV1 in OEA-mediated therapeutic effects, we also tested the actions of OEA in TRPV1- deficiency cells. We found that the effects of PEA on GST, TBARS and TUNEL were prevented by TRPV1 deletion in HL-1 cells transfected with TRPV1 siRNA (**Supplementary Figures S2A–C**). These results together with the data obtained from inhibitors studies indicated that OEA inhibited DIC through TRPV1 pathway activation.

OEA Promotes TRPV1-Mediated PI3K/ Akt Signaling in HL-1 Cardiomyocytes

TRPV1 is known to activate PI3K/Akt signaling and promote cells survival (Zhai et al., 2020). To verify that the PI3K/Akt

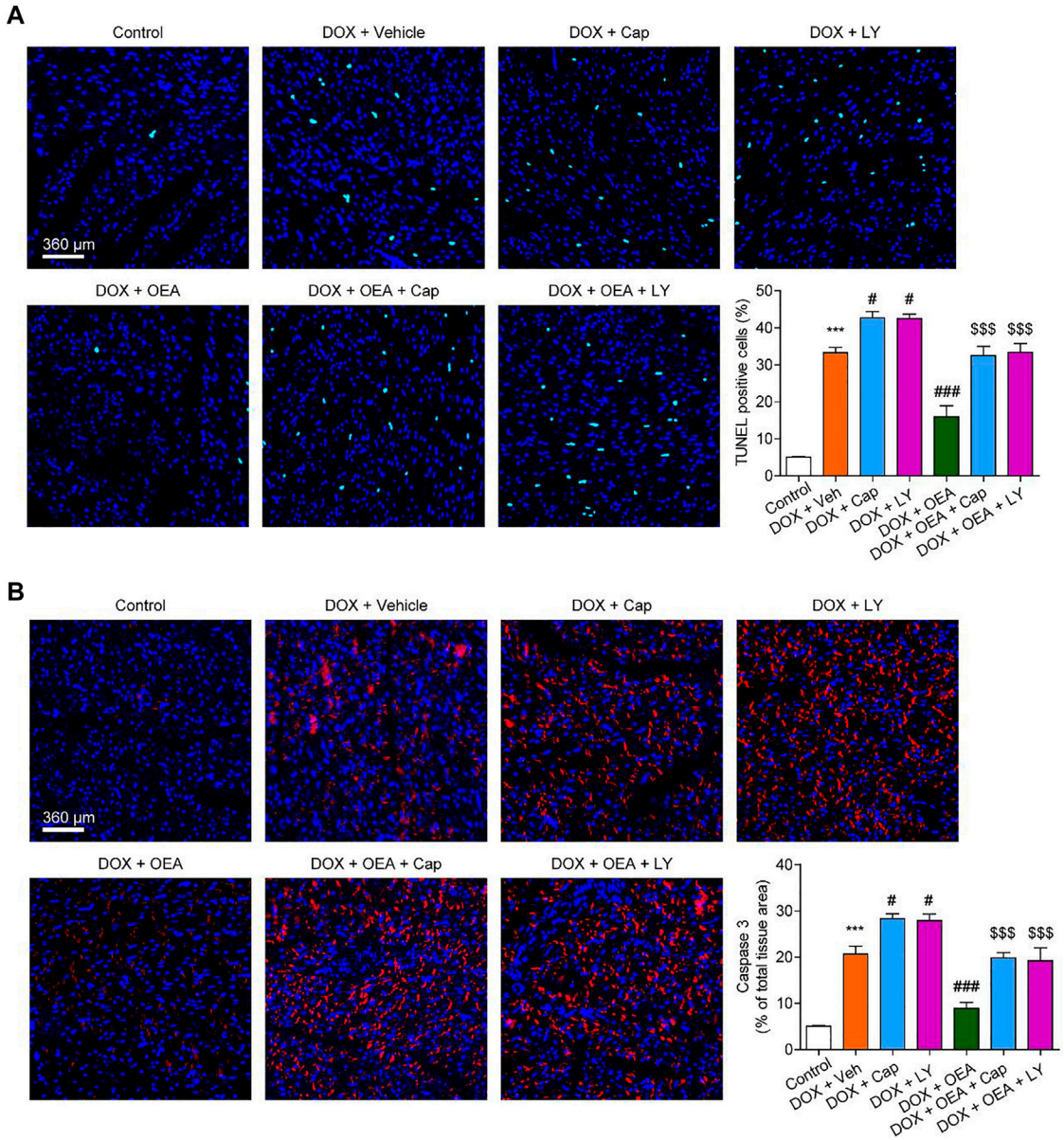

FIGURE 7 | OEA attenuates DOX-mediated myocardial oxidative stress in mice through a PI3K-dependent pathway. Mice with or without DOX (6 mg/kg, i. v.) challenge were treated with OEA (30 mg/kg, i. v.), capsazepine (5 mg/kg, i. v.) and LY294002 (10 mg/kg, **(I)** v.) for 14 days concurrently with DOX challenge. Heart tissues were isolated at day 15 for analysis. **(A)** Detection of apoptotic cells in mice cardiac tissues by TUNEL staining. TUNEL positive cells were counted. **(B)** Immunofluorescence staining of caspase three in myocardial tissues. Expression of caspase three were calculated. Data are expressed as mean ± SEM, $n = 6$. ***, $p < 0.001$ vs. control. #, $p < 0.05$ vs. DOX + vehicle. $$$, $p < 0.001$ vs. DOX + OEA.

signaling pathway activation is involved in the protective effects of OEA in DOX-treated cardiomyocytes, we examined PI3K and p-Akt expression on HL-1 cells that were cultured for 24 h in the absence or presence of OEA and/or the PI3K inhibitor, LY294002. As illustrated in **Figure 4**, DOX reduced PI3K expression in HL-1 cells, while OEA and nonivamide restored the PI3K expressions to normal levels. This effect of OEA was abolished by capsazepine. DOX also caused a reduction in cellular phosphorylated Akt (p-Akt) content, while treatment with OEA and nonivamide blocked the DOX-induced reduction of p-Akt levels. Inhibition of PI3K activity with LY294002 or antagonism of TRPV1 with capsazepine respectively reversed the effects of OEA. These data suggested that OEA promotes TRPV1-mediated PI3K/ Akt signaling in cardiomyocytes.

Next, we examined whether PI3K/ Akt signaling plays a role in the protective effects of OEA in HL-1 cardiomyocytes. As illustrated in **Figures 5A,B**, the antioxidant actions of OEA

were reversed by PI3K inhibitor LY294002. Moreover, OEA failed to increase cells viability and reduce cells apoptosis in LY294002-treated HL-1 cardiomyocytes (**Figures 5C–G**). Additionally, we also confirmed these results in adult derived primary human cardiomyocytes. As shown in **Supplementary Figure S3**, OEA effectively reduced cardiac oxidative stress and cells apoptosis in DOX-challenged cardiomyocytes, while capsazepine and LY294002 prevented these effects. These *in vitro* data confirm the essential role of TRPV1-mediated PI3K/ Akt signaling in the protective effects of OEA.

OEA Attenuates DIC in Mice Through a TRPV1-Mediated PI3K/ Akt Pathway

To further confirmed the role of TRPV1-mediated PI3K/ Akt signaling in OEA-mediated cardiac protection, we determined the effect of LY294002 and capsazepine in DOX-treated mice. As shown in **Figures 6**, **7**, treatment with LY294002 or capsazepine alone augmented DIC in mice. Furthermore, inhibition of PI3K activity with LY294002 or antagonism of TRPV1 with capsazepine, reversed the protective effect of OEA against DIC in cardiomyocytes, as demonstrated by myocardial fibrosis (**Figures 6A,B**), cardiac tissue damage (**Figures 6C,D**) and increased number of apoptotic cells (**Figure 7**). In summary, these results revealed that OEA attenuates DIC in mice through a TRPV1-mediated PI3K/ Akt pathway.

DISCUSSION

DOX is one of the most widely used chemotherapeutic anticancer drug (Al-Malky et al., 2020). However, prolonged clinical use of this compound has been associated to multiple serious effects, especially cardiovascular toxicity (Al-Malky et al., 2020). Mechanisms by which Dox promotes cardiac injury remains controversial. Enhanced oxidative stress and apoptosis dysregulation have been proposed to be involved in Dox-mediated cardiomyopathy (Renu et al., 2018). In this study, we observed that OEA alleviated DOX-induced cardiac dysfunction and cell apoptosis *in vitro* and *in vivo*. Furthermore, the protective effect of OEA was dependent on TRPV1-mediated PI3K/ Akt pathway, as inhibition of TRPV1 and PI3K abolished such effect.

Oxidative stress responses, including myocardial lipids peroxidation, DNA oxidative damage and generation of excessive ROS, have been reported to contribute to DIC (Minotti et al., 1996). Oxidative stress can activate serval apoptotic signaling pathways, such as p38/ JNK/ p53 MAPK signaling and NF-κB signaling, which trigger the activation of pro-apoptotic factors (Redza-Dutordoir and Averill-Bates, 2016; Das et al., 2018). Oxidative stress also endorses cell death by activating cardiolipin oxidation and increase mitochondrial permeability, which trigger caspase signaling and promote myocardial cell apoptosis (Circu and Aw, 2010; Redza-Dutordoir and Averill-Bates, 2016). In our study, OEA treatment significantly attenuated Dox-mediated oxidative stress in cardiac cells, evidenced from decreased expressions of TBARS and 8-OHdG, and increased levels of GST in OEA-treated cardiomyocytes, thus improved DIC.

OEA, an endogenous fatty acid amide, is the agonist of PPARα (IC_{50} = 0.12 μM) and TRPV1 (IC_{50} = 2 μM) (Ahern, 2003; Fu et al., 2003). The biological activities of OEA, such as control of food intake, anti-inflammation, neuro-protection and lipid metabolism, have been widely investigated (Bowen et al., 2017). To date, most of these effects have been shown to be mediated by the activation of PPARα, and the role of TRPV1 in OEA-mediated actions are less-well understood (Bowen et al., 2017). In our study, the effects of OEA were likely due to activation of TRPV1 but not PPARα. Supporting this conclusion, we found that the protective effects of OEA were abolished by the TRPV1 antagonist capsazepine, but not PPARα antagonist GW6471. In addition, activation of TRPV1 but not PPARα, reduced DIC. In accordance with our observation, Mahdieh Rahmatollahi et al. have shown that antagonism of PPARα improved DOX-induced atrial dysfunction (Rahmatollahi et al., 2016). Wei Ge et al. have reported that DOX-induced cardiac functional defect and apoptosis were reversed by the TRPV1 agonist SA13353 (Ge et al., 2016).

Recent literatures have provided important insight into the connection between TRPV1 to the cell proliferation and survival (Zhai et al., 2020). Of particular important mechanism is the activation of PI3K/ Akt by TRPV1 (Zhai et al., 2020). Consistent with these observations, we found that OEA increased expressions of PI3K and p-Akt in cardiomyocytes through a TRPV1-dependent way. Moreover, previous studies have shown that activation of PI3K/ Akt ameliorates doxorubicin-induced myocardial injury (Sun et al., 2014; Liu et al., 2016; Sahu et al., 2019; Nie et al., 2021). Our data confirmed the contribution of PI3K/ Akt signaling in OEA-mediated protective effects, thereby supporting the proposed mechanism that OEA alleviates DIC through a TRPV1-mediated PI3K/ Akt pathway. The present study has several limitations. First, the cardiac function parameters were not tested in the present study. Second, the other potential limitation of the present study is that our animal model is tumor-free. As a result, we cannot rule out potential effects of OEA on the anticancer effects of DOX. Thus, future studies should be carried out to confirm this action.

In summary, our results revealed that OEA protects cardiomyocytes against DOX-induced cytotoxicity through activation of TRPV1/ PI3K/ Akt signaling. Our results also identify OEA as a promising therapy for DIC.

DATA AVAILABILITY STATEMENT

The original contributions presented in the study are included in the article/**Supplementary Material**, further inquiries can be directed to the corresponding author.

ETHICS STATEMENT

The animal study was reviewed and approved by the Animal Care and Use Committee of Hainan Medical University.

AUTHOR CONTRIBUTIONS

YQ and JX conducted most of the experiments and helped with manuscript preparation. RZ and YL helped with data analysis. HW conceived the experiments and designed the experiments.

FUNDING

This work was supported by the foundation of Health and Family Planning Commission of Hannan Province of China (No. 20A200476).

SUPPLEMENTARY MATERIAL

The Supplementary Material for this article can be found online at: https://www.frontiersin.org/articles/10.3389/fphar.2022.863322/full#supplementary-material

REFERENCES

Aguilar Diaz De Leon, J., and Borges, C. R. (2020). Evaluation of Oxidative Stress in Biological Samples Using the Thiobarbituric Acid Reactive Substances Assay. *J. Vis. Exp.* 12, 159. doi:10.3791/61122

Ahern, G. P. (2003). Activation of TRPV1 by the Satiety Factor Oleoylethanolamide. *J. Biol. Chem.* 278, 30429–30434. doi:10.1074/jbc.M305051200

Al-Malky, H. S., Al Harthi, S. E., and Osman, A. M. (2020). Major Obstacles to Doxorubicin Therapy: Cardiotoxicity and Drug Resistance. *J. Oncol. Pharm. Pract.* 26, 434–444. doi:10.1177/1078155219877931

Bowen, K. J., Kris-Etherton, P. M., Shearer, G. C., West, S. G., Reddivari, L., and Jones, P. J. H. (2017). Oleic Acid-Derived Oleoylethanolamide: A Nutritional Science Perspective. *Prog. Lipid Res.* 67, 1–15. doi:10.1016/j.plipres.2017.04.001

Circu, M. L., and Aw, T. Y. (2010). Reactive Oxygen Species, Cellular Redox Systems, and Apoptosis. *Free Radic. Biol. Med.* 48, 749–762. doi:10.1016/j.freeradbiomed.2009.12.022

Das, S., Joardar, S., Manna, P., Dua, T. K., Bhattacharjee, N., Khanra, R., et al. (2018). Carnosic Acid, a Natural Diterpene, Attenuates Arsenic-Induced Hepatotoxicity via Reducing Oxidative Stress, MAPK Activation, and Apoptotic Cell Death Pathway. *Oxid Med. Cel Longev* 2018, 1421438. doi:10.1155/2018/1421438

Fu, J., Gaetani, S., Oveisi, F., Lo Verme, J., Serrano, A., Rodríguez De Fonseca, F., et al. (2003). Oleylethanolamide Regulates Feeding and Body Weight through Activation of the Nuclear Receptor PPAR-Alpha. *Nature* 425, 90–93. doi:10.1038/nature01921

Ge, W., Yuan, M., Ceylan, A. F., Wang, X., and Ren, J. (2016). Mitochondrial Aldehyde Dehydrogenase Protects against Doxorubicin Cardiotoxicity through a Transient Receptor Potential Channel Vanilloid 1-mediated Mechanism. *Biochim. Biophys. Acta* 1862, 622–634. doi:10.1016/j.bbadis.2015.12.014

Kalantary-Charvadeh, A., Sanajou, D., Hemmati-Dinarvand, M., Marandi, Y., Khojastehfard, M., Hajipour, H., et al. (2019). Micheliolide Protects against Doxorubicin-Induced Cardiotoxicity in Mice by Regulating PI3K/Akt/NF-kB Signaling Pathway. *Cardiovasc. Toxicol.* 19, 297–305. doi:10.1007/s12012-019-09511-2

Li, H., Li, X., Yang, B., Su, J., Cai, S., Huang, J., et al. (2021). The Retinoid X Receptor α Modulator K-80003 Suppresses Inflammatory and Catabolic Responses in a Rat Model of Osteoarthritis. *Sci. Rep.* 11, 16956. doi:10.1038/s41598-021-96517-y

Liang, X., Wang, S., Wang, L., Ceylan, A. F., Ren, J., and Zhang, Y. (2020). Mitophagy Inhibitor Liensinine Suppresses Doxorubicin-Induced Cardiotoxicity through Inhibition of Drp1-Mediated Maladaptive Mitochondrial Fission. *Pharmacol. Res.* 157, 104846. doi:10.1016/j.phrs.2020.104846

Liu, M. H., Zhang, Y., He, J., Tan, T. P., Wu, S. J., Guo, D. M., et al. (2016). Hydrogen Sulfide Protects H9c2 Cardiac Cells against Doxorubicin-Induced Cytotoxicity through the PI3K/Akt/FoxO3a Pathway. *Int. J. Mol. Med.* 37, 1661–1668. doi:10.3892/ijmm.2016.2563

Liu, Y., Zeng, L., Yang, Y., Chen, C., Wang, D., and Wang, H. (2020). Acyl-CoA Thioesterase 1 Prevents Cardiomyocytes from Doxorubicin-Induced Ferroptosis via Shaping the Lipid Composition. *Cell Death Dis* 11, 756. doi:10.1038/s41419-020-02948-2

Minotti, G., Mancuso, C., Frustaci, A., Mordente, A., Santini, S. A., Calafiore, A. M., et al. (1996). Paradoxical Inhibition of Cardiac Lipid Peroxidation in Cancer Patients Treated with Doxorubicin. Pharmacologic and Molecular Reappraisal of Anthracycline Cardiotoxicity. *J. Clin. Invest.* 98, 650–661. doi:10.1172/JCI118836

Nie, L., Liu, M., Chen, J., Wu, Q., Li, Y., Yi, J., et al. (2021). Hydrogen Sulfide Ameliorates Doxorubicininduced Myocardial Fibrosis in Rats via the PI3K/AKT/mTOR Pathway. *Mol. Med. Rep.* 23, 299. doi:10.3892/mmr.2021.11938

Pandey, R., Mousawy, K., Nagarkatti, M., and Nagarkatti, P. (2009). Endocannabinoids and Immune Regulation. *Pharmacol. Res.* 60, 85–92. doi:10.1016/j.phrs.2009.03.019

Rahmatollahi, M., Baram, S. M., Rahimian, R., Saeedi Saravi, S. S., and Dehpour, A. R. (2016). Peroxisome Proliferator-Activated Receptor-α Inhibition Protects against Doxorubicin-Induced Cardiotoxicity in Mice. *Cardiovasc. Toxicol.* 16, 244–250. doi:10.1007/s12012-015-9332-0

Redza-Dutordoir, M., and Averill-Bates, D. A. (2016). Activation of Apoptosis Signalling Pathways by Reactive Oxygen Species. *Biochim. Biophys. Acta* 1863, 2977–2992. doi:10.1016/j.bbamcr.2016.09.012

Renu, K., Vg, A., Pb, T. P., and Arunachalam, S. (2018). Molecular Mechanism of Doxorubicin-Induced Cardiomyopathy - an Update. *Eur. J. Pharmacol.* 818, 241–253. doi:10.1016/j.ejphar.2017.10.043

Sahu, R., Dua, T. K., Das, S., De Feo, V., and Dewanjee, S. (2019). Wheat Phenolics Suppress Doxorubicin-Induced Cardiotoxicity via Inhibition of Oxidative Stress, MAP Kinase Activation, NF-Kb Pathway, PI3K/Akt/mTOR Impairment, and Cardiac Apoptosis. *Food Chem. Toxicol.* 125, 503–519. doi:10.1016/j.fct.2019.01.034

Seifert, C. F., Nesser, M. E., and Thompson, D. F. (1994). Dexrazoxane in the Prevention of Doxorubicin-Induced Cardiotoxicity. *Ann. Pharmacother.* 28, 1063–1072. doi:10.1177/106002809402800912

Sun, X., Gu, J., Chi, M., Li, M., Lei, S., and Wang, G. (2014). Activation of PI3K-Akt through Taurine Is Critical for Propofol to Protect Rat Cardiomyocytes from Doxorubicin-Induced Toxicity. *Can. J. Physiol. Pharmacol.* 92, 155–161. doi:10.1139/cjpp-2013-0246

Sun, Z., Lu, W., Lin, N., Lin, H., Zhang, J., Ni, T., et al. (2020). Dihydromyricetin Alleviates Doxorubicin-Induced Cardiotoxicity by Inhibiting NLRP3 Inflammasome through Activation of SIRT1. *Biochem. Pharmacol.* 175, 113888. doi:10.1016/j.bcp.2020.113888

Tadokoro, T., Ikeda, M., Ide, T., Deguchi, H., Ikeda, S., Okabe, K., et al. (2020). Mitochondria-dependent Ferroptosis Plays a Pivotal Role in Doxorubicin Cardiotoxicity. *JCI Insight* 5, e132747. doi:10.1172/jci.insight.132747

Valavanidis, A., Vlachogianni, T., and Fiotakis, C. (2009). 8-hydroxy-2' -deoxyguanosine (8-OHdG): A Critical Biomarker of Oxidative Stress and Carcinogenesis. *J. Environ. Sci. Health C Environ. Carcinog Ecotoxicol Rev.* 27, 120–139. doi:10.1080/10590500902885684

Wu, K., Xiu, Y., Zhou, P., Qiu, Y., and Li, Y. (2019). A New Use for an Old Drug: Carmofur Attenuates Lipopolysaccharide (LPS)-Induced Acute Lung Injury via Inhibition of FAAH and NAAA Activities. *Front. Pharmacol.* 10, 818. doi:10.3389/fphar.2019.00818

Yang, L., Guo, H., Li, Y., Meng, X., Yan, L., Dan Zhang, Z., et al. (2016). Oleoylethanolamide Exerts Anti-inflammatory Effects on LPS-Induced THP-1 Cells by Enhancing PPARα Signaling and Inhibiting the NF-Kb and ERK1/2/AP-1/STAT3 Pathways. *Sci. Rep.* 6, 34611. doi:10.1038/srep34611

Zhai, K., Liskova, A., Kubatka, P., and Büsselberg, D. (2020). Calcium Entry through TRPV1: A Potential Target for the Regulation of Proliferation and Apoptosis in Cancerous and Healthy Cells. *Int. J. Mol. Sci.* 21, 4177. doi:10.3390/ijms21114177

Zhou, P., Xiang, L., Yang, Y., Wu, Y., Hu, T., Liu, X., et al. (2019). N-acylethanolamine Acid Amidase (NAAA) Inhibitor F215 as a Novel Therapeutic Agent for Osteoarthritis. *Pharmacol. Res.* 145, 104264. doi:10.1016/j.phrs.2019.104264

Zhou, Y., Yang, L., Ma, A., Zhang, X., Li, W., Yang, W., et al. (2012). Orally Administered Oleoylethanolamide Protects Mice from Focal Cerebral Ischemic Injury by Activating Peroxisome Proliferator-Activated Receptor α. *Neuropharmacology* 63, 242–249. doi:10.1016/j.neuropharm.2012.03.008

Conflict of Interest: The authors declare that the research was conducted in the absence of any commercial or financial relationships that could be construed as a potential conflict of interest.

frontiers | Frontiers in Pharmacology

ORIGINAL RESEARCH
published: 26 April 2022
doi: 10.3389/fphar.2022.872057

Dimethyl Fumarate Ameliorates Doxorubicin-Induced Cardiotoxicity By Activating the Nrf2 Pathway

*Xiaoliang Hu†, Cheng Li†, Qian Wang†, Zhixing Wei, Taizhong Chen, Yuepeng Wang and Yigang Li**

Department of Cardiology, Xinhua Hospital Affiliated to Shanghai Jiao Tong University School of Medicine, Shanghai, China

Doxorubicin (DOX) is limited in clinical application because of its cardiotoxicity. Oxidative stress and apoptosis are crucial in DOX-induced cardiac injury. Dimethyl fumarate (DMF) is an FDA-approved oral drug with powerful effects to reduce oxidative stress and apoptosis through the Nrf2 pathway. This study was aimed to determine whether DMF can protect against DOX-induced cardiac injury. We used both neonatal rat cardiomyocytes (NRCMs) *in vitro* and DOX-induced cardiac toxicity *in vivo* to explore the effects of DMF. The results showed that DMF significantly improved cell viability and morphology in NRCMs. In addition, DMF alleviated DOX-induced cardiac injury in rats, as evidenced by decreased CK-MB, LDH levels, improved survival rates, cardiac function, and pathological changes. Moreover, DMF significantly inhibited cardiac oxidative stress by reducing MDA levels and increasing GSH, SOD, and GSH-px levels. And DMF also inhibited DOX-induced cardiac apoptosis by modulating Bax, Bcl-2 and cleaved caspase-3 expression. Moreover, DMF exerted its protective effects against DOX by promoting Nrf2 nuclear translocation, which activated its downstream antioxidant gene Hmox1. Silencing of Nrf2 attenuated the protective effects of DMF in NRCMs as manifested by increased intracellular oxidative stress, elevated apoptosis levels, and decreased cell viability. In addition, DMF showed no protective effects on the viability of DOX-treated tumor cells, which suggested that DMF does not interfere with the antitumor effect of DOX *in vitro*. In conclusion, our data confirmed that DMF alleviated DOX-induced cardiotoxicity by regulating oxidative stress and apoptosis through the Nrf2 pathway. DMF may serve as a new candidate to alleviate DOX-related cardiotoxicity in the future.

Keywords: dimethyl fumarate, doxorubicin, oxidative stress, apoptosis, Nrf2 pathway

OPEN ACCESS

Edited by:
Zhi-Ren Zhang,
Harbin Medical University, China

Reviewed by:
Parames C. Sil,
Bose Institute, India
Eugenia Piragine,
University of Pisa, Italy

****Correspondence:***
Yigang Li
liyigang@xinhuamed.com.cn

†These authors have contributed equally to this work

Specialty section:
This article was submitted to Cardiovascular and Smooth Muscle Pharmacology, a section of the journal Frontiers in Pharmacology

Received: *09 February 2022*
Accepted: *21 March 2022*
Published: *26 April 2022*

Citation:
Hu X, Li C, Wang Q, Wei Z, Chen T, Wang Y and Li Y (2022) Dimethyl Fumarate Ameliorates Doxorubicin-Induced Cardiotoxicity By Activating the Nrf2 Pathway. Front. Pharmacol. 13:872057. doi: 10.3389/fphar.2022.872057

INTRODUCTION

Doxorubicin (DOX) is isolated from a mutated strain of Streptomyces peucetius var. caesius and is widely used in clinical for multiple malignant tumor treatment (Carvalho et al., 2009; Damiani et al., 2016). It is one of the most established and commonly used antineoplastic agents in various cancers, including pediatric cancer, leukemia, breast cancer, etc. Unfortunately, this drug can cause cardiotoxicity, including arrhythmia, hypotension, heart failure, and even late-onset cardiomyopathy (Nebigil and Desaubry, 2018). The incidence of heart failure will climb to 48% once the accumulation dose of DOX reaches 700 mg/m2 (Li and Hill, 2014). Thus, the application of DOX is limited despite its powerful anti-tumor characteristic. Currently, the only FDA-approved cardioprotective drug for DOX is dexrazoxane, which

does not interfere with DOX activity (Reichardt et al., 2018). The hydrolysis products of dexrazoxane could prevent the generation of cardiotoxic reactive oxygen species (ROS) by chelating intracellular iron. However, hematological toxicity such as severe leucopenia was more common in patients with dexrazoxane, which may interfere with chemotherapy (Wiseman and Spencer, 1998). The mechanisms of DOX-induced myocardial injury include oxidative stress, lipid peroxidation, DNA damage, mitochondrial injury, apoptosis, and autophagy disorder (Rawat et al., 2021). Among them, oxidative stress and apoptosis-mediated cardiomyocytes death are the leading cause of cytotoxicity (Octavia et al., 2012). Briefly, DOX produces massive ROS, which induces mitochondrial dysfunction and cardiomyocyte apoptosis (Kashfi et al., 1990; Schlame et al., 2000). Therefore, targeting oxidative stress and apoptosis should be effective against DOX-induced cardiotoxicity.

Dimethyl fumarate (DMF), known as Tecfidera, is an FDA-approved drug for severe psoriasis and relapsing multiple sclerosis (MS) since 1994 (Xu et al., 2015). DMF is a fumaric acid, which can mainly be hydrolyzed by esterase into monomethyl fumarate (MMF) with a half-life of 1 h. Both DMF and MMF exert similar pharmacological effects in several pathological conditions. Evidence suggests that DMF mainly exerts protective effects by activating the nuclear factor erythroid 2 (Nrf2) antioxidant pathway (Scannevin et al., 2012). Nrf2 is an important transcription factor responsible for regulating the redox balance within the cell. Under normal conditions, Nrf2 remains inactive in the cytoplasm due to its binding to the Keap1 protein and secondary ubiquitination degradation. However, DMF can oxidize the sulfhydryl groups of Keap1, thereby separating Keap1 from Nrf2. Then Nrf2 enters the nucleus to activate various powerful antioxidant genes, including heme oxygenase-1 (Hmox1), NAD (P) H-quinone dehydrogenase 1 (NQO-1), and glutathione Peptide-S-transferase 1 (GST-1) (Ma, 2013). Besides, DMF has a strong anti-inflammatory effect by inhibiting NF-κB activity and many inflammatory cytokines expressions such as iNOS, TNF-a, and IL6 (Wierinckx et al., 2005; Meili-Butz et al., 2008; Wilms et al., 2010; Scannevin et al., 2012). Given the powerful effects of regulating oxidative stress and inflammation, DMF has been already shown benefits in treating several diseases such as COPD (Cattani-Cavalieri et al., 2020), IBD (Li et al., 2020) and recently novel coronavirus (COVID-19) infection (Olagnier et al., 2020).

As a powerful drug to activate Nrf2, DMF has shown protective effects in several cardiac pathological models such as myocardial infarction, ischemia-reperfusion injury, and sepsis-induced cardiac dysfunction (Meili-Butz et al., 2008; Giustina et al., 2018; Mouton et al., 2021). Here we hypothesize that DMF might also protect against DOX-induced myocardial injury. However, this has not previously been reported. The objectives of the current study were to investigate whether DMF can protect against DOX-induced cardiac damage.

MATERIALS AND METHODS

Chemicals and Materials

DOX was obtained from Selleck. DMF was purchased from Selleck, which was dissolved in 0.8% Carboxymethyl cellulose (CMC) for *in vivo* tests and 0.1% dimethylsulfoxide (DMSO) for *in vitro* experiments. The nuclear and cytoplasmic protein extraction kits were purchased from KEYGEN Biotech. Co., Ltd. (Nanjing, China). Bicinchoninic acid (BCA) protein assay kit and cell lysis buffer kit were obtained from Beyotime Institute of Biotechnology (Jiangsu, China).

Primary (Neonatal Rat Cardiomyocytes) NRCMs Culture

NRCMs were isolated from the ventricles of 1- to 3-day-old neonatal Sprague–Dawley (SD) rats as previously described (Liu et al., 2014). Briefly, neonatal rat hearts were minced into 1-mm^3 pieces and were digested with 0.125% trypsin and 0.1% collagenase type I. Tow hours differential attachment culture was performed to separate cardiac fibroblasts from cardiomyocytes. Then NRCMs were cultured in medium with 5-BrdU. Through this method, the purity of cardiomyocytes could reach more than 90%. After incubation for 24 h, 90% of cardiomyocytes exhibited spontaneous pulsing, which indicated good viability.

Animals

Male-SD rats weighing 230–250 g (8-weeks old) were obtained from the Shanghai Jihui Laboratory Animal Care Co., Ltd (Shanghai, China) and maintained under SPF conditions in a controlled environment of 20–22 °C, with a 12/12 h light/dark cycle and 50–70% humidity, and food and water provided ad libitum. Rats were randomly divided into five groups: control groups, DOX-treated groups, solvent control groups, and DMF-treated groups. DMF was dissolved in 0.8% CMC and administered to rats by oral gavage, with CMC as solvent control. Based on preliminary data and previous studies, the rats were treated with DMF at a total daily dose of 40 mg/kg/d and 80 mg/kg/d twice a day (Li et al., 2018; Motterlini et al., 2019). The rats in DOX-treated groups were intraperitoneally injected with DOX (15 mg/kg diluted with 0.9% saline). The rats in solvent control groups and DMF-treated groups were pretreated with 0.8% CMC or DMF a week prior to DOX treatment (15 mg/kg diluted with 0.9% saline, intraperitoneally) and maintained until the end of the experiment. Six days after DOX treatment, all rats were sacrificed. The serum samples were obtained from blood by centrifugation (3000 r/min, 4°C) for 10 min, and the heart tissues were removed for further testing. All animal experiments were approved by the Institutional Review and Ethics Board of Shanghai Xinhua Hospital, Shanghai Jiao Tong University School of Medicine.

Echocardiography Analysis

Rats were anesthetized with 1% isoflurane inhalation and placed on a heated pad to maintain 37°C body temperature. The ejection fraction (EF) and fractional shortening (FS) were measured from M-mode images of echocardiography (Vivid 7; GE Medical, Milwaukee, WI, United States) with a 15 MHz transducer.

Cell Viability Evaluation

Cell counting kit 8 (CCK8) assay was performed according to the manufacturer's instructions. Briefly, after the cells were exposed to various treatments, CCK-8 (10 μl) was added to each well of the 96-well plate, and the plate was incubated for 4 h at 37°C. Cell viability was calculated by absorbance measurements at 450 nm using a Synergy H1 Multi-Mode Reader (BioTek, Winooski, VT, United States).

Hoechst 33258 Staining

Cells were seeded in the 24-well plates and were incubated with different interventions. At the end of the incubation period, cells were fixed, washed with PBS three times, and stained with Hoechst 33258 staining solution (Beyotime, Shang Hai, China) for 5 min at room temperature and observed by fluorescence microscope (OLYMPUS, Tokyo, Japan). Fragmented or condensed nuclei were considered apoptotic cells.

ROS Testing

At the end of different interventions, DCFH-DA (10 μM) was added in the well for 20 min induction at 37°C after removing the medium. The samples were observed using fluorescence microscopy (Olympus, Tokyo, Japan).

Immunofluorescence Staining

NRCMs were stained with antibodies against α-actinin (A5044,1: 100) and Nrf2 (ab137500,1:100), heart sections were stained with antibody against Nrf2 (ab137500,1:100) in a humidified box at 4°C overnight and followed by incubation with fluorescein-labeled secondary antibody for 1 h at 37°C. The cell nuclei were stained with DAPI for 5 min. All images were captured with a fluorescence microscope or scanner by Caseviewer software (3D Histech).

Measurement of CK-MB, LDH, ALT, Creatinine in Serum and MDA, SOD, GSH, and GSH- Px in Tissues

The CK-MB, LDH, ALT, creatinine levels in serum were detected using the commercial kits (Changchun Huili Biotech Co., Ltd.) according to the instructions. In addition, the heart tissues were placed in cold saline (1: 10, w/v) and then homogenized with a homogenizer machine. Next, the supernatant was obtained through centrifuging at 3000 r/min to detect the MDA, SOD, GSH, and GSH- Px levels in heart tissues according to the instructions (Jiancheng Biotech Co. Ltd, China).

Histopathologic Assay

Heart tissues were fixed in 10% formalin and embedded in paraffin, and then the sections were stained with hematoxylin-eosin (H&E) solution. Finally, images of the stained sections were obtained by Olympus microscope or scanner (3D Histech). The images were graded by the degree of myocardial necrosis and inflammatory cell infiltration according to the following standards: grade 0, normal; grade 1, lesion not exceeding 25%; grade 2, lesion between 25–50%; grade 3, lesion between 50–75%; grade 4, lesion exceeding 75% (Kanda et al., 2004). Six sections of one heart were graded by an experienced pathologist, who was blinded to the study design. The mean score of the six sections was recorded as the final cardiac pathology score.

Western Blot

The total protein samples from the cells and heart tissues were homogenized using RIPA lysis buffer containing protease and phosphatase inhibitors (Beyotime, Shang Hai, China). The protein concentrations of the samples were determined using a BCA Protein Assay Kit. After determining the contents, the proteins were separated by SDS-PAGE (8–12.5%) and then transferred to PVDF membranes (Millipore, Massachusetts, United States). After being blocked with 5% skim milk for 2 h at room temperature, the membranes were incubated with primary antibodies overnight at 4°C. The following antibodies were used. Hmox1 (10701-1-AP, 1:1000), Bax (50599-2-Ig, 1:2000), Bcl-2 (12789-1-AP, 1:1000), lamin B1 (12987-1-AP, 1:1000) were purchased from proteintech. Antibody against cleaved caspase-3 (9661, 1:1000) was from CST. Antibody against Nrf2 (ab137500, 1: 1000) was purchased from Abcam. Then the bands were incubated with secondary antibody for 1 h at room temperature. The protein bands on the membranes were detected using an enhanced chemiluminescence system (WBKLS0500; Millipore, Darmstadt, Germany). Intensity values of the relative protein levels were normalized to β-actin (*in vitro*) or α-tubulin (*in vivo*).

Real-Time PCR Analysis

Total RNA was extracted with RNAiso Plus (Takara, Kusatsu, Japan) from NRCMs and heart tissues. cDNA was synthesized using Evo M-MLV RT Kit (AG, Hunan, China). Quantitative real-time polymerase chain reaction (RT-PCR) was performed with Hieff® qPCR SYBR Green Master Mix (Yeasen, Shang Hai, China) on a QuantStudio 3 Real-Time PCR System (Applied Biosisytems, Waltham, MA, United States). The sequences of primers are shown in **Supplementary Table S1**.

Transfection of Nrf2-siRNA

siRNAs were synthesized by Ribobio (Guangzhou, China). We transfected Nrf2-siRNA or negative control siRNA using Rfect siRNA/miRNA Transfection Reagent (Baidai biotechnology, Changzhou, China) according to the manufacturer's instructions when cells reached 40–50%. The transfection efficiency was evaluated by Western blot. The used siRNA sequences are as follows: SiRNA1: CAAACAGAATGGACCTAAA;SiRNA2: GCAAGAAGCCAGATACAAA;SiRNA3: GGATGAAGAGACCGGAGAA.

Data Analysis

The data are expressed as the mean ± standard deviation (SD). Statistical analysis was performed with GraphPad Prism 5.0 software (San Diego, CA, United States). It was performed with one-way analysis of variance (ANOVA) followed by Tukey's posthoc test when comparing multiple groups, whereas differences within two groups were evaluated by Student's *t*-test. Survival analysis was performed using the Kaplan–Meier method. Statistical significance was defined as $p < 0.05$.

RESULTS

The Protective Effects of DMF Against DOX-Induced NRCMs Damage

Firstly, NRCMs purity was identified by immunofluorescence for α-actinin, a cardiomyocyte-specific marker (**Figure 1B**). Then the concentration-dependently cytotoxicity of DMF was evaluated by CCK8 assay. Compared with the control group, the viabilities of NRCMs were significantly reduced over 40 μM DMF for 24 h. As a result, we conducted concentrations of 10 and 20 μM DMF in this

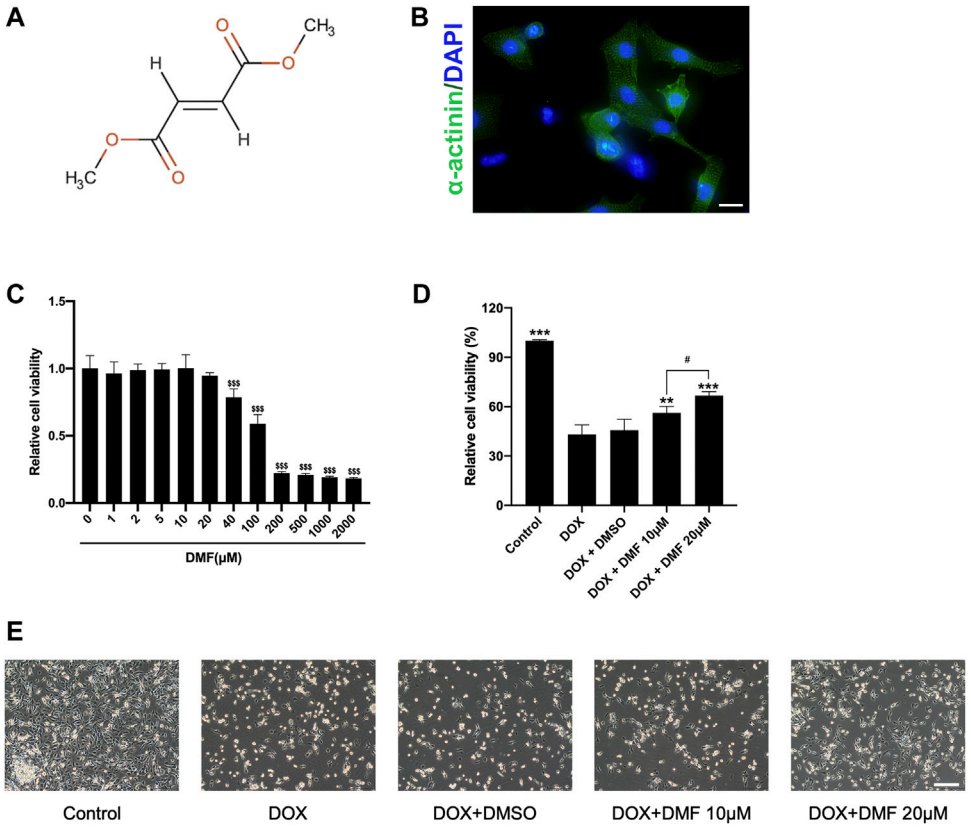

FIGURE 1 | DMF alleviates NRCMs damage against DOX. **(A)** Chemical structure of dimethyl fumarate. **(B)** Immunofluorescence of α-actinin in NRCMs (scale bar = 20 μm). **(C)** Cell viability of NRCMs with different concentrations of DMF ($n = 4$). **(D)** Changes in cell viability ($n = 4$). **(E)** Changes in cellular morphology ($n = 4$, scale bar = 50 μm). Data were presented as the mean ± SD. $^{\$\$\$}p < 0.001$, compared with the control group, $^{***}p < 0.001$, compared with the DOX group. $^{\#}p < 0.05$, compared with DOX + DMF 10 μM group.

research (**Figure 1C**). NRCMs were pre-treated with DMF for 4 h, then treated with 5 μM DOX for 48 h. Compared to the control group, DOX treatment caused a significant decrease in cell viability and impaired cell morphology. However, DMF could concentration-dependently improve the viability of NRCMs and cell morphology damage compared with the DOX group (**Figures 1D,E**). Furthermore, the solvent control of 0.1% DMSO showed no effects on the cells.

The Protective Effects of DMF Against DOX-Induced Cardiac Damage *In Vivo*

Treating rats with DOX resulted in about 67% mortality compared with the control group. However, pre-treatment with a 40 mg/kg DMF showed a mortality of 42% and 25% with a dose of 80 mg/kg (**Figure 2A**). The serum CK-MB and LDH levels in DOX groups increased compared with control groups. However, DMF dose-dependently decreased the serum CK-MB and LDH levels (**Figure 2B**). The pathology of DOX-induced myocardial injury mainly includes sarcoplasmic reticulum expansion, cardiomyocyte edema, fiber rupture, and massive inflammatory cell infiltration (Ferrans et al., 1997). Consistent with previous studies, DOX caused apparent myocardial tissue disturbance, necrosis, and massive inflammatory cell infiltration, as well as higher cardiac pathology scores, which were dose-dependently alleviated by DMF. The control solvents of 0.8% CMC showed no effects on animals (**Figure 2C**, **Supplementary Figure S1**).

Considering heart failure is the most severe side effect after DOX treatment, we evaluated indicators related to heart failure. We found that the body weight was dramatically reduced after DOX treatment and can be reversed with an increasing dose of DMF (**Figure 2D**). The heart weight/body weight ratio, a simple indicator of heart failure, was increased in the DOX group and can be dose-dependently reversed by DMF (**Figure 2E**). Furthermore, the echocardiography confirmed the cardiac function improvement in DMF after DOX treatment (**Figure 2F**).

DMF Inhibited Cardiac Oxidative Stress Caused by DOX

Given that oxidative stress is crucial in DOX-induced cardiac damage, we tested the oxidative stress levels *in vitro* and *in vivo*. The intracellular ROS level in NRCMs in the DOX group was remarkably increased compared with the control group and was decreased by DMF (**Figure 3A**). Then we measured some indicators representing tissue oxidative stress levels in heart tissue. MDA levels were elevated in DOX groups and were

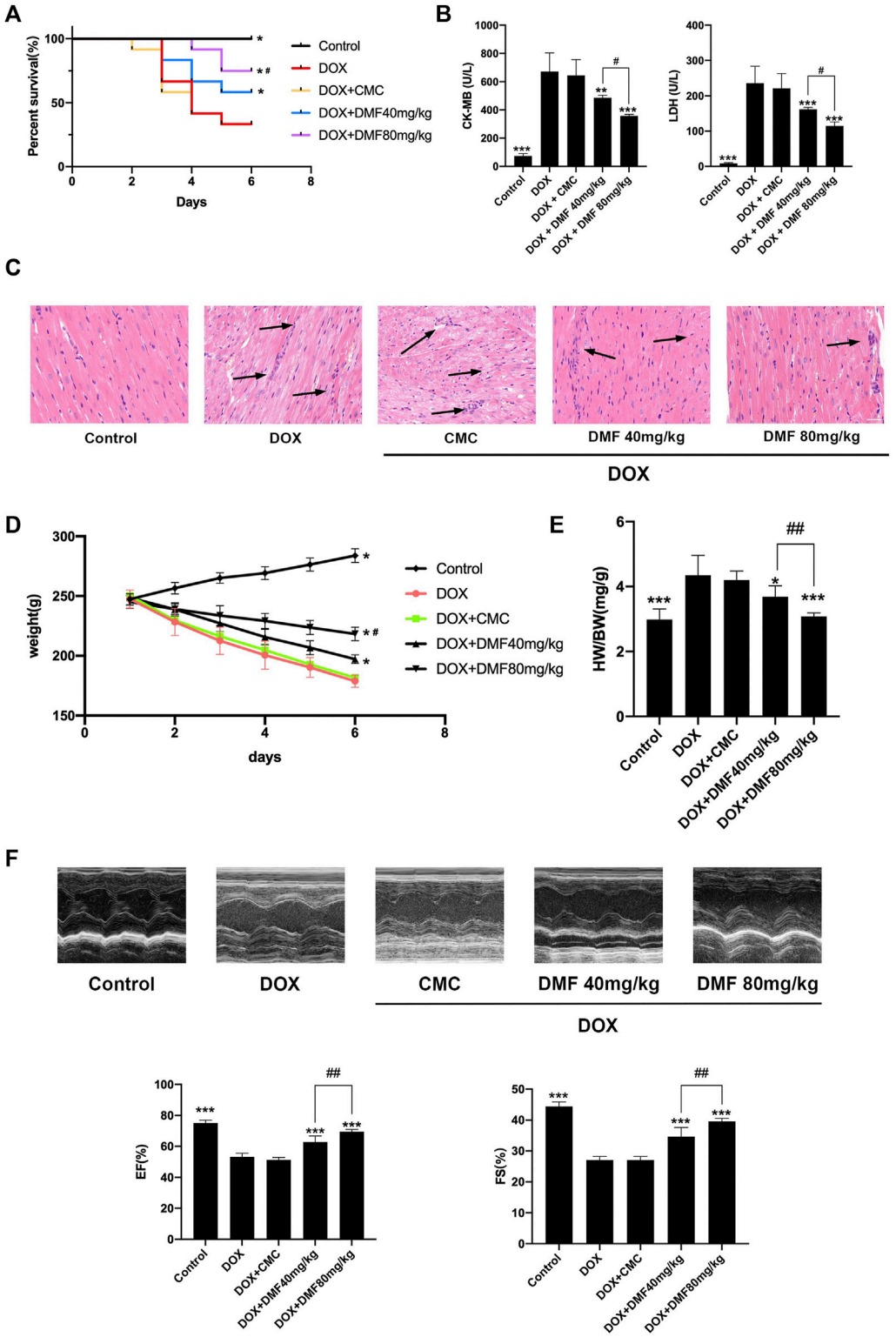

FIGURE 2 | DMF alleviated DOX-induced cardiac injury. **(A)** Effects of DMF on Kaplan-Meier survival curves ($n = 12$). **(B)** Changes in serum levels of CK-MB and LDH ($n = 6$). **(C)** Representative H&E staining of hearts (Black arrows indicate the cardiac injury sites, $n = 6$, scale bar = 20 μm) **(D)** Changes in the body weights ($n = 6$). **(E)** Changes in HW/BW (mg/g) ($n = 6$). **(F)** Representative M-mode echocardiograms and quantitative analysis of LVEF and FS($n = 5$). Data were presented as the mean ± SD. $^{*}p < 0.05$, $^{**}p < 0.01$, $^{***}p < 0.001$, compared with DOX group. $^{\#}p < 0.05$, $^{\#\#}p < 0.01$, compared with DOX + DMF 40 mg/kg group. HW: heart weight; BW: body weight.

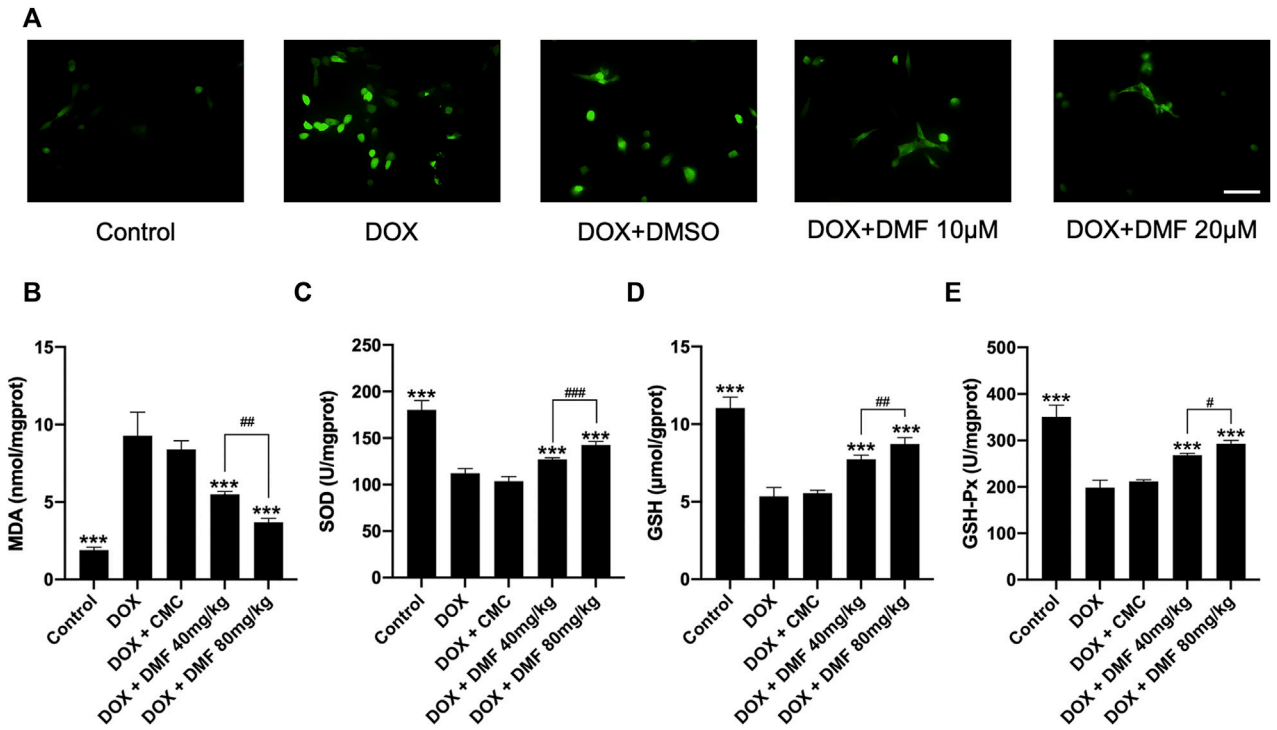

FIGURE 3 | DMF alleviated oxidative stress *in vitro* and *in vivo*. **(A)** Effects of DMF on cellular ROS level in NRCMs treated by DOX ($n = 5$, scale bar = 50 μm). **(B–E)** Effects of DMF on the levels of MDA, SOD, GSH, and GSH-Px in hearts after DOX treatment ($n = 6$). Data are presented as the mean ± SD. $^{***}p < 0.001$, compared with DOX group. $^{\#}p < 0.05$, $^{\#\#}p < 0.01$, $^{\#\#\#}p < 0.001$ compared with DOX + DMF 40 mg/kg.

significantly decreased by DMF. DMF restored the levels of SOD, GSH, and GSH-Px, which were downregulated in the DOX group (**Figures 3B–E**). These results indicated that DMF could alleviate DOX-induced oxidative stress *in vitro* and *vivo*.

DMF Alleviated DOX-Induced Cardiac Apoptosis

Apoptosis-related cardiomyocyte death is the leading cause of heart failure after DOX treatment, so we analyzed apoptosis indicators *in vitro* and *vivo*. The apoptotic cells were notably increased in the DOX group compared with the control group. However, treatment with DMF reduced the number of apoptotic cells (**Figure 4A**). Then, we evaluated the expression of apoptosis-related proteins. We found that administration of DOX increased the ratio of Bax/Bcl-2 and dramatically elevated the levels of cleaved caspase-3. In contrast, treatment with DMF notably decreased the Bax/Bcl-2 ratio and the levels of cleaved caspase-3 (**Figure 4B**). Consistent with results *in vitro*, DMF significantly reduced the ratio of Bax/Bcl-2 and the levels of cleaved caspase-3 in rats after DOX treatment (**Figure 4C**).

DMF Promotes Nrf2 Pathway Signaling

Nrf2 remains inactive in the cytoplasm under normal physiological conditions and enters the nucleus when activated. The expression levels of nuclear and cytoplasmic Nrf2 in NRCMs and heart tissues were assessed by western blotting. The results indicated that the expression levels of nuclear Nrf2 expression were significantly decreased, and the levels of cytoplasmic Nrf2 were slightly reduced in the DOX group. However, DMF significantly increased the expression levels of nuclear Nrf2 and decreased cytoplasmic Nrf2 levels (**Figures 5A,C**). These results suggested that DOX inhibited the entry of Nrf2 into the nucleus, which can be reversed by DMF. Then we further evaluated the Nrf2 translocation by immunofluorescence assay. Results *in vivo* confirmed that DOX significantly inhibited Nrf2 translocation, which can be dose-dependent reversed by DMF (**Figures 5B,D**). Hmox1 is one of the most powerful proteins in the Nrf2 pathway to defeat oxidative stress. We then tested its expression *in vitro* and *in vivo*. Results showed that DOX could significantly inhibit the expression of Hmox1, and DMF can dose-dependent increase it (**Figure 5E**). And other Nrf2 downstream antioxidant genes (NQO1, GCLC) showed similar changes (**Supplementary Figure S2**). These results indicated that DMF could activate the Nrf2 pathway by promoting Nrf2 transporting to the nucleus.

DMF Exerts Protective Effects Through Nrf2

To confirm the role of Nrf2 in the protective effects of DMF, the Nrf2-siRNA was conducted. Compared with the NC group, the protein levels of Nrf2 in NRCMs were most downregulated in the siRNA-2 group, which was used for further *in vitro* experiments

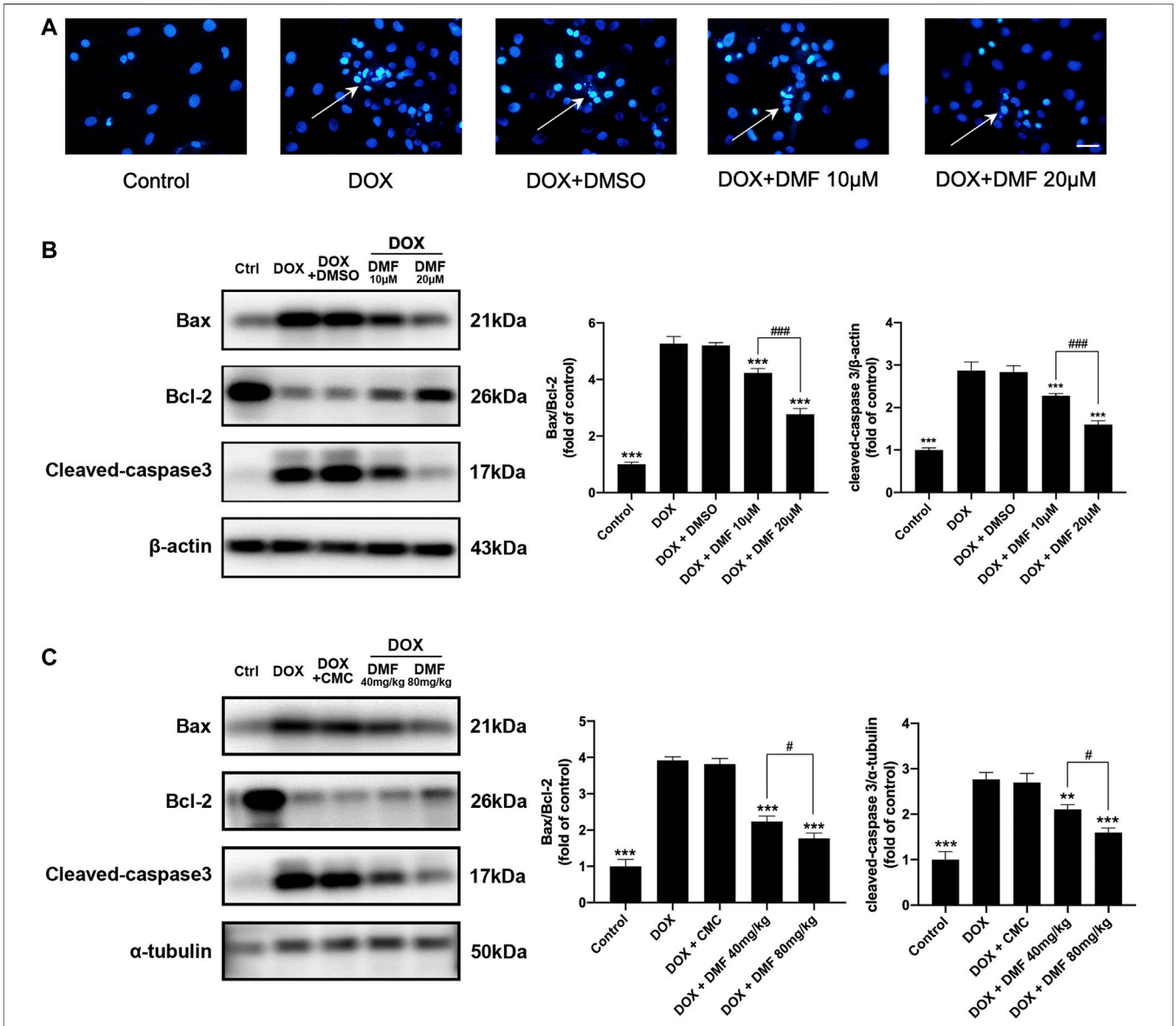

FIGURE 4 | DMF inhibited DOX-induced cardiac apoptosis. **(A)** Hoechst 33258 staining of NRCMs after DOX (White arrows indicate apoptotic cells, $n = 5$, scale bar = 50 μm). **(B)** Representative WB images and quantitative analysis of Bax/Bcl-2 ratio and cleaved caspase-3 in NRCMs ($n = 5$). **(C)** Representative WB images and quantitative analysis of Bax/Bcl-2 ratio and cleaved caspase-3 in rats ($n = 5$). All data were expressed by mean ± SD. $^{**}p < 0.01$, $^{***}p < 0.001$, compared with DOX group. $^{\#}p < 0.05$, $^{\#\#\#}p < 0.001$ compared with DOX + DMF 40 mg/kg or DOX + DMF 10 μM.

(**Figure 6A**). Transfection with Nrf2-siRNA reversed the cell viability improvements by DMF (**Figure 6B**). Moreover, the cell morphology damage, ROS level, apoptosis levels, and antioxidant genes expression were reserved after Nrf2 silencing (**Figures 6C,D**, **Supplementary Figure S3**). These results suggested that DMF protected against DOX through the Nrf2 pathway.

DMF Does Not Interfere With the Antitumor Ability of DOX

It was reported that Nrf2 activation could promote tumor cell proliferation and lead to chemotherapy resistance (Singh et al., 2016). So, we tested the effects of DMF on tumor cell viability after DOX treatment. Results showed that DMF exerted no protective effects on SHSY-5Y, RenCa, CT26. WT tumor cell lines after DOX (**Figure 7**).

DISCUSSION

DOX is a powerful and effective chemotherapeutic drug for solid and hematogenous cancer since 1969 (Damiani et al., 2016). However, the clinical utility of this drug is limited for its severe cardiotoxicity when it exceeds the cumulative dosage of 400–700 mg/m^2 for adults

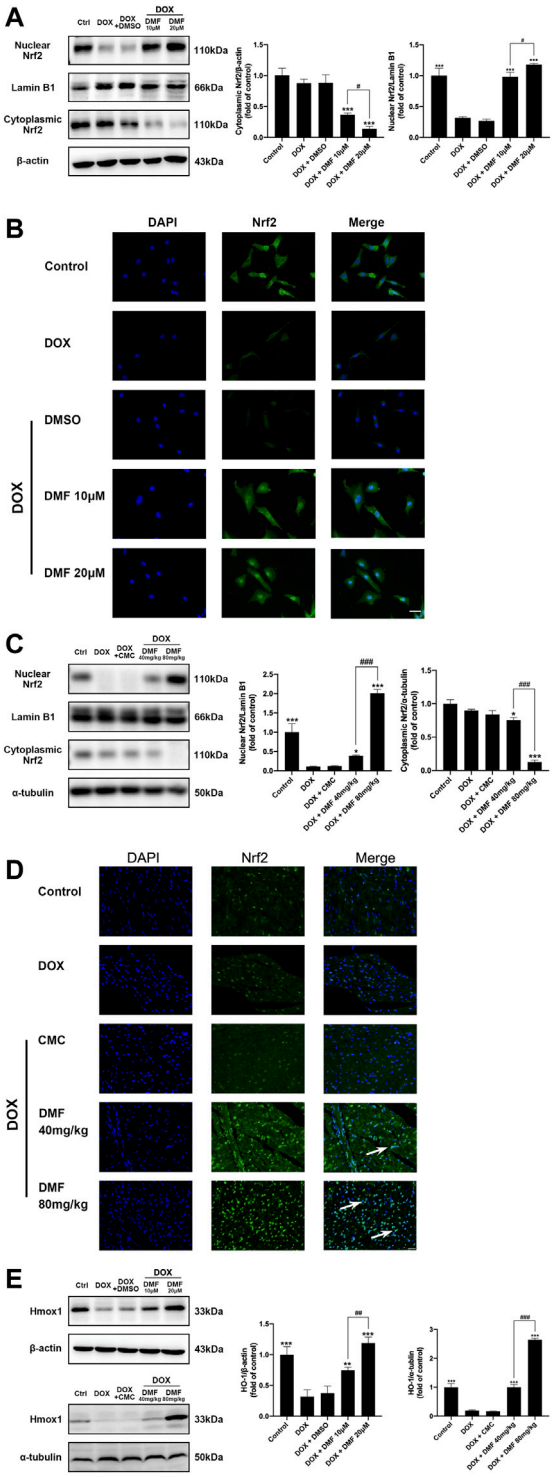

FIGURE 5 | Effect of DMF on Nrf2 signaling in NRCMs and rats after DOX treatment. **(A)** Representative WB images and quantitative analysis of nuclear and cytoplasmic Nrf2 expression in NRCMs. β-actin and Lamin B1 were served as cytoplasmic or nuclear internal controls, respectively (n = 5). **(B)** Location of Nrf2 in NRCMs using Immunofluorescence (n = 5, scale bar = 25 μm). **(C)** Representative WB images and quantitative analysis of nuclear and cytoplasmic Nrf2 expression in rats. α-tubulin and Lamin B1 were served as cytoplasmic or nuclear internal controls, respectively, (n = 5). **(D)** Location of Nrf2 in rats using immunofluorescence (White arrows indicate the nuclear entry of Nrf2, n = 5, scale bar = 20 μm). **(E)** Representative WB images and quantitative analysis of Hmox1 expression in NRCMs and rats (n = 5). Data are mean ± SD. $^{*}p < 0.05$, $^{**}p < 0.01$, $^{***}p < 0.001$, compared with DOX group. $^{\#}p < 0.05$, $^{\#\#}p < 0.01$, $^{\#\#\#}p < 0.001$ compared with DOX + DMF 10 μM or DOX + DMF 40 mg/kg.

(*Continued*)

and 300 mg/m^2 for children (Li and Hill, 2014). The cardiotoxicity mainly includes arrhythmia and congestive heart failure (Mitry and Edwards, 2016). However, the precise mechanism of DOX-induced cardiotoxicity is still elusive. Many mechanisms contribute to DOX cardiotoxicity, such as ROS overload, iron metabolism disorder, mitochondrial dysfunction, calcium dysregulation, inflammatory cascade, endothelial dysfunction, and apoptosis. Among those, oxidative stress plays a central role in DOX-induced cardiotoxicity. The abundant mitochondria within cardiomyocytes and inadequate endogenous antioxidant mechanism suggest that the heart is more susceptible to oxidative stress damage (Goffart et al., 2004).

After DOX administration, Massive ROS is produced during the redox cycle at complex I of the electron transport chain, leading to ATP synthesis disorder. In general, ROS-related enzymes within the mitochondria can reduce DOX to semiquinone, which can be readily reacted with oxygen to generate superoxide anions. Besides, DOX binds to free iron to generate iron-DOX complex, which can react with oxygen and catalyze Fenton reaction to produce massive ROS (Gutteridge, 1984; Simunek et al., 2009). The generated ROS then reacts with mitochondrial biomolecules (including lipids, proteins, and nucleic acids), disturbing mitochondrial function (Eder and Arriaga, 2006). Meanwhile, cardiomyocytes can reduce oxidative stress by some endogenous critical antioxidant enzymes, including SOD, GSH, GSH-Px. Among them, GSH and GSH-Px can catalyze the reduction of other peroxides, and SOD can reduce O^{2-} to low toxic H_2O_2 (Sugden and Clerk, 2006).

Nrf2 is a crucial intracellular oxidative stress regulator (Kopacz et al., 2020). Under oxidative stress, Nrf2 was depolymerized from Keap1 and translocated into the nucleus to activate various antioxidant genes (Hur and Gray, 2011; Kim et al., 2016). Nrf2 activation can alleviate arteriosclerosis, arrhythmia, and myocardial infarction by targeting ferroptosis, autophagy, programmed cell necrosis, and apoptosis (Chen, 2021). It was also reported that Nrf2 deficiency could aggravate cardiac injury after DOX treatment (Li et al., 2014).

As a powerful Nrf2 agonist, DMF would be speculated to alleviate cardiac oxidative stress caused by DOX. In the current study, DMF inhibited oxidative damage by downregulating levels of ROS *in vitro* and upregulating levels of SOD, GSH, GSH-Px *in vivo*. In addition, MDA, a significant ROS indicator, was significantly decreased by DMF. Then, the subcellular localization results of nrf2 suggested that DMF could promote nuclear translocation of Nrf2 and its downstream anti-oxidative gene (Hmox1) expression, which was inhibited by DOX. More importantly, the protective effects of DMF on oxidative stress

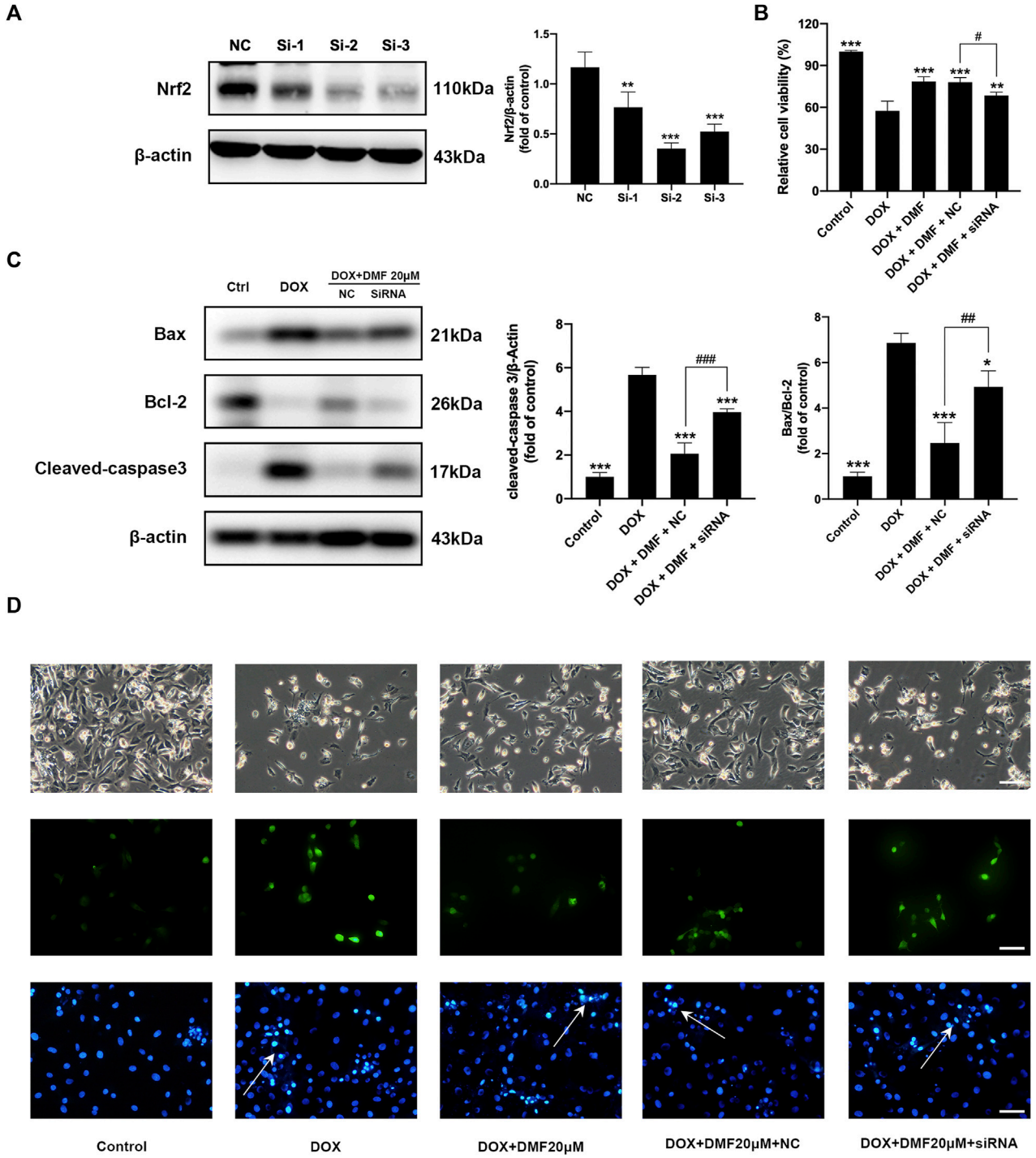

FIGURE 6 | Nrf2 silencing reversed the protective effects of DMF on DOX-induced NRCMs injury. **(A)** Representative WB images and quantitative analysis Nrf2 expression in NRCMs after siRNA transfection ($n = 5$). **(B)** Changes in cell viability in NRCMs ($n = 4$). **(C)** Representative WB images and quantitative analysis Bax/Bcl-2 ratio and cleaved caspase-3 expression in NRCMs ($n = 5$). **(D)** Changes in cell morphology ($n = 5$), ROS levels ($n = 5$), and Hoechst 33258 staining in NRCMs (White arrows indicate apoptotic cells, $n = 5$, scale bar = 50 μm). All data were expressed by mean ± SD. $^{*}p < 0.05$, $^{**}p < 0.01$, $^{***}p < 0.001$, compared with DOX or NC group. $^{\#}p < 0.05$, $^{\#\#}p < 0.01$, $^{\#\#\#}p < 0.001$ compared with DOX + DMF + NC group.

could be eliminated by Nrf2 silencing. Collectively, these results indicated that DMF inhibited oxidative stress caused by DOX through the Nrf2 pathway.

Besides, DOX can activate MAPK, p38, and JNK pathways, which leads to apoptosis by disrupting Bcl-2, Bax, cleaved caspase-9, and cleaved caspase-3 balance (Xu et al., 2005).

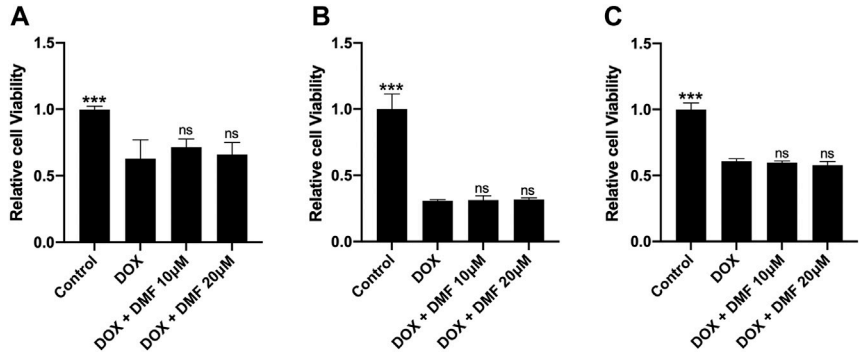

FIGURE 7 | Effects of DMF on antitumor efficacy of DOX in some tumor cell lines. **(A)** Cell viability of SH-SY5Y cell line (n = 4). **(B)** Cell viability of CT26. WT colon cancer cell line (n = 4). **(C)** Cell viability of renal cell adenocarcinoma (Renca) cell line (n = 4). All data were expressed by mean ± SD. ***p < 0.05 compared with DOX groups, ns (not significant).

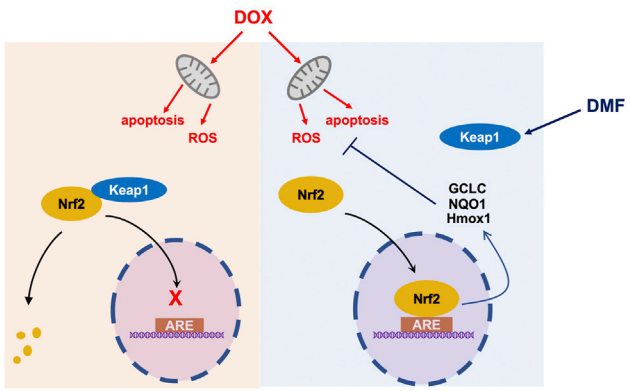

FIGURE 8 | A schematic diagram of protection of DMF against DOX-induced cardiotoxicity through Nrf2 pathway. ARE Antioxidant Response Element.

During apoptosis, caspase-3 is cleaved to an active form to degrade various functional proteins. Therefore, its activation is considered a sign of the inevitable stage of apoptosis (Crowley and Waterhouse, 2016). In our study, DOX activated the apoptosis pathway by increasing the Bax/Bcl-2 ratio and cleaved caspase-3 levels, which can be alleviated by DMF in a dose-dependent manner. Furthermore, Nrf2 silencing reversed the anti-apoptotic effects of DMF against DOX. These observations collectively indicate that DMF can attenuate apoptotic events caused by DOX through the Nrf2 pathway.

Recently, Fang reported that activating the Nrf2/Hmox1 pathway could aggravate cardiac ferroptosis in mice after DOX treatment by disturbing iron metabolism (Fang et al., 2019). However, the early Nrf2/Hmox1 activity (1 day after DOX treatment) and different DOX doses may not demonstrate the whole role of the Nrf2 pathway. Besides, ferroptosis is just one of various cell death types in cardiomyocytes induced by DOX. And DMF was reported to inhibit ferroptosis in multiple disease models by activating the Nrf2 pathway (Qiu et al., 2020; Zhang et al., 2020; Yan et al., 2021; Yang et al., 2021). Therefore, we need to further explore the relationship between the Nrf2/Hmox1 axis and ferroptosis in the heart after DOX treatment.

In addition to the heart, other organs, such as the skeletal muscle, brain, liver, and kidney, are also susceptible to oxidative stress caused by DOX. And kidney and liver are known to be the major metabolism organs for multiple drugs. Thus morphological and functional changes in the liver and kidneys were also examined. The results showed that DMF could also dose-dependently alleviate liver and kidney impairment caused by DOX (**Supplementary Figures S4, S5**). Together, we speculated that DMF is relatively safe and well-tolerated.

It was reported that Nrf2 activation could promote carcinogenesis and drug resistance (Hammad et al., 2019; DeBlasi and DeNicola, 2020). In this study, we didn't detect that DMF could interfere with the effects of DOX chemotherapy on three tumor cell lines. Besides, DMF has also been shown some anticancer abilities in serval cancers such as melanoma, breast cancer, colon cancer, and lung cancers by targeting Nrf2, NF-κB, ERK1/2, and miRNA pathway (Yamazoe et al., 2009; Xie et al., 2015; Kastrati et al., 2016). Moreover, several clinical trials have been conducted to test the antitumor effects of DMF (Saidu et al., 2019).

Gastrointestinal adverse events such as nausea, heartburn, vomiting, and diarrhea are common in patients taking DMF (Fox et al., 2012; Gold et al., 2012). In the DEFINE/CONFIRM trials, the incidence of gastrointestinal adverse events was approximately 40%, leading to treatment interruption in 4% of patients (Phillips et al., 2015). And those adverse reactions were also seen in patients treated with DOX (Hesketh, 2008). Therefore, we need to closely monitor gastrointestinal reactions and give appropriate management once the two drugs are used in combination.

However, we admitted that this study has some limitations. We only selected two concentrations of DMF for the *in vitro* studies and two doses of DMF for the *in vivo* study, which may not fully demonstrate the pharmacological effects of this drug. Moreover, DMF was also reported to regulate immune cell activity, inflammation, and metabolism in various pathological models (Kornberg et al., 2018; Zhao et al., 2020). We cannot rule out

that DMF may exert protective effects against DOX other than the Nrf2 pathway, which requires further exploration.

CONCLUSION

In conclusion, our data showed that the FDA-approved drug DMF notably alleviated DOX-caused cardiac injury by activating the Nrf2 pathway without interfering with the chemotherapy effect of DOX, which should be developed as a promising candidate for patients suffering from DOX-related cardiotoxicity (**Figure 8**).

DATA AVAILABILITY STATEMENT

The original contributions presented in the study are included in the article/**Supplementary Materials**, further inquiries can be directed to the corresponding author.

ETHICS STATEMENT

The animal study was reviewed and approved by Institutional Review and Ethics Board of Shanghai Xinhua Hospital, Shanghai Jiao Tong University School of Medicine.

AUTHOR CONTRIBUTIONS

XH, CL and QW contributed equally to this study. XH performed the experiments and organized the manuscript. CL and QW collected the data. ZW and TC helped to perform molecular biology experiments. YW and YL guided the overall thinking and the design of the experiment.

FUNDING

This study was sponsored by the State Key Program of National Natural Science Foundation of China (82130009), National Natural Science Foundation of China (81900293, 82070515, 81670414), Shanghai City Committee of Science and Technology Research Projects (201409005600), the Shanghai Sailing Program (19YF1431800), and Shanghai Leading Talent Program.

SUPPLEMENTARY MATERIAL

The Supplementary Material for this article can be found online at: https://www.frontiersin.org/articles/10.3389/fphar.2022.872057/full#supplementary-material

REFERENCES

Carvalho, C., Santos, R. X., Cardoso, S., Correia, S., Oliveira, P. J., Santos, M. S., et al. (2009). Doxorubicin: the Good, the Bad and the Ugly Effect. *Curr. Med. Chem.* 16 (25), 3267–3285. doi:10.2174/092986709788803312

Cattani-Cavalieri, I., da Maia Valença, H., Moraes, J. A., Brito-Gitirana, L., Romana-Souza, B., Schmidt, M., et al. (2020). Dimethyl Fumarate Attenuates Lung Inflammation and Oxidative Stress Induced by Chronic Exposure to Diesel Exhaust Particles in Mice. *Int. J. Mol. Sci.* 21 (24), 9658. doi:10.3390/ijms21249658

Chen, Q. M. (2021). Nrf2 for Cardiac protection: Pharmacological Options against Oxidative Stress. *Trends Pharmacol. Sci.* 42 (9), 729–744. doi:10.1016/j.tips.2021.06.005

Crowley, L. C., and Waterhouse, N. J. (2016). Detecting Cleaved Caspase-3 in Apoptotic Cells by Flow Cytometry. *Cold Spring Harb Protoc.* 2016 (11), 958–962. doi:10.1101/pdb.prot087312

Damiani, R. M., Moura, D. J., Viau, C. M., Caceres, R. A., Henriques, J. A. P., and Saffi, J. (2016). Pathways of Cardiac Toxicity: Comparison between Chemotherapeutic Drugs Doxorubicin and Mitoxantrone. *Arch. Toxicol.* 90 (9), 2063–2076. doi:10.1007/s00204-016-1759-y

DeBlasi, J. M., and DeNicola, G. M. (2020). Dissecting the Crosstalk between NRF2 Signaling and Metabolic Processes in Cancer. *Cancers (Basel)* 12 (10), 3023. doi:10.3390/cancers12103023

Eder, A. R., and Arriaga, E. A. (2006). Capillary Electrophoresis Monitors Enhancement in Subcellular Reactive Oxygen Species Production upon Treatment with Doxorubicin. *Chem. Res. Toxicol.* 19 (9), 1151–1159. doi:10.1021/tx060083i

Fang, X., Wang, H., Han, D., Xie, E., Yang, X., Wei, J., et al. (2019). Ferroptosis as a Target for protection against Cardiomyopathy. *Proc. Natl. Acad. Sci. U S A.* 116 (7), 2672–2680. doi:10.1073/pnas.1821022116

Ferrans, V. J., Clark, J. R., Zhang, J., Yu, Z. X., and Herman, E. H. (1997). Pathogenesis and Prevention of Doxorubicin Cardiomyopathy. *Tsitologiia* 39 (10), 928–937.

Fox, R. J., Miller, D. H., Phillips, J. T., Hutchinson, M., Havrdova, E., Kita, M., et al. (2012). Placebo-controlled Phase 3 Study of Oral BG-12 or Glatiramer in Multiple Sclerosis. *N. Engl. J. Med.* 367 (12), 1087–1097. doi:10.1056/NEJMoa1206328

Giustina, A. D., Bonfante, S., Zarbato, G. F., Danielski, L. G., Mathias, K., de Oliveira, A. N., Jr., et al. (2018). Dimethyl Fumarate Modulates Oxidative Stress and Inflammation in Organs after Sepsis in Rats. *Inflammation* 41 (1), 315–327. doi:10.1007/s10753-017-0689-z

Goffart, S., von Kleist-Retzow, J. C., and Wiesner, R. J. (2004). Regulation of Mitochondrial Proliferation in the Heart: Power-Plant Failure Contributes to Cardiac Failure in Hypertrophy. *Cardiovasc. Res.* 64 (2), 198–207. doi:10.1016/j.cardiores.2004.06.030

Gold, R., Kappos, L., Arnold, D. L., Bar-Or, A., Giovannoni, G., Selmaj, K., et al. (2012). Placebo-controlled Phase 3 Study of Oral BG-12 for Relapsing Multiple Sclerosis. *N. Engl. J. Med.* 367 (12), 1098–1107. doi:10.1056/NEJMoa1114287

Gutteridge, J. M. (1984). Lipid Peroxidation and Possible Hydroxyl Radical Formation Stimulated by the Self-Reduction of a Doxorubicin-Iron (III) Complex. *Biochem. Pharmacol.* 33 (11), 1725–1728. doi:10.1016/0006-2952(84)90340-x

Hammad, A., Namani, A., Elshaer, M., Wang, X. J., and Tang, X. (2019). "NRF2 Addiction" in Lung Cancer Cells and its Impact on Cancer Therapy. *Cancer Lett.* 467, 40–49. doi:10.1016/j.canlet.2019.09.016

Hesketh, P. J. (2008). Chemotherapy-induced Nausea and Vomiting. *N. Engl. J. Med.* 358 (23), 2482–2494. doi:10.1056/NEJMra0706547

Hur, W., and Gray, N. S. (2011). Small Molecule Modulators of Antioxidant Response Pathway. *Curr. Opin. Chem. Biol.* 15 (1), 162–173. doi:10.1016/j.cbpa.2010.12.009

Kanda, T., Takahashi, T., Kudo, S., Takeda, T., Tsugawa, H., and Takekoshi, N. (2004). Leptin Deficiency Enhances Myocardial Necrosis and Lethality in a Murine Model of Viral Myocarditis. *Life Sci.* 75 (12), 1435–1447. doi:10.1016/j.lfs.2004.03.012

Kashfi, K., Israel, M., Sweatman, T. W., Seshadri, R., and Cook, G. A. (1990). Inhibition of Mitochondrial Carnitine Palmitoyltransferases by Adriamycin and Adriamycin Analogues. *Biochem. Pharmacol.* 40 (7), 1441–1448. doi:10.1016/0006-2952(90)90438-q

Kastrati, I., Siklos, M. I., Calderon-Gierszal, E. L., El-Shennawy, L., Georgieva, G., Thayer, E. N., et al. (2016). Dimethyl Fumarate Inhibits the Nuclear Factor κB Pathway in Breast Cancer Cells by Covalent Modification of P65 Protein. *J. Biol. Chem.* 291 (7), 3639–3647. doi:10.1074/jbc.M115.679704

Kim, J. M., Ko, H., Kim, S. J., Shim, S. H., Ha, C. H., and Chang, H. I. (2016). Chemopreventive Properties of Genipin on AGS Cell Line via Induction of JNK/Nrf2/ARE Signaling Pathway. *J. Biochem. Mol. Toxicol.* 30 (1), 45–54. doi:10.1002/jbt.21741

Kopacz, A., Kloska, D., Forman, H. J., Jozkowicz, A., and Grochot-Przeczek, A. (2020). Beyond Repression of Nrf2: An Update on Keap1. *Free Radic. Biol. Med.* 157, 63–74. doi:10.1016/j.freeradbiomed.2020.03.023

Kornberg, M. D., Bhargava, P., Kim, P. M., Putluri, V., Snowman, A. M., Putluri, N., et al. (2018). Dimethyl Fumarate Targets GAPDH and Aerobic Glycolysis to Modulate Immunity. *Science* 360 (6387), 449–453. doi:10.1126/science.aan4665

Li, D. L., and Hill, J. A. (2014). Cardiomyocyte Autophagy and Cancer Chemotherapy. *J. Mol. Cel Cardiol.* 71, 54–61. doi:10.1016/j.yjmcc.2013.11.007

Li, S., Wang, W., Niu, T., Wang, H., Li, B., Shao, L., et al. (2014). Nrf2 Deficiency Exaggerates Doxorubicin-Induced Cardiotoxicity and Cardiac Dysfunction. *Oxid. Med. Cel Longev.* 2014, 748524. doi:10.1155/2014/748524

Li, Y., Ma, F., Li, H., Song, Y., Zhang, H., Jiang, Z., et al. (2018). Dimethyl Fumarate Accelerates Wound Healing under Diabetic Condition. *J. Mol. Endocrinol.* 61 (4), 163–172. doi:10.1530/JME-18-0102

Li, S., Takasu, C., Lau, H., Robles, L., Vo, K., Farzaneh, T., et al. (2020). Dimethyl Fumarate Alleviates Dextran Sulfate Sodium-Induced Colitis, through the Activation of Nrf2-Mediated Antioxidant and Anti-inflammatory Pathways. *Antioxidants (Basel)* 9 (4), 354. doi:10.3390/antiox9040354

Liu, C., Xue, R., Wu, D., Wu, L., Chen, C., Tan, W., et al. (2014). REDD1 Attenuates Cardiac Hypertrophy via Enhancing Autophagy. *Biochem. Biophys. Res. Commun.* 454 (1), 215–220. doi:10.1016/j.bbrc.2014.10.079

Ma, Q. (2013). Role of Nrf2 in Oxidative Stress and Toxicity. *Annu. Rev. Pharmacol. Toxicol.* 53, 401–426. doi:10.1146/annurev-pharmtox-011112-140320

Meili-Butz, S., Niermann, T., Fasler-Kan, E., Barbosa, V., Butz, N., John, D., et al. (2008). Dimethyl Fumarate, a Small Molecule Drug for Psoriasis, Inhibits Nuclear Factor-kappaB and Reduces Myocardial Infarct Size in Rats. *Eur. J. Pharmacol.* 586 (1-3), 251–258. doi:10.1016/j.ejphar.2008.02.038

Mitry, M. A., and Edwards, J. G. (2016). Doxorubicin Induced Heart Failure: Phenotype and Molecular Mechanisms. *Int. J. Cardiol. Heart Vasc.* 10, 17–24. doi:10.1016/j.ijcha.2015.11.004

Motterlini, R., Nikam, A., Manin, S., Ollivier, A., Wilson, J. L., Djouadi, S., et al. (2019). HYCO-3, a Dual CO-releaser/Nrf2 Activator, Reduces Tissue Inflammation in Mice Challenged with Lipopolysaccharide. *Redox Biol.* 20, 334–348. doi:10.1016/j.redox.2018.10.020

Mouton, A. J., Flynn, E. R., Moak, S. P., Aitken, N. M., Omoto, A. C. M., Li, X., et al. (2021). Dimethyl Fumarate Preserves Left Ventricular Infarct Integrity Following Myocardial Infarction via Modulation of Cardiac Macrophage and Fibroblast Oxidative Metabolism. *J. Mol. Cel Cardiol.* 158, 38–48. doi:10.1016/j.yjmcc.2021.05.008

Nebigil, C. G., and Désaubry, L. (2018). Updates in Anthracycline-Mediated Cardiotoxicity. *Front. Pharmacol.* 9, 1262. doi:10.3389/fphar.2018.01262

Octavia, Y., Tocchetti, C. G., Gabrielson, K. L., Janssens, S., Crijns, H. J., and Moens, A. L. (2012). Doxorubicin-induced Cardiomyopathy: from Molecular Mechanisms to Therapeutic Strategies. *J. Mol. Cel Cardiol.* 52 (6), 1213–1225. doi:10.1016/j.yjmcc.2012.03.006

Olagnier, D., Farahani, E., Thyrsted, J., Blay-Cadanet, J., Herengt, A., Idorn, M., et al. (2020). SARS-CoV2-mediated Suppression of NRF2-Signaling Reveals Potent Antiviral and Anti-inflammatory Activity of 4-Octyl-Itaconate and Dimethyl Fumarate. *Nat. Commun.* 11 (1), 4938. doi:10.1038/s41467-020-18764-3

Phillips, J. T., Selmaj, K., Gold, R., Fox, R. J., Havrdova, E., Giovannoni, G., et al. (2015). Clinical Significance of Gastrointestinal and Flushing Events in Patients with Multiple Sclerosis Treated with Delayed-Release Dimethyl Fumarate. *Int. J. MS Care* 17 (5), 236–243. doi:10.7224/1537-2073.2014-069

Qiu, Y. B., Wan, B. B., Liu, G., Wu, Y. X., Chen, D., Lu, M. D., et al. (2020). Nrf2 Protects against Seawater Drowning-Induced Acute Lung Injury via Inhibiting Ferroptosis. *Respir. Res.* 21 (1), 232. doi:10.1186/s12931-020-01500-2

Rawat, P. S., Jaiswal, A., Khurana, A., Bhatti, J. S., and Navik, U. (2021). Doxorubicin-induced Cardiotoxicity: An Update on the Molecular Mechanism and Novel Therapeutic Strategies for Effective Management. *Biomed. Pharmacother.* 139, 111708. doi:10.1016/j.biopha.2021.111708

Reichardt, P., Tabone, M. D., Mora, J., Morland, B., and Jones, R. L. (2018). Risk-benefit of Dexrazoxane for Preventing Anthracycline-Related Cardiotoxicity: Re-evaluating the European Labeling. *Future Oncol.* 14 (25), 2663–2676. doi:10.2217/fon-2018-0210

Saidu, N. E. B., Kavian, N., Leroy, K., Jacob, C., Nicco, C., Batteux, F., et al. (2019). Dimethyl Fumarate, a Two-Edged Drug: Current Status and Future Directions. *Med. Res. Rev.* 39 (5), 1923–1952. doi:10.1002/med.21567

Scannevin, R. H., Chollate, S., Jung, M. Y., Shackett, M., Patel, H., Bista, P., et al. (2012). Fumarates Promote Cytoprotection of central Nervous System Cells against Oxidative Stress via the Nuclear Factor (Erythroid-derived 2)-like 2 Pathway. *J. Pharmacol. Exp. Ther.* 341 (1), 274–284. doi:10.1124/jpet.111.190132

Schlame, M., Rua, D., and Greenberg, M. L. (2000). The Biosynthesis and Functional Role of Cardiolipin. *Prog. Lipid Res.* 39 (3), 257–288. doi:10.1016/s0163-7827(00)00005-9

Simunek, T., Stérba, M., Popelová, O., Adamcová, M., Hrdina, R., and Gersl, V. (2009). Anthracycline-induced Cardiotoxicity: Overview of Studies Examining the Roles of Oxidative Stress and Free Cellular Iron. *Pharmacol. Rep.* 61 (1), 154–171. doi:10.1016/s1734-1140(09)70018-0

Singh, A., Venkannagari, S., Oh, K. H., Zhang, Y. Q., Rohde, J. M., Liu, L., et al. (2016). Small Molecule Inhibitor of NRF2 Selectively Intervenes Therapeutic Resistance in KEAP1-Deficient NSCLC Tumors. *ACS Chem. Biol.* 11 (11), 3214–3225. doi:10.1021/acschembio.6b00651

Sugden, P. H., and Clerk, A. (2006). Oxidative Stress and Growth-Regulating Intracellular Signaling Pathways in Cardiac Myocytes. *Antioxid. Redox Signal.* 8 (11-12), 2111–2124. doi:10.1089/ars.2006.8.2111

Wierinckx, A., Brevé, J., Mercier, D., Schultzberg, M., Drukarch, B., and Van Dam, A. M. (2005). Detoxication Enzyme Inducers Modify Cytokine Production in Rat Mixed Glial Cells. *J. Neuroimmunol.* 166 (1-2), 132–143. doi:10.1016/j.jneuroim.2005.05.013

Wilms, H., Sievers, J., Rickert, U., Rostami-Yazdi, M., Mrowietz, U., and Lucius, R. (2010). Dimethylfumarate Inhibits Microglial and Astrocytic Inflammation by Suppressing the Synthesis of Nitric Oxide, IL-1beta, TNF-Alpha and IL-6 in an *In-Vitro* Model of Brain Inflammation. *J. Neuroinflammation* 7, 30. doi:10.1186/1742-2094-7-30

Wiseman, L. R., and Spencer, C. M. (1998). Dexrazoxane. A Review of its Use as a Cardioprotective Agent in Patients Receiving Anthracycline-Based Chemotherapy. *Drugs* 56 (3), 385–403. doi:10.2165/00003495-199856030-00009

Xie, X., Zhao, Y., Ma, C. Y., Xu, X. M., Zhang, Y. Q., Wang, C. G., et al. (2015). Dimethyl Fumarate Induces Necroptosis in colon Cancer Cells through GSH Depletion/ROS increase/MAPKs Activation Pathway. *Br. J. Pharmacol.* 172 (15), 3929–3943. doi:10.1111/bph.13184

Xu, X., Persson, H. L., and Richardson, D. R. (2005). Molecular Pharmacology of the Interaction of Anthracyclines with Iron. *Mol. Pharmacol.* 68 (2), 261–271. doi:10.1124/mol.105.013383

Xu, Z., Zhang, F., Sun, F., Gu, K., Dong, S., and He, D. (2015). Dimethyl Fumarate for Multiple Sclerosis. *Cochrane Database Syst. Rev.* 4, CD011076. doi:10.1002/14651858.CD011076.pub2

Yamazoe, Y., Tsubaki, M., Matsuoka, H., Satou, T., Itoh, T., Kusunoki, T., et al. (2009). Dimethylfumarate Inhibits Tumor Cell Invasion and Metastasis by Suppressing the Expression and Activities of Matrix Metalloproteinases in Melanoma Cells. *Cell Biol. Int.* 33 (10), 1087–1094. doi:10.1016/j.cellbi.2009.06.027

Yan, N., Xu, Z., Qu, C., and Zhang, J. (2021). Dimethyl Fumarate Improves Cognitive Deficits in Chronic Cerebral Hypoperfusion Rats by Alleviating Inflammation, Oxidative Stress, and Ferroptosis via NRF2/ARE/NF-κB Signal Pathway. *Int. Immunopharmacol.* 98, 107844. doi:10.1016/j.intimp.2021.107844

Yang, Y., Cai, F., Zhou, N., Liu, S., Wang, P., Zhang, S., et al. (2021). Dimethyl Fumarate Prevents Ferroptosis to Attenuate Acute Kidney Injury by Acting on NRF2. *Clin. Transl. Med.* 11 (4), e382. doi:10.1002/ctm2.382

Zhang, Y., Zhao, S., Fu, Y., Yan, L., Feng, Y., Chen, Y., et al. (2020). Computational Repositioning of Dimethyl Fumarate for Treating Alcoholic Liver Disease. *Cell Death Dis.* 11 (8), 641. doi:10.1038/s41419-020-02890-3

Zhao, J., Cheng, Z., Quan, X., Xie, Z., Zhang, L., and Ding, Z. (2020). Dimethyl Fumarate Protects Cardiomyocytes against Oxygen-Glucose Deprivation/reperfusion (OGD/R)-induced Inflammatory Response and Damages *via* Inhibition of Egr-1. *Int. Immunopharmacol.* 86, 106733. doi:10.1016/j.intimp.2020.106733

Conflict of Interest: The authors declare that the research was conducted in the absence of any commercial or financial relationships that could be construed as a potential conflict of interest.

Publisher's Note: All claims expressed in this article are solely those of the authors and do not necessarily represent those of their affiliated organizations, or those of the publisher, the editors and the reviewers. Any product that may be evaluated in this article, or claim that may be made by its manufacturer, is not guaranteed or endorsed by the publisher.

frontiers | Frontiers in Pharmacology

ORIGINAL RESEARCH
published: 28 April 2022
doi: 10.3389/fphar.2022.868393

Protective Effects of 6-Gingerol on Cardiotoxicity Induced by Arsenic Trioxide Through AMPK/SIRT1/PGC-1α Signaling Pathway

Xue Han[1†], Yakun Yang[1†], Muqing Zhang[2], Xi Chu[3], Bin Zheng[1], Chenxu Liu[1], Yucong Xue[2], Shengjiang Guan[4,5], Shijiang Sun[4]* and Qingzhong Jia[6]**

[1]School of Pharmacy, Hebei University of Chinese Medicine, Shijiazhuang, China, [2]College of Integrative Medicine, Hebei University of Chinese Medicine, Shijiazhuang, China, [3]The Fourth Hospital of Hebei Medical University, Shijiazhuang, China, [4]Affiliated Hospital, Hebei University of Chinese Medicine, Shijiazhuang, China, [5]School of Basic Medicine, Hebei University of Chinese Medicine, Shijiazhuang, China, [6]School of Pharmacy, Hebei Medical University, Shijiazhuang, China

OPEN ACCESS

Edited by:
Zhi-Ren Zhang,
Harbin Medical University, China

Reviewed by:
Xianju Huang,
South-Central University for Nationalities, China
Milton Prabu,
Annamalai University, India

***Correspondence:**
Shengjiang Guan
guanshengjiang123@126.com
Shijiang Sun
sunshijiang6909@163.com
Qingzhong Jia
qizhjia@hebmu.edu.cn

†These authors have contributed equally to this work

Specialty section:
This article was submitted to Cardiovascular and Smooth Muscle Pharmacology, a section of the journal Frontiers in Pharmacology

Received: 02 February 2022
Accepted: 28 March 2022
Published: 28 April 2022

Citation:
Han X, Yang Y, Zhang M, Chu X, Zheng B, Liu C, Xue Y, Guan S, Sun S and Jia Q (2022) Protective Effects of 6-Gingerol on Cardiotoxicity Induced by Arsenic Trioxide Through AMPK/SIRT1/PGC-1α Signaling Pathway. Front. Pharmacol. 13:868393. doi: 10.3389/fphar.2022.868393

Background and Objective: Arsenic trioxide (As_2O_3) induced cardiotoxicity to limit the clinical applications of the effective anticancer agent. 6-Gingerol (6G) is the main active ingredient of ginger, a food with many health benefits. The present study aims to investigate the potential pharmacological mechanisms of 6G on As_2O_3-induced myocardial injury.

Methods and Results: Fifty KunMing mice were divided into five groups (n = 10) receiving: 1) physiological saline; 2) 6G (20 mg/kg) alone; 3) As_2O_3 (5 mg/kg); 4) 6G (10 mg/kg) and As_2O_3 (5 mg/kg); 5) 6G (20 mg/kg) and As_2O_3 (5 mg/kg). 6G was given orally and As_2O_3 was given intraperitoneally once per day for seven consecutive days. Biochemical, histopathological, transmission electron microscopy, ELISA, and western blotting analyses were then performed. Based on the resultant data, As_2O_3 was found to induce cardiotoxicity in mice. 6G significantly ameliorated As_2O_3-induced heart injury, histopathological changes, oxidative stress, myocardial mitochondrial damage, inflammation, and cardiomyocyte apoptosis, while reversed As_2O_3-induced inhibition of the AMPK/SIRT1/PGC-1α pathway.

Conclusion: Our experimental results reveal that 6G effectively counteracts As_2O_3-induced cardiotoxicity including oxidative stress, inflammation and apoptosis, which might be attributed to its activation action on AMPK/SIRT1/PGC-1α signaling pathway.

Keywords: AMPK/SIRT1/PGC-1α pathway, arsenic trioxide, cardiotoxicity, 6-gingerol, oxidative stress

INTRODUCTION

As_2O_3 is a traditional Chinese medicine that has been used in China for more than 2,400 years. In recent years, reports have emerged that As_2O_3 may be effective at treating a wide array of cancers, and it has been used as a more suitable drug for the treatment of acute promyelocytic leukemia (Wang X. et al., 2021; Zong et al., 2021). However, As_2O_3 can cause various diseases such as cardiovascular disorder, and As_2O_3 toxicity presented significant obstacles to its clinical applications (Emadi and Gore, 2010). It has been reported that As_2O_3-induced cardiotoxicity is regulated by

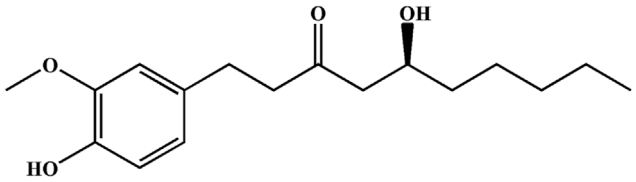

FIGURE 1 | Chemical structure of 6G.

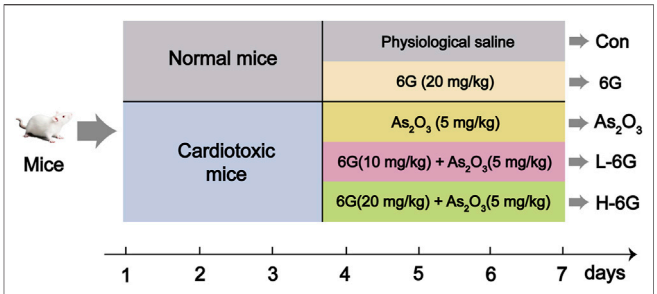

FIGURE 2 | Diagram of animal experimental design.

reactive oxygen species (ROS) (Ficker et al., 2004; Ghosh et al., 2009), which in turn leads to pro-/anti-oxidant imbalances, such as increased malondialdehyde (MDA) and decreased superoxide dismutase (SOD), glutathione (GSH) and catalase (CAT). Elevation of MDA is a very useful indicator of oxidative stress (C. Zhang et al., 2021). SOD, GSH and CAT are all important free radical scavengers that exert antioxidant functions and protect cells from damage (Birari et al., 2020). However, there is no definitive clinical drug to treat As_2O_3-induced cardiotoxicity.

As a highly conserved serine/threonine-protein kinase, AMP-activated protein kinase (AMPK) has a triggered effect on the metabolism of bioenergy (Salt and Hardie, 2017). When AMPK is activated, it could monitor the function of mitochondria and the energy status of the cell (Bechard et al., 2010) and regulate the activity of the silent information regulator 1 (SIRT1). Then the peroxisome proliferator-activated receptor-gamma coactivator one alpha (PGC-1α) is activated after activation of AMPK and SIRT1. The AMPK/SIRT1/PGC-1α pathway plays an important role in oxidative stress, and mitochondrial biosynthesis (Canto and Auwerx, 2009; Birari et al., 2020).

Ginger is a widely used spice that exhibits several health benefits. It is used as a home remedy in the treatment of stomach disorders with significant value (Haniadka et al., 2013; Seif et al., 2021). The gingerol-like compounds are the main bioactive substances in the non-volatile, pungent components of ginger. 6-Gingerol (6G) is one of the major components of total gingerols extracted from ginger (Luo et al., 2021), and its chemical structure of 6G is shown in **Figure 1**. Specifically, 6G has been shown to be potentially efficacious against cancer (Kapoor et al., 2016; Luna-Dulcey et al., 2018) and to possess anti-inflammatory and anti-apoptotic properties (Krell and Stebbing, 2012; Zhang et al., 2017). Previous studies by our group have shown the protective effect of 6G *in vitro* and *ex vivo* models, and proposed that the cardioprotective and antioxidant properties of 6G may be a result of decreased intracellular Ca^{2+} via the suppression of Ca^{2+} influx and contractility in ventricular myocytes and inhibition of the TLR4/MAPKs/NF-κB pathway (Han et al., 2019; Han et al., 2020). These studies indicate that 6G possesses cardioprotective potential, while the exact effects and potential protective mechanisms of 6G in As_2O_3-induced cardiotoxicity remain to be fully elucidated. Hence, the present study aimed to explore the effects and underlying pharmacological mechanisms of 6G on As_2O_3-induced oxidative stress, inflammation, and apoptosis of cells.

Herein, a mouse model of As_2O_3 induced-cardiotoxicity was established to explore whether 6G regulates oxidative stress, inflammation, and apoptosis via the AMPK/SIRT1/PGC-1α signaling pathway. To date, the role of 6G as an anti-cardiotoxic agent has not been demonstrated in As_2O_3-induced cardiotoxicity. Thus, our study explores the antioxidant and cardioprotective properties of 6G against As_2O_3-induced cardiotoxicity.

MATERIALS AND METHODS

Animals

In the current study, fifty male KunMing mice (20–25 g) were used. Before the experimental application, mice were housed at 23–25°C in 12 h light/dark cycles (50–55% relative humidity) and provided with free access to water and food. All experimental procedures regarding animals were complied with the guidelines of animal experiments from the Ethics Committee of Hebei University of Chinese Medicine (China, DWLL2021098).

Drugs and Chemicals

6G (purity >98%) was obtained from Alfa Biotechnology Co., Ltd. (Chengdu, China), and As_2O_3 (purity >98%) in the experiment was supplied by Shuanglu Pharmaceutical Co., Ltd. (Beijing, China). All other analytical grade reagents used in this study were provided by Sigma Chemical Company (MO, United States), unless otherwise specified.

Experimental Design

The dose selection of 6G (El-Bakly et al., 2012; Han et al., 2020) and As_2O_3 (Hemmati et al., 2018; Birari et al., 2020; Jin et al., 2020) in this study was based on our preliminary experiments and previous studies as well as doses used by other research groups in animal experiments. The experimental design of all animals is depicted in **Figure 2**. Mice were divided into five groups, which are described below (10 mice/group):

Group 1 (Con): Injected with physiological saline as a vehicle.

Group 2 (6G): Treated with 6G (20 mg/kg) orally for 7 days.

Group 3 (As_2O_3): Injected intraperitoneally with As_2O_3 (5 mg/kg) for 7 days.

Group 4 (L-6G): Daily treated with 6G (10 mg/kg) orally, then followed by injected intraperitoneally with As_2O_3 (5 mg/kg) for 7 days.

Group 5 (H-6G): Daily treated with 6G (20 mg/kg) orally, then followed by injected intraperitoneally with As_2O_3 (5 mg/kg) for 7 days.

Electrocardiography and Cardiac Weight Index Assessment

Briefly, mice were anesthetized with sodium urethane (1 g/kg). Electrocardiography was recorded using an electrocardiography recorder (Biological Signal Collection System, Chengdu Instrument Factory, China). Blood was then collected and subsequently the heart was removed, weighed and photographed. The heart weight-to-body weight ratio (cardiac weight index, CWI) was calculated.

Detection of Serum Biochemical Parameters

After electrocardiography, blood samples were centrifugated at 1,500 rpm for 5 min. The serum levels of lactate dehydrogenase (LDH), creatine kinase (CK), creatine kinase-MB (CK-MB) and cardiac troponin I (CTnI) were detected with an automatic biochemical analyzer (Shenzhen Kubel Biotechnology Co., LTD., China).

Evaluation of Histopathology

For examination, the hearts of mice were fixed in paraformaldehyde solution (4%), embedded in paraffin, cut into sections (5-μm-thick) by microtome, and stained with hematoxylin-eosin. The morphology of heart tissue was observed under ×20, ×200 and ×400 magnification with a light microscope (Nikon, Japan).

Assessments of ROS and Antioxidant Enzymes

A fluorescent probe dihydroethidium (DHE) (Servicebio, Wuhan, China) was used to detect the production of ROS in myocardial tissue. DHE staining solution was added into frozen sections and the slices were incubated at 37°C for 30 min. The treated sections were then washed with PBS three times for 5 min each and incubated with DAPI solution in a dark environment for 10 min. Finally, the sections were observed using a fluorescence microscope (Eclipse C1, Nikon, Tokyo, Japan).

The heart tissue samples were homogenized into a 10% (W/V) homogenate and obtained by centrifugation at 3,500 rpm for 10 min. Biochemical analyses were performed using the supernatant. Levels of SOD (A001-1), MDA (A003-1), GSH (A006-2) and CAT (A007-2) were obtained by commercially available kits (JianCheng, Nanjing, China), respectively, on the basis of the manufacturer's instructions.

Transmission Electron Microscope

The fresh heart samples were fixed in glutaraldehyde (4%) for 2 h and rinsed with phosphate buffer (0.1 M, pH 7.4). Briefly, after being washed with phosphate buffer three times, the myocardial tissues were post-fixed in osmium tetroxide (1%, 0.1 M) for 2 h, dehydrated, and embedded in Epon 812 (TAAB). After fixation, heart samples were stained with uranyl acetate and lead citrate and visualized with an electron microscope (HT7700, Hitachi, Japan).

Estimation of Inflammatory Cytokine Levels

ELISA testing was used to estimate inflammatory cytokine levels, including tumor necrosis factor-a (TNF-α) and interleukin-6 (IL-6). The samples of the heart were immediately homogenized in a tissue lysing device (Servicebio, Wuhan, China) and centrifuged at 3,000 rpm for 10 min at 4°C. The upper supernatant was used for all ELISA kit analyses. TNF-α (88-7324), and IL-6 (88-7064) contents were obtained from Thermo Fisher.

Western Blot Analysis of Apoptosis and AMPK/SIRT1/PGC-1α Signaling

Western blot analysis was carried out to detect the protein expressions of apoptosis-related indicators, including Bax, Bcl-2, Caspase-3, cleaved-Caspase-3, and members of the AMPK/SIRT1/PGC-1α pathway, as described previously (Han et al., 2020). Briefly, total protein was extracted, separated on SDS-PAGE gels (10%, Servicebio, China), transferred onto a PVDF membrane (Servicebio, China). The membranes were blocked with 5% (W/V) skimmed milk TBST (pH 7.3) for 1 h at 37°C and incubated overnight in 4°C with the major antibody of anti-Bcl-2 (dilution: 1:100,000) (Servicebio, China), anti-Bax (dilution: 1:1,000) (Affinity, United States), anti-Caspase-3 (dilution: 1:1,000) (Servicebio, China), anti-cleaved-Caspase-3 (dilution: 1:1,000) (Servicebio, China), anti-AMPK (dilution: 1:1,000) (BIOSS, United States), anti-Sirt1 (dilution: 1:1,000) (San Ying, China), and anti- PGC-1α (dilution: 1:1,000) (Servicebio, China). Then the immobilized primary antibody conjugated with the secondary antibody (dilution: 1: 5,000) (Servicebio, China) in TBST for 30 min at room temperature. After a thorough washing with TBST, proteins were visualized with ECL (Servicebio, China). Quantification of protein expression was performed using the analysis software of Alpha.

Statistical Analysis

Data are shown as mean ± SEM and analyzed via one-way analysis of variance (ANOVA), followed by Tukey's *post hoc* test using Origin Pro version 9.1 software. Statistical significance was accepted at a value of $p < 0.05$.

RESULTS

6G Ameliorated As_2O_3-Induced Heart Injury

The ECG, body mass, and heart index of mice are shown in **Figure 3**. Sample tracings of ECG from the experimental animals are shown in **Figure 3A**. Compared to the Con group, As_2O_3 induced a significant rise in heart rate and ST height (**Figure 3B**, $p < 0.01$). L-6G and H-6G induced a prominent decrease in both heart rate and ST height (**Figure 3B**, $p < 0.05$ or $p < 0.01$).

As_2O_3 administration induced cardiac enlargement, which presented as a brownish and swollen heart. However, L-6G and H-6G significantly improved this pathological condition, with an appearance similar to that of the Con group (**Figure 3C**). The CWI in the As_2O_3-treated mice was higher than in the Con group. In contrast, 6G treatment significantly reduced the level of CWI induced by As_2O_3 (**Figure 3C**, $p < 0.01$).

The results showed that administration of As_2O_3 induced a significant rise in the LDH, CK, CK-MB and CTnI levels relative to Con group (**Figure 4**, $p < 0.01$). On the other hand, treatment with L-6G and H-6G significantly decreased the levels of these cardiac markers relative to As_2O_3-treated mice ($p < 0.05$ or $p < 0.01$).

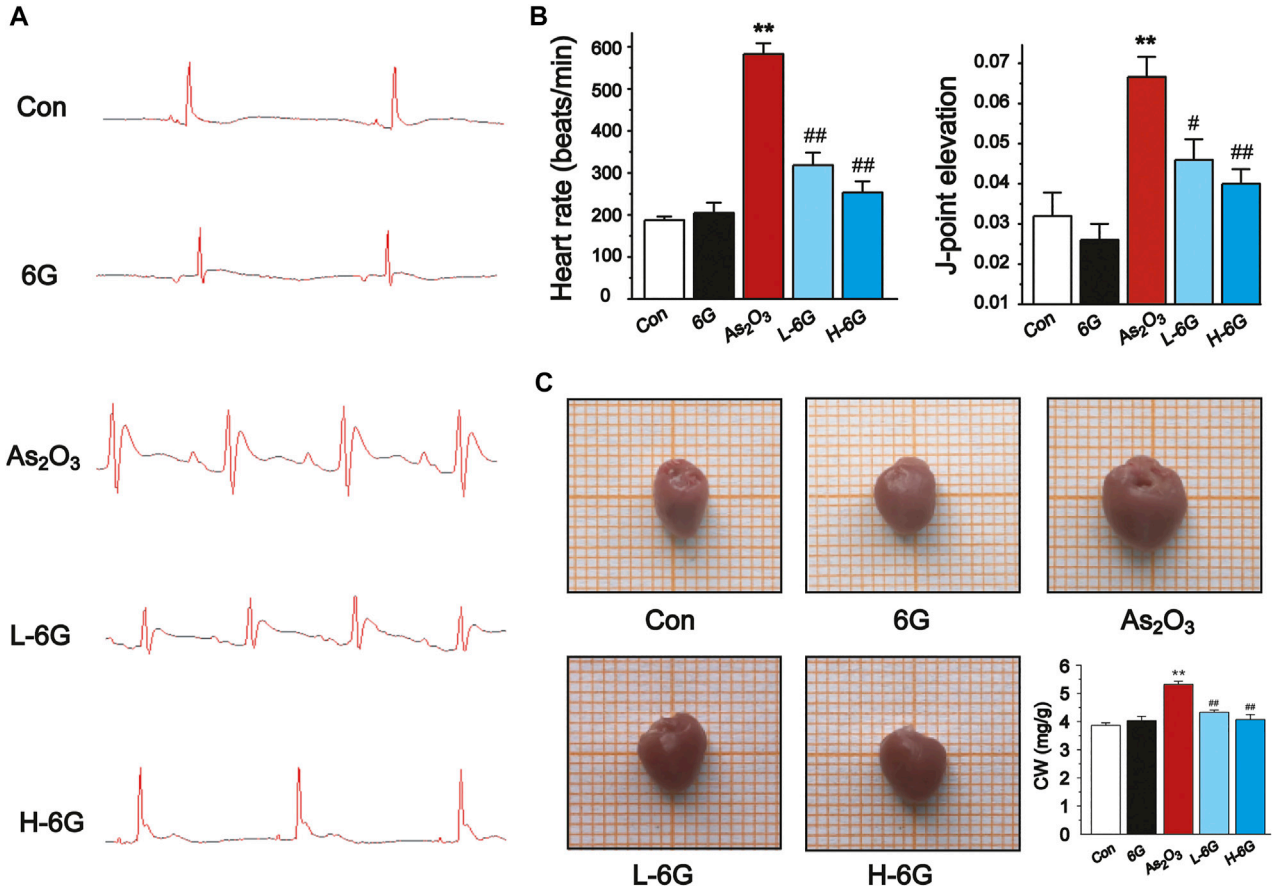

FIGURE 3 | Effect of 6G on ECG, heart rate, J-point elevation, and general appearance and coefficients. **(A)** Representative ECG waveforms were presented in each group. **(B)** 6G leads to a decrease in As_2O_3-induced heart rate acceleration and J-point elevation. **(C)** Representative pictures of the heart appearance and statistical analysis of CW were presented in each group. Data are represented as mean ± SEM, $n = 4–6$. $^{**}p < 0.01$ as in comparison to the Con group and $^{\#}p < 0.05$, $^{\#\#}p < 0.01$ as in comparison to the As_2O_3 group.

6G Improved As_2O_3-Induced Histopathological Changes

H&E staining, as shown in **Figure 5**, revealed typical myofibrillar structures in the Con group, while the myocardium of As_2O_3-treated mice suffered from inflammatory cell infiltration, edema, and cell necrosis. On the contrary, mice in the L-6G and H-6G groups partially alleviated the above pathological changes. Furthermore, the myocardial histoarchitecture of 6G-treated mice was similar to that of mice in the Con group.

6G Suppressed As_2O_3-Induced Oxidative Stress

As shown in **Figure 6A**, our data revealed that ROS levels in As_2O_3-treated mice were dramatically increased in comparison to the Con group. By contrast, ROS levels decreased in the L-6G and H-6G groups in comparison to the As_2O_3-treated mice.

The levels of oxidative stress in heart tissue homogenates were analyzed, and it was found that SOD, GSH and CAT levels decreased in As_2O_3-treated mice relative to the Con group, while MDA levels increased significantly ($p < 0.01$). Conversely, 6G treatment statistically increased the levels of SOD, GSH and CAT, as well as decreased the levels of MDA compared to the As_2O_3-treated mice (**Figures 6B–E**, $p < 0.05$ or $p < 0.01$).

6G Attenuated Myocardial Mitochondrial Damage

To investigate the protective effects of 6G on the ultrastructure of cardiomyocytes, transmission electron microscope was used to estimate the As_2O_3-induced cardiotoxicity. The data revealed no obvious morphological abnormalities in the Con and 6G groups. On the other hand, mitochondrial swelling and rupture of the mitochondrial membrane were found in As_2O_3-treated mice. However, treatment with L-6G and H-6G significantly alleviated pathological changes such as swelling of mitochondria and rupture of mitochondrial membranes (**Figure 7**).

6G Exerted Anti-Inflammatory Effects

ELISA analyses were performed to detect the inflammatory cytokines TNF-α and IL-6 in heart tissue homogenates. The

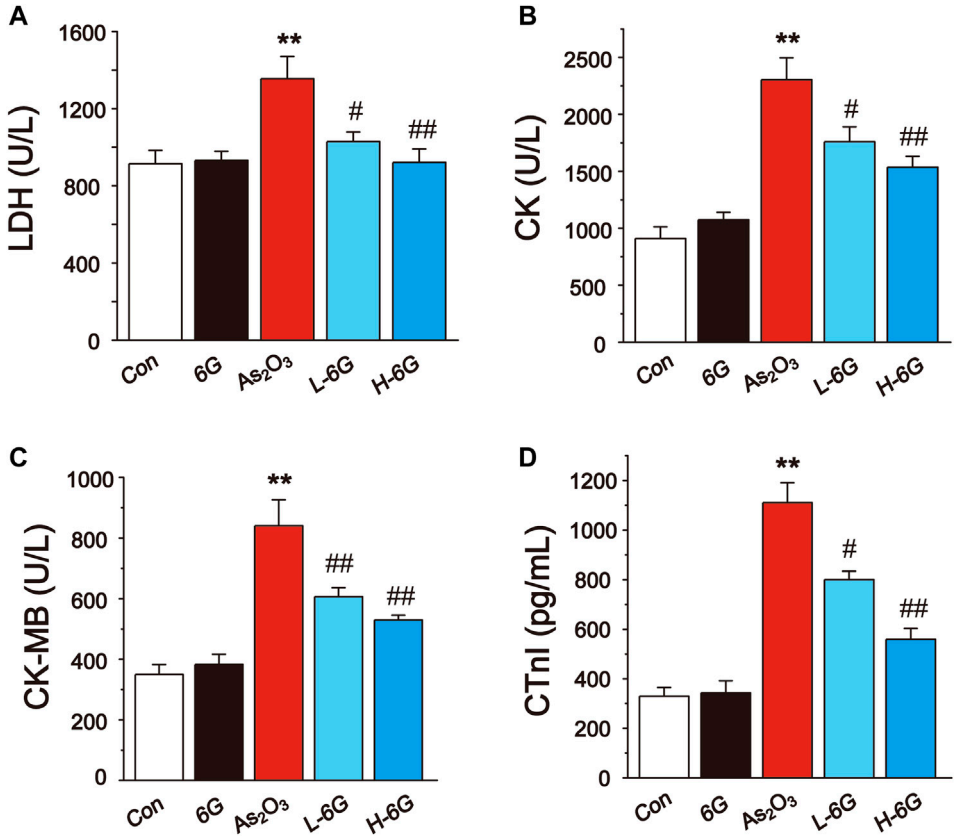

FIGURE 4 | Effect of 6G on the perturbed cardiac injury markers in As_2O_3-treated mice. The effects of 6G on serum concentration of LDH **(A)**, CK **(B)**, CK-MB **(C)** and CTnI **(D)** in each group. Data are expressed as mean ± SEM, $n = 6$. $^{*}p < 0.05$, $^{**}p < 0.01$ as in comparison to the Con group and $^{\#}p < 0.05$, $^{\#\#}p < 0.01$ as in comparison to the As_2O_3 group.

levels of TNF-α and IL-6 in As_2O_3-treated mice were significantly higher compared with mice in the Con group ($p < 0.01$). The levels of TNF-α and IL-6 in the 6G group were similar to those of the Con group. Treatment of L-6G and H-6G suppressed the As_2O_3-induced rise in levels of TNF-α and IL-6 ($p < 0.05$ or $p < 0.01$). The expression levels of these cytokines among the experimental groups are shown in **Figure 8**.

6G Inhibited As_2O_3-Induced Heart Apoptosis

Next, the expression levels of apoptosis-related markers were assessed to further elucidate the role of 6G in As_2O_3-induced cardiac dysfunction. As shown in **Figure 9**, Western blot analysis of apoptosis-related regulatory proteins revealed that the protein expression levels of Bax, Caspase-3 and cleaved-Caspase-3 and the ratio of Bax/Bcl-2 were obviously up-regulated, whereas the expression of Bcl-2 was down-regulated in As_2O_3-treated mice compared with mice in the Con group ($p < 0.01$). On the other hand, treatment with L-6G and H-6G significantly downregulated apoptosis-related regulatory proteins (i.e., Bax, Bax/Bcl-2, Caspase-3, and cleaved-Caspase-3) and upregulated the level of Bcl-2 compared with As_2O_3-treated mice (**Figure 9**, $p < 0.05$ or $p < 0.01$). Our findings indicated no significant change in mice treated with 6G alone relative to mice in the Con group.

6G Reversed As_2O_3-Induced Inhibition of the AMPK/SIRT1/PGC-1α Pathway

Finally, the expressions of AMPK, SIRT1 and PGC-1α in each group was examined by Western blot analysis to investigate the potential mechanism of action of 6G to alleviate As_2O_3-induced cardiotoxicity. Further analysis indicated that As_2O_3 significantly downregulated the expressions of AMPK, SIRT1, and PGC-1α, while treatment with L-6G and H-6G showed an inverse trend (**Figure 10**). Our data indicate that 6G can suppress As_2O_3-induced cardiotoxicity might be through activating of the AMPK/SIRT1/PGC-1α pathway.

DISCUSSION

As_2O_3, used in ancient Chinese medicine for more than 2,000 years, plays a vital role in the treatment of various diseases such

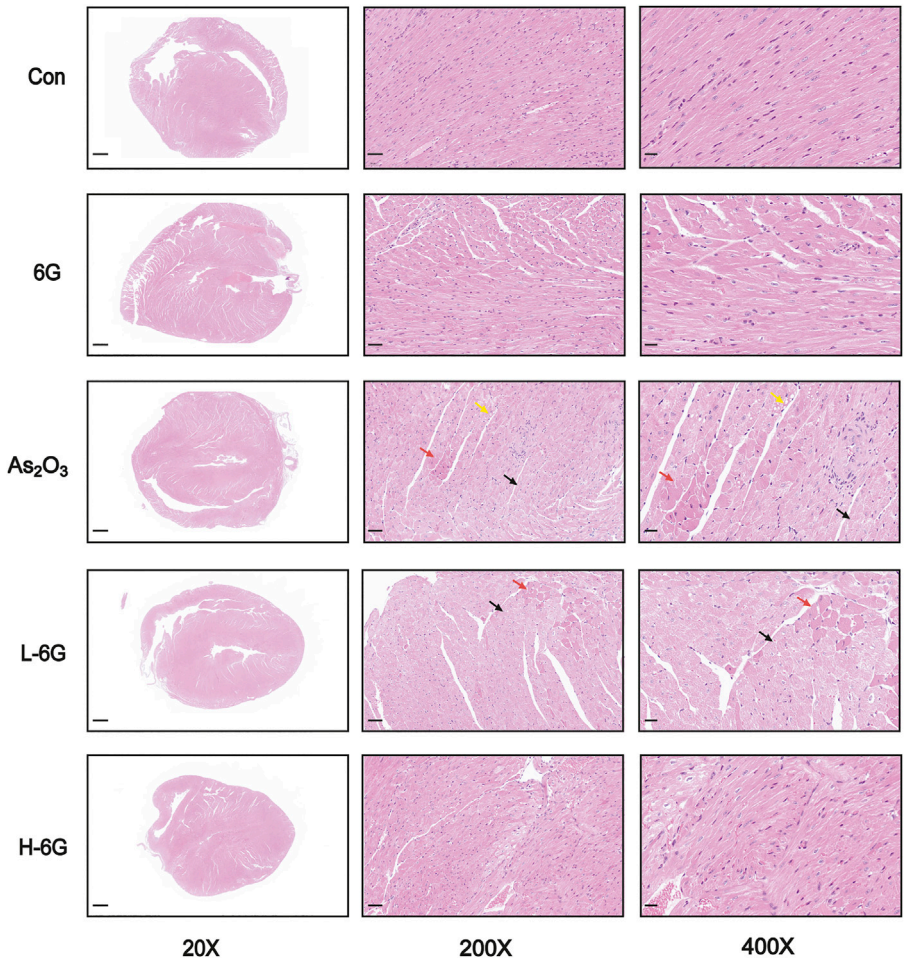

FIGURE 5 | Histological examination in each group. Red arrows represent cell necrosis, yellow arrows represent edema, and black arrows represent muscle fiber loss. $n = 6$.

as cancer (Hoonjan et al., 2018). Ginger is one of the oldest spices and is also used as a traditional Chinese medicine due to its many health benefits. The 6G extracted from ginger is the most pharmacologically active compound in gingerol (Luettig et al., 2016; de Lima et al., 2018). Our previous experimental findings have shown that 6G can effectively inhibit inflammation and apoptosis in cardiac fibrosis and myocardial injury (El-Bakly et al., 2012; Han et al., 2020). Furthermore, 6G was shown to be capable of reversing impaired insulin signaling in arsenic-intoxicated mice (Chakraborty et al., 2012). Moreover, consistent with previous research, our study found that 6G treatment can alleviate As_2O_3-induced heart injury in mice by reducing oxidative stress, the inflammatory response, and apoptosis. In addition, mice treated with 6G obtained these effects via activation of the AMPK/SIRT1/PGC-1α pathway.

The current study may help guide future research on 6G or suitable derivatives for the effective prevention of As_2O_3-induced cardiotoxicity. Evidence has amassed that heart rate and ST height are frequently used as important indicators for normal cardiac functioning and that elevated heart rate and ST segment changes indicate damage of the myocardium (Zenger et al., 2021). As_2O_3-induced myocardial injury is manifested by increased heart rate and ST-segment elevation (Sonawane et al., 2018). Our results showed that As_2O_3 treatment significantly increased heart rate and ST height, however, 6G reversed these pathological changes, suggesting that 6G protects myocardium from As_2O_3-induced injury (**Figure 3**). Meanwhile, the 6G-alone administration group was designed to observe changes in mice before and after 6G treatment. Our results showed no significant changes in mice treated with 6G alone compared to the Con group, indicating that 6G is a safe therapeutic agent.

The utilization of As_2O_3 in cancer patients causes various cardiotoxic effects (Yu et al., 2017). Serum levels of LDH and CK are indicators of myocardial damage and are frequently used to estimate cardiotoxicity (Saad et al., 2020). During cardiovascular disease or injury, the levels of CK-MB and CTnI in cardiac tissues are dramatically increased (Wang R. et al., 2021). We preliminarily analyzed the toxic effects of arsenic trioxide on the heart by the level of cardiac diagnostic markers. The data from

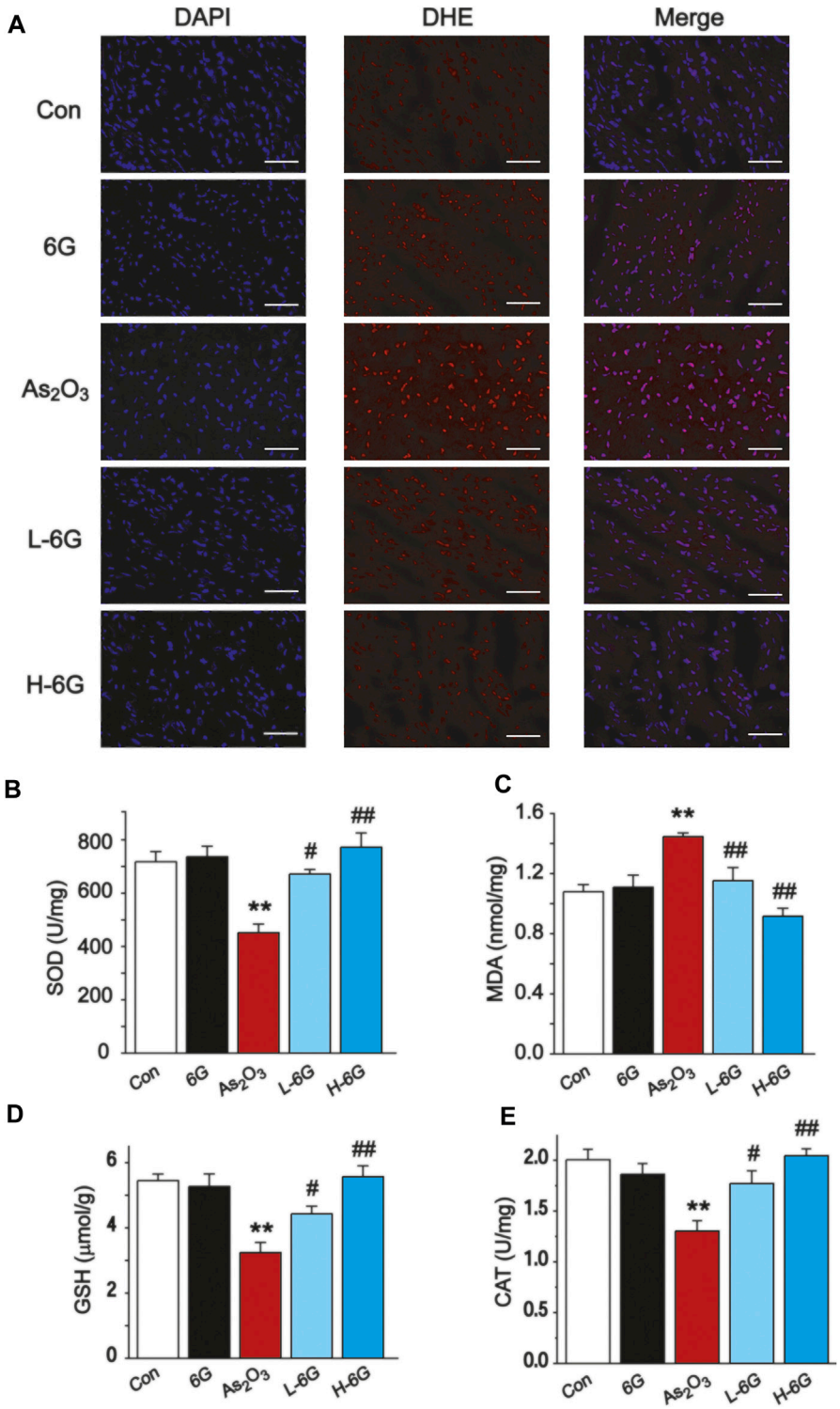

FIGURE 6 | Effect of 6G on oxidative stress in cardiac tissues. **(A)** Representative ROS fluorescence images in each group (400 ×, scale bar = 50 μm). The effects of 6G on the levels of SOD **(B)**, MDA **(C)**, GSH **(D)** and CAT **(E)** in myocardial tissues of each group. Data are presented as mean ± SEM, $n = 3$. $^{**}p < 0.01$ as in comparison to the Con group and $^{\#}p < 0.05$, $^{\#\#}p < 0.05$ as in comparison to the As_2O_3 group.

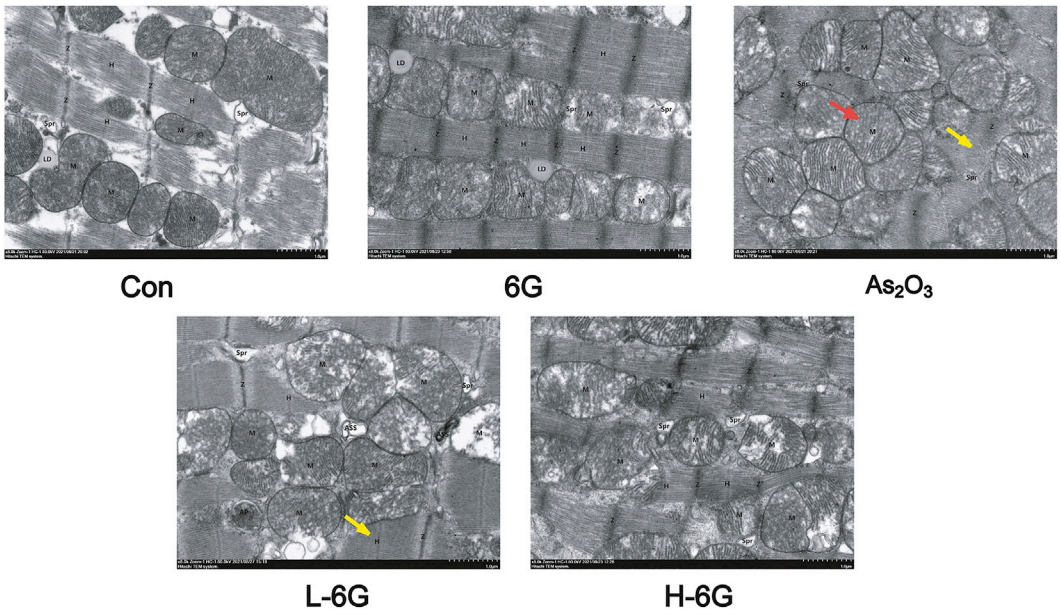

FIGURE 7 | Effect of 6G on the ultrastructure of cardiomyocytes. Representative TEM images show mitochondrial injury. Red arrows represent swelling of mitochondria and yellow arrows represent rupture of mitochondrial membranes. Scale bar = 500 nm.

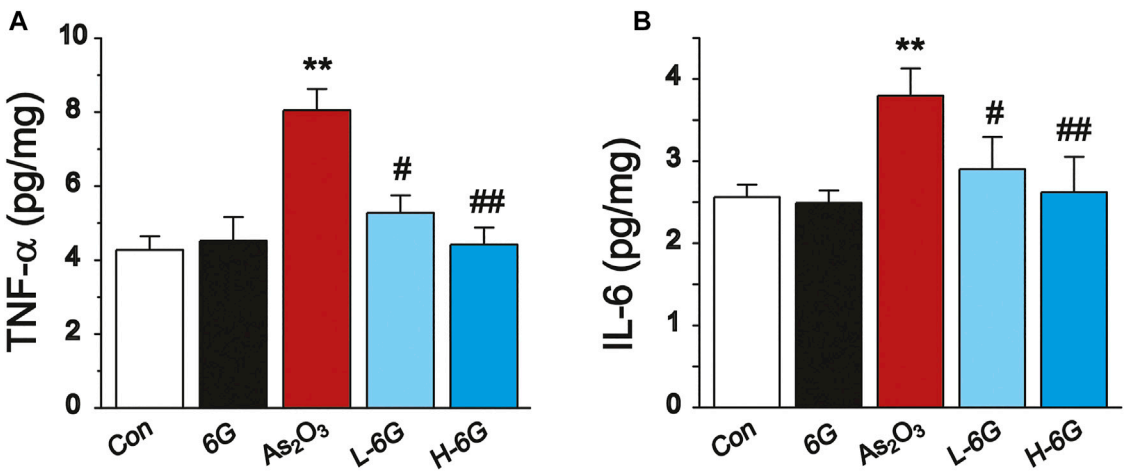

FIGURE 8 | ELISA analysis of inflammatory cytokines. The effects of 6G on the levels of TNF-α **(A)** and IL-6 **(B)** in myocardial tissues of each group. Data are expressed as mean ± SEM, $n = 3$. $^{**}p < 0.01$ as in comparison to the Con group and $^{\#}p < 0.05$, $^{\#\#}p < 0.05$ as in comparison to the As_2O_3 group.

our study demonstrate that As_2O_3 exposure increased serum levels of LDH, CK, CK-MB and CTnI. Elevated levels of these markers indicate cardiac damage, however, treatment with 6G can significantly reduce the levels of these indicators (**Figure 4**). We further observed the histopathological damage caused by As_2O_3. Results in the present study indicated that L-6G and H-6G treatment had curative effects on histopathological changes (**Figure 5**). Consistent with previous research, the protective effect of 6G, as determined by heart function markers, has been reported against ISO-induced cardiotoxicity (Han et al., 2020). 6G ((S)-5-hydroxy-1-(4-hydroxy-3-methoxyphenol)-3-decanone) extracted from ginger is the most pharmacologically active compound in gingerol, and the active part of the molecule is an aliphatic chain molecule containing a hydroxyl group (Yang et al., 2010; Wang et al., 2014). Due to its cardioprotective effect, 6G can be considered a promising molecule for the treatment of drug and chemical-induced cardiotoxicity and/or other cardiovascular diseases.

Production of reactive oxygen species, depletion of antioxidants, impairment of mitochondrial function, and

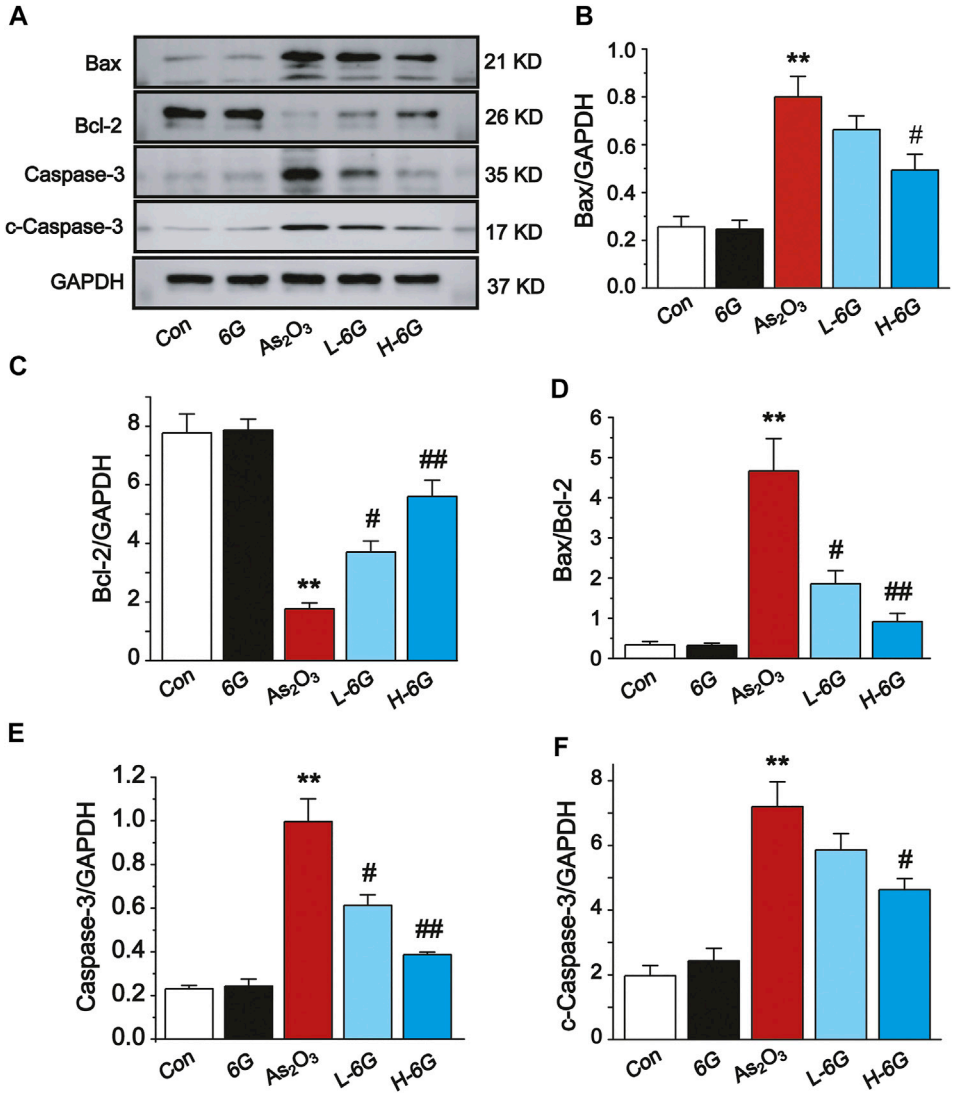

FIGURE 9 | Western blot analysis of Bcl-2, Bax, Caspase-3, and cleaved-Caspase-3 in cardiac homogenates prepared from mice, **(A)** The typical protein expression bands of each group. Bar graph of the expressions of Bax **(B)**, Bcl-2 **(C)**, Bax/Bcl-2 **(D)**, Caspase-3 **(E)** and c-Caspase-3 **(F)** in myocardial tissues. Data are expressed as mean ± SEM, $n = 3$. $^{**}p < 0.01$ as in comparison to the Con group and $^{\#}p < 0.05$, $^{\#\#}p < 0.05$ as in comparison to the As_2O_3 group.

induction of apoptosis are involved in the pathogenesis of cardiotoxicity caused by As_2O_3. Mitochondria are the major site of ROS production (Bugger and Pfeil, 2020), and exposure of As_2O_3 is able to induce overproduction of intracellular ROS, which triggers oxidative stress-related cascades, inflammatory responses, apoptosis, and cellular membrane damage (Zhong et al., 2021). The high levels of intracellular ROS in As_2O_3-treated mice were associated with the impaired mitochondrial reduction of molecular oxygen (Ahangarpour et al., 2017). The levels of SOD, CAT and GSH in the tissues indicated the extent of antioxidant defense. The results of the present study also demonstrate that As_2O_3 can generate large amounts of ROS, which leads to a significant decrease in the levels of antioxidants (SOD, GSH and CAT), as well as an increase in the levels of lipid peroxides MDA. This suggests that As_2O_3 induces cardiac injury by inducing oxygen radical production and reducing endogenous protective antioxidant capacity (**Figure 6**). Mitochondrial dysfunction is the main cause of As_2O_3-induced damage. 6G treatment could reduce the swelling of mitochondria and the breakage of mitochondrial membrane (**Figure 7**). Our results suggest that 6G could maintain mitochondrial function.

Excessive production of ROS and induction of oxidative stress-related signaling cascades result in the overproduction of pro-inflammatory mediators. TNF-α and IL-6, both of which play key roles in the inflammatory process (Forrester et al., 2018). Inflammatory cytokines were found to be upregulated in As_2O_3-induced cardiotoxicity. Our results are

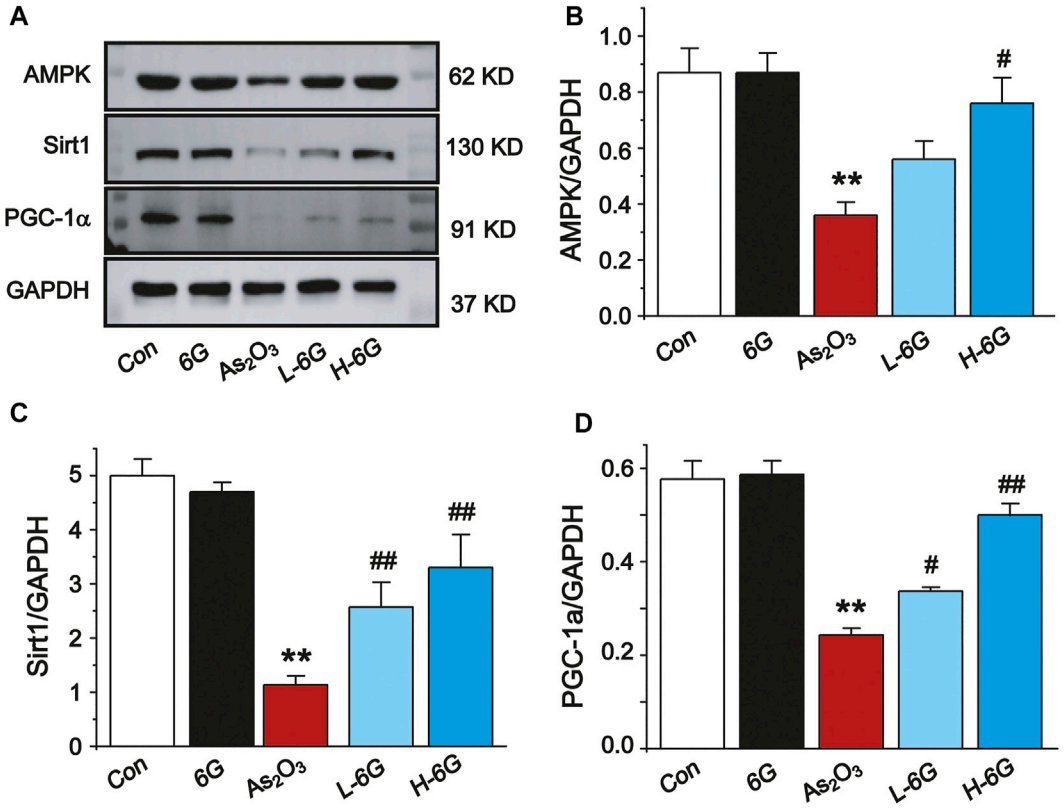

FIGURE 10 | Western blot analysis of AMPK, SIRT1, and PGC-1α in cardiac homogenates prepared from mice, **(A)** The typical protein expression bands of each group. Bar graph of the expressions of AMPK **(B)**, Sirt1 **(C)** and PGC-1α **(D)** in myocardial tissues. Data are expressed as mean ± SEM, $n = 3$. $^{**}p < 0.01$ as in comparison to the Con group and $^{\#}p < 0.05$, $^{\#\#}p < 0.05$ as in comparison to the As_2O_3 group.

in consistent with previous studies. Notably, TNF-α and IL-6 were significantly downregulated by 6G, suggesting that 6G exerts a significant anti-inflammatory effect by inhibiting the levels of TNF-α and IL-6 (**Figure 8**).

Oxidative stress caused by As_2O_3 results in dysfunction of mitochondria and apoptosis of cardiomyocytes, both of which contribute to the development of myocardial damage (Zhu and Zuo, 2013). It is well known that the apoptosis-related regulatory proteins Bax, Bcl-2, Caspase-3 and cleaved-Caspase-3 are closely associated with As_2O_3-induced cardiotoxicity. As a classical anti-apoptotic mediator, Bcl-2 can inhibit the activity of Caspase-3 which, in turn, inhibits cellular apoptosis. It is noteworthy that Bax upregulates the permeability of mitochondrial membranes, causing cytochrome c release, which induces cellular apoptosis through activation of Caspase-3 and cleaved-Caspase-3 (Polat and Karaboga, 2019). We also found that As_2O_3 induced apoptotic damage to the heart, as evidenced by notable increases in Caspase-3, Bax, and Bcl-2 expression and the Bax/Bcl-2 ratio in the heart of As_2O_3-treated mice. However, in the groups treated with 6G, Bax, Caspase-3, and cleaved-Caspase-3 levels were downregulated and the Bax/Bcl-2 ratio decreased in heart tissue, while Bcl-2 expression in heart tissue was upregulated relative to As_2O_3-treated mice (**Figure 9**).

The signaling cascade mediated by AMPK, SIRT1 and PGC-1α can inhibit ROS production and inflammatory cytokines (Thirupathi and de Souza, 2017). Thus, activation of the cascade may be an effective therapy against As_2O_3-induced damage. Multiple studies have shown that AMPK could affect the activity of the downstream molecules SIRT1 and PGC-1α, as well as the activation of AMPK and PGC-1α, which could also be regulated by SIRT1 (Tian et al., 2019). PGC-1α plays an important role in cardioprotective therapies and is highly expressed in cardiac myocytes (Lehman et al., 2000). Furthermore, PGC-1α is a key factor for myocardial mitochondrial biogenesis and for regulating the expression of the downstream proteins involved in oxidative stress (Choi et al., 2017; Di et al., 2018). SIRT1, a histone deacetylase, plays an important role in regulating a wide range of critical biological functions, including oxidative stress, energy metabolism, apoptosis, and autophagy. Our present study found that As_2O_3 significantly decreased the protein expressions of AMPK, SIRT1, and PGC-1α, whereas 6G upregulated the expressions of AMPK, SIRT1, and PGC-1α, enhanced SOD activities, and suppressed the production of ROS and MDA to maintain mitochondrial function and control oxidative stress (**Figures 10**, **11**).

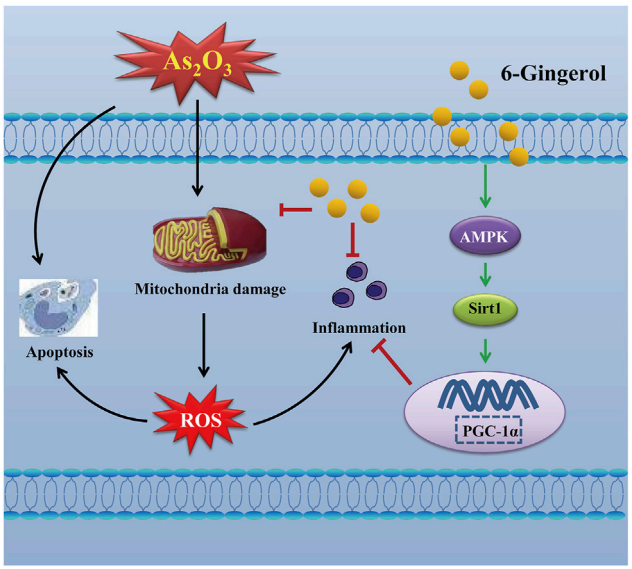

FIGURE 11 | Mechanism of 6G on As_2O_3-induced cardiotoxicity.

CONCLUSION

In line with these findings, the data generated by our study suggests that 6G treatment exerts cardioprotective effects by attenuating oxidative stress, inflammation, and apoptosis. 6G may be a promising therapeutic agent for the prevention of As_2O_3-induced cardiotoxicity, and the AMPK/SIRT1/PGC-1α pathway may be an effective target. Our experiments provide guidance for future studies on the efficacy of 6G or suitable derivatives in preventing the cardiotoxicity of anticancer drugs.

DATA AVAILABILITY STATEMENT

The original contributions presented in the study are included in the article/Supplementary Material, further inquiries can be directed to the corresponding authors.

ETHICS STATEMENT

The animal study was reviewed and approved by the Ethics Committee of Hebei University of Chinese Medicine.

AUTHOR CONTRIBUTIONS

Participated in research design: XH, YY, SG, SS, and QJ. Conducted experiments: XH, YY, MZ, and XC. Performed data analysis: XH, YY, BZ, CL, and YX. Wrote or contributed to the writing of the manuscript: XH, YY, SG, SS, and QJ.

FUNDING

This work was supported by the Natural Science Foundation of Hebei Province (No. H2021206352 and H2021423027) and Research Foundation of Administration of Traditional Chinese Medicine of Hebei Province (No. 2022097).

REFERENCES

Ahangarpour, A., Zeidooni, L., Rezaei, M., Alboghobeish, S., Samimi, A., and Oroojan, A. A. (2017). Protective Effect of Metformin on Toxicity of Butyric Acid and Arsenic in Isolated Liver Mitochondria and Langerhans Islets in Male Mice: an *In Vitro* Study. *Iran J. Basic Med. Sci.* 20 (12), 1297–1305. doi:10.22038/IJBMS.2017.9567

Bechard, L. J., Feldman, H. A., Gordon, C., Gura, K., Sonis, A., and Leung, K. (2010). A multi-center, Randomized, Controlled Trial of Parenteral Nutrition Titrated to Resting Energy Expenditure in Children Undergoing Hematopoietic Stem Cell Transplantation ("PNTREE"): Rationale and Design. *Contemp. Clin. Trials* 31 (2), 157–164. doi:10.1016/j.cct.2009.12.002

Birari, L. A., Mahajan, U. B., Patil, K. R., Patil, D. D., Bagul, N. A., Belemkar, S., et al. (2020). Aloin Protects against Arsenic Trioxide-Induced Myocardial Membrane Damage and Release of Inflammatory Cytokines. *Naunyn Schmiedebergs Arch. Pharmacol.* 393 (8), 1365–1372. doi:10.1007/s00210-020-01833-1

Bugger, H., and Pfeil, K. (2020). Mitochondrial ROS in Myocardial Ischemia Reperfusion and Remodeling. *Biochim. Biophys. Acta Mol. Basis Dis.* 1866 (7), 165768. doi:10.1016/j.bbadis.2020.165768

Canto, C., and Auwerx, J. (2009). PGC-1α, SIRT1 and AMPK, an Energy Sensing Network that Controls Energy Expenditure. *Curr. Opin. Lipidol.* 20 (2), 98–105. doi:10.1097/MOL.0b013e328328d0a4

Chakraborty, D., Mukherjee, A., Sikdar, S., Paul, A., Ghosh, S., and Khuda-Bukhsh, A. R. (2012). [6]-Gingerol Isolated from Ginger Attenuates Sodium Arsenite Induced Oxidative Stress and Plays a Corrective Role in Improving Insulin Signaling in Mice. *Toxicol. Lett.* 210 (1), 34–43. doi:10.1016/j.toxlet.2012.01.002

Choi, H. I., Kim, H. J., Park, J. S., Kim, I. J., Bae, E. H., Ma, S. K., et al. (2017). PGC-1alpha Attenuates Hydrogen Peroxide-Induced Apoptotic Cell Death by Upregulating Nrf-2 via GSK3beta Inactivation Mediated by Activated P38 in HK-2 Cells. *Sci. Rep.* 7 (1), 4319. doi:10.1038/s41598-017-04593-w

de Lima, R. M. T., Dos Reis, A. C., de Menezes, A. P. M., Santos, J. V. O., Filho, J., Ferreira, J. R. O., et al. (2018). Protective and Therapeutic Potential of Ginger (Zingiber Officinale) Extract and [6]-gingerol in Cancer: A Comprehensive Review. *Phytother Res.* 32 (10), 1885–1907. doi:10.1002/ptr.6134

Di, W., Lv, J., Jiang, S., Lu, C., Yang, Z., Ma, Z., et al. (2018). PGC-1: The Energetic Regulator in Cardiac Metabolism. *Curr. Issues Mol. Biol.* 28, 29–46. doi:10.21775/cimb.028.029

El-Bakly, W. M., Louka, M. L., El-Halawany, A. M., and Schaalan, M. F. (2012). 6-gingerol Ameliorated Doxorubicin-Induced Cardiotoxicity: Role of Nuclear Factor Kappa B and Protein Glycation. *Cancer Chemother. Pharmacol.* 70 (6), 833–841. doi:10.1007/s00280-012-1975-y

Emadi, A., and Gore, S. D. (2010). Arsenic Trioxide - an Old Drug Rediscovered. *Blood Rev.* 24 (4-5), 191–199. doi:10.1016/j.blre.2010.04.001

Ficker, E., Kuryshev, Y. A., Dennis, A. T., Obejero-Paz, C., Wang, L., Hawryluk, P., et al. (2004). Mechanisms of Arsenic-Induced Prolongation of Cardiac Repolarization. *Mol. Pharmacol.* 66 (1), 33–44. doi:10.1124/mol.66.1.33

Forrester, S. J., Kikuchi, D. S., Hernandes, M. S., Xu, Q., and Griendling, K. K. (2018). Reactive Oxygen Species in Metabolic and Inflammatory Signaling. *Circ. Res.* 122 (6), 877–902. doi:10.1161/CIRCRESAHA.117.311401

Ghosh, J., Das, J., Manna, P., and Sil, P. C. (2009). Taurine Prevents Arsenic-Induced Cardiac Oxidative Stress and Apoptotic Damage: Role of NF-Kb, P38 and JNK MAPK Pathway. *Toxicol. Appl. Pharmacol.* 240 (1), 73–87. doi:10.1016/j.taap.2009.07.008

Han, X., Liu, P., Liu, M., Wei, Z., Fan, S., Wang, X., et al. (2020). [6]-Gingerol Ameliorates ISO-Induced Myocardial Fibrosis by Reducing Oxidative Stress, Inflammation, and Apoptosis through Inhibition of TLR4/MAPKs/NF-Kb Pathway. *Mol. Nutr. Food Res.* 64 (13), e2000003. doi:10.1002/mnfr.202000003

Han, X., Zhang, Y., Liang, Y., Zhang, J., Li, M., Zhao, Z., et al. (2019). 6-Gingerol, an Active Pungent Component of Ginger, Inhibits L-type Ca(2+) Current, Contractility, and Ca(2+) Transients in Isolated Rat Ventricular Myocytes. *Food Sci. Nutr.* 7 (4), 1344–1352. doi:10.1002/fsn3.968

Haniadka, R., Saldanha, E., Sunita, V., Palatty, P. L., Fayad, R., and Baliga, M. S. (2013). A Review of the Gastroprotective Effects of Ginger (Zingiber Officinale Roscoe). *Food Funct.* 4 (6), 845–855. doi:10.1039/c3fo30337c

Hemmati, A. A., Olapour, S., Varzi, H. N., Khodayar, M. J., Dianat, M., Mohammadian, B., et al. (2018). Ellagic Acid Protects against Arsenic Trioxide-Induced Cardiotoxicity in Rat. *Hum. Exp. Toxicol.* 37 (4), 412–419. doi:10.1177/0960327117701986

Hoonjan, M., Jadhav, V., and Bhatt, P. (2018). Arsenic Trioxide: Insights into its Evolution to an Anticancer Agent. *J. Biol. Inorg. Chem.* 23 (3), 313–329. doi:10.1007/s00775-018-1537-9

Jin, W., Xue, Y., Xue, Y., Han, X., Song, Q., Zhang, J., et al. (2020). Tannic Acid Ameliorates Arsenic Trioxide-Induced Nephrotoxicity, Contribution of NF-Kb and Nrf2 Pathways. *Biomed. Pharmacother.* 126, 110047. doi:10.1016/j.biopha.2020.110047

Kapoor, V., Aggarwal, S., and Das, S. N. (2016). 6-Gingerol Mediates its Anti Tumor Activities in Human Oral and Cervical Cancer Cell Lines through Apoptosis and Cell Cycle Arrest. *Phytother Res.* 30 (4), 588–595. doi:10.1002/ptr.5561

Krell, J., and Stebbing, J. (2012). Ginger: the Root of Cancer Therapy? *Lancet Oncol.* 13 (3), 235–236. doi:10.1016/S1470-2045(12)70097-9

Lehman, J. J., Barger, P. M., Kovacs, A., Saffitz, J. E., Medeiros, D. M., and Kelly, D. P. (2000). Peroxisome Proliferator-Activated Receptor Gamma Coactivator-1 Promotes Cardiac Mitochondrial Biogenesis. *J. Clin. Invest.* 106 (7), 847–856. doi:10.1172/JCI10268

Luettig, J., Rosenthal, R., Lee, I. M., Krug, S. M., and Schulzke, J. D. (2016). The Ginger Component 6-shogaol Prevents TNF-α-Induced Barrier Loss via Inhibition of PI3K/Akt and NF-Kb Signaling. *Mol. Nutr. Food Res.* 60 (12), 2576–2586. doi:10.1002/mnfr.201600274

Luna-Dulcey, L., Tomasin, R., Naves, M. A., da Silva, J. A., and Cominetti, M. R. (2018). Autophagy-dependent Apoptosis Is Triggered by a Semi-synthetic [6]-gingerol Analogue in Triple Negative Breast Cancer Cells. *Oncotarget* 9 (56), 30787–30804. doi:10.18632/oncotarget.25704

Luo, J., Chen, J., Yang, C., Tan, J., Zhao, J., Jiang, N., et al. (2021). 6-Gingerol Protects against Cerebral Ischemia/reperfusion Injury by Inhibiting NLRP3 Inflammasome and Apoptosis via TRPV1/FAF1 Complex Dissociation-Mediated Autophagy. *Int. Immunopharmacol* 100, 108146. doi:10.1016/j.intimp.2021.108146

Polat, F. R., and Karaboga, I. (2019). Immunohistochemical Examination of Anti-inflammatory and Anti-apoptotic Effects of Hesperetin on Trinitrobenzene Sulfonic Acid Induced Colitis in Rats. *Biotech. Histochem.* 94 (3), 151–158. doi:10.1080/10520295.2018.1530454

Saad, S., Ahmad, I., Kawish, S. M., Khan, U. A., Ahmad, F. J., Ali, A., et al. (2020). Improved Cardioprotective Effects of Hesperidin Solid Lipid Nanoparticles Prepared by Supercritical Antisolvent Technology. *Colloids Surf. B Biointerfaces* 187, 110628. doi:10.1016/j.colsurfb.2019.110628

Salt, I. P., and Hardie, D. G. (2017). AMP-activated Protein Kinase: An Ubiquitous Signaling Pathway with Key Roles in the Cardiovascular System. *Circ. Res.* 120 (11), 1825–1841. doi:10.1161/CIRCRESAHA.117.309633

Seif, M., Abd El-Aziz, T., Sayed, M., and Wang, Z. (2021). Zingiber Officinale Ethanolic Extract Attenuates Oxidative Stress, Steroidogenic Gene Expression Alterations, and Testicular Histopathology Induced by Sodium Arsenite in Male Rats. *Environ. Sci. Pollut. Res. Int.* 28 (16), 19783–19798. doi:10.1007/s11356-020-11509-1

Sonawane, V. K., Mahajan, U. B., Shinde, S. D., Chatterjee, S., Chaudhari, S. S., Bhangale, H. A., et al. (2018). A Chemosensitizer Drug: Disulfiram Prevents Doxorubicin-Induced Cardiac Dysfunction and Oxidative Stress in Rats. *Cardiovasc. Toxicol.* 18 (5), 459–470. doi:10.1007/s12012-018-9458-y

Thirupathi, A., and de Souza, C. T. (2017). Multi-regulatory Network of ROS: the Interconnection of ROS, PGC-1 Alpha, and AMPK-SIRT1 during Exercise. *J. Physiol. Biochem.* 73 (4), 487–494. doi:10.1007/s13105-017-0576-y

Tian, L., Cao, W., Yue, R., Yuan, Y., Guo, X., Qin, D., et al. (2019). Pretreatment with Tilianin Improves Mitochondrial Energy Metabolism and Oxidative Stress in Rats with Myocardial Ischemia/reperfusion Injury via AMPK/SIRT1/PGC-1 Alpha Signaling Pathway. *J. Pharmacol. Sci.* 139 (4), 352–360. doi:10.1016/j.jphs.2019.02.008

Wang, R., Wang, N., Han, Y., Xu, J., and Xu, Z. (2021). Dulaglutide Alleviates LPS-Induced Injury in Cardiomyocytes. *ACS Omega* 6 (12), 8271–8278. doi:10.1021/acsomega.0c06326

Wang, S., Zhang, C., Yang, G., and Yang, Y. (2014). Biological Properties of 6-gingerol: a Brief Review. *Nat. Prod. Commun.* 9 (7), 1027–1030. doi:10.1177/1934578x1400900736

Wang, X., Qian, Z., Li, H., Chen, H., Lin, L., Guo, M., et al. (2021). Evaluation of Arsenic Species in Leukocytes and Granulocytes of Acute Promyelocytic Leukemia Patients Treated with Arsenic Trioxide. *J. Pharm. Biomed. Anal.* 203, 114201. doi:10.1016/j.jpba.2021.114201

Yang, G., Zhong, L., Jiang, L., Geng, C., Cao, J., Sun, X., et al. (2010). Genotoxic Effect of 6-gingerol on Human Hepatoma G2 Cells. *Chem. Biol. Interact* 185 (1), 12–17. doi:10.1016/j.cbi.2010.02.017

Yu, X., Wang, Z., Shu, Z., Li, Z., Ning, Y., Yun, K., et al. (2017). Effect and Mechanism of Sorbus Pohuashanensis (Hante) Hedl. Flavonoids Protect against Arsenic Trioxide-Induced Cardiotoxicity. *Biomed. Pharmacother.* 88, 1–10. doi:10.1016/j.biopha.2016.12.130

Zenger, B., Good, W. W., Bergquist, J. A., Rupp, L. C., Perez, M., Stoddard, G. J., et al. (2021). Transient Recovery of Epicardial and Torso ST-Segment Ischemic Signals during Cardiac Stress Tests: A Possible Physiological Mechanism. *J. Electrocardiol.* 69S, 38–44. doi:10.1016/j.jelectrocard.2021.07.007

Zhang, C., Wang, J., Qi, Q., Yang, L., Sun, P., and Yuan, X. (2021). Modulatory Effect of Fructooligosaccharide against Triphenyltin-Induced Oxidative Stress and Immune Suppression in Goldfish (Carassius auratus). *Ecotoxicol Environ. Saf.* 212, 111966. doi:10.1016/j.ecoenv.2021.111966

Zhang, F., Ma, N., Gao, Y. F., Sun, L. L., and Zhang, J. G. (2017). Therapeutic Effects of 6-Gingerol, 8-Gingerol, and 10-Gingerol on Dextran Sulfate Sodium-Induced Acute Ulcerative Colitis in Rats. *Phytother Res.* 31 (9), 1427–1432. doi:10.1002/ptr.5871

Zhong, G., Wan, F., Ning, Z., Wu, S., Jiang, X., Tang, Z., et al. (2021). The Protective Role of Autophagy against Arsenic Trioxide-Induced Cytotoxicity and ROS-dependent Pyroptosis in NCTC-1469 Cells. *J. Inorg. Biochem.* 217, 111396. doi:10.1016/j.jinorgbio.2021.111396

Zhu, X., and Zuo, L. (2013). Characterization of Oxygen Radical Formation Mechanism at Early Cardiac Ischemia. *Cell Death Dis* 4, e787. doi:10.1038/cddis.2013.313

Zong, L., Li, C., Shi, J., Yue, J., and Wang, X. (2021). FTIR Microspectroscopic Study of Biomacromolecular Changes in As2O3 Induced MGC803 Cells Apoptosis. *Spectrochim Acta A. Mol. Biomol. Spectrosc.* 263, 120220. doi:10.1016/j.saa.2021.120220

Conflict of Interest: The authors declare that the research was conducted in the absence of any commercial or financial relationships that could be construed as a potential conflict of interest.

Publisher's Note: All claims expressed in this article are solely those of the authors and do not necessarily represent those of their affiliated organizations, or those of the publisher, the editors and the reviewers. Any product that may be evaluated in this article, or claim that may be made by its manufacturer, is not guaranteed or endorsed by the publisher.

frontiers | Frontiers in Pharmacology

ORIGINAL RESEARCH
published: 13 May 2022
doi: 10.3389/fphar.2022.885699

Treatment-Related Coronary Disorders of Fluoropyrimidine Administration: A Systematic Review and Meta-Analysis

*Yajie Lu†, Shizhou Deng†, Qiongyi Dou, Wei Pan, Qingqing Liu, Hongchen Ji, Xiaowen Wang and Hong-Mei Zhang**

Department of Clinical Oncology, Xijing Hospital, Air Force Medical University of PLA, Xi'an, China

OPEN ACCESS

Edited by:
Ming-Ming Wu,
Harbin Medical University, China

Reviewed by:
Massimiliano Berretta,
University of Messina, Italy
Takahiro Kogawa,
Cancer Institute Hospital of Japanese Foundation for Cancer Research, Japan
Niansong Qian,
Urumqi General Hospital of PLA, China

***Correspondence:**
Hong-Mei Zhang
zhm@fmmu.edu.cn

†These authors have contributed equally to this work and share first authorship

Specialty section:
This article was submitted to Cardiovascular and Smooth Muscle Pharmacology, a section of the journal Frontiers in Pharmacology

Received: *28 February 2022*
Accepted: *07 April 2022*
Published: *13 May 2022*

Citation:
Lu Y, Deng S, Dou Q, Pan W, Liu Q, Ji H, Wang X and Zhang H-M (2022) Treatment-Related Coronary Disorders of Fluoropyrimidine Administration: A Systematic Review and Meta-Analysis. Front. Pharmacol. 13:885699. doi: 10.3389/fphar.2022.885699

Background: Coronary disorders are recognized as the most common manifestation of fluoropyrimidine-related cardiotoxicity in clinical practice. However, there are limited and conflicting data on the incidence and profiles of fluoropyrimidine-related coronary disorders. In this meta-analysis, we aimed to systematically assess the incidence of all-grade and grade 3 or higher fluoropyrimidine-related coronary disorders, and further explore the factors that influence its occurrence.

Methods: Studies reporting the fluoropyrimidine-related coronary disorders were retrieved from a systematic search of English literature in the PubMed, Web of Science, Medline, and Cochrane database from 1 Jan 2001, to 1 Jan 2022. The NIH assessment tool was used to evaluate the quality of each study. The data of basic study characteristics, treatment details, and results of coronary toxicities were extracted. According to the results of the heterogeneity test (I^2 and p-value statistic), a random-effect model or fixed-effect model was selected for the pooled analysis of the incidence of adverse coronary events. Subgroup analysis was conducted to further explore the risks influencing the occurrence of fluoropyrimidine-related coronary disorders. The stability and publication bias of our results were evaluated by sensitivity analysis and Egger test, respectively.

Results: A total of 63 studies were finally included in our pooled analysis, involving 25,577 patients. The pooled cumulative incidence of all-grade and grade 3 or higher coronary disorders was 2.75% (95% CI 1.89%–3.76%) and 1.00% (95% CI 0.62%–1.47%), respectively. The coronary disorders were most reported as myocardial ischemia (1.28%, 95% CI 0.42%–2.49%) and angina/chest pain (1.1%, 95% CI 0.54%–1.81%). Subgroup analysis revealed that studies in the female-only population seemed to have a lower incidence of fluoropyrimidine-related coronary disorders. The occurrence of adverse coronary events varied among different tumor types. Patients with esophageal cancer have the highest coronary toxicity (6.32%), while those with breast cancer have a relatively lower incidence (0.5%). Coronary disorders induced by 5-FU monotherapy are more frequent than that induced by capecitabine (3.31% vs. 1.21%, $p < 0.01$). Fluoropyrimidine combination therapy, whether combined with other chemotherapy drugs, targeted

therapy drugs, or radiotherapy, significantly increased the incidence of coronary complications ($p < 0.01$).

Conclusion: This meta-analysis has defined the incidence of fluoropyrimidine-related coronary disorders and depicted its epidemiological profiles for the first time, which may provide a reference for clinical practice in cancer management.

Keywords: coronary disorder, 5-FU, capecitabine, meta-analysis, fluoropyrimidine

INTRODUCTION

With the continuous development of chemotherapy, radiotherapy, and new treatment technologies, the survival of cancer patients has been greatly improved. Meanwhile, the cardiovascular toxicity related to anti-tumor therapy has become increasingly prominent, which is one of the important causes of death due to treatment-related complications (Curigliano et al., 2016). Cardio-Oncology, an emerging interdisciplinary field, focuses on cardiovascular disease in cancer patients, and has developed rapidly in recent years (Koutsoukis et al., 2018). The incidence and spectrum of cardiotoxicity vary widely by chemotherapeutic regimens. The cardiotoxicity of anthracyclines has been extensively studied and highly concerned over the past 2 decades (Lotrionte et al., 2013; Smith et al., 2010). However, fluoropyrimidine (5-fluorouracil (5-FU), capecitabine, S-1, Tas102, etc.) induced cardiotoxicity has not been attracted equal attention.

The coronary disorder is one of the typical adverse reactions induced by chemotherapy agents, such as 5-FU and capecitabine, which often refers to the transient contraction of coronary artery and thrombus formation, causing varying degrees of myocardial ischemia, and resulting in the clinical syndrome of angina pectoris, myocardial infarction, even sudden death (More et al., 2021). Chest pain with typical or atypical angina pectoris is the most prominent manifestation of the coronary disorder, which has directly been visualized during coronary angiography (Baldeo et al., 2018; Das et al., 2019; Gao et al., 2019).

Despite some studies that have focused on fluoropyrimidine-induced coronary disorder, most of them were conducted with small samples or just case reports (Karakulak et al., 2016; Ben-Yakov et al., 2017; Sedhom et al., 2017). The reported incidence of fluoropyrimidine-related coronary disorder varies from 0% to 35% (Pai and Nahata, 2000; Sara et al., 2018; Lestuzzi et al., 2020), which is a too wide range to provide valuable reference for clinical practice. In addition, some studies suggested that the occurrence of coronary disorder depended on the different fluoropyrimidine drugs, route of administrations, dosage schedules, and co-administered agents (Depetris et al., 2018; Kanduri et al., 2019). However, there is no consensus on the incidence, profiles, and risk factors of fluoropyrimidine-related coronary disorders. An accurate description of the incidence and epidemiological characteristics of coronary vasospasm is the basis for guiding clinical practice and is very crucial for the early identification and prevention of ischemic events caused by fluoropyrimidines. Obviously, the currently available data are not yet sufficient for drawing definite conclusions. Therefore, in this systematic review and meta-analysis, we are dedicated to comprehensively and systematically evaluating the incidence and epidemiological characteristics of fluoropyrimidine-induced coronary disorders and to further exploring the factors influencing its occurrence using a method of single-rate meta-analysis.

MATERIALS AND METHODS

The Definition of Coronary Disorder

The coronary disorder of interest in this study was defined as a group of symptoms represented by chest pain syndrome, including angina pectoris, myocardial ischemia, myocardial infarction, and acute coronary syndrome. The fluoropyrimidine-related coronary disorders were recognized by the new occurrence of a chest pain at rest in the presence of recent fluoropyrimidine administration with or without electrocardiogram (ECG) or biomarker changes.

Search Strategy and Selection Criteria

Literature search and study selection were conducted under the PRISMA guidelines. Studies reporting the fluoropyrimidine-related coronary disorders were retrieved from a systematic search of English literature in the PubMed, Web of Science, Medline, and Cochrane database from 1 Jan 2001 to 1 Jan 2022. The search strategy was determined after several pre-retrievals and finally combined the following two sorts of items: 1) "fluoropyrimidine" OR "5-FU" OR "capecitabine" OR "S-1" OR "Tas102"; 2) "cardiotoxicity" OR "coronary vasospasm" OR "chest pain" OR "angina" OR "myocardial ischemia" OR "myocardial infarction" OR "acute coronary syndrome." Studies had to meet the following inclusion criteria: 1) patients with a diagnosis of solid malignances; 2) articles explicitly reported the coronary disorders as defined above, and it is associated with fluorouracil-containing treatment; 3) the sample size was greater than 20; 4) the full-text was available; 5) prospective or retrospective clinical studies. Reviews, letters, comments, case report, meeting abstract were excluded.

Methodological Quality Assessment and Data Extraction

The quality of included studies was assessed using the quality assessment tool of the National Institutes of Health (NIH) (Nhlbi Study Quality Assessment Tools, 2020, **Supplementary Table S1**). The reviewers could select "YES," "NO," or "Cannot Determine/Not

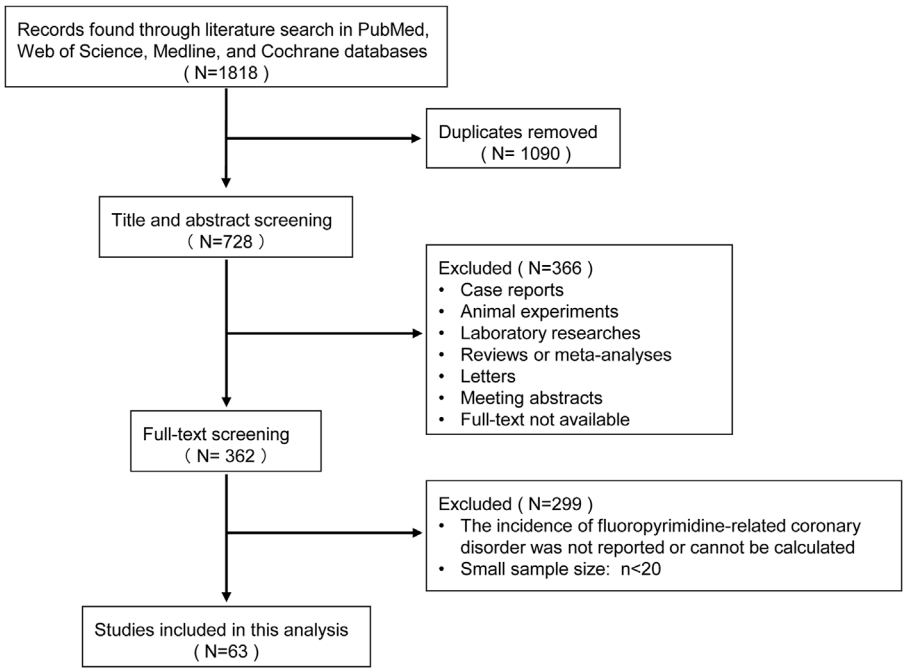

FIGURE 1 | The flow diagram for literature selection, screening, and inclusion.

Applicable/Not Reported" for each item in the list. Based on their responses, the quality of each study was graded as "good," "fair," or "poor." The incidences of fluoropyrimidine-related coronary disorders of all-grade and grade 3 or higher were the main outcomes in this meta-analysis. The data of basic characteristics (first-author, publication year, study design, country or region, age, gender, tumor type, and sample size), treatment details (treatment type, line, regimen, and dosage), and the incidence of fluoropyrimidine-related coronary disorders were extracted and documented. Two authors (Lu and Deng) independently searched the literature, assessed the quality of included studies, and extracted and cross-checked the data.

Statistical Analysis

The incidence of fluoropyrimidine-related coronary disorders in each study was shown as a percentage calculated using a division method ($\frac{the\ sum\ of\ cornary\ disorder}{the\ sum\ of\ total\ patients} \times 100\%$). The Cochran's chi-squared test reporting I^2 statistic and p-value was used to test heterogeneity, and if heterogeneity exists ($I^2 >$ 50% or $p < 0.1$), a random-effect model was conducted, otherwise, a fixed-effect model was adopted. The pooled incidence was achieved by a single rate meta-analysis method, shown as a proportion and 95 confidence intervals (CI). Subgroup analyses were performed based on study-level characteristics (e.g., publication period, study design, gender, age, tumor, treatment type, regimen, and so on) for all-grade and grade 3 or higher adverse coronary events. Sensitivity analyses were conducted to evaluate the stability of our results. Publication bias was shown by funnel plot symmetry and statistically checked using the Egger test. For all tests, p-values less than 0.05 were considered statistically significant. All the statistical process of this meta-analysis was performed using R software (version 4.0.6, MathSoft, Massachusetts) with "meta," "rmeta," and "metafor" packages.

RESULTS

Eligible Studies and Characteristics

A total of 1818 initial records were identified through a literature search. After title and abstract screening and full-text screening, 63 studies were finally included in this meta-analysis, involving 25,577 patients (**Figure 1**). The included populations covered more than 30 countries around the world, of which 5 were multi-country collaborations. Forty-seven (74.6%) of the 63 included articles were prospective studies, while the remaining 16 (25.4%) were retrospective in design. The tumor spectrum included colorectal cancer (number of studies: n = 25, 39.7%), breast cancer (n = 11, 17.5%), esophagus cancer (n = 4, 6.3%), gastric cancer (n = 3, 4.8%), and others (n = 9, 14.3%), the remaining 11 (17.5%) studies focused on mixed solid malignancies without distinguishing specific tumor categories. The included 63 studies consisted of 92 treatment arms, and their regimens included 5-FU/capecitabine mono chemotherapy (n = 20, 21.7%), 5-FU/capecitabine combined chemotherapy (n = 33, 35.9%), 5-FU/capecitabine based chemotherapy plus targeted therapy (n = 25, 27.2%), 5-FU/capecitabine based chemotherapy plus radiotherapy (n = 6, 6.5%), and the modified fluoropyrimidine agents S1 or TAS 102 (n = 2, 2.2%). According to the NIH quality assessment tools, 29 studies (46%) were rated as high quality, 34 (54%) fair

TABLE 1 | The characteristics of the included 64 studies.

No	Author	Year	Country/ Region	Sample size	Study design	Age	Gender (female %)	Tumor type	Regimen	Quality	References
1	Zafar A	2021	United States	4,019	retro	58 ± 13 64 ± 13	0.425 0.414	Mixed malignancies	5-FU or Cap based	Good	Zafar et al. (2021)
2	Mayer IA	2021	United States	198	pros	52 (26–76)	1	Breast cancer	Cap	Good	Mayer et al. (2021)
3	Chakravarthy AB	2020	United States	355	pros	54.3 ± 11.7 53.9 ± 9.9	0.348 0.376	Rectal cancer	mFOLFOX mFOLFOX + Bev	Fair	Chakravarthy et al. (2020)
4	Dyhl-Polk A (1)	2020	Denmark	108	retro	66 (35–81)	0.454	Colorectal or anal cancer	Coloretal cancer: 5-Fu or FOLFOX Metastatic: FOLFOX or FOLFIRI ± Cet or Pan Anal cancer: FP + RT	Fair	Dyhl-Polk et al. (2020a)
5	Delaloge S	2020	Multi-country	628	pros	18–70	1	Breast cancer	TX	Good	Delaloge et al. (2020)
6	Grierson P	2020	United States	16	pros	66 (42–73)	0.563	Pancreatic ductal adenocarcinoma	Cap + Tosedostat	Fair	Grierson et al. (2020)
7	Dyhl-Polk A (2)	2020	Denmark	2,236	retro	65 (21–85) 70 (22–93)	0.447 0.471	Colorectal cancer	5-FU based Cap based	Good	Dyhl-Polk et al. (2020b)
8	Raber I	2019	United States	177	retro	54–77	0.452	Mixed malignancies	5-FU or Cap based	Fair	Raber et al. (2019)
9	Jin X	2019	China	129	retro	>18	0.217	Gastric cancer	5-FU or Cap or S-1 based	Fair	Jin et al. (2019)
10	Primrose JN	2019	United Kingdom	213	pros	62 (55–68)	0.5	Biliary tract cancer	Cap	Good	Primrose et al. (2019)
11	Abdel-Rahman O	2019	Canada	3,223	pros	60.7 (11.4)	0.403	Colorectal cancer	FOLFOX or 5-FU based + Bev and/ or Pan	Good	Abdel-Rahman, (2019)
12	Hayashi Y	2019	Japan	80	pros	66.5 (62–73)	0.113	Esophageal cancer	5-FU/cisplatin + RT	Fair	Hayashi et al. (2019)
13	Peng J	2018	China	527	pros	57 (23–87)	0.339	Mixed malignancies	5-FU or Cap based	Good	Peng et al. (2018)
14	Chen EY	2018	China	47	pros	59.7 (21.4–80.1)	0.276	Colorectal cancer	FOLFIRI + Celecoxib	Good	Chen et al. (2018)
15	Kwakman JJM	2017	Netherlands	1973	pros	NA	NA	Colorectal cancer	Cap mono or based ± Bev	Good	Kwakman et al. (2017)
16	Turan T	2017	Turkey	32	pros	57	0.303	Mixed malignancies	5-FU based	Good	Turan et al. (2017)
17	Leicher LW	2017	Netherland	86	retro	69 (45–83)	0.523	Colorectal cancer	Cap	Fair	Leicher et al. (2017)
18	Zhang P	2017	China	397	pros	25–70	1	Breast cancer	Cap + Utidelone Cap	Good	Zhang et al. (2017)
19	Kerr RS	2016	Multi-country	1941	pros	65 (58–71)	0.427 0.429	Colorectal cancer	Cap + Bev Cap	Good	Kerr et al. (2016)
20	Winther SB	2016	Norway	71	retro	67–87	0.408	Colorectal cancer	SOX or S-1	Fair	Winther et al. (2016)
21	Polk A	2016	Denmark	452	retro	63 (28–88)	1	Breast cancer	Cap + Tra	Fair	Polk et al. (2016)
22	Mayer RJ	2015	United States	534	pros	63 (27–82)	0.389	Colorectal cancer	TAS102	Good	Mayer et al. (2015)
23	Lestuzzi C	2014	Germany	358	pros	57.5 (23–80)	NA	Mixed malignancies	5-FU or 5-FU based	Fair	Lestuzzi et al. (2014)
24	Tonyali O	2013	Turkey	37	retro	46 (30–75)	1	Breast cancer	TX + Tra	Fair	Tonyali et al. (2013)
25	Okines AFC	2013	United Kingdom	120	pros	62 (56–67) 64 (56–69)	0.321 0.182	Gastro-esophageal adenocarcinoma	ECX ECX + Bev	Good	Okines et al. (2013)

(Continued on following page)

TABLE 1 | (*Continued*) The characteristics of the included 64 studies.

No	Author	Year	Country/ Region	Sample size	Study design	Age	Gender (female %)	Tumor type	Regimen	Quality	References
26	Khan MA	2012	Pakistani	301	retro	47 (18–81)	0.249	Mixed malignancies	5-FU or 5-FU/ Cap based	Fair	Khan et al. (2012)
27	Martin M	2012	Multi-country	88	Pros	53 (32–82)	0.988	Breast cancer	Cap + Bev + Tra	Fair	Martin et al. (2012)
28	Petrini L	2012	Italy	39	pros	67 (41–83)	0.154	Hepatocellular carcinoma	5-FU + Sorafenib	Good	Petrini et al. (2012)
29	Koca D	2011	Turkey	52	pros	59	0.75	Mixed malignancies	Cap or Cap based + Lap	Fair	Koca et al. (2011)
30	Jensen SA	2010	Denmark	106	pros	64 (37–81)	0.556	Colorectal cancer	FOLFOX4	Good	Jensen et al. (2010)
31	Masi G	2010	Italy	57	pros	61 (34–75)	0.4	Colorectal cancer	FOLFOXIRI + Bev	Good	Masi et al. (2010)
32	Michalaki V	2010	Greece	29	pros	52 (34–70)	1	Breast cancer	TX + Tra	Good	Michalaki et al. (2010)
33	Chua YJ	2010	Australia	105	pros	64 (54–70)	0.46	Rectal cancer	XELOX	Good	Chua et al. (2010)
34	Baur M	2010	Austria	71	pros	62 (39–84)	0.394	Rectal cancer	5-FU based	Fair	Baur et al. (2010)
35	Joensuu H	2009	Multi-country	231	pros	≤65	1	Breast cancer	5-FU based + Tra 5-FU based	Good	Joensuu et al. (2009)
36	Skof E	2009	Slovenia	87	pros	63 (47–75) 62 (34–75)	0.366	Colorectal cancer	XELIRI FOLFIRI	Good	Skof et al. (2009)
37	Ardavanis A	2008	Greece	34	retro	69.5 (37–83)	0.47	Colorectal cancer	CapIRI + Bev	Fair	Ardavanis et al. (2008)
38	Kosmas C	2008	Greece	644	pros	66 (56–70)	NA	Mixed malignancies	5-FU based or Cap based	Good	Kosmas et al. (2008)
39	Yamamoto D	2008	Japan	59	pros	55 (42–70)	1	Breast cancer	Cap + Tra	Good	Yamamoto et al. (2008)
40	Machiels JP	2007	Belgium	40	pros	61 (34–78)	0.33	Rectal cancer	Cap + Cet + RT	Fair	Machiels et al. (2007)
41	Giantonio BJ	2007	United States	572	pros	62 (21–85) 60.8 (25–84)	0.395 0.392	Colorectal cancer	FOLFOX4 +Bev FOLFOX4	Good	Giantonio et al. (2007)
42	Yilmaz U	2007	Turkey	27	pros	54 (19–70)	0.444	Gastrointestinal cancer	LV5FU2	Fair	Yilmaz et al. (2007)
43	Emmanouilides C	2007	Greece	53	pros	65 (18–78)	0.434	Colorectal cancer	FOLFOX + Bev	Fair	Emmanouilides et al. (2007)
44	Geyer CE	2006	United States	324	pros	54 (26–80) 51 (28–83)	1	Breast cancer	Cap + Lap Cape	Good	Geyer et al. (2006)
45	Mambrini A	2006	Italy	211	pros	61 (21–79)	NA	Pancreatic cancer	FEC	Good	Mambrini et al. (2006)
46	Koopman M	2006	Netherland	393	pros	64 (27–84) 63 (35–79)	0.373 0.396	Colorectal cancer	Cap CapIRI	Good	Koopman et al. (2006)
47	Jensen SA	2006	Denmark	668	retro	NA	NA	Colorectal or gastric cancers	Cap Cap/Capatin/ Docetaxel 5-FU LV5FU2 FOLFOX-4	Fair	Jensen and Sorensen, (2006)
48	Yerushalmi R	2006	Israel	89	retro	66 (25–82) 62 (23–81)	0.418 0.5	Rectal cancer	Cap + RT 5-FU + RT	Fair	Yerushalmi et al. (2006)
49	Giordano KF	2006	United States	44	pros	57 (32–77)	0.114	Gastric or gastro-esophageal junction adenocarcinoma	TX	Fair	Giordano et al. (2006)
50	Jatoi A	2006	United States	46	pros	61 (32–80)	0.116	Esophageal or gastro-esophageal	XELOX	Fair	Jatoi et al. (2006)

(Continued on following page)

TABLE 1 | (*Continued*) The characteristics of the included 64 studies.

No	Author	Year	Country/ Region	Sample size	Study design	Age	Gender (female %)	Tumor type	Regimen	Quality	References
								junction adenocarcinoma			
51	Baghi M	2006	Germany	24	pros	60 (23–79)	0.042	Head and neck squamous cell carcinoma	TPF	Fair	Baghi et al. (2006)
562	Meydan N	2005	Turkey	231	retro	59 (23–87)	0.402	Mixed malignancies	LV5FU2	Fair	Meydan, (2005)
53	Lordick F	2005	Germany	48	pros	62 (41–75)	0.187	Gastric cancer	FUFOX	Fair	Lordick et al. (2005)
54	Ng M	2005	United Kingdom	153	pros	33–81	0.412	Colorectal cancer	CapeOx	Good	Ng et al. (2005)
55	Feliu J	2005	Spain	51	pros	76 (71–89)	0.392	Colorectal cancer	Cap	Fair	Feliu et al. (2005)
56	Wacker A	2003	Germany	102	pros	61.7 (39–78)	0.311	Mixed malignancies	5-FU or 5-FU based	Fair	Wacker et al. (2003)
57	Vaishampayan UN	2002	United States	32	retro	67.5 (45–84)	0.375	Gastrointestinal cancer	Cap + RT	Fair	Vaishampayan et al. (2002)
58	Tsavaris N	2002	Greece	427	retro	NA	NA	Mixed malignancies	5-Fu based	Fair	Tsavaris et al. (2002)
59	Van Cutsem E	2002	Switzerland	1,425	pros	NA NA NA	NA	Colorectal cancer Colorectal cancer Breast cancer	LV5FU2 Cap Cap	Fair	Van Cutsem et al. (2002)
60	Hartung G	2001	Germany	51	pros	60 (24–77)	0.25	Colorectal cancer	LV5FU2	Fair	Hartung et al. (2001)
61	Dencausse Y	2001	Germany	21	pros	30–80	0.333	Rectal cancer	LV5FU2+RT	Fair	Dencausse et al. (2001)
62	Peiffert D	2001	France	80	pros	≤75	0.837	Anal cancer	FP + RT	Fair	Peiffert et al. (2001)
63	Hoff PM	2001	Multi-country	605	pros	64 (23–86) 63 (24–87)	0.40 0.35	Colorectal cancer	Cap LV5FU2	Good	Hoff, (2001)

Notes: a, Mixed malignancies: including two or more tumor types, such as breast cancer, colorectal cancer, gastric cancer, head and neck cancer, and so on; NA: not available; RT: radiotherapy; Cap: Capecitabine; Bev: Bevacizumab; Cet: Cetuximab; Pan: Panitumumab; Tra, Trastuzumab; Lap, Lapatinib.

quality, and none was classified as poor (high risk of bias). The detailed characteristics of each included study are shown in **Table 1**.

The Incidence of 5-Fluorouracil Associated Coronary Artery Disorders

Using a random-effect model, the pooled incidence of all-grade fluoropyrimidine-related coronary disorders among 22,939 cases from 59 studies was 2.75% (95% CI 1.89%–3.76%) (**Figure 2A**). Thirty-three studies reported the incidence of grade 3 or higher fluoropyrimidine-related coronary disorders, involving a total of 14,135 cases, The pooled incidence of grade 3 or higher coronary disorders by meta-analysis, was 1.00% (95% CI 0.62%–1.47%) (**Figure 2B**).

Specific Reported Events of Coronary Disorders

Coronary disorders were frequently reported as angina/chest pain, myocardial infarction, myocardial ischemia, and acute coronary syndrome in our included literature. As shown in **Figure 3**, myocardial ischemia and angina/chest pain were the two most common adverse events, which have a pooled incidence of 1.28% (95% CI 0.42%–2.49%) and 1.1% (95% CI 0.54%–1.81%), respectively. Myocardial infarction and the acute coronary syndrome were less reported, with a pooled incidence of 0.38% (95% CI 0.16%–0.67%) and 0.14% (0–0.56%), respectively. Fourteen studies reported the typical ST-T changes on ECG with or without symptomatic coronary toxicities. A random-effect meta-analysis gave a pooled incidence of ST-T changes of 4.77% (95% CI 3.12%–7.28%), significantly higher than the incidence of adverse coronary events (2.75%). The changes of cardiac-specific serum enzymes were reported in 10 studies, including troponin, CK-MB, myoglobin, BNP, and copeptin, and the pooled overall incidence was 1.98% (95% CI 0.9%–4.36%).

Subgroup Analyses

Subgroup analyses were conducted to compare the incidence of all-grade and grade 3 or higher coronary disorders among different study-level moderators, and further identify the factors influencing the occurrence of adverse coronary events. The pooled incidence and 95% CI of coronary events in each subgroup were shown in **Table 2**, as well as the results of statistical comparisons between subgroups. A significant difference was identified among different publication periods (p = 0.02) for the incidence of all-grade coronary events, but

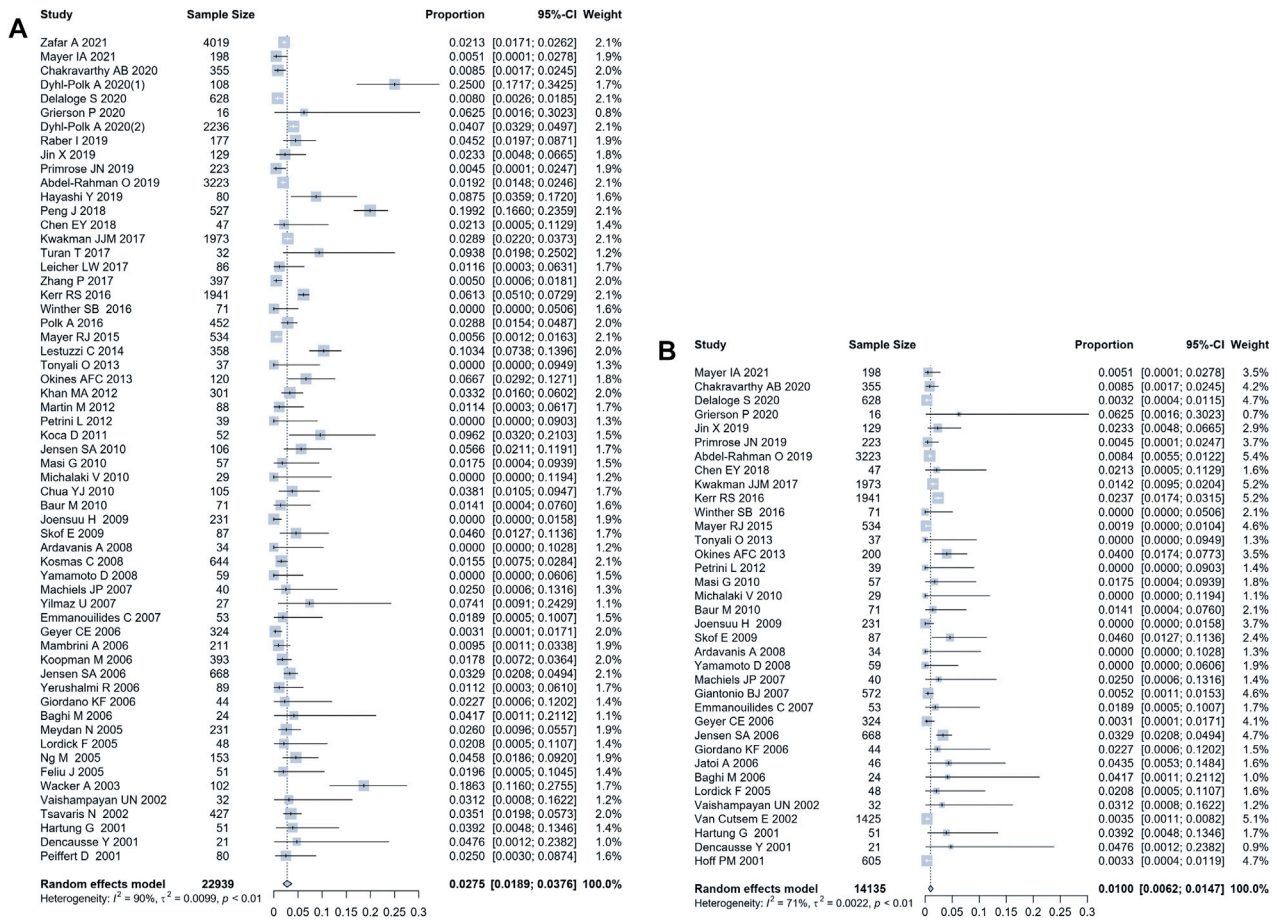

FIGURE 2 | Forest plot of the incidence of fluoropyrimidine-related coronary disorders. **(A)** the pooled incidence of all-grade adverse coronary events, by a random-effect model analysis, was 2.75% (95% CI 1.89%–3.76%); **(B)** the pooled incidence of grade 3 or higher adverse coronary events, by a random-effect model analysis, was and 1.00% (95% CI 0.62%–1.47%).

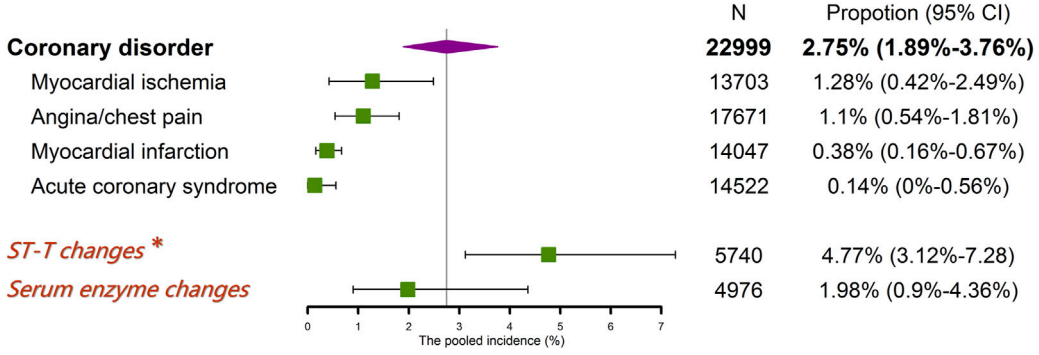

FIGURE 3 | The pooled incidence of specific reported events of coronary disorders. * a pooled incidence of 4.77% (95% CI 3.12%–7.28%), containing ST-T changes on ECG with or without symptomatic coronary toxicities.

not statistically significant for grade 3 or higher events (p = 0.65). We did not observe an obvious difference between prospective and retrospective study designs (all-grade: p = 0.58, grade 3 or higher: p = 0.21), nor between phase II and phase III clinical trials (all-grade: p = 0.24, grade 3 or higher: p = 0.18). There was also no significant difference between studies with good-quality and fair-quality (p = 0.43) for all-grade events, however, the good-quality studies had lower pooled incidence than fair-quality studies for

TABLE 2 | The pooled incidence of coronary disorder in each subgroup and the comparison results.

Subgroup	All-grade adverse coronary events			Grade 3 or higher adverse coronary events		
	Sample size (*N*)	Incidence (95%CI)	Comparison results	Sample size (*N*)	Incidence (95%CI)	Comparison results
Publication period						
2001–2005	1,196	4.27% (2.16%–7.06%)	$\chi^2 = 10.15$, $p = 0.02$*	1,329	0.92% (0.00%–3.26%)	$\chi^2 = 1.64$, $p = 0.65$
2006–2010	3,190	1.28% (0.65%–2.13%)		1767	1.12% (0.25%–2.40%)	
2011–2015	1,635	3.05% (0.93%–6.31%)		810	0.58% (0.00%–3.11%)	
2016–2022	16,978	3.37% (1.66%–5.65%)		8,804	0.72% (0.29%–1.28%)	
Study design						
Prospective study	13,950	3.02% (1.88%–4.42%)	$\chi^2 = 0.31$, $p = 0.58$	11,739	0.67% (0.26%–1.20%)	$\chi^2 = 1.55$, $p = 0.21$
Retrospective study	9,049	2.62% (1.98%–3.34%)		971	1.42% (0.30%–3.08%)	
Phase for clinical trials						
II	938	1.93% (1.14%–2.92%)	$\chi^2 = 1.41$, $p = 0.24$	711	0.15% (0.38%–2.62%)	$\chi^2 = 1.76$, $p = 0.18$
III	7,617	1.18% (0.49%–2.16%)		8,576	0.69% (0.29%–1.09%)	
Study quality						
Good	18,385	2.12% (1.08%–3.48%)	$\chi^2 = 1.67$, $p = 0.43$	10,970	0.58% (0.20%–1.10%)	$\chi^2 = 9.32$, $p < 0.01$*
Fair	4,162	3.35% (2.03%–4.98%)		1740	1.51% (0.70%–2.54%)	
Age						
No limitation	22,797	2.75% (1.87%–3.79%)	$\chi^2 = 0.04$, $p = 0.84$	12,639	0.78% (0.35%–1.33%)	$\chi^2 = 1.07$, $p = 0.30$
Old	202	2.17% (0.00%–10.00%)		71	0.00% (0.00%–5.06%)	
Gender						
All	20,556	3.48% (2.44%–4.70%)	$\chi^2 = 18.59$, $p < 0.01$*	11,204	1.09% (0.53%–1.78%)	$\chi^2 = 15.75$, $p < 0.01$*
Female-only	2,355	0.61% (0.15%–1.37%)		1,418	0.09% (0.00%–0.43%)	
Tumor type						
Esophagus cancer	244	6.32% (3.62%–9.71%)	$\chi^2 = 47.59$, $p < 0.01$*	290	3.51% (1.51%–6.14%)	$\chi^2 = 34.41$, $p < 0.01$*
Colorectal cancer	12,553	2.69% (1.57%–4.09%)		10,403	0.94% (0.39%–1.67%)	
Gastric cancer	177	2.26% (0.59%–4.96%)		177	2.13% (0.31%–5.05%)	
Pancreatic cancer	227	1.64% (0.00%–6.13%)		16	6.25% (0.16%–30.23%)	
Breast cancer	2,443	0.50% (0.11%–1.16%)		1,506	0.01% (0.00%–0.27%)	
Biliary tract cancer	223	0.45% (0.01%–2.47%)		223	0.45% (0.01%–2.47%)	
Others[a]						
Treatment type						
Adjuvant	3,703	1.36% (0.16%–3.36%)	$\chi^2 = 2.01$, $p = 0.37$	3,366	0.94% (0.32%–1.88%)	$\chi^2 = 3.84$, $p = 0.15$
Neoadjuvant	549	2.86% (1.50%–4.56%)		380	2.65% (1.16%–4.71%)	
For advanced/metastasis/relapse disease	925	1.70% (0.72%–2.97%)		933	1.10% (0.27%–2.48%)	
Regimen						
5-FU monotherapy	484	3.31% (1.46%–5.87%)	$\chi^2 = 28.65$, $p < 0.01$*	1,380	0.92% (0.00%–3.04%)	$\chi^2 = 15.79$, $p = 0.07$
Capecitabine monotherapy	2,627	1.21% (0.34%–2.59%)		3,059	0.75% (0.03%–1.36%)	
5-FU combined chemotherapy	2,993	4.31% (2.05%–7.35%)		706	1.2% (0.00%–4.31%)	
Capecitabine combined chemotherapy	3,956	2.69% (1.09%–4.98%)		1711	0.69% (0.00%–2.14%)	
5-FU based/targeted therapy	336	1.46% (0.46%–3.02%)		623	0.83% (0.14%–1.87%)	
Capecitabine based/targeted therapy	3,177	2.85% (1.75%–4.20%)		2,483	1.22% (0.46%–2.24%)	
5-FU based/radio	181	5.10% (1.58%–10.48%)		21	4.76% (0.12%–23.82%)	
Capecitabine based/radio	75	2.65% (0.25%–7.47%)		32	3.12% (0.08%–16.22%)	
S-1	71	0.00% (0.00%–5.06%)		71	0.00% (0.00%–5.06%)	
TAS 102	534	0.56% (0.12%–1.63%)		534	0.19% (0.00%–1.04%)	

Notes: *p < *0.05; a, "others" including liver cancer, gastrointestinal cancer, and head and neck cancer.*

the assessment of grade 3 or higher coronary events ($p < 0.01$). Notably, the female-only population (with breast cancer) reported lower pooled incidence than general populations, both in the assessment of all-grade ($p < 0.01$) and grade 3 or higher ($p < 0.01$) coronary disorders.

The pooled incidence of coronary disorders for all-grade or grade 3 or higher varied between tumor types (all-grade: $p < 0.01$, grade 3 or higher: $p < 0.01$). Fluoropyrimidine-related coronary disorders were most frequently in the treatment of esophageal cancer, with the all-grade incidence of 6.32% (95% CI 3.62%–9.71%). Fluoropyrimidines in the treatment of breast cancer, however, occupied the relatively lower coronary complications (all-grade: 0.50%, 95% CI 0.11%–1.16%) than colorectal cancer (all-grade: 2.69%, 95% CI 1.57%–4.09%) and esophagus cancer.

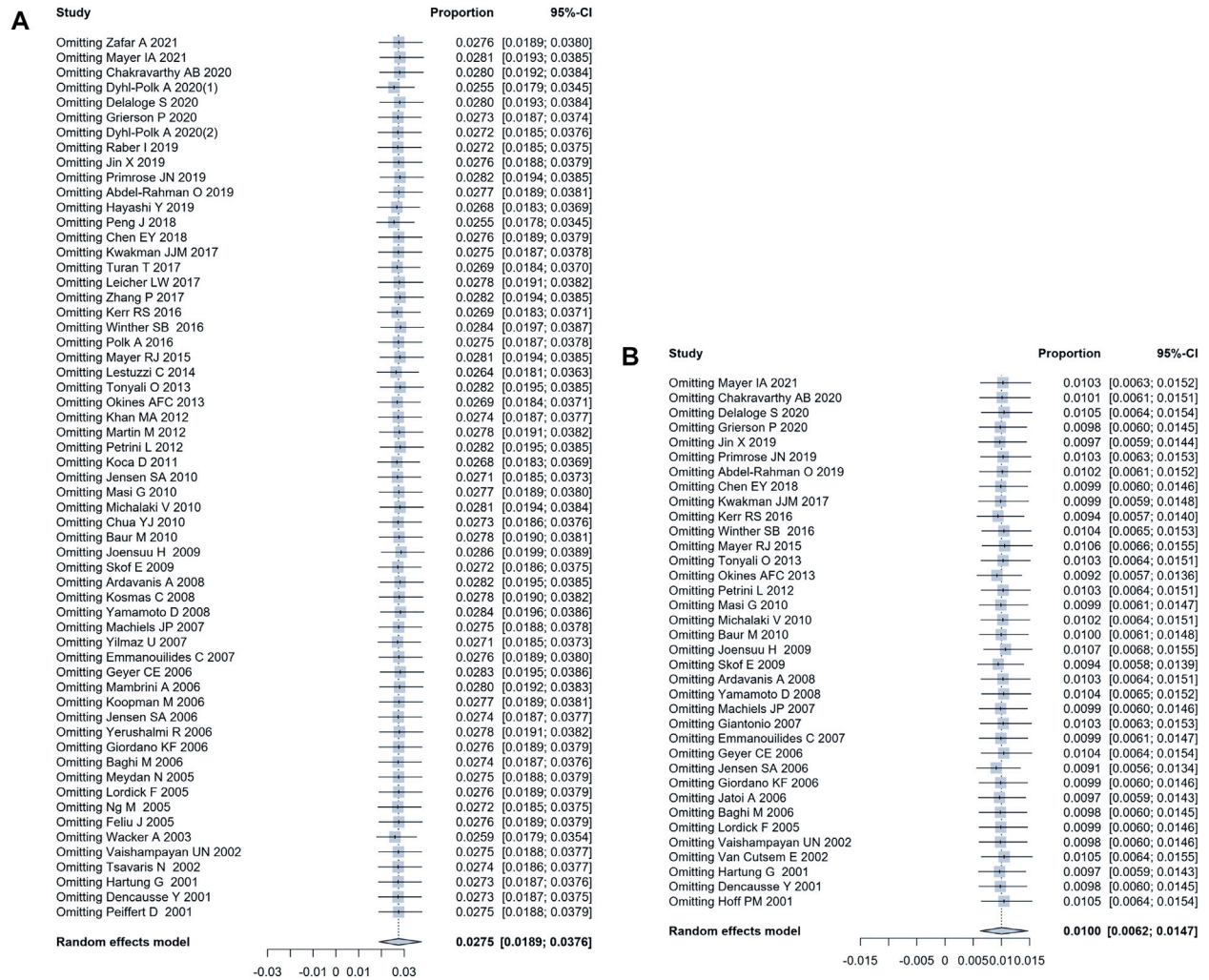

FIGURE 4 | The results of sensitive analysis. **(A)** the sensitive analysis of the incidence of all-grade coronary disorders indicated a variation between 2.64% and 2.86%; **(B)** the sensitive analysis of the incidence of grade 3 or higher coronary disorders indicated a variation between 0.92% and 1.07%.

The effect of treatment parameters on the incidence of coronary events was also analyzed. As a result, the administrations of fluoropyrimidine as neoadjuvant chemotherapy, adjuvant chemotherapy, or palliative treatment for advanced/metastasis/relapse disease did not significantly affect the occurrence of coronary events (all-grade: $p = 0.37$; grade 3 or higher: $p = 0.15$). However, the treatment regimen is closely related to the occurrence of coronary disorders (all-grade: $p < 0.01$; grade 3 or higher: $p = 0.07$). Coronary disorder induced by 5-FU is more frequent than that induced by capecitabine, both for all-grade (3.31% vs. 1.21%) and grade 3 or higher (0.92% vs. 0.75%). The 5-FU or capecitabine combined chemotherapy had a higher incidence of coronary events than 5-FU or capecitabine monotherapy (5-FU: 4.31% vs. 3.31%; capecitabine: 2.69% vs. 1.21%). The addition of targeted therapy drugs (e.g., bevacizumab, cetuximab, and trastuzumab) to capecitabine increased the risk of coronary disorder (all-grade; 2.85% vs. 1.21%; grade 3 or higher: 1.22% vs. 0.75%). Similarly, the addition of radiotherapy resulted in a significant increase in coronary toxicity, both for 5-FU (all-grade: 5.1% vs. 3.3%, grade 3 or higher: 4.76% vs. 0.92%) and capecitabine (all-grade: 2.65% vs. 1.21%, grade 3 or higher: 3.12% vs. 0.75%). Novel fluoropyrimidines, S-1 and Tas 102, demonstrated lower coronary toxicity (S-1: 0; Tas102: 0.56%), however, such data were derived from a limited number of studies.

Sensitive Analyses and Publication Bias

Sensitivity analyses were performed for the main outcome measures, all-grade and grade 3 or higher incidence of coronary disorders. In the all-grade and grade 3 or higher analyses, the variation of the pooled results after removing studies one by one was 2.64%–2.86% and 0.92%–1.07%, respectively (**Figure 4**), indicating that the conclusions of this meta-analysis were stable and reliable. The funnel plots and Egger tests did not show existing significant publication bias in the

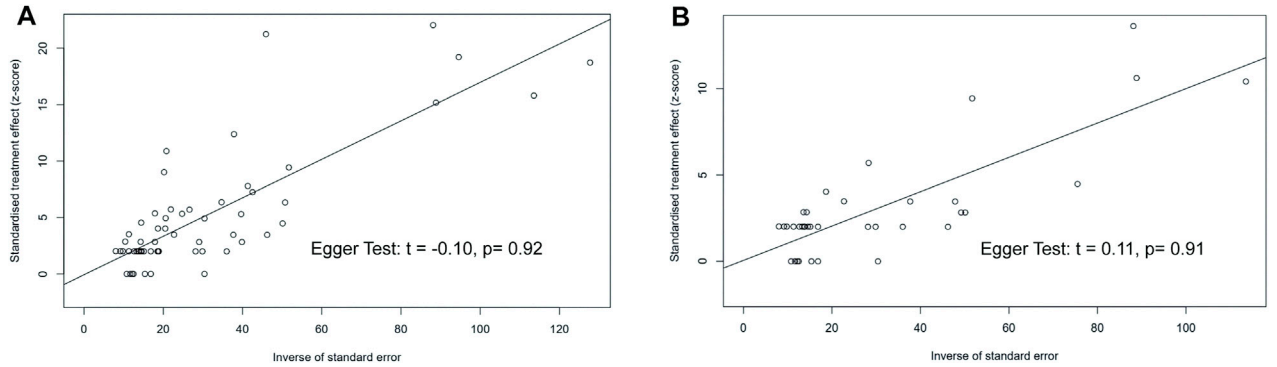

FIGURE 5 | Funnel plot and Egger test evaluating the publication bias of studies. The *p*-values of Egger test for all-grade and grade 3 or higher coronary disorder were 0.92 and 0.91, respectively, suggesting no significant publication bias.

evaluation of all-grade and grade 3 or higher coronary disorder in this meta-analysis (**Figure 5**).

DISCUSSION

Fluoropyrimidine, as a well-known class of pyrimidine antimetabolites, has been used in cancer treatment for more than half a century. Although numerous therapeutic strategies have been introduced in recent years, such as targeted therapy (Bedard et al., 2020), antiangiogenic therapy, and immunotherapy (Hegde and Chen, 2020), fluoropyrimidines are still one of the most effective and frequently used agents in the treatment of colorectal cancer, breast cancer, gastric cancer, and head and neck cancers, whether for neoadjuvant, adjuvant, advanced or maintenance therapy. Cardiotoxicity, especially coronary disorders caused by 5-FU and capecitabine remains a critical issue in cancer therapy that threatens patient survival and leads to the discontinuation of the medication. Unfortunately, there is no solid evidence worldwide about the incidence of fluoropyrimidine-related coronary disorders and the risk factors affecting its occurrence (Deac et al., 2020; Li et al., 2021). In this study, we systematically evaluated the incidence and profile of coronary disorder associated with fluoropyrimidines administration. To our best knowledge, this is the first comprehensive systematic review and meta-analysis on this topic.

The mechanism of fluoropyrimidine-induced cardiotoxicity has not yet been fully elucidated. Although several theories have been proposed, including vasoconstriction, endothelial injury, direct myocardial toxicity, and so on, the most predominant and important clinicopathological change was the disorder of coronary artery (Depetris et al., 2018; Mohammed et al., 2018; Chong and Ghosh, 2019). The coronary disorders defined in this study mainly refers to reversible cardiac ischemia caused by coronary vasospasm, and coronary atherosclerosis due to fluorouracil-induced coagulation problems was also included. There are several reported presentations of fluoropyrimidine-related coronary disorders, including atypical chest pain to typical angina, ACS, myocardial ischemia, and myocardial infarction. According to our results, myocardial ischemia (1.28%) and angina/chest pain (1.1%) are the most frequently reported. In fact, ischemia and angina/chest pain are not two independent adverse events. Chest pain with or without typical angina is often the primary clinical manifestation of acute cardiac ischemia or ACS, both of which are outcomes of coronary disorders. Thus, in this analysis, we focused on the overall coronary disorders consisting of angina/chest pain, myocardial ischemia and infarction, and ACS, rather than one of them.

Our results generated reliable data on the overall incidence of fluoropyrimidine-related coronary disorder of 2.7%, which revised the previous over-or under-estimation of 0–35%. The incidence of grade 3 or higher fluoropyrimidine reached 1%, accounting for 37% of the overall incidence, indicating that coronary disorder is one of the high-risk complications, which deserves special attention. The pooled results in our study were close to the data reported by Zafar et al. (2021), in which coronary disorders occurred in 2.16% of 4,019 patients treated with 5-FU. It should be noted that 14 of the 63 included studies observed ECG changes during fluoropyrimidine administration, with a pooled incidence of ST-T changes of 4.77%, remarkably exceeding the incidence of adverse coronary events (2.16%). Such inconsistency may be derived from the presence of asymptomatic ischemic ECG changes in some populations (Lounsbury et al., 2017). Therefore, continuous ECG monitoring should be recommended during fluoropyrimidine use, as early ST-T changes often indicate an impending adverse coronary event.

The results of our subgroup analysis showed a lower incidence of the coronary disorder in the female-only population, a phenomenon that has also been observed in other studies (Peng et al., 2018). Delaloge et al. (2020) reported 5 (0.8%) of 628 breast cancer patients treated with capecitabine developed coronary disorders in a phase III clinical trial. A similar low incidence (0.5%, 2/397) was also reported by Zhang et al. (2017) in 2017. Such gender differences may be associated with the protective effect of female hormones on the heart (Kurokawa et al., 2009; Gowd and Thompson, 2012; Costa et al., 2021). However, in this pooled analysis, the female-only population were breast cancer patients with capecitabine administration. We

believed that the characteristics in tumor type and medication should be mainly accounted for the lower coronary toxicity in the female-only population. In addition, a significant difference on the incidence of all-grade adverse coronary events was also observed among different publication periods. This discrepancy could be partly related to the way of drug administration, increased concomitant targeted therapy, and increased attention to cardiotoxicity.

We had observed a significant difference in fluoropyrimidine-related coronary disorders among different tumor types. However, these differences, to a great extent, should be attributed to the variability in treatment regimens among tumors. Capecitabine is an oral prodrug of 5-FU designed to be converted selectively in tumors. It is rapidly absorbed from the gut as an unchanged drug and then converted to the active form of 5-FU by carboxylesterase and thymidine phosphorylase (O'Connell et al., 2014). Therefore, the effect of capecitabine on the coronary is indirect, and our results seem to show that the incidence of capecitabine-caused coronary disorders is significantly lower than that of intravenous 5-FU. However, due to the lack of evidence of direct comparison between 5-FU and capecitabine, such a conclusion needs further confirmation. The coronary toxicity was distinctly varied from formulations or administration protocols of 5-FU or capecitabine. Combination therapy significantly increases coronary toxicity, whether combined with other chemotherapeutics or targeted therapy. The increased incidence of the coronary disorder in combination therapy may result from additive and synergistic toxic effects of different agents on the heart. As we know, anti-angiogenic targeted drugs (e.g., bevacizumab) also had adverse effects on the cardiovascular system (Economopoulou et al., 2015). Therefore, when combination regimens containing these agents were considered, more attention should be paid to the occurrence of coronary adverse events. On the other hand, radiotherapy covering or adjacent to the heart also significantly increases coronary toxicity of fluoropyrimidines. As in our meta-analysis, patients with esophageal cancer who received 5-FU combined with radiotherapy had the highest incidence of coronary disorder at 6.32%. Some studies further showed that radiotherapy increases not only short-term cardiotoxicity, but also long-term cardiotoxicity, such as pericarditis and pericardial effusion (Saunders and Anwar, 2019). Other fluoropyrimidine drugs, such as S-1 and TAS102, have shown a lower incidence of coronary disorders in our study and may be a safer option for patients. However, due to the limited number of cases included in the TAS102 and S1 analyses, more evidence is needed.

Admittedly, there were some limitations in this meta-analysis. First, heterogeneity was observed among the included studies. Although we have performed subgroup analyses and adopted a random-effect model to minimize the effects of the heterogeneity, its influence on the stability of the results cannot be eliminated. Second, it is difficult to clearly define and distinguish "coronary disorder," although in this study we included various manifestations such as angina, chest pain, myocardial infarction, myocardial ischemia, and ACS. Not all included studies have undertaken a comprehensive and targeted examination to identify these conditions, so the result may be an inevitable underestimation of the incidence. Furthermore, it is difficult to determine whether the referred coronary disorder was related to fluoropyrimidine-containing treatment. Although we only included studies that clearly indicated such a correlation, there is still a possibility that patients with spontaneous coronary disorder could be counted in the original study. Finally, several previous studies have reported the effects of age, race, smoking, history of heart disease, and other factors on fluoropyrimidine-related coronary toxicity. However, limited by the characteristics of the included studies in this meta-analysis, we did not have enough data to further analyze all possible moderators. Owing to the above limitations, the findings of this meta-analysis should be interpreted with carefully, and subsequent large-sample clinical studies are necessary.

CONCLUSION

In conclusion, this meta-analysis, which used a single-rate pooled analysis model, has defined the incidence of coronary disorders induced by fluoropyrimidine-based treatment, and depicted its epidemiological profiles. The occurrence of fluoropyrimidine-related coronary disorders is not a rare condition during fluoropyrimidine administration, which needs to be highly concerned. It varies among tumor types, and different treatment regimens may be associated with different incidence of adverse coronary events. This comprehensive overview of fluoropyrimidine-related coronary disorders can provide a reference for clinical practice in cancer management.

DATA AVAILABILITY STATEMENT

The original contributions presented in the study are included in the article/Supplementary Material, further inquiries can be directed to the corresponding author.

AUTHOR CONTRIBUTIONS

YL: literature retrieval, data extraction, literature quality evaluation, and article writing; SD: literature retrieval, data extraction, literature quality evaluation; QD, WP, and QL: data verification; HJ and XW: statistical analysis; H-MZ: study design and quality supervision.

SUPPLEMENTARY MATERIAL

The Supplementary Material for this article can be found online at: https://www.frontiersin.org/articles/10.3389/fphar.2022.885699/full#supplementary-material

REFERENCES

Abdel-Rahman, O. (2019). 5-Fluorouracil-related Cardiotoxicity; Findings from Five Randomized Studies of 5-Fluorouracil-Based Regimens in Metastatic Colorectal Cancer. *Clin. Colorectal Cancer* 18 (1), 58–63. doi:10.1016/j.clcc.2018.10.006

Ardavanis, A., Kountourakis, P., Mantzaris, I., Malliou, S., Doufexis, D., Sykoutri, D., et al. (2008). Bevacizumab Added to the Irinotecan and Capecitabine Combination for Advanced Colorectal Cancer: A Well-Tolerated, Active and Convenient Regimen. *Anticancer Res.* 28 (5B), 3087–3092. doi:10.1200/jco.2008.26.15_suppl.15085

Baghi, M., Hambek, M., Wagenblast, J., May, A., GstoettnerGstoettner, W., and Knecht, R. (2006). A Phase II Trial of Docetaxel, Cisplatin and 5-fluorouracil in Patients with Recurrent Squamous Cell Carcinoma of the Head and Neck (SCCHN). *Anticancer Res.* 26 (1B), 585–590. doi:10.1016/j.drugalcdep.2015.07.446

Baldeo, C., Baldeo, C., Mody, K., Seegobin, K., and Rollini, F. (2018). A Case of 5-Fluorouracil-Induced Coronary Artery Vasovasospasm in Rectal Adenocarcinoma. *J. Am. Coll. Cardiol.* 71S (11), 2324. doi:10.1016/S0735-1097(18)32865-1

Baur, M., Horvath, M., Stättner, S., Schratter-Sehn, A., Horvath, B., Sellner, F., et al. (2010). Chemoradiotherapy with 5-fluorouracil/leucovorin, Surgery and Adjuvant Chemotherapy for Locally Advanced Rectal Cancer. *Oncol. Lett.* 1 (1), 189–194. doi:10.3892/ol_00000035

Bedard, P. L., Hyman, D. M., Davids, M. S., and Siu, L. L. (2020). Small Molecules, Big Impact: 20 Years of Targeted Therapy in Oncology. *Lancet* 395 (10229), 1078–1088. doi:10.1016/S0140-6736(20)30164-1

Ben-Yakov, M., Mattu, A., Brady, W. J., and Dubbs, S. B. (2017). Prinzmetal Angina (Coronary Vasospasm) Associated with 5-fluorouracil Chemotherapy. *Am. J. Emerg. Med.* 35 (e37), 1038–e5. doi:10.1016/j.ajem.2017.02.046

Chakravarthy, A. B., Zhao, F., Meropol, N. J., Flynn, P. J., Wagner, L. I., Sloan, J., et al. (2020). Intergroup Randomized Phase III Study of Postoperative Oxaliplatin, 5-Fluorouracil, and Leucovorin versus Oxaliplatin, 5-Fluorouracil, Leucovorin, and Bevacizumab for Patients with Stage II or III Rectal Cancer Receiving Preoperative Chemoradiation: A Trial of the ECOG-ACRIN Research Group (E5204). *Oncologist* 25 (5), e798. doi:10.1634/theoncologist.2019-0437

Chen, E. Y., Blanke, C. D., Haller, D. G., Benson, A. B., Dragovich, T., Lenz, H. J., et al. (2018). A Phase II Study of Celecoxib with Irinotecan, 5-Fluorouracil, and Leucovorin in Patients with Previously Untreated Advanced or Metastatic Colorectal Cancer. *Am. J. Clin. Oncol.* 41 (12), 1193–1198. doi:10.1097/COC.0000000000000465

Chong, J. H., and Ghosh, A. K. (2019). Coronary Artery Vasospasm Induced by 5-fluorouracil: Proposed Mechanisms, Existing Management Options and Future Directions. *Interv. Cardiol.* 14 (2), 89–94. doi:10.15420/icr.2019.12

Chua, Y. J., Barbachano, Y., Cunningham, D., Oates, J. R., Brown, G., Wotherspoon, A., et al. (2010). Neoadjuvant Capecitabine and Oxaliplatin before Chemoradiotherapy and Total Mesorectal Excision in MRI-Defined Poor-Risk Rectal Cancer: a Phase 2 Trial. *Lancet Oncol.* 11 (3), 241–248. doi:10.1016/S1470-2045(09)70381-X

Costa, S., Saguner, A. M., Gasperetti, A., Akdis, D., Brunckhorst, C., and Duru, F. (2021). The Link between Sex Hormones and Susceptibility to Cardiac Arrhythmias: From Molecular Basis to Clinical Implications. *Front. Cardiovasc. Med.* 8, 644279. doi:10.3389/fcvm.2021.644279

Curigliano, G., Cardinale, D., Dent, S., Criscitiello, C., Aseyev, O., Lenihan, D., et al. (2016). Cardiotoxicity of Anticancer Treatments: Epidemiology, Detection, and Management. *CA Cancer J. Clin.* 66 (4), 309–325. doi:10.3322/caac.21341

Das, S. K., Das, A. K., and William, M. (2019). 5-Fluorouracil-induced Acute Coronary Syndrome. *Med. J. Aust.* 211 (6), 255–e1. doi:10.5694/mja2.50317

Deac, A. L., Burz, C. C., Bocsan, I. C., and Buzoianu, A. D. (2020). Fluoropyrimidine-induced Cardiotoxicity. *World J. Clin. Oncol.* 11 (12), 1008–1017. doi:10.5306/wjco.v11.i12.1008

Delaloge, S., Piccart, M., Rutgers, E., Litière, S., van 't Veer, L. J., van den Berkmortel, F., et al. (2020). Standard Anthracycline Based versus Docetaxel-Capecitabine in Early High Clinical And/or Genomic Risk Breast Cancer in the EORTC 10041/BIG 3-04 MINDACT Phase III Trial. *J. Clin. Oncol.* 38 (11), 1186–1197. doi:10.1200/JCO.19.01371

Dencausse, Y., Sturm, J., Hartung, G., Dietzler, P., Edler, L., Bambach, M., et al. (2001). Adjuvant Radio-Chemotherapy in Stage II-III Rectal Cancer with 24-hour Infusion of High-Dose 5-fluorouracil and Folinic Acid: Evaluation of Feasibility. *Onkologie* 24 (5), 476–480. doi:10.1159/000055129

Depetris, I., Marino, D., Bonzano, A., Cagnazzo, C., Filippi, R., Aglietta, M., et al. (2018). Fluoropyrimidine-induced Cardiotoxicity. *Crit. Rev. Oncol. Hematol.* 124, 1–10. doi:10.1016/j.critrevonc.2018.02.002

Dyhl-Polk, A., Schou, M., Vistisen, K. K., Sillesen, A. S., Serup-Hansen, E., Faber, J., et al. (2020a). Myocardial Ischemia Induced by 5-Fluorouracil: A Prospective Electrocardiographic and Cardiac Biomarker Study. *Oncologist* 26 (3), E403–E413. doi:10.1002/onco.13536

Dyhl-Polk, A., Vaage-Nilsen, M., Schou, M., Vistisen, K. K., Lund, C. M., Kümler, T., et al. (2020b). Incidence and Risk Markers of 5-fluorouracil and Capecitabine Cardiotoxicity in Patients with Colorectal Cancer. *Acta Oncol.* 59 (4), 475–483. doi:10.1080/0284186X.2019.1711164

Economopoulou, P., Kotsakis, A., Kapiris, I., and Kentepozidis, N. (2015). Cancer Therapy and Cardiovascular Risk: Focus on Bevacizumab. *Cancer Manag. Res.* 7, 133–143. doi:10.2147/CMAR.S77400

Emmanouilides, C., Sfakiotaki, G., Androulakis, N., Kalbakis, K., Christophylakis, C., Kalykaki, A., et al. (2007). Front-line Bevacizumab in Combination with Oxaliplatin, Leucovorin and 5-Fluorouracil (FOLFOX) in Patients with Metastatic Colorectal Cancer: a Multicenter Phase II Study. *BMC Cancer* 7 (91), 91. doi:10.1186/1471-2407-7-91

Feliu, J., Escudero, P., Llosa, F., Bolaños, M., Vicent, J. M., Yubero, A., et al. (2005). Capecitabine as First-Line Treatment for Patients Older Than 70 Years with Metastatic Colorectal Cancer: An Oncopaz Cooperative Group Study. *J. Clin. Oncol.* 23 (13), 3104–3111. doi:10.1200/JCO.2005.06.035

Gao, L., Tatsch, T., Sides, M., Willis, M., and Berbarie, R. (2019). 5-fluorouracil Induced Coronary Vasospasm and Non-ischemic Cardiomyopathy Presenting in the Same Patient. *J. Am. Coll. Cardiol.* 73 (9), 2477. doi:10.1016/S0735-1097(19)33083-9

Geyer, C. E., Forster, J., Lindquist, D., Chan, S., Romieu, C. G., Pienkowski, T., et al. (2006). Lapatinib Plus Capecitabine for HER2-Positive Advanced Breast Cancer. *N. Engl. J. Med.* 355 (26), 2733–2743. doi:10.1056/NEJMoa064320

Giantonio, B. J., Catalano, P. J., Meropol, N. J., O'Dwyer, P. J., Mitchell, E. P., Alberts, S. R., et al. (2007). Bevacizumab in Combination with Oxaliplatin, Fluorouracil, and Leucovorin (FOLFOX4) for Previously Treated Metastatic Colorectal Cancer: Results from the Eastern Cooperative Oncology Group Study E3200. *J. Clin. Oncol.* 25 (12), 1539–1544. doi:10.1200/JCO.2006.09.6305

Giordano, K. F., Jatoi, A., Stella, P. J., Foster, N., Tschetter, L. K., Alberts, S. R., et al. (2006). Docetaxel and Capecitabine in Patients with Metastatic Adenocarcinoma of the Stomach and Gastroesophageal junction: a Phase II Study from the North Central Cancer Treatment Group. *Ann. Oncol.* 17 (4), 652–656. doi:10.1093/annonc/mdl005

Gowd, B. M., and Thompson, P. D. (2012). Effect of Female Sex on Cardiac Arrhythmias. *Cardiol. Rev.* 20 (6), 297–303. doi:10.1097/CRD.0b013e318259294b

Grierson, P., Teague, A., Suresh, R., Lim, K. H., Amin, M., Pedersen, K., et al. (2020). Phase Ib/II Study Combining Tosedostat with Capecitabine in Patients with Advanced Pancreatic Adenocarcinoma. *J. Gastrointest. Oncol.* 11 (1), 61–67. doi:10.21037/jgo.2019.11.06

Hartung, G., Hofheinz, R. D., Wein, A., Riedel, C., Rost, A., Fritze, D., et al. (2001). Phase II Study of a Weekly 24-hour Infusion with 5-fluorouracil and Simultaneous Sodium-Folinic Acid in the First-Line Treatment of Metastatic Colorectal Cancer. *ONKOLOGIE* 24 (5), 457–462. doi:10.1159/000055126

Hayashi, Y., Iijima, H., Isohashi, F., Tsujii, Y., Fujinaga, T., Nagai, K., et al. (2019). The Heart's Exposure to Radiation Increases the Risk of Cardiac Toxicity after Chemoradiotherapy for Superficial Esophageal Cancer: a Retrospective Cohort Study. *BMC Cancer* 19 (1), 195. doi:10.1186/s12885-019-5421-y

Hegde, P. S., and Chen, D. S. (2020). Top 10 Challenges in Cancer Immunotherapy. *Immunity* 52 (1), 17–35. doi:10.1016/j.immuni.2019.12.011

Hoff, P. M., Ansari, R., Batist, G., Cox, J., Kocha, W., Kuperminc, M., et al. (20012001). Comparison of Oral Capecitabine versus Intravenous Fluorouracil Plus Leucovorin as First-Line Treatment in 605 Patients with Metastatic Colorectal Cancer: Results of a Randomized Phase III Study. *Jco* 19 (8), 2282–2292. doi:10.1200/JCO.2001.19.8.2282

Jatoi, A., Murphy, B. R., Foster, N. R., Nikcevich, D. A., Alberts, S. R., Knost, J. A., et al. (2006). Oxaliplatin and Capecitabine in Patients with Metastatic Adenocarcinoma of the Esophagus, Gastroesophageal junction and Gastric Cardia: a Phase II Study from the North Central Cancer Treatment Group. *Ann. Oncol.* 17 (1), 29–34. doi:10.1093/annonc/mdj063

Jensen, S. A., Hasbak, P., Mortensen, J., and Sørensen, J. B. (2010). Fluorouracil Induces Myocardial Ischemia with Increases of Plasma Brain Natriuretic Peptide and Lactic Acid but without Dysfunction of Left Ventricle. *J. Clin. Oncol.* 28 (36), 5280–5286. doi:10.1200/JCO.2009.27.3953

Jensen, S. A., and Sørensen, J. B. (2006). Risk Factors and Prevention of Cardiotoxicity Induced by 5-fluorouracil or Capecitabine. *Cancer Chemother. Pharmacol.* 58 (4), 487–493. doi:10.1007/s00280-005-0178-1

Jin, X., Bai, Y., Gao, L., and Wu, S. (2019). Incidence of and Risk Factors for Cardiotoxicity after Fluorouracil-Based Chemotherapy in Locally Advanced or Metastatic Gastric Cancer Patients. *Cancer Chemother. Pharmacol.* 84 (3), 599–607. doi:10.1007/s00280-019-03888-1

Joensuu, H., Bono, P., Kataja, V., Alanko, T., Kokko, R., Asola, R., et al. (2009). Fluorouracil, Epirubicin, and Cyclophosphamide with Either Docetaxel or Vinorelbine, with or without Trastuzumab, as Adjuvant Treatments of Breast Cancer: Final Results of the FinHer Trial. *J. Clin. Oncol.* 27 (34), 5685–5692. doi:10.1200/JCO.2008.21.4577

Kanduri, J., More, L. A., Godishala, A., and Asnani, A. (2019). Fluoropyrimidine-Associated Cardiotoxicity. *Cardiol. Clin.* 37 (4), 399–405. doi:10.1016/j.ccl.2019.07.004

Karakulak, U. N., Aladağ, E., Maharjan, N., and Övünç, K. (2016). Capecitabine-induced Coronary Artery Vasospasm in a Patient Who Previously Experienced a Similar Episode with Fluorouracil Therapy. *Turk Kardiyol Dern Ars* 44 (1), 71–74. doi:10.5543/tkda.2015.36005

Kerr, R. S., Love, S., Segelov, E., Johnstone, E., Falcon, B., Hewett, P., et al. (2016). Adjuvant Capecitabine Plus Bevacizumab versus Capecitabine Alone in Patients with Colorectal Cancer (QUASAR 2): an Open-Label, Randomised Phase 3 Trial. *Lancet Oncol.* 17 (11), 1543–1557. doi:10.1016/S1470-2045(16)30172-3

Khan, M. A., Masood, N., Husain, N., Ahmad, B., Aziz, T., and Naeem, A. (2012). A Retrospective Study of Cardiotoxicities Induced by 5-fluouracil (5-FU) and 5-FU Based Chemotherapy Regimens in Pakistani Adult Cancer Patients at Shaukat Khanum Memorial Cancer Hospital & Research Center. *J. Pak Med. Assoc.* 62 (5), 430–434.

Koca, D., Salman, T., Unek, I. T., Oztop, I., Ellidokuz, H., Eren, M., et al. (2011). Clinical and Electrocardiography Changes in Patients Treated with Capecitabine. *Chemotherapy* 57 (5), 381–387. doi:10.1159/000331645

Koopman, M., Antonini, N. F., Douma, J., Wals, J., Honkoop, A. H., Erdkamp, F. L., et al. (2006). Randomised Study of Sequential versus Combination Chemotherapy with Capecitabine, Irinotecan and Oxaliplatin in Advanced Colorectal Cancer, an Interim Safety Analysis. A Dutch Colorectal Cancer Group (DCCG) Phase III Study. *Ann. Oncol.* 17 (10), 1523–1528. doi:10.1093/annonc/mdl179

Kosmas, C., Kallistratos, M. S., Kopterides, P., Syrios, J., Skopelitis, H., Mylonakis, N., et al. (2008). Cardiotoxicity of Fluoropyrimidines in Different Schedules of Administration: a Prospective Study. *J. Cancer Res. Clin. Oncol.* 134 (1), 75–82. doi:10.1007/s00432-007-0250-9

Koutsoukis, A., Ntalianis, A., Repasos, E., Kastritis, E., Dimopoulos, M. A., and Paraskevaidis, I. (2018). Cardio-oncology: A Focus on Cardiotoxicity. *Eur. Cardiol.* 13 (1), 64–69. doi:10.15420/ecr.2017:17:2

Kurokawa, J., Suzuki, T., and Furukawa, T. (2009). New Aspects for the Treatment of Cardiac Diseases Based on the Diversity of Functional Controls on Cardiac Muscles: Acute Effects of Female Hormones on Cardiac Ion Channels and Cardiac Repolarization. *J. Pharmacol. Sci.* 109 (3), 334–340. doi:10.1254/jphs.08r23fm

Kwakman, J. J., Simkens, L. H., Mol, L., Kok, W. E., Koopman, M., and Punt, C. J. (2017). Incidence of Capecitabine-Related Cardiotoxicity in Different Treatment Schedules of Metastatic Colorectal Cancer: A Retrospective Analysis of the CAIRO Studies of the Dutch Colorectal Cancer Group. *Eur. J. Cancer* 76, 93–99. doi:10.1016/j.ejca.2017.02.009

Leicher, L. W., de Graaf, J. C., Coers, W., Tascilar, M., and de Groot, J. W. (2017). Tolerability of Capecitabine Monotherapy in Metastatic Colorectal Cancer: A Real-World Study. *Drugs R. D* 17 (1), 117–124. doi:10.1007/s40268-016-0154-8

Lestuzzi, C., Tartuferi, L., Viel, E., Buonadonna, A., Vaccher, E., and Berretta, M. (2020). Fluoropyrimidine-Associated Cardiotoxicity: Probably Not So Rare as it Seems. *Oncologist* 25 (8), e1254. doi:10.1634/theoncologist.2020-0053

Lestuzzi, C., Vaccher, E., Talamini, R., Lleshi, A., Meneguzzo, N., Viel, E., et al. (2014). Effort Myocardial Ischemia during Chemotherapy with 5-fluorouracil: an Underestimated Risk. *Ann. Oncol.* 25 (5), 1059–1064. doi:10.1093/annonc/mdu055

Li, C., Ngorsuraches, S., Chou, C., Chen, L., Qian, J., and Qian, J. (2021). Risk Factors of Fluoropyrimidine Induced Cardiotoxicity Among Cancer Patients: A Systematic Review and Meta-Analysis. *Crit. Rev. Oncology/Hematology* 162, 103346. doi:10.1016/j.critrevonc.2021.103346

Lordick, F., Lorenzen, S., Stollfuss, J., Vehling-Kaiser, U., Kullmann, F., Hentrich, M., et al. (2005). Phase II Study of Weekly Oxaliplatin Plus Infusional Fluorouracil and Folinic Acid (FUFOX Regimen) as First-Line Treatment in Metastatic Gastric Cancer. *Br. J. Cancer* 93 (2), 190–194. doi:10.1038/sj.bjc.6602697

Lotrionte, M., Biondi-Zoccai, G., Abbate, A., Lanzetta, G., D'Ascenzo, F., Malavasi, V., et al. (2013). Review and Meta-Analysis of Incidence and Clinical Predictors of Anthracycline Cardiotoxicity. *Am. J. Cardiol.* 112 (12), 1980–1984. doi:10.1016/j.amjcard.2013.08.026

Lounsbury, P., Elokda, A. S., Bunning, J. M., Arena, R., and Gordon, E. E. (2017). The Value of Detecting Asymptomatic Signs of Myocardial Ischemia in Patients with Coronary Artery Disease in Outpatient Cardiac Rehabilitation. *J. Cardiovasc. Nurs.* 32 (3), E1–E9. doi:10.1097/JCN.0000000000000380

Machiels, J. P., Sempoux, C., Scalliet, P., Coche, J. C., Humblet, Y., Van Cutsem, E., et al. (2007). Phase I/II Study of Preoperative Cetuximab, Capecitabine, and External Beam Radiotherapy in Patients with Rectal Cancer. *Ann. Oncol.* 18 (4), 738–744. doi:10.1093/annonc/mdl460

Mambrini, A., Sanguinetti, F., Pacetti, P., Caudana, R., Iacono, C., Guglielmi, A., et al. (2006). Intra-arterial Infusion of 5-fluorouracil, Leucovorin, Epirubicin and Carboplatin (FLEC Regimen) in Unresectable Pancreatic Cancer: Results of a Ten-Year Experience. *In Vivo* 20 (6A), 751–755. doi:10.1007/978-3-642-04346-8_23

Martín, M., Makhson, A., Gligorov, J., Lichinitser, M., Lluch, A., Semiglazov, V., et al. (2012). Phase II Study of Bevacizumab in Combination with Trastuzumab and Capecitabine as First-Line Treatment for HER-2-Positive Locally Recurrent or Metastatic Breast Cancer. *Oncologist* 17 (4), 469–475. doi:10.1634/theoncologist.2011-0344

Masi, G., Loupakis, F., Salvatore, L., Fornaro, L., Cremolini, C., Cupini, S., et al. (2010). Bevacizumab with FOLFOXIRI (Irinotecan, Oxaliplatin, Fluorouracil, and Folinate) as First-Line Treatment for Metastatic Colorectal Cancer: a Phase 2 Trial. *Lancet Oncol.* 11 (9), 845–852. doi:10.1016/S1470-2045(10)70175-3

Mayer, I. A., Zhao, F., Arteaga, C. L., Symmans, W. F., Park, B. H., Burnette, B. L., et al. (2021). Randomized Phase III Postoperative Trial of Platinum-Based Chemotherapy versus Capecitabine in Patients with Residual Triple-Negative Breast Cancer Following Neoadjuvant Chemotherapy: ECOG-ACRIN EA1131. *J. Clin. Oncol.* 39 (23), 2539–2551. doi:10.1200/JCO.21.00976

Mayer, R. J., Van Cutsem, E., Falcone, A., Yoshino, T., Garcia-Carbonero, R., Mizunuma, N., et al. (2015). Randomized Trial of TAS-102 for Refractory Metastatic Colorectal Cancer. *N. Engl. J. Med.* 372 (20), 1909–1919. doi:10.1056/nejmoa1414325

Meydan, N., Kundak, I., Yavuzsen, T., Oztop, I., Barutca, S., Yilmaz, U., et al. (2005). Cardiotoxicity of de Gramont's Regimen: Incidence, Clinical Characteristics and Long-term Follow-up. *Jpn. J. Clin. Oncol.* 35 (5), 265–270. doi:10.1093/jjco/hyi071

Michalaki, V., Fotiou, S., Gennatas, S., and Gennatas, C. (2010). Trastuzumab Plus Capecitabine and Docetaxel as First-Line Therapy for HER2-Positive Metastatic Breast Cancer: Phase II Results. *Anticancer Res.* 30 (7), 3051–3054. doi:10.1200/jco.2009.27.15_suppl.1111

Mohammed, R., Sallam, N., and El-Abhar, H. (2018). P47885-Fluorouracil Cardiotoxicity: the Role of Oxidative Stress, Apoptosis, Inflammation and Endothelial Dysfuction. *Eur. Heart J.* 39, 1003–1004. doi:10.1093/eurheartj/ehy563.P4788

More, L. A., Lane, S., and Asnani, A. (2021). 5-FU Cardiotoxicity: Vasospasm, Myocarditis, and Sudden Death. *Curr. Cardiol. Rep.* 23 (3), 17. doi:10.1007/s11886-021-01441-2

Ng, M., Cunningham, D., and Norman, A. R. (2005). The Frequency and Pattern of Cardiotoxicity Observed with Capecitabine Used in Conjunction with

Oxaliplatin in Patients Treated for Advanced Colorectal Cancer (CRC). *Eur. J. Cancer* 41 (11), 1542–1546. doi:10.1016/j.ejca.2005.03.027

Nhlbi Study Quality Assessment Tools (2020). *National Institutes of Health (NIH), National Heart, Lung, and Blood Institute (NHLBI)*. Bethesda, MD, USA. Available at: https://www.nhlbi.nih.gov/healthtopics/study-quality-assessment-tools (accessed on February 10, 2020).

O'Connell, M. J., Colangelo, L. H., Beart, R. W., Petrelli, N. J., Allegra, C. J., Sharif, S., et al. (2014). Capecitabine and Oxaliplatin in the Preoperative Multimodality Treatment of Rectal Cancer: Surgical End Points from National Surgical Adjuvant Breast and Bowel Project Trial R-04. *J. Clin. Oncol.* 32 (18), 1927–1934. doi:10.1200/JCO.2013.53.7753

Okines, A. F., Langley, R. E., Thompson, L. C., Stenning, S. P., Stevenson, L., Falk, S., et al. (2013). Bevacizumab with Peri-Operative Epirubicin, Cisplatin and Capecitabine (ECX) in Localised Gastro-Oesophageal Adenocarcinoma: a Safety Report. *Ann. Oncol.* 24 (3), 702–709. doi:10.1093/annonc/mds533

Pai, V. B., and Nahata, M. C. (2000). Cardiotoxicity of Chemotherapeutic Agents: Incidence, Treatment and Prevention. *Drug Saf.* 22 (4), 263–302. doi:10.2165/00002018-200022040-00002

Peiffert, D., Giovannini, M., Ducreux, M., Michel, P., François, E., Lemanski, C., et al. (2001). High-dose Radiation Therapy and Neoadjuvant Plus Concomitant Chemotherapy with 5-fluorouracil and Cisplatin in Patients with Locally Advanced Squamous-Cell Anal Canal Cancer: Final Results of a Phase II Study. *Ann. Oncol.* 12 (3), 397–404. doi:10.1023/A:1011107105538

Peng, J., Dong, C., Wang, C., Li, W., Yu, H., Zhang, M., et al. (2018). Cardiotoxicity of 5-fluorouracil and Capecitabine in Chinese Patients: a Prospective Study. *Cancer Commun. (Lond)* 38 (1), 22. doi:10.1186/s40880-018-0292-1

Petrini, I., Lencioni, M., Ricasoli, M., Iannopollo, M., Orlandini, C., Oliveri, F., et al. (2012). Phase II Trial of Sorafenib in Combination with 5-fluorouracil Infusion in Advanced Hepatocellular Carcinoma. *Cancer Chemother. Pharmacol.* 69 (3), 773–780. doi:10.1007/s00280-011-1753-2

Polk, A., Shahmarvand, N., Vistisen, K., Vaage-Nilsen, M., Larsen, F. O., Schou, M., et al. (2016). Incidence and Risk Factors for Capecitabine-Induced Symptomatic Cardiotoxicity: a Retrospective Study of 452 Consecutive Patients with Metastatic Breast Cancer. *BMJ Open* 6, e012798. doi:10.1136/bmjopen-2016-012798

Primrose, J. N., Fox, R. P., Palmer, D. H., Malik, H. Z., Prasad, R., Mirza, D., et al. (2019). Capecitabine Compared with Observation in Resected Biliary Tract Cancer (BILCAP): a Randomised, Controlled, Multicentre, Phase 3 Study. *Lancet Oncol.* 20 (5), 663–673. doi:10.1016/S1470-2045(18)30915-X

Raber, I., Warack, S., Kanduri, J., Pribish, A., Godishala, A., Abovich, A., et al. (2019). Fluoropyrimidine-Associated Cardiotoxicity: A Retrospective Case-Control Study. *Oncologist* 25 (3), E606–E609. doi:10.1634/theoncologist.2019-0762

Sara, J. D., Kaur, J., Khodadadi, R., Rehman, M., Lobo, R., Chakrabarti, S., et al. (2018). 5-fluorouracil and Cardiotoxicity: a Review. *Ther. Adv. Med. Oncol.* 10, 1758835918780140. doi:10.1177/1758835918780140

Saunders, S., and Anwar, M. (2019). Capecitabine-induced Myopericarditis - A Case Report and Review of Literature. *J. Oncol. Pharm. Pract.* 25 (4), 1006–1010. doi:10.1177/1078155218774871

Sedhom, D., Sedhom, R., and Khan, W. (2017). A Rare Case of Acute Coronary Syndrome Induced by Oral Capecitabine. *Am. J. Resp. Crit. Care* 195. doi:10.1016/S0735-1097(21)03914-0

Skof, E., Rebersek, M., Hlebanja, Z., and Ocvirk, J. (2009). Capecitabine Plus Irinotecan (XELIRI Regimen) Compared to 5-FU/LV Plus Irinotecan (FOLFIRI Regimen) as Neoadjuvant Treatment for Patients with Unresectable Liver-Only Metastases of Metastatic Colorectal Cancer: a Randomised Prospective Phase II Trial. *BMC Cancer* 9 (120), 120. doi:10.1186/1471-2407-9-120

Smith, L. A., Cornelius, V. R., Plummer, C. J., Levitt, G., Verrill, M., Canney, P., et al. (2010). Cardiotoxicity of Anthracycline Agents for the Treatment of Cancer: Systematic Review and Meta-Analysis of Randomised Controlled Trials. *BMC Cancer* 10, 337. doi:10.1186/1471-2407-10-337

Tonyali, O., Benekli, M., Berk, V., Coskun, U., Ozkan, M., Yildiz, R., et al. (2013). Efficacy and Toxicity of Trastuzumab and Paclitaxel Plus Capecitabine in the First-Line Treatment of HER2-Positive Metastatic Breast Cancer. *J. Cancer Res. Clin. Oncol.* 139 (6), 981–986. doi:10.1007/s00432-013-1409-1

Tsavaris, N., Kosmas, C., Vadiaka, M., Efremidis, M., Zinelis, A., Beldecos, D., et al. (2002). Cardiotoxicity Following Different Doses and Schedules of 5-fluorouracil Administration for Malignancy -- a Survey of 427 Patients. *Med. Sci. Monit.* 8 (6), PI51–7. doi:10.12659/MSM.936523

Turan, T., Agac, M. T., Aykan, A. Ç., Kul, S., Akyüz, A. R., Gökdeniz, T., et al. (2017). Usefulness of Heart-type Fatty Acid-Binding Protein and Myocardial Performance Index for Early Detection of 5-Fluorouracil Cardiotoxicity. *Angiology* 68 (1), 52–58. doi:10.1177/0003319716637516

Vaishampayan, U. N., Ben-Josef, E., Philip, P. A., Vaitkevicius, V. K., Du, W., Levin, K. J., et al. (2002). A Single-Institution Experience with Concurrent Capecitabine and Radiation Therapy in Gastrointestinal Malignancies. *Int. J. Radiat. Oncol. Biol. Phys.* 53, 675–679. (PII S0360-9(02)02772-43). doi:10.1016/S0360-3016(02)02772-4

Van Cutsem, E., Hoff, P. M., Blum, J. L., Abt, M., and Osterwalder, B. (2002). Incidence of Cardiotoxicity with the Oral Fluoropyrimidine Capecitabine Is Typical of that Reported with 5-fluorouracil. *Ann. Oncol.* 13, 484–485. doi:10.1093/annonc/mdf108

Wacker, A., Lersch, C., Scherpinski, U., Reindl, L., and Seyfarth, M. (2003). High Incidence of Angina Pectoris in Patients Treated with 5-fluorouracil. A Planned Surveillance Study with 102 Patients. *ONCOLOGY* 65 (2), 108–112. doi:10.1159/000072334

Winther, S. B., Zubcevic, K., Qvortrup, C., Vestermark, L. W., Jensen, H. A., Krogh, M., et al. (2016). Experience with S-1 in Older Caucasian Patients with Metastatic Colorectal Cancer (mCRC): Findings from an Observational Chart Review. *Acta Oncol.* 55 (7), 881–885. doi:10.3109/0284186X.2016.1161825

Yamamoto, D., Iwase, S., Kitamura, K., Odagiri, H., Yamamoto, C., and Nagumo, Y. (2008). A Phase II Study of Trastuzumab and Capecitabine for Patients with HER2-Overexpressing Metastatic Breast Cancer: Japan Breast Cancer Research Network (JBCRN) 00 Trial. *Cancer Chemother. Pharmacol.* 61 (3), 509–514. doi:10.1007/s00280-007-0497-5

Yerushalmi, R., Idelevich, E., Dror, Y., Stemmer, S. M., Figer, A., Sulkes, A., et al. (2006). Preoperative Chemoradiation in Rectal Cancer: Retrospective Comparison between Capecitabine and Continuous Infusion of 5-fluorouracil. *J. Surg. Oncol.* 93 (7), 529–533. doi:10.1002/jso.20503

Yilmaz, U., Oztop, I., Ciloglu, A., Okan, T., Tekin, U., Yaren, A., et al. (2007). 5-Fluorouracil Increases the Number and Complexity of Premature Complexes in the Heart: a Prospective Study Using Ambulatory ECG Monitoring. *Int. J. Clin. Pract.* 61 (5), 795–801. doi:10.1111/j.1742-1241.2007.01323.x

Zafar, A., Drobni, Z. D., Mosarla, R., Alvi, R. M., Lei, M., Lou, U. Y., et al. (2021). The Incidence, Risk Factors, and Outcomes with 5-Fluorouracil-Associated Coronary Vasospasm. *JACC CardioOncol* 3 (1), 101–109. doi:10.1016/j.jaccao.2020.12.005

Zhang, P., Sun, T., Zhang, Q., Yuan, Z., Jiang, Z., Wang, X. J., et al. (2017). Utidelone Plus Capecitabine versus Capecitabine Alone for Heavily Pretreated Metastatic Breast Cancer Refractory to Anthracyclines and Taxanes: a Multicentre, Open-Label, Superiority, Phase 3, Randomised Controlled Trial. *Lancet Oncol.* 18 (3), 371–383. doi:10.1016/S1470-2045(17)30088-8

Conflict of Interest: The authors declare that the research was conducted in the absence of any commercial or financial relationships that could be construed as a potential conflict of interest.

Publisher's Note: All claims expressed in this article are solely those of the authors and do not necessarily represent those of their affiliated organizations or those of the publisher, the editors, and the reviewers. Any product that may be evaluated in this article, or claim that may be made by its manufacturer, is not guaranteed or endorsed by the publisher.

frontiers | Frontiers in Pharmacology

ORIGINAL RESEARCH
published: 23 May 2022
doi: 10.3389/fphar.2022.901887

Characteristics and Predictors of Venous Thromboembolism Among Lymphoma Patients Undergoing Chemotherapy: A Cohort Study in China

Yue Chen[1†], Haike Lei[2†], Wei Wang[1], Jie Zhu[1], Chensi Zeng[1], Zhuo Lu[1], Luchun Li[1], Dairong Li[1], Bo Long[1] and Haixia Liu[1*]*

[1]Chongqing Key Laboratory of Translational Research for Cancer Metastasis and Individualized Treatment, Chongqing University Cancer Hospital, Chongqing, China, [2]Chongqing Cancer Multi-Omics Big Data Application Engineering Research Center, Chongqing University Cancer Hospital, Chongqing, China

Background: Venous thromboembolism (VTE) is a potential complication among lymphoma patients. We evaluated the incidence rate and predictors of VTE in lymphoma patients undergoing chemotherapy.

Methods: The present study retrospectively studied 1,069 patients with lymphoma who were treated with chemotherapy from 2018 to 2020. We investigated clinical predictors of VTE among all patients. The follow-up results were obtained *via* telephone communication and from inpatient and outpatient records.

Results: A total of 1,069 patients underwent chemotherapy for lymphoma. During a mean follow-up of 23.1 months, 52 (4.9%) patients developed VTE. According to a multivariate analysis, the five variables found to be independently associated with VTE were male sex (HR 2.273, 95% CI 1.197–4.316, $p = 0.012$), age >64-years-old (HR 2.256, 95% CI 1.017–5.005, $p = 0.045$), the number of cycles of chemotherapy (HR 4.579, 95% CI 1.173–17.883, $p = 0.029$), platelet count ≥350 × 10^9/L (HR 2.533, 95% CI 1.187–5.406, $p = 0.016$), and D-dimer >0.5 mg/L (HR 4.367, 95% CI 2.124–8.981, $p < 0.001$).

Conclusion: This population-based study confirms the risk factors for VTE among patients with lymphoma who underwent chemotherapy and confirms that targeted thromboprophylaxis may reduce the burden of VTE in this population.

Keywords: VTE, lymphoma patients, chemotherapy, prospective cohort, targeted thromboprophylaxis

OPEN ACCESS

Edited by:
Ming-Ming Wu,
Harbin Medical University, China

Reviewed by:
Tong Liu,
Tianjin Medical University, China
Yuhui Zhang,
Chinese Academy of Medical Sciences and Peking Union Medical College, China
Chunyu Zeng,
Daping Hospital, China

***Correspondence:**
Haixia Liu
haixial222@163.com
Bo Long
rbolong@163.com

[†]These authors have contributed equally to this work and share first authorship

Specialty section:
This article was submitted to Cardiovascular and Smooth Muscle Pharmacology, a section of the journal Frontiers in Pharmacology

Received: *22 March 2022*
Accepted: *05 May 2022*
Published: *23 May 2022*

Citation:
Chen Y, Lei H, Wang W, Zhu J, Zeng C, Lu Z, Li L, Li D, Long B and Liu H (2022) Characteristics and Predictors of Venous Thromboembolism Among Lymphoma Patients Undergoing Chemotherapy: A Cohort Study in China. Front. Pharmacol. 13:901887. doi: 10.3389/fphar.2022.901887

INTRODUCTION

Venous thromboembolism (VTE), including deep vein thrombosis (DVT) and pulmonary embolism (PE), is a common complication of lymphoma, with an incidence of 1.5%–59.5% (Goldschmidt et al., 2003; Zhou et al., 2010). A prospective study on newly diagnosed lymphoma patients in Asia found a 1-year VTE incidence of 7.9% (Park et al., 2012). Another meta-analysis of 29 independent cohorts, including 18,018 patients and 1,149 events, found a VTE incidence rate of 5.3% in adult patients with lymphoma. Among these lymphoma patients, the incidence rate of VTE for patients with non-

Hodgkin lymphoma (NHL) was 6.5%, which is significantly greater than that observed for patients with Hodgkin lymphoma (HL) (4.7%) (Caruso et al., 2010). Compared to patients with several other types of cancer, patients with lymphoma are at significantly higher risk for VTE, especially those undergoing chemotherapy, for whom the VTE incidence rate may reach 15% or higher (Caruso et al., 2010; Falanga et al., 2012).

The development of VTE is related to various factors, including patient characteristics (i.e., bedridden status, central venous catheter use, older age, and prior history of venous thrombosis), disease status (i.e., surgery, comorbidities, coagulation function, and tumor progression), and therapeutic effects (i.e., chemotherapy, targeted therapy, and immunotherapy) (Reitsma et al., 2012; Timp et al., 2013; Mahajan et al., 2019). These factors have a significant impact on quality of life, additional anticoagulant therapy, increased risk of bleeding, financial burden, and tumor treatment, and the most serious consequence is increased mortality. Therefore, it is important to evaluate the clinical characteristics and risk factors associated with VTE among patients with lymphoma, as VTE has a considerable impact on the patient's condition.

In this retrospective study, we aimed to clarify the clinical and laboratory variables, disease status, and treatment approaches that increase VTE risk in patients with lymphoma.

PATIENTS AND METHODS

Study Population

Patients with lymphoma who underwent chemotherapy at the Chongqing University Cancer Hospital from January 2018 to December 2020 were considered possible candidates for the present study. The diagnosis of lymphoma was confirmed by histopathology, and the diagnostic criteria were based on the WHO classification. The exclusion criteria were as follows: juvenile patients (<18-years-old), patients with VTE, patients with other infectious or hematological malignancies as complications, and patients who refused or were unable to participate in the study. The present study was performed according to the guidelines of the Declaration of Helsinki and was approved by the Ethics Committee of The Chongqing University Cancer Hospital. Written informed consent was obtained from all subjects.

VTE Diagnosis

VTE was defined only as a primary event, with an objective diagnosis of DVT and/or PE being performed during chemotherapy. DVT (lower extremity thrombosis, upper extremity thrombosis, central venous catheter thrombosis, portal vein thrombosis) was confirmed by color and Doppler ultrasound examination or venogram. PE was confirmed by ventilation/perfusion scan and/or computed tomography angiography.

Data Collection

General, diagnostic and treatment information was collected for all patients. The specific data collected included age, sex, body mass index (BMI), histological type, Ann Arbor stage, Eastern Cooperative Oncology Group (ECOG) performance status, central venous catheter blood cell count, coagulation index, chemotherapy regimens, number of cycles of chemotherapy, and thrombosis location. All patients were routinely followed up *via* telephone communication, outpatient visits or hospitalization information. Telephone follow-ups were performed every 6 months after discharge. Patients were followed from the time of diagnosis until the development of VTE, death, loss to follow-up, whichever came first.

Statistical Analysis

All statistical analyses were performed using SPSS 26.0 software. Patient demographics and clinical characteristics were summarized with descriptive statistics. Count data were compared using the $\chi 2$ test. Normally distributed measurement data were compared using an independent sample t test, and nonnormally distributed measurement data were compared using a corrected t test. Univariate and multivariate Cox regression analyses were used to identify the predictors associated with VTE in patients with lymphoma who underwent chemotherapy. $p < 0.05$ was considered statistically significant.

RESULTS

A total of 1,069 patients (635 males, 59.5%) with a mean age of 55.6 ± 14.4 years were included in the analyses from January 2018 to December 2020. Hodgkin lymphoma was diagnosed in 106 patients (9.9%), B-cell lymphoma was diagnosed in 788 patients (73.7%), T-cell lymphoma was diagnosed in 87 patients (8.1%), and NK/T-cell lymphoma was diagnosed in 88 patients (8.2%). Most patients had a good ECOG performance status (≤ECOG grade 1: 83.7%), while approximately 64.3% of patients had Ann Arbor stage III/IV disease. Only 6.3% of all patients received a central venous catheter (CVC). The most common chemotherapy regimen used was R-CHOP (rituximab, cyclophosphamide, adriamycin, vincristine and prednisone) or CHOP. However, 92.4% of patients with HL received the ABVD (adriamycin, bleomycin, vinblastine and dacarbazine) regimen. Ninety percent of patients had only 1-5 cycles of chemotherapy (**Table 1**).

During a mean follow-up of 23.1 months, 52 (4.9%) patients were diagnosed with VTE, and all the patients had DVT. Hodgkin lymphoma and non-Hodgkin lymphoma accounted for 6.7 and 4.7% of VTE patients, respectively. These patients developed VTE while undergoing chemotherapy, with a median time to event of 3.45 months. All episodes of VTE occurred after chemotherapy treatment was initiated.

Univariate competing risks regression demonstrated that male sex (hazard ratio [HR] 1.919, 95% confidence interval [CI] 1.039–3.542, $p = 0.037$), age >64-years-old (HR 2.438 95% CI 1.153–5.157, $p = 0.020$), 6–10 cycles of chemotherapy (HR 2.916, 95% CI 1.304–6.518, $p = 0.009$), platelet count

TABLE 1 | Clinical characteristics of lymphoma patients with or without VTE.

Characteristics	Total (%)	VTE (%)	No VTE (%)	*p* Value
Subjects, n	1069 (100)	52 (4.9)	1017 (95.1)	
Males, n (%)	635 (59.4)	38 (73.1)	597 (58.7)	0.043
Age, (years)				0.000
≤45	228 (21.3)	9 (17.3)	219 (21.5)	
46–64	506 (47.3)	14 (26.9)	492 (48.4)	
>64	335 (31.4)	29 (55.8)	306 (30.1)	
BMI, (kg/m^2)	23.3 ± 3.6	23.2 ± 3.2	23.3 ± 3.6	0.960
ECOG, n (%)				0.018
0	337 (31.5)	21 (40.4)	316 (31.1)	
1	558 (52.2)	18 (34.6)	540 (53.1)	
2	167 (15.6)	11 (6.6)	156 (15.3)	
3	7 (0.7)	2 (3.8)	5 (0.5)	
Ann Arbor, n (%)				
I	120 (11.2)	9 (17.3)	111 (10.9)	0.480
II	261 (24.4)	11 (21.2)	250 (24.6)	
III	228 (21.3)	8 (17.3)	219 (21.5)	
IV	460 (43)	23 (44.2)	437 (43)	
Central venous catheter, n (%)	67 (6.3)	3 (5.8)	64 (6.3)	0.879
White blood cell count (>11×10^9/L), n (%)	974 (91.1)	48 (92.3)	926 (91.1)	0.750
Hemoglobin (<100 g/L), n (%)	190 (17.8)	15 (28.8)	175 (17.2)	0.032
Platelet count (≥350×10^9/L), n (%)	101 (9.4)	9 (17.3)	93 (9)	0.047
D-dimer (>0.5 mg/L), n (%)	544 (50.9)	42 (80.8)	10 (19.2)	0.000
Histological type, n (%)				0.059
Hodgkin lymphoma	106 (9.9)	7 (13.5)	99 (9.7)	
B-cell lymphoma	788 (73.7)	32 (61.5)	756 (74.3)	
T-cell lymphoma	87 (8.1)	9 (17.3)	78 (7.7)	
NK/T-cell lymphoma	88 (8.2)	4 (7.7)	84 (8.3)	
Chemotherapy regimens, n (%)				0.160
ABVD	98 (9.2)	6 (11.5)	92 (9)	
CHOP/R-CHOP	590 (55.2)	26 (50)	564 (55.5)	
P-GEMOX	56 (5.2)	3 (5.8)	53 (5.2)	
DICE/R-DICE	30 (2.8)	3 (5.8)	27 (2.7)	
R-EPOCH	47 (4.4)	0	47 (4.6)	
GDP/R-GDP	51 (4.8)	6 (11.5)	45 (4.4)	
BR	7 (0.7)	0	7 (0.7)	
Others	19,017.8)	8 (15.4)	182 (17.9)	
Cycles of chemotherapy, n (%)				0.001
1–5	996 (93.2)	42 (80.8)	954 (93.8)	
6–10	52 (4.8)	7 (13.5)	45 (4.4)	
≥11	21 (2.0)	3 (5.7)	18 (1.8)	

BMI, body mass index; VTE, venous thromboembolism; ECOG, eastern cooperative oncology group; ABVD, adriamycin, bleomycin, vinblastine and dacarbazine; R-CHOP, rituximab, cyclophosphamide, doxorubicin, vincristine and prednisone; P-GEMOX, pegaspargase, gemcitabine and oxaliplatin; R-DICE, rituximab, cisplatin, ifosfamide, etoposide and dexamethasone; R-EPOCH, rituximab, etoposide phosphate, prednisone, vincristine sulfate, cyclophosphamide and doxorubicin hydrochloride; R-GDP, rituximab, gemcitabine, dexamethasone and cisplatin; BR, bendamustine and rituximab.

≥350 × 10^9/L (HR 2.229, 95% CI 1.085–4.580, $p = 0.029$), and D-dimer >0.5 mg/L (HR 4.593, 95% CI 2.229–9.176, $p < 0.001$) were associated with an increased risk of developing VTE. Body mass index, ECOG grade, Ann Arbor stage, CVC, white blood cell count, hemoglobin count and chemotherapy regimen were not associated with VTE development. To exclude the influence of confounding factors, all possible risk factors were added to the multivariate model. Conclusively, male sex (HR 2.273, 95% CI 1.197–4.316, $p = 0.012$), age >64-years-old (HR 2.256, 95% CI 1.017–5.005, $p = 0.045$), number of cycles of chemotherapy (HR 4.579, 95% CI 1.173–17.883, $p = 0.029$), platelet count ≥350 × 10^9/L (HR 2.533, 95% CI 1.187–5.406, $p = 0.016$), and D-dimer >0.5 mg/L (HR 4.367, 95% CI 2.124–8.981, $p < 0.001$) were still statistically significant (**Table 2**; **Figure 1**).

DISCUSSION

The incidence of and risk factors for VTE among adult patients with lymphoma were investigated in the present study. A VTE incidence of 4.9% supported the similar prevalence (4%) found in another retrospective study, which included the second-largest population of lymphoma patients analyzed for VTE risk in California (Mahajan et al., 2014). The rate of VTE was 6.7% in patients with HL and 4.7% in patients with NHL, differing from a previous study (Caruso et al., 2010). A possible reason for the difference was that our research focused on patients who underwent chemotherapy and excluded many NHL patients undergoing other types of treatment, such as surgery and targeted therapies. Another reason may be related to regional differences.

TABLE 2 | HRs (95% confidence intervals) for risk factors associated with venous thromboembolism.

Variables	Univariate		Multivariate[a]	
	HR (95%CI)	P	HR (95%CI)	P
Male sex	1.919 (1.039–3.542)	0.037	2.273 (1.197–4.316)	0.012
Age				
≤45	1 (ref.)			
46–64	0.730 (0.316–1.687)	0.461	0.769 (0.323–1.830)	0.553
>64	2.438 (1.153–5.157)	0.020	2.256 (1.017–5.005)	0.045
Cycles of chemotherapy				
1–5	1 (ref.)			
6–10	2.916 (1.304–6.518)	0.009	3.790 (1.566–9.171)	0.003
≥11	3.129 (0.965–10.141)	0.057	4.579 (1.173–17.883)	0.029
Platelet count ≥350 × 109/L	2.229 (1.085–4.580)	0.029	2.533 (1.187–5.406)	0.016
D-dimer >0.5 mg/L	4.593 (2.229–9.176)	<0.001	4.367 (2.124–8.981)	<0.001

[a]*Adjusted for age, sex, BMI, ECOG, ann arbor, central venous catheter, white blood cell count, hemoglobin, platelet count, D-dimer, histological type, chemotherapy regimens, and cycles of chemotherapy.*

In terms of individual risk factors, we reported male sex, age >64-years-old, increased cycles of chemotherapy, platelet count ≥350 × 10^9/L and D-dimer >0.5 mg/L as potential risk factors for developing VTE. This finding was in accordance with a previous study that identified female sex, older age, ECOG performance scores ≥2 and anemia (hemoglobin <100 g/L) as predictors of VTE (Byun et al., 2019). A previous study also suggested that patients with platelet abnormalities prior to undergoing chemotherapy and patients at Ann Arbor stage III/IV were associated with a significantly higher risk of developing VTE (Li et al., 2021).

Several previous studies suggested that older age is a risk factor for cancer-associated VTE. Park et al. identified age >60 years as a risk factor for VTE in patients with diffuse large B-cell lymphoma (Park et al., 2012). Another study from Asia also reported a similar conclusion in primary central nervous system lymphoma patients who underwent chemotherapy (Byun et al., 2019). A recent analysis, which included 16,755 patients with NHL, confirmed that those who were aged ≥45 years and above had an increased risk of VTE (Mahajan et al., 2014). In the present study, we discovered a positive relationship between age >64-years-old and VTE, which is consistent with the aforementioned studies.

Male sex might be a potential risk factor for VTE in patients with lymphoma in the present study. Our research showed a 2.27-fold higher risk of VTE in male patients than in female patients. However, a study including 304 lymphoma patients who received chemotherapy investigated the risk of VTE occurring in women and found that it was significantly higher than that in other patients. The results of another study that included seven academic centers in Korea also suggested that female sex was independently associated with VTE in patients with primary central nervous system lymphoma (Byun et al., 2019). Although these results were inconsistent with our study, the data are far from conclusive. Several other studies did not find an association between female sex and the risk for VTE (Sanfilippo et al., 2016; Rupa-Matysek et al., 2017; Hohaus et al., 2018; Rupa-Matysek et al., 2018).

A platelet count ≥350 × 10^9/L is a component of the Khorana Risk score for VTE development in cancer patients and is considered to increase the risk of VTE (Khorana et al., 2008). Li et al. suggested that an abnormal platelet count (<125 or >350 × 10^9/L) increased the risk of VTE by more than 60 times (Li et al., 2021). Platelet abnormalities are an independent risk factor for VTE in lymphoma patients, but little is known about the pathophysiological mechanism underlying this relationship. This might be related to the expression and release of some cytokines by tumor cells, leading to the activation of platelet and coagulation pathways. Additionally, tumor cells can secrete some inflammatory cytokines, such as tumor necrosis factor α and interleukin-β, which can result in platelet activation and the expression of a procoagulant phenotype by endothelial cells (Falanga et al., 2009).

In our study, we found that increasing the number of cycles of chemotherapy led to a higher risk of VTE in lymphoma patients. The incidence of VTE in patients who underwent more than 10 cycles of chemotherapy was significantly higher than that in patients who underwent 1-5 cycles of chemotherapy. The results supported findings from several studies showing a relationship between chemotherapy and the risk of VTE (Horsted et al., 2012; Sanfilippo et al., 2016). A prior study including 2,650 patients who underwent orchiectomy for testicular cancer also suggested that an increasing number of chemotherapy cycles was an independent risk factor for VTE (Robinson et al., 2020). Many chemotherapeutic drugs are known to be associated with VTE. The increasing number of cycles of chemotherapy leading to the development of VTE may be related to drug accumulation effects.

D-dimer is a typical marker of VTE and is widely used in clinical practice. Several studies confirmed a correlation between D-dimer levels and VTE in hematologic malignancies (Ay et al., 2009; Libourel et al., 2016). Libourel et al. showed that the risk of VTE among patients with D-dimer >4.0 mg/L was 32 times higher than that among patients with D-dimer ≤0.5 mg/L (Libourel et al., 2016). Another study of 111 patients from the Vienna Cancer and Thrombosis Study (CATS) with hematologic malignancies (lymphoma and multiple myeloma) demonstrated that elevated D-dimer levels (>1.4 mg/L) were associated with an increased risk of VTE (Ay et al., 2009). Notwithstanding, data to support a cutoff for increased D-dimer levels in routine

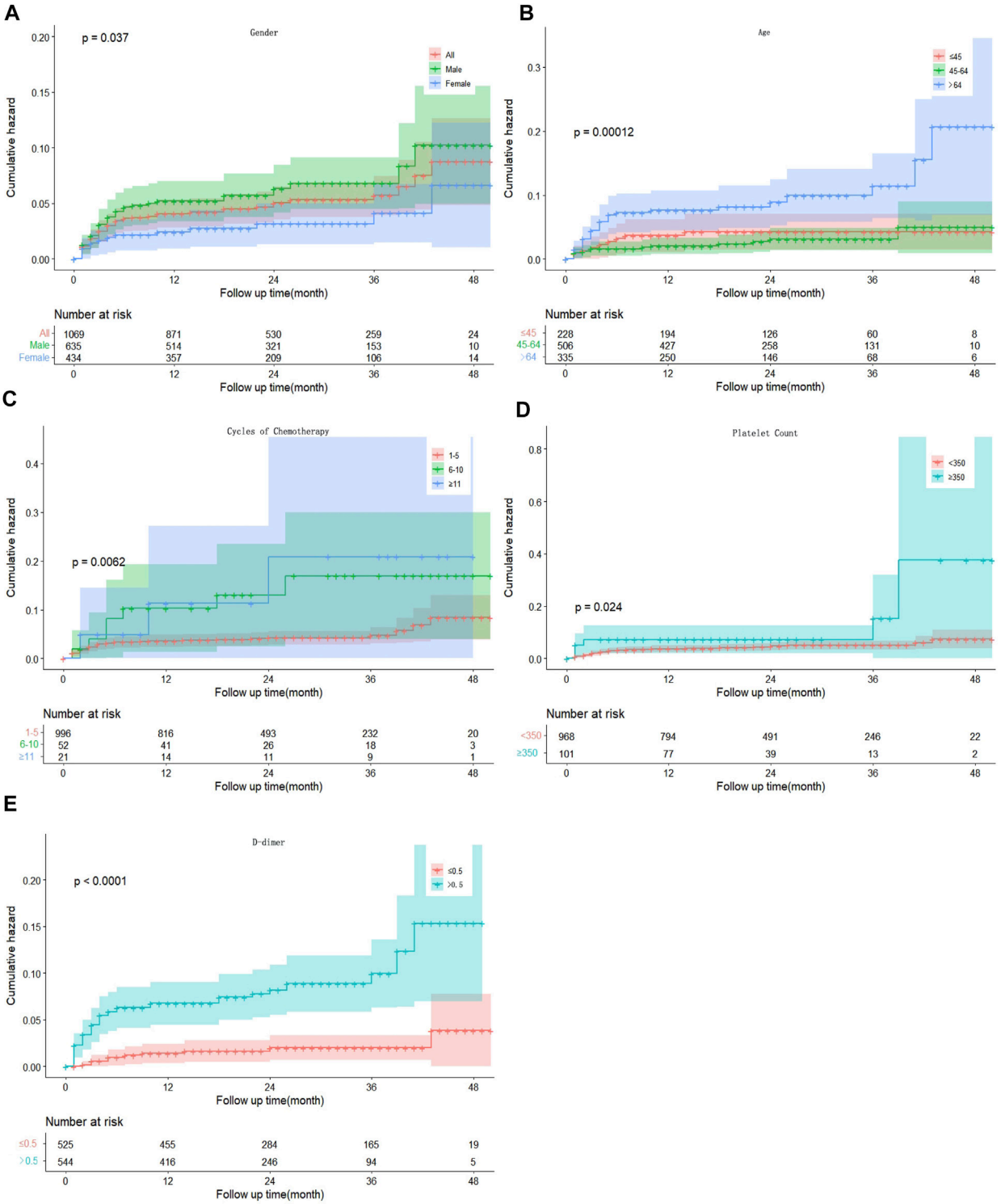

FIGURE 1 | Kaplan–Meier curves for the cumulative incidence of VTE patients by sex **(A)**, age **(B)**, cycles of chemotherapy **(C)**, platelet count **(D)** and D-dimer concentration **(E)**. VTE, venous thromboembolism.

clinical decision-making are currently lacking. However, there is a well-established trend that increasing D-dimer levels lead to an increased risk of thrombosis.

The current research was a single-center retrospective study. We confirmed the risk factors for VTE among patients with lymphoma who underwent chemotherapy. Compared to other risk models (i.e., the Khorana score, the ONKOTEV score and the TiC-Onco score), age, sex, and the number of cycles of chemotherapy were included as predictors. Although the study had a small sample size from a single center, these variables were more available clinically, which provided a reference for future research. The limitations of this study are related to regional bias and the small sample size. Another limitation was the possible omission of asymptomatic VTE due to this follow-up method. Since it was a retrospective study, some variables, such as VTE history and hospitalization status, were not available, which might affect the results. The strength of our study was an adequate follow-up. Multicenter, large-scale cohorts with more statistical power are needed to validate the findings of the present study, which will help to verify effective predictors and implement early intervention to improve the quality of life and prolong the survival of patients.

CONCLUSION

In this paper, we demonstrated that male sex, older age, an increased number of cycles of chemotherapy, a platelet count $\geq 350\times10^9$/L and a D-dimer >0.5 mg/L were associated with VTE incidence in lymphoma patients. Early VTE identification and intervention are critically important for clinical practice.

DATA AVAILABILITY STATEMENT

The original contributions presented in the study are included in the article/supplementary materials, further inquiries can be directed to the corresponding authors.

ETHICS STATEMENT

The present study was performed according to the guidelines of the Declaration of Helsinki and was approved by the Ethics Committee of The Chongqing University Cancer Hospital. Written informed consent was obtained from all subjects.

AUTHOR CONTRIBUTIONS

YC and HL conceived and designed the study. WW, JZ, and CZ collected and assembled the data and were responsible for privacy management. ZL and LL cleaned the data and analyzed and implemented the algorithm. YC, HL, DL, and BL interpreted the data. BL and HL were responsible for the literature review. YC, BL, and HL drafted the manuscript. All authors revised the manuscript for important intellectual content.

FUNDING

This work was supported by the Fundamental Research Funds for the Central Universities (2019CDYGYB014).

REFERENCES

Ay, C., Vormittag, R., Dunkler, D., Simanek, R., Chiriac, A. L., Drach, J., et al. (2009). D-dimer and Prothrombin Fragment 1 + 2 Predict Venous Thromboembolism in Patients with Cancer: Results from the Vienna Cancer and Thrombosis Study. *J. Clin. Oncol.* 27 (25), 4124–4129. doi:10.1200/JCO.2008.21.7752

Byun, J. M., Hong, J., Yoon, S. S., Koh, Y., Ock, C. Y., Kim, T. M., et al. (2019). Incidence and Characteristics of Venous Thromboembolism in Asian Patients with Primary Central Nervous System Lymphoma Undergoing Chemotherapy. *Thromb. Res.* 183, 131–135. doi:10.1016/j.thromres.2019.10.002

Caruso, V., Di Castelnuovo, A., Meschengieser, S., Lazzari, M. A., de Gaetano, G., Storti, S., et al. (2010). Thrombotic Complications in Adult Patients with Lymphoma: a Meta-Analysis of 29 Independent Cohorts Including 18 018 Patients and 1149 Events. *Blood* 115 (26), 5322–5328. doi:10.1182/blood-2010-01-258624

Falanga, A., Marchetti, M., and Russo, L. (2012). Venous Thromboembolism in the Hematologic Malignancies. *Curr. Opin. Oncol.* 24 (6), 702–710. doi:10.1097/CCO.0b013e3283592331

Falanga, A., Panova-Noeva, M., and Russo, L. (2009). Procoagulant Mechanisms in Tumour Cells. *Best. Pract. Res. Clin. Haematol.* 22 (1), 49–60. doi:10.1016/j.beha.2008.12.009

Goldschmidt, N., Linetsky, E., Shalom, E., Varon, D., and Siegal, T. (2003). High Incidence of Thromboembolism in Patients with Central Nervous System Lymphoma. *Cancer* 98 (6), 1239–1242. doi:10.1002/cncr.11623

Hohaus, S., Tisi, M. C., Bartolomei, F., Cuccaro, A., Maiolo, E., Alma, E., et al. (2018). Risk Factors for Venous Thromboembolism in Patients with Lymphoma Requiring Hospitalization. *Blood Cancer J.* 8 (6), 54. doi:10.1038/s41408-018-0096-1

Horsted, F., West, J., and Grainge, M. J. (2012). Risk of Venous Thromboembolism in Patients with Cancer: a Systematic Review and Meta-Analysis. *PLoS Med.* 9 (7), e1001275. doi:10.1371/journal.pmed.1001275

Khorana, A. A., Kuderer, N. M., Culakova, E., Lyman, G. H., and Francis, C. W. (2008). Development and Validation of a Predictive Model for Chemotherapy-Associated Thrombosis. *Blood* 111 (10), 4902–4907. doi:10.1182/blood-2007-10-116327

Li, X., Hou, S. L., Li, X., Li, L., Lian, K., Cui, J. Y., et al. (2021). Risk Factors of Thromboembolism in Lymphoma Patients Undergoing Chemotherapy and its Clinical Significance. *Clin. Appl. Thromb. Hemost.* 27, 37923. doi:10.1177/10760296211037923

Libourel, E. J., Klerk, C. P. W., van Norden, Y., de Maat, M. P. M., Kruip, M. J., Sonneveld, P., et al. (2016). Disseminated Intravascular Coagulation at Diagnosis Is a Strong Predictor for Thrombosis in Acute Myeloid Leukemia. *Blood* 128 (14), 1854–1861. doi:10.1182/blood-2016-02-701094

Mahajan, A., Brunson, A., White, R., and Wun, T. (2019). The Epidemiology of Cancer-Associated Venous Thromboembolism: An Update. *Semin. Thromb. Hemost.* 45 (4), 321–325. doi:10.1055/s-0039-1688494

Mahajan, A., Wun, T., Chew, H., and White, R. H. (2014). Lymphoma and Venous Thromboembolism: Influence on Mortality. *Thromb. Res.* 133 Suppl 2 (Suppl. 2), S23–S28. doi:10.1016/S0049-3848(14)50004-7

Park, L. C., Woo, S. Y., Kim, S., Jeon, H., Ko, Y. H., Kim, S. J., et al. (2012). Incidence, Risk Factors and Clinical Features of Venous Thromboembolism in Newly Diagnosed Lymphoma Patients: Results from a Prospective Cohort Study with Asian Population. *Thromb. Res.* 130 (3), e6–12. doi:10.1016/j.thromres.2012.03.019

Reitsma, P. H., Versteeg, H. H., and Middeldorp, S. (2012). Mechanistic View of Risk Factors for Venous Thromboembolism. *Arterioscler. Thromb. Vasc. Biol.* 32 (3), 563–568. doi:10.1161/ATVBAHA.111.242818

Robinson, A. G., Wei, X., Karim, S., Raphael, M. J., Bedard, P. L., and Booth, C. M. (2020). Venous Thromboembolism during Chemotherapy for Testicular Cancer: A Population-Based Study. *Clin. Oncol. R. Coll. Radiol.* 32 (10), e188–e193. doi:10.1016/j.clon.2020.03.013

Rupa-Matysek, J., Gil, L., Kaźmierczak, M., Barańska, M., and Komarnicki, M. (2017). Prediction of Venous Thromboembolism in Newly Diagnosed Patients Treated for Lymphoid Malignancies: Validation of the Khorana Risk Score. *Med. Oncol.* 35 (1), 5. doi:10.1007/s12032-017-1065-4

Rupa-Matysek, J., Lidia, G., and Komarinicki, M. (2018). Evaluation of the ThroLy Score for the Prediction of Venous Thromboembolism in Newly Diagnosed Patients Treated for Lymphoid Malignancies in Clinical Practice. *Cancer Med* 7, 2868. doi:10.1002/cam4.1540

Sanfilippo, K. M., Wang, T. F., Gage, B. F., Luo, S., Riedell, P., and Carson, K. R. (2016). Incidence of Venous Thromboembolism in Patients with Non-hodgkin Lymphoma. *Thromb. Res.* 143, 86–90. doi:10.1016/j.thromres.2016.05.008

Timp, J. F., Braekkan, S. K., Versteeg, H. H., and Cannegieter, S. C. (2013). Epidemiology of Cancer-Associated Venous Thrombosis. *Blood* 122 (10), 1712–1723. doi:10.1182/blood-2013-04-460121

Zhou, X., Teegala, S., Huen, A., Ji, Y., Fayad, L., Hagemeister, F. B., et al. (2010). Incidence and Risk Factors of Venous Thromboembolic Events in Lymphoma. *Am. J. Med.* 123 (10), 935–941. doi:10.1016/j.amjmed.2010.05.021

Conflict of Interest: The authors declare that the research was conducted in the absence of any commercial or financial relationships that could be construed as a potential conflict of interest.

Publisher's Note: All claims expressed in this article are solely those of the authors and do not necessarily represent those of their affiliated organizations, or those of the publisher, the editors and the reviewers. Any product that may be evaluated in this article, or claim that may be made by its manufacturer, is not guaranteed or endorsed by the publisher.

frontiers | Frontiers in Pharmacology

ORIGINAL RESEARCH
published: 07 June 2022
doi: 10.3389/fphar.2022.850053

Cariporide Attenuates Doxorubicin-Induced Cardiotoxicity in Rats by Inhibiting Oxidative Stress, Inflammation and Apoptosis Partly Through Regulation of Akt/GSK-3β and Sirt1 Signaling Pathway

Wenli Liao[1†], *Zhiwei Rao*[2†], *Lingling Wu*[1], *Yong Chen*[2*] *and Cairong Li*[1*]

[1]National Demonstration Center for Experimental General Medicine Education, Xianning Medical College, Hubei University of Science and Technology, Xianning, China, [2]Central Hospital of Xianning, The First Affiliate Hospital of Hubei University of Science and Technology, Xianning, China

OPEN ACCESS

Edited by:
Jun Pu,
Shanghai Jiao Tong University, China

Reviewed by:
Sabzali Javadov,
University of Puerto Rico, Puerto Rico
Chi Keung Lam,
University of Delaware, United States

***Correspondence:**
Cairong Li
xnlcr@163.com
Yong Chen
xncheny@163.com

[†]These authors have contributed equally to this work

Specialty section:
This article was submitted to Cardiovascular and Smooth Muscle Pharmacology, a section of the journal Frontiers in Pharmacology

Received: 07 January 2022
Accepted: 12 April 2022
Published: 07 June 2022

Citation:
Liao W, Rao Z, Wu L, Chen Y and Li C (2022) Cariporide Attenuates Doxorubicin-Induced Cardiotoxicity in Rats by Inhibiting Oxidative Stress, Inflammation and Apoptosis Partly Through Regulation of Akt/GSK-3β and Sirt1 Signaling Pathway. Front. Pharmacol. 13:850053. doi: 10.3389/fphar.2022.850053

Background: Doxorubicin (DOX) is a potent chemotherapeutic agent with limited usage due to its cumulative cardiotoxicity. The Na^+/H^+ exchanger isoform 1 (NHE1) is a known regulator of oxidative stress, inflammation, and apoptosis. The present study was designed to investigate the possible protective effect of cariporide (CAR), a selective inhibitor of NHE1, against DOX-induced cardiotoxicity in rats.

Methods: Male Sprague-Dawley rats were intraperitoneally injected with DOX to induce cardiac toxicity and CAR was given orally for treatment. The injured H9c2 cell model was established by incubation with DOX *in vitro*. Echocardiography, as well as morphological and ultra-structural examination were performed to evaluate cardiac function and histopathological changes. The biochemical parameters were determined according to the manufacturer's guideline of kits. ROS were assessed by using an immunofluorescence assay. The serum levels and mRNA expressions of inflammatory cytokines were measured by using ELISA or qRT-PCR. Cardiac cell apoptosis and H9c2 cell viability were tested by TUNEL or MTT method respectively. The protein expressions of Cleaved-Caspase-3, Bcl-2, Bax, Akt, GSK-3β, and Sirt1 were detected by western blot.

Results: Treatment with CAR protected against DOX-induced body weight changes, impairment of heart function, leakage of cardiac enzymes, and heart histopathological damage. In addition, CAR significantly attenuated oxidative stress and inhibited the levels and mRNA expressions of inflammatory cytokines (TNF-α, IL-6, IL-18, and IL-1β), which were increased by DOX treatment. Moreover, CAR significantly suppressed myocardial apoptosis and Cleaved-Caspase-3 protein expression induced by DOX, which was in agreement with the increased Bcl-2/Bax ratio. Also, DOX suppressed phosphorylation of Akt and GSK-3β, which was significantly reversed by administration of CAR. Furthermore, CAR treatment prevented DOX-induced down-regulation of Sirt1 at the protein level *in vitro*

and *in vivo*. Finally, Sirt1 inhibitor reversed the protective effects of CAR, as evidenced by reduced cell viability and Sirt1 protein expression *in vitro*.

Conclusion: Taken together, we provide evidence for the first time in the current study that CAR exerts potent protective effects against DOX-induced cardiotoxicity in rats. This cardio-protective effect is attributed to suppressing oxidative stress, inflammation, and apoptosis, at least in part, through regulation of Akt/GSK-3β and Sirt1 signaling pathway, which has not been reported to date.

Keywords: cariporide, doxorubicin, cardiotoxicity, apoptosis, SIRT1, Na+/H+ exchanger isoform 1

INTRODUCTION

As an anthracycline drug, doxorubicin (DOX) is one of the most extensively used chemotherapeutic agents for treatment of various cancers including leukemia, lymphoma, breast cancer, and other solid tumors (Rivankar, 2014). Unfortunately, despite its remarkable anticancer activity, the clinical application of DOX is markedly limited by its serious cardiotoxicity, which is characterized by electrocardiographic changes, cardiac arrhythmia, and irreversible degenerative cardiomyopathy (Smith et al., 2010). DOX-induced cardiotoxicity can occur immediately, within months, or even years after DOX treatment (Alkreathy et al., 2010). The exact molecular mechanisms responsible for DOX-induced cardiotoxicity are still not fully understood, and few drugs have been tested clinically to alleviate DOX-induced cardiotoxicity. Numerous studies have implicated that reactive oxygen species (ROS) generation, mitochondrial dysfunction, inflammation, apoptosis and various signaling pathways were convincingly shown to be crucial in DOX-induced cardiotoxicity (Mukhopadhyay et al., 2007; Meeran et al., 2019; Chen et al., 2020).

Sirtuin 1 (Sirt1), an NAD^+-dependent histone deacetylase, plays important roles in multiple biological processes including longevity, stress response, and cell survival. It has been well established that Sirt1 was involved in redox regulation, cell apoptosis, as well as inflammation (Hwang et al., 2013), and the protein level of Sirt1 increased in response to DOX injection (Zhang et al., 2011). Some evidence supports that PI3K-Akt-GSK3β signaling pathway is necessary for endoplasmic reticulum stress-induced Sirt1 activation (Koga et al., 2015), and the protective role of PI3K/Akt signaling pathway is found in DOX-induced cardiac dysfunction (Wen et al., 2019). The activation of PI3K/Akt signaling pathway can suppress DOX-induced cardiomyocyte apoptosis. In particular, GSK-3β is a downstream effector of PI3K/Akt signaling pathway and can lead to the mitochondrial permeability transition pore opening and subsequently apoptosis (Townsend et al., 2007). As DOX still remains a mainstay of many chemotherapeutic regimens, further investigation of its cardiotoxicity and how to prevent it is warranted.

Cariporide (CAR) is a selective Na+/H+ exchanger isoform 1 (NHE1) inhibitor, which can significantly improve DOX sensitivity in a xenograft model, specifically enhancing tumor growth inhibition and reducing tumor volume (Chen et al., 2019). CAR also reverses burn-induced intracellular Na + accumulation and cell apoptosis involved in PI3K/Akt and p38 MAPK pathways (Fang et al., 2020). Inhibition of NHE1 exerts potent cardioprotective effects against ischemia/reperfusion-induced heart injury through activation of Akt/GSK-3β survival pathway (Jung et al., 2010). Additionally, gene inactivation of NHE1 attenuates transient focal cerebral ischemia induced-apoptosis and mitochondrial injury (Wang et al., 2008). NHE1 inhibition also ameliorates peripheral diabetic nephropathy, as well as alleviates atherosclerotic lesion growth and promotes plaque stability by inhibiting the inflammatory reaction (Li et al., 2014). Moreover, inhibition of NHE1 by its inhibitor amiloride significantly enhances the intracellular accumulation of DOX in DOX-resistant human colon cancer cells and thereby increases their treatment (Miraglia et al., 2005). A recent study reported that citronellal could ameliorate DOX-induced cardiotoxicity by inhibiting the NHE1-mediated oxidative stress, apoptosis in rats (Liu X. et al., 2021). Considering the effects of NHE1 in oxidative stress, inflammation, apoptosis and sensitivity of DOX, we hypothesized that its selective inhibitor CAR not only enhanced the anticancer effect of DOX, but also might have the protective effect against DOX-induced cardiotoxicity.

Therefore, the present study was undertaken to investigate the protective effects of CAR against DOX-induced cardiotoxicity in rats, and to elucidate the underlying mechanisms of its cardioprotective effects. Our findings demonstrated that CAR could alleviate DOX-induced cardiotoxicity via suppression of oxidative stress, inflammation and apoptosis, which was at least partially through regulation of Akt/GSK-3β and Sirt1 signaling pathway. The potent protective effects of CAR against DOX-induced cardiotoxicity in rats have not been reported to date, and it is the first time to report Sirt1 signaling pathway is involved in the cardio-protective effect of CAR. These results reveal a novel role of CAR in DOX-induced cardiotoxicity and suggest that NHE1 may be a therapeutic target for lessening DOX-induced cardiac damage.

MATERIALS AND METHODS

Materials

CAR was purchased from Santa Cruz Biotechnology (Santa Cruz, CA, United States). DOX and nicotinamide were purchased from Aladdin Technology (Shanghai, China). Anti-Bcl-2, anti-Bax,

anti-Akt, anti-GSK-3β, anti-phospho-Akt, anti-phospho-GSK-3β, anti-Sirt1, and anti-GAPDH were purchased from Santa Cruz Biotechnology (Santa Cruz, CA, United States). The test kits of creatine kinase-MB fraction (CK-MB), lactate dehydrogenase (LDH), malondialdehyde (MDA), superoxide dismutase (SOD), glutathione peroxidase (GSH-Px) and catalase (CAT) were purchased from Nanjing Jiancheng Biotechnology Institute (Nanjing, China). The CCK-8 kit was purchased from Wuhan Saiweier Biotechnology Co., Ltd (Wuhan, China). The test kit of cTnT was purchased from Milliplex Company (Darmstadt, Germany). The ELISA test kits of tumor necrosis factor-alpha (TNF-α), interleukin-6 (IL-6), interleukin-18 (IL-18) and interleukin-1β (IL-1β) were purchased from Dakewe Biotec Company (Beijing, China). The *In Situ* Cell Death Detection Kit was purchased from Roche Company (Mannheim, Germany). TRIzol reagent was purchased from Invitrogen Corporation (Carlsbad, CA, United States). All other chemicals were purchased in the highest grade available from Sigma-Aldrich Corporation (St. Louis, MO, United States).

Animals and Experimental Design

Thirty-two adult male Sprague-Dawley rats weighing 280–310 g were obtained from the Experimental Animal Research Center of Hubei Province (Certificate No. SCXK [E] 2015–0018, Wuhan, China). All animal procedures and experiments described in this study were approved by the Review Committee for the Use of Human or Animal Subjects of Hubei University of Science and Technology. The animals were housed under controlled environmental conditions of humidity (40%–50%) and temperature (25 ± 2°C) with natural light and dark cycles (12 h: 12 h) and were allowed free access to food and water.

Rats were randomly divided into four groups (8 per group): Control group (CON), DOX group (DOX), DOX with CAR treatment group (DOX + CAR), and CAR group (CAR). Rats in CON group were received standard laboratory diet and drinking water. Rats in DOX group were intraperitoneally (i.p.) injected with DOX (2.5 mg/kg, every other day) over a period of 12 days for a cumulative dose of 15 mg/kg as described previously (Siveski-Iliskovic et al., 1994). Rats in DOX + CAR group were injected with DOX (i.p.) at a dose of 2.5 mg/kg every other day for a cumulative dose of 15 mg/kg and simultaneously treated with CAR (1 mg kg^{-1} day^{-1}) once a day over a period of 12 days. Rats in CAR group were treated with CAR (1 mg kg^{-1} day^{-1}) once a day over a period of 12 days.

Detection of Myocardial Injury Markers

The levels of myocardial enzymes CK-MB, and LDH activities in the serum, which were considered as the pivotal diagnostic indicators of myocardial injury, were tested following the manufacturer's protocols (Nanjing Jiancheng Biotechnology Institute, China). The level of cTnT was measured according to the manufacturer's guideline (Milliplex Company, Darmstadt, Germany).

Assessment of Left Ventricular Function

At the end of the experiment, transthoracic echocardiography was performed in all groups under isoflurane (1%–3%) anesthesia using an echocardiography system (Vevo 2100, VisualSonics, Canada). The echocardiography parameters were as follows: left ventricular end-diastolic diameter (LVEDD) and left ventricular end-systolic diameter (LVESD). To assess left ventricular systolic function, the ejection fraction (EF) and fractional shortening (FS) were also calculated.

Morphological and Ultra-Structural Examination

The left ventricles of the heart samples were removed and fixed by immersion in 10% formalin. Subsequently, parts of the left ventricles were embedded in paraffin wax, cut into 3-μm-thick sections, stained with hematoxylin-eosin (HE) staining or Masson's staining respectively, and examined under a light microscope (CKX41, 170 Olympus, Tokyo, Japan) at total magnifications of ×400 by a pathologist blinded to this study. For ultra-structural examination, the samples were immersed with 2.5% glutaraldehyde for 2 h and were fixed in 1% osmic acid for 3 h. After embedding in paraffin, ultra-thin sections (60–80 nm) were stained with 3% uranyl acetate and lead citrate, and were then examined by transmission electron microscope (TEM, HT7700 120 kv, HITACHI, Japan). The qualitative analysis of histopathological changes was performed as none (-) to severe (+++) according to the degree of inflammation, myocardial disorganization, and myofibrillar loss, which are listed in **Table 1**. The scoring system was as follows (-) no damage, (+) mild damage, (++) moderate damage, and (+++) severe damage.

Assessment of Biochemical Parameters

The content of MDA and the activities of antioxidant enzymes including SOD, GSH-Px, and CAT in heart homogenates were measured according to the manufacturer's instructions (Nanjing Jiancheng Biotechnology Institute, China). The levels of TNF-α, IL-6, IL-18, and IL-1β in serum were determined with ELISA test kits from Dakewe Biotec Company (Beijing, China) following the manufacturer's protocols.

Cell Culture and Detection of Cellular ROS

The H9c2 cell line was purchased from the China Center for Type Culture Collection (CCTCC, China), and cultured in Dulbecco's modified Eagle's medium with fetal bovine serum (10%), streptomycin (1%), and penicillin. The culture conditions contained a humidified atmosphere (95% air and 5% CO_2 at 37°C). The H9c2 cells were incubated with DOX (1 μmol/L) for 72 h with or without CAR(5 μmol/L) and Sirt1 inhibitor (nicotinamide, 10 μmol/L). The cell viability was detected by a CCK-8 kit. The ROS-level was measured by dihydroethidium (DHE, Beyotime Biotechnology, China), an indicative fluorescence probe, which was used to detect intracellular superoxide anions.

Quantitative Real-Time PCR

Total RNAs were extracted from cardiac tissues by using the TRIzol reagent (TaKaRa, Japan) according to the manufacturer's instructions. cDNA synthesis was performed with HiScriptIIQ RT SuperMix (Vazyme, China) according to the manufacturer's instructions. Quantitative RT-PCR was performed with ChamQ

TABLE 1 | Effect of CAR on morphological changes as assessed by histopathological examination of hearts from the DOX-treated rats.

Groups	n	Inflammation	Myocardial Disorganization	Interstitial Fibrosis
CON	12	(-)	(-)	(-)
DOX	9	(+) to (++)	(++) to (+++)	(+) to (++)
DOX + CAR	13	(-) to (+)	(+) to (++)	(-) to (+)
CAR	12	(-)	(-)	(-)

(–): none; (+): mild; (++): moderate; (+++): severe.

SYBR qPCR Master Mix (Vazyme, China) according to the protocol. GAPDH was used as the reference gene.

Terminal Deoxynucleotidyl Transferase-Mediated dUTP Nick End-Labelling Assay

Cardiac apoptotic cells were tested by TUNEL staining which was often used for detecting DNA fragmentation. The TUNEL assay was performed according to the manufacturer's protocol and instructions provided in the *In Situ* Cell Death Detection Kit supplied by Roche Company (Mannheim, Germany). The results were examined and the apoptotic index was calculated under a light microscope (CKX41, 170 Olympus, Tokyo, Japan) at a total magnification of ×400 by a pathologist blinded to this study.

Western Blot Analysis

Equal amounts of protein from hippocampal homogenates were separated by 10% SDS-PAGE gels and then transferred to PVDF membranes. The membranes were blocked for 1 h at room temperature in 5% non fat milk. After being incubated overnight at 4°C with the appropriate primary antibodies including Bcl-2, Bax, phospho-Akt, Akt, phospho-GSK-3β, GSK-3β, Sirt1, and GAPDH (Santa Cruz, CA, United States), the membranes were washed 15 min with TBST three times and then incubated with the secondary antibody for 1 h at room temperature. The blots were then imaged using ECL assay kits (Dalian Meilun Biotech Co., Ltd, China). The band intensities were quantified using NIH ImageJ 1.50 software and normalized to the quantity of GAPDH in each sample lane. All assays were performed at least three times.

Statistics

The values are expressed as means ± SEM. Data were analyzed One-way ANOVA followed by post hoc Tukey's test by employing GraphPad Prism Version 5.0. p values of 0.05 or less were considered to be statistically significant.

RESULTS

CAR Reinstated Body Weight and Myocardial Marker Enzymes in DOX-Induced Cardiotoxicity in Rats

As compared to CON group, the body weight dramatically decreased in DOX group ($p < 0.01$ vs. CON, **Figure 1A**). Administration of CAR resulted in a significant prevention of DOX-induced decrease in body weight ($p < 0.01$ vs. DOX, **Figure 1A**). To further confirm the protective effects of CAR against DOX-induced cardiotoxicity, we tested the serum levels of cardiac enzymes (CK-MB, LDH, and cTnT), which represented the biochemical markers of myocardial injury. As shown in **Figures 1B–D**, treatment with DOX caused significantly elevated serum levels of CK-MB, LDH, and cTnT as compared to CON group ($p < 0.01$ vs. CON for all). Administration of CAR ($10\ mg\ kg^{-1}\ day^{-1}$) caused a reversal of DOX-induced increase in serum cardiac enzymes ($p < 0.01$ vs. DOX for all). Moreover, no significant changes in body weight and serum cardiac enzymes were observed in CAR group as compared to CON group, demonstrating that the dose of CAR used in this study ($10\ mg\ kg^{-1}\ day^{-1}$) did not affect body weight and myocardial marker enzymes of the rats.

CAR Prevented DOX-Induced Left Ventricular Dysfunction

Next, we conducted an echocardiography analysis of left ventricular function. Representative pictures of heart function were shown in **Figure 1E**. Administration of DOX resulted in a significant increase of LVEDD and LVESD ($p < 0.05$, $p < 0.05$ vs. CON), both of which were preserved by CAR treatment ($p < 0.05$, $p < 0.05$ vs. DOX, **Figures 1F,G**). Furthermore, FS and EF, the index of left ventricular systolic function, decreased dramatically in DOX group ($p < 0.05$, $p < 0.01$ vs. CON). CAR treatment significantly ameliorated the reduction of FS and EF caused by DOX ($p < 0.05$, $p < 0.05$ vs. DOX, **Figures 1H,I**). In addition, CAR alone had no effect on left ventricular function. These data suggest that CAR can ameliorate the impairment of heart function induced by DOX.

Histopathological and Ultra-structural Analysis by HE Staining, Masson's Staining, and TEM

To assess cardiac morphological alterations, sections of rat heart tissue were stained with HE or Masson's staining, and examined by light microscopy. As shown in **Figure 3**, DOX-induced cardiotoxicity was characterized by mild focal inflammation, myofibrillar loss, swelling, and fibrosis. Our results revealed that CAR treatment significantly

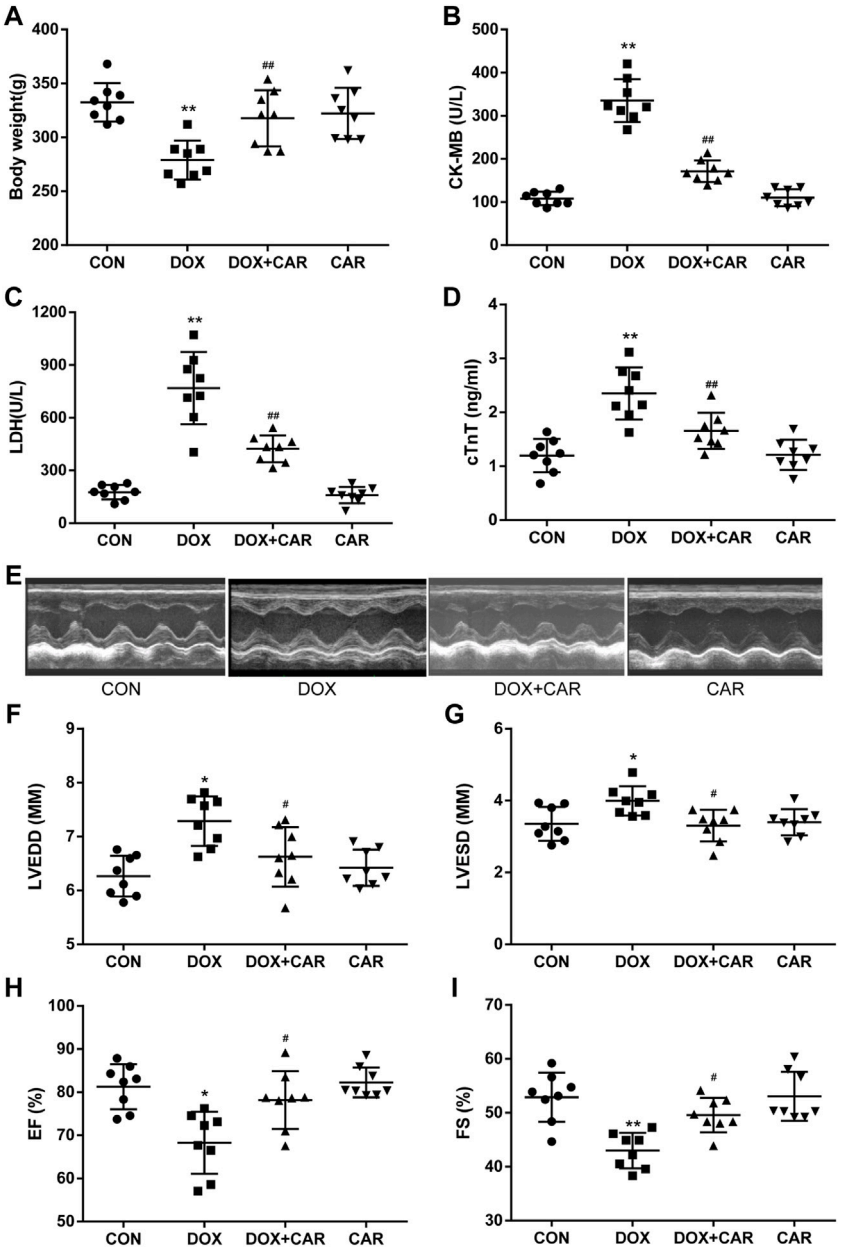

FIGURE 1 | CAR reinstated body weight, myocardial marker enzymes and left ventricular dysfunction in DOX-induced cardiotoxicity in rats. **(A)** body weight, **(B)** LDH, **(C)** CK-MB, **(D)** cTnT, **(E)** Representative pictures of heart function, **(F)** LVEDD, **(G)** LVESD, **(H)** EF, and **(I)** FS. Quantitative data are means ± SEM (n = 8). One-way ANOVA followed by post hoc Tukey's test. *$p < 0.05$, **$p < 0.01$ vs. CON; #$p < 0.05$, ##$p < 0.01$ vs. DOX.

ameliorated DOX-induced lesions on myocardial morphology (**Figure 3A**), and mitigated the cardiac fibrosis (**Figure 3B**). TEM performed for the myocardium showed that treatment with DOX caused marked ultra-structural aberration leading to myofibrillar disintegration, damage of Z-band and M-band, and irregular mitochondria (**Figures 3C,D**). The qualitative analysis of histopathological changes were shown in **Table 1**. Treatment with CAR markedly improved the irregular and disintegrated sarcomere, restored the Z-band and M-band, and reduced the damaged mitochondria.

CAR Alleviated Oxidative Stress Induced by DOX

It is well established that oxidative stress plays a critical role in DOX-induced cardiotoxicity. Therefore we investigated the effects of CAR on markers of oxidative stress, including MDA and the antioxidant enzymes (SOD, GSH-Px, and CAT). As expected, DOX administration resulted in a significant increased level of MDA and a significant decreased activities of SOD, GSH-Px, and CAT as compared to CON group ($p < 0.01$, $p < 0.01$, $p < 0.01$, $p < 0.05$ vs. CON). However, treatment with

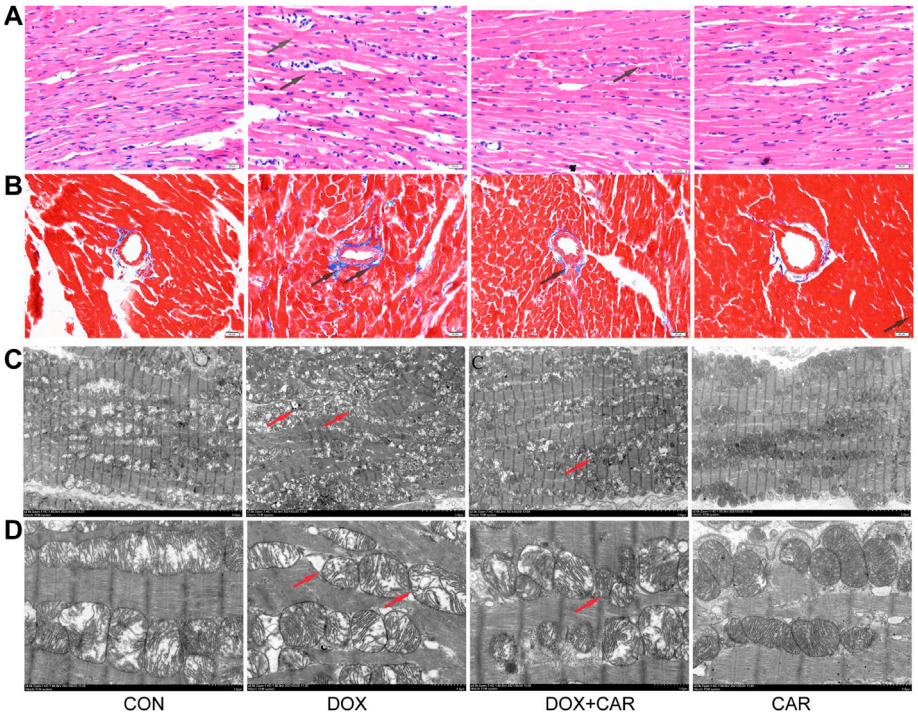

FIGURE 2 | CAR attenuated the pathological alterations in myocardial tissues of DOX-treated hearts. Representative pictures of myocardial tissue sections stained with H&E and Masson (magnification = ×400) **(A)** H&E staining, **(B)** Masson; n = 3, Bar = 20 μm. Representative images of myocardial tissue sections tested by TEM **(C)**, the magnification is 1.5 K times (Scale = 5 μm). Representative images of myocardial tissue sections tested by TEM **(D)**, the magnification is 5.0 K times (Scale = 2 μm).

CAR significantly prevented DOX-induced increased level of MDA and decreased activities of SOD, GSH-Px, and CAT ($p < 0.01$, $p < 0.01$, $p < 0.01$, $p < 0.05$ vs. DOX, **Figures 3A–D**). Administration of CAR alone had no significant effect on the level of MDA or the activities of SOD, GSH-Px, and CAT as compared to CON group.

DOX-induced ROS level *in vitro* was also detected by using DHE as a fluorescent probe. The results showed that H9c2 cells treated with DOX alone showed greater red fluorescence, indicating that DOX treatment led a clear increase in intracellular ROS levels. On the other hand, the red fluorescence in the cells treated with the combination of DOX and CAR exhibited largely reduced brightness when compared with those cells treated with DOX only, demonstrating that CAR could prevent intracellular ROS production (**Figure 3E**). These results suggest that CAR may protect against DOX-induced cardiotoxicity at least partially through suppression of oxidative stress.

Effect of CAR on Inflammation Following DOX-Induced Cardiotoxicity

Since several inflammatory cytokines are associated with the pathological injury caused by DOX-induced cardiotoxicity, the serum levels and mRNA expressions of TNF-α, IL-6, IL-18, and IL-1β in heart tissues were then tested. As expected, the serum levels and cardiac mRNA expressions of TNF-α, IL-6, IL-18, and IL-1β were dramatically elevated in DOX group ($p < 0.01$ vs. CON for all, Figures A, B, C, and D indicated serum levels of TNF-α, IL-6, IL-18, and IL-1β; Fig. E, F, G and H indicated mRNA of TNF-α, IL-6, IL-18, and IL-1β). On the other hand, treatment with CAR protected against DOX-induced increase of serum levels and cardiac mRNA expressions of TNF-α, IL-6, IL-18, and IL-1β (serum levels $p < 0.01$, $p < 0.01$, $p < 0.01$, $p < 0.05$; mRNA expressions $p < 0.05$ vs. DOX for all). Administration of CAR alone did not significantly alter the serum levels and cardiac mRNA expressions of these inflammatory cytokines. Therefore, in addition to preventing DOX-induced oxidative stress, CAR may also prevent DOX-induced cardiotoxicity via downregulation of pathological inflammatory cytokines.

CAR Inhibited Cardiomyocyte Apoptosis Induced by DOX

As DOX-induced cardiotoxicity is known to involve in the induction of apoptosis in cardiomyocytes, we tested whether the protective effect of CAR included the ability to prevent cardiomyocyte apoptosis by using TUNEL staining of heart tissues. As shown in **Figure 5A**, DOX caused a significant increase of apoptotic cells (pink staining) compared to CON group ($p < 0.01$ vs. CON, **Figure 5B**). CAR treatment was able to partially prevent DOX-induced increase of cardiomyocyte apoptosis ($p < 0.05$ vs. DOX), while CAR treatment alone had no significant effect.

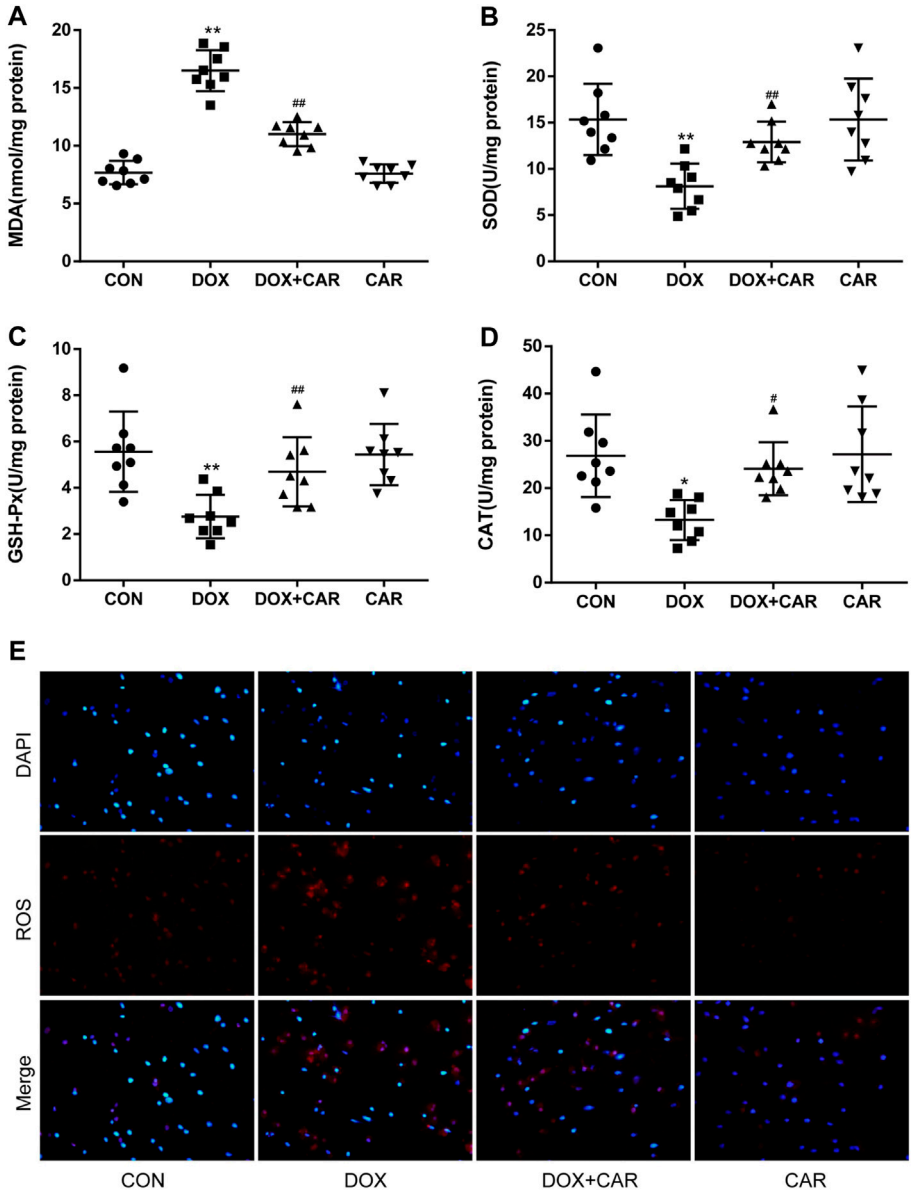

FIGURE 3 | CAR alleviated oxidative stress in myocardial tissues in rat and H9c2 cells treated with DOX. Quantitative analysis **(A)** MDA, **(B)** SOD, **(C)** GSH-Px, and **(D)** CAT. Representative images of cells stained with DAPI and DHE **(E)**, Scale = 20 μm. Quantitative data are means ± SEM (n = 8). One-way ANOVA followed by post hoc Tukey's test. *p < 0.05, **p < 0.01 vs. CON; #p < 0.05, ##p < 0.01 vs. DOX.

To further investigate the ability of CAR to prevent DOX-induced apoptosis, we analyzed the apoptosis related proteins including Bcl-2, Bax and Cleaved-Caspase-3 in heart tissues using Western blot. As shown in **Figures 5C**, administration of DOX resulted insignificant increased expressions of Bax and Cleaved-Caspase-3, whereas the Bcl-2 protein level was significantly decreased. In contrast, CAR treatment markedly reversed DOX-mediated protein changes of Bcl-2, Bax and Cleaved-Caspase-3, as well as partially normalized the Bcl-2/Bax ratio (p < 0.05, p < 0.05 vs. DOX). No significant differences were detected in the protein levels of Bcl-2, Bax, and Cleaved-Caspase-3 between CAR and CON groups. It is tempting to speculate that this phenomenon may partially explain CAR's ability to prevent DOX-induced cardiotoxicity by reducing apoptosis in cardiomyocytes.

Effect of CAR on Akt/GSK-3β Signaling Following DOX-Induced Cardiotoxicity

As previous studies have indicated that the cardioprotective and anti-hypertrophic effects of NHE1 inhibition were involved in the activation of Akt/GSK-3β signaling pathway (Javadov et al., 2009; Jung et al., 2010), we investigated the phosphorylation levels of Akt and its downstream target protein GSK-3β by Western blot.

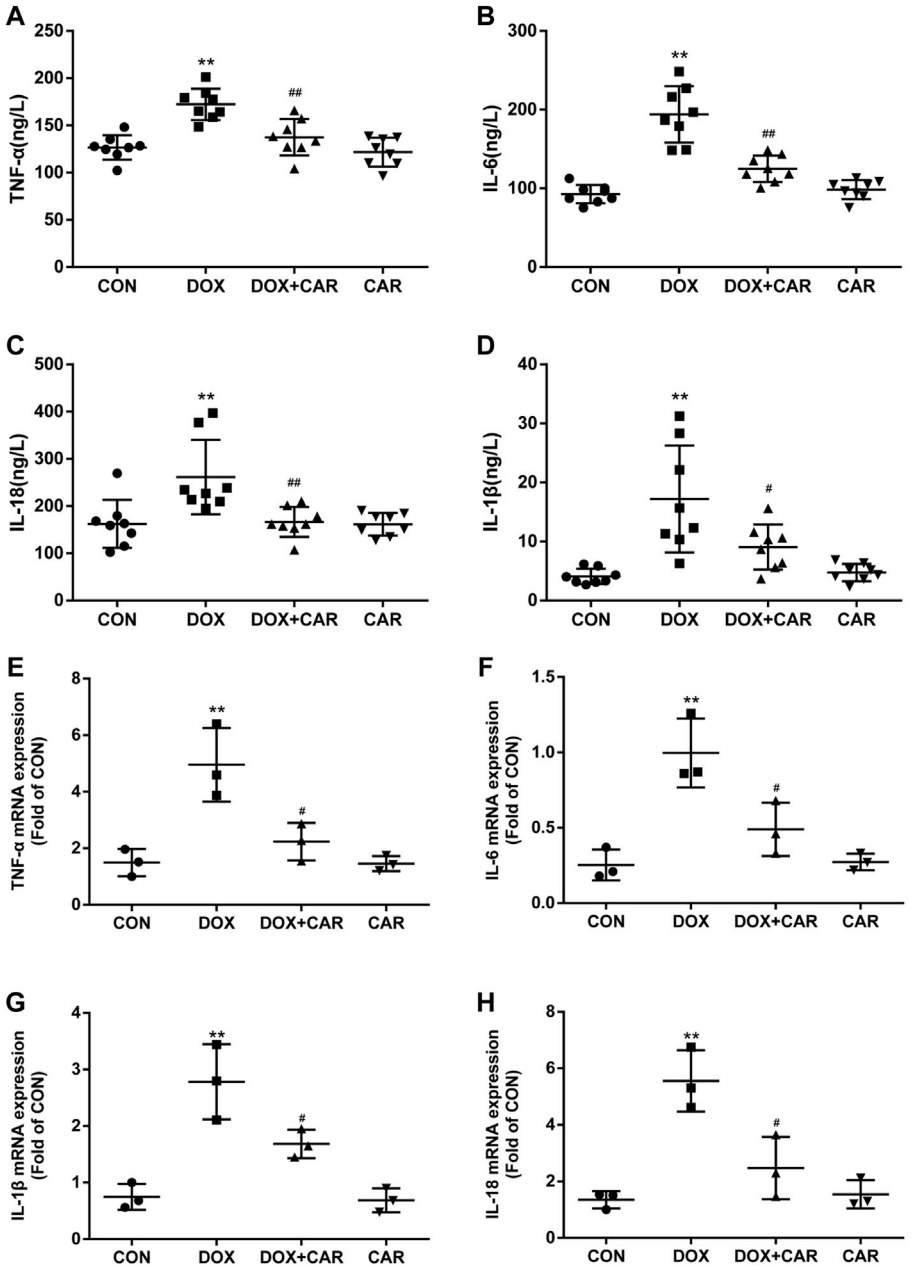

FIGURE 4 | CAR alleviated the serum levels and mRNA expressions of inflammatory cytokines in DOX-treated rats. Quantitative analysis of serum levels **(A)** TNF-α, **(B)** IL-6, **(C)** IL-18 and **(D)** IL-1β; Quantitative data are means ± SEM (n = 8). Quantitative analysis of mRNA expressions **(E)** TNF-α, **(F)** IL-6, (G) IL-18 and **(H)** IL-1β. Quantitative data are means ± SEM (n = 3). One-way ANOVA followed by post hoc Tukey's test. $^{**}p < 0.01$ vs. CON; $\#p < 0.05$, $\#\#p < 0.01$ vs. DOX.

As shown in **Figures 6A,B**, the phosphorylation levels of Akt and GSK-3β significantly decreased by administration of DOX. In contrast, treatment with CAR attenuated DOX-induced decrease in phosphorylation of both Akt and GSK-3β ($p < 0.05$, $p < 0.05$ vs. DOX, **Figures 6C,D**). None of DOX or CAR significantly altered the total Akt and GSK-3β protein levels. These data suggest that CAR may protect against DOX-induced cardiotoxicity via activating Akt/GSK-3β survival signaling pathway.

Sirt1 Involved in the Cardioprotective Effect of CAR Against DOX-Induced Cardiotoxicity

Previous studies have revealed that Sirt1 was decreased in DOX treated heart or H9c2 cardiac cells (Zhang S. et al., 2021; Liu Y. et al., 2021; Zhang WB. et al., 2021), and PI3K-Akt-GSK3β signaling pathway is required for Sirt1 induction by endoplasmic reticulum stress (Koga et al., 2015), we then tested the protein expression of Sirt1. Both in DOX treated

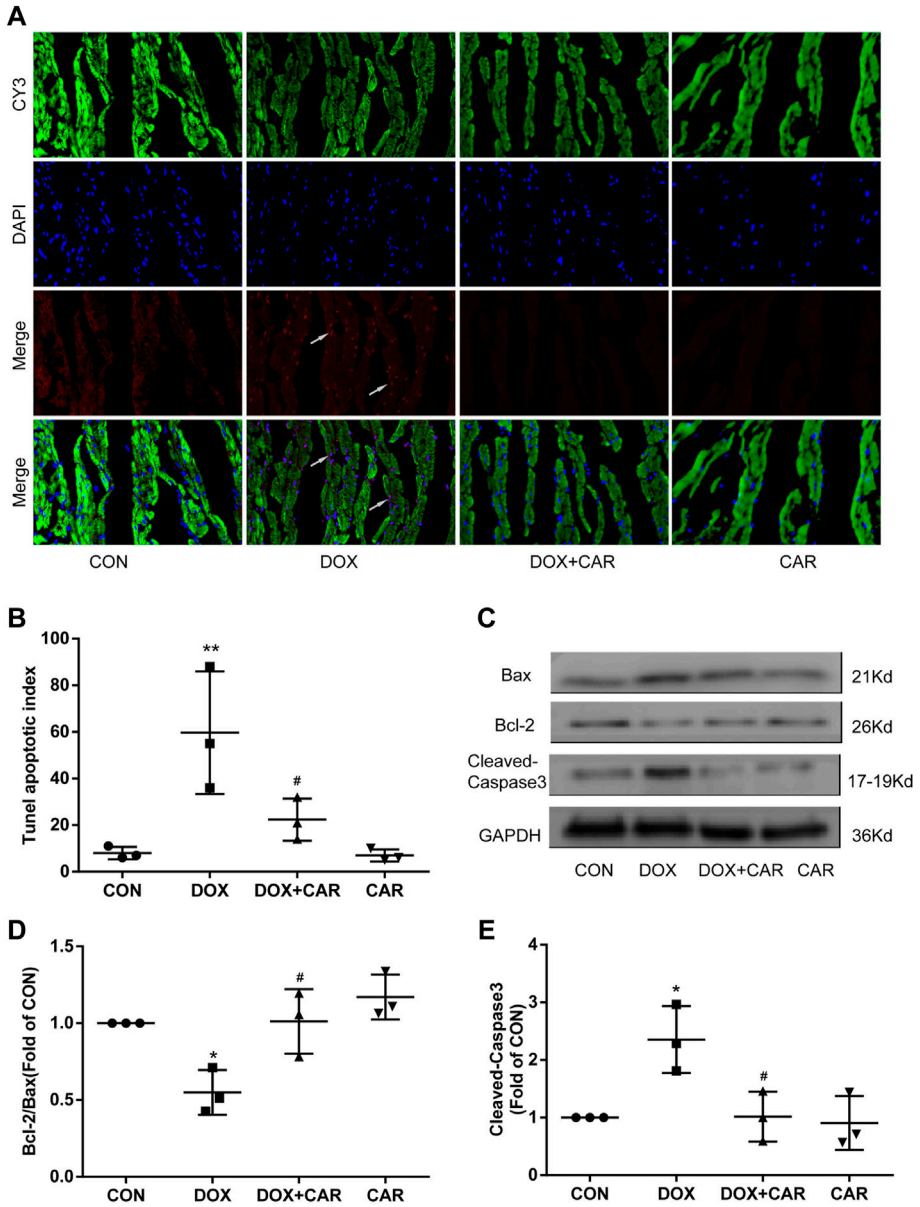

FIGURE 5 | CAR inhibited cardiomyocyte apoptosis induced by DOX. **(A)**: Representative pictures of the TUNEL assay, **(B)**: Histogram representing quantitative analysis of the apoptotic index, **(C)**: Representative western blots of Bcl-2, Bax and Cleaved-Caspase-3, **(D)**: Histogram representing the quantitative analysis of the ratio of Bcl-2/Bax, **(E)**: Histogram representing the quantitative analysis of Cleaved-Caspase-3. Quantitative data are means ± SEM (n = 3). *$p < 0.05$, **$p < 0.01$ vs. CON; #$p < 0.05$ vs. DOX.

mice and H9c2 cell, the protein expressions of Sirt1 decreased significantly, which were restored by CAR treatment ($p < 0.05$, $p < 0.05$ vs. DOX, **Figures 7A–D**). Nicotinamide, an inhibitor of Sirt1, reversed the protective effect of CAR by downregulating the protein expression of Sirt1 and reducing H9c2 cell viability ($p < 0.05$, vs. DOX, **Figure 7E**, G; $p > 0.05$ vs. DOX + CAR, and **Figure 7F**). These data suggest that activating Sirt1 pathway may mediate the cardioprotective role of CAR against DOX-induced cardiotoxicity.

DISCUSSION

Here, we demonstrated for the first time that CAR treatment suppressed DOX-induced cardiotoxicity, as indicated by improving cardiac function, reducing oxidative damage, inhibiting inflammatory response, and alleviating myocardial apoptosis. In addition, we found that Akt/GSK-3β signaling pathway was involved in the protective effects of CAR. Furthermore, the results from the present study also

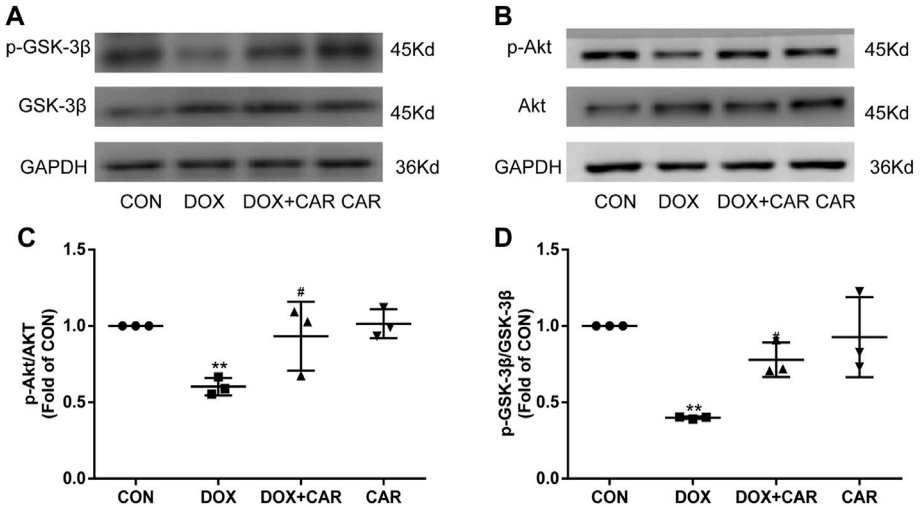

FIGURE 6 | Effect of CAR on Akt/GSK-3β signaling following DOX-induced cardiotoxicity. **(A)**: Representative western blots of GSK-3β, **(B)**: Representative western blots of Akt, **(C)**: Histogram representing the quantitative analysis of GSK-3β, **(D)**: Histogram representing the quantitative analysis of Akt. Quantitative data are means ± SEM (n = 3). $^{**}p < 0.01$ vs. CON; $\#p < 0.05 < 0.01$ vs. DOX.

demonstrated that these protective effects of CAR were mediated by the activation of Sirt1 *in vivo* and *in vitro*, and Sirt1 inhibition abolished CAR treatment-mediated cardiac protection. Collectively, our data suggest that CAR may be a potential therapeutic drug and NHE1 may be a potential therapeutic target for the prevention and treatment of DOX-induced cardiotoxicity.

Doxorubicin is a well-established chemotherapeutic agent widely used in the treatment of hematological malignancies and solid tumors. Unfortunately, there are numerous serious toxicities associated with DOX treatment, particularly on the cardiovascular system, which severely limits its clinical use. The dose of DOX used in the present study (15 mg/kg) was comparable with the typical dose given to cancer patients (Venturini et al., 1996; Xiao et al., 2012). Our data demonstrated that this dosage of DOX resulted in cardiotoxicity in rats as evidenced by decreased body weight, elevated serum levels of cardiotoxicity biomarker enzymes, as well as alterations in heart function and cardiac histopathological damage. On the contrary, administration of CAR increased the body weight, attenuated the increased levels of serum CK-MB, LDH, and cTnT, improved the impairment of left ventricular function, as well as ameliorated the histopathological damage of the heart caused by DOX treatment, suggesting that CAR exerted a prominent protective effect against DOX-induced cardiotoxicity. In addition, the dose of CAR used in this experiment (10 mg kg^{-1} day^{-1}) did not cause any cardiotoxicity, thus warranting further investigation into the possible molecular mechanisms underlying its cardioprotective effects.

Given the established role of oxidative stress in DOX-induced cardiotoxicity (Xu et al., 2001; Zhang et al., 2017), we first investigated the effect of CAR on biomarkers of oxidative stress in heart tissues. Excessive production of free radicals can cause oxidative damage to nearly all types of biological molecules, leading to numerous disease states (Halliwell and Gutteridge, 1990). Over-production of ROS leads to damage of nuclear and mitochondrial DNA, altered calcium homeostasis, decreased protein synthesis, and cardiomyocyte death. Numerous oxidative stress markers, including lipidperoxidation and lipid aldehydes, are found in heart tissues after DOX treatment (Chaiswing et al., 2004; Zhang et al., 2017). In agreement with this, our results showed that DOX-induced cardiotoxicity in rats was associated with significant increase of cardiac MDA level as well as reduced activities of the cardiac antioxidant enzymes (GSH-Px, SOD, and CAT). Notably, treatment with CAR significantly inhibited MDA production and prevented the decreased activities of cardiac GSH-Px, SOD, and CAT in rats subjected to DOX. A recent study indicated that DOX-induced ROS production in the H9c2 cells quantified with a fluorescent probe was inhibited by treatment with pinocembrin (Sangweni et al., 2020). In our results, H9c2 cells treated with DOX exhibited a clear increase in intracellular ROS level, which was reversed by CAR treatment. Therefore, suppressing oxidative stress may be one of the primary mechanisms by which CAR protects against DOX-induced cardiotoxicity.

In addition to directly causing deleterious effects, oxidative stress in the heart can also lead to inflammation, which is known to be involved in a variety of cardiovascular diseases, including atherosclerosis, atrial fibrillation, and inflammatory cardiomyopathies. Prior research has suggested that there is a strong association between cardiac oxidative stress and inflammatory cytokine release after DOX treatment (Bien et al., 2007). TNF-α, IL-6, IL-18, and IL-1β are the common proinflammatory cytokines involved in DOX-induced cardiotoxicity and are increased in individuals who have cardiac dysfunction (Miettinen et al., 2008; Tamariz and Hare, 2010). In agreement with the prior studies (Wang et al., 2016), we found that DOX application in rats led to increased serum levels and cardiac mRNA expressions of TNF-α, IL-6, IL-18, and IL-1β. CAR treatment prevented the increased serum levels of these proinflammatory cytokines and their cardiac mRNA expressions.

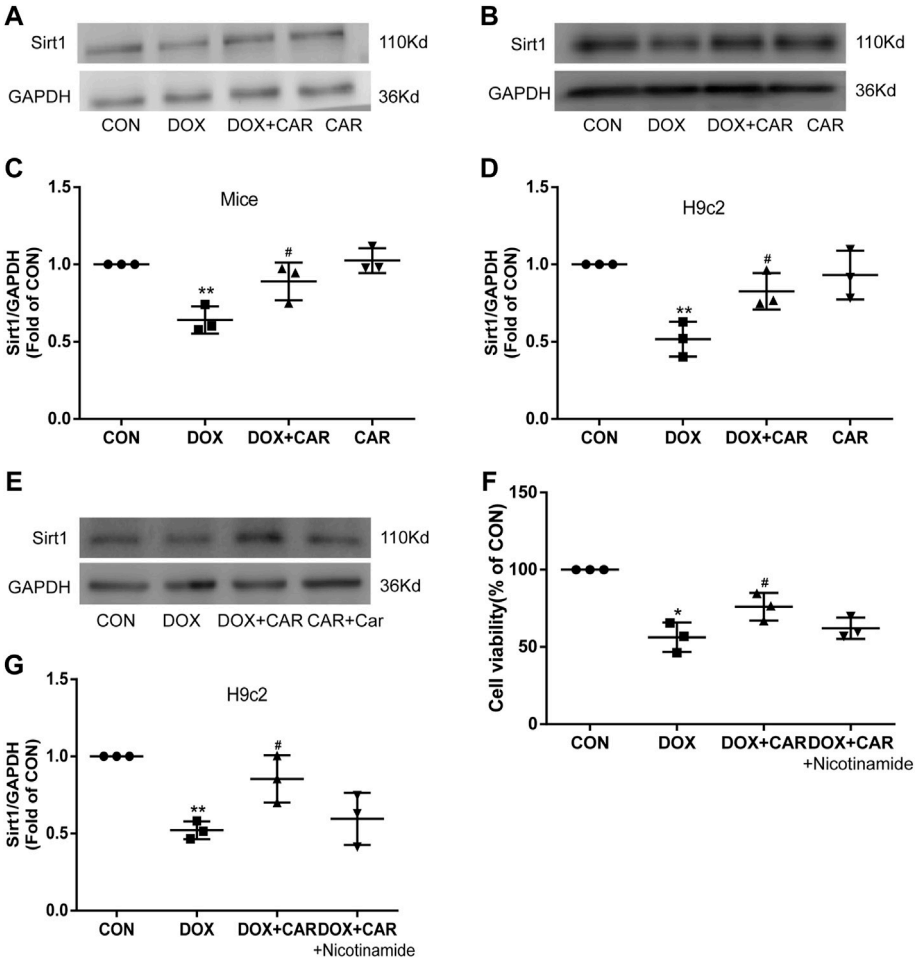

FIGURE 7 | Sirt1 was involved in the cardioprotective effect of CAR against DOX-induced cardiotoxicity. **(A)**: Representative western blots of Sirt1 in cardiac tissues of mice, **(B)**: Representative western blots of Sirt1 in H9c2 cells, **(C)**: Histogram representing the quantitative analysis of Sirt1 in cardiac tissues of mice, **(D)**: Histogram representing the quantitative analysis of Sirt1 in H9c2 cells, **(E)**: Representative Western blots of Sirt1 in H9c2 cells treated with the inhibitor, **(F)**: The cell viability measured by CCK-8, **(G)**: Histogram representing the quantitative analysis of Sirt1 in H9c2 cells treated with inhibitor. Quantitative data are means ± SEM (n = 3). $^{*}p < 0.05$, $^{**}p < 0.01$ vs. CON; $\#p < 0.05$ vs. DOX.

It is interesting to speculate that alongside its antioxidant effects, anti-inflammatory properties may be also responsible for the protective effect of CAR against DOX-induced cardiotoxicity.

Beyond the damage inflicted by ROS and inflammation, myocardial apoptosis is believed to be the fundamental basis of DOX-induced cardiotoxicity (Kalay et al., 2006). β-Hydroxybutyrate, a small lipid-derived molecule derived from increased free fatty, could protect against DOX-induced cardiotoxicity by inhibiting cell apoptosis and oxidative stress and maintaining mitochondrial membrane integrity (Liu et al., 2020). Also, CAR treatment has been found to significantly suppress the induction of TUNEL-positive cardiomyocytes in cardiac hypoxia/reoxygenation. Therefore, we also examined the effect of CAR on myocardial apoptosis induced by DOX. As differential induction of apoptosis in cardiomyocytes caused by DOX treatment has been reported in different experimental animal models (Hou et al., 2006; Ruan et al., 2015; Argun et al., 2016), we observed increased TUNEL-positive cardiomyocytes following DOX treatment over a period of 12 days in rats, consistent with a previous study (Argun et al., 2016). Importantly, CAR treatment significantly inhibited DOX-induced myocardial cell apoptosis, thereby improving its myocardial toxicity.

In many cell types, apoptosis is regulated by Bcl-2 protein family. The pro-apoptotic Bax protein and anti-apoptotic Bcl-2 protein play a major role in determining whether or not cells undergo apoptosis. The translocation of Bax from the cytoplasm to mitochondria results in cytochrome c release from the mitochondria to promote apoptosis, while Bcl-2 can prevent the release of cytochrome c from mitochondria and suppress apoptosis progression (Scorrano and Korsmeyer, 2003). A recent study found that DOX administration increased Bax expression and decreased Bcl-2 expression in H9c2 cells (Liu et al., 2016). Prior research also suggested that CAR reduced mitochondrial Ca2+, the number of PI and TUNEL positive cells, cytosolic cytochrome c, caspase-3 activity, and ratio of Bax and Bcl-2 in

primary cultured neonatal rat cardiomyocytes subjected to hypoxia/re-oxygenation (Sun et al., 2004). Our results revealed that treatment with DOX significantly reduced Bcl-2/Bax ratio and elevated the Cleaved-Caspase-3 protein expression in the heart, which was reversed significantly by administration of CAR. These results highly suggest that the cardioprotective effect of CAR is also due to its ability to regulate the levels of apoptosis related proteins. However, non-caspase-dependent apoptotic pathways can also be activated under DOX or cardiac IR condition, as evidenced by AIF translocation to the nuclei in H9c2 cardiomyoblasts treated with DOX (Moreira et al., 2014) and intracytosolic translocation of AIF and endonuclease G during cardiac ischemia (Yang et al., 2017). Therefore, whether AIF and mitochondrial endonuclease G are involved in the cardioprotective effect of Car against DOX-induced cardiotoxicity needs to be further studied.

Cell survival signaling pathways, including Akt, GSK-3β and ERK1/2, are known regulators of myocardial cell survival (Li et al., 2009), suggesting that they may be pharmacological targets for the prevention of myocardial cell apoptosis under stress conditions. Notably, it has previously been shown that DOX treatment caused a remarkable reduction of Akt and GSK3β phosphorylation in mouse heart (Prysyazhna et al., 2016), and erythropoietin protects against DOX-induced cardiotoxicity by activating PI3K-Akt-GSK-3β signaling pathway, thereby reducing cardiomyocyte apoptosis (Kim et al., 2008). Shenmai injection, one of the patented traditional Chinese medicine, prevents DOX-induced cardiotoxicity through activation of PI3K/Akt/GSK-3β signaling pathway (Li et al., 2020). In agreement with prior studies, we also observed that Akt and GSK-3β phosphorylation reduced in DOX-treated hearts. Treatment with CAR significantly attenuated DOX-induced decreased phosphorylated protein expressions of Akt and GSK-3β.

Sirt1 has been suggested to play key roles in redox regulation, cell apoptosis, and inflammation (Hwang et al., 2013). A previous study showed that exposure to DOX of H9c2 cells leads to cellular injury and the reduction of Sirt1 (Liu et al., 2016). Sirt1 is also highly expressed in cardiomyocytes and involved in DOX-induced cardiotoxicity (Dolinsky, 2017). Inconsistent with these findings, we also found that DOX reduced Sirt1 protein levels *in vivo* and *in vitro*. However, Zhang (Zhang et al., 2011) reported that Sirt1 level was slightly increased by DOX treatment, and resveratrol attenuated DOX-induced cardiomyocyte apoptosis in mice through up-regulation of Sirt1. The inconsistent expressions of SIRT1 under DOX condition may be related to the different animals used and the different action time of DOX, which may need further discussion. Of note, restoration of the expression of Sirt1 by CAR treatment could improve cardiac function and attenuate DOX-related cardiac injury in mice. Moreover, inhibition of Sirt1 by nicotinamide offset the protective effects provided by CAR treatment against DOX-induced H9c2 injury. These findings suggest that CAR exerts cardiac protection partially via activating Sirt1 signaling pathway. Sirt3, another NAD + -dependent histone deacetylase, restores mitochondrial respiratory chain defects, and cell viability of DOX treated cardiomyocytes (Blasco et al., 2018). Also, NHE-1 inhibitor EMD-87580 improves cardiac mitochondrial function through regulation of mitochondrial biogenesis during posti nfarction remodeling in these hearts (Javadov et al., 2006b), and attenuates the hypertrophic phenotype via improving mitochondrial integrity and decreasing generation of mitochondrial-derived reactive oxygen species (Javadov et al., 2006a). These evidences provide the relationship between DOX cardiotoxicity and Sirt3 or mitochondrial biogenesis. Further studies are needed to clarify the precise mechanism Sirt3 and mitochondrial biogenesis in the cardioprotective effect of CAR against DOX-induced cardiotoxicity.

CONCLUSION

We demonstrate for the first time that CAR, a selective inhibitor of NHE1, exerts protective effects against DOX-induced cardiotoxicity via its antioxidant, anti-inflammatory, and anti-apoptotic activities. The results from the present study also demonstrate a role for Akt/GSK-3β and Sirt1 signaling pathway in the cardioprotective effects of CAR, and suggest that CAR may be a potential therapeutic drug and NHE1 may be a potential therapeutic target for the prevention and treatment of DOX-induced cardiotoxicity.

DATA AVAILABILITY STATEMENT

The original contributions presented in the study are included in the article/supplementary material, further inquiries can be directed to the corresponding authors.

ETHICS STATEMENT

The animal study was reviewed and approved by Review Committee for the Use of Human or Animal Subjects of Hubei University of Science and Technology.

AUTHOR CONTRIBUTIONS

CL and YC conceived and designed the experiments; WL performed the experiments; LW contributed to reagents; CL and ZR wrote the manuscript. All authors gave final approval and agree to be accountable for all aspects of work ensuring integrity and accuracy.

FUNDING

This work was supported by the grants from Hubei University of Science and Technology (2021WG03, 2022T01), Hubei Provincial Health Commission (WJ 2021M090), Department of Education of Hubei Province (T201921, B2021225), Xianning Science and Technology Bureau (2020ZRKX02, 2021ZRKX039) and the Natural Science Foundation of Hubei Province (2020CFB866).

REFERENCES

Alkreathy, H., Damanhouri, Z. A., Ahmed, N., Slevin, M., Ali, S. S., and Osman, A. M. (2010). Aged Garlic Extract Protects against Doxorubicin-Induced Cardiotoxicity in Rats. *Food Chem. Toxicol.* 48 (3), 951–956. doi:10.1016/j.fct.2010.01.005

Argun, M., Üzüm, K., Sönmez, M. F., Özyurt, A., Derya, K., Çilenk, K. T., et al. (2016). Cardioprotective Effect of Metformin against Doxorubicin Cardiotoxicity in Rats. *Anatol. J. Cardiol.* 16 (4), 234–241. doi:10.5152/akd.2015.6185

Bien, S., Riad, A., Ritter, C. A., Gratz, M., Olshausen, F., Westermann, D., et al. (2007). The Endothelin Receptor Blocker Bosentan Inhibits Doxorubicin-Induced Cardiomyopathy. *Cancer Res.* 67 (21), 10428–10435. doi:10.1158/0008-5472.CAN-07-1344

Blasco, N., Cámara, Y., Núñez, E., Beà, A., Barés, G., Forné, C., et al. (2018). Cardiomyocyte Hypertrophy Induced by Endonuclease G Deficiency Requires Reactive Oxygen Radicals Accumulation and Is Inhibitable by the Micropeptide Humanin. *Redox Biol.* 16, 146–156. doi:10.1016/j.redox.2018.02.021

Chaiswing, L., Cole, M. P., St Clair, D. K., Ittarat, W., Szweda, L. I., and Oberley, T. D. (2004). Oxidative Damage Precedes Nitrative Damage in Adriamycin-Induced Cardiac Mitochondrial Injury. *Toxicol. Pathol.* 32 (5), 536–547. doi:10.1080/01926230490502601

Chen, Q., Liu, Y., Zhu, X. L., Feng, F., Yang, H., and Xu, W. (2019). Increased NHE1 Expression Is Targeted by Specific Inhibitor Cariporide to Sensitize Resistant Breast Cancer Cells to Doxorubicin *In Vitro* and *In Vivo*. *BMC Cancer* 19 (1), 211. doi:10.1186/s12885-019-5397-7

Chen, Y., Huang, T., Shi, W., Fang, J., Deng, H., and Cui, G. (2020). Potential Targets for Intervention against Doxorubicin-Induced Cardiotoxicity Based on Genetic Studies: a Systematic Review of the Literature. *J. Mol. Cell. Cardiol.* 138, 88–98. doi:10.1016/j.yjmcc.2019.11.150

Dolinsky, V. W. (2017). The Role of Sirtuins in Mitochondrial Function and Doxorubicin-Induced Cardiac Dysfunction. *Biol. Chem.* 398 (9), 955–974. doi:10.1515/hsz-2016-0316

Fang, Z., Zhang, D., Yao, L., Wu, G., Zhang, Z., Deng, X., et al. (2020). Burn-Induced Apoptosis of Pulmonary Microvascular Endothelial Cell Is NHE1 Dependent and Regulated by PI3K-Akt and P38 MAPK Pathways. *Shock* 54 (6), 819–827. doi:10.1097/SHK.0000000000001573

Halliwell, B., and Gutteridge, J. M. (1990). Role of Free Radicals and Catalytic Metal Ions in Human Disease: an Overview. *Methods Enzymol.* 186, 1–85. doi:10.1016/0076-6879(90)86093-b

Hou, X. W., Son, J., Wang, Y., Ru, Y. X., Lian, Q., Majiti, W., et al. (2006). Granulocyte Colony-Stimulating Factor Reduces Cardiomyocyte Apoptosis and Improves Cardiac Function in Adriamycin-Induced Cardiomyopathy in Rats. *Cardiovasc Drugs Ther.* 20 (2), 85–91. doi:10.1007/s10557-006-7652-9

Hwang, J. W., Yao, H., Caito, S., Sundar, I. K., and Rahman, I. (2013). Redox Regulation of SIRT1 in Inflammation and Cellular Senescence. *Free Radic. Biol. Med.* 61, 95–110. doi:10.1016/j.freeradbiomed.2013.03.015

Javadov, S., Baetz, D., Rajapurohitam, V., Zeidan, A., Kirshenbaum, L. A., and Karmazyn, M. (2006a). Antihypertrophic Effect of Na+/H+ Exchanger Isoform 1 Inhibition Is Mediated by Reduced Mitogen-Activated Protein Kinase Activation Secondary to Improved Mitochondrial Integrity and Decreased Generation of Mitochondrial-Derived Reactive Oxygen Species. *J. Pharmacol. Exp. Ther.* 317 (3), 1036–1043. doi:10.1124/jpet.105.100107

Javadov, S., Purdham, D. M., Zeidan, A., and Karmazyn, M. (2006b). NHE-1 Inhibition Improves Cardiac Mitochondrial Function through Regulation of Mitochondrial Biogenesis during Postinfarction Remodeling. *Am. J. Physiol. Heart Circ. Physiol.* 291 (4), H1722–H1730. doi:10.1152/ajpheart.00159.2006

Javadov, S., Rajapurohitam, V., Kilić, A., Zeidan, A., Choi, A., and Karmazyn, M. (2009). Anti-hypertrophic Effect of NHE-1 Inhibition Involves GSK-3beta-dependent Attenuation of Mitochondrial Dysfunction. *J. Mol. Cell. Cardiol.* 46 (6), 998–1007. doi:10.1016/j.yjmcc.2008.12.023

Jung, I. S., Lee, S. H., Yang, M. K., Park, J. W., Yi, K. Y., Yoo, S. E., et al. (2010). Cardioprotective Effects of the Novel Na+/H+ Exchanger-1 Inhibitor KR-32560 in a Perfused Rat Heart Model of Global Ischemia and Reperfusion: Involvement of the Akt-GSK-3beta Cell Survival Pathway and Antioxidant Enzyme. *Arch. Pharm. Res.* 33 (8), 1241–1251. doi:10.1007/s12272-010-0815-z

Kalay, N., Basar, E., Ozdogru, I., Er, O., Cetinkaya, Y., Dogan, A., et al. (2006). Protective Effects of Carvedilol against Anthracycline-Induced Cardiomyopathy. *J. Am. Coll. Cardiol.* 48 (11), 2258–2262. doi:10.1016/j.jacc.2006.07.052

Kim, K. H., Oudit, G. Y., and Backx, P. H. (2008). Erythropoietin Protects against Doxorubicin-Induced Cardiomyopathy via a Phosphatidylinositol 3-kinase-dependent Pathway. *J. Pharmacol. Exp. Ther.* 324 (1), 160–169. doi:10.1124/jpet.107.125773

Koga, T., Suico, M. A., Shimasaki, S., Watanabe, E., Kai, Y., Koyama, K., et al. (2015). Endoplasmic Reticulum (ER) Stress Induces Sirtuin 1 (SIRT1) Expression via the PI3K-Akt-Gsk3β Signaling Pathway and Promotes Hepatocellular Injury. *J. Biol. Chem.* 290 (51), 30366–30374. doi:10.1074/jbc.M115.664169

Li, J. F., Chen, S., Feng, J. D., Zhang, M. Y., and Liu, X. X. (2014). Probucol via Inhibition of NHE1 Attenuates LPS-Accelerated Atherosclerosis and Promotes Plaque Stability *In Vivo*. *Exp. Mol. Pathol.* 96 (2), 250–256. doi:10.1016/j.yexmp.2014.02.010

Li, L., Li, J., Wang, Q., Zhao, X., Yang, D., Niu, L., et al. (2020). Shenmai Injection Protects against Doxorubicin-Induced Cardiotoxicity via Maintaining Mitochondrial Homeostasis. *Front. Pharmacol.* 11, 815. doi:10.3389/fphar.2020.00815

Li, X. M., Ma, Y. T., Yang, Y. N., Liu, F., Chen, B. D., Han, W., et al. (2009). Downregulation of Survival Signalling Pathways and Increased Apoptosis in the Transition of Pressure Overload-Induced Cardiac Hypertrophy to Heart Failure. *Clin. Exp. Pharmacol. Physiol.* 36 (11), 1054–1061. doi:10.1111/j.1440-1681.2009.05243.x

Liu, M. H., Lin, X. L., Guo, D. M., Zhang, Y., Yuan, C., Tan, T. P., et al. (2016). Resveratrol Protects Cardiomyocytes from Doxorubicin-Induced Apoptosis through the AMPK/P53 Pathway. *Mol. Med. Rep.* 13 (2), 1281–1286. doi:10.3892/mmr.2015.4665

Liu, X., Qiu, Y., Huang, N., Liu, Y. h., Wang, H. H., Yu, Y. N., et al. (2021a). Citronellal Alleviates Doxorubicin-induced Cardiotoxicity by Suppressing Oxidative Stress and Apoptosis via Na +/H + Exchanger-1 Inhibition. *J Biochem. Mol. Tox* 36, e22971. doi:10.1002/jbt.22971

Liu, Y., Wei, X., Wu, M., Xu, J., Xu, B., and Kang, L. (2020). Cardioprotective Roles of β-Hydroxybutyrate against Doxorubicin Induced Cardiotoxicity. *Front. Pharmacol.* 11, 603596. doi:10.3389/fphar.2020.603596

Liu, Y., Zhou, L., Du, B., Liu, Y., Xing, J., Guo, S., et al. (2021b). Protection against Doxorubicin-Related Cardiotoxicity by Jaceosidin Involves the Sirt1 Signaling Pathway. *Oxid. Med. Cell. Longev.* 2021, 9984330. doi:10.1155/2021/9984330

Meeran, M. F. N., Al Taee, H., Azimullah, S., Tariq, S., Adeghate, E., and Ojha, S. (2019). β-Caryophyllene, a Natural Bicyclic Sesquiterpene Attenuates Doxorubicin-Induced Chronic Cardiotoxicity via Activation of Myocardial Cannabinoid Type-2 (CB2) Receptors in Rats. *Chem. Biol. Interact.* 304, 158–167. doi:10.1016/j.cbi.2019.02.028

Miettinen, K. H., Lassus, J., Harjola, V. P., Siirilä-Waris, K., Melin, J., Punnonen, K. R., et al. (2008). Prognostic Role of Pro- and Anti-inflammatory Cytokines and Their Polymorphisms in Acute Decompensated Heart Failure. *Eur. J. Heart Fail* 10 (4), 396–403. doi:10.1016/j.ejheart.2008.02.008

Miraglia, E., Viarisio, D., Riganti, C., Costamagna, C., Ghigo, D., and Bosia, A. (2005). Na+/H+ Exchanger Activity Is Increased in Doxorubicin-Resistant Human Colon Cancer Cells and its Modulation Modifies the Sensitivity of the Cells to Doxorubicin. *Int. J. Cancer* 115 (6), 924–929. doi:10.1002/ijc.20959

Moreira, A. C., Branco, A. F., Sampaio, S. F., Cunha-Oliveira, T., Martins, T. R., Holy, J., et al. (2014). Mitochondrial Apoptosis-Inducing Factor Is Involved in Doxorubicin-Induced Toxicity on H9c2 Cardiomyoblasts. *Biochim. Biophys. Acta* 1842 (12 Pt A), 2468–2478. doi:10.1016/j.bbadis.2014.09.015

Mukhopadhyay, P., Bátkai, S., Rajesh, M., Czifra, N., Harvey-White, J., Haskó, G., et al. (2007). Pharmacological Inhibition of CB1 Cannabinoid Receptor Protects against Doxorubicin-Induced Cardiotoxicity. *J. Am. Coll. Cardiol.* 50 (6), 528–536. doi:10.1016/j.jacc.2007.03.057

Prysyazhna, O., Burgoyne, J. R., Scotcher, J., Grover, S., Kass, D., and Eaton, P. (2016). Phosphodiesterase 5 Inhibition Limits Doxorubicin-Induced Heart Failure by Attenuating Protein Kinase G Iα Oxidation. *J. Biol. Chem.* 291 (33), 17427–17436. doi:10.1074/jbc.M116.724070

Rivankar, S. (2014). An Overview of Doxorubicin Formulations in Cancer Therapy. *J. Cancer Res. Ther.* 10 (4), 853–858. doi:10.4103/0973-1482.139267

Ruan, Y., Dong, C., Patel, J., Duan, C., Wang, X., Wu, X., et al. (2015). SIRT1 Suppresses Doxorubicin-Induced Cardiotoxicity by Regulating the Oxidative Stress and p38MAPK Pathways. *Cell. Physiol. Biochem.* 35 (3), 1116–1124. doi:10.1159/000373937

Sangweni, N. F., Moremane, M., Riedel, S., van Vuuren, D., Huisamen, B., Mabasa, L., et al. (2020). The Prophylactic Effect of Pinocembrin against Doxorubicin-Induced Cardiotoxicity in an *In Vitro* H9c2 Cell Model. *Front. Pharmacol.* 11, 1172. doi:10.3389/fphar.2020.01172

Scorrano, L., and Korsmeyer, S. J. (2003). Mechanisms of Cytochrome C Release by Proapoptotic BCL-2 Family Members. *Biochem. Biophys. Res. Commun.* 304 (3), 437–444. doi:10.1016/s0006-291x(03)00615-6

Siveski-Iliskovic, N., Kaul, N., and Singal, P. K. (1994). Probucol Promotes Endogenous Antioxidants and Provides Protection against Adriamycin-Induced Cardiomyopathy in Rats. *Circulation* 89 (6), 2829–2835. doi:10.1161/01.cir.89.6.2829

Smith, M. A., Seibel, N. L., Altekruse, S. F., Ries, L. A., Melbert, D. L., O'Leary, M., et al. (2010). Outcomes for Children and Adolescents with Cancer: Challenges for the Twenty-First Century. *J. Clin. Oncol.* 28 (15), 2625–2634. doi:10.1200/JCO.2009.27.0421

Sun, H. Y., Wang, N. P., Halkos, M. E., Kerendi, F., Kin, H., Wang, R. X., et al. (2004). Involvement of Na+/H+ Exchanger in Hypoxia/re-Oxygenation-Induced Neonatal Rat Cardiomyocyte Apoptosis. *Eur. J. Pharmacol.* 486 (2), 121–131. doi:10.1016/j.ejphar.2003.12.016

Tamariz, L., and Hare, J. M. (2010). Inflammatory Cytokines in Heart Failure: Roles in Aetiology and Utility as Biomarkers. *Eur. Heart J.* 31 (7), 768–770. doi:10.1093/eurheartj/ehq014

Townsend, P. A., Davidson, S. M., Clarke, S. J., Khaliulin, I., Carroll, C. J., Scarabelli, T. M., et al. (2007). Urocortin Prevents Mitochondrial Permeability Transition in Response to Reperfusion Injury Indirectly by Reducing Oxidative Stress. *Am. J. Physiol. Heart Circ. Physiol.* 293 (2), H928–H938. doi:10.1152/ajpheart.01135.2006

Venturini, M., Del Mastro, L., Testore, F., Danova, M., Garrone, O., Lanfranco, C., et al. (1996). Erythropoietin and Granulocyte-Macrophage Colony-Stimulating Factor Allow Acceleration and Dose Escalation of Cyclophosphamide/epidoxorubicin/5-Fluorouracil Chemotherapy: a Dose-Finding Study in Patients with Advanced Breast Cancer. *Cancer Chemother. Pharmacol.* 38 (6), 487–494. doi:10.1007/s002800050516

Wang, Y., Luo, J., Chen, X., Chen, H., Cramer, S. W., and Sun, D. (2008). Gene Inactivation of Na+/H+ Exchanger Isoform 1 Attenuates Apoptosis and Mitochondrial Damage Following Transient Focal Cerebral Ischemia. *Eur. J. Neurosci.* 28 (1), 51–61. doi:10.1111/j.1460-9568.2008.06304.x

Wang, Z. Q., Chen, M. T., Zhang, R., Zhang, Y., Li, W., and Li, Y. G. (2016). Docosahexaenoic Acid Attenuates Doxorubicin-Induced Cytotoxicity and Inflammation by Suppressing NF-κB/iNOS/NO Signaling Pathway Activation in H9C2 Cardiac Cells. *J. Cardiovasc Pharmacol.* 67 (4), 283–289. doi:10.1097/FJC.0000000000000350

Wen, J., Zhang, L., Liu, H., Wang, J., Li, J., Yang, Y., et al. (2019). Salsolinol Attenuates Doxorubicin-Induced Chronic Heart Failure in Rats and Improves Mitochondrial Function in H9c2 Cardiomyocytes. *Front. Pharmacol.* 10, 1135. doi:10.3389/fphar.2019.01135

Xiao, J., Sun, G. B., Sun, B., Wu, Y., He, L., Wang, X., et al. (2012). Kaempferol Protects against Doxorubicin-Induced Cardiotoxicity *In Vivo* and *In Vitro*. *Toxicology* 292 (1), 53–62. doi:10.1016/j.tox.2011.11.018

Xu, M. F., Tang, P. L., Qian, Z. M., and Ashraf, M. (2001). Effects by Doxorubicin on the Myocardium Are Mediated by Oxygen Free Radicals. *Life Sci.* 68 (8), 889–901. doi:10.1016/s0024-3205(00)00990-5

Yang, S., Zhao, X., Xu, H., Chen, F., Xu, Y., Li, Z., et al. (2017). AKT2 Blocks Nucleus Translocation of Apoptosis-Inducing Factor (AIF) and Endonuclease G (EndoG) while Promoting Caspase Activation during Cardiac Ischemia. *Int. J. Mol. Sci.* 18 (3). doi:10.3390/ijms18030565

Zhang, C., Feng, Y., Qu, S., Wei, X., Zhu, H., Luo, Q., et al. (2011). Resveratrol Attenuates Doxorubicin-Induced Cardiomyocyte Apoptosis in Mice through SIRT1-Mediated Deacetylation of P53. *Cardiovasc Res.* 90 (3), 538–545. doi:10.1093/cvr/cvr022

Zhang, S., Wu, P., Liu, J., Du, Y., and Yang, Z. (2021a). Roflumilast Attenuates Doxorubicin-Induced Cardiotoxicity by Targeting Inflammation and Cellular Senescence in Cardiomyocytes Mediated by SIRT1. *Drug Des. Devel Ther.* 15, 87–97. doi:10.2147/DDDT.S269029

Zhang, W. B., Zheng, Y. F., and Wu, Y. G. (2021b). Protective Effects of Oroxylin A against Doxorubicin-Induced Cardiotoxicity via the Activation of Sirt1 in Mice. *Oxid. Med. Cell. Longev.* 2021, 6610543. doi:10.1155/2021/6610543

Zhang, Y. Y., Yi, M., and Huang, Y. P. (2017). Oxymatrine Ameliorates Doxorubicin-Induced Cardiotoxicity in Rats. *Cell. Physiol. Biochem.* 43 (2), 626–635. doi:10.1159/000480471

Conflict of Interest: The authors declare that the research was conducted in the absence of any commercial or financial relationships that could be construed as a potential conflict of interest.

Publisher's Note: All claims expressed in this article are solely those of the authors and do not necessarily represent those of their affiliated organizations, or those of the publisher, the editors and the reviewers. Any product that may be evaluated in this article, or claim that may be made by its manufacturer, is not guaranteed or endorsed by the publisher.

frontiers | Frontiers in Pharmacology

TYPE Case Report
PUBLISHED 01 August 2022
DOI 10.3389/fphar.2022.890546

OPEN ACCESS

EDITED BY
Zhi-Ren Zhang,
Harbin Medical University, China

REVIEWED BY
Chunxia Su,
Department of Oncology, China
Jijin Lin,
Guangdong Academy of Medical Sciences, China

*CORRESPONDENCE
Hui Huang,
huangh8@mail.sysu.edu.cn

SPECIALTY SECTION
This article was submitted to Cardiovascular and Smooth Muscle Pharmacology, a section of the journal Frontiers in Pharmacology

RECEIVED 06 March 2022
ACCEPTED 28 June 2022
PUBLISHED 01 August 2022

CITATION
Pan W, Yin L, Guo Y, Pan D and Huang H (2022), Case Report: Good cardiac tolerance to Toripalimab in a CVD patient with oral melanoma. *Front. Pharmacol.* 13:890546. doi: 10.3389/fphar.2022.890546

Case Report: Good cardiac tolerance to Toripalimab in a CVD patient with oral melanoma

Wei Pan[1], Li Yin[1], Yadi Guo[1], Dachao Pan[2] and Hui Huang[1]*

[1]Cardiovascular Department, The Eighth Affiliated Hospital, Sun Yat-Sen University, Shenzhen, China, [2]Oncology Department, The Eighth Affiliated Hospital, Sun Yat-Sen University, Shenzhen, China

Primary oral melanoma is extremely rare, and the prognosis is very poor. With the development of immunotherapy, melanoma's treatment landscape changed dramatically. Toripalimab, a recombinant programmed death receptor 1 (PD-1) monoclonal antibody, has been approved as second-line therapy for metastatic melanoma. However, the cardiac toxicity of Toripalimab is seldom reported. This article describes the application of Toripalimab on a patient who suffered from primary oral melanoma accompanied with arrhythmic mitral valve prolapse (AMVP).

Case Summary: A 55-year-old Chinese female was diagnosed with BRAF wild-type oral malignant melanoma by excisional biopsy and genetic test. The melanoma quickly progressed after complete tumor resection. Combined therapy after surgical resection was applied to control the progression of melanoma. Due to this patient's basic cardiovascular situation, sacubitril–valsartan, spironolactone, and bisoprolol were used to maintain cardiac function. After five antitumor treatment courses, we re-evaluated the patient systemically from the symptom, physical examination, and auxiliary examination. The result showed that the patient who received Toripalimab combined with chemotherapy and radiotherapy did not present severe side effects on the cardiovascular system. The cardiac function remained well.

Conclusions: This case provided evidence of Toripalimab combined with chemotherapy on melanoma patients with complex cardiovascular diseases. Toripalimab demonstrated a manageable safety profile and durable clinical response. In addition, the standard CHF treatment plays a vital role in the protection of cardiac function. In a cancer patient with complex cardiovascular diseases, standard prophylactic CHF treatment should be applied at an early stage.

KEYWORDS

melanoma, immunotherapy, cancer treatment, arrhythmic mitral valve prolapse, cardiovascular toxicity

Introduction

Melanoma is a severe malignant tumor derived from the skin and mucous membrane with its aggressive behavior and less favorable prognosis (Moțățăianu et al., 2019). The epidemiological data showed that the incidence of this cancer elevated rapidly globally, and the overall 5-year survival rate for mucosal melanomas is 0%–45% (Yde et al., 2018). However, the management of melanoma patients is a complex and evolving issue. Recent data indicate that immunotherapy may improve this situation in the years to come. Anti-CTLA-4 and anti-PD-1/PD-L1 blockade in mucosal melanoma have been evaluated in recent studies. PD-1 monoclonal antibody is considered as a safe, feasible, and effective therapy for patients with metastatic melanoma (Carreau and Pavlick, 2019; Goldberg et al., 2020). However, some cardiovascular events such as myocarditis, myocardial infarction, pericardial effusion, pericarditis, arrhythmia, cardiac tamponade, and acute heart failure have been recently reported (Läubli et al., 2015; Moreira et al., 2019). Though the cardiovascular side effects are relatively rare, they can be severe and potentially fatal when they develop. So a close collaboration between cardiologists and oncologists is needed to help cancer patients receiving the PD-1 antibody, especially when treating patients with basic cardiovascular disease. Toripalimab is one of the promising anti-PD-1 antibodies, which was warranted by its efficacy and safety in the treatment of melanoma (Tang et al., 2020a). Nevertheless, the cardiac tolerance of Toripalimab is still unknown because of insufficient evidence. Here, we reported a case of metastatic melanoma with Toripalimab treatment combined with chemotherapy, who suffered from long-lasting heart valve disease and arrhythmia. Under standard management of cardiovascular diseases, the patient presented good cardiac tolerance in the antitumor treatment of melanoma.

Case description

A 55-year-old woman was admitted to the hospital in December 2019, with a chief complaint of repeated gingival bleeding for 2 months. She also had a history of mitral prolapse and mitral regurgitation, as well as a history of premature ventricular contraction. Before this admission, she received a standard prophylactic therapy including

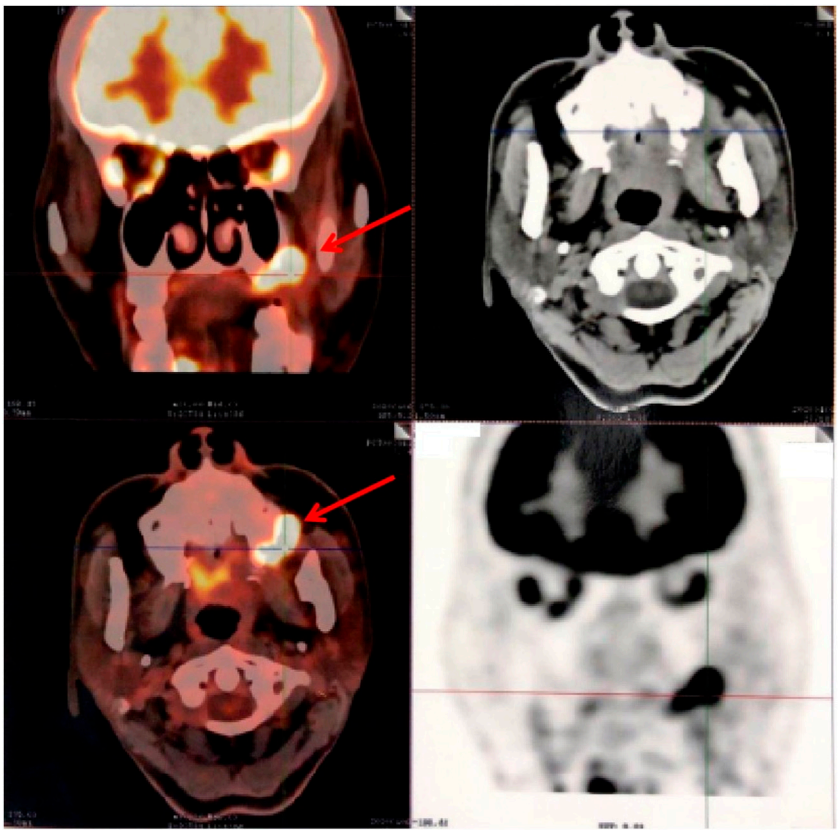

FIGURE 1
PET-CT axial view shows metabolic hyperactivity of the maxillary mass on the left lateral wall.

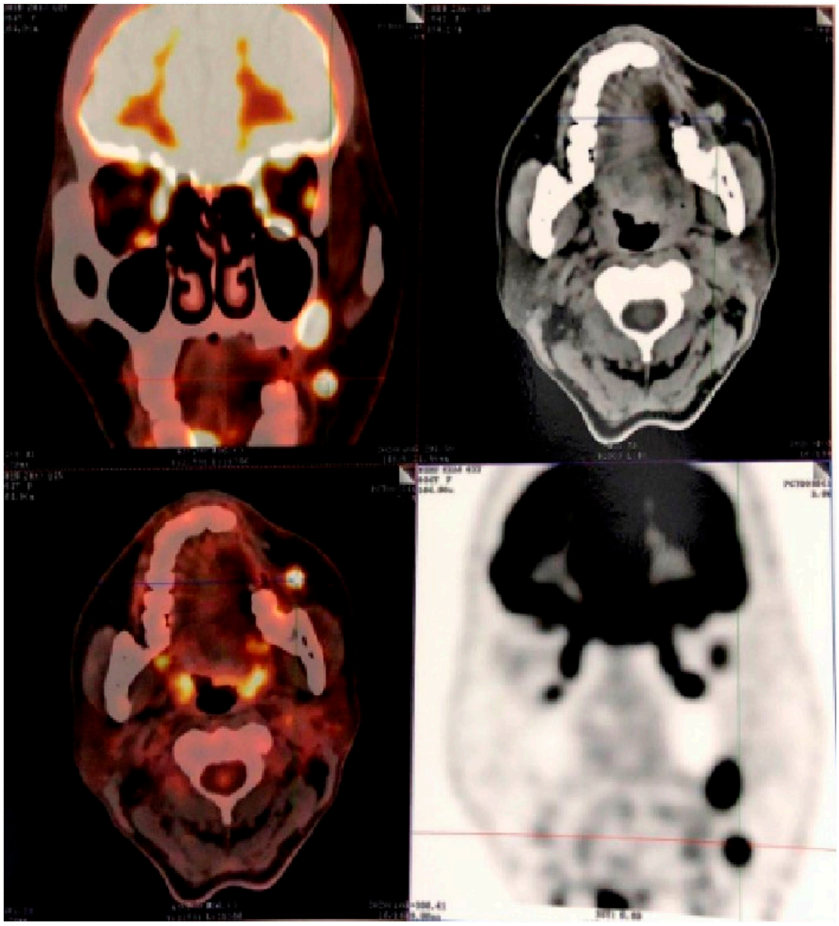

FIGURE 2
PET-CT axial view shows metabolic hyperactivity of the lymph node mass on the left side.

sacubitril–valsartan, spironolactone, and bisoprolol to prevent heart failure. There are no symptoms of chest stuffiness, chest pain, dyspnea, etc. Exercise tolerance is well maintained with a preserved left ventricular ejection fraction (LVEF). Her heart rate was well controlled in a range of 60–70 beats/min. A 24-h Holter electrocardiogram (ECG) at baseline showed sinus rhythm with an average heart rate of 53 bpm. There were 11,619 isolated ventricular ectopic beats (VEBs), and a total of 26 nonsustained ventricular tachycardia events were registered. A rapidly growing mass at the left posterior edentulous maxillary alveolar ridge was found and excised for histopathology analysis after the careful oral examination. The biopsy specimen revealed a sheet of pleomorphic epithelioid tumor cells interspersed with melanophages with melanin pigmentation. Then the tumor cells were stained positive for human melanoma black (HMB)-45, melan-A, and S-100 protein by immunohistochemical analysis, which concluded the diagnosis of malignant melanoma. Computed tomography results revealed the destruction of the maxillary bone and the formation of soft tissue mass–like lesions. Therefore, complete removal of the tumor, including the mass of the parotid gland as well as the left lateral neck dissection, was operated quickly for neoplasm staging and the treatment of melanoma. Further molecular analysis and positron emission tomography/computed tomography (PET/CT) showed that this melanoma was a stage IIIc, pT4N3M0, BRAF wild-type melanoma with the lymph node metastasis (Figure 1). Though there was no clinical or radiologic evidence of the liver, bone, cerebral, or pulmonary metastasis at the moment (Figures 1, 2), the surgical therapy seemed to fail because of the rapid progress of melanoma in the lymph node (Figure 3). Due to this reason, the strategy of chemotherapy combined with immunotherapy was initiated. Temozolomide combined with Toripalimab was chosen for this patient. Considering that the patient suffered from basic cardiovascular diseases, biomarkers such as cardiac troponin I (cTnI) and N-terminal pro B-type natriuretic peptide (NT-proBNP) were detected regularly during the antitumor course (Table 1). ECG (Figure 4) and ultrasonic cardiogram (UCG)

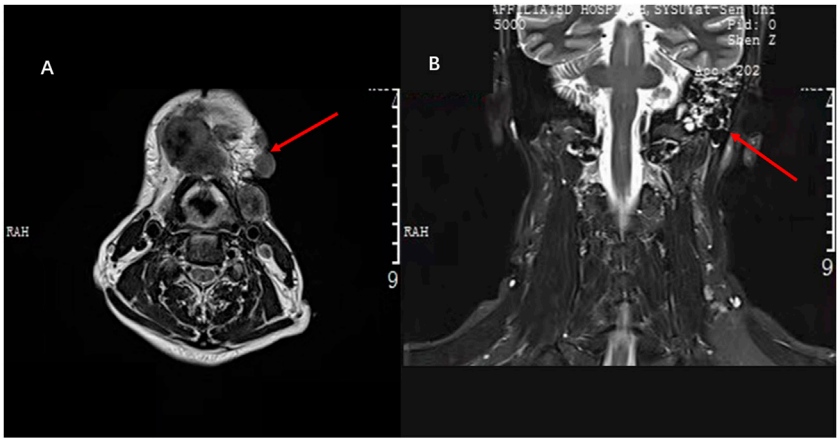

FIGURE 3
MRI image of metastatic melanoma. **(A)** T2-weighted axial image shows soft tissue mass with ill-defined borders involving the left lateral wall and cervical lymph node metastasis. The lesion is causing compression of oropharynx. **(B)** Post contrast T2-weighted coronal image shows the enlarged cervical lymph node.

TABLE 1 Levels of myocardial enzymes and NT-proBNP before and after immunotherapy in the patient.

Courses after immunotherapy)	Myo (ng/ml)	CK-MB(ng/ml)	cTnI (ng/ml)	NT-proBNP(pg/ml)
0	27.1	0.47	<0.012	173
1	27.6	0.69	<0.012	157
2	21.2	0.35	<0.012	138
3	25.1	0.54	<0.012	229
4	25.9	0.59	<0.012	165
5	21.5	0.3	<0.012	188

(Figure 5) were also performed to evaluate the cardiac function. A 24-h Holter ECG after immunotherapy showed sinus rhythm with an average heart rate of 49 bpm. There were 524 isolated VEBs. The treatment for the prevention of HF was continually conferred during the five courses of antitumor therapy with temozolomide and Toripalimab. The total time of five-course combined therapy was more than 6 months, and there were no cardiovascular events such as myocarditis, myocardial infarction, pericardial effusion, pericarditis, arrhythmia, or occurrence of cardiac tamponade. The aforementioned cardiovascular indexes evaluated that there were no abnormal changes observed in this female patient. It showed good cardiac tolerance to Toripalimab in combination with chemotherapy under the protection of cardiovascular regimen.

Discussion

Metastatic melanoma, especially derived from primary oral melanoma, is a rare and aggressive category of cancer with a high mortality rate and a poor prognosis (Moțățăianu et al., 2019). Treatment with ICIs has improved clinical outcomes in multiple types of cancer (Yoneda et al., 2018; Shi et al., 2020; Keenan and Tolaney, 2020), especially in the treatment of melanoma (Robert et al., 2020), but the combined effects of immunotherapy and chemotherapy have not been sufficiently studied. In addition, as the mechanism of immunotherapy is to recognize and target cancer cells by attacking the immune system directly, it may also cause damages to the normal tissues. Previous studies found that unlike most immune-related adverse events, which are common, reversible, and can be treated effectively with glucocorticoid therapy, cardiovascular side effects are usually uncommon but with severe consequences and sometimes may lead to sudden death. Cardiotoxic side effects such as autoimmune myocarditis, pericarditis, and vasculitis have been reported in patients interfering with the CTLA-4 and PD-1 axes (Weyand et al., 2018; Spisarová, 2020; Lal et al., 2021; Fu et al., 2020). Therefore, side effects caused by ICIs have begun to attract widespread concerns.

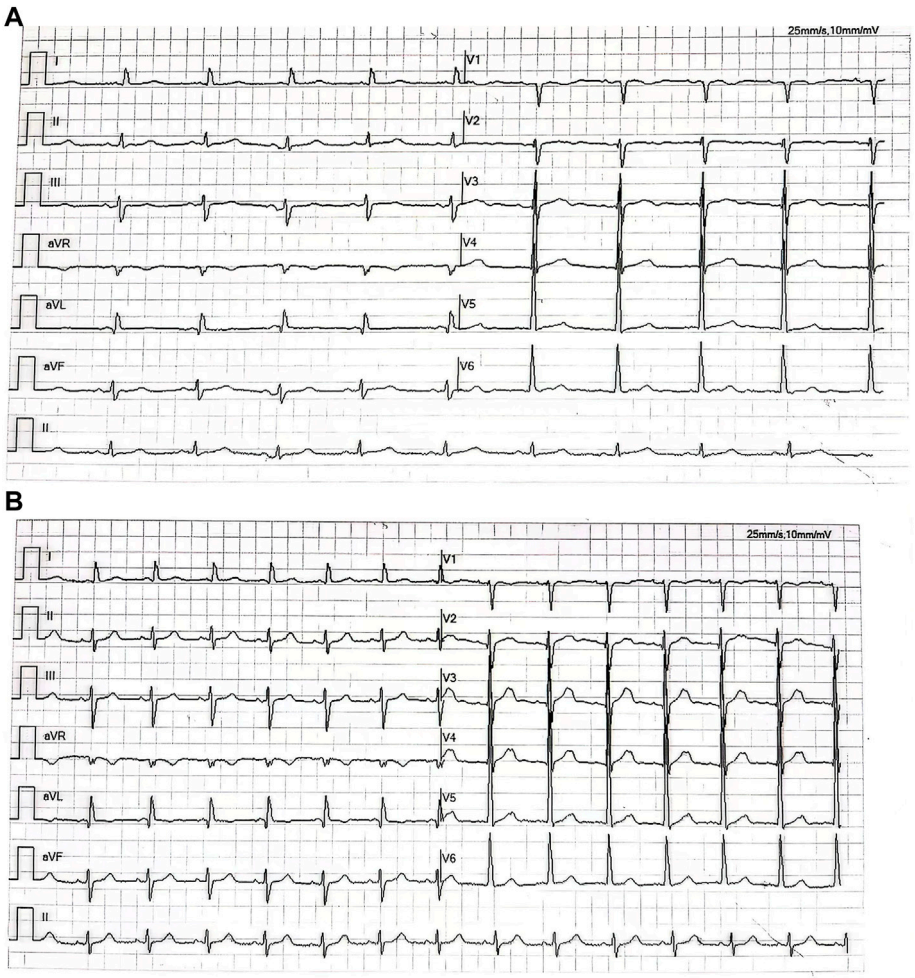

FIGURE 4
(A) Electrocardiogram shows the sinus rhythm with high voltage on the V5 lead before the antitumor therapy. **(B)** Electrocardiogram shows sinus rhythm with high voltage on the V5 lead after the five-course antitumor therapy.

As we all know, therapeutic antibodies against programmed death receptor 1 (PD-1) are considered to be efficient and safe therapy in metastatic melanoma. Theoretically, interference with the CTLA-4 and PD-1 axes can lead to serious and potentially fatal cardiovascular toxicity. The POLARIS-01 multicenter phase II trial was designed to evaluate safety and efficacy of Toripalimab in advanced Chinese patients with melanoma who had failed in systemic treatments. The result showed that patients with positive PD-L1 staining in tumor biopsies had significantly improved ORR (38.5% vs. 11.9%, $p = 0.0065$), PFS (7.7 months vs. 2.7 months, $p = 0.013$), and OS (not reached vs. 14.4 months, $p = 0.0005$) than PD-L1-negative patients which confirmed the safety of Toripalimab (Tang et al., 2020). However, cardiovascular toxicity is rarely reported in Toripalimab, not to mention the situation when treated with PD-1 together with chemotherapy in metastatic melanoma patients with basic cardiovascular diseases. In this case report, the female patient diagnosed with metastatic melanoma also suffered from AMVP. AMVP was defined as the disease of mitral valve prolapse (MVP) with ventricular arrhythmias (VAs) on Holter monitoring, including inverted or biphasic T waves, QT dispersion, QT prolongation, and premature ventricular contractions originating from the left ventricular out flow tract and papillary muscles (Essayagh et al., 2020). From ECG, we could read the situation of this patient who satisfies the diagnostic standard of AMVP. Recent RCTs suggested that sudden cardiac death (SCD) could occur earlier in the course of MVP from complex arrhythmias (Basso et al., 2015). Some risk factors have been proposed, including female sex, bileaflet prolapse, mitral annulus dilatation and disjunction, T wave inversion in the inferolateral leads, frequent and complex PVCs, and presence of papillary muscle fibrosis. By risk stratification, this patient is at a high risk of cardiovascular events such as heart failure and SCD.

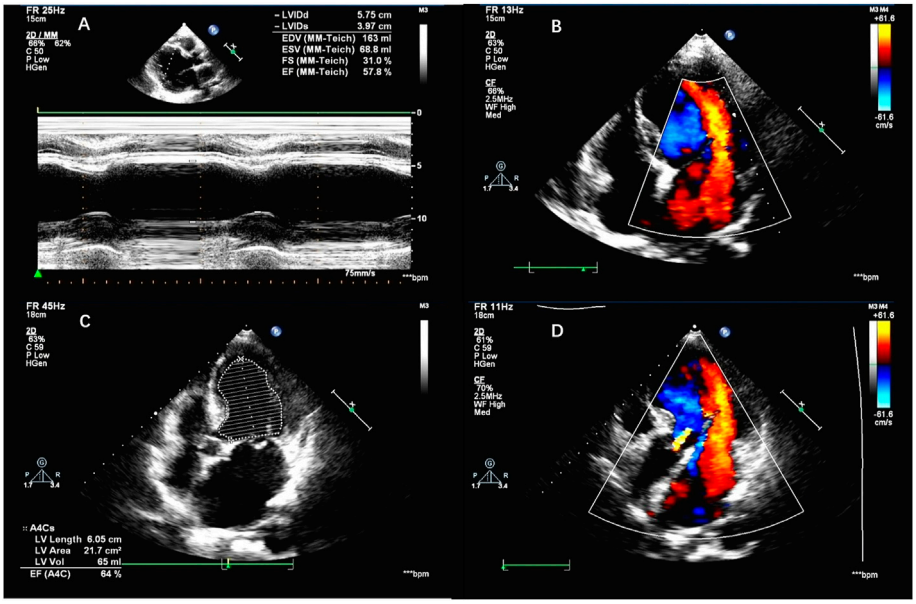

FIGURE 5
(A,B) Echocardiography before the antitumor therapy. **(C,D)** Echocardiography after the five-course antitumor therapy.

TABLE 2 Timeline of the medical process.

Time	Course of disease
October. 2019	Repeated gingival bleeding
December. 2019	Diagnosis of melanoma by pathological report
January. 2020	Cervical lymph node metastasis
AprIL. 2020	Toripalimab combined with temozolomide (1st course)
May 2020-June. 2020	Radiotherapy
July. 2020-August 2020	Toripalimab combined with temozolomide (2nd–5th course)

TABLE 3 Parameters of the echocardiography.

Parameter	Before the immunotherapy	After five-course of immunotherapy
AO	31 mm	34 mm
LA	42 mm	47 mm
LVSd	10 mm	9 mm
LVPWd	9 mm	8 mm
LVIDd	57 mm	64 mm
LVEF	57%	64%
RVIDd	26 mm	21 mm

AO, aorta; LA, left atrium; IVSd, interventricular septum dim; LVPWd, left ventricular posterior wall dimension; LVIDd, Left ventricular end diastolic dimension; LVEF, Left ventricular ejection fraction; RVIDd, Right ventricular end diastolic dimension.

(Miller et al., 2018). Due to a lack of evidence, current guidelines, unfortunately, cannot provide specific indications for AMVP patients, and guidelines only recommend secondary prevention in the case of the non-surgery population as in our case. By applying sacubitril–valsartan, spironolactone, and bisoprolol, the condition of this patient is under good control. But the mass of melanoma progressed so fast that the complete removal of the tumor had no effect on this patient. In recent years, anti-PD-1 monotherapy is accepted as a first-line treatment for non–small–cell lung cancer (NSCLC) and other types of tumors and is approved by NCCN and EMSO (Hsu et al., 2019; Eguren-Santamaria et al., 2020; Leighl et al., 2021). Combined therapy with the anti-PD-1 antibody, including targeted therapy, immune agents, and chemotherapy has been tested in clinical trials or even in clinical practice (Davar et al., 2021; Janjigian et al., 2021). So under careful observation, the strategy of Toripalimab combined with temozolomide was applied to treat melanoma.

Surprisingly, after five courses of antitumor treatment, the patient presented good cardiac tolerance to our strategy. The total timeline of the medical process is shown in Table 2. There was no symptom of arrhythmia or other discomforts that appeared during the therapeutic process. There were no obvious changes observed from echocardiography (Table 3) and other auxiliary examinations, which means that the cardiac function was maintained in good condition. This case provides the first evidence of PD-1 combined with chemotherapy applied in the metastatic melanoma patient with AMVP. As we know, mitral valve prolapse (MVP) is a well-studied, mostly benign, phenomenon that can be caused by degenerative valve disease (mitral valve prolapse), left ventricular impairment and dilatation (in coronary artery disease or dilated cardiomyopathy), and infective endocarditis (Flachskampf and Daniel, 2006). In this case, we noticed that the patient not only suffered from MVP but also

ventricular arrhythmia. According to a recent clinical study, though the pathophysiology of AMVP remains incompletely defined and uncertain, the outcome of AMVP was rarely severely observed by Holter monitoring. Most of the AMVP was independently associated with the phenotype dominated by mitral annulus disjunction, marked leaflet redundancy, and repolarization abnormalities (Essayagh et al., 2020). Considering that long-term arrhythmia results in notable excess mortality and reduced event-free survival, a well-designed study is necessary for further research. Toripalimab is proven to be safe to use for the AMVP patient without increasing the risk of heart failure or arrhythmia. We also confirmed the importance of standard prophylactic anti-CHF therapy, including angiotensin receptor neprilysin inhibitors (ARNIs), mineralocorticoid receptor antagonists (MRAs), and β-blockers during the treatment of antitumor (Edelmann et al., 2018). In conclusion, it is always a big challenge when a cardiologist faces the management and decision-making of a metastatic melanoma patient with basic cardiovascular diseases due to the lack of specific recommendations. The current case aimed at creating further awareness on reducing the cardiovascular risk through comprehensive therapy. Careful surveillance, prompt recognition, and appropriate treatment will become increasingly important. A close collaboration between cardiologists and oncologists is needed to improve the outcomes and survival of complex patients.

Data availability statement

The original contributions presented in the study are included in the article Material. Further inquiries can be directed to the corresponding author.

Ethics statement

Written informed consent was obtained from the individual(s) for the publication of any potentially identifiable images or data included in this article.

Author contributions

WP and HH contributed to the conception and design of the study. LY and DP organized the database. WP wrote the first draft of the manuscript. YG wrote some sections of the manuscript. All authors contributed to the article and approved the submitted version.

Funding

This study was supported by the Science and Technology Planning Project of Shenzhen Municipality (No. JCYJ20180306173433984).

Acknowledgments

The contribution with the image data by Yu Xia, MD, is greatly appreciated.

Conflict of interest

The authors declare that the research was conducted in the absence of any commercial or financial relationships that could be construed as a potential conflict of interest.

Publisher's note

All claims expressed in this article are solely those of the authors and do not necessarily represent those of their affiliated organizations, or those of the publisher, the editors, and the reviewers. Any product that may be evaluated in this article, or claim that may be made by its manufacturer, is not guaranteed or endorsed by the publisher.

References

Basso, C., Perazzolo Marra, M., Rizzo, S., De Lazzari, M., Giorgi, B., Cipriani, A., et al. (2015). Arrhythmic mitral valve prolapse and sudden cardiac death. *Circulation* 132 (7), 556–566. doi:10.1161/CIRCULATIONAHA.115.016291

Carreau, N. A., and Pavlick, A. C. (2019). Nivolumab and ipilimumab: Immunotherapy for treatment of malignant melanoma. *Future Oncol.* 15 (4), 349–358. doi:10.2217/fon-2018-0607

Davar, D., Dzutsev, A. K., McCulloch, J. A., Rodrigues, R. R., Chauvin, J. M., Morrison, R. M., et al. (2021). Fecal microbiota transplant overcomes resistance to anti-PD-1 therapy in melanoma patients. *Science* 371 (6529), 595–602. doi:10.1126/science.abf3363

Edelmann, F., Knosalla, C., Mörike, K., Muth, C., Prien, P., Störk, S., et al. (2018). Chronic heart failure. *Dtsch. Arztebl. Int.* 115 (8), 124–130. doi:10.3238/arztebl.2018.0124

Eguren-Santamaria, I., Sanmamed, M. F., Goldberg, S. B., Kluger, H. M., Idoate, M. A., Lu, B. Y., et al. (2020). PD-1/PD-L1 blockers in NSCLC brain metastases: Challenging paradigms and clinical practice. *Clin. Cancer Res.* 26 (16), 4186–4197. doi:10.1158/1078-0432.CCR-20-0798

Essayagh, B., Sabbag, A., Antoine, C., Benfari, G., Yang, L. T., Maalouf, J., et al. (2020). Presentation and outcome of arrhythmic mitral valve prolapse. *J. Am. Coll. Cardiol.* 76 (6), 637–649. doi:10.1016/j.jacc.2020.06.029

Flachskampf, F. A., and Daniel, W. G. (2006). [Mitral regurgitation]. *Internist (Berl)* 47 (3), 275–283. quiz 284-5. German. doi:10.1007/s00108-005-1529-z

Fu, Y., Zou, T., Shen, X., Nelson, P. J., Li, J., Wu, C., et al. (2020). Lipid metabolism in cancer progression and therapeutic strategies. *MedComm.* 2 (1), 27–59. doi:10.1002/mco2.27

Goldberg, S. B., Schalper, K. A., Gettinger, S. N., Mahajan, A., Herbst, R. S., Chiang, A. C., et al. (2020). Pembrolizumab for management of patients with NSCLC and brain metastases: Long-term results and biomarker analysis from a non-randomised, open-label, phase 2 trial. *Lancet. Oncol.* 21 (5), 655–663. doi:10.1016/S1470-2045(20)30111-X

Hsu, P. C., Jablons, D. M., Yang, C. T., and You, L. (2019). Epidermal growth factor receptor (EGFR) pathway, yes-associated protein (YAP) and the regulation of programmed death-ligand 1 (PD-L1) in non-small cell lung cancer (NSCLC). *Int. J. Mol. Sci.* 20 (15), 3821. doi:10.3390/ijms20153821

Janjigian, Y. Y., Shitara, K., Moehler, M., Garrido, M., Salman, P., Shen, L., et al. (2021). First-line nivolumab plus chemotherapy versus chemotherapy alone for advanced gastric, gastro-oesophageal junction, and oesophageal adenocarcinoma (CheckMate 649): A randomised, open-label, phase 3 trial. *Lancet* 398 (10294), 27–40. doi:10.1016/S0140-6736(21)00797-2

Keenan, T. E., and Tolaney, S. M. (2020). Role of immunotherapy in triple-negative breast cancer. *J. Natl. Compr. Canc. Netw.* 18 (4), 479–489. doi:10.6004/jnccn.2020.7554

Lal, J. C., Brown, S. A., Collier, P., and Cheng, F. (2021). A retrospective analysis of cardiovascular adverse events associated with immune checkpoint inhibitors. *Cardiooncology.* 7 (1), 19. doi:10.1186/s40959-021-00106-x

Läubli, H., Balmelli, C., Bossard, M., Pfister, O., Glatz, K., Zippelius, A., et al. (2015). Acute heart failure due to autoimmune myocarditis under pembrolizumab treatment for metastatic melanoma. *J. Immunother. Cancer* 3, 11. doi:10.1186/s40425-015-0057-1

Leighl, N. B., Redman, M. W., Rizvi, N., Hirsch, F. R., Mack, P. C., Schwartz, L. H., et al. (2021). Phase II study of durvalumab plus tremelimumab as therapy for patients with previously treated anti-PD-1/PD-L1 resistant stage IV squamous cell lung cancer (Lung-MAP substudy S1400F, NCT03373760). *J. Immunother. Cancer* 9 (8), e002973. doi:10.1136/jitc-2021-002973

Miller, M. A., Dukkipati, S. R., Turagam, M., Liao, S. L., Adams, D. H., Reddy, V. Y., et al. (2018). Arrhythmic mitral valve prolapse: JACC review topic of the week. *J. Am. Coll. Cardiol.* 72 (23 Pt A), 2904–2914. doi:10.1016/j.jacc.2018.09.048

Moreira, A., Loquai, C., Pföhler, C., Kähler, K. C., Knauss, S., Heppt, M. V., et al. (2019). Myositis and neuromuscular side-effects induced by immune checkpoint inhibitors. *Eur. J. Cancer* 106, 12–23. doi:10.1016/j.ejca.2018.09.033

Moţăţăianu, A. I., Maier, M. S., Chinezu, L., Bărcuţean, L. I., Voidăzan, T. S., Bajkó, Z., et al. (2019). Malignant melanoma-the most severe skin cancer and neurological pathology. *Rom. J. Morphol. Embryol.* 60 (4), 1207–1214.

Robert, C., Marabelle, A., Herrscher, H., Caramella, C., Rouby, P., Fizazi, K., et al. (2020). Immunotherapy discontinuation - How, and when? Data from melanoma as a paradigm. *Nat. Rev. Clin. Oncol.* 17 (11), 707–715. doi:10.1038/s41571-020-0399-6

Shi, R., Tang, Y.-Q., and Miao, H. (2020). Metabolism in tumor microenvironment: Implications for cancer immunotherapy. *MedComm.* 1 (1), 47–68. doi:10.1002/mco2.6

Spisarová, M. (2020). Immunotherapy-associated myocarditis. *Klin. Onkol.* 33 (1), 20–22. English. doi:10.14735/amko202020

Tang, B., Chi, Z., Chen, Y., Liu, X., Wu, D., Chen, J., et al. (2020). Safety, efficacy, and biomarker analysis of Toripalimab in previously treated advanced melanoma: Results of the POLARIS-01 multicenter phase II trial. *Clin. Cancer Res.* 26 (16), 4250–4259. doi:10.1158/1078-0432.CCR-19-3922

Tang, B., Chi, Z., and Guo, J. (2020). Toripalimab for the treatment of melanoma. *Expert Opin. Biol. Ther.* 20 (8), 863–869. doi:10.1080/14712598.2020.1762561

Weyand, C. M., Berry, G. J., and Goronzy, J. J. (2018). The immunoinhibitory PD-1/PD-L1 pathway in inflammatory blood vessel disease. *J. Leukoc. Biol.* 103 (3), 565–575. doi:10.1189/jlb.3MA0717-283

Yde, S. S., Sjoegren, P., Heje, M., and Stolle, L. B. (2018). Mucosal melanoma: A literature review. *Curr. Oncol. Rep.* 20 (3), 28. doi:10.1007/s11912-018-0675-0

Yoneda, K., Imanishi, N., Ichiki, Y., and Tanaka, F. (2018). Immune checkpoint inhibitors (ICIs) in non-small cell lung cancer (NSCLC). *J. UOEH* 40 (2), 173–189. doi:10.7888/juoeh.40.173

frontiers | Frontiers in Pharmacology

ORIGINAL RESEARCH
published: 04 August 2022
doi: 10.3389/fphar.2022.883600

Cardiac Safety in Breast Cancer Patients Receiving Pegylated Liposome Doxorubicin Sequential Anti-HER2 Monoclonal Antibody Therapy

Ping Huang[1†], Jia-huan Huang[1,2†], Ya-bing Zheng[1], Wen-ming Cao[1], Xi-ying Shao[1], Jun-qing Chen[1], Yuan Huang[1], Guang-liang Li[1], K Sharma[3], Huan-huan Zhou[1], Xiao-jia Wang[1], Hong-chuan Jin[4]* and Zhan-hong Chen[1]**

[1]Department of Breast Medical Oncology, The Cancer Hospital of the University of Chinese Academy of Sciences (Zhejiang Cancer Hospital), Institute of Basic Medicine and Cancer (IBMC), Chinese Academy of Sciences, Hangzhou, China, [2]Department of Internal Medicine, Second Clinical Medical College of Zhejiang Chinese Medical University, Hangzhou, China, [3]ICardioOncology (Official Cardio-Oncology Organization in China), Shanghai, China, [4]Sir Run Run Shaw Hospital, Zhejiang University School of Medicine, Hangzhou, China

Background: Cardiotoxicity associated with the sequential use of anthracyclines followed by trastuzumab is common in adjuvant therapy of patients with HER2-positive early breast cancer (eBC). However, the cardiac safety of trastuzumab concurrent with pegylated liposomal doxorubicin (PLD) is relatively less studied.

Method: Clinical data of patients with HER2-positive eBC treated with PLD and cyclophosphamide (PLD-C) followed by taxanes plus trastuzumab ± pertuzumab (TH or TPH) who then completed standard anti-HER2 treatment for 12 months from June 2012 to August 2021 were retrospectively collected. The primary endpoints were clinical and subclinical cardiotoxicity.

Result: In total, 70 eligible patients were enrolled. Among them, 55 patients (78.6%) received PLD-C → TH and 15 patients (21.4%) received PLD-C → TPH. The median follow-up time was 41.8 months. Until August 2021, only two patients had recurrent or metastatic diseases, with 2-year and 5-year disease-free survivals of 98.6% and 96.8%, respectively. Clinical cardiotoxicity occurred in six patients (8.6%), and all of them had an absolute decline of ≥16% from baseline left ventricular ejection fraction (LVEF) but not below the lower limit of normal (LLN = 50%). Subclinical cardiotoxicity events occurred in 17 patients (24.3%), and all of them had absolute declines of ≥10% and <16% from baseline LVEF but not below the LLN. No patients were interrupted from treatment, and all patients completed anti-HER2 treatment for 12 months. The sharpest decrease in LVEF was observed at 18 months after the start of PLD treatment. The cumulative incidences of clinical and subclinical cardiotoxicity were 9.8% and 28.3%, respectively. In the univariate analysis, body mass index, age, left chest wall radiotherapy, and ongoing cardiovascular risk factors were not significantly associated

OPEN ACCESS

Edited by:
Zhi-Ren Zhang,
Harbin Medical University, China

Reviewed by:
Tanaya Vaidya,
AbbVie (United States), United States
Mayel Gharanei,
Simon Fraser University, Canada

***Correspondence:**
Zhan-hong Chen
czred@sina.com
Hong-chuan Jin
jinhc@zju.edu.cn
Xiao-jia Wang
wxiaojia0803@163.com

†These authors have contributed equally to this work and share first authorship

Specialty section:
This article was submitted to Cardiovascular and Smooth Muscle Pharmacology, a section of the journal Frontiers in Pharmacology

Received: 25 February 2022
Accepted: 23 June 2022
Published: 04 August 2022

Citation:
Huang P, Huang J-h, Zheng Y-b, Cao W-m, Shao X-y, Chen J-q, Huang Y, Li G-l, Sharma K, Zhou H-h, Wang X-j, Jin H-c and Chen Z-h (2022) Cardiac Safety in Breast Cancer Patients Receiving Pegylated Liposome Doxorubicin Sequential Anti-HER2 Monoclonal Antibody Therapy. Front. Pharmacol. 13:883600. doi: 10.3389/fphar.2022.883600

with clinical or subclinical cardiotoxicity ($p > 0.05$). No patients had congestive heart failure or death caused by PLD or anti-HER2 treatment.

Conclusion: The sequential use of PLD and trastuzumab showed a lower incidence of clinical cardiotoxicity, presented as asymptomatic decreased LVEF, compared with the results obtained in previous clinical studies using conventional anthracycline, taxanes and trastuzumab. The study regimen demonstrated good cardiac tolerance and is an alternative strategy for cardioprotection in patients with HER2-positive eBC.

Keywords: cardiotoxicity, early breast cancer, HER2-positive, pegylated liposomal doxorubicin, trastuzumab

INTRODUCTION

Breast cancer is the most common type of malignant tumor and the leading cause of death in women worldwide (Sung et al., 2021). The use of chemotherapy has significantly improved both mortality and morbidity outcomes in breast cancer patients. Anthracyclines are widely used in the treatment of hematological malignancies and solid tumors, with powerful antitumor effects and indispensability (Nicolazzi et al., 2018). However, cardiotoxicity is a serious side effect of these kinds of drugs, which limits their clinical application (Schwentner et al., 2016). Pegylated liposomal doxorubicin (PLD) is a new dosage form of doxorubicin confined in liposomes, which can form a stable three-dimensional structure when polyethylene glycol is grafted onto the surface (stealth liposome) (Gabizon et al., 2008). Pegylated liposomal encapsulation reduces the plasma levels of free doxorubicin and may reduce drug delivery to normal tissues, which can in turn reduce cardiotoxicity (Gil-Gil et al., 2021). Results from clinical data revealed that PLD showed a similar efficacy to doxorubicin with a lower incidence of cardiotoxicity when administered in either advanced or (neo)adjuvant stages of treatment (O'Brien et al., 2004; Liu et al., 2021).

Human epidermal growth factor receptor 2 (HER2) is overexpressed in approximately 20–25% of breast cancer cases, which is associated with poor prognosis (Lynce et al., 2017). However, remarkable progress of trastuzumab plus chemotherapy as adjuvant treatment has significantly improved the survival rates of female breast cancer patients (Slamon et al., 2011; Goldhirsch et al., 2013; Perez et al., 2014; Cameron et al., 2017). Further development in the administration of dual anti-HER2 therapy with trastuzumab and pertuzumab shows great outcomes in (neo)adjuvant as well as metastatic settings (Baselga et al., 2012; Gianni et al., 2012; von Minckwitz et al., 2017). Trastuzumab is also associated with an increased risk of cardiotoxicity, particularly when administered in combination with anthracycline-based therapy. Cardiotoxicity, in this instance, would be manifested as symptomatic congestive heart failure (CHF) or asymptomatic decline of left ventricular ejection fraction (LVEF) (Seidman et al., 2002).

Previous studies have reported that 3–7% of patients who were receiving trastuzumab exhibited cardiac dysfunction in various forms (Seidman et al., 2002). When pertuzumab was combined with trastuzumab and chemotherapy, its cardiac safety was similar to that of trastuzumab alone (Swain et al., 2013; Yu et al., 2016). Nevertheless, limited data are available on the cardiac safety of PLD-based treatment administered sequentially with trastuzumab ± pertuzumab for the adjuvant treatment of HER2-positive early breast cancer (eBC) patients. Therefore, in this study, we aimed to explore strategies to reduce the cardiotoxicity of anthracycline sequential trastuzumab treatment and to clarify the cardiac safety and efficacy of PLD sequential trastuzumab treatment in adjuvant therapy.

PATIENTS AND METHODS

Patients and Study Design

Baseline clinical data as well as posttreatment patient assessment data were retrospectively collected, including the LVEF, electrocardiogram (ECG) status, and efficacy, in patients with HER2-positive eBC treated with PLD-C (PLD plus cyclophosphamide) followed by TH (taxanes with trastuzumab) or TPH (taxanes with trastuzumab and pertuzumab) who then completed standard anti-HER2 treatment for a total of 12 months from June 2012 to August 2021.

Eligibility

Inclusion criteria were patients with HER2-positive eBC diagnosed by pathology who had been treated with radical surgery, age of ≥18 years, and sequential use of PLD and trastuzumab ± pertuzumab. LVEF was evaluated at least twice at our center before and after treatment by 2D echocardiography.

Patients were excluded if they had metastatic disease or severe CHF (NYHA III–IV).

Cardiac Monitoring

LVEF monitoring was performed before chemotherapy and every 3 months, where ECG including preanthracycline and pretrastuzumab was collected at multiple timepoints and sequentially throughout the therapy.

Definition of Cardiotoxicity

Clinical cardiotoxicity caused by cancer therapy is defined as ① symptomatic CHF; ② an asymptomatic absolute decline of ≥16% from baseline LVEF; ③ an asymptomatic absolute decline of 10–15% from baseline LVEF to below the lower limit of normal (LLN = 50%); and ④ LVEF<45% (in these situations, antitumor therapy should be halted for more than 4 weeks, and LVEF needs to be rechecked at an interval of 3–4 weeks). Signs associated with CHF consist of S3 rhythm gallops and/or tachycardia (Yu et al.,

2015). Subclinical cardiotoxicity is defined as ① an asymptomatic absolute decline of ≥10% and <16% from baseline LVEF and ② an asymptomatic absolute decline of <10% to below the LLN (LLN = 50%) (in these situations, antitumor therapy continued, and LVEF needs to be rechecked at an interval of 3–4 weeks) (Yu et al., 2015). Adverse events (AEs) were also monitored continuously and graded according to the National Cancer Institute Common Terminology Criteria for Adverse Events (NCI-CTCAE) v4.0.

Interruption of Anti-HER2 Treatment and Efficacy Endpoint

Interruption of anti-HER2 treatment was defined as interruption of one or more doses or ≥6 weeks between doses.

The efficacy endpoint was disease-free survival (DFS), defined as the time from the first date of surgery to the first date of disease progression or August 2021.

Adjuvant Treatment Plan and Dosage

Patients received PLD-C (PLD 25 mg/m^2 on day 1 plus cyclophosphamide 600 mg/m^2 on day 1) every 3 weeks for four cycles, followed by taxanes (paclitaxel 80 mg/m^2 on day 1 or docetaxel 75–100 mg/m^2 on day 1 or nab-paclitaxel 125 mg/m^2 on day 1, 8) every 3 weeks for four cycles plus anti-HER2 therapy (trastuzumab was given at an initial dose of 8 mg/kg, followed by 6 mg/kg; pertuzumab was given at an initial dose of 840 mg, followed by 420 mg) every 3 weeks. Patients were allowed to complete 12 months of trastuzumab ± pertuzumab maintenance treatment until unacceptable toxicity levels were registered, or if/when there were signs of disease progression.

Statistical Analysis

The normally distributed continuous data were expressed as mean ± standard deviation. Qualitative data were expressed as frequency and percentage. Chi-square (χ^2) test of significance was used to compare proportions between qualitative parameters. The Kaplan–Meier method was used to estimate the percentage of DFS at 2 and 5 years. A p-value of <0.05 was considered statistically significant. Data were analyzed using Statistical Program for Social Science version 25.0.

RESULTS

Patient Characteristics

In total, 70 eligible patients were enrolled. The mean age was 54.0 years (range 30–70 years), and 63 patients (90.0%) were younger than 65 years. All patients underwent breast surgery, either modified radical mastectomy (88.6%) or conservative surgery (11.4%). Of note, 41 patients (58.6%) received radiation therapy, of which 20 patients (48.8%) received left chest wall radiotherapy. Among all the patients, 55 patients (78.6%) received PLD-C followed by TH and 15 patients (21.4%) received PLD-C followed by TPH. Of all cases, 14 patients (20.0%) had at least one cardiovascular risk factor, including hypertension, diabetes, or dyslipidemia.

TABLE 1 | Patients baseline characteristics (N = 70).

Patient characteristic	N (%)
Median age, years (range)	54 (30–70)
BMI (kg/m^2)	23.0 ± 2.6
Histologic type	
Ductal carcinoma	65 (92.9)
Metaplastic carcinoma	3 (4.3)
Mucinous carcinoma	2 (2.9)
Tumor size (cm)	2.2 (0.5–11.0)
Histologically positive nodes, median (range)	1 (0–20)
0	29 (41.4)
1–3	27 (38.6)
≥4	14 (20.0)
Estrogen receptor status	
Positive	31 (44.3)
Negative	39 (5.7)
Progesterone receptor status	
Positive	22 (31.4)
Negative	48 (68.6)
Surgery type	
Mastectomy	62 (88.6)
Breast conserving	8 (11.4)
Radiotherapy	
Yes	41 (58.6)
No	29 (41.4)
Adjuvant regimens	
AC→T/DH	55 (78.6)
AC→ T/D/PHPt	15 (21.4)
Cardiovascular risk factors	
Yes	14 (20.0)
No	56 (80.0)

Numbers are mean ± standard deviation for continuous variables (unless otherwise specified), and N (%) for categorical variables; T: Paclitaxel; D: Docetaxel; P: nab-paclitaxel.

The concrete baseline characteristics of patients are listed in **Table 1**.

Cardiotoxicity Analysis

During the observation period, clinical cardiotoxicity occurred in six patients (8.6%), and all of them were observed to have an absolute decline of ≥16% from baseline LVEF but not below the LLN (LLN = 50%). Subclinical cardiotoxicity events occurred in 17 patients (24.3%), and all these patients had absolute declines of ≥10% and <16% from baseline LVEF but not below the LLN (LLN = 50%).

One patient developed syncope after the first cycle of PLD-C, and ECG studies further showed evidence of third-degree atrioventricular block, which was considered to be related to previous bradycardia. The patient underwent cardiac pacemaker implantation soon after but still completed the remaining seven cycles of chemotherapy and 1-year trastuzumab therapy. There was no cardiotoxicity manifested as a decrease in LVEF in this patient. No other patients were observed to have CHF, and there were no deaths caused by PLD or anti-HER2 drugs.

By August 2021, no patients were interrupted from treatment, and all patients completed anti-HER2 treatment for 12 months.

The mean baselines of pre-AC and pre-H/HP LVEF were 71.7 ± 4.4% and 70.3 ± 4.1%, respectively. During the treatment period, the sharpest decrease in LVEF was observed within

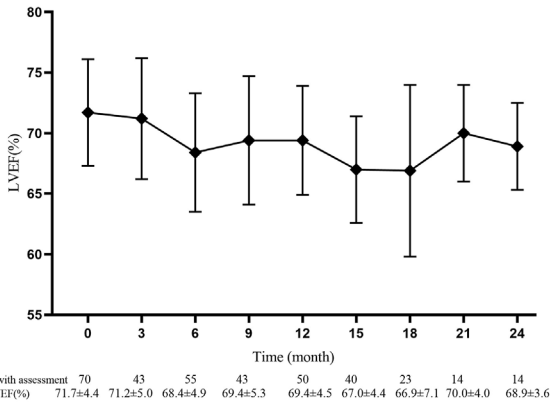

FIGURE 1 | Pre-anthracycline baseline and value of left ventricular ejection fraction in 70 patients at each monitoring timepoint. Data are presented as mean ± standard deviation.

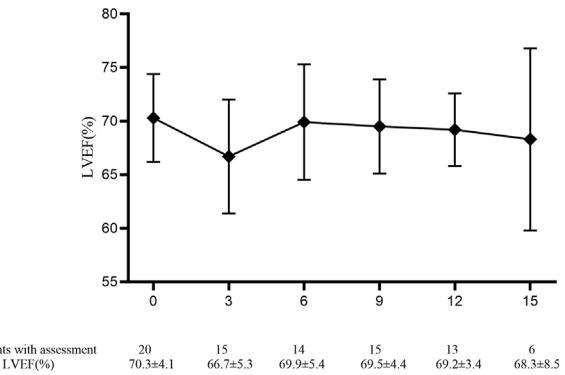

FIGURE 2 | Pre-trastuzumab baseline and value of left ventricular ejection fraction percentage in 20 patients at each monitoring timepoint. Data are presented as mean ± standard deviation.

18 months after the start of PLD treatment, which was equivalent to that within 15 months after the start of 12-month trastuzumab treatment (**Figures 1** and **2**). At each monitoring timepoint, the incidence of cardiotoxicity was the highest at the 18th month after the start of PLD or at the 15th month after the start of trastuzumab treatment, which was 8.7% (**Table 2**). LVEF began to recover at the 21st month after starting PLD treatment, which was the same as that observed at the 18th month after patients started trastuzumab treatment. The cumulative incidence of clinical cardiotoxicity-related events within 6 years was 9.8% and that of subclinical cardiotoxicity-related events within 6 years was 28.3% (**Figure 3**).

Survival Analysis

Until August 2021, only two patients developed local recurrent or metastatic diseases. In total, 57 patients were followed up for 2 years, and the 2-year DFS was 98.6%. Moreover, 18 patients were followed up for 5 years, and the 5-year DFS was 96.8% (**Figure 4**).

The main cardiac safety and efficacy results of this study were compared with other pivotal adjuvant treatments of eBC using anti-HER2 monoclonal therapy and summarized, as presented in **Table 3**.

Analysis of Factors Affecting Cardiotoxicity

In the univariate analysis, body mass index (BMI; <25, ≥25 kg/m^2), age (<60, ≥60 years), left chest wall radiotherapy, and ongoing cardiovascular risk factors were not significantly associated with clinical or subclinical cardiotoxicity ($p > 0.05$); the results are listed in **Tables 4** and **5**.

Echocardiogram Parameter Changes

The most frequent cardiac disorder reported by echocardiogram was left ventricular diastolic dysfunction, which was more common in the no-cardiotoxicity group (70.3%) than in the cardiotoxicity group (66.7%). Left ventricular systolic dysfunction events had an incidence of 33.3% in the cardiotoxicity group (**Table 6**).

Electrocardiogram Changes

In the cardiotoxicity group, ECG changes mainly included T-wave changes (83.3%), sinus bradycardia (50.0%), ST-TU segment changes (33.3%), ST-T segment changes (16.7%), and T-U segment changes (16.7%). The concrete disorders are listed in **Table 6**.

DISCUSSION

Over recent years, the application of anthracyclines sequentially with anti-HER2 therapy has shown to significantly improve the survival rates and prognoses of patients (Slamon et al., 2011). However, cardiotoxicity, as the major cause of breast cancer deaths, even without symptoms, may significantly limit the possibility of tumor treatment (Patnaik et al., 2011). In clinical practice, LVEF measured by echocardiography is used as an index to evaluate cardiotoxicity due to its accessibility.

TABLE 2 | Changes in left ventricular ejection fraction are divided into two groups, and the number of cases is listed.

△LVEF (LVEF-base)	3M(n = 43)	6M(n = 55)	9M(n = 43)	12M(n = 50)	15M(n = 40)	18M(n = 23)	21M(n = 14)	24M(n = 14)
10%~15%	3 (7.0%)	2 (3.6%)	4 (9.3%)	0 (0)	4 (10.0%)	4 (17.4%)	0 (0)	0 (0)
≥16%	1 (2.3%)	2 (3.6%)	0 (0)	0 (0)	1 (2.5%)	2 (8.7%)	0 (0)	0 (0)

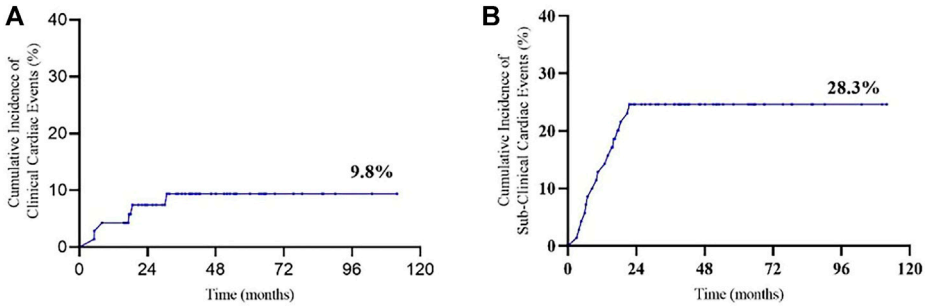

FIGURE 3 | Cumulative incidence of cardiac events: **(A)** clinical cardiotoxicity and **(B)** subclinical cardiotoxicity.

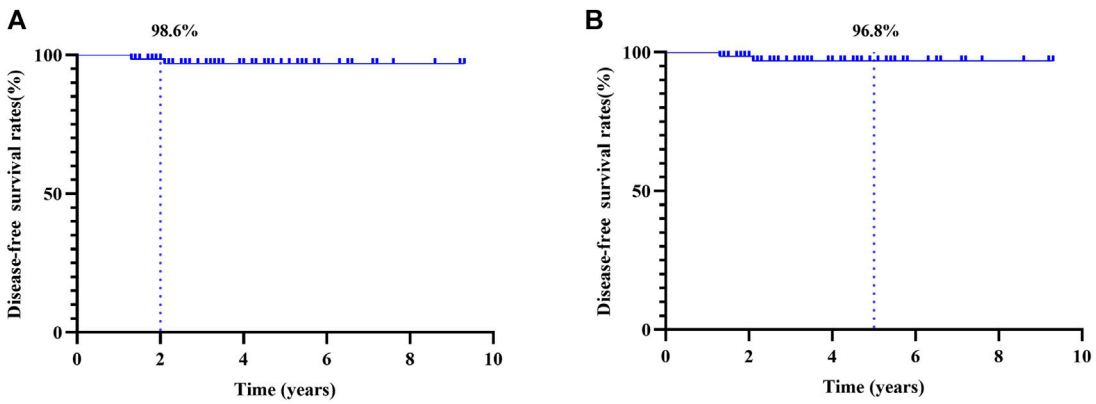

FIGURE 4 | Kaplan–Meier curves for disease-free survival (DFS): **(A)** 2-year DFS and **(B)** 5-year DFS.

TABLE 3 | Summary of the cardiac safety and efficacy results of our study compared with other pivotal adjuvant trastuzumab trials.

Trial	Design	Median follow-up times	DFS	Severe CHF/CD	LVEF absolute decline from baseline	References
NCCTG N9831 (N = 1944)	arm B: AC (q3w x 4) →P (qw x 12)-H (qw x 52) arm C: AC (q3w x 4) →P (qw x 12) + H (qw x 12) →H (qw x40)	9.2-year	arm B: 80.1% (5-year) arm C: 84.5% (5-year)	arm B 2.8% arm C 3.7%	≥15%:arm B 14.6% ≥ 15%:arm C 18.7%	Advani et al. (2016)
NSABPB-31/ N9831	AC→PH	8.4-year	73.7% (10-year)	2.0%	NR	Perez et al. (2014)
NSABP B-31 (N = 2043)	arm B: AC (q3w x 4) → P (q3w x 4 or qw x 12) + H (qw x 12) →H (qw x 40)	7-year	NR	arm B 3.9%	≥10%: 35.3% ≥ 15%: 14.6%	Romond et al. (2012)
BCIRG-006 (N = 3,222)	arm B: AC (q3w x 4) →TXT (q3w x 4) + H (qw x 12) → H (q3w x 13) arm C: Cb + TXT (q3w x 6) + H (qw x 18) →H (q3w x 12)	10-year	arm B: 84% (5-year) arm C: 81% (5-year)	arm B: 2.0% arm C: 0.4%	≥10%:18.6% ≥ 10%:9.4%	Slamon et al. (2011)
HERA (N = 5,102)	arm B: A-based (A-T 26%; T-free 68%) → H (1-year q3w)	11-year	69% (10-year)	1%	≥10%:4.4%	Cameron et al. (2017)
Our study (N = 70)	PLD-C →TH/TPH (q3w) → finished H/PH treatment for a total of 12 months	3.5-year	98.6% (2-year) 96.8% (5-year)	0%	≥16%:8.6% ≥ 10% and<16:24.3%	

Abbreviations: A, doxorubicin; C, cyclophosphamide; P, paclitaxel; TXT, docetaxel; T, taxanes; H, trastuzumab; PH, pertuzumab and trastuzumab; CE, cardiac events; CD, cardiac death; carboplatin: Cb; CHF: congestive heart failure; DFS, disease-free survival; LVEF, left ventricular ejection fraction; NSABP, National Surgical Adjuvant Breast and Bowel Project; NCCTG, North Central Cancer Treatment Group; BCIRG, Breast Cancer International Research Group; HERA, herceptin adjuvant trial; qw, every week; q3w, every 3 weeks; NR, not reported. The chemotherapy regimens involved in these pivotal studies were all conventional doses.

TABLE 4 | Univariate chi-square analyses for influencing factors of clinical cardiotoxicity according to patients' characteristics.

Patient characteristics	Cardiotoxicity (n = 6)	No cardiotoxicity (n = 64)	χ2	P
Age			0.000	1.000
<60 years	4 (66.7%)	47 (73.4%)		
≥60 years	2 (33.3%)	17 (26.6%)		
Left chest wall radiotherapy			0.000	1.000
yes	2 (33.3%)	18 (28.1%)		
no	4 (66.7%)	46 (71.9%)		
Cardiovascular risk factors			0.103	0.749
yes	2 (33.3%)	12 (18.7%)		
no	4 (66.7%)	52 (81.3%)		
BMI			0.000	1.000
<25 kg/m^2	5 (83.3%)	52 (81.3%)		
≥25 kg/m^2	1 (16.70%)	12 (18.7%)		

TABLE 5 | Univariate chi-square analyses for influencing factors of subclinical cardiotoxicity according to patients' characteristics.

Patient characteristics	Cardiotoxicity (n = 17)	No cardiotoxicity (n = 53)	χ2	P
Age			0.000	1.000
<60 years	12 (70.6%)	35 (73.6%)		
≥60 years	5 (29.4%)	14 (26.4%)		
Left chest wall radiotherapy			0.157	0.692
yes	6 (24.3%)	14 (26.4%)		
no	11 (64.7%)	39 (73.6%)		
Cardiovascular risk factors			0.000	1.000
yes	3 (17.6%)	11 (20.8%)		
no	14 (82.4%)	42 (79.2%)		
BMI			0.000	1.000
<25 kg/m^2	14 (82.4%)	43 (81.1%)		
≥25 kg/m^2	3 (17.6%)	10 \(18.9%)		

TABLE 6 | Cardiac disorders (NCI-CTCAEv4.0, all grades).

Adverse event (n, %)	Cardiotoxicity (n = 6)	No cardiotoxicity (n = 64)
LVDD	4 (66.7%)	45 (70.3%)
LVSD	1 (16.7%)	1 (1.6%)
ST segment changes	0 (0.0%)	3 (4.7%)
Twave changes	5 (83.3%)	34 (53.1%)
ST-T segment changes	1 (16.7%)	14 (21.9%)
ST-T-U segment changes	2 (33.3%)	19 (29.7%)
T-U segment changes	1 (16.7%)	10 (15.6%)
Atrial premature beat ventricular premature beat	0 (0.0%) 0(0.0%)	9 (14.1%) 1 (1.6%)
Sinus tachycardia	0 (0.0%)	3 (4.7%)
Sinus bradycardia Sinus arrhythmia	3(50.0%) 0(0.0%)	5 (7.8%) 5 (7.8%)
Atrial fibrillation Cardiomegaly Bundle branch block right	0(0.0%) 0(0.0%) 0(0.0%)	0(0.0%) 0(0.0%) 8 (12.5%)
Extrasystoles	0 (0.0%)	0 (0.0%)
PR interval prolongation	0 (0.0%)	3 (4.7%)
QT interval prolongation	0 (0.0%)	2 (3.1%)

Abbreviations: LVSD, left ventricular systolic dysfunction; LVDD, left ventricular diastolic dysfunction.

PLD has been demonstrated to have equivalent efficacy but significantly less cardiotoxicity than conventional doxorubicin. In a phase III study, the cardiotoxicity rates were 3.9% and 18.8% with PLD and doxorubicin, respectively (O'Brien et al., 2004). A retrospective study compared the use of traditional anthracyclines and PLD in neoadjuvant therapy for patients with breast cancer. The study revealed higher pathologic complete response rates and lower incidences of cardiotoxicity in PLD-based cohorts (Liu et al., 2021). Therefore, it can be considered that the risk of cardiac toxicity after PLD sequential trastuzumab therapy is slightly higher than that of PLD monotherapy, but it is acceptable. Dual-target therapy with the addition of pertuzumab did not increase the incidence of cardiac-related AEs in either metastatic or neoadjuvant studies (Gianni et al., 2012; Schneeweiss et al., 2013).

PLD-C is not a standard protocol for breast cancer in adjuvant chemotherapy. However, due to the individualized treatment of cancer, some patients choose PLD as an alternative drug to anthracycline in adjuvant therapy. Through the narration of the physician in charge of these cases, the main reasons for these patients to choose PLD in our center include the following: 1) to avoid obvious hair loss caused by initial chemotherapy, 2) to avoid stronger nausea and vomiting symptoms, 3) to avoid the potential risk of developing febrile neutropenia, and 4) consideration of the potential to reduce the incidence of lifetime cardiotoxicity.

In this retrospective cohort study, PLD-C followed by anti-HER2 therapy as adjuvant therapy was effective and safe in a population of HER2-positive eBC patients. This study demonstrated that these schemes had a low risk for cardiotoxicity with slight clinical cardiotoxicity compared with treatments in previous clinical studies containing conventional anthracycline, taxanes, and trastuzumab (**Table 3**).

As described in **Table 3**, the NCCTG N9831 trial randomized patients between two arms in the adjuvant setting with AC followed by paclitaxel either with sequential or concurrent trastuzumab, and at a median follow-up of 9.2 years, the reported incidence of CHF or cardiac death (CD) was 2.8% in arm B (AC followed by paclitaxel and then trastuzumab) and 3.7% in arm C (AC followed by paclitaxel concurrent with trastuzumab) (Advani et al., 2016). In the NSABP-B31 study, at a median follow-up of 7 years, the incidence of severe CHF/CD was 3.9% in the arm with AC followed by TH. An independent retrospective review of the B-31 and N9831 trials demonstrated a 2.0% incidence of symptomatic CHF or CD in the trastuzumab-containing arm (Romond et al., 2012). In the BCIRG-006 study, at a median follow-up of 10 years, the incidence of CHF or CD was 2.0% in the arm with AC followed by docetaxel and trastuzumab (Slamon et al., 2011). While in our study, at a median follow-up of 3.5 years, the incidence of CHF or CD was 0% in the groups with PLD-C followed by TH/TPH (q3w). In the NCCTGN9831 and NSABPB-31 trials, LVEF reductions ≥15% from baseline were 14.6% (NCCTG N9831 arm B) and 18.7% (NCCTG N9831 arm C), respectively (Romond et al., 2012; Advani et al., 2016). While in our study, LVEF reduction ≥16% from baseline was 8.6%, where cardiotoxicity halved in value. Subclinical cardiotoxicity in the NSABP B-31 and BCIRG-006 studies using anthracyclines and trastuzumab was similar to that in our study (Slamon et al., 2011; Romond et al., 2012). This indicates that although PLD is used, cardiotoxicity monitoring is still necessary. In the HERA study, because 68% of patients did not use taxanes, the subclinical cardiotoxicity was relatively low (4.4%) (Cameron et al., 2017). In the NCCTGN9831 study, the 5-year DFS rates were 80.1% (arm B) and 84.5% (arm C) (Advani et al., 2016). In the BCIRG-006 study, the 5-year DFS rates were 84% (arm B:AC-TH group) and 81% (arm C:TCH group), respectively (Slamon et al., 2011). While in our study, the 5-year DFS was 96.8%, suggesting that patients had improved survival. It is worth noting that all patients completed PLD-C followed by TH or TPH every 3 weeks, which reflects the excellent tolerance; this may be related to higher DFS and efficiency.

The NCCTG N9831 trial demonstrated that age ≥60 years, registration LVEF <65%, and use of antihypertensive medications were associated with an increased risk of cardiac events, while radiation therapy, BMI, or ethnicity were not statistically significant (Advani et al., 2016). In the NSABP-B31 trial, LVEF (50–54%), age (≥60 years), and receiving antihypertensive medications and radiotherapy were also not statistically significant (Romond et al., 2012). The CANTO study indicated that obesity appeared to be associated with an important increase in risk-related cardiotoxicity in eBC patients (Kaboré and Guenancia, 2019). In our study, since the basal LVEF of the patients was not low and the incidence of cardiotoxicity was low, it was less possible to conclude that cardiotoxicity was related to BMI (<25, ≥25 kg/m^2), age (<60, ≥60 years), radiotherapy, ongoing cardiovascular risk factors, or LVEF at baseline.

Our study had several limitations as follows. This study was a retrospective study, the test population was of a small sample size, and the LVEF values were not available for all patients at all corresponding observation points, leading to the possibility that the results showed a reduced incidence of cardiotoxicity. Due to the lack of necessary baseline or follow-up LVEF measurements, many patients had to be excluded, resulting in some selection bias. Therefore, as a future consideration, a prospective cohort study to further clarify the precise incidence and outcome of PLD sequential trastuzumab cardiotoxicity is worth carrying out.

CONCLUSION

PLD sequential trastuzumab treatment reduces cardiotoxicity by nearly half compared with traditional anthracyclines, which is well tolerated. Most patients can complete the established treatment plans, which may have a positive effect on survival; this merits further exploration and may become an alternative strategy for cardioprotection in patients with HER2-positive eBC.

DATA AVAILABILITY STATEMENT

The raw data supporting the conclusions of this article will be made available by the authors, without undue reservation.

ETHICS STATEMENT

The studies involving human participants were reviewed and approved by the Ethics Board of Zhejiang Cancer Hospital. Written informed consent for participation was not required for this study in accordance with the national legislation and institutional requirements.

AUTHOR CONTRIBUTIONS

PH and J-HH were involved in conception of the study, participated in the design of the study, collected cases, and

performed statistical analysis. PH, JH-H, and KS wrote the first draft of the manuscript. Z-HC, Y-BZ, W-MC, X-YS, J-QC, YH, G-LL, and H-HZ collected cases and performed statistical analysis. Z-HC, H-CJ, and X-JW designed this study. All authors contributed to the manuscript and revised, read, and approved the submitted version.

FUNDING

This work was partly supported by Zhejiang Province's Scientific Research Foundation of Traditional Chinese Medicine, China (2020ZB034), and Medical Science and Technology Project of Zhejiang Province, China (2020KY492).

REFERENCES

Advani, P. P., Ballman, K. V., Dockter, T. J., Colon-Otero, G., and Perez, E. A. (2016). Long-Term Cardiac Safety Analysis of NCCTG N9831 (Alliance) Adjuvant Trastuzumab Trial. *J. Clin. Oncol.* 34, 581–587. doi:10.1200/JCO.2015.61.8413

Baselga, J., Cortés, J., Kim, S. B., Im, S. A., Hegg, R., Im, Y. H., et al. (2012). Pertuzumab Plus Trastuzumab Plus Docetaxel for Metastatic Breast Cancer. *N. Engl. J. Med.* 366, 109–119. doi:10.1056/NEJMoa1113216

Cameron, D., Piccart-Gebhart, M. J., Gelber, R. D., Procter, M., Goldhirsch, A., de Azambuja, E., et al. (2017). 11 Years' Follow-Up of Trastuzumab after Adjuvant Chemotherapy in HER2-Positive Early Breast Cancer: Final Analysis of the HERceptin Adjuvant (HERA) Trial. *Lancet* 389, 1195–1205. doi:10.1016/S0140-6736(16)32616-2

Gabizon, A., Isacson, R., Rosengarten, O., Tzemach, D., Shmeeda, H., and Sapir, R. (2008). An Open-Label Study to Evaluate Dose and Cycle Dependence of the Pharmacokinetics of Pegylated Liposomal Doxorubicin. *Cancer Chemother. Pharmacol.* 61, 695–702. doi:10.1007/s00280-007-0525-5

Gianni, L., Pienkowski, T., Im, Y. H., Roman, L., Tseng, L. M., Liu, M. C., et al. (2012). Efficacy and Safety of Neoadjuvant Pertuzumab and Trastuzumab in Women with Locally Advanced, Inflammatory, or Early HER2-Positive Breast Cancer (NeoSphere): a Randomised Multicentre, Open-Label, Phase 2 Trial. *Lancet Oncol.* 13, 25–32. doi:10.1016/S1470-2045(11)70336-9

Gil-Gil, M. J., Bellet, M., Bergamino, M., Morales, S., Barnadas, A., Manso, L., et al. (2021). Long-Term Cardiac Safety and Survival Outcomes of Neoadjuvant Pegylated Liposomal Doxorubicin in Elderly Patients or Prone to Cardiotoxicity and Triple Negative Breast Cancer. Final Results of the Multicentre Phase II CAPRICE Study. *Front. Oncol.* 11, 645026. doi:10.3389/fonc.2021.645026

Goldhirsch, A., Gelber, R. D., Piccart-Gebhart, M. J., de Azambuja, E., Procter, M., Suter, T. M., et al. (2013). 2 Years versus 1 Year of Adjuvant Trastuzumab for HER2-Positive Breast Cancer (HERA): an Open-Label, Randomised Controlled Trial. *Lancet* 382, 1021–1028. doi:10.1016/S0140-6736(13)61094-6

Kaboré, E. G., Guenancia, C., Vaz-Luis, I., Di Meglio, A., Pistilli, B., Coutant, C., et al. (2019). Association of Body Mass Index and Cardiotoxicity Related to Anthracyclines and Trastuzumab in Early Breast Cancer: French CANTO Cohort Study. *PLoS Med.* 16, e1002989. doi:10.1371/journal.pmed.1002989

Liu, W., Chen, W., Zhang, X., Zhao, P., Fan, Z., Bi, L., et al. (2021). Higher Efficacy and Reduced Adverse Reactions in Neoadjuvant Chemotherapy for Breast Cancer by Using Pegylated Liposomal Doxorubicin Compared with Pirarubicin. *Sci. Rep.* 11, 199. doi:10.1038/s41598-020-80415-w

Lynce, F., Barac, A., Tan, M. T., Asch, F. M., Smith, K. L., Dang, C., et al. (2017). SAFE-HEaRt: Rationale and Design of a Pilot Study Investigating Cardiac Safety of HER2 Targeted Therapy in Patients with HER2-Positive Breast Cancer and Reduced Left Ventricular Function. *Oncologist* 22, 518–525. doi:10.1634/theoncologist.2016-0412

Nicolazzi, M. A., Carnicelli, A., Fuorlo, M., Scaldaferri, A., Masetti, R., Landolfi, R., et al. (2018). Anthracycline and Trastuzumab-Induced Cardiotoxicity in Breast Cancer. *Eur. Rev. Med. Pharmacol. Sci.* 22, 2175–2185. doi:10.26355/eurrev_201804_14752

O'Brien, M. E., Wigler, N., Inbar, M., Rosso, R., Grischke, E., Santoro, A., et al. (2004). Reduced Cardiotoxicity and Comparable Efficacy in a Phase III Trial of Pegylated Liposomal Doxorubicin HCl (CAELYX/Doxil) versus Conventional Doxorubicin for First-Line Treatment of Metastatic Breast Cancer. *Ann. Oncol.* 15, 440–449. doi:10.1093/annonc/mdh097

Patnaik, J. L., Byers, T., Diguiseppi, C., Dabelea, D., and Denberg, T. D. (2011). Cardiovascular Disease Competes with Breast Cancer as the Leading Cause of Death for Older Females Diagnosed with Breast Cancer: a Retrospective Cohort Study. *Breast Cancer Res.* 13, R64. doi:10.1186/bcr2901

Perez, E. A., Romond, E. H., Suman, V. J., Jeong, J. H., Sledge, G., Geyer, C. E., JR., et al. (2014). Trastuzumab Plus Adjuvant Chemotherapy for Human Epidermal Growth Factor Receptor 2-positive Breast Cancer: Planned Joint Analysis of Overall Survival from NSABP B-31 and NCCTG N9831. *J. Clin. Oncol.* 32, 3744–3752. doi:10.1200/JCO.2014.55.5730

Romond, E. H., Jeong, J. H., Rastogi, P., Swain, S. M., Geyer, C. E., JR., Ewer, M. S., et al. (2012). Seven-year Follow-Up Assessment of Cardiac Function in NSABP B-31, a Randomized Trial Comparing Doxorubicin and Cyclophosphamide Followed by Paclitaxel (ACP) with ACP Plus Trastuzumab as Adjuvant Therapy for Patients with Node-Positive, Human Epidermal Growth Factor Receptor 2-positive Breast Cancer. *J. Clin. Oncol.* 30, 3792–3799. doi:10.1200/JCO.2011.40.0010

Schneeweiss, A., Chia, S., Hickish, T., Harvey, V., Eniu, A., Hegg, R., et al. (2013). Pertuzumab Plus Trastuzumab in Combination with Standard Neoadjuvant Anthracycline-Containing and Anthracycline-free Chemotherapy Regimens in Patients with HER2-Positive Early Breast Cancer: a Randomized Phase II Cardiac Safety Study (TRYPHAENA). *Ann. Oncol.* 24, 2278–2284. doi:10.1093/annonc/mdt182

Schwentner, L., Harbeck, N., Singer, S., Eichler, M., Rack, B., Forstbauer, H., et al. (2016). Short Term Quality of Life with Epirubicin-Fluorouracil-Cyclophosphamid (FEC) and Sequential Epirubicin/cyclophosphamid-Docetaxel (EC-DOC) Chemotherapy in Patients with Primary Breast Cancer - Results from the Prospective Multi-Center Randomized ADEBAR Trial. *Breast* 27, 69–77. doi:10.1016/j.breast.2016.03.003

Seidman, A., Hudis, C., Pierri, M. K., Shak, S., Paton, V., Ashby, M., et al. (2002). Cardiac Dysfunction in the Trastuzumab Clinical Trials Experience. *J. Clin. Oncol.* 20, 1215–1221. doi:10.1200/JCO.2002.20.5.1215

Slamon, D., Eiermann, W., Robert, N., Pienkowski, T., Martin, M., Press, M., et al. (2011). Adjuvant Trastuzumab in HER2-Positive Breast Cancer. *N. Engl. J. Med.* 365, 1273–1283. doi:10.1056/NEJMoa0910383

Sung, H., Ferlay, J., Siegel, R. L., Laversanne, M., Soerjomataram, I., Jemal, A., et al. (2021). Global Cancer Statistics 2020: GLOBOCAN Estimates of Incidence and Mortality Worldwide for 36 Cancers in 185 Countries. *CA Cancer J. Clin.* 71, 209–249. doi:10.3322/caac.21660

Swain, S. M., Ewer, M. S., Cortés, J., Amadori, D., Miles, D., Knott, A., et al. (2013). Cardiac Tolerability of Pertuzumab Plus Trastuzumab Plus Docetaxel in Patients with HER2-Positive Metastatic Breast Cancer in CLEOPATRA: a Randomized, Double-Blind, Placebo-Controlled Phase III Study. *Oncologist* 18, 257–264. doi:10.1634/theoncologist.2012-0448

von Minckwitz, G., Procter, M., de Azambuja, E., Zardavas, D., Benyunes, M., Viale, G., et al. (2017). Adjuvant Pertuzumab and Trastuzumab in Early HER2-Positive Breast Cancer. *N. Engl. J. Med.* 377, 122–131. doi:10.1056/NEJMoa1703643

Yu, A. F., Manrique, C., Pun, S., Liu, J. E., Mara, E., Fleisher, M., et al. (2016). Cardiac Safety of Paclitaxel Plus Trastuzumab and Pertuzumab in Patients with HER2-Positive Metastatic Breast Cancer. *Oncologist* 21, 418–424. doi:10.1634/theoncologist.2015-0321

Yu, A. F., Yadav, N. U., Lung, B. Y., Eaton, A. A., Thaler, H. T., Hudis, C. A., et al. (2015). Trastuzumab Interruption and Treatment-Induced Cardiotoxicity in

Early HER2-Positive Breast Cancer. *Breast Cancer Res. Treat.* 149, 489–495. doi:10.1007/s10549-014-3253-7

Conflict of Interest: The authors declare that the research was conducted in the absence of any commercial or financial relationships that could be construed as a potential conflict of interest.

Publisher's Note: All claims expressed in this article are solely those of the authors and do not necessarily represent those of their affiliated organizations, or those of the publisher, the editors, and the reviewers. Any product that may be evaluated in this article, or claim that may be made by its manufacturer, is not guaranteed or endorsed by the publisher.

frontiers | Frontiers in Pharmacology

TYPE Original Research
PUBLISHED 08 September 2022
DOI 10.3389/fphar.2022.873614

OPEN ACCESS

EDITED BY
Zhi-Ren Zhang,
Harbin Medical University, China

REVIEWED BY
Yong Fen Qi,
Peking University, China
Tamer M. A. Mohamed,
University of Louisville, United States
Firdos Ahmad,
University of Sharjah, United Arab Emirates

*CORRESPONDENCE
Zijie Cheng,
cheng.zijie@zs-hospital.sh.cn
Lingmei Qian,
lmqian@shsmu.edu.cn

†These authors have contributed equally to this work

SPECIALTY SECTION
This article was submitted to Cardiovascular and Smooth Muscle Pharmacology, a section of the journal Frontiers in Pharmacology

RECEIVED 11 February 2022
ACCEPTED 29 July 2022
PUBLISHED 08 September 2022

CITATION
Wang X, Zhang L, Feng M, Xu Z, Cheng Z and Qian L (2022), ELA-11 protects the heart against oxidative stress injury induced apoptosis through ERK/MAPK and PI3K/AKT signaling pathways. *Front. Pharmacol.* 13:873614. doi: 10.3389/fphar.2022.873614

ELA-11 protects the heart against oxidative stress injury induced apoptosis through ERK/MAPK and PI3K/AKT signaling pathways

Xuejun Wang[1,2†], Li Zhang[1†], Mengwen Feng[2], Zhongqing Xu[1], Zijie Cheng[1,2*] and Lingmei Qian[1,2*]

[1]Hongqiao International Institute of Medicine, Tongren Hospital, Shanghai Jiao Tong University School of Medicine, Shanghai, China, [2]Department of Cardiology, The First Affiliated Hospital of Nanjing Medical University, Nanjing, China

Increasing evidence revealed that apoptosis and oxidative stress injury were associated with the pathophysiology of doxorubicin (DOX)-induced myocardial injury. ELABELA (ELA) is a newly identified peptide with 32 amino acids, can reduce hypertension with exogenous infusion. However, the effect of 11-residue furn-cleaved fragment (ELA-11) is still unclear. We first administrated ELA-11 in DOX-injured mice and measured the cardiac function and investigated the effect of ELA-11 *in vivo*. We found that ELA-11 alleviated heart injury induced by DOX and inhibited cardiac tissues from apoptosis. *In vitro*, ELA-11 regulated the sensitivity towards apoptosis induced by oxidative stress with DOX treatment through PI3K/AKT and ERK/MAPK signaling pathway. Similarly, ELA-11 inhibited oxidative stress-induced apoptosis in cobalt chloride ($CoCl_2$)-injured cardiomyocytes. Moreover, ELA-11 protected cardiomyocyte by interacting with Apelin receptor (APJ) by using 4-oxo-6-((pyrimidin-2-ylthio) methyl)-4H-pyran-3-yl 4-nitrobenzoate (ML221). Hence, our results indicated a protective role of ELA-11 in oxidative stress-induced apoptosis in DOX-induced myocardial injury.

KEYWORDS

ELA-11, doxorubicin, heart failure, apoptosis, oxidative stress

Abbreviations: LDH, lactate dehydrogenase; ROS, relative oxygen species; TUNEL assay, terminal-deoxynucleotidyl transferase (TdT)-mediated dUTP-biotin nick end-labeling assay; ELISA, enzyme-linked immunosorbent assay; DOX, doxorubicin; $CoCl_2$, cobalt chloride; MDA, malondialdehyde; SOD, superoxide dismutase; ERK, extracellular signal-related kinase; JNK, Jun amino-terminal kinase; PI3K, phosphatidylinositol 3 kinase; AKT, protein kinase B; JC-1, tetrechloro-tetraethylbenzimidazol carbocyanine iodide; ML221, 4-oxo-6-((pyrimidin-2-ylthio) methyl)-4H-pyran-3-yl 4-nitrobenzoate; Scr, scramble; AA, amino acid; EF, ejection fraction; FS, fractional shortening; LVEDs, left ventricular end-systolic dimension; APJ, Apelin receptor (APJ).

Introduction

Myocardial injury caused by chemotherapy drugs is a major reason that affecting the prognosis of tumor patients (Zhang et al., 2019). Statistically, 70% of patients in worldwide have different degrees of cardio-toxic reactions during chemotherapy, and these symptoms will accompany them for life (Leemasawat et al., 2020). In China, nearly 30% of cancer patients die from cardiovascular diseases. The most common cardio-toxicity caused by anthracycline is heart failure, with an incidence of 48% (Wu et al., 2017). It is known that the mechanism of doxorubicin (DOX)-induced cardiotoxicity is very complex, which involving pathological processes such as cell apoptosis, oxygen free radical damage, iron ion metabolism disorder, calcium overload and metabolic disorder (Kostrzewa-Nowak et al., 2005; Govender et al., 2014; Eid et al., 2021). Oxygen free radical injury is one of the representative theories of cardiotoxic injury caused by DOX (Ma et al., 2020). Cytochrome P450 reductase and a variety of reductases can produce superoxide free radicals (O2-) and reduce anthraquinone of DOX to form quinone-semiquinone cycle, leading to lipid peroxidation of mitochondria and microsomes, then damages myocardial cells (Yuan et al., 2020). Due to the decreased content of antioxidant enzymes in cardiomyocytes, a large number of reactive oxygen species and free radicals are generated to induce the oxidative stress response of cardiomyocytes and aggravate the damage of cardiomyocytes (Carrasco et al., 2021). Free radicals generated by DOX activated NAD(P)H oxidases [NAD(P)H oxidases, NOXs] can also activate the apoptosis pathway of cardiac myocytes and cause cell death (Wang et al., 2018). Furthermore, Pharmacological strategies that inhibit apoptosis and oxidative stress injury can protect patients from chemotherapeutic drug-induced myocardial damage.

Oxidative stress is an accompaniment of apoptosis through activating mitochondrial dysfunction, the death receptor pathway or endoplasmic reticulum stress (Dai et al., 2014). When cells are stimulated by oxidative stress, the accumulation of oxidizing substances such as free radicals can damage organelles and activate cell death program (Lüscher, 2015). Recent studies have demonstrated that the increase of intracellular ROS levels could put cells in a state of constitutive oxidative stress, leading to cell apoptosis (Lee et al., 2019). Targeting cell death pathways before oxidative stress manifestation can alleviate oxidative impairment by prevented free radicals which could potentially pave the way for new therapeutics through against oxidative stress induced apoptosis (Münzel et al., 2010; Malla et al., 2020).

It is well known that peptides produced by proteasomes degradation can play a protective role *in vivo* and act as endogenous ligands or receptors to mediate a variety of signaling pathways (Ye et al., 2019). For example, endorphins as an endogenous peptide which can ease pain, like morphine and analgesic (Paes et al., 2019). Angiotensin II binds to angiotensin receptors to regulate water-salt balance and blood pressure in heart and kidney (Johnson et al., 2017). Furthermore, natriuretic peptide family members can be used to diagnose heart failure (Brady et al., 2019). In conclusion, peptides play indispensable roles in regulating physiological function and pathophysiological process.

It has been reported that a conserved gene, AK092578, is predicted to encode a 54aa hormone with a signal peptide (Yang et al., 2017). This hormone is highly conserved among multiple species which is named ELABELA (ELA) or toddler (Read et al., 2019). As an early endogenous ligand of the Apelin receptor (APJ), ELA is essential for heart development. In recent studies, it has been suggested that a 32-amino-acid mature peptide (ELA-32) can be decomposed to produce endogenous fragments including ELA-21 and ELA-11 (Chen et al., 2017). Studies have proved that ELA-32 and ELA-11 could inhibit renal ischemia-reperfusion (I/R) injury, and ELA-21 could significantly increase angiogenesis, promoted cardiomyocyte proliferation and reduced apoptosis and heart fibrosis near the infarct area (Xu, 2021). Recent study has clarified that Elabela (19–32) could ameliorate doxorubicin (DOX)-induced cardiotoxicity by promoting autophagic flux through TFEB pathway (Chen et al., 2022). However, the effect and mechanism of ELA-11 in DOX-induced cardiac injury is unclear.

The PI3K-AKT signaling pathway is a classical signaling pathway that regulates apoptosis (Brady et al., 2019). PI (3, 4, 5) P_3 is an intracellular second messenger in the cell that is required for the transfer of protein kinase B (AKT) to the membrane for activation (Lin et al., 2019). Phosphorylation of AKT mediates insulin and various growth factors to induce cell growth and promotes cell survival through numerous channels (Song et al., 2018). ELA-11 induced ERK/MAPK is a classical anti-apoptotic signaling pathway. When the downstream phosphorylation of ERK is activated, it inhibits the process of apoptosis.

In present study, we found that ELA-11 could attenuate DOX-induced free radical production, which protected cardiomyocytes against oxidative stress-induced apoptosis. Mechanistically, ELA-11 inhibited oxidative stress-induced apoptosis by suppressing mitochondrial membrane potential mediated by ERK/MAPK and PI3K/AKT signaling pathways. Moreover, ELA-11 acted as a protective role in DOX-induced cardiac injury by targeting APJ.

Materials and methods

Cell culture

Rat primary cardiomyocytes were extracted from rats 24 h after birth. The blood, fat, connective tissues and heart tissue sections were separated and digested with trypsin at 37°C at 60 rpm for 15 min. The solution was removed, and the digestion was repeated three times. The cell-containing digested fluids were placed in a centrifuge tube and centrifuged together after passing

through a 180-mesh filters. The cells were resuspended in 10 ml DMEM containing 10% horse serum (HS, Gibco, United States) and incubated in a 10 cm^2 dish for 1.5 h. The cell suspension was removed, and the cells ($5–6 \times 10^5$ cells per dish) were inoculated into a new dish as previously described. When cell adhered to about 80%, 1uM ELA-11 was added to the culture media. After 12 h of co-incubation with DOX, experimental verification was carried out.

Animals

Male C57BL/6J mice (6–8 weeks of age, 20–22 g) were obtained from the Model Animal Research Center of Nanjing University (Nanjing, Jiangsu, China), and all procedures used were approved by the ethical committee of Nanjing Medical University. All animals were housed at 20–25°C and 50%–70% relative humidity. The experimental mice were randomly divided into four groups. Before injected with 5 mg/kg DOX by intraperitoneal injection for five consecutive weeks, 10 mg/kg ELA-11 was injected to mice through veil tail for 7 days, after which electrocardiograms were obtained and the mice were sacrificed. The mice were treated according to the experimental requirements. All animal experiments complied with the Guide for the Care and Use of Laboratory Animals published by the National Institutes of Health (NIH Publications No. 85-23, revised 1996).

Cell-in-cell experiment

We chemically synthesized FITC-labeled, incubated cells with ELA-11 for 1 h at 37°C and 5% CO_2 atmosphere. The localization of ELA-11 was observed by fluorescence microscopy.

Cell counting kit-8 assay

Thousand cells were inoculated into each well of the 96-well plate, ELA-11, DOX or $CoCl_2$ was added into the plates respectively after cells were adhered. Measured the absorbance at 450OD. Cell viability (%) = [OD (experimental group)–OD (blank group)]/[OD (control group)–OD (blank group)] * 100%.

Cell death rates

Trypan blue staining was used to calculate the mortality of the primary cells. The cells were collected at different times (0, 6, 12, 18, 24 or 36 h) and stained with the dye from a trypan blue staining cell viability assay kit to determine the cell death rate. At different concentrations of DOX (0.1, 0.5, 1, 2, and 5 μM) and $CoCl_2$ (200, 400, 600, 800 and 1,000 μM), measurements were taken according to the manufacturer's instructions.

Lactate dehydrogenase level detection

Levels of lactate dehydrogenase (LDH) released were detected in serum using an LDH release assay kit according to the manufacturer's protocol.

Terminal-deoxynucleotidyl transferase-mediated dUTP-biotin nick end-labeling staining assay

The rate of apoptosis can be was detected by a TUNEL staining kit. The cells were seeded (1×10^5 cells per well) in 6-well dishes. After the treatments described above were performed, the cells were washed once with phosphate-buffered saline (PBS) and fixed with 4% paraformaldehyde. Apoptotic cells were visualized with TUNEL staining according to the manufacturer's protocol. TUNEL fluorescence intensity/DAPI fluorescence density was used to calculate the percentage of positive cells, and the density was evaluated using ImageJ software 1.26 (Wayne Rasband, National Institutes of Health, Bethesda, MD, United States).

Tetrechloro-tetraethylbenzimidazol carbocyanine iodide assay

The mitochondrial membrane potential was measured by a mitochondrial membrane potential assay kit with JC-1 according to the manufacturer's instructions. The cells were cultured in serum-free DMEM containing (×1) JC-1 staining working fluid at 37°C for 20 min. Then, the cells were washed twice with JC-1 buffer, after which 2 ml DMEM was added, and then the cells were photographed with a fluorescence microscope (BX61; Olympus Corporation, Tokyo, Japan). The JC-1 density was assessed by ImageJ software and calculated upon normalization to the control.

Reactive oxygen species measurement

The levels of intracellular ROS were determined using a relative oxygen species assay kit following the instructions. Cells were incubated in serum-free DMEM containing 0.1% DCFH-DA at 37°C for 20 min, washed with serum-free DMEM three times and photographed with a fluorescence microscope.

Western blot

Proteins were isolated from cells using lysis buffer (containing RIPA and 1% PMSF). Protein quantification was performed using a BCA protein detection kit (23229; Thermo

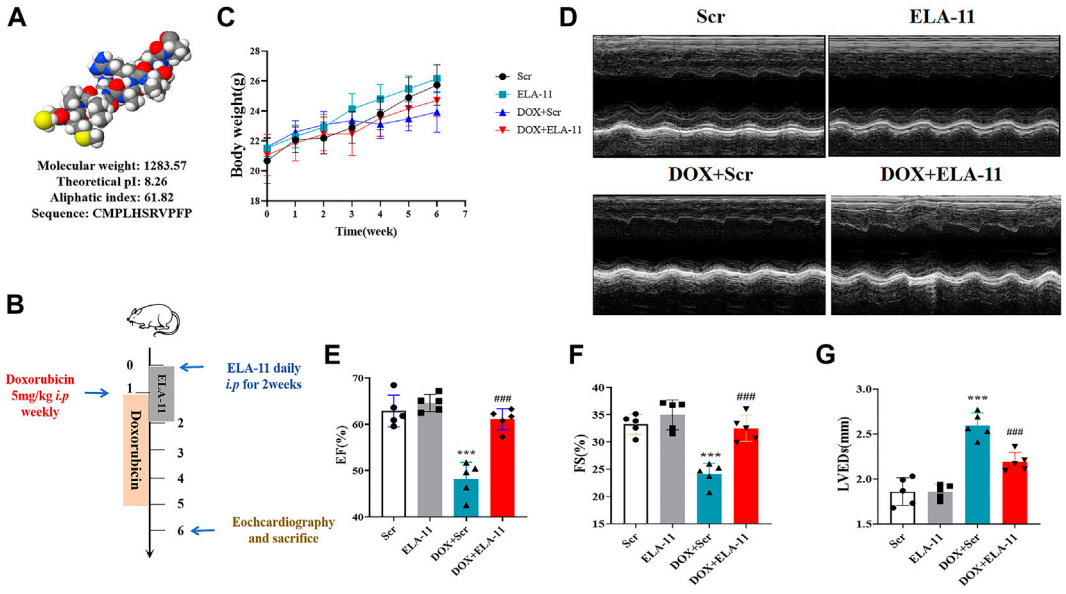

FIGURE 1
Function of ELA-11 in doxorubicin-injured model. **(A)** The biological characteristics of ELA. **(B)** Schematic map for DOX-induced mice cardiac injury model. **(C)** The body weight of mice in four groups during the experiment. **(D)** The representative echocardiograms of DOX-induced cardiac injured group. **(E)** EF value for echocardiography. **(F)** FS value for echocardiography. **(G)** LVEDs value for echocardiography. ***$p < 0.001$ and $^{###}p < 0.001$, one-way ANOVA, N = 5 mice per group.

Fisher Scientific). Protein samples of the same mass were separated on 10% SDS-PAGE gels and transferred to nitrocellulose membranes (Millipore, Billerica, MA, United States), which were blocked with 5% skim milk and then incubated with specific primary antibodies. Caspase-3 (14220T, 1:1000), PARP (9532T, 1:1000), β-actin (3700S, 1:1000), GAPDH (5174T, 1:1000), AKT (4685S, 1:1000), p-AKT (4060T, 1:2000), PI3K (4249T, 1:1000), ERK (4695T, 1:1000) and p-ERK (4370T, 1:1000) were purchased from Cell signaling Technology. The anti-rabbit (SA00001-2, 1:10000), PI3K (20584-1-AP, 1:1000) and anti-mouse (SA00001-1, 1:10000) secondary antibody were purchase from Proteintech. FluorChem M system was used to quantify the positive bands representing proteins involved in the orchestrated immune responses (ProteinSimple, San Jose, CA, United States).

Malondialdehyde, superoxide dismutase, and glutathione peroxidase assay

Cellular oxidative stress was determined by detecting the state of intracellular oxidation and reduction. Lipid peroxidation Malondialdehyde (MDA) assay (Beyotime, Nanjing, China) and total superoxide dismutase assay (Beyotime, Nanjing, China) were measured by following the manufacturer's instructions. glutathione peroxidase (GSH-Px) assay kit was purchased from Elabscience. The cell supernatant was collected, and the standard substance was prepared and diluted according to the instructions, the concentration of each well was 600, 400, 200, 100, and 50 U/L, respectively. The tested samples were added to the plate and mixed, then incubated at 37°C for 30 min. Wash plates, add enzyme and chromogenic reaction were proceeded according to the instructions. After incubating at 37°C for 15 min, the absorbance of each well was measured at 450 nm wavelength.

Echocardiography

Post DOX and ELA-11 administration, all the mice were subjected to M-mode echocardiography to assess heart function. All animal experiments complied with the Guide for the Care and Use of Laboratory Animals published by the National Institutes of Health (NIH Publications No. 85-23, revised 1996).

Enzyme-linked immunosorbent assay

Serum Creatine kinase isoenzyme (CKMB) and B-type natriuretic peptide (BNP) level in mice heart tissue was determined by a commercially available Enzyme-linked immunosorbent assay (ELISA) kit (Mlbio, Shanghai, China) according to the manufacturer's instructions.

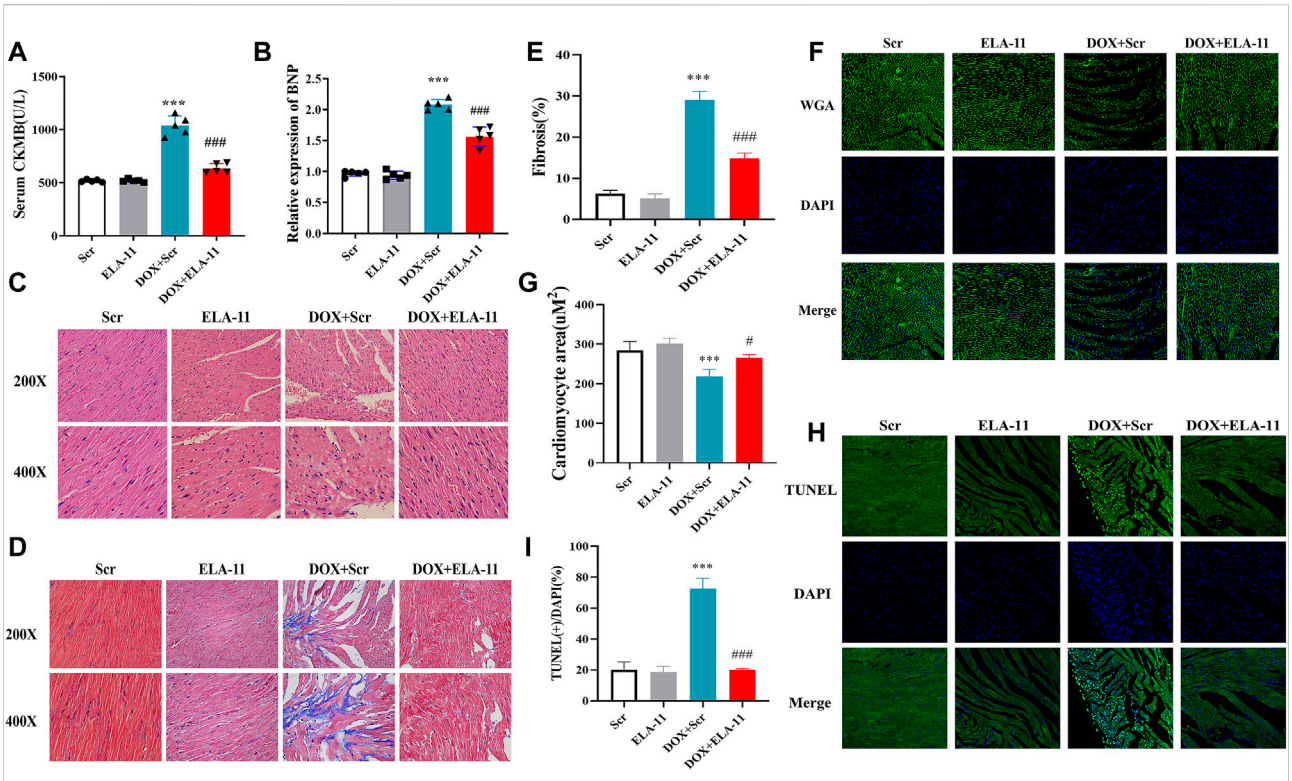

FIGURE 2
ELA-11 protects doxorubicin-injured heart in vivo. **(A)** Serum CKMB release in DOX-injured model. **(B)** Serum BNP release in DOX-injured model. **(C)** Representative photographs of HE staining. **(D)** Representative photographs of Masson staining. **(E,F)** Representative photographs of WGA staining and its quantitative data. **(G,H)** Representative photographs of TUNEL staining and its quantitative data. ***$p < 0.001$ and $^{###}p < 0.001$, one-way ANOVA, N = 5 mice per group.

Hematoxylin & Eosin (H&E) Staining

Obtained the cardiac tissues and fixed them in 4% paraformaldehyde for 7 days after the blood in the heart cavity was pumped out. The tissue was transparent with ethanol and xylene. Soak the transparent tissue into melted paraffin for embedding. After cooling and solidification, they were cut into five micron slices and placed in hot water to flatten and then pasted onto slides and dried in a 45°C incubator. Before staining, paraffin was removed again, and Hematoxylin and eosin dyes were respectively used for staining, which made the nucleus and intracellular ribosomes stained blue and purple by Hematoxylin (H). The cytoplasm is stained red or reddish with Eosin (E).

Masson staining

Obtained and sectioned tissue according to the above method. Weigert sapwood semen was used for staining nuclear for 5–10 min, and ponceau acid fuchsin solution was used for 5–10 min after washing. Soaked with 2% glacial acetic acid solution for 30 s, and differentiate with 1% phosphomolybdate solution for 3–5 min. Then, the slices were dyed with aniline blue for 5 min, and bathed again with 0.2% glacial acetic acid solution for 30 s. Finally, the slices were sealed with 95% alcohol, anhydrous alcohol, xylene transparent and neutral gum.

Wheat germ agglutinin staining

Obtained and sectioned tissue according to the above method. Placed the section in the antigen repair buffer of pH 8.0, then the section was decolorized with PBS after cooled naturally. A histochemical pen was used to draw circles around the tissues and Wheat germ agglutinin (WGA) staining buffer was added into the circles, and the cells were incubated for 30 min at 37°C. The nucleus was stained with DAPI. Sealed the section, then collected the images under fluorescence microscope.

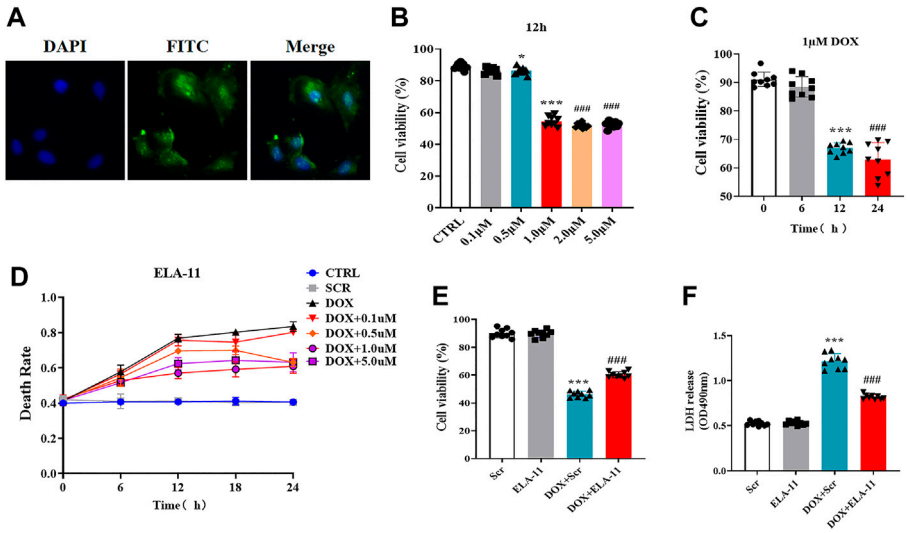

FIGURE 3
ELA-11 attenuates doxorubicin-induced injury in rat primary cardiomyocytes. **(A)** The location of ELA-11 in rat primary cardiomyocytes. **(B)** Trypan blue assay for cell death with different concentration of DOX with different duration (N = 9 per group). **(C)** The cell viability of 1 uM DOX in different duration (N = 9 per group). **(D)** Cell viability of ELA-11 with different concentration for 12 h (N = 9 per group). **(E)** Cell viability in DOX-induced cardiomyocyte model (N = 9 per group). **(F)** LDH release in DOX-induced cardiomyocyte model (N = 9 per group). ***$p < 0.001$ and $^{###}p < 10.001$, one-way ANOVA.

Statistical analysis

All results are expressed as the mean ± SD. Comparisons between multiple groups were performed by one-way analysis of variance (ANOVA), and $p < 0.05$ (*), $p < 0.01$ (**) and $p < 0.001$ (***) were considered significant. All experiments were repeated at least three times unless otherwise specified. All data was analyzed by GraphPad Prism software.

Results

Function of ELA-11 in doxorubicin-injured model

To understand the shape of ELA-11 in molecular chain, we predicted its structure by I-TASSER server (https://zhanggroup.org/I-TASSER/) and analyzed the biological characteristics through Expasy (https://www.expasy.org/) (Figure 1A). We found that ELA-11 possessed the advantages of light molecular weight and high lipid solubility. Hence, we investigated the effect of ELA-11 in DOX-induced cardiac injury *in vivo* (Figure 1B). We weighed the mice every 2 weeks for 10 weeks, the result demonstrated that the weight of DOX-induced group began to decrease after 6 weeks, scramble (scr) peptide could not affect cell death, but DOX increased cell death since week 5. Compared with DOX, ELA-11 could increase weight index significantly (Figure 1C). Next, the echocardiographic results suggested that DOX reduced ejection fraction (EF) and fractional shortening (FS), but increased left ventricular end-systolic dimension (LVED) significantly, however, ELA-11 increased EF and FS, and decreased left ventricular end-systolic dimension (LVED) significantly compared with DOX + Scr group (Figures 1D–G). These results demonstrated that ELA-11 could inhibit DOX-induced injury *in vivo*.

ELA-11 protects doxorubicin-injured heart in vivo

Then, our results demonstrated that the release of CKMB and BNP in blood serum increased significantly in DOX + Scr treated group compared with Scr group, but ELA-11 decreased CKMB and BNP release significantly (Figures 2A,B). To further identify the effect of ELA-11 *in vivo*, we collected organs to perform pathological examination. HE staining results indicated that myocardial fibers in DOX-treated group were in disordered arrangement and cardiomyocytes were changed into vacuolated compared with Scr group, but there was less disarrayed myocardial fibers and vacuolated cells in DOX + ELA-11 treated group (Figure 2C). The evidence from Masson staining suggested that fibrosis was significantly increased by DOX but reduced by ELA-11 (Figures 2D,E). To figure out the cardiomyocyte areas of the four groups, WGA staining results demonstrated that the cardiomyocyte area decreased

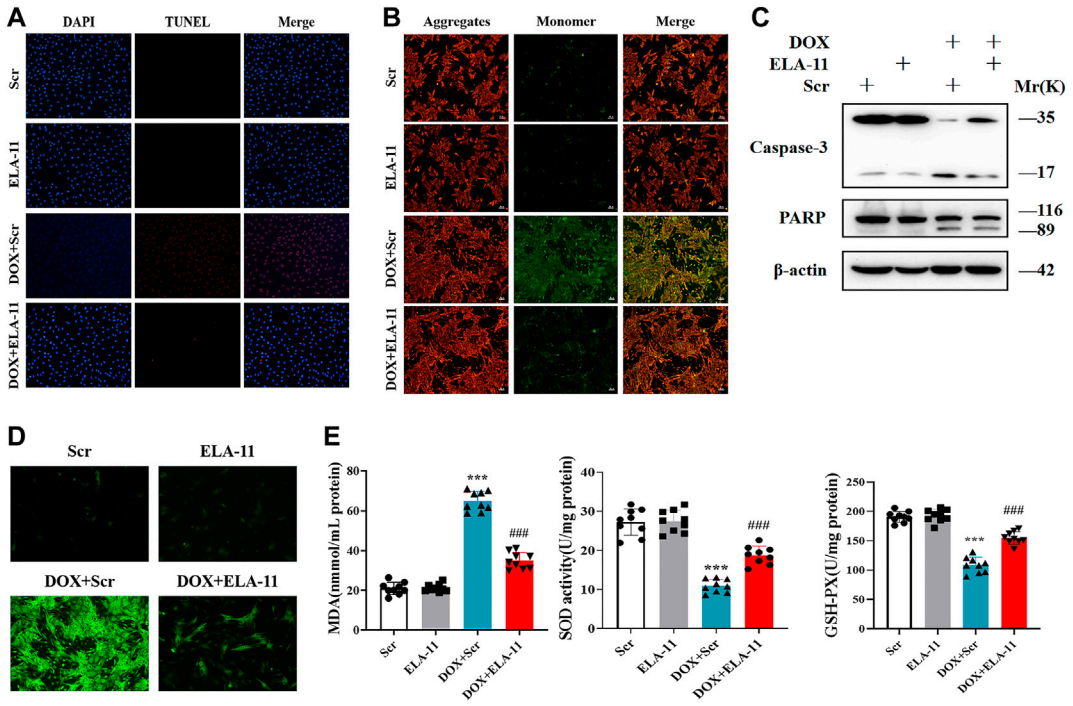

FIGURE 4
ELA-11 inhibits DOX-induced cardiac injury through oxidative stress -induced apoptosis. **(A)** Representative photographs of TUNEL staining in DOX- induced cardiomyocyte injury (N = 9 per group). **(B)** Representative photographs of JC-1 in DOX-induced cardiomyocyte injury. **(C)** The expression of PARP and caspase-3 in DOX-induced cardio-myocyte injury by western blot. **(D)** Representative photographs of ROS in DOX-induced cardio-myocyte injury. **(E)** Detection of MDA production, SOD activity and GSH-PX release in DOX-induced cardiomyocyte injury (N = 9 per group). ***$p < 0.001$ and $^{###}$ $p < 0.001$, one-way ANOVA.

significantly in DOX-treated group compared with the Scr group, but ELA-11 significantly rescued cardiomyocyte area (Figures 2F,G). TUNEL staining showed a significant increase in the apoptosis rate in the myocardium in the DOX + Scr group, and it generally decreased to the level in DOX mice administered with ELA-11 (Figures 2H,I). These results demonstrated that ELA-11 might have a protective role in DOX-induced cardiac injury.

ELA-11 attenuates doxorubicin-induced injury in rat primary cardiomyocytes

To determine the effect of ELA-11 *in vitro*, we first cultured rat primary cardiomyocytes with ELA-11, we found that ELA-11 could enter into the cytoplasm (Figure 3A). To figure out the optimal concentration of DOX, we incubated DOX with different concentrations (0.1, 0.5, 1, 2, and 5 uM) for 12 h, CCK-8 results demonstrated that 0.5 uM DOX could reduce cell viability, but 1, 2, and 5 uM decreased cell viability more significantly and there were no difference among 1, 2 and 5 uM DOX (Figure 3B). Then CCK-8 results manifested that 1 uM DOX cultured for 12 and 24 h could effectively reduce the cell survival rate, however there was no statistic difference between the two groups (Figure 3C). To figure out whether ELA-11 could affect cell survival, we cultured ELA-11 with different duration times (0, 6, 12, and 24 h) and concentrations (0.1, 0.5, 1, 2, and 5 uM). Then trypan blue dyeing results demonstrated that 0.5 uM ELA-11 decreased cell death at 24 h, 1 uM, and 5 uM ELA-11 both could decrease cell death at 12 h. But there was no significant difference among the groups (Figure 3D). Next, we cultured 1 uM ELA-11 before DOX treatment for 12 h and found ELA-11 could significantly increase cell viability compared with DOX + Scr group (Figure 3E). And LDH results indicated that ELA-11 inhibited DOX-induced cardiotoxicity (Figure 3F). Our study revealed that ELA-11 could attenuate DOX-induced injury in rat primary cardiomyocytes.

ELA-11 inhibits doxorubicin-induced cardiac injury through oxidative stress-induced apoptosis

Based on the effect of ELA-11 *in vivo*, we further detected the apoptosis level by TUNEL, the results revealed that the number of apoptotic cells was increased in the DOX-induced group but

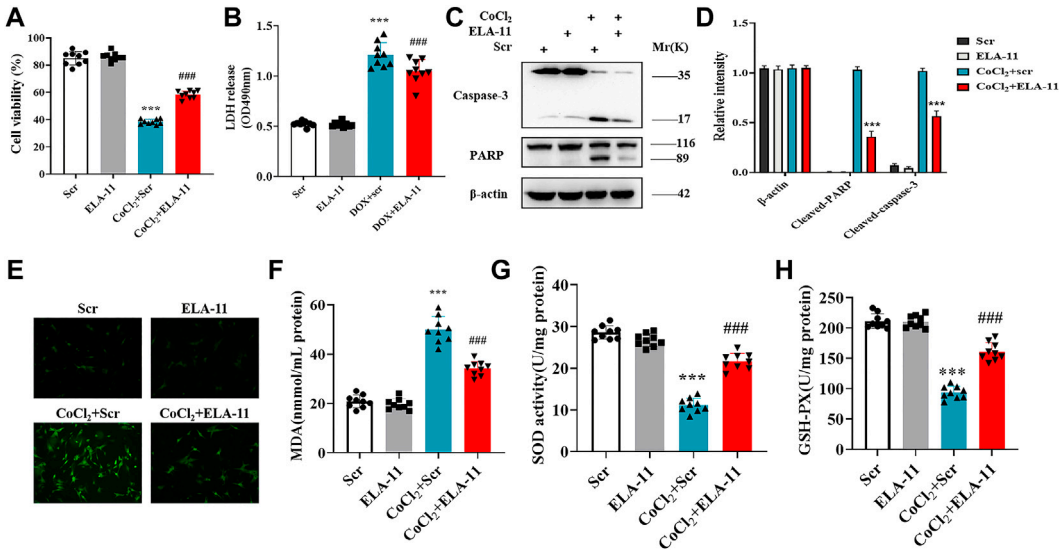

FIGURE 5
ELA-11 protected cardiomyocytes against oxidative stress-induced apoptosis in $CoCl_2$ model. **(A)** Cell viability in $CoCl_2$ -induced cardiomyocyte model. **(B)** LDH release in $CoCl_2$ -induced cardiomyocyte oxidative stress injury (N = 9 per group). **(C,D)** The expression of PARP and caspase-3 in $CoCl_2$ -induced cardiomyocyte oxidative stress injury by western blot. **(E)** Representative photographs of ROS production in $CoCl_2$ -induced cardiomyocyte oxidative stress injury. **(F–H)** Detection of MDA production, SOD activity and GSH -PX release in $CoCl_2$ -induced cardiomyocyte oxidative stress injury (N = 9 per group). ***$p < 0.001$ and $^{###}p < 0.001$, one-way ANOVA.

reduced after ELA-11 co-treatment (Figure 4A). Furthermore, DOX reduced mitochondrial membrane potential compared with scr group, but ELA-11 elevated mitochondrial membrane potential compared with DOX treatment (Figure 4B). The western blot results revealed that cleaved caspase-3 and PARP were activated by DOX, but ELA-11 reduced the elevated expression of cleaved caspase-3 and PARP (Figure 4C). Next, ROS release results indicated that ELA-11 attenuated DOX-induced free radical production (Figure 4D). Furthermore, we evaluated cellular oxidative stress levels by MDA production, SOD activity and GSH-Px content. Our results demonstrated that DOX increased MDA production and reduced SOD activity and GSH-Pxproduction, but ELA-11 inhibited MDA production, promoted SOD activity and GSH-Px production (Figure 4E). Therefore, ELA-11 could inhibit DOX-induced injury by attenuating oxidative stress-induced apoptosis.

ELA-11 protected cardiomyocytes against oxidative stress-induced apoptosis in $CoCl_2$ model

To validate the role of ELA-11 in another oxidative stress model, we further constructed chemical ischemic model in rat primary cardiomyocytes. Our results indicated that ELA-11 protected cardiomyocytes from $CoCl_2$-induced injury (Figures 5A,B). Then western blot evidence proved that ELA-11 could inhibit $CoCl_2$-induced cardiac apoptosis (Figures 5C,D). Furthermore, ELA-11 inhibited ROS production with $CoCl_2$ treatment (Figure 5E). And ELA-11 inhibited superoxide production and peroxidase activity (Figures 5F–H). Our results further proved ELA-11 protected cardiac injury in $CoCl_2$ model mediated by oxidative stress-induced apoptosis.

ELA-11 attenuated cardiac injury through ERK/MAPK and PI3K/AKT signaling pathway

We further verified the possible signaling pathway of ELA-11 in rat primary cardiomyocytes by Western blot. We first determined the expression of p38, JNK and ERK, however, the result showed that there was no expression of JNK and p38 (data not shown), but phosphorylated ERK was down-regulated by DOX and ERK protein phosphorylation was activated upon ELA-11 treatment compared with DOX (Figures 6A,B). Next, we found that DOX also down-regulated the expression of phosphorylated AKT and PI3K, but ELA-11 activated phosphorylation of AKT and PI3K protein expression (Figures 6C–E). When $CoCl_2$ was blunted, the phosphorylation of ERK, AKT and PI3K protein expression was downregulated. With intervention of ELA-11, ELA-11 activated the expression of ERK, AKT and PI3K phosphorylated proteins after $CoCl_2$ treatment in rat primary cardiomyocytes (Figures 6F–J). These

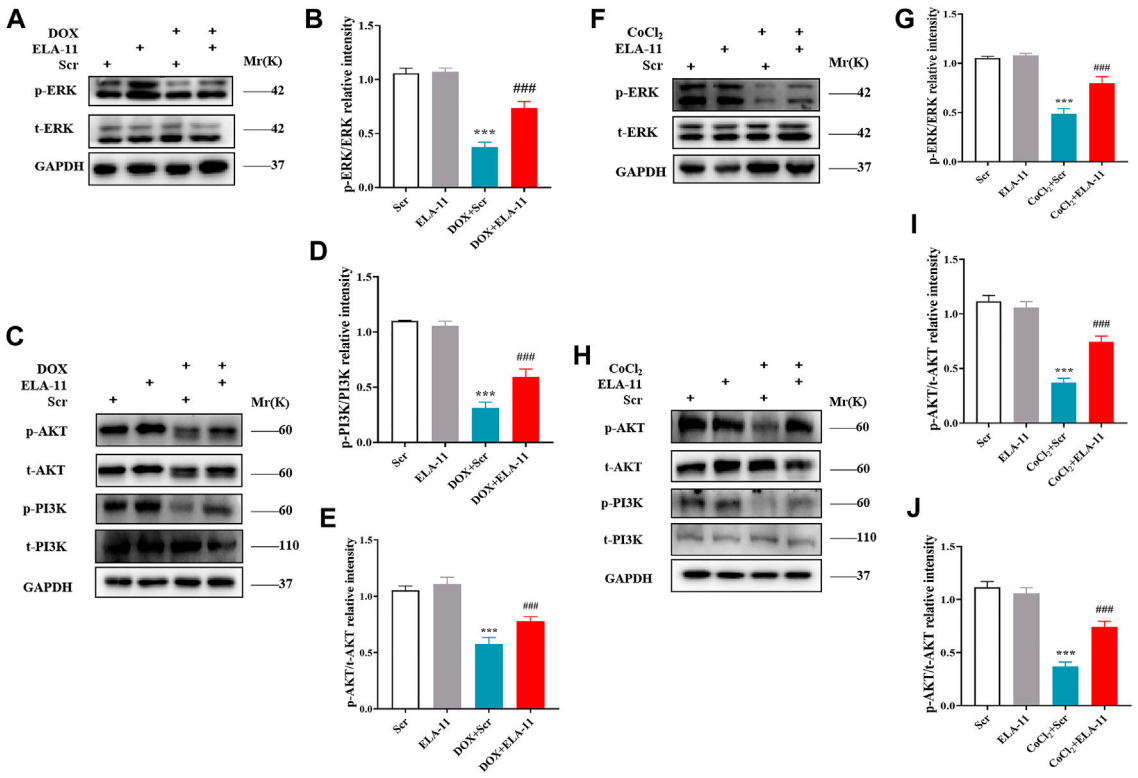

FIGURE 6
ELA-11 attenuated cardiac injury through ERK/MAPK and PI3K/AKT signaling pathway. **(A)** The expression of ERK in DOX-induced cardiac injury by western blot. **(B)** The quantitative data for western blot. **(C–E)** The expression of PI3K and AKT in DOX-induced cardiac injury by western blot and its quantitative data. **(F,G)** Western blot analyzed the expression the expression of ERK in CoCl2 -induced cardiac injury and its quantitative data. **(H–J)** Western blot analyzed the expression the expression of PI3K and AKT in $CoCl_2$ -induced cardiac injury and its quantitative data. ***$p <$ 0.001 and $^{###}p < 0.001$, one-way ANOVA.

results revealed that ELA-11 protected cardiomyocytes from apoptosis through the ERK/MAPK and PI3K/AKT signaling pathways.

ELA-11 protects cardiomyocytes by binding apelin receptor

4- oxo-6-((pyrimidin-2-ylthio) methyl)-4H-pyran-3-yl4-nitrobenzoate (ML221) is the first reported APJ antagonist which exerts antagonistic effect mainly by inhibiting cAMP and recruiting β-arrestin by ELA-11. Report has shown that ML221 has potential to attenuate the activation and signaling of the APJ receptor and reduce elabela-induced microvascular endothelial cell proliferation (Godoy-Parejo et al., 2019). To determine the role of ML221, we used to detect its interaction with ELA-11 by Western blot. We found that ML221 inhibited the effect of ELA-11 on cardiomyocyte apoptosis after DOX administration (Figures 7A,B). We wondered whether ML221 was involved in the ERK/MAPK and PI3K/AKT signaling pathways when the cells were treated with DOX, and western blot results demonstrated that ML221 significantly decreased the phosphorylation of AKT, PI3K, and ERK proteins compared with ELA-11, when ELA-11 and ML221 co-incubation with DOX, the ability of ELA-11 to activate phosphorylated ERK, PI3K and AKT was inhibited (Figures 7C–G). Furthermore, we found that ML221 could also inhibit the effect of ELA-11 in $CoCl_2$-induced apoptosi s (Figures 7H,I). The phosphorylation of AKT, PI3K and ERK proteins was significantly up-regulated after co-treatment with ML221 and ELA-11 in $CoCl_2$ model (Figures 7J,K,L–N). These results suggested that ELA-11 inhibited apoptosis by binding to APJ. Finally, we drew a pattern diagram of ELA-11 for inhibiting apoptosis and oxidative stress injury in cardiomyocytes (Figures 8).

Discussion

Our current study revealed that ELA-11 has a protective effect on apoptosis and attenuates DOX-induced cardiotoxicity *in vitro* and *in vivo*. Furthermore, we demonstrated that ELA-11

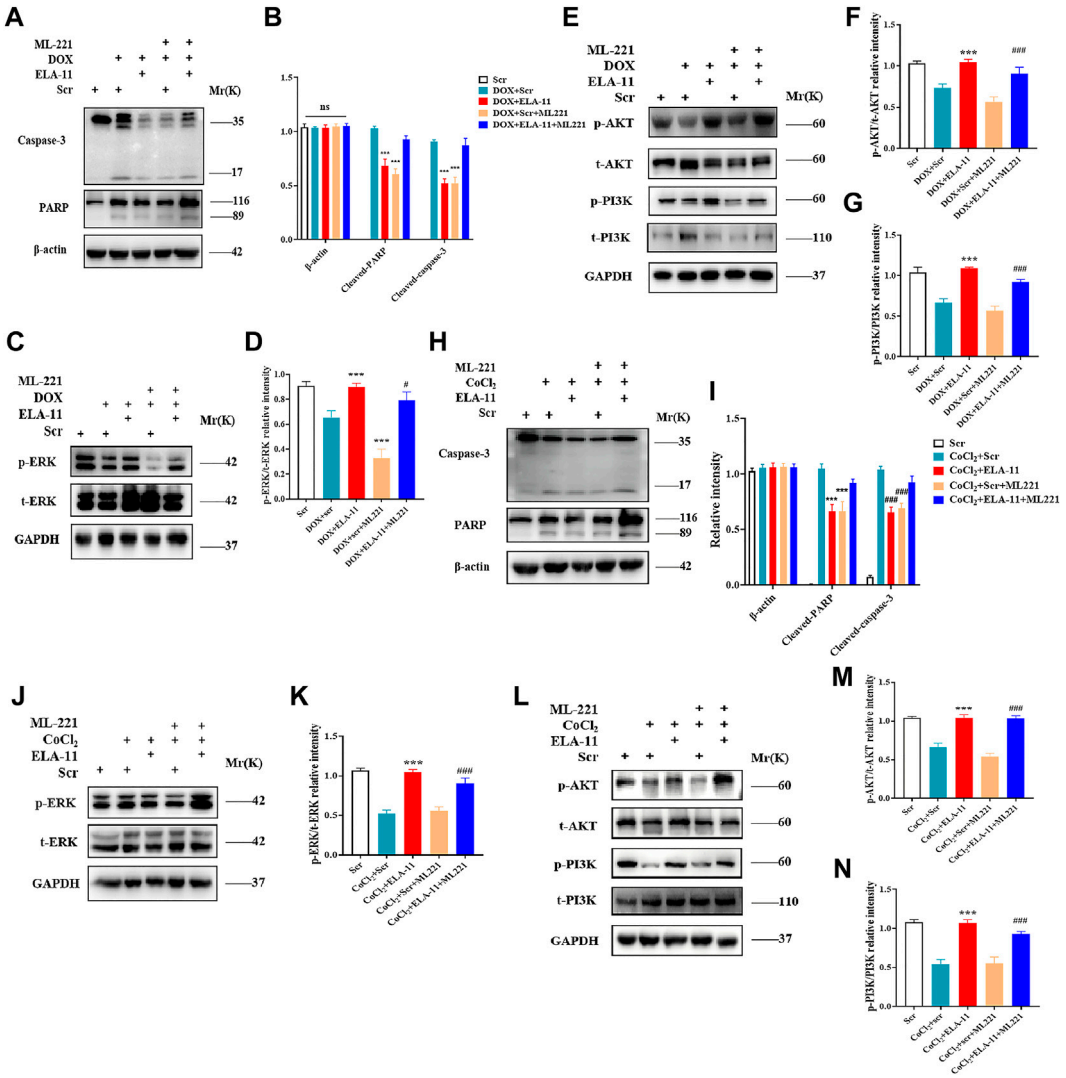

FIGURE 7
ELA-11 protects cardiomyocytes by binding APJ. **(A,B)** Western blot result of PARP and caspase-3 with ML221 treatment in DOX-induced group and its quantiied data. **(C,D)** Western blot result of ERK with ML221 treatment in DOX -induced group and its quantiied data. **(E–G)** Western blot and quantiied data for PI3K and AKT in DOX-induced group. **(H,I)** The expression of PARP and casapse-3 in $CoCl_2$ -induced group by western blot and quantiied. **(J,K)** The expression of ERK in $CoCl_2$ -induced group by western blot and quantiied. **(L–N)** The expression of PI3K and AKT in $CoCl_2$ -induced group with quantiied data. ***$p < 0.001$, and $^{###}$ $p < 0.001$, one-way ANOVA.

attenuated oxidative stress-induced apoptosis through ERK/MAPK and PI3K/AKT signaling pathways by targeting APJ. ERK/MAPK and PI3K/AKT signaling pathways is regarded as a promising molecular mechanism in apoptosis, proliferation and differentiation. Our findings provide evidence of the molecular mechanism by which the ELA-11 peptide inhibits oxidative stress-induced apoptosis, indicating its potential use for DOX-induced cardiotoxicity.

Many known bioactive substances secreted by heart, including ANP, have been indicated to be involved in the regulation of cardiovascular disease and sensitive as indicators of disease monitoring (Ishimaru et al., 2017). In addition, endocrine-derived peptides play a dispensable role in different pathological processes and engage in organ crosstalk. For instance, a vasoactive intestinal polypeptide of 28 amino acids is released by intestinal neurons (Reginauld et al., 2019). Its level of variation is related to a variety of human diseases. It is worth observing that some long peptides can be cleaved into smaller peptides that have more consequential functions than those of longer peptides.

Because of the cardiac toxicity caused by DOX, its clinical application is severely limited (Sun et al., 2019). Apoptosis and

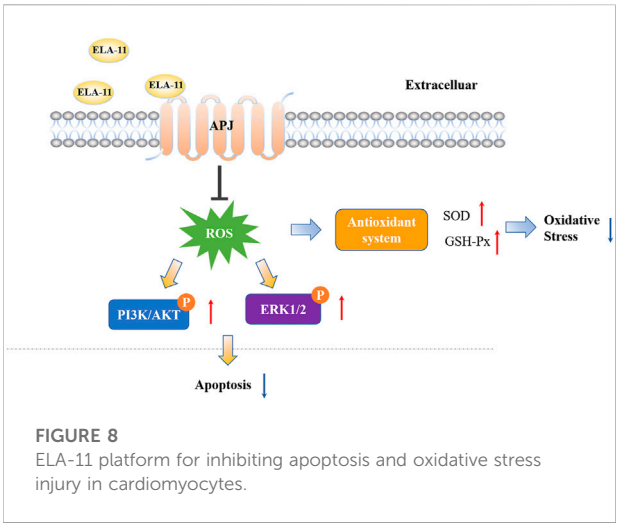

FIGURE 8
ELA-11 platform for inhibiting apoptosis and oxidative stress injury in cardiomyocytes.

oxidative stress injury induced by DOX came into our insight. $CoCl_2$ is a classic and effective compound used to simulate hypoxic and ischemic processes (Ma et al., 2020). In consistence with previous studies, our study has demonstrated that DOX and $CoCl_2$ can induce apoptosis and oxidative stress injury. APJ receptor is an essential orphan G protein-coupled receptor super-family. Previous studies have demonstrated that ELA-21 and ELA-32 involved in heart development and stem cell maintenance (Dai et al., 2008). ELA-11 is the shortest peptide in ELABELA family and may retain the functional peptide to perform biological functions (Ma et al., 2021). We proved that ELA-11 can also protect cardiac function by interacting with APJ.

As an endogenous ligand of Apelin, APJ plays a cardiovascular protective role by binding to different G protein subtypes and trigger multiple signaling pathways, such as AMPK, PI3K/Akt or MAPK signaling pathways (Li et al., 2021). Elabela was first identified as a novel ligand of APJ receptor in zebrafish embryos. The Ela-APJ axis is critical to a variety of biological processes and has been shown to regulate humoral homeostasis, myocardial contractility, vasodilation, angiogenesis, cell differentiation, apoptosis, oxidative stress, cardiorenal fibrosis and dysfunction (Sato et al., 2017). In human embryonic stem cells, Elabela can activate PI3K/Akt/MTORC1 signaling pathway to regulate self-renewal and survival of stem cells (Ho et al., 2015). As we all know that DOX induced cardiotoxicity involves a variety of molecular mechanisms, including energy metabolism, oxidative stress, and programmed cell death (Tocchetti et al., 2014). The excessed ROS can be effectively eliminated by the antioxidant defense system in physiological status (Zhang et al., 2022). However, when the antioxidant defense system is unable to consume excessive levels of ROS, cytotoxic signaling pathways will activate, leading to DNA damage, mitochondrial dysfunction and abnormal cellular calcium homeostasis.

Oxidative stress irritates the activity of ion exchangers, including Na+/H+ exchangers (NHE-1) and transient receptor potentials melastain 2 (TRPM2), resulting in overload of cell serum and mitochondrial Ca2+. Overloaded Ca2+ leads to activation of mitochondrial Ca2+ sensitive dehydrogenase and massive production of respiratory metabolic chain substrate NADH, which again promotes ROS production (Javadov et al., 2008). This cycle eventually leads to dyshomeostasis, apoptosis, inflammatory responses and other pathological process. Hence, ROS overproduction is the main event of oxidative stress injury (Schieber and Chandel, 2014). Mechanically, as an essential signaling pathway of G-protein-coupled receptors, APJ can activates RAF-1 to phosphorylate threonine and tyrosine through PI3K/AKT, and ultimately activate ERK1 and ERK2 (i.e., p44MAPK and p42MAPK) (Chiu et al., 2013). Therefore, AKT and ERK signaling pathways play a key role in oxidative stress response.

Multiple evidence indicated that mitochondrial permeability conversion pore (mPTP) plays a key role in regulating cardiac apoptosis under pathological conditions (Hou et al., 2022). Changes in intracellular pH, mitochondrial membrane potential or reactive oxygen species can regulate THE opening of mPTP (Ahmad et al., 2019). Glycogen synthase kinase (GSK)-3α/β is a serine/threonine kinase that regulates the opening of mPTP and participates in the apoptosis process of cardiomyocytes (Ahmad et al., 2014). The activation of PI3K/AKT signaling pathway may regulate the activation of GSK-3 downstream protein. Knock down the expression of GSK-3 in adult cardiomyocyte can lead to mitotic catastrophe which resulting in fatal dilated cardiomyopathy (Zhou et al., 2016; Ahmad and Woodgett, 2020). And inhibition of GSK-3αmay be a novel strategy for limited adverse ventricular remodeling and dysfunction after myocardial infarction in future treatment (Lal et al., 2015). Whether GSK-3 can play a role in DOX induced cardiotoxicity will be further explored in future studies.

Although recent studies have shown that the short peptide ELABELA (19–32) can ameliorate DOX-induced cardiotoxicity by promoting autophagic flux through TFEB pathway, ELA-11, shorter than ELABELA (19–32) reduced ROS release, thereby inhibiting mitochondrial oxidative stress and further inhibiting apoptosis of cardiomyocytes. Furthermore, In our study, the results supported that ELA-11 resisted cardiotoxicity by inhibiting apoptosis and oxidative stress by activating PI3K, AKT and ERK phosphorylation.

Our study also has some limitations. First, more clinical samples are needed to determine the exact window of time of interactions for clinical application. Second, whether the modification of ELA-11 influences its function in cardiovascular diseases needs further evaluation.

Data availability statement

The original contributions presented in the study are included in the article/Supplementary Materials, further inquiries can be directed to the corresponding authors.

Ethics statement

The animal study was reviewed and approved by the Peptide and doxorubicin-induced cardiotoxicity.

Author contributions

LQ designed the research. XW, LZ, and MF performed the experiments. ZX analyzed the data. XW and ZC wrote the manuscript. LQ and ZC supervised the work.

Funding

This work was supported by the National Natural Science Foundation of China (Grant No. 81873540), Jiangsu provincial key research and development program (Grant No. BE2019752), Changning Science and Technology Commission (CNKW2020Y06) and Technology Transfer and Promotion Project of School of Medicine, Shanghai Jiaotong University (ZT202013).

Conflict of interest

The authors declare that the research was conducted in the absence of any commercial or financial relationships that could be construed as a potential conflict of interest.

Publisher's note

All claims expressed in this article are solely those of the authors and do not necessarily represent those of their affiliated organizations, or those of the publisher, the editors and the reviewers. Any product that may be evaluated in this article, or claim that may be made by its manufacturer, is not guaranteed or endorsed by the publisher.

Supplementary material

The Supplementary Material for this article can be found online at: https://www.frontiersin.org/articles/10.3389/fphar.2022.873614/full#supplementary-material

References

Ahmad, F., Lal, H., Zhou, J., Vagnozzi, R. J., Yu, J. E., Shang, X., et al. (2014). Cardiomyocyte-specific deletion of Gsk3α mitigates post-myocardial infarction remodeling, contractile dysfunction, and heart failure. *J. Am. Coll. Cardiol.* 64 (7), 696–706. doi:10.1016/j.jacc.2014.04.068

Ahmad, F., Singh, A. P., Tomar, D., Rahmani, M., Zhang, Q., Woodgett, J. R., et al. (2019). Cardiomyocyte-GSK-3α promotes mPTP opening and heart failure in mice with chronic pressure overload. *J. Mol. Cell. Cardiol.* 130, 65–75. doi:10.1016/j.yjmcc.2019.03.020

Ahmad, F., and Woodgett, J. R. (2020). Emerging roles of GSK-3α in pathophysiology: Emphasis on cardio-metabolic disorders. *Biochim. Biophys. Acta. Mol. Cell. Res.* 1867 (2), 118616. doi:10.1016/j.bbamcr.2019.118616

Brady, D., Grapputo, A., Romoli, O., and Sandrelli, F. (2019). Insect cecropins, antimicrobial peptides with potential therapeutic applications. *Int. J. Mol. Sci.* 20 (23), 5862. doi:10.3390/ijms20235862

Carrasco, R., Castillo, R. L., Gormaz, J. G., Carrillo, M., and Thavendiranathan, P. (2021). Role of oxidative stress in the mechanisms of anthracycline-induced cardiotoxicity: Effects of preventive strategies. *Oxid. Med. Cell. Longev.* 2021, 8863789. doi:10.1155/2021/8863789

Chen, D., Yu, W., Zhong, C., Hong, Q., Huang, G., Que, D., et al. (2022). Elabela ameliorates doxorubicin-induced cardiotoxicity by promoting autophagic flux through TFEB pathway. *Pharmacol. Res.* 178, 106186. doi:10.1016/j.phrs.2022.106186

Chen, H., Wang, L., Wang, W., Cheng, C., Zhang, Y., Zhou, Y., et al. (2017). ELABELA and an ELABELA fragment protect against AKI. *J. Am. Soc. Nephrol.* 28 (9), 2694–2707. doi:10.1681/ASN.2016111210

Chiu, C. F., Ho, M. Y., Peng, J. M., Hung, S. W., Lee, W. H., Liang, C. M., et al. (2013). Raf activation by Ras and promotion of cellular metastasis require phosphorylation of prohibitin in the raft domain of the plasma membrane. *Oncogene* 32 (6), 777–787. doi:10.1038/onc.2012.86

Dai, C., Li, J., Tang, S., Li, J., and Xiao, X. (2014). Colistin-induced nephrotoxicity in mice involves the mitochondrial, death receptor, and endoplasmic reticulum pathways. *Antimicrob. Agents Chemother.* 58 (7), 4075–4085. doi:10.1128/AAC.00070-14

Dai, M., Cui, P., Yu, M., Han, J., Li, H., and Xiu, R. (2008). Melatonin modulates the expression of VEGF and HIF-1 alpha induced by CoCl2 in cultured cancer cells. *J. Pineal Res.* 44 (2), 121–126. doi:10.1111/j.1600-079X.2007.00498.x

Eid, B. G., El-Shitany, N. A. E., and Neamatallah, T. (2021). Trimetazidine improved adriamycin-induced cardiomyopathy by downregulating TNF-α, BAX, and VEGF immunoexpression via an antioxidant mechanism. *Environ. Toxicol.* 36, 1217–1225. doi:10.1002/tox.23120

Godoy-Parejo, C., Deng, C., Liu, W., and Chen, G. (2019). Insulin stimulates PI3K/AKT and cell adhesion to promote the survival of individualized human embryonic stem cells. *Stem Cells* 37 (8), 1030–1041. doi:10.1002/stem.3026

Govender, J., Loos, B., Marais, E., and Engelbrecht, A. M. (2014). Mitochondrial catastrophe during doxorubicin-induced cardiotoxicity: A review of the protective role of melatonin. *J. Pineal Res.* 57 (4), 367–380. doi:10.1111/jpi.12176

Ho, L., Tan, S. Y., Wee, S., Wu, Y., Tan, S. J., Ramakrishna, N. B., et al. (2015). ELABELA is an endogenous growth factor that sustains hESC self-renewal via the PI3K/AKT pathway. *Cell. Stem Cell.* 17 (4), 435–447. doi:10.1016/j.stem.2015.08.010

Hou, D., Hu, F., Mao, Y., Yan, L., Zhang, Y., Zheng, Z., et al. (2022). Cationic antimicrobial peptide NRC-03 induces oral squamous cell carcinoma cell apoptosis via CypD-mPTP axis-mediated mitochondrial oxidative stress. *Redox Biol.* 54, 102355. doi:10.1016/j.redox.2022.102355

Ishimaru, Y., Shibagaki, F., Yamamuro, A., Yoshioka, Y., and Maeda, S. (2017). An apelin receptor antagonist prevents pathological retinal angiogenesis with ischemic retinopathy in mice. *Sci. Rep.* 7 (1), 15062. doi:10.1038/s41598-017-15602-3

Javadov, S., Choi, A., Rajapurohitam, V., Zeidan, A., Basnakian, A. G., and Karmazyn, M. (2008). NHE-1 inhibition-induced cardioprotection against

ischaemia/reperfusion is associated with attenuation of the mitochondrial permeability transition. *Cardiovasc. Res.* 77 (2), 416–424. doi:10.1093/cvr/cvm039

Johnson, T. A., Milan-Lobo, L., Che, T., Ferwerda, M., Lambu, E., McIntosh, N. L., et al. (2017). Identification of the first marine-derived opioid receptor "balanced" agonist with a signaling profile that resembles the endorphins. *ACS Chem. Neurosci.* 8 (3), 473–485. doi:10.1021/acschemneuro.6b00167

Kostrzewa-Nowak, D., Paine, M. J., Wolf, C. R., and Tarasiuk, J. (2005). The role of bioreductive activation of doxorubicin in cytotoxic activity against leukaemia HL60-sensitive cell line and its multidrug-resistant sublines. *Br. J. Cancer* 93 (1), 89–97. doi:10.1038/sj.bjc.6602639

Lal, H., Ahmad, F., Woodgett, J., and Force, T. (2015). The GSK-3 family as therapeutic target for myocardial diseases. *Circ. Res.* 116 (1), 138–149. doi:10.1161/CIRCRESAHA.116.303613

Lee, D., Lee, S. H., Noh, I., Oh, E., Ryu, H., Ha, J., et al. (2019). A helical polypeptide-based potassium ionophore induces endoplasmic reticulum stress-mediated apoptosis by perturbing ion homeostasis. *Adv. Sci.* 6 (14), 1801995. doi:10.1002/advs.201801995

Leemasawat, K., Phrommintikul, A., Chattipakorn, S. C., and Chattipakorn, N. (2020). Mechanisms and potential interventions associated with the cardiotoxicity of ErbB2-targeted drugs: Insights from *in vitro*, *in vivo*, and clinical studies in breast cancer patients. *Cell. Mol. Life Sci.* 77 (8), 1571–1589. doi:10.1007/s00018-019-03340-w

Li, M., Qi, Z., Zhang, J., Zhu, K., and Wang, Y. (2021). Effect and mechanism of Si-Miao-Yong-An on vasa vasorum remodeling in ApoE-/- mice with atherosclerosis vulnerable plague. *Front. Pharmacol.* 12, 634611. doi:10.3389/fphar.2021.634611

Lin, Z., Tian, X. Y., Huang, X. X., He, L. L., and Xu, F. (2019). microRNA-186 inhibition of PI3K-AKT pathway via SPP1 inhibits chondrocyte apoptosis in mice with osteoarthritis. *J. Cell. Physiol.* 234 (5), 6042–6053. doi:10.1002/jcp.27225

Lüscher, T. F. (2015). Ageing, inflammation, and oxidative stress: Final common pathways of cardiovascular disease. *Eur. Heart J.* 36 (48), 3381–3383. doi:10.1093/eurheartj/ehv679

Ma, Z., Zhao, L., Martin, S., Zhang, Y., Dong, Y., Zhong, J. C., et al. (2021). Lower plasma elabela levels in hypertensive patients with heart failure predict the occurrence of major adverse cardiac events: A preliminary study. *Front. Cardiovasc. Med.* 8, 638468. doi:10.3389/fcvm.2021.638468

Ma, Z. G., Kong, C. Y., Wu, H. M., Song, P., Zhang, X., Yuan, Y. P., et al. (2020). Toll-like receptor 5 deficiency diminishes doxorubicin-induced acute cardiotoxicity in mice. *Theranostics* 10 (24), 11013–11025. doi:10.7150/thno.47516

Malla, J. A., Umesh, R. M., Yousf, S., Mane, S., Sharma, S., Lahiri, M., et al. (2020). A glutathione activatable ion channel induces apoptosis in cancer cells by depleting intracellular glutathione levels. *Angew. Chem. Int. Ed. Engl.* 59 (20), 7944–7952. doi:10.1002/anie.202000961

Münzel, T., Gori, T., Bruno, R. M., and Taddei, S. (2010). Is oxidative stress a therapeutic target in cardiovascular disease? *Eur. Heart J.* 31 (22), 2741–2748. doi:10.1093/eurheartj/ehq396

Paes, W., Leonov, G., Partridge, T., Chikata, T., Murakoshi, H., Frangou, A., et al. (2019). Contribution of proteasome-catalyzed peptide cis-splicing to viral targeting by CD8+ T cells in HIV-1 infection. *Proc. Natl. Acad. Sci. U. S. A.* 116 (49), 24748–24759. doi:10.1073/pnas.1911622116

Read, C., Nyimanu, D., Williams, T. L., Huggins, D. J., Sulentic, P., Macrae, R. G. C., et al. (2019). International union of basic and clinical Pharmacology. CVII. Structure and Pharmacology of the apelin receptor with a recommendation that elabela/toddler is a second endogenous peptide ligand. *Pharmacol. Rev.* 71 (4), 467–502. doi:10.1124/pr.119.017533

Reginauld, S. H., Cannone, V., Iyer, S., Scott, C., Bailey, K., Schaefer, J., et al. (2019). Differential regulation of ANP and BNP in acute decompensated heart failure: Deficiency of ANP. *JACC. Heart Fail.* 7 (10), 891–898. doi:10.1016/j.jchf.2019.05.012

Sato, T., Sato, C., Kadowaki, A., Watanabe, H., Ho, L., Ishida, J., et al. (2017). ELABELA-APJ axis protects from pressure overload heart failure and angiotensin II-induced cardiac damage. *Cardiovasc. Res.* 113 (7), 760–769. doi:10.1093/cvr/cvx061

Schieber, M., and Chandel, N. S. (2014). ROS function in redox signaling and oxidative stress. *Curr. Biol.* 24 (10), R453–R462. doi:10.1016/j.cub.2014.03.034

Song, H. P., Chu, Z. G., Zhang, D. X., Dang, Y. M., and Zhang, Q. (2018). PI3K-AKT pathway protects cardiomyocytes against hypoxia-induced apoptosis by MitoKATP-mediated mitochondrial translocation of pAKT. *Cell. Physiol. biochem.* 49 (2), 717–727. doi:10.1159/000493037

Sun, X., Guo, C., Zhao, F., Zhu, J., Xu, Y., Liu, Z. Q., et al. (2019). Vasoactive intestinal peptide stabilizes intestinal immune homeostasis through maintaining interleukin-10 expression in regulatory B cells. *Theranostics* 9 (10), 2800–2811. doi:10.7150/thno.34414

Tocchetti, C. G., Carpi, A., Coppola, C., Quintavalle, C., Rea, D., Campesan, M., et al. (2014). Ranolazine protects from doxorubicin-induced oxidative stress and cardiac dysfunction. *Eur. J. Heart Fail.* 16 (4), 358–366. doi:10.1002/ejhf.50

Wang, Y., Lei, T., Yuan, J., Wu, Y., Shen, X., Gao, J., et al. (2018). GCN2 deficiency ameliorates doxorubicin-induced cardiotoxicity by decreasing cardiomyocyte apoptosis and myocardial oxidative stress. *Redox Biol.* 17, 25–34. doi:10.1016/j.redox.2018.04.009

Wu, S. P., Tam, M., Vega, R. M., Perez, C. A., and Gerber, N. K. (2017). Effect of breast irradiation on cardiac disease in women enrolled in BCIRG-001 at 10-year follow-up. *Int. J. Radiat. Oncol. Biol. Phys.* 99 (3), 541–548. doi:10.1016/j.ijrobp.2017.06.018

Xu, C. (2021). The elabela in hypertension, cardiovascular disease, renal disease, and preeclampsia: An update. *J. Hypertens.* 39 (1), 12–22. doi:10.1097/HJH.0000000000002591

Yang, P., Read, C., Kuc, R. E., Buonincontri, G., Southwood, M., Torella, R., et al. (2017). Elabela/toddler is an endogenous agonist of the apelin APJ receptor in the adult cardiovascular system, and exogenous administration of the peptide compensates for the downregulation of its expression in pulmonary arterial hypertension. *Circulation* 135 (12), 1160–1173. doi:10.1161/CIRCULATIONAHA.116.023218

Ye, N., Zhang, N., Zhang, Y., Qian, H., Wu, B., and Sun, Y. (2019). Cul4a as a new interaction protein of PARP1 inhibits oxidative stress-induced H9c2 cell apoptosis. *Oxid. Med. Cell. Longev.* 2019, 4273261. doi:10.1155/2019/4273261

Yuan, Y., Fan, S., Shu, L., Huang, W., Xie, L., Bi, C., et al. (2020). Exploration the mechanism of doxorubicin-induced heart failure in rats by integration of proteomics and metabolomics data. *Front. Pharmacol.* 11, 600561. doi:10.3389/fphar.2020.600561

Zhang, S., Li, Z. T., Liu, M., Wang, J. R., Xu, M. Q., Li, Z. Y., et al. (2019). Anti-tumour activity of low molecular weight heparin doxorubicin nanoparticles for histone H1 high-expressive prostate cancer PC-3M cells. *J. Control. Release* 295, 102–117. doi:10.1016/j.jconrel.2018.12.034

Zhang, T., Wang, Y., Ma, X., Ouyang, Z., Deng, L., Shen, S., et al. (2022). Melatonin alleviates copper toxicity via improving ROS metabolism and antioxidant defense response in tomato seedlings. *Antioxidants (Basel)* 11 (4), 758. doi:10.3390/antiox11040758

Zhou, J., Ahmad, F., Parikh, S., Hoffman, N. E., Rajan, S., Verma, V. K., et al. (2016). Loss of adult cardiac myocyte GSK-3 leads to mitotic catastrophe resulting in fatal dilated cardiomyopathy. *Circ. Res.* 118 (8), 1208–1222. doi:10.1161/CIRCRESAHA.116.308544

Advantages of publishing in Frontiers

OPEN ACCESS
Articles are free to read for greatest visibility and readership

FAST PUBLICATION
Around 90 days from submission to decision

HIGH QUALITY PEER-REVIEW
Rigorous, collaborative, and constructive peer-review

TRANSPARENT PEER-REVIEW
Editors and reviewers acknowledged by name on published articles

Frontiers
Avenue du Tribunal-Fédéral 34
1005 Lausanne | Switzerland

Visit us: www.frontiersin.org
Contact us: frontiersin.org/about/contact

REPRODUCIBILITY OF RESEARCH
Support open data and methods to enhance research reproducibility

DIGITAL PUBLISHING
Articles designed for optimal readership across devices

FOLLOW US
@frontiersin

IMPACT METRICS
Advanced article metrics track visibility across digital media

EXTENSIVE PROMOTION
Marketing and promotion of impactful research

LOOP RESEARCH NETWORK
Our network increases your article's readership